Edited by
Lukas Tamm

WILEY-VCH

Protein-Lipid Interactions

From Membrane Domains to Cellular Networks

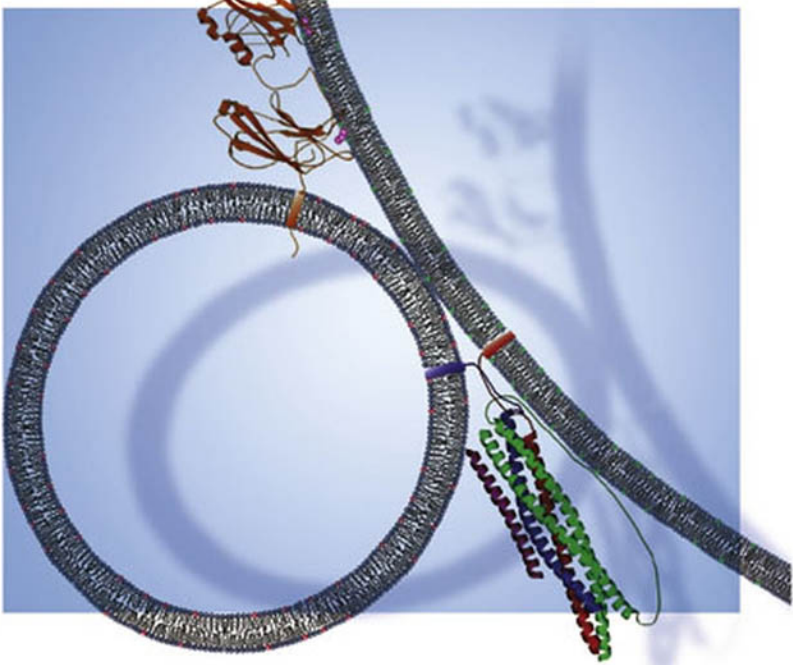

Protein–Lipid Interactions

Edited by
Lukas K. Tamm

Further Titles of Interest:

Johannes Buchner, Thomas Kiefhaber (Eds.)

Protein Folding Handbook
(5 Volumes)

2005
ISBN 3-527-30784-2

Giovanni Cesareni, Mario Gimona, Marius Sudol, Michael Yaffe (Eds.)

Modular Protein Domains

2004
ISBN 3-527-30813-X

Yoshihito Yawata

Cell Membrane
The Red Blood Cell as a Model

2003
ISBN 3-527-30463-0

Asim K. Duttaroy, Friedrich Spener (Eds.)

Cellular Proteins and Their Fatty Acids in Health and Disease

2003
ISBN 3-527-30437-1

Joachim K. Seydel, Michael Wiese, Raimund Mannhold, Hugo Kubinyi, Gerd Volkers (Eds.)

Drug-Membrane Interactions
Analysis, Drug Distribution, Modeling

2002
ISBN 3-527-30427-4

Protein–Lipid Interactions

From Membrane Domains to Cellular Networks

Edited by
Lukas K. Tamm

WILEY-VCH Verlag GmbH & Co. KGaA

Editor:

Prof. Dr. Lukas K. Tamm
Professor of Molecular Physiology
and Biological Physics
University of Virginia
PO Box 800736
Charlottesville, VA 22908-0736
USA

Library of Congress Card No.: applied for

British Library Cataloguing-in-Publication Data: A catalogue record for this book is available from the British Library.

Die Deutsche Bibliothek – CIP Cataloguing-in-Publication Data: A catalogue record for this publication is available from Die Deutsche Bibliothek

Cover illustration 4t Werbeagentur GmbH, Darmstadt
Composition K+V Fotosatz GmbH, Beerfelden
Printing betz-druck GmbH, Darmstadt
Bookbinding Litges & Dopf Buchbinderei GmbH, Heppenheim

Printed in the Federal Republic of Germany

ISBN-13: 978-3-527-31151-4
ISBN-10: 3-527-31151-3

To
Evelyne, Nicolas, and Yannick

Preface

Membranes define cells and many organelles within cells. Along with the genetic material, cellular membranes are arguably the most important cell components that carry out thousands of essential functions that define life, from the most primitive microorganisms through the plant and animal kingdoms up to man. Membranes are involved in such diverse cellular functions as transport of nutrients, ion conduction, photosynthesis, respiration and ATP synthesis, signal transduction, vision, hearing, cell migration, fertilization, development, and many more.

For about half a century now, we know that the basic building block of biological membranes is the lipid bilayer. Embedded in the fluid lipid bilayer are proteins of various shapes and traits. This volume illuminates from physical, chemical and biological angles the numerous – mostly quite weak – interactions between lipids, proteins, and proteins and lipids that define the delicate, highly dynamic and yet so stable fabric that gives biological membranes their shape and function.

Even though the basic bimolecular leaflet structure of membranes has been discovered many decades ago, more recent research has considerably refined the early "fluid mosaic" model of the structure of biomembranes. As briefly recounted in Chapter 1, it has been recognized that the membrane-water "interface" occupies a considerable fraction of the entire membrane volume that has many previously under-appreciated consequences, for example, on how proteins interact with membranes or become inserted into membranes. It has also become increasingly clear that the "fluid mosaic" model does not suffice to describe lateral heterogeneities that exist in biological membranes and that affect many membrane functions – for example, in signal transduction, protein sorting, endocytosis, or the budding of enveloped viruses. Biological evidence points to a membrane structure that is laterally highly organized, while still retaining predominantly liquid characteristics. In physical terms, membranes could be considered to consist of a mosaic of fluid grains of different degrees of pseudo two-dimensional liquid order. Our current level of understanding and consequences of this membrane structure of organized fluid domains on various micro- and nanoscopic length scales are summarized in Chapters 13 and 14. Some answers emerge from this research on why cells make many lipids with different properties, but the long-standing question why cells make as many lipids as they do (literally thousands) is still not answered by even the most recent research in this rapidly evolving field.

The four chapters collected in Part 1 illuminate how proteins are inserted into biological and model membranes. Since the crowded environment of a cell membrane, namely the laterally and vertically compartmentalized lipid bilayer, is so different from the crowded aqueous environment of the cytoplasm, the folding and insertion of membrane proteins proceeds along very different biological pathways and according to very different physical principles than the folding of soluble proteins. The major building blocks of membrane proteins are α-helices and β-sheets and the generation and insertion of these elements of secondary structure are described in Chapters 1 to 3, respectively. Chapter 4 focuses on what happens when membrane protein folding goes wrong and causes disease.

Not only do lipids shape proteins, but proteins also shape lipids. The two chapters in Part 2 focus on this problem and illuminate how specific lipids can be dramatically distorted on membrane protein surfaces as seen by x-ray crystallography, but also how lipid-protein interactions can be highly dynamic at these interfaces when examined by nuclear magnetic resonance techniques.

Many diseases, including some that are unleashed by biological terrorism agents, are caused by protein toxins that have to breach the cell membrane to reach their point of action. Examples include diphtheria and anthrax toxins. Other toxins such as those from staphylococci, clostridiae, or sea anemones are toxic because of their pore forming activities in membranes. Since these proteins are facultative membrane proteins that can exist in soluble and membrane-bound forms, they offer interesting avenues to study membrane protein insertion in addition to studying their mechanism of pore formation and toxicity. Chapters 7 and 8 deal with these mechanisms and Chapter 9 gives an overview of the action of antimicrobial peptides on membranes.

Viruses constitute another class of biological agents that cause disease. While very little is known on how non-enveloped viruses breach cell membranes, membrane-enveloped viruses enter cells by membrane fusion. Chapter 12 recounts how viral fusion proteins have evolved to orchestrate the formation of fusion pores through which viral nucleocapsids and viral genomes are delivered into the cell cytoplasm. Just as viruses gain cell entry by membrane fusion, some cells fuse with one another to generate multinucleated cells. This occurs in fertilization, but also in development – for example when myotubes are formed in muscle development or when epithelial cells fuse in nematode development as summarized in Chapter 10. The molecular mechanisms that govern intracellular membrane fusion, which is essential for the biogenesis of organelles, exocytosis and synaptic transmission are summarized in Chapter 11.

Many cellular proteins are targeted to membranes in response to signals from the outside or from within the cell. Switching between membrane-bound and soluble forms of these proteins regulates a huge number of metabolic responses that impact on cell growth, migration, and development. The volume closes with a collection of Chapters that describe how different protein modules are recruited and bind to membrane surfaces. Chapter 15 gives a broad overview over the many families of membrane targeting domains that are present in eukaryot-

ic cells. Chapter 16 focuses on the mechanisms of membrane interactions of one of these families, namely the C2 domains. Chapter 17 illustrates with two prominent examples how some of these domains cooperate to form allosteric molecular switches on membrane surfaces.

I would like to express my gratitude to the contributing authors, to Ann Folsom for her able handling of the manuscripts, to Volker Kiessling for the design of the cover figure, and to Frank Weinreich and Waltraud Wüst, Wiley-VCH, for their invitation to edit a book on this topic and their dedication and professionalism in producing this book.

July 2005 *Lukas K. Tamm*

Contents

List of Contributors

Dr. Gregor Anderluh
Department of Biology
University of Ljubljana
Večna pot 111
1000 Ljubljana
Slovenia

Dr. Ashish Arora
Department of Molecular
and Structural Biology
Central Drug Research Institute
Chattar Manzil Palace
P.O. Box 173
M.G. Marg, Lucknow 226001, UP
India

Kirsten Bacia
Biophysics/BioTec
Technical University Dresden
Tatzberg 47–51
01307 Dresden
Germany

Prof. Paula J. Booth
Membrane Protein Folding Group
Department of Biochemistry
University of Bristol
University Walk
Bristol, BS8 1TD
UK

Prof. David S. Cafiso
Department of Chemistry
University of Virginia
McCormick Road
Charlottesville, VA 22908-4319
USA

Dr. Bertram Canagarajah
Laboratory of Molecular Biology
National Institute of Diabetes
and Digestive and Kidney Diseases
National Institutes of Health
US Department of Health
and Human Services
50 South Drive
Bethesda, MD 20892
USA

Dr. Leonid V. Chernomordik
Laboratory of Cellular and Molecular
Biophysics
Section on Membrane Biology
National Institute of Child Health
and Human Development
National Institutes of Health
10 Center Drive, Building 10
Bethesda, MD 20892-1855
USA

Prof. Wonhwa Cho
Department of Chemistry (M/C 111)
University of Illinois at Chicago
845 W. Taylor Street
Chicago, IL 60607-7061
USA

Tara Hessa
Department of Biochemistry
and Biophysics
Stockholm University
10691 Stockholm
Sweden

Dr. Alejandro P. Heuck
Department of Medical Biochemistry
and Genetics
Texas A&M University System
Health Science Center
116 Reynolds Medical Building
College Station, TX 77843-1114
USA

Dr. James H. Hurley
Laboratory of Molecular Biology
National Institute of Diabetes
and Digestive and Kidney Diseases
National Institutes of Health
US Department of Health
and Human Services
50 South Drive
Bethesda, MD 20892
USA

Prof. Reinhard Jahn
Department of Neurobiology
Max Planck Institute for Biophysical
Chemistry
37077 Göttingen
Germany

Prof. Arthur E. Johnson
College of Medicine
Texas A&M University System
Health Science Center
116 Reynolds Medical Building
College Station, TX 77843-1114
USA

Dr. Nicoletta Kahya
Biophysics/BioTec
Technical University Dresden
Tatzberg 47–51
01307 Dresden
Germany

Priv.-Doz. Jörg H. Kleinschmidt
Department of Biology (M 694)
University of Konstanz
78457 Konstanz
Germany

Junko Kondo
Institute for Frontier Medicine
Kyoto University
Shougoin, Sakyo-ku
Kyoto 606-8507
Japan

Prof. Akihiro Kusumi
Institute for Frontier Medicine
Kyoto University
Shougoin, Sakyo-ku
Kyoto 606-8507
Japan

Alex L. Lai
Department of Molecular Physiology
and Biological Physics
University of Virginia
1300 Jefferson Park Avenue
P.O. Box 800736
Charlottesville, VA 22908-0736
USA

Prof. Jeremy H. Lakey
Institute of Cell and Molecular Biosciences
University of Newcastle-upon-Tyne
Framlington Place
Newcastle-upon-Tyne, NE2 4HH
UK

Dr. Yinling Li
Department of Molecular Physiology and Biological Physics
University of Virginia
1300 Jefferson Park Avenue
P.O. Box 800736
Charlottesville, VA 22908-0736
USA

Dr. Nobuhiro Morone
Department of Ultrastructural Research
National Center of Neurology and Psychiatry
Kodaira, Tokyo 187-8502
Japan

Prof. Benjamin Podbilewicz
Department of Biology
Technion Israel Institute of Technology, Technion City
Haifa 32000
Israel

Prof. Charles R. Sanders
Department of Biochemistry and Center for Structural Biology
Room 5110C, MRB III
Vanderbilt University
Nashville, TN 37027
USA

Prof. Petra Schwille
Biophysics/BioTec
Technical University Dresden
Tatzberg 47–51
01307 Dresden
Germany

Prof. Yechiel Shai
Department of Biological Chemistry
The Weizmann Institute of Science
Rehovot 76100
Israel

Dr. William J. Smith
Cell Biology and Metabolism Branch
National Institute of Child Health and Human Development
National Institutes of Health
US Department of Health and Human Services
50 South Drive
Bethesda, MD 20892
USA

Dr. Robert V. Stahelin
Department of Chemistry (M/C 111)
University of Illinois at Chicago
845 W. Taylor Street
Chicago, IL 60607-7061
USA

Prof. Kenichi Suzuki
Institute for Frontier Medicine
Kyoto University
Shougoin, Sakyo-ku
Kyoto 606-8507
Japan

Prof. Lukas K. Tamm
Department of Molecular Physiology and Biological Physics
University of Virginia
1300 Jefferson Park Avenue
P.O. Box 800736
Charlottesville, VA 22908-0736
USA

Yasuhiro Umemura
Institute for Frontier Medicine
Kyoto University
Shougoin, Sakyo-ku
Kyoto 606-8507
Japan

Dr. Olga Vites
Department of Neurobiology
Max Planck Institute for Biophysical Chemistry
37077 Göttingen
Germany

Prof. Gunnar von Heijne
Department of Biochemistry and Biophysics
Stockholm University
10691 Stockholm
Sweden

Prof. Stephen H. White
Department of Physiology and Biophysics
Medical Sciences I-D346
University of California at Irvine
Irvine, CA 92697-4560
USA

Prof. Michael C. Wiener
Department of Molecular Physiology and Biological Physics
University of Virginia
1300 Jefferson Park Avenue
P.O. Box 800736
Charlottesville, VA 22908-0736
USA

Part 1
How Lipids Shape Proteins

1
Lipid Bilayers, Translocons and the Shaping of Polypeptide Structure

Stephen H. White, Tara Hessa, and Gunnar von Heijne

1.1
Introduction

Constitutive membrane proteins (MPs) come to equilibrium with the lipid bilayer and water, after transmembrane (TM) insertion, through the translocation machinery of cells. The prediction of their three-dimensional structure from the amino acid sequence should emerge from a comprehensive understanding of the physical chemistry of protein–lipid interactions. The most fundamental physical principle is that TM helices are composed predominantly of non-polar amino acids. Bacteriorhodopsin [1], comprised of seven TM helices packed neatly into a bundle, is generally taken as the archetypal MP. Its apparent simplicity has led to a simple prediction paradigm that involves first identifying hydrophobic TM segments using hydropathy plots (reviewed in [2]) and then applying helix-packing constraints [3]. This optimistic assessment has been seriously challenged by the three-dimensional structure of the ClC chloride channel published in 2002 [4] (Fig. 1.1 A). The jumble of helices buried within the membrane mocks bacteriorhodopsin's simplicity. Not only do the 17-odd helices vary greatly in length and tilt, some form TM structures in end-to-end arrangements in the manner of the aquaporin family of transporters (reviewed in [5]). Hydropathy plots fail to identify the complex topology correctly. This failure is not limited to the ClC channel alone, as shown by the three-dimensional structure of the KvAP voltage-gated potassium channel [6]. The S1–S4 voltage sensing region is not comprised of the simple TM helices as surmised from hydropathy plot analyses. Rather, this region appears to be dominated by a helical hairpin arrangement that can move within the lipid bilayer in response to changes of membrane potential. These new structures force a re-evaluation of the structure-prediction problem.

What is missing from the present approach? One thing may be attention to the mechanisms of biological assembly. Constitutive α-helical MPs are as-

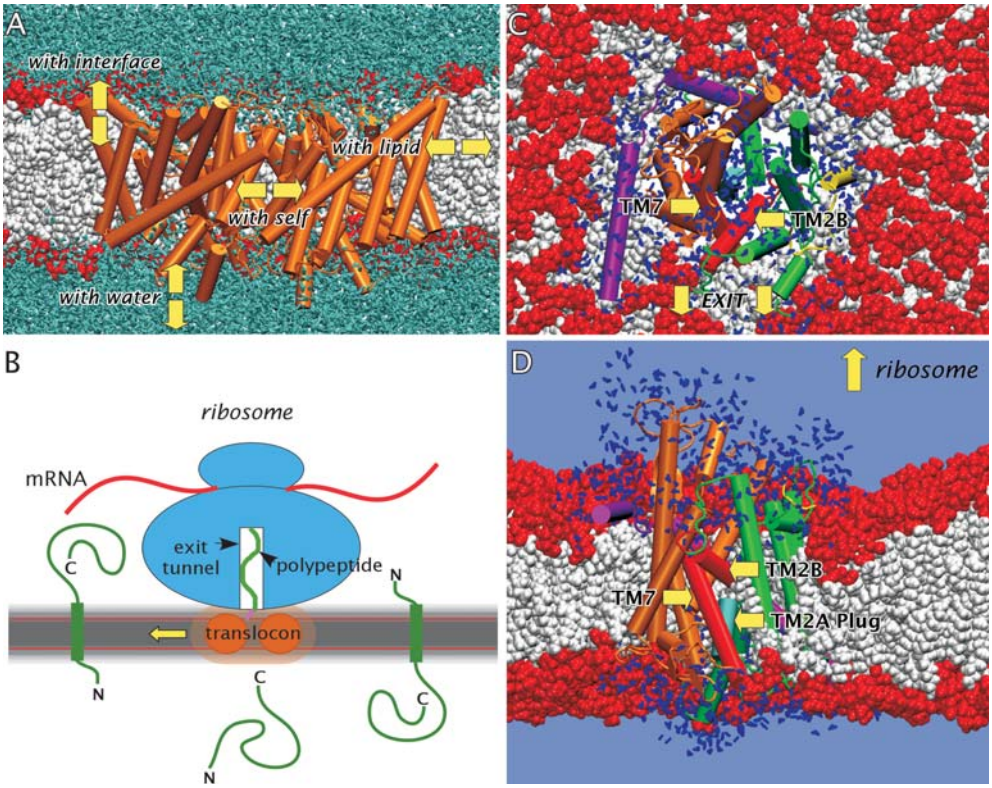

Fig. 1.1 Examples of MPs in lipid bilayers. In the molecular images, phospholipid headgroups are red and acyl chains are white. (A) An image of the ClC chloride channel [4, 111] embedded in a lipid bilayer (red and white) surrounded by water (aquamarine). The topology of this complex protein defies predictions using hydropathy plots. The yellow arrows highlight the components of the intrinsic interactions that must be understood quantitatively in order to predict the three-dimensional structure from the amino acid sequence. Intrinsic interactions are those involving the full-length polypeptide sequence, the lipid bilayer and water. The image was produced from a MD simulation of ClC in a POPC bilayer, courtesy of Dr. Alfredo Freites at UC Irvine.
(B) Schematic representation of the translocation or insertion of TM helices by a translocon receiving an elongating polypeptide chain from a ribosome. Polypeptide chains destined for translocation across the ER (center green chain) of eukaryotes or the plasma membrane of prokaryotes lack a segment of sufficient hydrophobicity and length to be identified by the translocon as a TM helix. The topology of a TM segment [112] is determined by charge interactions [113] with the translocon complex (Sec61 in eukaryotes, SecY in bacteria). Several recent reviews discuss translocon-guided insertion of MPs [9–14, 114]. The schematic image is based upon Fig. 1 of [9].
(C and D) Structure of the SecY complex from *Methanococcus jannaschii* [7] that has been embedded in a POPC lipid bilayer using MD methods. A view of SecY normal to the bilayer plane looked at from the ribosome is shown in (C), while (D) shows a view along the bilayer plane looking into the so-called "gate" formed by helices TM2B and TM7. Nascent TM helices move into the bilayer through this gate. The translocon is in a closed state, because the structure was determined in the absence of an elongating polypeptide. The TM2A "plug helix" apparently seals the translocon in the absence of nascent peptide to prevent TM movement of ions. Waters within 5 Å of SecY are identified by the blue triangles. The images were prepared from a MD simulation, courtesy of Dr. Alfredo Freites at UC Irvine. All molecular graphics images were produced using Visual Molecular Dynamics (VMD) [115].

sembled in membranes by means of a translocation/insertion process that involves physical engagement of a ribosome (Fig. 1.1 B) with the translocon complex [7–9] – itself a MP [9–12] (Fig. 1.1 C and D). Polypeptide segments destined for insertion as TM segments are identified by the translocon–bilayer system and shunted into the bilayer (reviewed in [9–15]). After release into the membrane's bilayer fabric and disassembly of the ribosome–translocon machinery, a MP resides stably in a thermodynamic free energy minimum (evidence reviewed in [16, 17]). This outline of MP assembly suggests two fundamental categories of protein–lipid interactions that require consideration in structure-prediction algorithms: intrinsic and formative.

Intrinsic interactions are those responsible for the stability and structure of the full-length polypeptide chain after synthesis. These interactions, which produce the final shaping of MP structure, include interactions of the polypeptide chain with itself, water, the bilayer hydrocarbon core (HC), the bilayer interfaces (IFs) and, in some cases, cofactors (Fig. 1.1 A). Several recent reviews [17–21] provide extensive discussions of the evolution, structure and thermodynamic stability of MPs. An overview of intrinsic interactions that stabilize α-helical MPs is provided in Section 1.2. The basic thermodynamic principles of α-helical MPs, except for helix–helix interactions, apply also to β-barrel MPs, but this class of MPs will not be considered here. The interested reader should consult two excellent recent reviews on β-barrel MPs [21, 22].

The second category of interactions that require consideration in structure-prediction algorithms, formative interactions, involve interactions of elongating polypeptides with the translocon as well as the lipid bilayer. These interactions, which lead to the selection of a polypeptide segment for shunting into the bilayer, are the subject of Section 1.3. Recent experiments [23] have revealed the basic selection rules, and the recent structure of the bacterial (SecY) translocon [7, 8] (shown embedded in a lipid bilayer in Fig. 1.1 C and D) provides a structural context for the underlying formative interactions. The basic selection rules indicate that our understanding of the intrinsic interactions is incomplete.

1.2
Membrane Proteins: Intrinsic Interactions

1.2.1
Physical Determinants of Membrane Protein Stability: The Bilayer Milieu

Two influences are paramount in shaping polypeptide structure in membranes. First, as indicated in Fig. 1.2, the membrane's bilayer fabric has two chemically distinct regions: HC and IFs. IF structure and chemistry must be important because the specificity of protein signaling and targeting by membrane-binding domains could not exist otherwise [24], as discussed in detail in Chapters 15 to 17. Second, the high energetic cost of dehydrating the peptide bond, as when transferring it to a non-polar phase, causes it to dominate structure formation

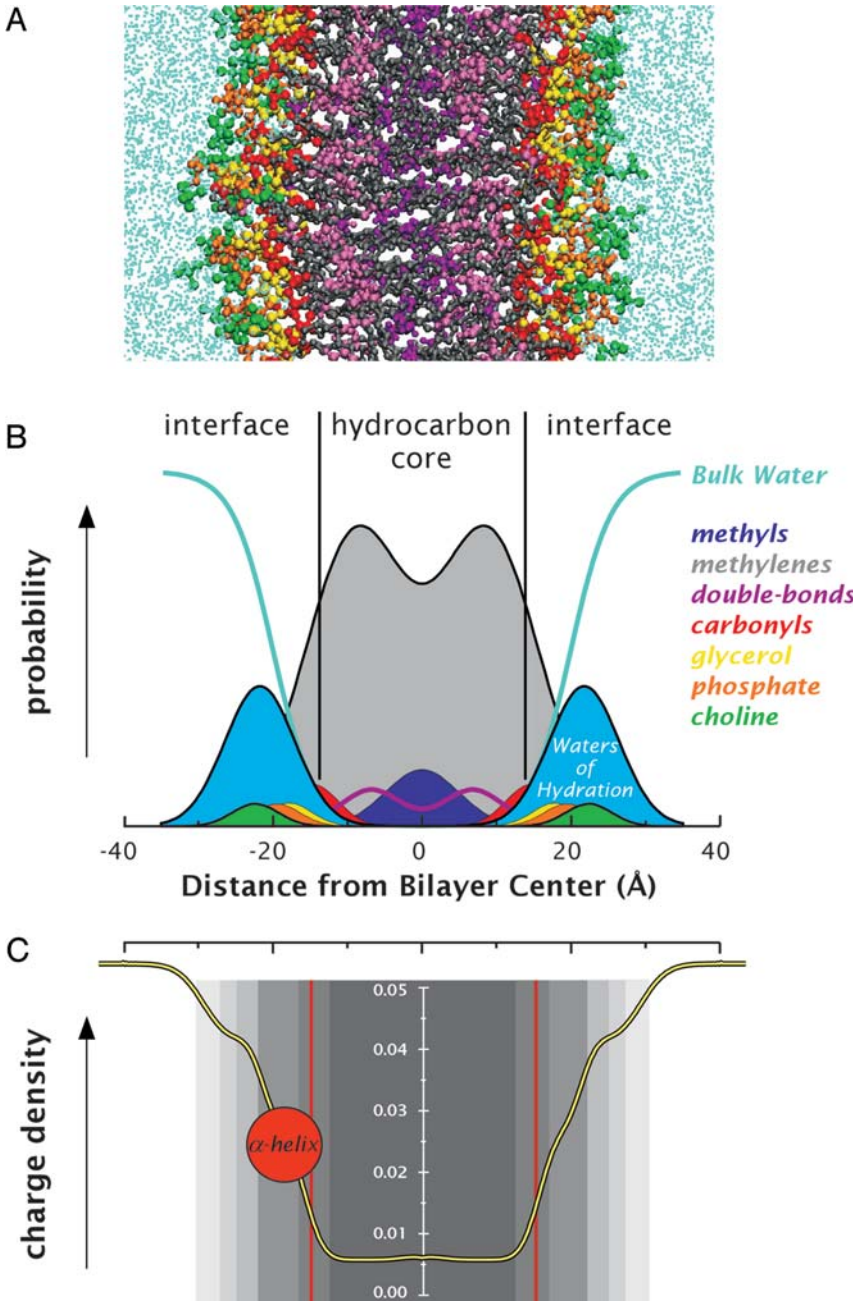
A
B
interface
hydrocarbon core
interface
Bulk Water
methyls
methylenes
double-bonds
carbonyls
glycerol
phosphate
choline
probability
Waters of Hydration
-40
-20
0
20
40
Distance from Bilayer Center (Å)
C
charge density
α-helix
0.05
0.04
0.03
0.02
0.01
0.00

[25], as summarized in Fig. 1.3. The only permissible TM structural motifs of MPs are α-helices and β-barrels, because internal hydrogen bonding ameliorates this cost (see below).

As membranes must be in a fluid state for normal cell function, only the structure of fluid (L_α phase) bilayers is relevant to understanding how membranes mold proteins. However, atomic-resolution images of fluid membranes are precluded due to their high thermal disorder (Fig. 1.2 A). Nevertheless, fundamental and useful structural information can be obtained from multilamellar bilayers (liquid crystals) dispersed in water or deposited on surfaces [26–29]. Their one-dimensional crystallinity perpendicular to the bilayer plane allows the distribution of matter along the bilayer normal to be determined by combined X-ray and neutron diffraction measurements (liquid crystallography; reviewed in [30, 31]). The resulting "structure" consists of a collection of time-averaged probability distribution curves of water and lipid component groups (carbonyls, phosphates, etc.), representing projections of three-dimensional motions onto the bilayer normal. Fig. 1.2 B shows the liquid-crystallographic structure of an L_α phase dioleoylphosphatidylcholine (DOPC) bilayer [32].

Three features of this structure are important. First, the widths of the probability densities reveal the great thermal disorder of fluid membranes. Second, the combined thermal thickness of the IFs (defined by the distribution of the waters of hydration) is approximately equal to the 30-Å thickness of the HC. The thermal thickness of a single IF (around 15 Å) can easily accommodate an α-helix parallel to the membrane plane. The common cartoons of bilayers that assign a diminutive thickness to the bilayer IFs are thus misleading. Third, the thermally disordered IFs are highly heterogeneous chemically. A polypeptide chain in an IF must experience dramatic variations in environmental polarity

Fig. 1.2 The liquid-crystalline structure of a fluid DOPC bilayer.
(A) Molecular graphics image of DOPC taken from a MD simulation by Ryan Benz at UC Irvine. The color scheme for the component groups (carbonyls, phosphates, water, etc.) is given in (B). The image was prepared by S. White using VMD [115].
(B) Liquid-crystallographic structure of a fluid DOPC lipid bilayer [32]. The "structure" of the bilayer is comprised of a collection of transbilayer Gaussian probability distribution functions representing the lipid components that account for the entire contents of the bilayer unit cell. The areas under the curves correspond to the number of constituent groups per lipid represented by the distributions (one phosphate, two carbonyls, four methyls, etc.). The widths of the Gaussians measure the thermal motions of the lipid components and are simply related to crystallographic *B* factors [39, 40, 116]. The thermal motion of the bilayer is extreme: lipid-component *B* factors are typically around 150 $Å^2$, compared to around 30 $Å^2$ for atoms in protein crystals.
(C) Polarity profile (yellow curve) of the DOPC bilayer (above) computed from the absolute values of atomic partial charges [33]. The end-on view in (B) of an α-helix with diameter $\sim$10 Å – typical for MP helices [87] – shows the approximate location of the helical axes of the amphipathic-helix peptides Ac-18A-NH_2 [40] and melittin [39], as determined by a novel, absolute-scale X-ray diffraction method (reviewed in [117]). Panels (B) and (C) have been adapted from reviews by White and Wimley [17, 33, 118].

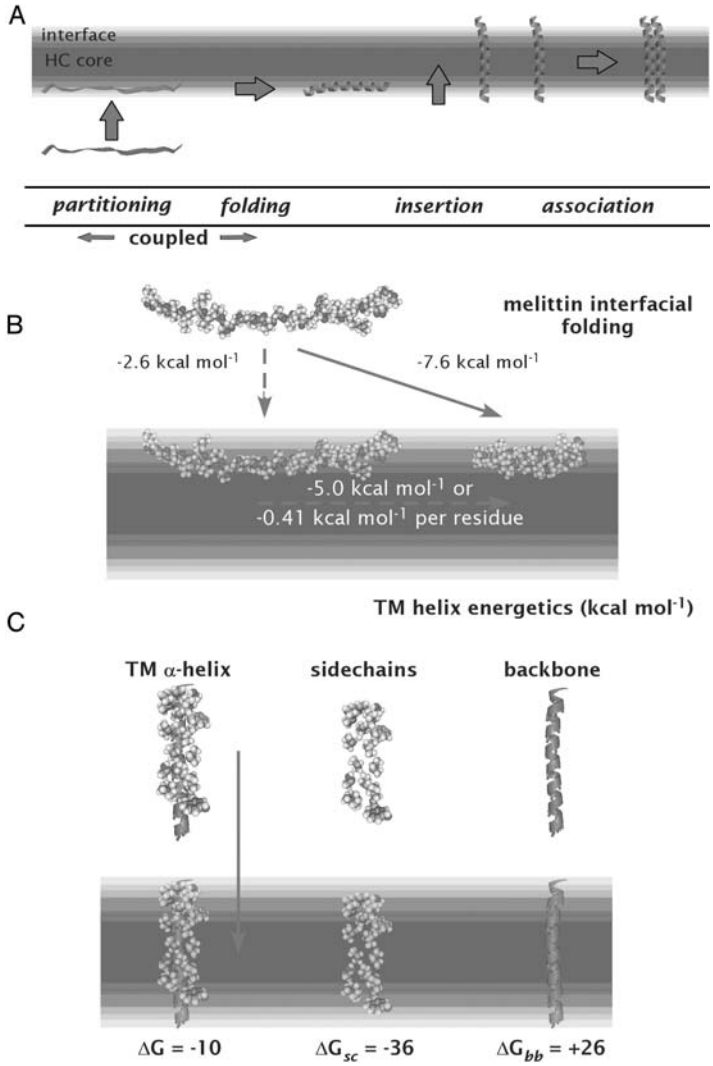

Fig. 1.3 Energetics of peptide interactions with lipid bilayers.
(A) Schematic representation of the shaping of protein structure through polypeptide–bilayer interactions. Based upon the four-step thermodynamic cycle of Wimley and White [17] for describing the partitioning, folding, insertion and association of α-helical polypeptides. The aqueous insolubility of MPs, folded or unfolded, precludes direct determinations of interaction free energies. The only route to understanding the energetics of MP stability is through studies of small, water-soluble peptides [62, 64, 65, 68]. The association of TM helices is probably driven by van der Waals interactions, giving rise to knob-into-hole packing [84–86, 119]. The GxxxG motif is especially important in helix–helix interactions in membranes [90, 91].
(B) Energetics of secondary structure formation by melittin at the bilayer IF [65]. Unfolded peptides are driven toward the folded state in the IF because hydrogen-bond formation dramatically lowers the cost of peptide-bond partitioning, which is the

over a short distance due to the steep changes in chemical composition, as illustrated by the yellow curve in the lower half of Fig. 1.2 C [33]. As the regions of first contact, the IFs are especially important in the folding and insertion of non-constitutive MPs, such as diphtheria toxin [34, 35] and to the activity of surface-binding enzymes, such as phospholipases [36–38]. However, for reasons discussed below, they are also likely to be important in translocon-assisted folding of MPs.

Experimentally determined bilayer structures such as the one in Fig. 1.2 C are essential for understanding thermodynamic measurements of peptide–bilayer interactions at the molecular level. Recent extension of the liquid-crystallographic methods to bilayers containing peptides such as melittin [39] and other amphipathic peptides [40] makes this a practical possibility. However, there are numerous other X-ray and neutron diffraction approaches that provide important information about the molecular interactions of peptides with lipid bilayers [41–47]. Molecular dynamics (MD) simulations of bilayers [48–51] (Fig. 1.2 A) are rapidly becoming an essential structural tool for examining lipid–protein interactions at the atomic scale [52–57]. The future offers the prospect of combining bilayer diffraction data with MD simulations in order to arrive at experimentally validated MD simulations of fluid lipid bilayers [58]. This approach should allow one to convert the static one-dimensional images obtained by diffraction (Fig. 1.2 B) into dynamic, three-dimensional structures for examining peptide–lipid interactions in atomic detail.

1.2.2 Physical Determinants of Membrane Protein Stability: Energetics of Peptides in Bilayers

Experimental exploration of the stability of intact MPs is problematic due to their general insolubility. One approach to stability is to "divide and conquer" by

dominant determinant of whole-residue partitioning. The free energy reduction accompanying secondary structure formation by melittin is around 0.4 kcal mol^{-1} per residue [64, 65], but may be as low as 0.1 kcal mol^{-1} for other peptides [120]. Although small, such changes in aggregate can be large. For example, the folding of 12 residues of 26-residue melittin into an α-helical conformation causes the folded state to be favored over the unfolded state by around 5 kcal mol^{-1}. To put this number in perspective, the ratio of folded to unfolded peptide is around 4700.

(C) The energetics of TM helix insertion based upon the work of Wimley and White [68] and Jayasinghe et al. [72]. Estimated relative free energy contributions of the side-chains (ΔG_{sc}) and backbone (ΔG_{bb}) to the helix-insertion energetics of glycophorin A [73]. The net side-chain contribution (relative to glycine) was computed using the *n*-octanol hydrophobicity scale of Wimley et al. [74]. The per-residue cost of partitioning a polyglycine α-helix is +1.15 kcal mol^{-1} [72]. (Adapted from reviews by White et al. [19] and White [20]).

studying the membrane interactions of fragments of MPs, i.e. peptides. Because MPs are equilibrium structures, one is free to describe the interactions by any convenient set of experimentally accessible thermodynamic pathways, irrespective of the biological synthetic pathway. One particularly useful set of pathways is the so-called four-step model [17] (Fig. 1.3 A), which is a logical combination of the early three-step model of Jacobs and White [59] and the two-stage model of Popot and Engelman [60], in which TM helices are first "established" across the membrane and then assemble into functional structures (helix association; reviewed in [61]). Although these pathways do not mirror the actual biological assembly process of MPs, they are nevertheless useful for guiding biological experiments, because they provide a thermodynamic context within which biological processes must proceed.

In the four-step model (Fig. 1.3 A), the free energy reference state is taken as the unfolded protein in an IF. However, this state cannot actually be achieved with MPs because of the solubility problems. Nor can it be achieved with small non-constitutive membrane-active peptides, such as melittin, because binding usually induces secondary structure (partitioning-folding coupling). It can be defined for phosphatidylcholine (PC) IFs by means of an experiment-based interfacial free energy (hydrophobicity) scale [62] derived from partitioning into 1-palmitoyl-2-oleolyl-phosphatidylcholine (POPC) bilayers of tri- and pentapeptides [59, 62] that have no secondary structure in the aqueous or interfacial phases. This scale (Fig. 1.4 A), which includes the peptide bonds as well as the side-chains, allows calculation of the virtual free energy of transfer of an unfolded chain into an IF. For peptides that cannot form regular secondary structure, such as the antimicrobial peptide indolicidin, the scale predicts observed free energies of transfer with remarkable accuracy [63]. This validates it for computing virtual partitioning free energies of proteins into PC IFs. Similar scales are needed for other lipids and lipid mixtures.

The high cost of interfacial partitioning of the peptide bond [62], 1.2 kcal mol^{-1}, explains the origin of partitioning-folding coupling and it also explains why the IF is a potent catalysis of secondary structure formation. Wimley et al. [64] showed for interfacial β-sheet formation that hydrogen-bond formation reduces the cost of peptide partitioning by about 0.5 kcal mol^{-1} per peptide bond. The folding of melittin into an amphipathic α-helix on POPC membranes involves a per-residue reduction of about 0.4 kcal mol^{-1} [65] (Fig. 1.3 B). The folding of other peptides may involve smaller per-residue values [66, 67]. The cumulative effect of these relatively small per-residue free energy reductions can be very large when tens or hundreds of residues are involved.

The energetics of TM helix stability also depend critically on the partitioning cost of peptide bonds (Fig. 1.3 C). Determination of the energetics of TM α-helix insertion, which is necessary for predicting structure, is difficult because nonpolar helices tend to aggregate in both aqueous and interfacial phases [68]. The broad energetic issues are clear [69], however. Computational studies [70, 71] suggest that the transfer free energy ΔG_{CONH} of a non-hydrogen-bonded peptide bond from water to alkane is +6.4 kcal mol^{-1}, compared to only +2.1 kcal mol^{-1}

for the transfer free energy $\Delta G_{\mathrm{Hbond}}$ of a hydrogen-bonded peptide bond. The per-residue free energy cost of disrupting hydrogen bonds in a membrane is therefore about 4 kcal mol^{-1}. A 20-amino-acid TM helix would thus cost 80 kcal mol^{-1} to unfold within a membrane, which explains why unfolded polypeptide chains cannot exist in a TM configuration.

As discussed in detail elsewhere [19, 72], $\Delta G_{\mathrm{Hbond}}$ sets the threshold for TM stability as well as the so-called decision level in hydropathy plots [2]. The free energy of transfer of non-polar side-chains dramatically favors helix insertion, while the transfer cost of the helical backbone dramatically disfavors insertion. For example [19], the favorable (hydrophobic effect) free energy for the insertion of the single membrane-spanning helix of glycophorin A [73] is estimated to be –36 kcal mol^{-1}, whereas the cost ΔG_{bb} of dehydrating the helix backbone is +26 kcal mol^{-1} (Fig. 1.3 C). The net free energy ΔG_{TM} favoring insertion is thus –10 kcal mol^{-1}. As is common in so many biological equilibria, the free energy minimum is the small difference of two relatively large opposing energetic terms. Uncertainties in the per-residue cost of backbone insertion will have a major effect on estimates of TM helix stability, the interpretation of hydropathy plots, and the establishment of the minimum value of side-chain hydrophobicity required for stability. An uncertainty of 0.5 kcal mol^{-1}, for example, would cause an uncertainty of about 10 kcal mol^{-1} in ΔG_{TM}!

What is the most likely estimate of $\Delta G_{\mathrm{Hbond}}$? The practical number is the cost $\Delta G^{\mathrm{helix}}_{\mathrm{glycyl}}$ of transferring a single glycyl unit of a polyglycine α-helix into the bilayer HC. Electrostatic calculations [71] and the octanol partitioning study of Wimley et al. [74] suggested that $\Delta G^{\mathrm{helix}}_{\mathrm{glycyl}} = +1.25$ kcal mol^{-1}, which is the basis for the calculation of ΔG_{bb}. The cost of transferring a random-coil glycyl unit into *n*-octanol [74] is +1.15 kcal mol^{-1}, which suggested that the *n*-octanol whole-residue hydrophobicity scale [17] (Fig. 1.4 B) derived from partitioning data of Wimley et al. [74] might be a good measure of $\Delta G^{\mathrm{helix}}_{\mathrm{glycyl}}$. This hypothesis was borne out by a study [72] of known TM helices cataloged in the MPtopo database of MPs of known topology [75], accessible via *http://blanco.biomol.uci.edu/mptopo*. This study showed that +1.15 kcal mol^{-1} is indeed the best estimate of $\Delta G^{\mathrm{helix}}_{\mathrm{glycyl}}$. Using this value, TM helices for MPs of known three-dimensional structure could be identified with high accuracy in the 2001 edition of MPtopo. This scale also includes free energy values for protonated and deprotonated forms of Asp, Glu and His. In addition, Wimley et al. [76] determined the free energies of partitioning salt-bridges into octanol, which are believed to be good estimates for partitioning into membranes [72]. This has led to the augmented Wimley–White (aWW) hydrophobicity scale [72] that forms the basis for a useful hydropathy-based tool, MPEx, for analyzing MP protein stability. MPEx is available as an on-line java applet at *http://blanco.biomol.uci.edu/mpex*. However, the scale fails miserably in the prediction of the topology of the ClC chloride channel (Fig. 1.1 A), indicating the need to understand the translocon-assisted folding of MPs. Nevertheless, the WW experiment-based whole-residue hydrophobicity scales [62, 72, 74], Fig. 1.4 [A (ΔG_{IF}) and B (ΔG_{WW} or ΔG_{oct})], provide a solid starting point for understanding the physical stability of MPs. The

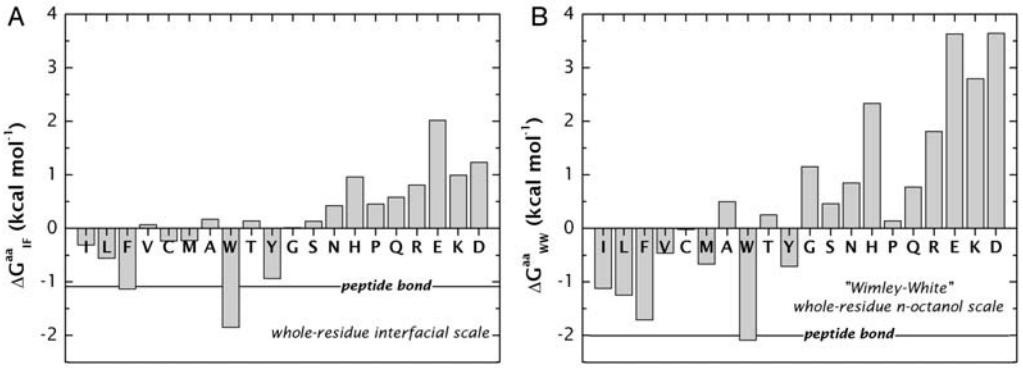
A
B
ΔG^aa_IF (kcal mol^-1)
ΔG^aa_WW (kcal mol^-1)
L F V C M A W T Y G S N H P Q R E K D
I L F V C M A W T Y G S N H P Q R E K D
peptide bond
whole-residue interfacial scale
"Wimley-White"
whole-residue n-octanol scale

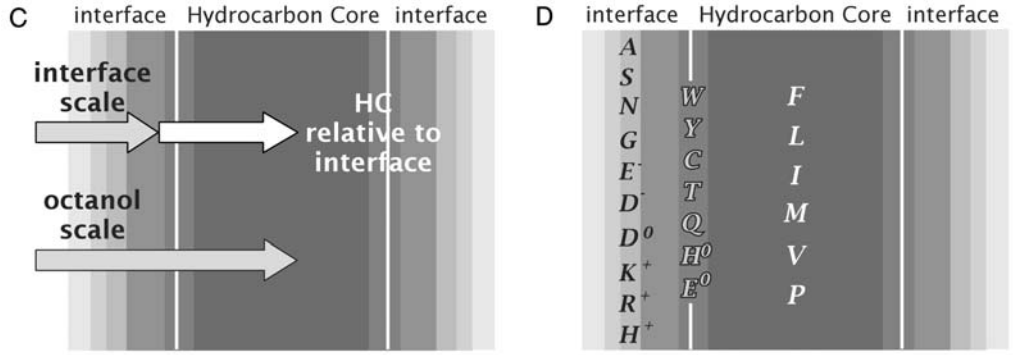
C
D
interface
Hydrocarbon Core
interface
interface scale
octanol scale
HC relative to interface
A S N G E- D- D0 K+ R+ H+
W Y C T Q H0 E0
F L I M V P

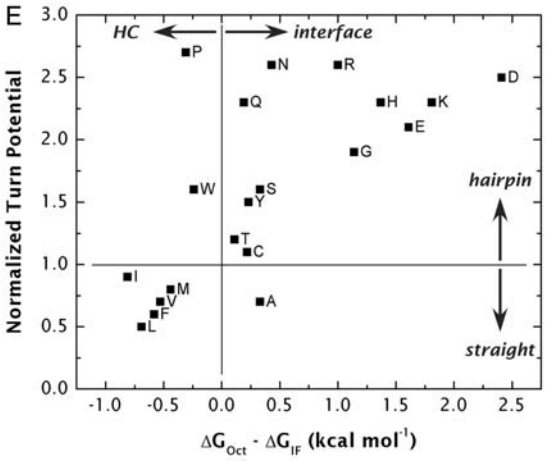
E
HC
interface
hairpin
straight
Normalized Turn Potential
ΔG_Oct - ΔG_IF (kcal mol^-1)

whole-residue WW scale provides an important connection between physical chemistry and biology (see below).

When the two scales are used together (Fig. 1.4 C), one can estimate the preference of a polypeptide segment for the HC as an α-helix relative to the membrane IF as an unfolded chain. The "octanol–IF" scale, $\Delta G_{oct-IF} = \Delta G_{oct} - \Delta G_{IF}$, divides the amino acid residues into three groups (Fig. 1.4 D): strongly IF preferring, strongly HC preferring and those that are borderline ($|\Delta G_{oct-IF}| \leq 0.25$ kcal mol^{-1}). The octanol–IF scale provided insights into translocon-assisted folding [77–79] and was the stimulus for undertaking a detailed examination of the recognition of TM helices by the endoplasmic reticulum (ER) translocon (see below) [23].

1.2.3 Physical Determinants of Membrane Protein Stability: Helix–Helix Interactions in Bilayers

The hydrophobic effect is generally considered to be the major driving force for compacting soluble proteins [80]. However, it cannot be the force driving compaction (association) of TM α-helices. Because the hydrophobic effect arises solely from dehydration of non-polar surfaces [81], it is expended after helices are established across the membrane. Helix association is most likely driven primarily by van der Waals forces; more specifically, the London dispersion force (reviewed in [17, 18]). But why would van der Waals forces be stronger between helices than between helices and lipids?

Extensive work [82–86] on dimer formation of glycophorin A in detergents reveals the answer: knob-into-hole packing that allows more efficient packing between helices than between helices and lipids. Tight, knob-into-hole packing has been found to be a general characteristic of helical-bundle MPs as well [87,

Fig. 1.4 Summary of experiment-based hydrophobicity scales that are useful for understanding MP stability and translocon-assisted folding.
(A) The WW interfacial hydrophobicity scale determined from measurements of the partitioning of short peptides into phosphatidylcholine vesicles [62].
(B) The WW octanol hydrophobicity scale determined from the partitioning of short peptides into *n*-octanol [74] that predicts the stability of TM helices [72]. The free energy values along the abscissa are ordered in the same manner as in Fig. 1.6 A.
(C) The basis for deriving the octanol–IF scale ($\Delta G_{oct-IF} = \Delta G_{oct} - \Delta G_{IF}$) from the scales shown in (A and B). Numerical values for all of the scales can be obtained at http://blanco.biomol.uci.edu/hydrophobicity_scales.html.
(D) The ΔG_{oct-IF} scale divides the natural amino acid residues into three classes based upon their relative propensities for the HC and the membrane IF.
(E) A plot of the normalized turn propensity for helical hairpin formation [78] versus the octanol–IF hydrophobicity scale. There is a clear correlation between the turn propensity and ΔG_{oct-IF} hydrophobicity. Those residues that favor the conversion of a long (about 40 amino acids), single-spanning polyleucine TM helix into a helical hairpin (two TM helices separated by a tight turn) are generally the same ones that favor the membrane IF. See text for discussion.
(Adapted from a review by White [20]).

88]. For glycophorin A dimerization, knob-into-hole packing is facilitated by the GxxxG motif, in which the glycines permit close approach of the helices. The substitution of larger residues for glycine prevents the close approach and, hence, dimerization [82, 85, 86]. The so-called TOX–CAT method [89] has made it possible to sample the amino acid motifs preferred in helix–helix association in biological membranes by using randomized sequence libraries [90]. The GxxxG motif is among a significant number of motifs that permit close packing. A statistical survey of MP sequences disclosed that these motifs are very common in MPs [91].

Dimerization studies of glycophorin in detergent micelles [85] do not permit the absolute free energy of association to be determined, because of the large free energy changes associated with micelle stability. However, estimates [17] suggest 1–5 kcal mol^{-1} as the free energy cost of separating a helix from a helix bundle within the bilayer environment. The cost of breaking hydrogen bonds within the bilayer HC (above) implies that hydrogen bonding between α-helices could provide a strong stabilizing force for helix association. This is borne out by recent studies of synthetic TM peptides designed to hydrogen bond to one another [92, 93]. Interhelical hydrogen bonds, however, are not common in MPs (reviewed in [17]). Indeed, lacking the specificity of knob-into-hole packing, they could be hazardous because of their tendency to cause promiscuous aggregation [18], although they are probably important in the association of TM signaling proteins [94].

1.3
Membrane Proteins: Formative Interactions

1.3.1
Connecting Translocon-assisted Folding to Physical Hydrophobicity Scales: The Interfacial Connection

The literature on translocon-assisted MP folding has been reviewed extensively in the past several years [9–14]. Here it is sufficient to note that the signal recognition particle (SRP) targets nascent ribosome-bound membrane and secreted proteins to the translocon complex (Sec61 in eukaryotes, SecY in bacteria), whereupon membrane integration and folding occurs, provided that the nascent protein has at least one run of amino acids with sufficient hydrophobicity to form a TM helix/stop-transfer sequence (Fig. 1.1 B). Otherwise, the protein is secreted across the membrane. An important topic, reviewed elsewhere [9, 95, 96], is the physical basis for topology determination of the initial TM segment.

There have been two points of view about translocon-assisted membrane integration, discussed extensively by Johnson [14]. The "sequential" point-of-view visualizes the translocon as having a large-diameter tunnel (around 50 Å) into which the nascent protein chain is secreted during folding, in preparation for insertion into the lipid bilayer via a passageway through the wall of the translocon. A crucial feature of this scheme is that the ribosome must make a tight seal with the translocon in order to prevent ion leakage. There is a growing body of evidence, however,

that the alternate "concerted" scheme, in which the translocon complex and the lipid work together, is more likely (reviewed in [9]). Two low-resolution (around 15 Å) images of ribosome–translocon assemblies indicate significant gaps between the ribosome and translocon [97, 98], which eliminates the possibility of a tight seal. It appears that sealing must be provided in some way by the nascent peptide within the translocon itself. The structure of an archaeal SecY translocon, composed of 10 TM segments, strongly supports this view (Fig. 1.1 C and D). The nascent TM segment apparently emerges laterally through a gate formed principally by helices TM2B and TM7. A short "plug" helix (TM2A) serves to seal the translocon in the absence of a nascent chain. Site-specific photo-cross-linking studies [99] show that the nascent chain can cross-link with lipids well before the termination of translation, implying that the growing chain interacts with both the translocon and neighboring lipids during folding. Heinrich et al. [100] concluded that the integration of TM domains occurs through a lipid-partitioning process as a result of the TM segment being in contact with the lipid as soon as it arrives in the translocon channel. However, integration into the membrane can occur only if a polypeptide segment has the right properties, such as sufficient hydrophobicity.

What is the minimum hydrophobicity required for a 20-amino-acid stop-transfer segment to be integrated into the lipid bilayer? Chen and Kendall [101] examined this question for *Escherichia coli* by attaching artificial stop-transfer sequences to alkaline phosphatase, which is a water-soluble protein that is normally secreted across the membrane. Potential stop-transfer sequences (21 amino acids) composed of Leu and Ala in various ratios were introduced into an internal position of the enzyme by cassette mutagenesis. The threshold value of hydrophobicity for integration was found to be 16 Ala and five Leu. This is exactly the threshold predicted by the WW octanol-based hydrophobicity scale, as shown by Jayasinghe et al. [72]. This establishes a close relationship between the WW octanol scale and translocon-assisted TM helix insertion.

There is also indirect evidence for a relationship between interfacial hydrophobicity and translocon-mediated folding. Nilsson and von Heijne [102] made the interesting observation that a Leu39Val hydrophobic sequence introduced into leader peptidase was incorporated into the membranes of dog pancreas microsomes as a single TM helix. The fact that this helix is twice the length of the typical TM helix strongly supports the idea of early contact of the growing chain with membrane lipids. The more striking observation, however, was that the introduction of a single proline into the center of the Leu39Val segment caused it to be inserted as a helical hairpin. That is, the proline induced the formation of two TM segments separated by a tight turn. Expanding on this observation, Monné et al. [77, 78] established a turn-propensity scale by introducing one or two of each of the natural amino acids into the center of a 40-residue polyleucine sequence. The residues with a favorable turn potential were found to be, in decreasing order, Pro, Asn, Arg, Asp, His, Gln, Lys, Glu and Gly. Except for Pro, which commonly occurs within TM helices of ordinary length [103], these are the residues in the WW ΔG_{oct-IF} scale (Fig. 1.4 D) that have a strong IF preference. Another misfit is Ala, which has a low turn potential but a significant

interfacial preference. The relationship between turn potential and the octanol–IF scale is shown in Fig. 1.4 E. The correlation coefficient between the scales is 0.67, meaning that there is not a strict linear relationship. This is not surprising because turn potential is affected by the length of the long polyleucine segment and the number of residues of a given type introduced into the segment's center [78]. For example, unlike the Leu39Val, a single proline placed in the center of a Leu29Val sequence does not induce hairpin formation.

A closer connection between turn potential and the WW ΔG_{oct-IF} scale was disclosed by studies of turn induction by runs of Ala residues placed in the center of polyleucine segments [79]. A run of around four alanines was found to induce helical hairpins efficiently in hydrophobic segments as short as 34 residues. Furthermore, glycosylation mapping revealed a slight preference of alanine for the membrane IF, consistent with the WW ΔG_{oct-IF} scale.

These various studies support the idea that the translocon and lipid bilayer work in concert to integrate hydrophobic segments into membranes, which strengthens the lipid-partitioning model of Rapoport et al. [100]. In addition, the studies establish a direct link between physical hydrophobicity scales and translocon-assisted folding. An early study [104] of the relationship between biophysical hydrophobicity and translocon-mediated integration found that popular hydrophobicity scales of the time could not accurately predict the hydrophobic threshold for stop-transfer activity. The reason is now understood [72]. Prior to the WW experiment-based whole-residue scales, no hydrophobicity scale took into account the cost of dehydrating the helix backbone. As result, side-chain-only scales dramatically over-predict TM helices in MPs of known structure. If one thinks of the threshold for insertion as the mid-point of a Boltzmann probability curve (see below), side-chain-only scales will cause the apparent threshold to have a positive ΔG, rather than the expected value of zero. Indeed, Sääf et al. [104] found the mean per-residue hydrophobicity threshold to be approximately +1.5 kcal mol^{-1}, which is about the cost of dehydrating the peptide bond. Had the partitioning cost of the peptide bond been appreciated at the time and taken into account, the threshold then would have been very close to $\Delta G = 0$. With the availability of experiment-based physical scales that account reasonably well for both interfacial and HC partitioning, it became possible to design more finely tuned TM helices for probing translocon-assisted folding [23], described below.

1.3.2
Connecting Translocon-assisted Folding to Physical Hydrophobicity Scales: Transmembrane Insertion of Helices

Important new insights into TM helix insertion have been obtained by Hessa et al. [23] using an *in vitro* expression system [104] that permits quantitative assessment of the membrane insertion efficiency of model TM segments. Specifically, they examined the integration into membranes of dog pancreas rough microsomes of designed polypeptide segments. These segments were engineered into the luminal P2 domain of the integral MP leader peptidase (Lep) (Fig. 1.5 A–C).

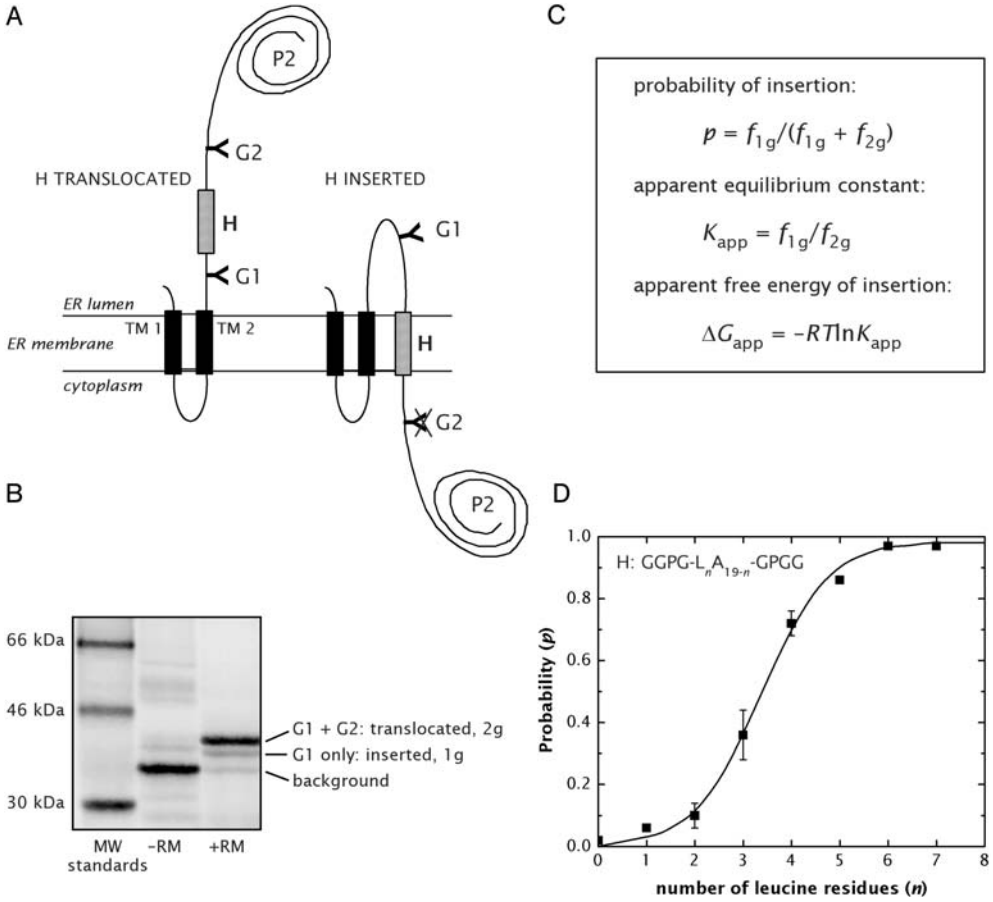

Fig. 1.5 Integration of designed TM segments (H-segments) into the ER using dog pancreas microsomal membranes. This system was used to explore systematically the hydrophobicity requirements for TM helix integration via the Sec61 translocon [23]. (A) Wild-type leader peptidase (Lep) from *E. coli* has two N-terminal TM segments (TM1 and TM2) and a large luminal domain (P2). H-segments were inserted between residues 226 and 253 in the P2 domain. Glycosylation acceptor sites (G1 and G2) were placed in positions flanking the H-segment. For H-segments that integrate into the membrane, only the G1 site is glycosylated (right), whereas both the G1 and G2 sites are glycosylated for H-segments that do not integrate into the membrane (left). (Based upon Hessa et al. [23]). (B) An example of sodium dodecylsulfate gels used in the determination of the extent of glycosylation of Lep/H-segment constructs. Plasmids encoding the Lep/H-segment constructs were transcribed and translated *in vitro* in the absence (–RM) and presence (+RM) of dog pancreas rough microsomes. Data from Hessa et al. [23]. (C) Equations used by Hessa et al. [23] for the analysis of gels of the type shown in (B). (D) Mean probability of insertion, p, for H-segments with n=0–7 Leu residues in H-segments of the form GGPG-(L$_n$A$_{19-n}$)-GPGG. The curve is the best-fit Boltzmann distribution, which suggests equilibrium between the inserted and translocated H-segments. (Data re-plotted from Hessa et al. [23]).

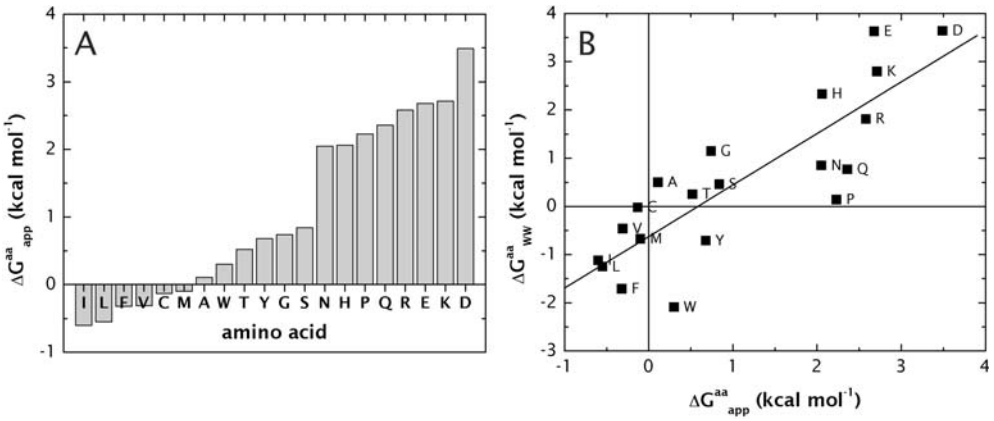

Fig. 1.6 Biological and biophysical hydrophobicity scales.
(A) ΔG^{aa}_{app} scale derived by Hessa et al. [23] from H-segments (Fig. 1.5) with the indicated amino acid placed in the middle of the 19-residue hydrophobic stretch.
(B) Correlation between ΔG^{aa}_{app} and the WW water/octanol free energy scale (ΔG^{aa}_{WW}) (Fig. 1.4 B). (Data re-plotted from Hessa et al. [23]).

The first step in the analysis was to test the hypothesis that the WW octanol scale had correctly identified the minimum hydrophobicity required for TM helix stability. Initial measurements were thus made by testing H-segments of the design GGPG-(L_nA_{19-n})-GPGG with $n=0$–7. As shown in Fig. 1.5 D, the probability of insertion, $p(n)$, conforms accurately to a Boltzmann distribution, which shows that translocon-mediated insertion has the appearance of an equilibrium process.

A "biological" hydrophobicity scale (ΔG^{aa}_{app}) could be derived from studies on H-segments in which each of the 20 naturally occurring amino acids were placed in the middle position of the segment. As seen in Fig. 1.6 A, Ile, Leu, Phe and Val promote membrane insertion ($\Delta G^{aa}_{app}<0$), Cys, Met and Ala have $\Delta G^{aa}_{app}\sim 0$, and all polar and charged residues have $\Delta G^{aa}_{app}>0$. The correlation between the ΔG^{aa}_{app} scale and the WW octanol scale is shown in Fig. 1.6 B. Considering the complexity of the biological system, the two scales correlate surprisingly well. The overall high correspondence between the two scales indicates that the recognition of TM segments by the translocon involves direct interaction between the segment and the surrounding lipid [100].

The ΔG^{aa}_{app} biological scale is strictly valid only for residues placed in the middle of the H-segment. To explore the role of residue position, Hessa et al. also performed symmetric "scans" in which a pair of residues of a given kind were moved symmetrically from the center of the H-segment towards its N- and C-termini. The results are summarized in Fig. 1.7 A – while the contributions from apolar residues do not vary much with position within the H-segment, Trp and Tyr strongly reduce membrane insertion when placed centrally, but be-

come much less unfavorable as they are moved apart. This positional dependency is even stronger for charged residues such as Lys and Asp. The positional effects are consistent with the relative preferences of Trp, Tyr and charged residues for the bilayer IF (Fig. 1.4), suggesting the importance of interactions of elongating peptides with the lipid bilayer.

The position dependence observed by Hessa et al. [23] had another important characteristic. Namely, the probability of helix insertion was sensitive to amphiphilicity of the elongating peptide as an *α*-helix (Fig. 1.7 B). Helices with a low hydrophobic moment [105] had a higher insertion probability than those with a high hydrophobic moment, as though the polar surface had a more favorable interaction energy with the translocon than the non-polar surface.

Overall, the results of Hessa et al. [23] suggest that direct protein–lipid interactions are essential for the recognition of TM helices by the translocon, and support models based on a partitioning of the TM helices between the Sec61 translocon and the surrounding lipid. The details of the partitioning process remain to be determined, but presumably the open state of the translocon is a highly dynamic one that permits rapid sampling of the translocon–bilayer IF by the translocating polypeptide. The results also provide a starting point for quantitative modeling of the membrane insertion of TM segments. However, Hessa et al. caution that the base ΔG^{aa}_{app} scale alone (Fig. 1.6 A) is not appropriate for calculating membrane insertion efficiency of natural polypeptide segments because of the strong positional dependence of ΔG^{aa}_{app}.

The importance of including the position dependence was especially apparent in a related study by Hessa et al. [106] of the TM insertion of the voltage sensor of the KvAP voltage-gated potassium channel [6]. The critical element in the sensor domains in virtually all voltage-gated ion channels is the S4 helix, which contains at least four regularly spaced Arg residues interspersed with hydrophobic residues. Voltage activation has been suggested to involve movement of S4 through the lipid bilayer in response to membrane depolarization [107]. This mechanism is controversial, because of the presumed cost of burying charges in the HC of the lipid bilayer [108]. To examine this issue, Hessa et al. [106] measured the insertion efficiency of an H-segment containing the arginine-rich region of the KvAP S4 helix (Fig. 1.7 C). The measured ΔG_{app} was found to be only 0.5 kcal mol^{-1} rather than the value of 3.9 kcal mol^{-1} computed from the biological hydrophobicity scale (Fig. 1.6 A). However, when measurements of the position dependence of ΔG^{Arg}_{app} were taken into account, the computed value of ΔG_{app} agreed closely with the measured value. The position dependence of ΔG^{aa}_{app} is clearly extremely important. However, it is surprising, because the HC of the bilayer has always been assumed to behave as a uniform alkyl liquid.

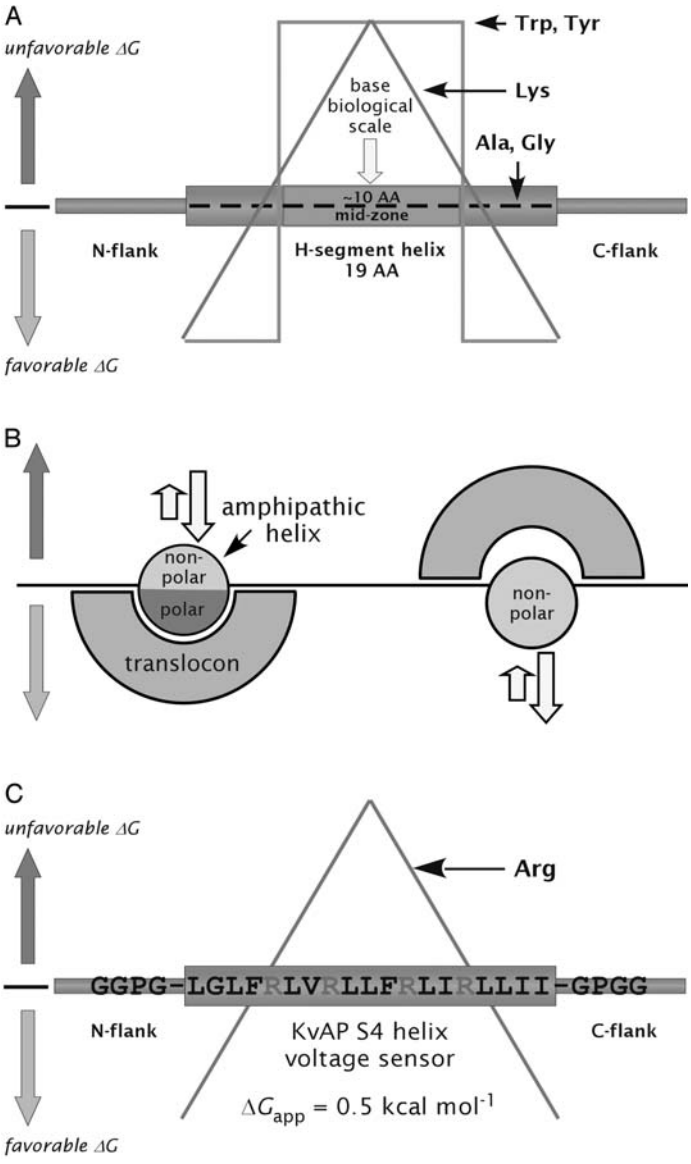
A
unfavorable ΔG
Trp, Tyr
base
biological
scale
Lys
Ala, Gly
~10 AA
mid-zone
N-flank
H-segment helix
19 AA
C-flank
favorable ΔG
B
amphipathic
helix
non-
polar
polar
translocon
non-
polar
C
unfavorable ΔG
Arg
GGPG-LGLFRLVRLLFRLIRLLII-GPGG
N-flank
KvAP S4 helix
voltage sensor
C-flank
ΔG_app = 0.5 kcal mol-1
favorable ΔG

Fig. 1.7

1.4 Perspectives

The lipid bilayer presents a complex environment for the folding and stability of MPs. Much progress has been made in describing and understanding this environment, and in teasing out the basic thermodynamic principles of its interactions with peptides. Yet, despite our progress with model systems, our understanding of the details of protein–lipid interactions *in vivo* remain woefully inadequate, as revealed by the studies of translocon-assisted insertion of TM helices [23, 106]. The dogma of the past 25 years or so has been that the HC of the lipid bilayer is simply a thin alkyl film that is strictly off-limits to charged amino acids because of the Born charging energy [109]. It has certainly dominated thinking about the energetics of ion channel voltage sensors [108].

The new information that has emerged from the studies of translocon-assisted protein folding tells us that the lipid bilayer has greater possibilities for lipid–protein interactions than previously thought. The dependence of the insertion energetics of polar residues on position within TM helices reveals this most clearly. The ease with which the S4 helix of the KvAP potassium channel voltage sensor can be inserted across the ER membrane seems astounding at first. However, in the context of diphtheria toxin, the result is not so surprising. The T-domain of diphtheria toxin is capable, on its own, of translocating large portions of itself (including highly charged helices) and the water-soluble catalytic domain across endosomal membranes spontaneously in response to lowered pH [110]. Just how this can be accomplished is a mystery that may, at its core, be related to the high structural integrity of the lipid bilayer, an integrity that

Fig. 1.7 Summary of the basic code used by the ER translocon to identify TM segments based upon the findings of Hessa et al. [23, 106]. As noted in Fig. 1.6, the biological ΔG^{aa}_{app} scale is based upon values obtained from amino acids placed in the center of the H-segment. The results of Hessa et al. reveal very strong dependences upon amino acid position, contrary to the implicit assumption of hydropathy plot analyses that the position of an amino acid within a bilayer-spanning helix does not matter.
(A) The ΔG^{aa}_{app} values for some amino acids such as Gly and Ala are little affected by position within the TM segment. The ΔG^{aa}_{app} values for the aromatic residues Trp and Tyr, on the other hand, depend strongly on position. They are very unfavorable in the central 10-amino-acid zone, but become quite favorable toward the ends, consistent with the strong interfacial preference of aromatic amino acids. Interestingly, Phe does not show this effect. Its behavior is about the same as that of Leu. ΔG^{aa}_{app} values for charged residues, which can be placed in the middle of a TM segment in the presence of a sufficiently large number of Leu residues, show an even stronger dependence than Trp and Tyr. The positional penalty declines almost linearly as the residue is moved toward either end of the helix.
(B) TM helices with low hydrophobic moments (low amphiphilicity) are released into the bilayer interior from the translocon more readily than helices with high amphiphilicity.
(C) Surprisingly, the KvAP potassium channel voltage sensor (S4 helix) can be inserted across the ER membrane with good efficiency, despite the presence of four arginines. The strong positional dependence of ΔG^{Arg}_{app} makes this possible [106].

prevails despite great thermal motion. Understanding and describing the lipid bilayer and its interactions with proteins from this perspective is one of the important challenges ahead.

Acknowledgments

This work was supported by grants from the National Institute of General Medical Sciences (GM46823 and GM68002) to S.H.W., and the Swedish Cancer Foundation, the Swedish Research Council, and the Marianne and Marcus Wallenberg Foundation to G.v.H.

References

1 J.K. Lanyi, B. Schobert, *J. Mol. Biol.* **2003**, *328*, 439–450.
2 S.H. White, Hydropathy plots and the prediction of membrane protein topology. In *Membrane Protein Structure: Experimental Approaches*, White, S.H. (ed.). New York: Oxford University Press, **1994**, pp. 97–124.
3 J.U. Bowie, *Protein Sci.* **1999**, *8*, 2711–2719.
4 R. Dutzler, E.B. Campbell, M. Cadene, B.T. Chait, R. MacKinnon, *Nature* **2002**, *415*, 287–294.
5 R.M. Stroud, L.J.W. Miercke, J. O'Connell, S. Khademi, J.K. Lee, J. Remis, W. Harries, Y. Robles, D. Akhavan, *Curr. Opin. Struct. Biol.* **2003**, *13*, 424–431.
6 Y.X. Jiang, A. Lee, J.Y. Chen, V. Ruta, M. Cadene, B.T. Chait, R. MacKinnon, *Nature* **2003**, *423*, 33–41.
7 B. Van den Berg, W.M. Clemons, Jr, I. Collinson, Y. Modis, E. Hartmann, S.C. Harrison, T.A. Rapoport, *Nature* **2004**, 427, 36–44.
8 W.M. Clemons, Jr, J.-F. Ménétret, C.W. Akey, T.A. Rapoport, *Curr. Opin. Struc. Biol.* **2004**, *14*, 390–396.
9 S.H. White, G. von Heijne, *Curr. Opin. Struct. Biol.* **2004**, *14*, 397–404.
10 A.J.M. Driessen, E.H. Manting, C. van der Does, *Nat. Struct. Biol.* **2001**, *8*, 492–498.
11 R.E. Dalbey, G. von Heijne (eds), *Protein Targeting Transport and Translocation.* New York: Academic Press, **2002**.
12 S. Pfeffer, *Cell* **2003**, *112*, 507–517.
13 E. Bibi, *Trends Biochem. Sci.* **1998**, *23*, 51–55.
14 A.E. Johnson, M.A. van Waes, *Annu. Rev. Cell Dev. Biol.* **1999**, *15*, 799–842.
15 G. von Heijne, *Adv. Protein Chem.* **2003**, *63*, 1–18.
16 M.A. Lemmon, D.M. Engelman, *Q. Rev. Biophys.* **1994**, *27*, 157–218.
17 S.H. White, W.C. Wimley, *Annu. Rev. Biophys. Biomol. Struct.* **1999**, *28*, 319–365.
18 J.-L. Popot, D.M. Engelman, *Annu. Rev. Biochem.* **2000**, *69*, 881–922.
19 S.H. White, A.S. Ladokhin, S. Jayasinghe, K. Hristova, *J. Biol. Chem.* **2001**, *276*, 32395–32398.
20 S.H. White, *FEBS Lett.* **2003**, *555*, 116–121.
21 L.K. Tamm, H. Hong, Folding of membrane proteins. In *Protein Folding Handbook I*, Buchner, J., Kiefhaber, T. (eds). Weinheim: Wiley-VCH, **2004**, pp. 994–1027.
22 L.K. Tamm, A. Arora, J.H. Kleinschmidt, *J. Biol. Chem.* **2001**, *276*, 32399–32402.
23 T. Hessa, H. Kim, K. Bihlmaler, C. Lundin, J. Boekel, H. Andersson, I. Nilsson, S.H. White, G. von Heijne, *Nature* **2005**, *433*, 377–381.
24 J.H. Hurley, S. Misra, *Annu. Rev. Biophys. Biomol. Struct.* **2000**, *29*, 49–79.
25 Y. Liu, D.W. Bolen, *Biochemistry* **1995**, *34*, 12884–12891.
26 S. Tristram-Nagle, H.I. Petrache, J.F. Nagle, *Biophys. J.* **1998**, *75*, 917–925.
27 H.I. Petrache, S. Tristram-Nagle, J.F. Nagle, *Chem. Phys. Lipids* **1998**, *95*, 83–94.
28 J.F. Nagle, S. Tristram-Nagle, *Curr. Opin. Struct. Biol.* **2000**, *10*, 474–480.

29 J. F. Nagle, S. Tristram-Nagle, *Biochim. Biophys. Acta* **2001**, *1469*, 159–195.

30 S. H. White, M. C. Wiener, Determination of the structure of fluid lipid bilayer membranes. In *Permeability and Stability of Lipid Bilayers*, Disalvo, E. A., Simon, S. A. (eds). Boca Raton: CRC Press, **1995**, pp. 1–19.

31 S. H. White, M. C. Wiener, The liquid-crystallographic structure of fluid lipid bilayer membranes. In *Membrane Structure and Dynamics*, Merz, K. M., Roux, B. (eds). Boston: Birkhäuser, **1996**, pp. 127–144.

32 M. C. Wiener, S. H. White, *Biophys. J.* **1992**, *61*, 434–447.

33 S. H. White, W. C. Wimley, *Biochim. Biophys. Acta* **1998**, *1376*, 339–352.

34 A. S. Ladokhin, R. Legmann, R. J. Collier, S. H. White, *Biochemistry* **2004**, *43*, 7451–7458.

35 M. P. Rosconi, G. Zhao, E. London, *Biochemistry* **2004**, *43*, 9127–9139.

36 M. H. Gelb, W. H. Cho, D. C. Wilton, *Curr. Opin. Struct. Biol.* **1999**, *9*, 428–432.

37 J. G. Bollinger, K. Diraviyam, F. Ghomashchi, D. Murray, M. H. Gelb, *Biochemistry* **2004**, *43*, 13293–13304.

38 A. A. Frazier, M. A. Wisner, N. J. Malmberg, K. G. Victor, G. E. Fanucci, E. A. Nalefski, J. J. Falke, D. S. Cafiso, *Biochemistry* **2002**, *41*, 6282–6292.

39 K. Hristova, C. E. Dempsey, S. H. White, *Biophys. J.* **2001**, *80*, 801–811.

40 K. Hristova, W. C. Wimley, V. K. Mishra, G. M. Anantharamaiah, J. P. Segrest, S. H. White, *J. Mol. Biol.* **1999**, *290*, 99–117.

41 K. He, S. J. Ludtke, D. L. Worcester, H. W. Huang, *Biophys. J.* **1996**, *70*, 2659–2666.

42 L. Yang, T. M. Weiss, R. I. Lehrer, H. W. Huang, *Biophys. J.* **2000**, *79*, 2002–2009.

43 W. T. Heller, A. J. Waring, R. I. Lehrer, T. A. Harroun, T. M. Weiss, L. Yang, H. W. Huang, *Biochemistry* **2000**, *39*, 139–145.

44 J. P. Bradshaw, M. J. M. Darkes, T. A. Harroun, J. Katsaras, R. M. Epand, *Biochemistry* **2000**, *39*, 6581–6585.

45 T. M. Weiss, P. C. A. van der Wel, J. A. Killian, R. E. Koeppe, II, H. W. Huang, *Biophys. J.* **2003**, *84*, 379–385.

46 J. P. Bradshaw, S. M. A. Davies, T. Hauss, *Biophys. J.* **1998**, *75*, 889–895.

47 F.-Y. Chen, M.-T. Lee, H. W. Huang, *Biophys. J.* **2003**, *84*, 3751–3758.

48 R. W. Pastor, *Curr. Opin. Struct. Biol.* **1994**, *4*, 486–492.

49 D. P. Tieleman, S. J. Marrink, H. J. C. Berendsen, *Biochim. Biophys. Acta* **1997**, *1331*, 235–270.

50 L. R. Forrest, M. S. P. Sansom, *Curr. Opin. Struct. Biol.* **2000**, *10*, 174–181.

51 S. E. Feller, *Curr. Opin. Colloid Interface Sci.* **2000**, *5*, 217–223.

52 S. S. Deol, P. J. Bond, C. Domene, M. S. P. Sansom, *Biophys. J.* **2004**, *87*, 3737–3749.

53 S. E. Feller, K. Gawrisch, T. B. Woolf, *J. Am. Chem. Soc.* **2003**, *125*, 4434–4435.

54 D. P. Tieleman, B. Hess, M. S. P. Sansom, *Biophys. J.* **2002**, *83*, 2393–2407.

55 F. Q. Zhu, E. Tajkhorshid, K. Schulten, *Biophys. J.* **2004**, *86*, 50–57.

56 S. Bernèche, B. Roux, *Nature* **2001**, *414*, 73–77.

57 D. J. Tobias, Membrane simulations. In *Computational Biochemistry and Biophysics*, Becker, O. M., MacKerell, A. D., Jr, Roux, B., Watanabe, M. (eds). New York: Marcel Dekker, **2001**, pp. 465–496.

58 R. W. Benz, F. Castro-Román, D. J. Tobias, S. H. White, *Biophys. J.* **2005**, in press.

59 R. E. Jacobs, S. H. White, *Biochemistry* **1989**, *28*, 3421–3437.

60 J.-L. Popot, D. M. Engelman, *Biochemistry* **1990**, *29*, 4031–4037.

61 A. R. Curran, D. M. Engelman, *Curr. Opin. Struct. Biol.* **2003**, *13*, 412–417.

62 W. C. Wimley, S. H. White, *Nat. Struct. Biol.* **1996**, *3*, 842–848.

63 A. S. Ladokhin, S. H. White, *J. Mol. Biol.* **2001**, *309*, 543–552.

64 W. C. Wimley, K. Hristova, A. S. Ladokhin, L. Silvestro, P. H. Axelsen, S. H. White, *J. Mol. Biol.* **1998**, *277*, 1091–1110.

65 A. S. Ladokhin, S. H. White, *J. Mol. Biol.* **1999**, *285*, 1363–1369.

66 T. Wieprecht, M. Beyermann, J. Seelig, *Biochemistry* **1999**, *38*, 10377–10387.

67 Y. Li, X. Han, L. K. Tamm, *Biochemistry* **2003**, *42*, 7245–7251.

68 W. C. Wimley, S. H. White, *Biochemistry* **2000**, *39*, 4432–4442.

69 M. A. Roseman, *J. Mol. Biol.* **1988**, *201*, 621–625.

70 N. Ben-Tal, D. Sitkoff, I. A. Topol, A.-S. Yang, S. K. Burt, B. Honig, *J. Phys. Chem. B* **1997**, *101*, 450–457.

71 N. Ben-Tal, A. Ben-Shaul, A. Nicholls, B. Honig, *Biophys. J.* **1996**, *70*, 1803–1812.

72 S. Jayasinghe, K. Hristova, S. H. White, *J. Mol. Biol.* **2001**, *312*, 927–934.

73 J. P. Segrest, R. L. Jackson, V. T. Marchesi, R. B. Guyer, W. Terry, *Biochem. Biophys. Res. Commun.* **1972**, *49*, 964–969.

74 W. C. Wimley, T. P. Creamer, S. H. White, *Biochemistry* **1996**, *35*, 5109–5124.

75 S. Jayasinghe, K. Hristova, S. H. White, *Protein Sci.* **2001**, *10*, 455–458.

76 W. C. Wimley, K. Gawrisch, T. P. Creamer, S. H. White, *Proc. Natl Acad. Sci. USA* **1996**, *93*, 2985–2990.

77 M. Monné, M. Hermansson, G. von Heijne, *J. Mol. Biol.* **1999**, *288*, 141–145.

78 M. Monné, I. M. Nilsson, A. Elofsson, G. von Heijne, *J. Mol. Biol.* **1999**, *293*, 807–814.

79 I. M. Nilsson, A. E. Johnson, G. von Heijne, *J. Biol. Chem.* **2003**, *278*, 29389–29393.

80 K. A. Dill, *Biochemistry* **1990**, *29*, 7133–7155.

81 C. Tanford, *The Hydrophobic Effect: Formation of Micelles and Biological Membranes*. New York: Wiley, **1973**.

82 M. A. Lemmon, J. M. Flanagan, J. F. Hunt, B. D. Adair, B. J. Bormann, C. E. Dempsey, D. M. Engelman, *J. Biol. Chem.* **1992**, *267*, 7683–7689.

83 M. A. Lemmon, H. R. Treutlein, P. D. Adams, A. T. Brünger, D. M. Engelman, *Nat. Struct. Biol.* **1994**, *1*, 157–163.

84 K. R. MacKenzie, J. H. Prestegard, D. M. Engelman, *Science* **1997**, *276*, 131–133.

85 K. G. Fleming, A. L. Ackerman, D. M. Engelman, *J. Mol. Biol.* **1997**, *272*, 266–275.

86 K. R. MacKenzie, D. M. Engelman, *Proc. Natl Acad. Sci. USA* **1998**, *95*, 3583–3590.

87 J. U. Bowie, *J. Mol. Biol.* **1997**, *272*, 780–789.

88 D. Langosch, J. Heringa, *Proteins* **1998**, *31*, 150–159.

89 W. P. Russ, D. M. Engelman, *Proc. Natl Acad. Sci. USA* **1999**, *96*, 863–868.

90 W. P. Russ, D. M. Engelman, *J. Mol. Biol.* **2000**, *296*, 911–919.

91 A. Senes, M. Gerstein, D. M. Engelman, *J. Mol. Biol.* **2000**, *296*, 921–936.

92 F. X. Zhou, M. J. Cocco, W. P. Russ, A. T. Brunger, D. M. Engelman, *Nat. Struct. Biol.* **2000**, *7*, 154–160.

93 C. Choma, H. Gratkowski, J. D. Lear, W. F. DeGrado, *Nat. Struct. Biol.* **2000**, *7*, 161–166.

94 S. O. Smith, C. S. Smith, B. J. Bormann, *Nat. Struct. Biol.* **1996**, *3*, 252–258.

95 A. Kuhn, M. Spiess, Membrane protein insertion into bacterial membranes and the endoplasmic reticulum. In *Protein Targeting Transport and Translocation*, Dalbey, R. E., von Heijne, G. (eds). New York: Academic Press, **2002**, pp. 107–130.

96 V. Goder, M. Spiess, *FEBS Lett.* **2001**, *504*, 87–93.

97 R. Beckmann, C. M. T. Spahn, N. Eswar, J. Helmers, P. A. Penczek, A. Sali, J. Frank, G. Blobel, *Cell* **2001**, *107*, 361–372.

98 D. G. Morgan, J.-F. Ménétret, A. Neuhof, T. A. Rapoport, C. W. Akey, *J. Mol. Biol.* **2002**, *324*, 871–886.

99 W. Mothes, S. U. Heinrich, R. Graf, I. M. Nilsson, G. von Heijne, J. Brunner, T. A. Rapoport, *Cell* **1997**, *89*, 523–533.

100 S. U. Heinrich, W. Mothes, J. Brunner, T. A. Rapoport, *Cell* **2000**, *102*, 233–244.

101 H. Chen, D. A. Kendall, *J. Biol. Chem.* **1995**, *270*, 14115–14122.

102 I. M. Nilsson, G. von Heijne, *J. Mol. Biol.* **1998**, *284*, 1185–1189.

103 K. A. Williams, C. M. Deber, *Biochemistry* **1991**, *30*, 8919–8923.

104 A. Sääf, E. Wallin, G. von Heijne, *Eur. J. Biochem.* **1998**, *251*, 821–829.

105 D. Eisenberg, R. M. Weiss, T. C. Terwilliger, *Proc. Natl Acad. Sci. USA* **1984**, *81*, 140–144.

106 T. Hessa, S. H. White, G. von Heijne, *Science* **2005**, *307*, 1427.

107 Y.X. Jiang, V. Ruta, J.Y. Chen, A. Lee, R. MacKinnon, *Nature* **2003**, 42–48.

108 M. Grabe, H. Lecar, Y.N. Jan, L.Y. Jan, *Proc. Natl Acad. Sci. USA* **2004**, *101*, 17640–17645.

109 A. Parsegian, *Nature* **1969**, *221*, 844–846.

110 K.J. Oh, L. Senzel, R.J. Collier, A. Finkelstein, *Proc. Natl Acad. Sci. USA* **1999**, *96*, 8467–8470.

111 R. Dutzler, E.B. Campbell, R. MacKinnon, *Science* **2003**, *300*, 108–112.

112 C.D. Snow, H. Nguyen, V.S. Pande, M. Gruebele, *Nature* **2002**, *420*, 102–106.

113 V. Goder, T. Junne, M. Spiess, *Mol. Biol. Cell* **2004**, *15*, 1470–1478.

114 D.J. Schnell, D.N. Hebert, *Cell* **2003**, *112*, 491–505.

115 W. Humphrey, W. Dalke, K. Schulten, *J. Mol. Graphics* **1996**, *14*, 33–38.

116 M.C. Wiener, S.H. White, *Biophys. J.* **1991**, *59*, 162–173.

117 S.H. White, K. Hristova, Peptides in lipid bilayers: determination of location by absolute-scale X-ray refinement. In *Lipid Bilayers. Structure and Interactions*, Katsaras, J., Gutberlet, T. (eds). Berlin: Springer, **2000**, pp. 189–206.

118 S.H. White, W.C. Wimley, *Curr. Opin. Struct. Biol.* **1994**, *4*, 79–86.

119 I.T. Arkin, K.R. MacKenzie, L. Fisher, S. Aimoto, D.M. Engelman, S.O. Smith, *Nat. Struct. Biol.* **1996**, *3*, 240–243.

120 T. Wieprecht, O. Apostolov, M. Beyermann, J. Seelig, *J. Mol. Biol.* **1999**, *294*, 785–794.

2
Folding and Stability of Monomeric β-Barrel Membrane Proteins

Jörg H. Kleinschmidt

2.1
Introduction

Integral membrane proteins fall into two different classes that can be distinguished by their transmembrane secondary structure: α-helical and β-barrel proteins. Within the hydrophobic core of the membrane, all hydrogen-bonding donors and acceptors of the polypeptide backbone form hydrogen bonds. The nonpolar side-chains face the hydrophobic acyl chains of the membrane lipids. While the more abundant α-helical transmembrane proteins are found in the cytoplasmic (or inner) membranes, the integral membrane proteins with β-barrel structures are known from outer membranes of bacteria, mitochondria and chloroplasts. The β-barrel is characterized by the number of antiparallel β-strands and by the shear number, which is a measure for the inclination angle of the β-strands against the barrel axis. The outer membrane proteins (OMPs) of bacteria form transmembrane β-barrels with even numbers of β-strands ranging from 8 to 22 with shear numbers from 8 to 24 [1]. The strands are tilted by 36–44 ° relative to the barrel axis [1, 2]. Examples are OmpA [3, 4], OmpX [5–7], NspA [8], and PagP [9, 10] (8 β-strands); OmpT [11] (10 β-strands); NalP [12] and OmPlA [13] (12 β-strands); FadL [14] (14 β-strands); Omp32 [15], matrix porin [16], OmpF [17] and PhoE [18] (16 β-strands); maltoporin (LamB) [19] and sucrose porin (ScrY) [20] (18 β-strands); and FepA [21], BtuB [22, 23] and FhuA [24, 25] (22 β-strands). Monomers (OmpA, FhuA and OmpG [26]), dimers (OmPlA) and trimers (OmpF and PhoE) are known. The β-barrel membrane proteins serve a wide range of different functions. They can be non-specific diffusion pores (OmpA, OmpC and OmpF), specific pores (LamB and ScrY), active transporters (FhuA, FepA and BtuB), enzymes such as proteases (OmpT), lipases (OmPlA), acyltransferases (PagP) or, like TolC, involved in solute efflux [27]. Some examples of β-barrel membrane proteins are shown in Fig. 2.1. Recently developed screening algorithms for the genomic identification of β-barrel

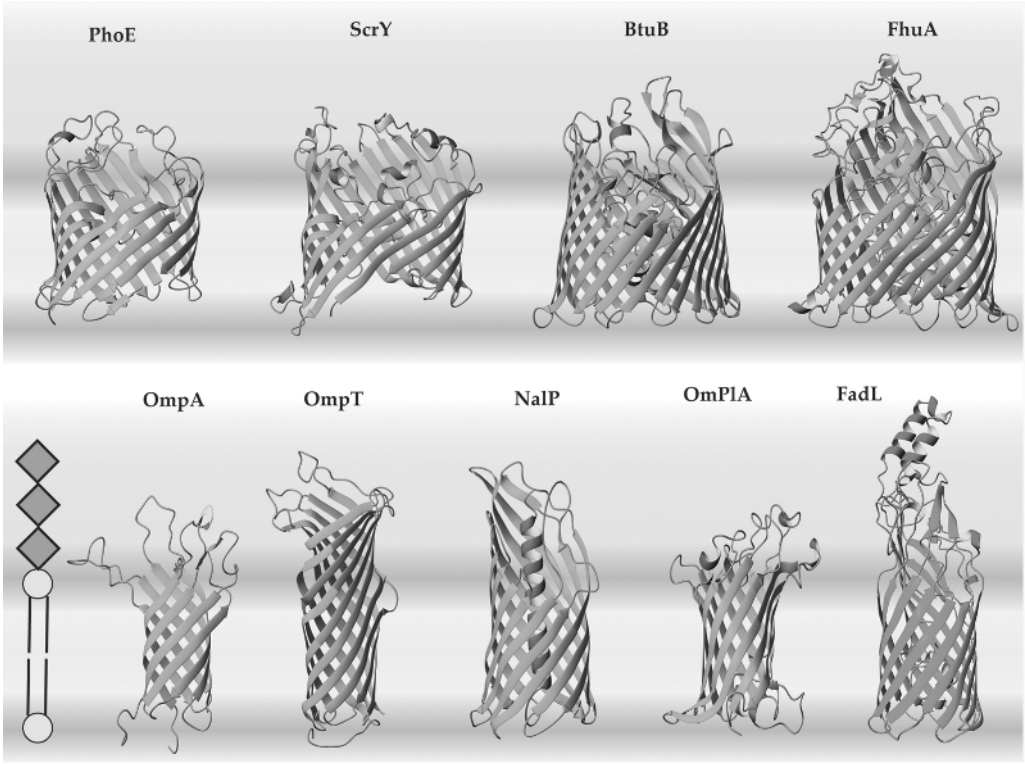

Fig. 2.1 Some representative crystal structures of β-barrel membrane proteins of the outer membranes of bacteria are shown. Transmembrane β-barrels have an even number of antiparallel transmembrane strands, which is eight for OmpA (shown here is the nuclear magnetic resonance structure from [3]; for the crystal structure, see [4, 94]), 10 for OmpT [11], 12 for NalP [12] and OmPlA [13], 14 for FadL [14], 16 for PhoE [18], 18 for ScrY [11], and 22 for BtuB [22] and FhuA [24]. OmpA is a small ion channel [73], OmpT is a protease, NalP is an autotransporter, FadL is a long-chain fatty acid transporter, PhoE is a diffusion pore, ScrY is a sucrose-specific porin and OmPlA is a phospholipase. BtuB and FhuA are active transporters for ferrichrome iron and vitamin B_{12} uptake, respectively. OMPs of mitochondria are predicted to form similar transmembrane β-barrels. Examples are the voltage-dependent anion channels, out of which more than a dozen have been sequenced [144]. Protein structures were generated with MolMol [145].

membrane proteins indicate that there are many still not characterized OMPs, e.g. in the genomes of *Escherichia coli* and *Pseudomonas aeruginosa* [28, 29]. Soluble bacterial toxins that can insert into membranes, such as α-hemolysine from *Staphylococcus aureus* [30] and perfringolysine O from *Clostridium perfringens* [31, 32], also form β-barrels, but these are oligomeric. This chapter focuses on the stability and folding of monomeric β-barrels from bacteria. For reviews on the membrane insertion and assembly of pore forming toxins, see, e.g. [33–35]. For

a review on the oligmeric β-barrels from mycobacteria, such as MspA from *Mycobacterium smegmatis* [36], see, e.g. [37].

2.2
Stability of β-Barrel Membrane Proteins

Since most membrane proteins have a high thermal stability and are difficult to unfold in solution [38], it is not easy to experimentally determine the free energy of membrane insertion and folding of integral membrane proteins, which is equivalent to the free energy of unfolding from the membrane. Exceptions have been the β-barrel membrane proteins, which are generally characterized by a relatively low average hydrophobicity and can therefore be completely solubilized in concentrated solutions of a chemical denaturant, e.g. urea. The thermodynamic stability of the ferric enterobactin receptor (FepA) was studied after solubilization of FepA in detergent micelles and a recent study on the stability of OmpA in lipid bilayers indicated that bilayer properties strongly influence the stability of integral membrane proteins.

2.2.1
Thermodynamic Stability of FepA in Detergent Micelles

The first report on the thermodynamic stability of integral β-barrel membrane proteins by equilibrium unfolding experiments came from Feix and coworkers, who determined the free energy of unfolding of FepA in Triton X-100 detergent micelles [39]. Unfolding was induced with increasing concentrations of urea or, alternatively, of guanidinium chloride as chemical denaturants. The linearity of the dependence of unfolding equilibria on the denaturant concentration has been demonstrated many times for soluble proteins [40–43] and was confirmed for FepA unfolding from Triton X-100 detergent micelles [39] and later for OmpA from phospholipid bilayers [44]. The free energy of unfolding in absence of denaturant, $\Delta G^{\circ}_{U}(H_2O)$, could therefore be extrapolated from the free energies of unfolding in presence of different concentrations of denaturant, ΔG°_{U} ([denaturant]), according to

$$\Delta G^{\circ}_{U}(H_2O) = \Delta G^{\circ}_{U}([\text{denaturant}]) + m \cdot [\text{denaturant}]$$

where the m value is independent of the denaturant concentration, but a specific parameter that depends on the protein, the denaturant, the solvents (aqueous solutions of soluble proteins, solutions of detergent micelle/membrane protein complexes or solutions of membrane proteins in lipid vesicles) and on other parameters, such as temperature and pH. The m value can be linked to the increase of the denaturant exposed surface upon protein unfolding and is also a measure for the cooperativity of unfolding [45, 46]. Using site-directed spin-labeling (SDSL) electron spin resonance (ESR) spectroscopy, Klug et al. [39] reported a free energy $\Delta G^{\circ}_{U}(H_2O) = 6.05 \pm 0.6$ kcal mol^{-1} at 22 °C and pH 7.2 for

unfolding of FepA from Triton X-100 detergent micelles with an equilibrium transition midpoint at 5.5 M urea and an *m*-value of 1.1 ± 0.1 kcal mol^{-1} M^{-1}. They obtained a similar value, $\Delta G^{\circ}_{U}(H_2O) = 6.4$ kcal mol^{-1}, when unfolding was performed using guanidinium chloride (GdnHCl), but with a transition midpoint at 2.0 ± 0.1 M GdnHCl and an *m*-value of 3.3 ± 0.1 kcal mol^{-1} M^{-1}. The free energy of unfolding of FepA from Triton X-100 corresponded well with the free energies of unfolding of many water-soluble globular proteins, such as myoglobin, lysozyme, ribonuclease or barnase, which all have $\Delta G^{\circ}_{U}(H_2O)$ values in the range of 5–10 kcal mol^{-1} [42, 43, 47, 48].

Using SDSL ESR spectroscopy, the local stabilities of FepA along the fourth transmembrane β-strand (residues 244–256) were determined at pH 7 and at room temperature after solubilizing FepA in 2% Triton X-100 [49]. The stability of the β-strand and the cooperativity of unfolding were maximal for amino acid residues near the center of the β-strand at residue 250. A single-site cysteine mutant that was spin-labeled at this position and ESR spectroscopy were used to determine a stability of $\Delta G^{\circ}_{U}(H_2O) = 9.4$ kcal mol^{-1} ($m = 5.8$ kcal mol^{-1} M^{-1}) at this location in FepA. When determined for additionally prepared single-site cysteine mutants, the stability of the β-strand decreased from residue 250 towards residue 244 [$\Delta G^{\circ}_{U}(H_2O) = 7.1$ kcal mol^{-1}, $m = 3.3$ kcal mol^{-1} M^{-1}] and towards residue 256 [$\Delta G^{\circ}_{U}(H_2O) = 2.4$ kcal mol^{-1}, $m = 1.3$ kcal mol^{-1} M^{-1}], respectively [49].

2.2.2 Thermodynamic Stability of OmpA in Phospholipids Bilayers

First experimental data on the thermodynamic stability of an integral membrane protein in lipid bilayers was presented recently by Hong and Tamm [44] for OmpA. Since OmpA folds quantitatively at pH 10 from a fully denatured state in 8 M urea upon dilution of the denaturant in the presence of preformed lipid bilayers of phosphatidylcholine [50, 51] or mixtures of phosphatidylcholine and phosphatidylglycerol [52], Hong and Tamm studied the equilibrium unfolding of OmpA from model membranes using intrinsic fluorescence spectroscopy. Unfolding/folding equilibria were studied at 37.5 °C, i.e. above the gel-to-liquid-crystalline phase transition temperature of the phospholipids and with small unilamellar vesicles (SUVs) prepared by ultrasonication. It was found that the free energy of unfolding of OmpA from lipid bilayers depends on the length of the fatty acyl chains and on the headgroup of the phospholipid. In a reference bilayer, composed of 92.5% palmitoyloleoylphosphatidylcholine ($C_{16:0}C_{18:1}$PC) and 7.5% palmitoyloleoylphosphatidylglycerol ($C_{16:0}C_{18:1}$PG) the free energy of unfolding was $\Delta G^{0}_{U}(H_2O) = 3.4$ kcal mol^{-1} (pH 10, 37.5 °C, $m = 1.1$ kcal mol^{-1} M^{-1}). The study nicely demonstrated the large dependence of the thermodynamic stability of OmpA on the composition of the lipid bilayer and on the chemical structure of the lipids, highlighting the important role of membrane phospholipids in the stabilization of integral membrane proteins. Based on the reference bilayer, the effects of the lipid chain length, degree of unsaturation of the acyl chains and lipid headgroup were investigated by varying the content of such a phospholipid at the

expense of $C_{16:0}C_{18:1}$PC and at constant 7.5% $C_{16:0}C_{18:1}$PG in this lipid bilayer. The stability $\Delta G^{\circ}_{U}(H_2O)$ of OmpA decreased with decreasing chain length of the phospholipids upon incorporation of increasing percentages of short-chain lipids (*di*$C_{10:0}$PC to *di*$C_{14:0}$PC). When phospholipids with longer acyl chains (e.g. $C_{18:0}C_{18:1}$PC) were incorporated, the stability of OmpA increased with increasing amounts of $C_{18:0}C_{18:1}$PC. An even stronger stability increase was observed, when the phosphatidylcholine lipid $C_{16:0}C_{18:1}$PC was replaced by the corresponding phosphatidylethanolamine ($C_{16:0}C_{18:1}$PE). For example, the free energies of OmpA unfolding from membranes composed of 7.5% $C_{16:0}C_{18:1}$PG and 62.5% $C_{16:0}C_{18:1}$PC host lipids and 30% of guest lipid were $\Delta G^{\circ}_{U}(H_2O) = 5.0$ kcal mol^{-1} with $C_{16:0}C_{18:1}$PE, $\Delta G^{\circ}_{U}(H_2O) = 3.9$ kcal mol^{-1} with $C_{18:0}C_{18:1}$PC, $\Delta G^{\circ}_{U}(H_2O) = 2.9$ kcal mol^{-1} with *di*$C_{12:0}$PC or *di*$C_{14:0}$PC and $\Delta G^{\circ}_{U}(H_2O) = 2.2$ kcal mol^{-1} with *di*$C_{10:0}$PC. For each lipid species, the dependence of $\Delta G^{\circ}_{U}(H_2O)$ on the concentration of this lipid appeared to be linear, when increased at the expense of $C_{16:0}C_{18:1}$PC in bilayers containing a constant amount of 7.5% of $C_{16:0}C_{18:1}$PG. Surprisingly, when lipids with two unsaturated acyl chains were incorporated into the reference bilayer, values for $\Delta G^{\circ}_{U}(H_2O)$ increased with decreasing length of the fatty acyl chains, reversing the effect seen for saturated and mono-unsaturated lipids. Two unsaturated acyl chains in a diacylphospholipid induce smaller elastic moduli and larger curvature stresses in lipid bilayers [53], which might explain these observations.

2.2.3
Thermal Stability of FhuA in Detergent Micelles

The thermal stability of ferric hydroxamate uptake protein A (FhuA) in *N*,*N*-dimethyl-*N*-lauryl amine *N*-oxide (LDAO) detergent micelles was recently studied by Bonhivers et al. [54]. FhuA showed two unfolding maxima in differential scanning calorimetry. In the absence of the ferrichrome iron ligand, wild-type (wt)-FhuA unfolding maxima were at $T_1 = 65\,^{\circ}$C and at $T_2 = 74.4\,^{\circ}$C with corresponding enthalpies of 140 and 160 kcal mol^{-1} [54], suggesting that there are two autonomous folding units in FhuA. In presence of ferrichrome iron, the first transition was shifted up to 71.4 °C, while T_2 remained constant. A mutant form, FhuAΔ21–128, in which a large part of the N-terminal cork domain was removed, showed only one transition at 62 °C and an enthalpy of 200 kcal mol^{-1}, independent of the presence of ferrichrome iron. This indicated that ferrichrome iron stabilized the cork domain and that the cork domain stabilized the 22-stranded β-barrel. However, reversibility of unfolding was not investigated and free energies of unfolding were not determined. Klug et al. had previously found that ferric enterobactin has limited stability at room temperature and, therefore, they could not compare the effect of this ligand on the thermodynamic stability of FepA. However, they also reported that the unfolding kinetics of FepA were slower in presence of ferric enterobactin [39], indicating a stabilizing effect of ferric enterobactin on FepA, which is consistent with the effect of ferrichrome iron on the denaturation temperature of FhuA [54].

2.3 Insertion and Folding of Transmembrane β-Barrel Proteins

2.3.1 Insertion and Folding of β-Barrel Membrane Proteins in Micelles

First *in vitro* refolding studies of integral membrane proteins were performed by Henning et al. in 1978 and demonstrated that the eight-stranded β-barrel OmpA develops native structure when incubated with lipopolysaccharide (LPS) and Triton X-100 after dilution of the denaturants sodium dodecylsulfate (SDS) or urea [55]. Similarly, Dornmair et al. [56] showed that after heat-induced unfolding in SDS micelles, OmpA refolds into micelles of the detergent octylglucoside even in the absence of LPS. These results on the β-barrel OmpA, and the successful refolding of bacteriorhodopsin that consists of a bundle of seven transmembrane α-helices and was first refolded by Khorana et al. in 1981 [57], suggest that the information for the formation of native structure in integral membrane proteins is contained in their amino acid sequence, as previously described by the Anfinsen paradigm for soluble proteins [58].

2.3.2 Oriented Insertion and Folding into Phospholipid Bilayers

Surrey and Jähnig [51] showed that OmpA spontaneously inserts and folds into phospholipid bilayers. Oriented insertion and folding of OmpA into lipid bilayers in absence of detergent was observed when unfolded OmpA in 8 M urea was reacted with SUVs of dimyristoylphosphatidylcholine (diC$_{14:0}$PC) under concurrent strong dilution of the urea. The insertion of OmpA into vesicles was oriented, because trypsin digestion resulted in a 24-kDa fragment, while the full-length OmpA (35 kDa) was no longer observed. Translocation of the periplasmic domain of OmpA across the lipid bilayer into the inside of the vesicle would have lead to a full protection of OmpA from trypsin digestion. The 24-kDa fragment corresponded to the membrane inserted β-barrel domain (19 kDa) and a smaller part of the periplasmic domain, which was largely digested by trypsin. In contrast, only 50% of detergent-refolded OmpA that was reconstituted into diC$_{14:0}$PC vesicles after refolding into micelles could be digested with trypsin, indicating random orientation of the periplasmic domain inside and outside of the phospholipid vesicles [51]. Since OmpA assumed a random orientation after micelle-bilayer fusion [51], it is unlikely that OmpA would first fold into LPS micelles in the periplasm, which then fuse with the outer membrane as first proposed for PhoE based on the appearance of a folded monomer in mixed micelles of LPS and Triton X-100 *in vitro* [59]. However, a PhoE mutant was later shown to fold *in vivo* and also *in vitro* into LDAO micelles, but not into mixed micelles of Triton X-100 and LPS, leading to doubts about the existence of a folded monomeric intermediate of PhoE in LPS *in vivo* [60].

For direct oriented insertion of OmpA into the bilayers, the preformed lipid-vesicles had to be in the lamellar-disordered (liquid-crystalline) phase and the vesicles had to be sonicated [52, 61]. By contrast, insertion and folding did not complete when the lipid bilayers were in the lamellar-ordered (gel) phase or when refolding attempts were made with *di*$C_{14:0}$PC bilayers of large unilamellar vesicles (LUVs) that were prepared by extrusion through membranes of pore size 100 nm [62]. Similarly, folding and trimerization of OmpF [63] was observed after interaction of urea-unfolded OmpF with preformed lipid bilayers in the absence of detergent. Membrane inserted dimers of OmpF were detected transiently. *In vitro*, the folding yields of OmpF into lipid bilayers are small (below around 30%) even under optimized conditions [63] and when compared to OmpA, which quantitatively folds at pH 10.

2.3.3
Assemblies of Amphiphiles Induce Structure Formation in β-Barrel Membrane Proteins

To determine basic principles for the folding of β-barrel transmembrane proteins, folding of OmpA was examined with a large set of different phospholipids and detergents at different concentrations [50]. Folding of OmpA was successful with 64 different detergents, and phospholipids that had very different compositions of the polar headgroup did not carry a net charge and had a hydrophobic carbon chain length ranging from seven to 14 carbon atoms. Kleinschmidt et al. [50] demonstrated that for OmpA folding, the concentrations of these detergents or phospholipids must be above the critical micelle concentration (CMC), demonstrating that a supramolecular assembly (micelles or lipid bilayers) with a hydrophobic interior is the minimal requirement for the formation of a β-barrel transmembrane domain. OmpA did not fold into micelles of SDS that have a strong negative surface charge. Kleinschmidt et al. [50] monitored folding of OmpA by circular dichroism (CD) spectroscopy and by electrophoretic mobility measurements. Both methods indicate that after exposure to amphiphiles with short hydrophobic chains (with 14 or fewer carbons), OmpA assumes either both secondary and tertiary structure (i.e. the native state) or no structure at all, dependent on the presence of supramolecular assemblies (micelles, bilayers). OmpA folding into micelles is a thermodynamically controlled two-state process [50]. The necessary presence of amphiphiles (lipids, detergents) above the critical concentration for assembly (CCA) to induce the formation of native secondary and tertiary structure in OmpA also indicated that β-barrel structure does not develop while detergent or lipid monomers are adsorbed to a newly formed hydrophobic surface of the protein. (The term CCA is defined here to describe the amphiphile concentration at which a geometrically unique, water-soluble supramolecular assembly is formed, which can be a micelle, a lipid vesicle or even an inverted or cubic lipid phase. The CCA is identical to the CMC in the special case of micelle forming detergents. The CCA does not refer to the formation of random aggregates, e.g. misfolded membrane proteins.) To the con-

trary, a hydrophobic core of a micelle or bilayer must be present to allow folding of OmpA. Conlan and Bayley [64] reported later that another OMP, OmpG, folds into a range of detergents such as Genapol X-080, Triton X-100, *n*-dodecyl-β-D-maltoside, Tween 20 and octylglucoside. However, OmpG did neither fold into *n*-dodecylphosphocholine nor into the negatively charged detergents SDS and sodium cholate. Similar to OmpA, the detergent concentrations had to be above the CMC for OmpG folding [64]. Different detergents have also been used for refolding of other β-barrel membrane proteins for subsequent membrane protein crystallization (for an overview, see, e.g. [65]).

2.3.4 Electrophoresis as a Tool to Monitor Insertion and Folding of β-Barrel Membrane Proteins

SDS-polyacrylamide gel electrophoresis (PAGE) according to Laemmli [66] has been very useful to monitor the folding of OmpA into detergent micelles or lipid bilayers, provided that the samples are not boiled prior to electrophoresis [50–52, 55, 56, 62, 67–69]. If samples are not heat denatured, the folded and denatured OMPs migrate differently. For OmpA, Henning and coworkers described this property as heat modifiability [55]. It has been reported later also for other OMPs of bacteria such as FhuA [70] or OmpG [26, 64, 71]. Native OmpA, for example, migrates at 30 kDa, whereas unfolded OmpA migrates at 35 kDa [55]. Up to the present, all structural and functional experiments have shown a strict correlation between the 30-kDa form and structurally intact, fully functional OmpA. These previous studies included analysis of the OmpA structure by Raman, Fourier transform IR (FTIR) and CD spectroscopy [50–52, 56, 61, 72], biochemical digestion experiments [51, 67], and functional assays such as phage inactivation [55] and single-channel conductivity measurements [73].

It is possible to determine the kinetics of native structure formation in OmpA (and probably also in other OMPs) using the different electrophoretic mobilities of folded and unfolded OmpA, because OmpA folding can be inhibited by SDS and SDS does not unfold OmpA unless samples are boiled [52, 62, 67]. In an assay to determine the folding kinetics of OmpA, SDS was added to small volumes of the reaction mixture that were taken out at defined times after initiation of folding. In these samples, SDS bound quickly to folded and unfolded OmpA and stopped further OmpA folding [62, 67]. Finally, the fractions of folded OmpA in all samples were determined by cold SDS-PAGE (i.e. without heat-denaturing the samples). The fractions of folded OmpA at each time were estimated by densitometric analyses of the bands of folded and of unfolded OmpA, thus monitoring the formation of tertiary structure in OmpA as a function of time [kinetics of tertiary structure formation by electrophoresis (KTSE)].

2.3.5
pH and Lipid Headgroup Dependence of the Folding of β-Barrel Membrane Proteins

Although OmpA folded quantitatively into a wide range of neutral detergents, it did not fold into negatively charged SDS micelles at neutral or basic pH (cf. [56]). The negative charge of SDS could not be the only reason for lack of folding into these micelles, since OmpA folded partially into micelles of negatively charged LPS at pH 7 [68] and also into bilayers containing negatively charged phosphatidylglycerol [68, 74]. Surrey and Jähnig reported that OmpA folding yields reached 100% in neutral bilayers of $di C_{14:0}PC$ at pH 10, but were only around 70% at neutral pH [52]. The increased folding yield at pH 10 was very likely a consequence of an increased negative surface charge of OmpA ($pI = 5.9$) at pH 10 that increased the solubility of OmpA, i.e. suppresses the aggregation side-reaction. Surrey and Jähnig reported further that OmpA folding yields were again much lower at the even higher pH 12 [52]. They concluded that upon deprotonation of the arginine side-chains of OmpA, the increased negative net charge or negative surface potential of OmpA is too high to allow structure formation. Charge–charge repulsions between the negative surface potential of SDS micelles and negative charges on OmpA might have been the reason why OmpA did not fold into SDS micelles. The relatively small headgroup of SDS in comparison with the negatively charged LPS or phosphatidylglycerol causes a higher charge density on the surface of the SDS micelle, preventing insertion and folding of OmpA, which is negatively charged above pH 5.9.

2.4
Kinetics of Membrane Protein Folding

2.4.1
Rate Law for β-Barrel Membrane Protein Folding and Lipid Acyl Chain Length Dependence

The rate law of OmpA folding into a range of different phospholipid bilayers was determined using the method of initial rates. Kleinschmidt and Tamm [62] found that the folding kinetics of OmpA into LUVs of short-chain phospholipids and also into SUVs of $di C_{18:1}PC$ at 40 °C follow a single-step second-order rate law. The folding kinetics of OmpA could be approximated with a pseudo-first-order rate law, if the lipid concentration was high compared to the protein concentration (above a lipid/protein ratio of 90). With this approximation, a rate constant was observed that was identical to the product of the second-order rate constant and the lipid concentration. When fitted with a second-order rate law, the kinetic rate constants did neither depend on the lipid nor on the protein concentration, if the lipid/protein ratio was above around 90 mol mol^{-1}, while the first-order rate constant depended on the lipid concentration. However, the

second-order rate constants strongly depended on the acyl chain lengths of the lipids. When OmpA folding into bilayers of diC$_{12}$PC was monitored by fluorescence spectroscopy, this rate constant was $k_{2ord} \sim 0.4$ l mol^{-1} s^{-1}, while it was $k_{2ord} \sim 5.2$ l mol^{-1} s^{-1} for OmpA folding into bilayers of diC$_{11:0}$PC and $k_{2ord} \sim 30$ l mol^{-1} s^{-1} for OmpA folding into diC$_{10:0}$PC bilayers [62].

2.4.2
Synchronized Kinetics of Secondary and Tertiary Structure Formation of the β-Barrel OmpA

The kinetics of membrane insertion and structure formation of OmpA initiated by denaturant dilution in the presence of preformed lipid bilayers may also be monitored by CD spectroscopy or by KTSE. When the kinetics of secondary structure formation were measured for OmpA insertion and folding into LUVs of saturated short-chain phospholipids, a similar dependence of the rate constants on the length of the hydrophobic acyl chains of the lipids was observed as by fluorescence spectroscopy. However, the second-order rate constants were generally smaller than the corresponding rate constants of the fluorescence time courses [62]. Secondary structure formation was fastest with diC$_{10:0}$PC and slowest with diC$_{12:0}$PC as determined from the CD kinetics at 204 nm. When OmpA was reacted with preformed lipid bilayers (LUVs) of diC$_{14:0}$PC or diC$_{18:1}$PC, the CD signals did not change with time, indicating no changes in the secondary structure of OmpA upon incubation with these lipids.

2.4.3
Interaction of OmpA with the Lipid Bilayer is Faster than the Formation of Folded OmpA

When folding kinetics were analyzed using KTSE assays to determine the rate constants of tertiary structure formation, observations corresponded to those made by CD spectroscopy. The folding kinetics of OmpA were dependent on the length of the hydrophobic chains, but OmpA did not fold when the experiments were performed with diC$_{14:0}$PC or diC$_{18:1}$PC. The OmpA folding kinetics into diC$_{12:0}$PC bilayers at different concentrations were fitted to a second-order rate law and second-order rate constants were determined. Over a range of different lipid concentrations, the second-order rate constants obtained by KTSE were practically indistinguishable from the second-order rate constants of secondary structure formation. The rate constants of the secondary and tertiary structure formation of OmpA in diC$_{12:0}$PC were both $^{s/t}k_{2ord} \sim 0.090$ l mol^{-1} s^{-1}. By contrast, the second-order rate constant obtained from the fluorescence time courses of the OmpA folding kinetics into this lipid was about 4- to 5-fold higher ($^{pla}k_{2ord} \sim 0.4$ l mol^{-1} s^{-1}), indicating that the adsorption and insertion of the fluorescent Trp residues of OmpA into the hydrophobic core of the lipid bilayer were faster than the formation of the fully folded form of OmpA. Four of the five Trps of OmpA are at the front end of the β-barrel and presumably interacted first with the

hydrophobic core of the membrane, leading to fast fluorescence kinetics compared to the CD kinetics and kinetics of tertiary structure formation by electrophoresis. Together, these results indicated that the formation of the β-strands and the formation of the β-barrel of OmpA take place in parallel and are a consequence of the insertion of the membrane protein into the lipid bilayer. The previous observation that a preformed supramolecular amphiphile assembly is necessary for structure formation in OmpA was therefore further detailed by a kinetic characterization of the faster rates of interaction of OmpA with the lipid bilayer and by the slower rates of secondary and tertiary structure formation in OmpA.

2.5
Folding Mechanism of the β-Barrel of OmpA into DOPC Bilayers

2.5.1
Multistep Folding Kinetics and Temperature Dependence of OmpA Folding

Early folding experiments with urea-unfolded OmpA and membranes of $di C_{14:0}$PC indicated that OmpA folds into lipid bilayers of SUVs prepared by sonication, but not into bilayers of LUVs with a diameter of 100 nm prepared by extrusion [51, 52]. Lipids with longer chains such as $di C_{14:0}$PC and dioleoylphosphatidylcholine ($di C_{18:1}$PC) required the preparation of SUVs by ultrasonication and temperatures greater than around 25–28 °C for successful OmpA insertion and folding [51, 67].

Lipid bilayers of SUVs have a high surface curvature and intrinsic curvature stress. This leads to an increase of the hydrophobic surface that is exposed to OmpA after it is adsorbed at the membrane water interface, facilitating insertion of OmpA into SUVs compared to insertion of OmpA into bilayers of LUVs, where curvature stress is much lower and no insertion was observed. The folding kinetics of OmpA into SUVs of $di C_{14:0}$PC or $di C_{18:1}$PC were slower compared to the folding kinetics into LUVs of short chain phospholipids and strongly temperature dependent [62]. The fluorescence kinetics of OmpA folding that could still be fitted to a single-step pseudo first-order rate law at 40 °C [62, 67] were more complex when the temperature for folding was 30 °C or less. A single-step rate law was not sufficient to describe the kinetics [67]. Insertion and folding of OmpA into bilayers of $di C_{18:1}$PC (SUVs) was characterized by at least three kinetic phases, when experiments were performed at temperatures between 2 and 40 °C. These phases could be approximated by pseudo-first-order kinetics at a lipid/protein ratio of 400. Two folding steps could be distinguished by monitoring the fluorescence time courses at 30 °C. The first (faster) step was only weakly temperature dependent ($k_1 = 0.16\ \text{min}^{-1}$ at 0.5 mM lipid). The second step was up to two orders of magnitude slower at low temperatures, but the rate constant approached the rate constant of the first step at higher temperatures (around $0.0058\ \text{min}^{-1}$ at 2 °C and around $0.048–0.14\ \text{min}^{-1}$ at 40 °C, in the presence of 0.5 mM lipid). The activation energy for the slower process was

46 ± 4 kJ mol^{-1} [67]. An even slower phase of OmpA folding was observed by KTSE assays, indicating that tertiary structure formation was slowest with a rate constant $k_3 = 0.9 \times 10^{-2}$ min^{-1} (at 3.6 mM lipid and at 40 °C) [67]. This is consistent with the smaller rate constants of secondary and tertiary structure formation in comparison to the rate constants of protein association with the lipid bilayer, which were later observed for OmpA folding into LUVs of short-chain phospholipids [62] (see Section 2.4.3). The kinetic phases that were observed for OmpA folding into *di*$C_{18:1}$PC bilayers (SUVs) suggest that at least two membrane-bound OmpA folding intermediates exist when OmpA folds and inserts into lipid bilayers with 14 or more carbons in the hydrophobic acyl chains. These membrane-bound intermediates could be stabilized in fluid *di*$C_{18:1}$PC bilayers at low temperatures between 2 and 25 °C (the temperature for the phase transition of *di*$C_{18:1}$PC from the lamellar-ordered to the lamellar-disordered liquid-crystalline phase is $T_c = -18$ °C). The low-temperature intermediates could be rapidly converted to fully inserted, native OmpA, as demonstrated by temperature jump experiments [67].

2.5.2
Characterization of Folding Intermediates by Fluorescence Quenching

Tryptophan fluorescence quenching by brominated phospholipids (see, e.g. [75–82]) or by lipid spin-labels (see, e.g. [83–88]) traditionally has been very valuable to determine characteristic elements of the transmembrane topology and lipid–protein interactions of integral membrane proteins. To further characterize the folding process of OmpA, we combined this method with the study of the folding kinetics of OmpA into bilayers (SUVs) of *di*$C_{18:1}$PC [89, 90]. The average positions of the five fluorescent Trps of OmpA were characterized for the membrane-bound folding intermediates that were previously implicated by the discovery of multistep folding kinetics [67]. A new method was developed by studying the kinetics of the refolding process in combination with the Trp fluorescence quenching at different depths in the lipid bilayer [90] using membrane embedded quenchers. The positions of fluorescent Trps with reference to the center of the phospholipid bilayer can be determined using a set of membrane integrated fluorescence quenchers that carry either two vicinal bromines or alternatively a doxyl group at the *sn*-2 acyl chain of the phospholipid. When in close proximity to the fluorescent Trp residues of integral membrane proteins, these groups quench the Trp fluorescence. The positions of the bromines in 1-palmitoyl-2-(4,5-dibromo-)stearoyl-*sn*-glycero-3-phosphocholine (4,5-DiBrPC), 6,7-DiBrPC, 9,10-DiBrPC and 11,12-DiBrPC are known from X-ray diffraction to be 12.8, 11.0, 8.3 and 6.5 Å from the center of the lipid bilayer [91, 92]. The fluorescence intensity of the Trps of OmpA was measured as a function of time after initiation of OmpA folding by dilution of the denaturant in presence of preformed lipid bilayers containing one of the brominated lipids as a fluorescence quencher. In a set of four equivalent folding experiments, bilayers were used that contained 30 mol% of one of the four brominated lipids and 70%

di$C_{18:1}$PC. The fluorescence intensities in the four different time courses of OmpA folding in presence of each of the four brominated lipids were subsequently normalized by division with fluorescence intensities obtained upon OmpA folding into bilayers of 100% *di*$C_{18:1}$PC (i.e. in the absence of any quencher). Thus, depth-dependent quenching profiles were obtained at each time after initiation of OmpA folding. From these profiles, the vertical location of Trp in the membrane in projection to the bilayer normal was then determined using the parallax method [88, 93] or the distribution analysis [81, 82].

A large set of experiments was performed in the temperature range between 2 and 40 °C. At each selected temperature, the average distances of the Trps to the center of the lipid bilayer were determined as a function of time. Therefore, we called this method time-resolved distance determinations by Trp fluorescence quenching (TDFQ) [90]. Previously unidentified folding intermediates on the pathway of OmpA insertion and folding into lipid bilayers were detected, trapped and characterized. Three membrane-bound intermediates were described, in which the average distances of the Trps from the bilayer center were 14–16, 10–11 and 0–5 Å, respectively [90]. The first folding intermediate was stable at 2 °C for at least 1 h. A second intermediate was characterized at temperatures between 7 and 20 °C. The Trps moved 4–5 Å closer to the center of the bilayer at this stage. Subsequently, in an intermediate that was observed at 26–28 °C, the Trps moved another 5–11 Å closer to the center of the bilayer. This intermediate appeared to be less stable. The distribution parameter, calculated from distribution analysis, was largest for the Trp distribution of this intermediate. This was a consequence of the mechanism of folding and of the structure of folded OmpA [3, 4, 94]. The large distribution parameter observed for this intermediate was consistent with experiments on single Trp mutants of OmpA [89] (see below). Trp7 has to remain in the first leaflet of the lipid bilayer, while the other Trps must be translocated across the bilayer to the second leaflet. Therefore, with symmetrically incorporated brominated lipids as fluorescence quenchers, the largest distribution parameter was observed when the four translocating Trps are in the center of the lipid bilayer. Formation of the native structure of OmpA was observed at temperatures above about 28 °C. In the end of these kinetic experiments, all five Trps were finally located on average about 9 to 10 Å from the bilayer center, Trp7 in the periplasmic leaflet and the other four Trps in the outer leaflet of the outer membrane.

When KTSE experiments were performed to monitor OmpA folding at 30 °C, a 32-kDa band was observed in the first few minutes of OmpA folding [67]. The folding conditions for this experiment were nearly identical to those of the fluorescence quenching experiments at 28–30 °C. Therefore, this 32-kDa form is very likely identical to the third folding intermediate of OmpA, in which the average Trp-location is 0–5 Å from the center of the lipid bilayer. The comparison indicated that in this intermediate, a significant part of the *β*-barrel had formed, which is resistant to treatment with SDS at room temperature.

2.5.3 The β-Barrel Domain of OmpA Folds and Inserts by a Concerted Mechanism

TDFQ experiments were subsequently performed with the five different single Trp mutants of OmpA. These mutants were prepared by site-directed mutagenesis [89], and contained each a single Trp and four phenylalanines in the five Trp positions of the wild-type protein. All mutants were isolated from the *E. coli* outer membrane and refolded *in vitro* into lipid bilayers. Time-resolved distance determinations (TDFQ) for each of the single Trp mutants of OmpA gave more structural detail on the folding mechanism of OmpA. TDFQ experiments were carried out at selected temperatures between 2 and 40 °C [89]. When kinetic experiments were performed below 30 °C, each of the five Trps approached a distance of 10–11 Å from the bilayer center in the end of the fluorescence time course of OmpA folding. The distance decrease with time was observed even at 40 °C for Trp7. The TDFQ results showed that Trp7 did not migrate any closer to the bilayer center than around 10 Å independent of the experimental conditions. However, Trp15, Trp57, Trp102 and Trp143 were detected very close to the center of the lipid bilayer in the first minutes of refolding at temperatures of 30, 32, 35 and 30 °C, respectively. TDFQ experiments performed at 40 °C resolved the last two steps of OmpA refolding, and the translocation rate constants of the first phase of fast distance change were 0.55, 0.46, 0.26 and 0.43 min^{-1} for Trp15, Trp57, Trp102 and Trp143, respectively. The four Trps crossed the center of the bilayer and approached distances of around 10 Å from the bilayer center in the final folding step of OmpA. These experiments demonstrated that Trp15, Trp57, Trp102 and Trp143 are similarly located in three folding intermediates that were also observed previously for wild-type OmpA. The similar distances of these Trps from the membrane center in each of the membrane-bound folding intermediates indicate a simultaneous translocation of the transmembrane segments of OmpA, coupled to the formation of the β-barrel structure upon insertion.

The results of these kinetic studies on the folding mechanism of OmpA may be used to develop a tentative model of OmpA folding (Fig. 2.2): the time courses of OmpA folding into phospholipid bilayers (LUVs) of $di C_{12:0}PC$ indicated that β-strand secondary and β-barrel tertiary structure formation are synchronized with the same rate constant [62], which is lower than the rate constant of the fluorescence time course of OmpA adsorption to the lipid bilayer. Strongly temperature dependent kinetics were observed and several kinetic phases were distinguished, when folding of OmpA was investigated with lipid bilayers of $di C_{18:1}PC$ (SUVs), which is a phospholipid with comparably long hydrophobic chains. OmpA first adsorbs to the water–membrane interface (intermediate A) and the intrinsic fluorescence of OmpA increases strongly due to the partitioning of the fluorescent Trps into the less polar environment at the membrane–water interface. Subsequently, the slower phase of the fluorescence changes reflect the migration of the Trps from the membrane–water interface into the hydrophobic core of the lipid bilayer. The translocation of the Trps across the bilayer is best monitored with membrane inserted fluorescence

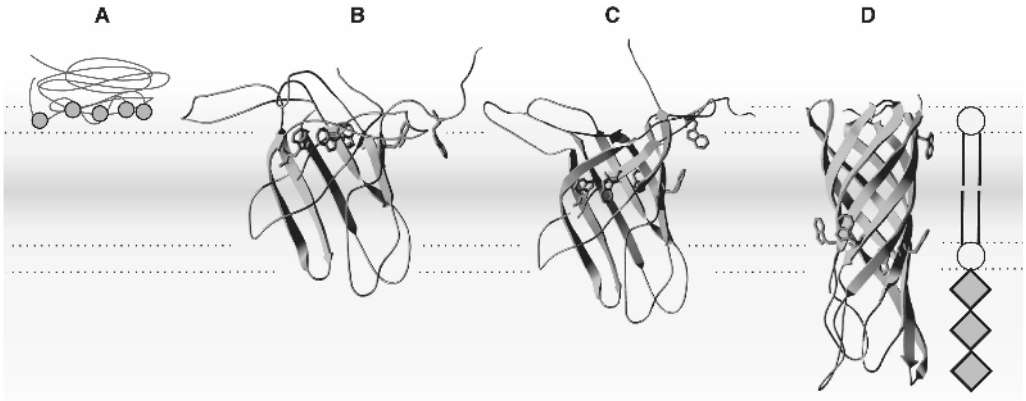

Locations of the Tryptophans of OmpA in Folding Intermediates identified by TDFQ:

Tryptophan	Distance to the Center of the Lipid Bilayer			
	I_{M1} (A) ⟶	I_{M2} (B) ⟶	I_{M3} (C) ⟶	N (D)
(7)	~14-16 Å	~10 Å	~10 Å	~10 Å
(15, 57, 102, 143)		~10 Å	~0-5 Å	~10 Å

Fig. 2.2 Folding model of OmpA. The kinetics of β-sheet secondary and β-barrel tertiary structure formation in OmpA have the same rate constants and are coupled to the insertion of OmpA into the lipid bilayer [62, 89, 90]. The locations of the five Trps in the three identified membrane-bound folding intermediates and in the completely refolded state of OmpA [89, 90] are shown. Additional details, such as the translocation of the long polar loops across the lipid bilayer, must still be determined. OmpA structures were generated with DeepView [146, 147].

quenchers, since the intrinsic Trp fluorescence does not change much during Trp migration through the 30-Å hydrophobic core of *di*$C_{18:1}$PC. The average location of the Trps of 14–16 Å from the bilayer center after adsorption to the membrane-water interface was determined by TDFQ experiments at 2 °C [90]. At temperatures of 5–25 °C, this initial phase of folding was fast and followed by a second, slower phase, in which the Trps move into more hydrophobic regions at a distance of about 10 Å from the bilayer center. The observed folding intermediate (B) is quite stable. A third membrane-bound intermediate (C) was identified at 27–29 °C. In this intermediate, all Trps, except Trp7, are detected a distance of 0–5 Å from the bilayers center in the first minutes of OmpA folding. Trp7 remains at the same location as in intermediate B. Very likely, this intermediate is identical to the 32-kDa form of OmpA that was previously observed by KTSE experiments [67]. Finally, at temperatures above 28–30 °C, Trp15, Trp57, Trp102 and Trp143 move away from the center of the bilayer to a distance of about 10 Å. This distance of the Trp residues of OmpA compares well with the X-ray and nuclear magnetic resonance structures of OmpA [3, 4]. The basic elements of the model in Fig. 2.2 are the synchronized kinetics of second-

ary and tertiary structure formation, the simultaneous migration of the Trps that cross the bilayer center, and the migration of Trp7, which does not translocate. However, more structural information is needed to improve this preliminary model. For example, it is not known how the residues of the polar loops of OmpA cross the hydrophobic core of the lipid bilayer.

2.6 Protein–Lipid Interactions at the Interface of β-Barrel Membrane Proteins

2.6.1 Stoichiometry of the Lipid–Protein Interface

To resolve the interactions between membrane lipids and fully inserted and folded β-barrel membrane proteins in detail, Ramakrishnan et al. [95] investigated the stoichiometry and lipid selectivity of the eight-stranded OmpA and the 22-stranded FhuA in dimyristoylphosphatidylglycerol ($di C_{14:0}$PG) bilayers by electron spin resonance (ESR) spectroscopy, a method that was very successfully applied previously to investigate lipid–protein interactions of α-helical membrane proteins (see, e.g. [96]). Spin-labeled lipids of different headgroup compositions, but with the same fatty acyl chains, were incorporated into $di C_{14:0}$PG bilayers with either OmpA or FhuA. ESR spectra of bilayers containing 1 mol% of phosphatidylglycerol carrying the doxyl group at C-14 of the *sn*-2 acyl chain (14-PGSL), were recorded at 30 °C, i.e. above the gel-to-liquid-crystalline phase transition temperature of $di C_{14:0}$PG. Difference spectroscopy demonstrated that the spectra had two components when either OmpA or FhuA was present in the lipid bilayer. The two components corresponded to protein-immobilized lipid spin-labels and to mobile spin-labels in the $di C_{14:0}$PG host matrix. Similar components of spin-label spectra were described previously in a wide range of studies with α-helical membrane proteins [96–99]. The ratio of mobile/immobile lipid populations was proportional to the lipid/protein ratio. From this linear dependence, it was possible to calculate the number of lipids in contact with the protein. Stoichiometries of 11 lipids/OmpA and of 32 lipids/FhuA, respectively, were found for the protein–lipid molecular interface [95].

2.6.2 Lipid Selectivity of β-Barrel Membrane Proteins

The ESR spectra also demonstrated that lipids with different chemical structure of their polar headgroups have different affinities to associate with the integral β-barrel membrane proteins. A quantitative analysis of the ESR spectra resulted in the relative association constants of the different lipid species with FhuA and OmpA [95]. For OmpA, the lipid headgroup selectivity was phosphatidic acid > phosphatidylglycerol > phosphatidylcholine > phosphatidylethanolamine > phosphatidylserine > diacylglycerol > stearic acid. For FhuA, the selectivity pattern was stearic acid > phosphatidic acid > phosphatidylcholine > phosphatidylglycerol > phospha-

tidylserine > phosphatidylethanolamine > diacyl glycerol. The strong difference in the selectivity for stearic acid was explained by a different protonation state of stearic acid in association with OmpA as compared to FhuA in the negatively charged $di C_{14:0}$PG host bilayer. Since $di C_{14:0}$PG bilayers have a strongly negative electrostatic surface potential, stearic acid is expected to be protonated at pH 7. In reconstituted bilayers of FhuA, the negative surface potential is locally neutralized in regions of high positive charge on FhuA, leading to the ionized form of stearic acid [100]. Representations of the surface electrostatics of the crystal structures of OmpA and FhuA indicate an excess of positive charges on the extracellular, but not on the periplasmic surface of the two proteins, which is more pronounced for FhuA. This may explain the overall selectivity of these β-barrels for negatively charged lipids. On the extracellular side of OmpA, basic side-chains, Lys64(β_3), Lys73(β_4), Arg103(β_5) and Lys113(β_6) are located in extensions of the β-strands facing the lipid headgroup region. These side-chains may probably cause the observed selectivity of OmpA for the negatively charged phospholipids. It is likely that this cluster of positively charged lysine and arginine residues also forms a binding site for the negatively charged LPS, similar to the one identified in FhuA [24, 101], which contains Lys306(β_7), Lys351(β_8), Arg382(β_9) and Lys437(β_{10}). FhuA also has a marked selectivity for negatively charged phospholipids [95]. For both OmpA and FhuA, the relative association constant for phosphatidylglycerol is about 2 times greater than the relative association constant of phosphatidylethanolamine, indicating that phosphatidylglycerol is the preferred lipid at the interface to the OMPs in the outer membranes of bacteria, especially in mutant strains that do not contain LPS [102, 103]. Similar clusters of positively charged residues that form a binding site for negatively charged LPS have also been observed in other OMPs such as OmpT [104, 105].

2.7
Orientation of β-Barrel Membrane Proteins in Lipid Bilayers

2.7.1
Lipid Dependence of the β-Barrel Orientation Relative to the Membrane

The orientation of the β-barrel membrane proteins OmpA and FhuA and their order parameters have been determined recently from IR dichroism studies [100]. The tilt angle of the barrel axis relative to the membrane normal, α (i.e. the mean effective inclinations of the β-sheets relative to the membrane normal), depended on the thickness of the lipid bilayer and decreased in fluid bilayers from $\alpha = 45^\circ$ for $di C_{12:0}$PC to $\alpha = 30^\circ$ for $di C_{17:0}$PC in case of the eight-stranded β-barrel domain of OmpA (residues 0–176 of OmpA). The barrel tilt angle, α, was generally smaller for the 22-stranded β-barrel domain of FhuAΔ5–160, ranging from $\alpha = 36^\circ$ in $di C_{12:0}$PC to $\alpha = 21^\circ$ in $di C_{17:0}$PC. The protein order parameters in these fluid bilayers increased for OmpA0–176 from 0.25 (in $di C_{12}$PC) to 0.61 (in $di C_{17:0}$PC) and increased for FhuAΔ5–160 from 0.48

(in diC$_{12}$PC) to 0.80 (in diC$_{17:0}$PC). The lipid order parameters exhibited little systematic change with lipid chain length [100]. Also, in the case of OmpA and OmpA0–176, differences between data for fluid and gel-phase bilayers were not large, but barrel tilts were considerably smaller and order parameters larger for FhuAΔ5–160 in fluid than in gel-phase bilayers. The greater freedom of orientation of OmpA in thin lipid bilayers correlates well with faster rates of insertion and folding observed with thin bilayers [62]. Since the β-barrel domain of FhuA has a much larger cross-section (39 Å×46 Å [24]) than OmpA (with an outer diameter of 24 Å [94]), the membrane ordering is greater for FhuA [100].

2.7.2
Inclination of the β-Strands Relative to the β-Barrel Axis in Lipid Bilayers

The tilt angles, β, of the β-strands relative to the barrel axis were $\beta = 44^\circ$ for OmpA0–176 and $\beta = 44.5^\circ$ for FhuAΔ5–160, when determined from attenuated total internal reflection (ATR)-FTIR spectra. For comparison, strand tilt angles relative to the barrel axis were $\beta = 43.1^\circ$ for OmpA0–171 [4, 94, 106] and $\beta = 38.3$ for FhuAΔ5–160 [24, 106] when calculated from the crystal structures. The slightly larger strand tilts obtained for FhuA were interpreted as a slight relaxation of the FhuAΔ5–160 structure relative to the packing of the whole protein in the crystal [100]. Ramakrishnan et al. [100] also estimated the sheet twist, $\theta = 18^\circ$ (wt-OmpA) and $\theta = 6^\circ$ (FhuAΔ5–160), and strand coiling, $\varepsilon = 10^\circ$ (wt-OmpA) and $\varepsilon = 4^\circ$ (FhuAΔ5–160) from the β-strand tilts, β, that were obtained from the dichroic ratios of ATR-FTIR spectra. The values were in agreement with the estimates from the X-ray crystal structures, suggesting similar β-barrel geometries of OmpA and FhuA in lipid membranes and X-ray crystals.

Analysis of the FTIR spectra of wt-OmpA and OmpAΔ5–160 [100] showed that the overall percentage of β-sheet secondary structure in wt-OmpA was 59%, while a β-sheet content of 63% was deduced from the crystal structure of OmpA0–171 [4]. Ramakrishnan et al. [100] therefore concluded that about 55% of the periplasmic domain of OmpA must also be of β-sheet secondary structure. Interestingly, the crystal structure of the 127 residue C-terminal domain of RmpM, which is homologous to the periplasmic domain of OmpA with about 35% sequence identity, contains 25% β-strands and 25% β-turns [107].

2.7.3
Hydrophobic Matching of the β-Barrel and the Lipid Bilayer

The tilts of the strands can be used to deduce information about the hydrophobic thickness of lipid bilayer. The hydrophobicity analysis [72] of the OmpA barrel showed that the hydrophobic region, which is delimited by two aromatic girdles, is comprised of an average of five outward facing residues in each of the strands of the OmpA transmembrane domain. With the rise of 3.45 Å per residue [108] and an average tilt angle of 44°, the hydrophobic thickness can be estimated to around 25 Å, which agrees well with estimates for several OMPs of

E. coli [109]. When the acyl chain length dependence of the lipid affinity of another OMP, OmpF, was investigated by fluorescence spectroscopy [110], a maximum affinity was found for $di C_{14:1}PC$, with a progressive decrease for lipids with longer acyl chains. The double bond reduces the bilayer thickness, which is comparable for $di C_{14:1}PC$ and $di C_{12:0}PC$ [111], to about 24 nm. This is consistent with the thickness derived from β-strand tilt angles.

2.8 *In vivo* Requirements for the Folding of OMPs

2.8.1 Amino Acid Sequence Constraints for OmpA Folding *in vivo*

Koebnik [112] tested constraints within the amino acid sequence that limit the folding of OmpA *in vivo*. In this study, OMPs assembled efficiently into the outer membrane only when at least four of the five residues pointing to the hydrophobic chains of the membrane lipids were hydrophobic. In addition, none of the three central residues of a β-strand could be charged. The amino acid sidechains facing the inside of the small eight-stranded β-barrel of OmpA could not be large and proline residues were not well tolerated in the β-strands.

Two complementary OmpA fragments that were split at the second or third periplasmic turn could be co-expressed in *E. coli* and assembled efficiently with all termini located in the periplasmic space [113]. When pairs of the transmembrane β-strands were permuted on the DNA level, only the three possible circular permutations led to correctly assembled OmpA variants, although their assembly was less efficient than the assembly of OmpA [114].

2.8.2 Periplasmic Chaperones

The biochemical requirement for the *in vitro* folding of β-barrel membrane proteins OmpA [50, 56], OmpG [64], OmpF [63], PhoE [115] and others from a denatured state in urea appears to be a supramolecular assembly of amphiphiles [50, 69]. While the presence of a supramolecular assembly of detergents or lipids is a minimal requirement for the *in vitro* folding of β-barrel membrane proteins such as OmpA, additional components may be necessary *in vivo*. For instance, it is not clear how OMPs are successfully targeted to the outer membrane, and how insertion and finally folding of other OMPs takes place, which exhibited poor folding yields *in vitro*, such as OmpF [63] and FhuA (Pocanschi and Kleinschmidt, in preparation). Poor *in vitro* refolding upon denaturant dilution in presence of preformed phospholipid bilayers appears to be a consequence of the fast aggregation of OMPs, which competes with bilayer insertion and folding. *In vivo*, molecular chaperones keep the OMPs soluble in the periplasm [116, 117] before they become part of the outer membrane. The chaper-

ones are likely more efficient to prevent OMP aggregation in comparison to the denaturant urea that has been used in folding studies *in vitro* and that must be diluted before OMPs can insert and fold into model membranes. *In vivo*, there must also be a targeting mechanism that prevents the insertion of OMPs from the periplasm into the cytoplasmic membrane and specifically directs them to the outer membrane. It may be possible that differences in the physicochemical properties of the inner and outer membrane are responsible for the targeting of β-barrel membrane proteins to the outer membrane. For instance, the average hydrophobic thicknesses of the proteins of the outer membrane (22–24 Å) [62, 109] and of the inner membrane (around 26–29 Å) [109] of *E. coli* are different. In fact, *in vitro* experiments also showed that insertion and folding of OmpA into thin membranes are faster then into phospholipid bilayers with a thicker hydrophobic core [62]. The outer membrane contains mostly LPS in the outer leaflet. LPS has relatively short hydrocarbon chains, which are partially hydroxylated close to the glucosamine backbone at C-3, lowering the hydrophobic thickness of the outer membrane. Whether this difference in the hydrophobic thicknesses of the inner and outer membranes is really relevant for targeting of OMPs to the outer membrane, remains to be clarified. Most likely, proteins are involved in proper targeting of OMPs to the outer membrane. Several periplasmic proteins and LPS have been demonstrated to interact with OMPs in the periplasm. OMPs of Gram-negative bacteria are translocated across the cytoplasmic membrane into the periplasm in a mostly unfolded form by the SecA/E/Y/G export system (for recent reviews, see, e.g. [118, 119]). In the periplasm, the signal sequence is cleaved off by a signal peptidase. Genetic studies on possible periplasmic chaperones and biophysical assays with these chaperones and soluble proteins as their substrates suggested that for example SurA (45 kDa) [120–122] and FkpA (26 kDa) [123–125] have a role in the targeting and assembly of OMPs. In these studies, the periplasmic chaperones prevented the aggregation of soluble proteins. *In vivo*, the concentrations of some OMPs in the outer membrane of *E. coli* were decreased, when the genes of the periplasmic proteins Skp [46] or SurA [120, 121] were deleted. Representatives of three different families of peptidyl-prolyl *cis*/*trans* isomerases were found in the periplasm. Examples are the parvulin-type SurA [122, 123], the FKBP-type FkpA [123–126] and the cyclophilin-type PpiA (RotA, 18 kDa) [127]. SurA bound the 18-stranded LamB *in vitro* [122].

2.8.3
Insertion and Folding of the β-Barrel OmpA is Assisted by Skp and LPS

Direct biochemical evidence for a chaperone-assisted three-step delivery pathway of OmpA to a model membrane was first given by Bulieris et al. [68]. It was demonstrated that the periplasmic chaperone Skp [116, 128–131] keeps OmpA soluble *in vitro* at pH 7 in an unfolded form even when the denaturant urea was diluted out. Skp was also shown to prevent the premature folding of OmpA into LPS micelles and to inhibit the folding of OmpA into phospholipid bilayers composed of phosphatidylethanolamine, phosphatidylglycerol and phosphatidylcholine [68].

Only when Skp complexes with unfolded OmpA were reacted with LPS in a second stage, a folding competent form of OmpA was formed that efficiently inserted and folded into phospholipid bilayers in a third stage. In this Skp/LPS-assisted folding pathway, Bulieris et al. observed faster folding kinetics and higher yields of folded OmpA in comparison to the direct folding of OmpA into the same lipid bilayers upon urea dilution in absence of Skp and LPS. In the sole presence of either Skp or LPS, the kinetics of insertion and folding were inhibited (Fig. 2.3). The higher folding yields of OmpA from the complex with Skp and LPS (in comparison to OmpA folding from the urea denatured state) may be a consequence of faster Skp binding to unfolded OmpA in solution in comparison to the folding of OmpA into lipid bilayers. Faster rates of Skp binding in solution would result in relatively lower amounts of aggregated OmpA, thus increasing the amounts of OmpA available for folding. However, Bulieris et al. [68] also showed that LPS is required for the efficient OmpA insertion from complexes with Skp into lipid bilayers. In their study, unfolded OmpA bound LPS or Skp or both. The binding stoichiometries were 25 molecules of LPS with a binding constant of

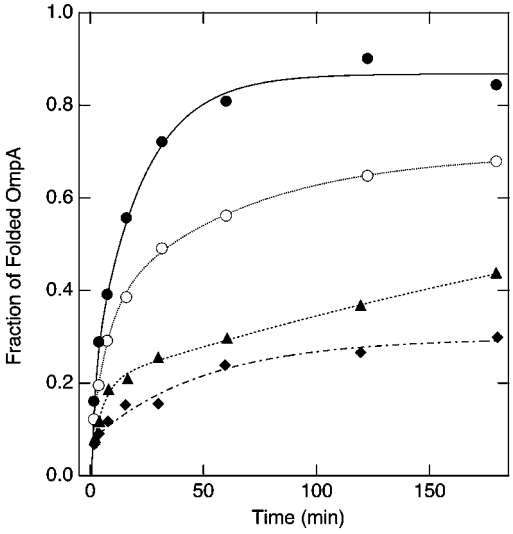

Fig. 2.3 Folding of OmpA into lipid bilayers requires both, Skp and LPS (adapted from [68]). Data shown correspond to Omp folding experiments into lipid bilayers, 30 min after dilution of the denaturant urea, in the absence of Skp and LPS (open circles), in the presence of Skp (diamonds), in the presence of LPS (triangles), and in the presence of both Skp and LPS (solid circles). The folding kinetics were fastest and folding yields were highest when both Skp and LPS were present. Folding was inhibited when either Skp or LPS were absent. The folding kinetics in presence of Skp and LPS also compare favorably with the folding kinetics from the urea-denatured state in the absence of Skp and LPS, indicating that OmpA is insertion competent *in vivo*, in the absence of urea, when in complex with Skp and LPS. The work also indicated that OmpA did not develop native structure when complexed with Skp and LPS, but only in the presence of lipid bilayers.

$K_{LPS} \sim 1.2 \pm 0.7\ mM^{-1}$ (i.e. with a free energy of binding $\Delta G = -8.3 \pm 0.3$ kcal mol^{-1}) and three molecules of Skp with a much larger binding constant of $K_{Skp} \sim 46 \pm 30\ mM^{-1}$ (i.e. with $\Delta G = -10.3 \pm 0.5$ kcal mol^{-1}) [68]. The 8- to 150-fold greater OmpA binding constant of Skp explains that Skp prevents the folding of OmpA upon addition of LPS micelles. However, LPS was necessary to promote efficient folding of OmpA into preformed phospholipid membranes at optimal stoichiometries of 0.5–1.7 mol LPS mol Skp^{-1} and 3 mol Skp mol unfolded $OmpA^{-1}$. For fast kinetics and high yields of membrane insertion and folding of OmpA, about 1.5–5 mol LPS bound to Skp/OmpA complexes (i.e. much lower amounts than observed in absence of Skp) [68]. Interestingly CD spectroscopy and KTSE assays indicated that large amounts of secondary and tertiary structure in OmpA only form in the third stage of the assembly pathway, upon addition of phospholipid bilayers [68], suggesting that Skp and LPS deliver OmpA to the membrane, which is absolutely needed for the formation of secondary and tertiary structure in OmpA.

The interaction of the OmpA/Skp/LPS complex with the lipid bilayer is apparently the most important event to initiate folding of OmpA in presence of chaperones and LPS as a folding catalyst. The described assisted folding pathway and discovered 3:1 stoichiometry for Skp binding to OmpA [68] was later supported by the observation that Skp is trimeric in solution [132] and by the description of the crystal structure of Skp and a putative LPS binding site in Skp [133, 134] (Fig. 2.4 A). One LPS binding site per Skp monomer is consistent with the observation of optimal folding kinetics of OmpA from an OmpA/Skp/LPS complex at 0.5–1.7 mol LPS mol Skp^{-1} [68]. In this case, a 1:1 stoichiometry perhaps indicates that LPS only binds to the LPS binding site of Skp and OmpA is completely shielded from interactions with LPS. A current folding model for this assisted OmpA folding pathway is shown in Fig. 2.5.

A second periplasmic protein, the survival factor A, SurA [123], has been demonstrated to affect OMP assembly. *E. coli* mutants, in which the *surA* gene was deleted, had reduced concentrations of OmpA and LamB in the outer membrane [120, 121]. SurA functions as a peptidyl-prolyl *cis*/*trans* isomerase and as a molecular chaperone [122]. The crystal structure of SurA [135] is shown in Fig. 2.4 B. Genetic evidence suggests that SurA and Skp act as chaperones that are involved in parallel pathways of OMP targeting to the outer membrane [136].

2.8.4 Role of Omp85 in Targeting or Assembly of β-Barrel Membrane Proteins

The Skp/LPS-assisted folding pathway is not the only pathway for OMP folding, because in initial experiments, the folding of the 22-stranded β-barrel FhuA was not facilitated in the presence of Skp and LPS (Pocanschi and Kleinschmidt, unpublished data). There is genetic evidence for a parallel folding pathway involving the periplasmic SurA. The double deletion of the genes *skp* and *surA* is lethal to the bacteria [122, 136]. Also, the assembly of TolC does neither require

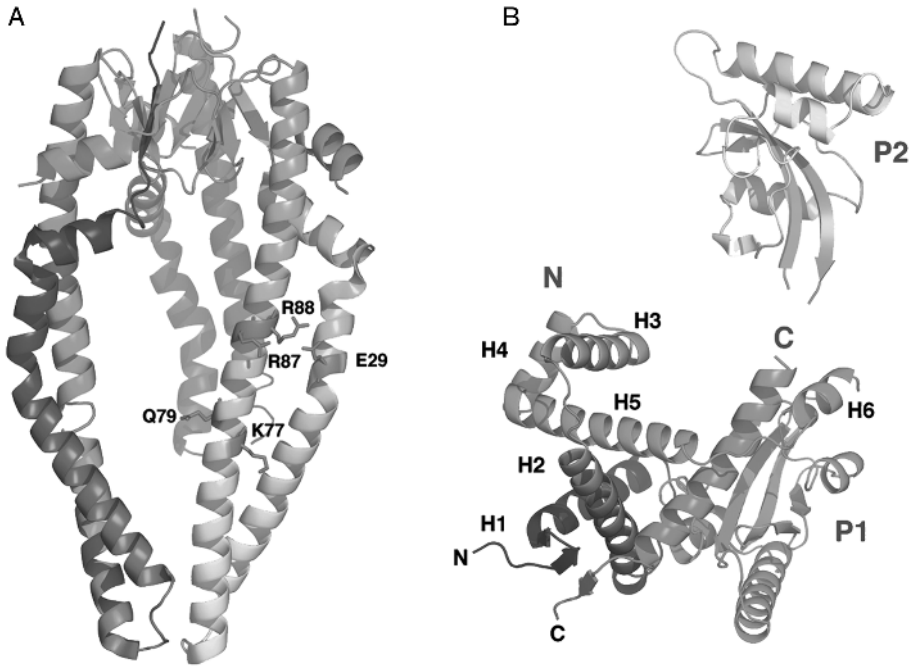

Fig. 2.4 (A) Crystal structure of the Skp trimer (PDB entry 1SG2 [134]). The Skp trimer consists of a tightly packed 12-stranded β-barrel that is surrounded by C-terminal α-helices of the three subunits that point away from the barrel in form of tentacles that are about 65 Å long. These tentacles form a cavity that may take up the unfolded OMP. The outside surface of the helical domain of Skp is highly basic. Each monomer of the trimeric Skp has a putative LPS binding site [133] (Skp structure entry 1UM2 in the PDB). The LPS-binding site was found using a previously identified LPS-binding motif [101], and consists of K77, R87 and R88. This motif matches the LPS-binding motif in FhuA with residues K306, K351 and R382 (see Section 2.6.2) and a root mean square deviation of 1.75 Å for the Cα–Cγ atoms was calculated [133]. Q99 in Skp may also form a hydrogen bond to an LPS phosphate, completing the four-residue LPS-binding motif. (B) Crystal structure of survival factor A, SurA (PDB entry 1M5Y [135]). The N-terminal domain (N) is composed of the α-helices H1 to H6 (residues 1–148) and connected to peptidyl-prolyl *cis*/*trans* isomerase (PPI) domain P1 (residues 149–260). The P2 domain (residues 261–369) connects to the C-terminal domain C (residues 370–428, colored in red). It has been demonstrated that a mutant SurAN(-Ct), which does not contain the two PPIase domains and is composed of the N and C domains only, functions like a chaperone [122]. This SurA "core domain" has been proposed to bind the tripeptide motif aromatic–random–aromatic, which is prevalent in the aromatic girdles of β-barrel membrane proteins [148]. Figures were created with PyMOL [149].

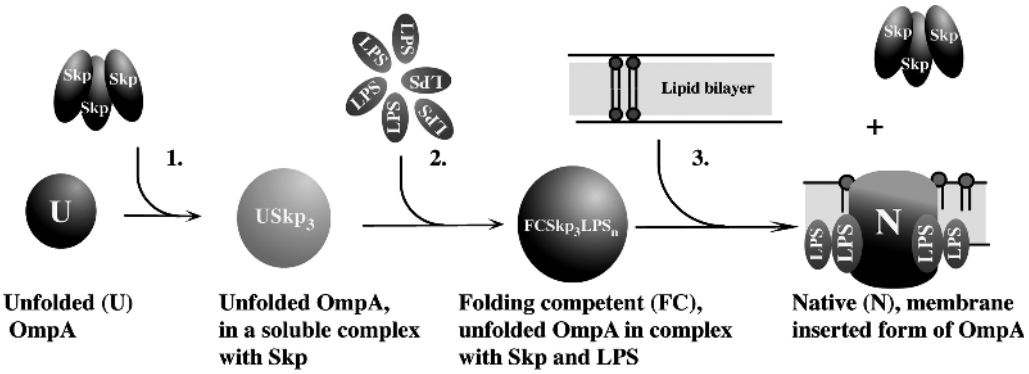

Fig. 2.5 A model of the Skp/LPS-assisted folding pathway of the β-barrel protein OmpA of the outer membrane of *E. coli* is depicted. After translocation across the cytoplasmic membrane by the SecA/E/G/Y system in unfolded form (U), OmpA binds three molecules of the trimeric Skp, which is a periplasmic chaperone and keeps OmpA soluble in an unfolded state ($USkp_3$). The complex of unfolded OmpA and Skp interacts with LPS molecules to form a folding competent intermediate of OmpA ($FCSkp_3LPS_n$). In the final step, folding competent OmpA inserts and folds into the lipid bilayer (adapted from [69]).

Skp nor SurA [137]. Recently, an OMP, Omp85, has been demonstrated to be essential for the targeting of integral membrane proteins to the outer membrane [138] and, similarly, Tob55 has been demonstrated to be essential for targeting porins to the outer membrane of mitochondria [139, 140]. Omp85 was necessary for the viability of the bacteria and deletion of the *omp85* gene from the chromosome lead to an accumulation of OMPs in non-native, probably aggregated form. The lack of insertion of the OMPs was further confirmed by immunofluorescence microscopy, which showed strongly reduced surface labeling with antibodies directed against OMPs. Omp85 may therefore be involved either in targeting of OMPs towards or in OMP insertion into the outer membrane, or in both. Alternatively, it was also suggested that the effect of Omp85 may be an indirect one and that Omp85 is instead involved in lipid transport to the outer membrane [141]. This role for Omp85 was proposed, because the *omp85* gene is co-transcribed with several downstream genes involved in lipid or LPS synthesis. Also, OMPs still appeared in fractions of the high density outer membrane fraction after sucrose density centrifugation, while LPS and phospholipids accumulated in the lower density inner membrane fraction, arguing against a role of Omp85 in OMP assembly according to ref. [141]. However, the gene cluster that includes *omp85* also includes *skp*, which codes for the chaperone Skp that is well known for its role in OMP transport [68, 116, 130], but also has a binding site for LPS [133]. Based on the elimination of OMPs from the outer membrane after deletion of the gene for Omp85, it has been proposed that prior to folding, OMPs first insert into a channel formed by the membrane-embedded domain of Omp85, which then laterally opens to allow the stable insertion of

the OMP into the bilayer of the membrane [142]. The proposed role of Omp85 as a translocon-like channel for OMP assembly raises several interesting questions: As has been recently pointed out [143], the lateral opening of the transmembrane channel would involve breaking several hydrogen bonds between the transmembrane β-strands of Omp85, a process that is energetically very unfavorable in the hydrophobic lipid environment of the membrane. If individual β-strands would be released from the Omp85 transmembrane channel, the hydrophilic residues and the polar amide and carbonyl groups of these strands would be exposed to the hydrophobic membrane environment in addition to those of the laterally opened Omp85 channel. On the other hand, the channel would be too small to contain a large β-barrel such as FhuA. Another question would be, how would Omp85 adjust to the large differences in the diameters of the β-barrels of the various OMPs? Further experiments are clearly needed to really clarify possible effects of Omp85 in the stages of structure formation and β-barrel membrane protein integration. Instead of a direct involvement of Omp85 in the structure formation of OMPs, it appears more likely that Omp85 is needed for targeting of the OMPs to the outer membrane. In lack of direct experimental evidence for a role of Omp85 in membrane insertion and structure formation, the proposed translocon-like model for the action of Omp85 currently appears speculative or premature. When folding is analyzed by methods that directly report on the formation of secondary and tertiary structure in OMPs as well as on the degree of membrane insertion, folding and insertion of OMPs definitely also take place in absence of Omp85, by a concerted mechanism that is simply induced by lipid–protein interactions [62, 89, 90].

2.9 Outlook

Although the exploration of insertion and folding of β-barrel membrane proteins into membranes has made progress in recent years, our knowledge about the process is still very limited and many new questions have surfaced with the discovery of OMP targeting and/or folding machineries that exist in the periplasm, and apparently also in the outer membrane [143]. While Skp and SurA were demonstrated to improve membrane insertion and folding of OmpA *in vitro*, these chaperones had no significant effects on the insertion and folding of some other OMPs into preformed lipid bilayers. It will be interesting to note which additional chaperones will be discovered that assist the OMP assembly process in well-defined *in vitro* experiments. It will then be necessary to investigate whether these proteins are directly involved in the generation of structure in OMPs or whether they are key elements for the targeting of OMPs to the surface of the outer membrane, where OMP insertion into the phospholipid bilayer is then mediated by lipid–protein interactions. Some OMPs, e.g. OmpA, do not absolutely require folding machinery for quantitative folding *in vitro* from a urea-denatured state. However, *in vivo*, i.e. in the absence of urea, chaperones such as Skp must prevent the hy-

drophobic collapse and misfolding of OMPs, and deliver them to the outer membrane. In the case of OmpA, insertion and folding appear to be driven by the interaction of a chaperone–OmpA complex with the lipid bilayer and apparently can take place in absence of membrane-integrated proteins that act as folding machinery [68]. The folding kinetics of OmpA *in vitro* greatly depend on the properties of the lipid bilayer. These properties may be modulated by peripherally bound or by intrinsic membrane proteins. Skp, for example, is highly basic and may modulate the surface properties of the periplasmic leaflet of the outer membrane, which contains phosphatidylglycerol that is negatively charged. Future studies on the insertion and folding of β-barrel membrane proteins must therefore also include investigations on how periplasmic proteins modify the properties of the periplasmic surface of the outer membrane. In addition, more detailed information must be obtained on structure formation in OMPs. For example, it is not clear how the polar loops of the OMPs translocate across the hydrophobic core of the bilayer, and what role lipid–protein and protein–protein interactions have in this context.

References

1 G. E. Schulz. *Biochim. Biophys. Acta* **2002**, *1565*, 308–317.
2 D. Marsh, T. Páli. *Biophys. J.* **2001**, *80*, 305–312.
3 A. Arora, F. Abildgaard, J. H. Bushweller, L. K. Tamm. *Nat. Struct. Biol.* **2001**, *8*, 334–338.
4 A. Pautsch, G. E. Schulz. *J. Mol. Biol.* **2000**, *298*, 273–282.
5 J. Vogt, G. E. Schulz. *Struct. Fold. Des.* **1999**, *7*, 1301–1309.
6 C. Fernandez, K. Adeishvili, K. Wüthrich. *Proc. Natl Acad. Sci. USA* **2001**, *98*, 2358–2363.
7 C. Hilty, G. Wider, C. Fernández, K. Wüthrich. *ChemBiochem* **2004**, *5*, 467–473.
8 L. Vandeputte-Rutten, M. P. Bos, J. Tommassen, P. Gros. *J. Biol. Chem.* **2003**, *278*, 24825–24830.
9 P. M. Hwang, W. Y. Choy, E. I. Lo, L. Chen, J. D. Forman-Kay, C. R. Raetz, G. G. Privé, R. E. Bishop, L. E. Kay. *Proc. Natl Acad. Sci. USA* **2002**, *99*, 13560–13565.
10 V. E. Ahn, E. I. Lo, C. K. Engel, L. Chen, P. M. Hwang, L. E. Kay, R. E. Bishop, G. G. Privé. *EMBO J.* **2004**, *23*, 2931–2941.
11 L. Vandeputte-Rutten, R. A. Kramer, J. Kroon, N. Dekker, M. R. Egmond, P. Gros. *EMBO J.* **2001**, *20*, 5033–5039.
12 C. J. Oomen, P. Van Ulsen, P. Van Gelder, M. Feijen, J. Tommassen, P. Gros. *EMBO J.* **2004**, *23*, 1257–1266.
13 H. J. Snijder, I. Ubarretxena-Belandia, M. Blaauw, K. H. Kalk, H. M. Verheij, M. R. Egmond, N. Dekker, B. W. Dijkstra. *Nature* **1999**, *401*, 717–721.
14 B. van den Berg, P. N. Black, W. M. Clemons, Jr., T. A. Rapoport. *Science* **2004**, *304*, 1506–1509.
15 K. Zeth, K. Diederichs, W. Welte, H. Engelhardt. *Struct. Fold. Des.* **2000**, *8*, 981–992.
16 M. S. Weiss, A. Kreusch, E. Schiltz, U. Nestel, W. Welte, J. Weckesser, G. E. Schulz. *FEBS Lett.* **1991**, *280*, 379–382.
17 S. W. Cowan, R. M. Garavito, J. N. Jansonius, J. A. Jenkins, R. Karlsson, N. Konig, E. F. Pai, R. A. Pauptit, P. J. Rizkallah, J. P. Rosenbusch, et al. *Structure* **1995**, *3*, 1041–1050.
18 S. W. Cowan, T. Schirmer, G. Rummel, M. Steiert, R. Ghosh, R. A. Pauptit, J. N. Jansonius, J. P. Rosenbusch. *Nature* **1992**, *358*, 727–733.

19 T. Schirmer, T. A. Keller, Y. F. Wang, J. P. Rosenbusch. *Science* **1995**, *267*, 512–514.

20 D. Forst, W. Welte, T. Wacker, K. Diederichs. *Nat. Struct. Biol.* **1998**, *5*, 37–46.

21 S. K. Buchanan, B. S. Smith, L. Venkatramani, D. Xia, L. Esser, M. Palnitkar, R. Chakraborty, D. van der Helm, J. Deisenhofer. *Nat. Struct. Biol.* **1999**, *6*, 56–63.

22 D. P. Chimento, A. K. Mohanty, R. J. Kadner, M. C. Wiener. *Acta Crystallogr. D Biol. Crystallogr.* **2003**, *59*, 509–511.

23 G. Kurisu, S. D. Zakharov, M. V. Zhalnina, S. Bano, V. Y. Eroukova, T. I. Rokitskaya, Y. N. Antonenko, M. C. Wiener, W. A. Cramer. *Nat. Struct. Biol.* **2003**, *10*, 948–954.

24 A. D. Ferguson, E. Hofmann, J. W. Coulton, K. Diederichs, W. Welte. *Science* **1998**, *282*, 2215–2220.

25 K. P. Locher, B. Rees, R. Koebnik, A. Mitschler, L. Moulinier, J. P. Rosenbusch, D. Moras. *Cell* **1998**, *95*, 771–778.

26 S. Conlan, Y. Zhang, S. Cheley, H. Bayley. *Biochemistry* **2000**, *39*, 11845–11854.

27 V. Koronakis, A. Sharff, E. Koronakis, B. Luisi, C. Hughes. *Nature* **2000**, *405*, 914–919.

28 W. C. Wimley. *Protein Sci.* **2002**, *11*, 301–312.

29 W. C. Wimley. *Curr. Opin. Struct. Biol.* **2003**, *13*, 404–411.

30 L. Song, M. R. Hobaugh, C. Shustak, S. Cheley, H. Bayley, J. E. Gouaux. *Science* **1996**, *274*, 1859–1866.

31 A. P. Heuck, E. M. Hotze, R. K. Tweten, A. E. Johnson. *Mol. Cell.* **2000**, *6*, 1233–1242.

32 L. A. Shepard, A. P. Heuck, B. D. Hamman, J. Rossjohn, M. W. Parker, K. R. Ryan, A. E. Johnson, R. K. Tweten. *Biochemistry* **1998**, *37*, 14563–14574.

33 G. Menestrina, M. Dalla Serra, M. Comai, M. Coraiola, G. Viero, S. Werner, D. A. Colin, H. Monteil, G. Prevost. *FEBS Lett* **2003**, *552*, 54–60.

34 M. Montoya, E. Gouaux. *Biochim. Biophys. Acta.* **2003**, *1609*, 19–27.

35 A. P. Heuck, R. K. Tweten, A. E. Johnson. *Biochemistry* **2001**, *40*, 9065–9073.

36 M. Faller, M. Niederweis, G. E. Schulz. *Science* **2004**, *303*, 1189–1192.

37 M. Niederweis. *Mol. Microbiol.* **2003**, *49*, 1167–1177.

38 T. Haltia, E. Freire. *Biochim. Biophys. Acta* **1995**, *1241*, 295–322.

39 C. S. Klug, W. Su, J. Liu, P. E. Klebba, J. B. Feix. *Biochemistry* **1995**, *34*, 14230–14236.

40 J. A. Schellman. *Biopolymers* **1978**, *17*, 1235–1248.

41 C. N. Pace. *Methods Enzymol.* **1986**, *131*, 266–280.

42 F. Ahmad, C. C. Bigelow. *J. Biol. Chem.* **1982**, *257*, 12935–12938.

43 M. Yao, D. W. Bolen. *Biochemistry* **1995**, *34*, 3771–3781.

44 H. Hong, L. K. Tamm. *Proc. Natl Acad. Sci. USA* **2004**, *101*, 4065–4070.

45 D. Shortle. *Adv. Protein Chem.* **1995**, *46*, 217–247.

46 J. K. Myers, C. N. Pace, J. M. Scholtz. *Protein Sci* **1995**, *4*, 2138–2148.

47 C. N. Pace, K. E. Vanderburg. *Biochemistry* **1979**, *18*, 288–292.

48 L. Serrano, A. Horovitz, B. Avron, M. Bycroft, A. R. Fersht. *Biochemistry* **1990**, *29*, 9343–9352.

49 C. S. Klug, J. B. Feix. *Protein Sci.* **1998**, *7*, 1469–1476.

50 J. H. Kleinschmidt, M. C. Wiener, L. K. Tamm. *Protein Sci.* **1999**, *8*, 2065–2071.

51 T. Surrey, F. Jähnig. *Proc. Natl. Acad. Sci. USA* **1992**, *89*, 7457–7461.

52 T. Surrey, F. Jähnig. *J. Biol. Chem.* **1995**, *270*, 28199–28203.

53 J. A. Szule, N. L. Fuller, R. P. Rand. *Biophys. J.* **2002**, *83*, 977–984.

54 M. Bonhivers, M. Desmadril, G. S. Moeck, P. Boulanger, A. Colomer-Pallas, L. Letellier. *Biochemistry* **2001**, *40*, 2606–2613.

55 M. Schweizer, I. Hindennach, W. Garten, U. Henning. *Eur. J. Biochem.* **1978**, *82*, 211–217.

56 K. Dornmair, H. Kiefer, F. Jähnig. *J. Biol. Chem.* **1990**, *265*, 18907–18911.

57 K. S. Huang, H. Bayley, M. J. Liao, E. London, H. G. Khorana. *J. Biol. Chem.* **1981**, *256*, 3802–3809.

58 C. B. Anfinsen. *Science* **1973**, *181*, 223–230.

59 H. de Cock, J. Tommassen. *EMBO J.* **1996**, *15*, 5567–5573.

60 C. Jansen, M. Heutink, J. Tommassen, H. de Cock. *Eur. J. Biochem.* **2000**, *267*, 3792–3800.

61 N. A. Rodionova, S. A. Tatulian, T. Surrey, F. Jähnig, L. K. Tamm. *Biochemistry* **1995**, *34*, 1921–1929.

62 J. H. Kleinschmidt, L. K. Tamm. *J. Mol. Biol.* **2002**, *324*, 319–330.

63 T. Surrey, A. Schmid, F. Jähnig. *Biochemistry* **1996**, *35*, 2283–2288.

64 S. Conlan, H. Bayley. *Biochemistry* **2003**, *42*, 9453–9465.

65 S. K. Buchanan. *Curr. Opin. Struct. Biol.* **1999**, *9*, 455–461.

66 U. K. Laemmli. *Nature* **1970**, *227*, 680–685.

67 J. H. Kleinschmidt, L. K. Tamm. *Biochemistry* **1996**, *35*, 12993–13000.

68 P. V. Bulieris, S. Behrens, O. Holst, J. H. Kleinschmidt. *J. Biol. Chem.* **2003**, *278*, 9092–9099.

69 J. H. Kleinschmidt. *Cell. Mol. Life Sci.* **2003**, *60*, 1547–1558.

70 K. P. Locher, J. P. Rosenbusch. *Eur. J. Biochem.* **1997**, *247*, 770–775.

71 M. Behlau, D. J. Mills, H. Quader, W. Kühlbrandt, J. Vonck. *J. Mol. Biol.* **2001**, *305*, 71–77.

72 H. Vogel, F. Jähnig. *J. Mol. Biol.* **1986**, *190*, 191–199.

73 A. Arora, D. Rinehart, G. Szabo, L. K. Tamm. *J. Biol. Chem.* **2000**, *275*, 1594–1600.

74 R. Freudl, H. Schwarz, Y. D. Stierhof, K. Gamon, I. Hindennach, U. Henning. *J. Biol. Chem.* **1986**, *261*, 11355–11361.

75 S. J. Alvis, I. M. Williamson, J. M. East, A. G. Lee. *Biophys. J.* **2003**, *85*, 3828–3838.

76 A. S. Ladokhin. *Anal. Biochem.* **1999**, *276*, 65–71.

77 T. Markello, A. Zlotnick, J. Everett, J. Tennyson, P. W. Holloway. *Biochemistry* **1985**, *24*, 2895–2901.

78 E. J. Bolen, P. W. Holloway. *Biochemistry* **1990**, *29*, 9638–9643.

79 J. Everett, A. Zlotnick, J. Tennyson, P. W. Holloway. *J. Biol. Chem.* **1986**, *261*, 6725–6729.

80 I. M. Williamson, S. J. Alvis, J. M. East, A. G. Lee. *Biophys. J.* **2002**, *83*, 2026–2038.

81 A. S. Ladokhin, P. W. Holloway. *Biophys. J.* **1995**, *69*, 506–517.

82 A. S. Ladokhin. *Biophys. J.* **1999**, *76*, 946–955.

83 M. E. Fastenberg, H. Shogomori, X. Xu, D. A. Brown, E. London. *Biochemistry* **2003**, *42*, 12376–12390.

84 B. Piknova, D. Marsh, T. E. Thompson. *Biophys. J.* **1997**, *72*, 2660–2668.

85 F. S. Abrams, E. London. *Biochemistry* **1993**, *32*, 10826–10831.

86 M. J. Prieto, M. Castanho, A. Coutinho, A. Ortiz, F. J. Aranda, J. C. Gómez-Fernandéz. *Chem. Phys. Lipids* **1994**, *69*, 75–85.

87 A. Cruz, C. Casals, I. Plasencia, D. Marsh, J. Pérez-Gil. *Biochemistry* **1998**, *37*, 9488–9496.

88 F. S. Abrams, E. London. *Biochemistry* **1992**, *31*, 5312–5322.

89 J. H. Kleinschmidt, T. den Blaauwen, A. Driessen, L. K. Tamm. *Biochemistry* **1999**, *38*, 5006–5016.

90 J. H. Kleinschmidt, L. K. Tamm. *Biochemistry* **1999**, *38*, 4996–5005.

91 T. J. McIntosh, P. W. Holloway. *Biochemistry* **1987**, *26*, 1783–1788.

92 M. C. Wiener, S. H. White. *Biochemistry* **1991**, *30*, 6997–7008.

93 A. Chattopadhyay, E. London. *Biochemistry* **1987**, *26*, 39–45.

94 A. Pautsch, G. E. Schulz. *Nat. Struct. Biol.* **1998**, *5*, 1013–1017.

95 M. Ramakrishnan, C. L. Pocanschi, J. H. Kleinschmidt, D. Marsh. *Biochemistry* **2004**, *43*, 11630–11636.

96 D. Marsh, L. I. Horváth. *Biochim. Biophys. Acta* **1998**, *1376*, 267–296.

97 J. H. Kleinschmidt, G. L. Powell, D. Marsh. *Biochemistry* **1998**, *37*, 11579–11585.

98 J. E. Mahaney, J. Kleinschmidt, D. Marsh, D. D. Thomas. *Biophys. J.* **1992**, *63*, 1513–1522.

99 M. B. Sankaram, P. J. Brophy, D. Marsh. *Biochemistry* **1991**, *30*, 5866–5873.

100 M. Ramakrishnan, J. Qu, C. L. Pocanschi, J. H. Kleinschmidt, D. Marsh. *Biochemistry* **2005**, *44*, 3515–3523.

101 A. D. Ferguson, W. Welte, E. Hofmann, B. Lindner, O. Holst, J. W. Coulton, K. Diederichs. *Structure* **2000**, *8*, 585–592.

102 L. Steeghs, H. de Cock, E. Evers, B. Zomer, J. Tommassen, P. van der Ley. *EMBO J.* **2001**, *20*, 6937–6945.

103 P. van der Ley, L. Steeghs. *J. Endotoxin Res.* **2003**, *9*, 124–128.

104 K. Brandenburg, P. Garidel, A. B. Schromm, J. Andrä, A. Kramer, M. Egmond, A. Wiese. *Eur. Biophys. J.* **2005**, *34*, 28–41.

105 R. A. Kramer, K. Brandenburg, L. Vandeputte-Rutten, M. Werkhoven, P. Gros, N. Dekker, M. R. Egmond. *Eur. J. Biochem.* **2002**, *269*, 1746–1752.

106 T. Páli, D. Marsh. *Biophys. J.* **2001**, *80*, 2789–2797.

107 S. Grizot, S. K. Buchanan. *Mol. Microbiol.* **2004**, *51*, 1027–1037.

108 S. Arnott, S. D. Dover, A. Elliott. *J. Mol. Biol.* **1967**, *30*, 201–208.

109 A. G. Lee. *Biochim. Biophys. Acta* **2003**, *1612*, 1–40.

110 A. H. O'Keeffe, J. M. East, A. G. Lee. *Biophys. J.* **2000**, *79*, 2066–2074.

111 B. A. Lewis, D. M. Engelman. *J. Mol. Biol.* **1983**, *166*, 211–217.

112 R. Koebnik. *J. Mol. Biol.* **1999**, *285*, 1801–1810.

113 R. Koebnik. *EMBO J.* **1996**, *15*, 3529–3537.

114 R. Koebnik, L. Krämer. *J. Mol. Biol.* **1995**, *250*, 617–626.

115 H. de Cock, S. van Blokland, J. Tommassen. *J. Biol. Chem.* **1996**, *271*, 12885–12890.

116 U. Schäfer, K. Beck, M. Müller. *J. Biol. Chem.* **1999**, *274*, 24567–24574.

117 M. Müller, H. G. Koch, K. Beck, U. Schäfer. *Prog Nucleic Acid Res. Mol. Biol.* **2001**, *66*, 107–157.

118 E. H. Manting, A. J. Driessen. *Mol. Microbiol.* **2000**, *37*, 226–238.

119 P. N. Danese, T. J. Silhavy. *Annu. Rev. Genet.* **1998**, *32*, 59–94.

120 S. W. Lazar, R. Kolter. *J. Bacteriol.* **1996**, *178*, 1770–1773.

121 P. E. Rouvière, C. A. Gross. *Genes Dev.* **1996**, *10*, 3170–3182.

122 S. Behrens, R. Maier, H. de Cock, F. X. Schmid, C. A. Gross. *EMBO J.* **2001**, *20*, 285–294.

123 D. Missiakas, J. M. Betton, S. Raina. *Mol. Microbiol.* **1996**, *21*, 871–884.

124 K. Ramm, A. Plückthun. *J. Biol. Chem.* **2000**, *275*, 17106–17113.

125 H. Bothmann, A. Plückthun. *J. Biol. Chem.* **2000**, *275*, 17100–17105.

126 K. Ramm, A. Plückthun. *J. Mol. Biol.* **2001**, *310*, 485–498.

127 J. Liu, C. T. Walsh. *Proc. Natl Acad. Sci. USA* **1990**, *87*, 4028–4032.

128 N. Harms, G. Koningstein, W. Dontje, M. Müller, B. Oudega, J. Luirink, H. de Cock. *J. Biol. Chem.* **2001**, *276*, 18804–18811.

129 H. Bothmann, A. Plückthun. *Nat. Biotechnol.* **1998**, *16*, 376–380.

130 R. Chen, U. Henning. *Mol. Microbiol.* **1996**, *19*, 1287–1294.

131 H. de Cock, U. Schäfer, M. Potgeter, R. Demel, M. Müller, J. Tommassen. *Eur. J. Biochem.* **1999**, *259*, 96–103.

132 M. Schlapschy, M. K. Dommel, K. Hadian, M. Fogarasi, I. P. Korndörfer, A. Skerra. *Biol. Chem.* **2004**, *385*, 137–143.

133 T. A. Walton, M. C. Sousa. *Mol. Cell* **2004**, *15*, 367–374.

134 I. P. Korndörfer, M. K. Dommel, A. Skerra. *Nat. Struct. Mol. Biol.* **2004**, *11*, 1015–1020.

135 E. Bitto, D. B. McKay. *Structure* **2002**, *10*, 1489–1498.

136 A. E. Rizzitello, J. R. Harper, T. J. Silhavy. *J. Bacteriol.* **2001**, *183*, 6794–6800.

137 J. Werner, A. M. Augustus, R. Misra. *J. Bacteriol.* **2003**, *185*, 6540–6547.

138 R. Voulhoux, M. P. Bos, J. Geurtsen, M. Mols, J. Tommassen. *Science* **2003**, *299*, 262–265.

139 S. A. Paschen, T. Waizenegger, T. Stan, M. Preuss, M. Cyrklaff, K. Hell, D. Rapaport, W. Neupert. *Nature* **2003**, *426*, 862–866.

140 T. Waizenegger, S. J. Habib, M. Lech, D. Mokranjac, S. A. Paschen, K. Hell, W. Neupert, D. Rapaport. *EMBO Rep.* **2004**, *5*, 704–709.

141 S. Genevrois, L. Steeghs, P. Roholl, J. J. Letesson, P. van der Ley. *EMBO J.* **2003**, *22*, 1780–1789.

142 R. Voulhoux, J. Tommassen. *Res. Microbiol.* **2004**, *155*, 129–135.

143 A. E. Johnson, R. E. Jensen. *Nat. Struct. Mol. Biol.* **2004**, *11*, 113–114.

144 L. Heins, H. Mentzel, A. Schmid, R. Benz, U. K. Schmitz. *J. Biol. Chem.* **1994**, *269*, 26402–26410.

145 R. Koradi, M. Billeter, K. Wüthrich. *J. Mol. Graph.* **1996**, *14*, 51–55, 29–32.

146 N. Guex, M.C. Peitsch. *Electrophoresis* **1997**, *18*, 2714–2723.

147 T. Schwede, J. Kopp, N. Guex, M.C. Peitsch. *Nucleic Acids Res.* **2003**, *31*, 3381–3385.

148 E. Bitto, D.B. McKay. *J. Biol. Chem.* **2003**, *278*, 49316–49322.

149 W.L. Delano. *The PyMOL User's Manual.* DeLano Scientific, San Carlos, CA, **2002**.

3
A Paradigm of Membrane Protein Folding: Principles, Kinetics and Stability of Bacteriorhodopsin Folding

Paula J. Booth

3.1
Introduction

Bacteriorhodopsin is one of the most intensively studied integral membrane proteins. The stability of the protein, together with the ease of obtaining large amounts of pure protein, made it a center of attention after its discovery over 30 years ago. The deceptively simple, but very efficient, process of light-driven proton transport by bacteriorhodopsin meant it also rapidly became the subject of intensive research into the mechanism of ion transport. As a result, bacteriorhodopsin has provided the highest-resolution structures of ground and intermediate states involved in any membrane transport process. Such milestones are due to the ability to develop new technologies using bacteriorhodopsin as a test bed and many techniques that are in use today were originally initiated on bacteriorhodopsin. There are numerous examples: it was the first integral membrane protein on which extensive mutagenesis was carried out [1–3], two-dimensional electron crystallography was applied initially to the naturally occurring two-dimensional lattice of bacteriorhodopsin in its native membrane [4] and ultrafast time-resolved optical methods developed apace to probe the dynamics of the protein-pumping reaction [5–8]. The development of this array of tools was possible due to the ease of handling bacteriorhodopsin – a factor that naturally led to this membrane protein becoming pivotal in studies of membrane protein folding [9, 10]. Bacteriorhodopsin was the first integral membrane protein to be fully unfolded and refolded *in vitro*, a feat achieved in the early 1980s [9, 11]. Bacteriorhodopsin remains the only transmembrane α-helical protein that can be manipulated in this manner.

Bacteriorhodopsin consists of an apoprotein, bacterio-opsin together with a retinal cofactor. The protein folds to a tightly packed bundle of seven transmembrane α-helices (referred to as helices A–G, see Fig. 3.1) with retinal bound covalently within the helix bundle, through a Schiff base link to a Lys residue on helix G [12]. It is the only protein constituent of the purple membrane of *Halobacterium salinarium*, where it exists as a hexagonal array of trimers [13, 14].

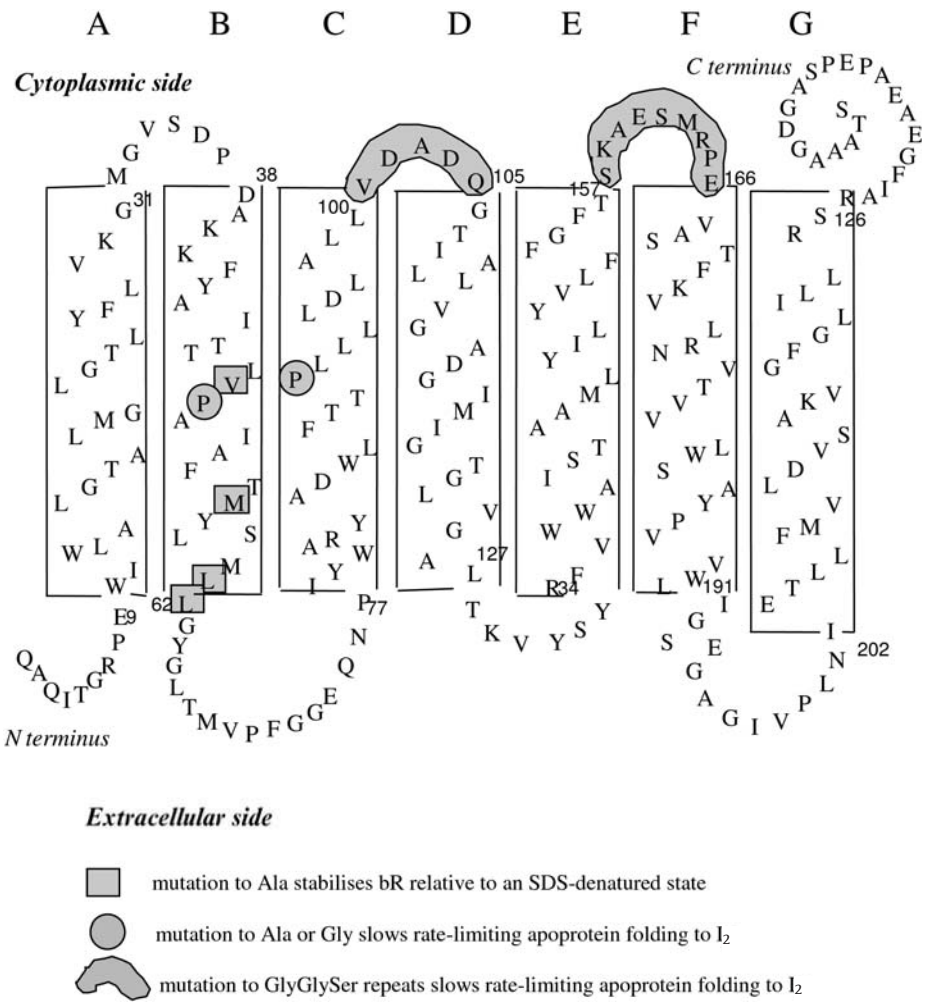

Fig. 3.1 Two-dimensional representation of the secondary structure of bacteriorhodopsin showing the amino acid sequence. Boxed regions approximate the regions of transmembrane α helices. Some of the mutations referred to in the text are highlighted together with their effect on particular aspects of folding.

Studies on the folding of bacteriorhodopsin range from *in vitro* kinetic and stability studies on the mature polypeptide in detergents, lipids or the native membrane to cotranslational investigations in the native environment (for detailed reviews, see [15, 16]). A common theme of the studies that will be discussed in this chapter is the identification of intermediates states and determination of reaction mechanisms. Bacteriorhodopsin has led the field in this respect and has given us the clearest picture of the forces stabilizing an integral

membrane helical protein. As ever, the protein has been the testing ground for methods that are now beginning to be translated to other proteins. The methods for measuring *in vitro* folding kinetics have successfully been applied to other membrane proteins and single-molecule studies on the unfolding of the protein are now being applied to more complex transport proteins.

3.2 Principles of Transmembrane α-Helical Membrane Protein Folding: A Thermodynamic Model for Bacteriorhodopsin

Experiments on bacteriorhodopsin were one of the dominating factors behind the "two-stage" model developed in 1990 by Popot and Engelman [17]. The first stage of this model involves insertion and formation of transmembrane helices, which can be considered as stable, folding domains. The second stage involves the interaction of these preformed helices to form the folded protein. This is a thermodynamic model, which does not necessarily represent an *in vitro* or *in vivo* mechanism for folding. Folding of helical membrane proteins, including bacteriorhodopsin, is unlikely to be this simple and indeed work on bacteriorhodopsin itself shows that the individual helices of the protein are not necessarily independently stable in lipid bilayers [18]. The two-stage model has recently been extended to accommodate additional complexity in folding [19]. A third stage has been suggested for the folding of helix-connecting loops or cofactor binding, after critical helix interactions have occurred. These additional steps have been identified in bacteriorhodopsin. It had, for example, been known for some time that the bacteriorhodopsin polypeptide could fold to attain the native helix content in the absence of retinal, and that retinal binding required this initial apoprotein folding [9, 11]. The helix-connecting loops of bacteriorhodopsin also contribute to the efficient folding and stability of the protein [20, 21].

The two (or three)-stage model provides a framework from which to approach helical protein folding in membranes. An important feature postulated by the model is that there will be stable entities or intermediate states of helical membrane proteins. These states can be used as starting points in kinetic or reversible folding experiments. The intermediate states do not necessarily contain independent helices of the protein as predicted directly from the model; however a core helical content may be necessary for the protein to fold upon. This is reflected in some of the early experiments used to develop the two-stage model. Protein fragments, where the protein is cut in a helix-connecting loop, of bacteriorhodopsin can fold to a native-like, functional state [22, 23]. This shows that certain helix connections are not absolutely required for protein folding and that helix–helix interactions play a key role. A more comprehensive study of this phenomenon followed, whereby all two to five helix fragments of bacteriorhodopsin were overexpressed and their ability to associate and bind retinal was tested [24]. All pairs of complementary fragments (AB and C–G; A–C and D–G; A–D and E–G; A–E and FG: see Fig. 3.1) could assemble to give a functional state. However, not all

the fragments could fold correctly on their own. Notably, the C-terminal fragments (E–G and FG) folded to structures with low helix content, with the FG fragment containing about 20% β structure. This suggests that the first five helices of bacteriorhodopsin (A–E) may be able to fold according to the two-stage model, but the last two helices are probably stabilized by interaction with a preformed five-helix core. Other experiments on bacteriorhodopsin have involved the measurement of the kinetics and thermodynamics of folding from a sodium dodecylsulfate (SDS)-denatured state of the protein [25, 26]. A strong oxidizing organic acid, such as trifluoroethanoic acid, is required to denature bacterio-opsin fully. Transfer of this acid-denatured state into SDS turned out to be a crucial step in the refolding of the protein [11]. SDS induces helical structure in most proteins and the SDS state of bacterio-opsin has just over half the native-helix content [9, 27]. Precisely which parts of the protein are helical is unknown, but it seems likely that much of the A and B helices are formed in SDS. This is very likely to represent the critical core of helical structure that is necessary for refolding, which is in line with the ideas of the two-stage model, as discussed earlier. This function of SDS to stabilize a core helix content could also be the reason why it enables folding of other helical membrane proteins as well as bacteriorhodopsin [28, 29].

The emphasis of the two-stage model on helix, helix interactions has led to several advances in the understanding of factors stabilizing helical membrane proteins as well as driving the specific helix interactions required in protein folding. One of the most influential studies has been that on the glycophorin dimer which led to the identification of the GlyxxxGly dimerization motif [30]. Glycophorin has a single transmembrane helix, but forms an unusually stable dimer with a very specific interaction between the transmembrane helices of the monomers. Saturation mutagenesis of the transmembrane helix led to the identification of this dimerization motif involving Gly residues, which enable close backbone contacts between the two helices. This motif has since been found in other membrane proteins and has led to considerable interest in the GlyxxxGly motif as a framework for transmembrane helix association. Other studies in this area have investigated the role of polar interactions in helix association, especially Asn residues and hydrogen bonds to Cα backbone atoms [31].

3.3 Bacteriorhodopsin Stability

Bacteriorhodopsin is a very stable protein. The native environment in the purple membrane of *H. salinarium* is a hexagonal array of protein trimers. Some of the factors contributing to this stability have been investigated, e.g. helix interactions between different monomers [32]. Calorimetric studies have found that the protein unfolds irreversibly from this trimeric state at around 95 °C [33], while the monomeric protein in detergent/lipid micelles denatures at around 70 °C [34]. In both cases a similar enthalpy contribution has been estimated (of around +400 kJ mol^{-1} for the unfolding), with only a relatively small contri-

bution (around –20 kJ mol^{-1}) to the overall stability of the protein in purple membrane coming from the hexagonal lattice and trimer interactions [35].

The following sections focus on investigations into the stability of bacteriorhodopsin monomers.

3.3.1 Side-chain Contributions to Helix Interactions and the Role of Pro

Thermodynamic studies on bacteriorhodopsin have centered on the reversible unfolding that is possible with an SDS-denatured state. The pioneering studies of Khorana's laboratory in the 1980s first showed the requirement of SDS to refold bacteriorhodopsin from a fully denatured state in trifluoroacetic acid. Many seminal papers in the folding field emerged from Khorana's lab during this decade, based on folding the SDS state into mixed lipid/detergent [L-*α*-1,2-dimyristoylphosphatidylcholine (DMPC)/{3-[(3-cholamidopropyl)dimethylammonio-1-propanesulfonate} (CHAPS)] micelles (see, e.g. [1, 2, 9, 11, 36–43]). Bowie et al. have recently used this reversible SDS refolding approach in a further study on the thermodynamic stability of bacteriorhodopsin [44]. This recent report by Bowie investigated the contributions that side-chains of helix B make to the stability of bacteriorhodopsin. Sites throughout this helix were mutated in turn to Ala and the contribution to the free energy of formation of bacteriorhodopsin from an SDS denatured state was determined. This free energy change was determined from equilibrium denaturation curves where purple membrane samples were denatured in different concentrations of SDS. Helix B was chosen for the Ala stability scan because this helix makes the least interactions of all the helices with the retinal cofactor, and thus helix B is more likely to reveal helix–helix interactions rather than helix–retinal interactions. This study gives us one of the most detailed insights to date on specific contributions to membrane protein stability with several new findings. Ala substitutions in the middle of helix B, especially those pointing towards other helices, or into the helical bundle of bacteriorhodopsin, destabilized the protein. An interesting correlation was found with the area of the mutated side-chain and the change in free energy. The protein was stabilized to the same extent as a water-soluble protein, per unit area of side-chain buried during folding. This is somewhat unexpected, since side-chain burial in water-soluble proteins is related to the hydrophobic effect as non-polar groups are removed from the surrounding water. Furthermore, there is little difference in the free energy contribution per unit area of side-chain buried between polar or apolar residues in bacteriorhodopsin, implying a dominant role for van der Waals forces in the protein stability. Another intriguing result from the work was that four of the Ala mutations (Lys61Ala and Lys62Ala at the extracellular side of the helix, as well as Val49A and Met56Ala) stabilized the folding state, although this may result from alterations in the unfolded rather than folded state. Nevertheless, stabilizing mutations have been found before in membrane proteins [45], which suggests that the proteins may not be optimized for stability in the membrane.

The Ala scan of bacteriorhodopsin stability also produced another somewhat unexpected result from the mutation of the Pro in the centre of helix B (Pro50) to Ala (see Fig. 3.1). Pro in transmembrane helices invariably cause kinks in the helices and Pro50 was thought to be the cause of the kink seen in the helix B. Thus, the removal of Pro50 could be expected to destabilize the folded state. However, the substitution of this Pro by Ala had no effect on stability. Moreover, a crystal structure of the Pro50Ala mutant revealed that helix B has the same kink in both wild-type and mutant. It therefore seems that other tertiary contacts stabilize the helix distortion, rather than Pro alone. Mutation of this Pro on helix B, as well as the Pro in the centre of helix C, to Ala or Gly, does affect the rate of bacteriorhodopsin folding [46]. The rate-limiting folding step of bacterio-opsin results in formation of an intermediate state that contains seven transmembrane helices, and is a critical state for retinal binding. The mutation of either Pro in helix B or C (see Fig. 3.1) slows this rate-limiting folding step. Thus the Pro residues could lower the transition state barrier to folding by aiding formation of inter-helix contacts that contribute to the helix kink.

3.3.2 Helix-connecting Loops

The two-stage model for folding emphasizes the inherent stability of transmembrane helices and the role of helix association in driving folding, with helix-connecting loops playing a minor part. Over the years, however, the contribution of these loops to the specificity and stability of the final protein fold has begun to emerge. Early studies focused on a break in the protein in the loop between helices B and C, since this could be achieved relatively easily by protease digestion [22, 23]. The resulting AB and C–G fragments re-associated and bound retinal efficiently to form a functional protein. A calorimetric study of the protein in native purple membrane with this cut in the BC loop revealed a decrease in the unfolding enthalpy of about 180 kJ mol^{-1}, showing the loop does make a significant contribution to protein stability and it was concluded this contribution has an entropic as well as enthalpic origin [21, 47]. The BC loop seems to have some β-sheet structure, while the CD, DE and FG loops show order in the crystal structures, and the remaining AB and EF loops seem to be more disordered [12, 48–50]. The contribution of each helix-connecting loop in the protein has since been assessed in a more detailed study where each loop in turn was mutated to a structureless linker consisting of repeat Gly–Gly–Ser sequences of the same length as the original loop (see Fig. 3.1) [20]. As predicted from the earlier studies on bacteriorhodopsin fragments, all the mutant bacteriorhodopsins with these changes in one of their loops could fold to a functional state. The stability of the folded bacterio-opsin, apoprotein state, in detergent/lipid micelles (i.e. with native helix content, but no retinal) was determined over time for each loop mutant. In addition, the stability of fully folded bacteriorhodopsin (with correctly bound retinal) was assessed by resistance to denaturation in SDS. All of the loop mutants, except those with changes in the DE and BC loop, were

found to destabilize the protein in both the apoprotein and bacteriorhodopsin states (although changes in the BC loop caused a blue-shifted retinal chromophore band, dependent on conditions). The mutations to the cytoplasmic AB, CD and EF loops decreased the stability of the protein to the same extent in the bacteriorhodopsin state, while the AB mutant was slightly more stable than the CD and EF mutants in the apoprotein state. The extracellular FG loop made different contributions to protein stability depending on whether retinal was bound or not. The FG loop mutant was more stable than the three cytoplasmic loop mutants in the apoprotein state, but the least stable mutant in the bacteriorhodopsin state. Overall these results therefore indicate that the inter-helix loop connections, particularly AB, CD, EF and FG, stabilize the partly and fully folded states of the protein and do not act as merely as covalent linkers to keep the helices in close proximity. A study of the folding kinetics of these loop mutants suggested that the CD and EF loops may contribute to the transition state for rate-limiting folding of the apoprotein, while the FG loop is involved in final folding and covalent retinal binding [51].

3.4
Pulling the Protein Out of the Membrane

Intriguing results have emerged from dynamic force spectroscopy studies on bacteriorhodopsin [52]. This technique involves pulling bacteriorhodopsin out of the native purple membrane by attaching the protein to an atomic force microscope tip. Individual proteins can be pulled out of the array within the membrane and seem to uncoil as they do so. The method enables the force required to extend the polypeptide by a certain amount to be measured, at a particular applied force. The magnitude of the applied force is important, since the dissociation time of the bond being broken depends critically on how fast a force is applied to it [53]. Several studies have now appeared on globular, water-soluble proteins that are forging a way ahead in this field [54–56]. Bacteriorhodopsin has provided the first application of forced unfolding to a membrane protein. A range of different force–extension curves (for a constant loading rate of applied force) are observed for bacteriorhodopsin, taken as evidence that different molecules unfold by different pathways [52, 57, 58]. Selecting those molecules that are seen to extend to the full length predicted for totally unfolded bacteriorhodopsin (i.e. a fully extended bacteriorhodopsin polypeptide) gives some deceptively simple results. The protein seems to unfold stepwise, with the helices unfolding and being pulled from the membrane sequentially. Moreover, the results can be fit to a simple model involving a two state transition between folded and fully extended polypeptide. The experiments are carried out with the extracellular surface of the protein adhered to a mica surface while the protein is pulled from the cytoplasmic C-terminus. The majority of peaks in the force–extension curves are assigned to helices leaving the membrane in pairs. However, additional peaks can just be resolved in the data that seem to correspond to the helices and loops also unfolding individually in a

significant proportion of molecules. Thus, although helices G and F (together with the FG loop) are pulled out of the membrane together, peaks are also seen in the force curve that fit to a model whereby helix G unfolds first. This unfolding of G is followed by another peak that could correspond to the extracellular FG loop stretching and being pulled into the membrane, then helix F unfolds and is pulled out of the membrane together with the cytoplasmic EF loop [58] (see Fig. 3.1). Similar peaks patterns are seen for the other helix pairs, indicating that the extracellular loops present a barrier to unfolding, while the cytoplasmic loops do not. The barriers perhaps then reflect the fact that whilst both types of loops are hydrophilic, only the extracellular ones have to be pulled through the hydrophobic membrane.

These forced unfolding experiments give information on the force required to pull a helix out of the membrane and the data are interpreted as extending the helix in the membrane before/during pulling it out. This pulling process therefore requires the breaking of helix–helix interactions and helix–retinal interactions, as well as backbone hydrogen bonds within the helix so that the helix can fully extend and is then pulled through the membrane and out. The method does not appear to be particularly sensitive to lateral, helix–helix interactions, possibly because the breaking of backbone hydrogen bonds and subsequent exposure of the polar peptide bonds to the membrane interior, together with pulling side-chains through the hydrophobic interior, pose larger energetic barriers. The method of pulling from the C-terminus also favors the helices emerging in pairs, i.e. pulling and extending two helices together with their connecting loop (that initially starts on the opposite side of the membrane) until the next loop is reached that does not have to go through the membrane. The same type of pairwise helix unfolding has also been seen when a different membrane protein, a 12-helix sodium-proton antiporter is pulled out of reconstituted two-dimensional crystal samples [59].

3.5 Bacteriorhodopsin Folding Kinetics

Bacteriorhodopsin has provided an incredible opportunity to study the folding mechanism of an integral membrane protein. Kinetic studies are required to determine the underlying folding mechanism. The kinetics of bacteriorhodopsin folding or assembly have been investigated in several environments, ranging from *in vitro* cotranslation off the ribosome and mature protein assembly in the native membrane to folding from a denatured state into artificial detergent or lipid systems (for reviews, see [15, 16, 25, 60]). Much of this work has been possible as a result of the remarkable feats of two groups in the 1970s and 1980s that placed folding studies of bacteriorhodopsin in a unique position. Following on from the successful isolation of bacteriorhodopsin [13, 61], Oesterhelt went on to show that binding of the retinal cofactor in a native purple membrane environment was reversible [62]. Since then a sequence of detailed studies on

this retinal binding event and the associated protein structural changes have emerged (e.g. [63–67] and see [16]). Meanwhile Khorana et al. used bacteriorhodopsin to demonstrate for the first time that a membrane protein could be refolded from a denatured state *in vitro* [9, 11]. This led to the development of a successful overexpression system for the protein in *Escherichia coli* [2, 37, 41, 68, 69], and the exchange of every amino acid in the protein for folding, stability and functional work well ahead of any other helical membrane protein. The demonstration of refolding by Khorana was also instrumental in the development of a series of methods to probe the folding mechanism by detailed kinetic studies *in vitro* [25, 70].

3.5.1
Cotranslational Insertion

There is little detail on bacteriorhodopsin insertion and folding *in vivo*. Elegant studies on the active translation of the protein *in vivo* are consistent with polypeptide insertion and folding occurring cotranslationally as the protein comes off the ribosome [71, 72]. Halobacteria also appear to contain a signal recognition-like particle that may be involved in translation and insertion of membrane-associated proteins. This possible insertion mechanism of bacteriorhodopsin is thus in line with cotranslational insertion of many other polytopic membrane proteins via secretory translocase machinery.

The active translation studies took advantage of the accessibility of the extracellular side of the protein to external reagents. Halobacterial strains were created with a unique cysteine in the N-terminal extracellular domain or one of the extracellular loops [71]. The translocation of these regions across the membrane, during translation, was then detected by derivatizing the cysteine with a membrane impermeant compound. Almost 80 amino acids were found to have been synthesized before the N-terminal cysteine was translocated, showing that the N-terminus inserts cotranslationally [72]. The results from the cysteine substitutions in the other extracellular loops showed that the N-terminal domain, the BC loop and the FG loop are translocated in order from the N-terminus to the C-terminus, with the FG loop being translocated post-translationally. Overall the results suggest that cotranslational insertion and folding of the N-terminal, A helix aids folding of the remaining helices. This is also consistent with the results from the *in vitro* folding and fragment work discussed earlier where the A and B helices, or an A–E fragment, seem to facilitate folding of the remainder of the protein.

3.5.2
Retinal Binding Studies to Apomembrane

Extensive biophysical studies have been carried out on retinal binding to apoprotein in membrane samples [13, 16, 62, 66, 67, 73]. This latter apoprotein membrane state is formed either by bleaching purple membrane or from a retinal deficient bacterial strain. The apomembrane contains bacterio-opsin that is

probably arranged in trimers, but lacks the characteristic crystalline array of purple membrane. The protein secondary structure in the apomembrane and purple membrane states seems to be very similar. The tertiary structures of the apomembrane state has not been investigated in detail, but significant tilting of the helices from the membrane normal has been noted in this state [74]. Formation of purple membrane is achieved either by addition of all-*trans* retinal to the apomembrane or by photoisomerization of 9-*cis* retinal already non-covalently bound to the apomembrane. (This 9-*cis* isomer cannot bind to give functional protein, but binding and formation of purple membrane is triggered by the photoisomerization to all-*trans* retinal that does bind to give a functional state.) These studies take advantage of the color changes that occur during retinal binding [62–64, 66]. All-*trans* retinal is found to bind to apomembrane in two stages to form purple membrane. First, retinal is fixed within its binding site and ring-chain planarization of the cofactor occurs, resulting in a red shift of the retinal absorption band from about 380 to about 400 nm. A further red shift of the absorption band is then observed giving an intermediate with an absorption band with maxima at 430 and 460 nm. Retinal is non-covalently bound within its binding pocket in both the 400- and 430/46-nm states. Finally, retinal binds covalently and the characteristic 560 nm purple band is observed. It has also been possible to follow some of the secondary structure and side-chain protonation changes that occur during these retinal-binding reactions by Fourier transform IR difference spectroscopy [67]. Protonation changes were observed with pK_a shifts for two apparent proton-binding groups from pK_as of 4.6 and 7.1 in the apomembrane state to 2.8 and 8.9, respectively, in purple membrane. These proton-binding groups were suggested to result from a hydrogen-bonded network in the protein. The purple membrane resulting from retinal addition to apomembrane also shows some interesting differences to native purple membrane. One difference is that the Schiff base link of the retinal to Lys216 on helix G is different. Thus, the Schiff base of native purple membrane has a high pK_a of about 13. In contrast lower pK_as of 9 or 8.5 have been found for purple membrane that has been generated by addition of retinal to apomembrane. A higher pK_a above 10 was found for the *in vivo* formation of purple membrane, when retinal was added to the retinal-deficient cells during cell growth. This is suggested to reflect a different packing of the helices in the apomembrane state as compared to purple membrane and may be connected with the lack of the crystalline array of bacteriorhodopsin in the apomembrane state [75]. Thus, when retinal is present during synthesis of the purple membrane the helices can fold more tightly round the retinal than when retinal is added to apomembrane after cell growth and apomembrane isolation. Nevertheless, the apomembrane studies show that the protein is potentially stable in the absence of the cofactor and that retinal is not required for polypeptide folding.

3.5.3
Unfolding, Refolding and Kinetic Studies *in vitro*

A wealth of information has emerged from a series of kinetic studies on the folding of bacteriorhodopsin *in vitro* [10]. These have focused on folding bacteriorhodopsin from a partly denatured state in SDS into several different detergent micelles or lipid vesicles. Kinetic measurements are achieved with millisecond time resolution by simply mixing the SDS-denatured protein with a renaturing solution [29, 70]. A variety of renaturing solutions have been used successfully, to obtain 70–100% refolding yields in a few minutes. These renaturing conditions include mixed detergent/lipid micelles, mixed lipid/lipid micelles and lipid vesicles, all of which contain the retinal cofactor.

The refolding kinetics of SDS-denatured bacterio-opsin in DMPC/CHAPS, DMPC/L-*α*-1,2-dihexanoylphosphatidylcholine (DHPC) micelles and L-*α*-1,2-dipalmitoleoylphosphatidylcholine (DPoPC) vesicles, in the presence of all-*trans* retinal, have been investigated by time-resolved fluorescence and absorption spectroscopy, together with some far UV protein circular dichroism studies (for reviews, see [10, 25]). The yield of folded protein is assessed *in situ* using absorption spectroscopy to monitor the formation of native-like, purple chromophore [9, 11, 76]. The folding reaction occurs in mixed SDS/DMPC/DHPC micelles or SDS/DPoPC vesicles and probably all of the SDS partitions into the micelles or vesicles.

The simplest, sequential reaction scheme that accounts for the kinetic data in DMPC/DHPC micelles or lipid vesicles is:

$$\mathrm{bO} \rightleftharpoons \mathrm{I_1} \leftrightarrow \mathrm{I_2} \overset{\overset{\mathrm{R}}{\searrow}}{\rightleftharpoons} \mathrm{I_R} \leftrightarrow \mathrm{bR}$$

bO is the SDS denatured state, and I_1 and I_2 are intermediates that form prior to retinal binding. Parallel folding routes are omitted for simplicity (although, there is for example evidence for at least two folding routes from I_2 to bacteriorhodopsin [77]). All-*trans* retinal (R) binds to I_2 non-covalently to give I_R. This is followed by formation of the covalent link with Lys216 (on a timescale of minutes) to give bacteriorhodopsin with covalently bound, all-*trans* retinal. Isomerization of retinal then occurs within the binding pocket to give bacteriorhodopsin that contains a mixture of all-*trans* and 13-*cis* retinal. I_R seems to consist of at least two observable states one where the retinal absorption band is similar to that of free retinal at about 380 nm (I_{R380}) and one where the retinal band is red-shifted to 440 nm (I_{R440}). I_{R380} seems to form and decay in parallel with I_{R440} and with the same observed kinetics. This could result from a distribution of protein conformers in I_2 and I_R (and probably bO) that have slightly different protonation equilibria of their side-chains and can interconvert by thermal energy. Alternatively, the I_R states could differ in polypeptide conformation or have altered protonation states of individual residues (or bound solvent ions) near the retinal with no difference in polypeptide conformation.

One difficulty in kinetic studies is differentiating protein-folding events from changes in the detergent/lipid environment. This is further complicated by the lack of definitive and specific probes for the changes in protein structure, as well as the dynamics of the micelles and vesicles themselves. The apparent rate of stopped-flow mixing of the SDS micelles and the renaturing micelles or vesicles can be determined by two methods: (1) using fluorescence dyes or tryptophan, the fluorescence of which increase in the more hydrophobic lipid moieties [78], and (2) by time-resolving the light scattered by the micelles or vesicles [79]. In micelle folding experiments, these approaches have revealed two kinetic phases with rates of about 100 and 2 s^{-1} on stopped-flow mixing of SDS and DMPC/CHAPS micelles. The faster time constant seems to reflect mixing of the SDS and DMPC/CHAPS micelles, whilst the slower one involves some further molecular rearrangement of the SDS/DMPC/CHAPS micelles. Kinetic measurements in lipid vesicles are even more complicated. Time constants similar to those for mixing of SDS and DMPC/CHAPS micelles are also observed on stopped-flow mixing of SDS micelles and lipid vesicles. Additional time constants (minutes to hours) can also be resolved, which correspond to very subtle changes in light scattering and the degree of which depends on the vesicle composition [15, 29, 76]. Not surprisingly changes in bO fluorescence are also observed with these micelle/vesicle mixing time constants during the folding reaction, but it remains to be determined how much protein folding actually occurs. An increase in protein fluorescence is observed during the fastest, 100 s^{-1}, mixing phase. This could reflect an increase in the hydrophobic environment of the protein's aromatic residues as a result of either protein folding or the SDS-solubilized protein coming into contact with the more hydrophobic DMPC/CHAPS micelles or lipid vesicles. The 2 s^{-1} event is also observed as a change in protein fluorescence that has been tentatively assigned to the formation of an intermediate, I_1 [25].

All the kinetic folding experiments thus far point to the apoprotein intermediate I_2 being key to the folding process and a prerequisite for retinal binding. Formation of I_2 is rate limiting in apoprotein folding [29, 70, 78]. At least two I_2 states (I_{2a} and I_{2b}) seem to be present when folding in lipid vesicles. The additional intermediate is probably due to the greater internal two-dimensional pressure present in these lipid vesicles as compared to micelles. The changes in protein secondary structure have been time-resolved during this stage of folding in micelles by far UV circular dichroism [27]. The SDS-denatured bO state has an α-helical content of about four transmembrane helices, whilst the remaining equivalent of three transmembrane α-helices are disordered. The secondary structure of I_2 is native-like and corresponds to seven transmembrane α-helices. Far-UV circular dichroism experiments have shown that at least 30 or so amino acids fold to α-helices during I_2 formation. This has been suggested to reflect either folding and insertion of parts of helices F and G or folding of helix ends (for reviews, see [10, 25, 80]). There are some indications that the seven-transmembrane apoprotein intermediate, I_2 also contains some helix–helix interactions and possibly the inter-helix hydrogen bonds [46]. Single point mutations

of Pro50 (near the centre of helix B) or Pro91 (near the centre of helix C) (see Fig. 3.1) to either Ala or Gly result in a 5- to 7-fold slowing of the rate of folding to I_2. Proline residues occur at kinks in α-helices, which are probably important in helix packing and cofactor binding sites. Furthermore, the backbone nitrogen of Pro cannot hydrogen bond within the helix and therefore leaves a free backbone carbonyl group four residues higher up in the helix. These backbone carbonyl groups in bacteriorhodopsin, which are free of intra-helical hydrogen bonds as a result of Pro50 and 91, are involved in inter-helix hydrogen bonds (via waters) between helices B and G, and helices C and D [12]. The slowing of the rate-limiting step that occurs when either of these Pros is mutated could suggest that this folding step involves helix–helix interactions and possibly these hydrogen bonds. However it should be noted that removal of Pro50 does not remove the kink in the helix [44].

3.6 Controlling Membrane Protein Folding

The rate of bacteriorhodopsin folding can be controlled by manipulating particular characteristics of the refolding lipid environment [15, 76, 80–82]. Again, it appears that the rate-limiting folding to the key intermediate I_2 is altered. Biological membranes contain a variety of lipids, with phosphatidylcholine (PC) and phosphatidylethanolamine (PE) lipids being some of the most common. The liquid crystalline behavior of these lipids in water is well understood allowing the mechanical properties of PC and PE bilayers to be manipulated. PC lipids tend to form flat bilayers whereas PE lipids have a stronger tendency (than PC lipids with the same chains) to form phases where the lipid monolayer interface bends towards water, and are thus often referred to as "non-bilayer" lipids. The introduction of a PE lipid into a PC bilayer increases the propensity for each monolayer to curve towards water (see Fig. 3.2). However, this desire for monolayer curvature is frustrated because bilayers require flat monolayers. As a result there is an increase in the stored curvature elastic energy of the PC/PE bilayers with increasing PE content (until eventually a critical PE composition is achieved and a phase transition occurs to a non-bilayer phase). Bilayer curvature stress is also affected by the lipid chain composition, and this can also be used to manipulate the stored stress within a bilayer. Unsaturated lipid chains contain more *cis* double bonds, which kink the chains and increase the desire for monolayer curvature.

Bacteriorhodopsin has been folded into lipid vesicles with different curvature stress [76, 81], achieved by altering the lipid composition as outlined above. Altering the bilayer stress alters the refolding rates and the amount of folded protein. Decreasing the curvature stress of PC bilayers (by altering chain composition) increases the yield of correctly folded bacteriorhodopsin, up to 100%. Conversely, increasing the curvature stress of PC bilayers (through addition of PE or the proportion of lipids with saturated chains) decreases the yield of bacterio-

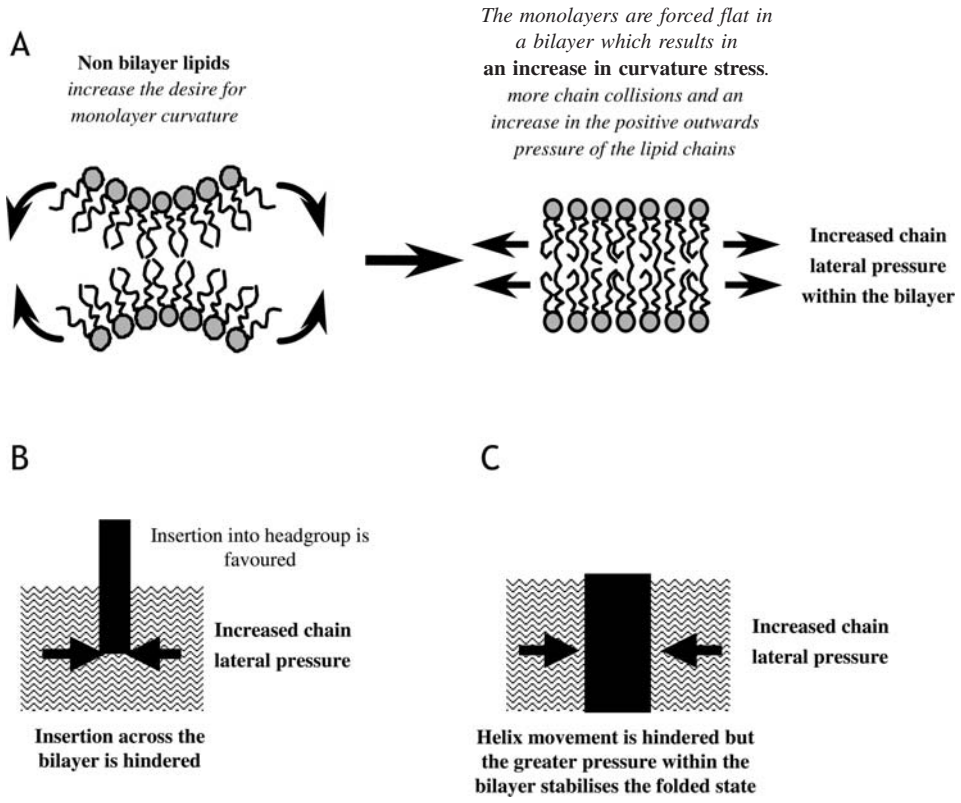

Fig. 3.2 Schematic diagrams illustrating stored curvature stress in lipid bilayers and its affect on helix insertion and lateral movement. (A) The effect of non-bilayer lipids on the stored curvature stress and chain lateral pressure. The effect of increased curvature stress and chain lateral pressure on (B) transmembrane insertion and (C) lateral motion of transmembrane helices.

rhodopsin. This decrease seems to be caused by a decrease in the amount of key apoprotein intermediates (I_{2a} and I_{2b}) that have to form prior to retinal binding and formation of bacteriorhodpsin. This suggests that the increase in stress hinders the insertion of the protein from SDS into the PC/PE bilayers. Such hindered insertion is consistent with work on the insertion of a synthetic transmembrane helix from an aqueous state into PC bilayers [83]. The activation energy for insertion of this helix was found to increase as the stored curvature elastic stress of the bilayers was increased. The increase in curvature elastic stress is directly related to an increase in the two-dimensional pressure parallel to the bilayer interface that is exerted by chain-chain collisions in the hydrophobic core of the bilayer. This lateral chain pressure will hinder the insertion of a protein or peptide across the bilayer (see Fig. 3.2 B).

3.7 Conclusions

3.7.1 Summary of Bacteriorhodopsin Folding

The folding mechanism of bacteriorhodopsin does not strictly follow the two-stage model. It seems more likely that a critical helix core forms first, possibly involving helices A–E. One folding scheme that is consistent with the data discussed here is presented in Fig. 3.3. This scheme relates to the detailed kinetic studies from an SDS state; however, several aspects are based on other work. Thus, the kinetic studies have identified intermediates in the folding reaction, but cannot assign these to the formation of particular structural features. As a result, the concept of the five helices A–E folding first is based on the studies on protein fragments. An intermediate state, I_2, with a native helix structure then forms and this seems to be required before retinal binds to give the final functional state. Therefore, the protein does not require the cofactor to fold nor does secondary and tertiary structure formation occur sequentially. A similar series of intermediate states is observed whether the protein folds into micelles or lipid bilayer vesicles, or whether amino acid substitutions are made in the protein. These latter substitutions can be fairly drastic, including substituting the helix-connecting loops with Gly–Gly–Ser repeats or changing Pro in helices to Ala. This indicates that the overall folding mechanism is insensitive to such changes, presumably because they do not significantly perturb the critical helical core formation nor are they the sole interactions involved in folding and intermediate formation. However, individual interactions and folding steps are sensitive to the changes in the bilayer or amino acids. A critical step in formation of bacteriorhodopsin is the formation of the I_2 intermediate(s). This intermediate contains native secondary structure and some tertiary interactions and thus is probably a largely folded apoprotein state, with the final folding of the protein occurring as retinal binds. Formation of I_2 is sensitive to bilayer and amino acid changes, with the changes affecting the rate of this folding step. The mutation of the Pro in the centre of helix B or C slows this rate-limiting folding. Thus, the Pro residues could aid formation of inter-helix contacts, suggesting that folding to I_2 involves some helix–helix association. Mutations of the cytoplasmic CD and EF loops also slow the folding to I_2, which suggests the structure of these loops is important in I_2 formation. This could be due to the fact that I_2 folding involves helix packing, or folding of the helix ends together with these loops or the insertion of some helices (e.g. F and G) that then allows the loops to fold correctly.

Formation of I_2 is also sensitive to changes in the bilayer curvature stress. Increasing the stress decreases the folding yield and a study of the folding kinetics sheds some light on this. The main factor is that when the bilayer stress is too high, the insertion of the protein across the bilayer is hindered and this prevents all the protein inserting. Curvature stress also affects the rates of folding events within the bilayer, particularly helix packing and protein, retinal association.

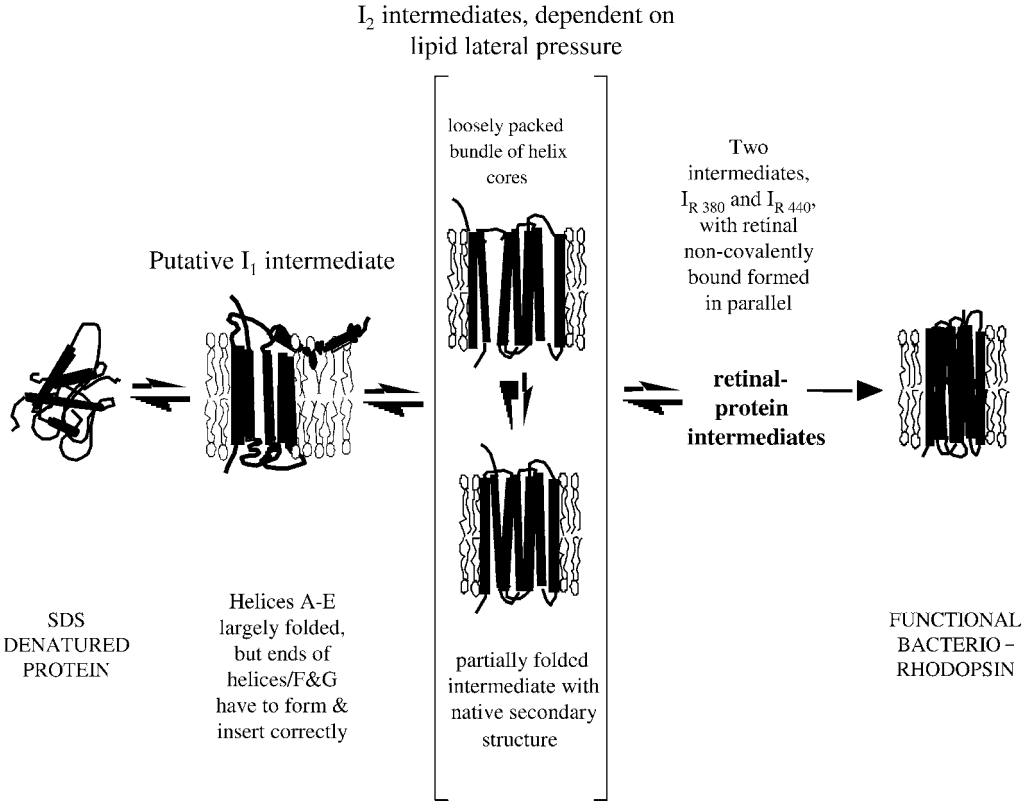

Fig. 3.3 One possible scheme for the folding of bacteriorhodopsin in lipid bilayer vesicles. The apoprotein, bO, folds from a state in SDS to give the I_2 states (I_{2a} and I_{2b}), both of which are shown here with seven transmembrane helical structure. Retinal then binds and this eventually results in bacteriorhodpsin formation. Apoprotein folding to I_2 may proceed via another intermediate, I_1, and could involve helix extension, tilting and packing or some helix insertion. This scheme proposes that A–E are largely formed at this point. The difference in the two I_2 states is unknown, but seems to be dependent on the lateral pressure exerted on the helix bundle by the lipid chains. This lateral pressure could affect helix insertion or helix packing. Although we only show here a difference in helix packing between I_{2a} and I_{2b}, there could also be a difference in the number of transmembrane helices. Retinal binds to I_2 to give two retinal, protein intermediates, I_{R380} and I_{R440}, which form and decay with identical rates. Both these intermediates have retinal non-covalently bound, but have different absorption maxima of 380 or 440 nm, respectively. This reaction scheme is only one possible scheme that does not include all kinetic stages for clarity.

3.7.2 Implications for Transmembrane α-Helical Membrane Protein Folding

The folding of bacteriorhodopsin has been more widely studied than any other α-helical membrane protein. The work has advanced studies of membrane protein folding in four main ways: (1) by providing detailed information on an integral membrane protein, (2) by providing some general principles in membrane protein folding, (3) by acting as a test bed for hypotheses and the design of new experimental systems, and (4) in the development of methods to probe membrane protein folding.

Protein folding has traditionally been dominated by studies on water-soluble proteins. The seminal work of Anfinsen, which opened the way for *in vitro* studies of folding mechanisms, started over 40 years ago [84, 85]. The advances of Khorana et al. on the refolding of bacteriorhodopsin some 20–25 years ago [9, 11] meant that helical membrane proteins could enter the fray. The first "fast" kinetic studies on the folding of a membrane protein, i.e. with millisecond time resolution, were reported in the mid 1990s [70] and revealed transient folding intermediates for bacteriorhodopsin. Gradually, over the last 10 years or so, studies on other helical membrane proteins have been undertaken, frequently following directly from the approaches taken with the pioneering bacteriorhodopsin work. Thus, similar studies of the kinetics of folding from an SDS state into detergent micelles have been reported for the major plant light harvesting protein, LHCII [86–89], and the *E. coli* disulfide binding protein, DsbB [90]. Following on from the demonstration several years ago that the *E. coli* enzyme, diacylglycerol kinase, can be refolded into detergent or lipids directly from a denatured state in urea [91], detailed folding kinetic studies have now been reported on this process [92–94].

Bacteriorhodopsin has also led the way in other aspects of folding. The extensive mutagenesis work of Khorana's laboratory led to a vast amount of information on the contribution of individual amino acids to the protein fold, stability and function. Taken together with other advances in membrane protein and protein folding research, this has recently enabled Bowie to perform a systematic study into the specific interactions of amino acid side-chains of a single helix to the protein folding and stability [44]. Khorana also used his experience with bacteriorhodopsin to investigate the role of single point amino acid changes in rhodopsin folding [69]. Notably, extensive studies on rhodopsin mutants showed that folding of the three domains of this receptor protein, i.e. cytoplasmic, membrane and intradiscal, is coupled [95–100]. Furthermore, the group demonstrated that single point mutations associated with retina degeneration diseases cause misfolding of the protein *in vitro*; one of the first demonstrations of misfolding of a membrane protein in disease [101]. As a final example of bacteriorhodopsin as a paradigm for technique application, it has been the focus of the first mechanical unfolding studies [52].

Bacteriorhodopsin has also provided the opportunity to demonstrate that a generic, mechanical property of the basic fabric of cell membranes, the lipid bilayer,

affects folding events [76, 81]. This has ramifications for a variety of *in vitro* situations as well as *in vivo*. Several properties of bilayers such as headgroup interactions and lateral pressure – all of which are encompassed in the stored curvature stress – affect folding. There seem to be different optimal stresses for different stages of folding. A relaxed bilayer is appropriate for optimizing the amount of transbilayer protein that inserts. However, there seems to be some critical stress or chain lateral pressure for optimal rates of folding. Folding events slow down if the stress is increased too much. This can be thought of as an increase in the microviscosity within the bilayer that hinders lateral movement of transmembrane helices. Thus, the maximum yield does not necessarily correlate with the maximum rate or stability of final folded protein and this knowledge can be used to guide the design of successful folding systems for membrane proteins. It also implies that curvature stress will affect reconstitution of membrane proteins and indeed this has recently been demonstrated [102].

With regard to biogenesis *in vivo,* whilst much of the mechanism remains to be determined, the latest structural and functional models imply that helices will probably form inside the translocon, cotranslationally, and emerge laterally into the bilayer [103, 104]. However, for polytopic proteins that span the bilayer several times, the helices may well leave the translocon individually or in small groups with the final helix packing and folding occurring in the bilayer. Thus, there is the distinct possibility that mechanical properties of the membrane play a role here/are optimized for helix packing. Moreover, membrane proteins frequently do not reside in the membrane where they are made. Thus, proteins initially inserted into the endoplasmic reticulum can end up in the plasma membrane. The different membranes have different compositions and different curvature stresses, which could affect folding.

A tremendous amount of information has resulted from folding studies on bacteriorhodopsin. It is still the only helical membrane protein for which molecular-level information on folding can be obtained and thus work on the protein should undoubtedly continue. A challenge now, however, is to translate the methods to other membrane proteins and to derive general rules for folding. The recent increase in the number of near-atomic-resolution crystal structures of helical membrane proteins augers well. Amongst other things, we now need to establish reversible refolding conditions for these membrane proteins as well as lipid bilayer folding systems.

Acknowledgments

I thank all the people in my research group who have contributed to our bacteriorhodopsin folding work. In particular, Rachael Curran was the originator of much of the lipid work and skillfully translated the concept into reality, Samantha Allen continued this work and performed near-impossible experiments with tremendous precision, and Hui Lu made critical contributions to the detailed kinetic studies. In addition, I am very grateful to my collaborators who have contributed to the work my laboratory has done on bacteriorhodopsin and the ideas presented here. I thank Richard Templer for his insight into lipid proper-

ties and their potential for modulating folding; Sabine Flitsch and Gobind Khorana who generously shared their knowledge of bacteriorhodopsin and assisted with the first kinetic folding experiments; and Bonnie Wallace for expert advice on circular dicrhoism measurements and David Klug who was a great help with kinetic data analyses. I also acknowledge colleagues and support from the Departments of Biochemistry at Oxford, Imperial and Bristol. Bacteriorhodopsin research in my lab has been supported by the Wellcome Trust, The Royal Society and the BBSRC.

References

1 Nassel, M., Mogi, T., Karnik, S., Khorana, H. **1987**. Structure–function studies on bacteriorhodopsin. *J. Biol. Chem. 262*, 9264–9270.

2 Karnik, S.S., Nassal, M., Doi, T., Jay, E., Sgaramella, V., Khorana, H.G. **1987**. Structure–function studies on bacteriorhodopsin. II. Improved expression of the bacterio-opsin gene in *Escherichia coli*. *J. Biol. Chem. 262*, 9255–9263.

3 Dunn, R.J., Hackett, N.R., McCoy, J.M., Chao, B.H., Kimura, K., Khorana, H.G. **1987**. Structure–function studies on bacteriorhodopsin. I. Expression of the bacterio-opsin gene in *Escherichia coli*. *J. Biol. Chem. 262*, 9246–9254.

4 Henderson, R., Baldwin, J.M., Ceska, T.A., Zemlin, F., Beckmann, E., Downing, K.H. **1990**. Model for the structure of bacteriorhodopsin based on high-resolution electron cryo-microscopy. *J. Mol. Biol. 213*, 899–929.

5 Gerwert, K., Souvignier, G., Hess, B. **1990**. Simultaneous monitoring of light-induced changes in protein side group protonation, chromophore isomerization, and backbone motion of bacteriorhodopsin by time-resolved Fourier-transform infrared spectroscopy. *Proc. Natl Acad. Sci. USA 87*, 9774–9778.

6 Delaney, J.K., Brack, T.L., Atkinson, G.H., Ottolenghi, M., Steinberg, G., Sheves, M. **1995**. Primary picosecond molecular events in the photoreaction of the BR5. 12 artificial bacteriorhodopsin pigment. *Proc. Natl Acad. Sci. USA 92*, 2101–2105.

7 Herbst, J., Heyne, K., Diller, R. **2002**. Femtosecond infrared spectroscopy of bacteriorhodopsin chromophore isomerization. *Science 297*, 822–825.

8 Mathies, R.A., Lin, S. W., Ames, J.B., Pollard, W.T. **1991**. From femtoseconds to biology: mechanism of bacteriorhodopsin's light-driven proton pump. *Ann. Rev. Biophys. Biophys. Chem. 20*, 491–518.

9 London, E., Khorana, H.G. **1982**. Denaturation and renaturation of bacteriorhodopsin in detergents and lipid–detergent mixtures. *J. Biol. Chem. 257*, 7003–7011.

10 Booth, P.J. **2000**. Unravelling the folding of bacteriorhodopsin. *Biochim. Biophys. Acta 1460*. 4–14.

11 Huang, K.-S., Bayley, H., Liao, M.-J., London, E., Khorana, H.G. **1981**. Refolding of an integral membrane protein. Denaturation, renaturation and reconstitution of intact bacteriorhodopsin and two proteolytic fragments. *J. Biol. Chem. 256*, 3802–3809.

12 Luecke, H., Schobert, B., Richter, H.-T., Cartailler, J.-P., Lanyi, J.K. **1999**. Structure of bacteriorhodopsin at 1.55 Å resolution. *J. Mol. Biol. 291*, 899–911.

13 Oesterhelt, D., Stoeckenius, W. **1971**. Rhodopsin-like protein from the purple membrane of *Halobacterium halobium*. *Nat. New Biol. 233*, 149–152.

14 Stoeckenius, W., Lozier, R.H., Bohomolni, R.A. **1979**. Bacteriorhodopsin and the purple membrane of halobacteria. *Biochim. Biophys. Acta 505*, 215–278.

15 Booth, P.J., Templer, R.H., Meijberg, J. W., Allen, S.J., Lorch, M., Curran, A.R. **2001**. *In vitro* studies of membrane protein folding. *Crit. Rev. Biochem. Mol. Biol. 36*, 501–603.

16 Haupts, U., Tittor, J., Oesterhelt, D. **1999**. Closing in on bacteriorhodopsin: progress in understanding the molecule. *Annu. Rev. Biophys. Biomol. Struct. 28*, 367–399.

17 Popot, J.-L., Engelman, D.M. **1990**. Membrane protein folding and oligomerization: the two stage model. *Biochemistry 29*, 4031–4037.

18 Hunt, J.F., Earnest, T.N., Bousche, O., Kalghati, K., Reilly, K., Horváth, C., Rothschild, K.J., Engelman, D.M. **1997**. A biophysical study of integral membrane protein folding. *Biochemistry 36*, 15156–15176.

19 Engelman, D.M., Chen, Y., Chin, C.N., Curran, A.R., Dixon, A.M., Dupuy, A.D., Lee, A.S., Lehnert, U., Matthews, E.E., Reshetnyak, Y.K., Senes, A., Popot, J.L. **2003**. Membrane protein folding: beyond the two stage model. *FEBS Lett. 555*, 122–125.

20 Kim, J.-M., Booth, P.J., Allen, S.J., Khorana, H.G. **2001**. Structure and function in bacteriorhodopsin: the role of the interhelical loops in the folding and stability of bacteriorhodopsin. *J. Mol. Biol. 308*, 409–422.

21 Kahn, T.W., Sturtevant, J.M., Engelman, D.M. **1992**. Thermodynamic measurements of the contributions of helix-connecting loops and of retinal to the stability of bacteriorhodopsin. *Biochemistry 31*, 8829–8839.

22 Liao, M.-J., London, E., Khorana, H.G. **1983**. Regeneration of the native bacteriorhodopsin structure from two chymotryptic fragments. *J. Biol. Chem. 258*, 9949–9955.

23 Popot, J.-L., Gerchman, S.-E., Engelman, D.M. **1987**. Refolding of bacteriorhodopsin in lipid bilayers. A thermodynamically controlled two-stage process. *J. Mol. Biol. 198*, 655–676.

24 Marti, T. **1998**. Refolding of bacteriorhodopsin from expressed polypeptide fragments. *J. Biol. Chem. 273*, 9312–9322.

25 Booth, P.J. **1997**. Folding α helical membrane proteins: kinetic studies on bacteriorhodopsin. *Fold Design 2*, R85–R92.

26 Chen, G.Q., Gouaux, E. **1999**. Probing the folding and unfolding of wild-type and mutant forms of bacteriorhodopsin in micellar solutions: evaluation of reversible unfolding conditions. *Biochemistry 38*, 15380–15387.

27 Riley, M.L., Wallace, B.A., Flitsch, S.L., Booth, P.J. **1997**. Slow α helical formation during folding of a membrane protein. *Biochemistry 36*, 192–196.

28 Valiyaveetil, F.I., MacKinnon, R., Muir, T.W. **2002**. Semisynthesis and folding of the potassium channel KcsA. *J. Am. Chem. Soc. 124*, 9113–9120.

29 Allen, S.J., Curran, A.R., Templer, R.H., Meijberg, W., Booth, P.J. **2004**. Folding kinetics of an α helical membrane protein in phospholipid bilayer vesicles. *J. Mol. Biol. 342*, 1279–1291.

30 Lemmon, M.A., Treutlein, H.R., Adams, P.D., Brünger, A.T., Engelman, D.M. **1994**. A dimerization motif for transmembrane α-helices. *Nat. Struct. Biol. 1*, 157–163.

31 Curran, A.R., Engelman, D.M. **2003**. Sequence motifs, polar interactions and conformational changes in helical membrane proteins. *Curr. Opin. Struct. Biol. 13*, 412–417.

32 Isenbarger, T.A., Krebs, M.P. **1999**. Role of helix–helix interactions in assembly of the bacteriorhodopsin lattice. *Biochemistry 38*, 9023–9030.

33 Jackson, M.B., Sturtevant, J.M. **1978**. Phase transitions of the purple membranes of *Halobacterium halobium*. *Biochemistry 17*, 911–915.

34 Brouillette, C.G., McMichens, R.B., Stern, L.J., Khorana, H.G. **1989**. Structure and thermal stability of monomeric bacteriorhodopsin in mixed phospholipid/detergent micelles. *Proteins 5*, 38–46.

35 Haltia, T., Freire, E. **1995**. Forces and factors that contribute to the structural stability of membrane proteins. *Biochim. Biophys. Acta 1241*. 295–322.

36 Mogi, T., Stern, L.J., Marti, T., Chao, B., Khorana, H.G. **1988**. Aspartic Acid substitutions affect proton translocation by bacteriorhodopsin. *Proc. Natl Acad. Sci. USA 85*, 4148–4152.

37 Khorana, H.G. **1988**. Bacteriorhodopsin, a membrane protein that uses light to translocate protons. *J. Biol. Chem. 263*, 7439–7442.

38 Flitsch, S.L., Khorana, H.G. **1989**. Structural studies on transmembrane proteins. 1. Model study using bacterio-

rhodopsin mutants containing single cysteine residues. *Biochemistry 28*, 7800–7805.

39 Mogi, T., Stern, L.J., Chao, B.H., Khorana, H.G. **1989**. Structure–function studies on bacteriorhodopsin. VII Substitutions of the membrane-embedded prolines 50, 91 and 186: the effects are determined by the substituting amino acids. *J. Biol. Chem. 264*, 14192–14196.

40 Mogi, T., Marti, T., Khorana, H.G. **1989**. Structure–function studies on bacteriorhodopsin. IX. Substitutions of tryptophan residues affect protein–retinal interactions in bacteriorhodopsin. *J. Biol. Chem. 24*, 14197–14201.

41 Braiman, M.S., Stern, L.J., Chao, B.H., Khorana, H.G. **1987**. Structure–function studies on bacteriorhodopsin. IV. Purification and renaturation of bacterio-opsin polypeptide expressed in *Escherichia coli*. *J. Biol. Chem. 262*, 9271–9276.

42 Hackett, N.R., Stern, L.J., Chao, B., Kronis, K.A., Khorana, H.G. **1987**. Structure–function studies on bacteriorhodopsin. V. Effects of amino acid substitutions in the putative helix F. *J. Biol. Chem. 262*, 9277–9284.

43 Stern, L.J., Khorana, H.G. **1989**. Structure–function studies on bacteriorhodopsin. X. Individual substitutions of arginine residues by glutamine affect chromophore formation, photocycle and proton translocation. *J. Biol. Chem. 264*, 14202–14208.

44 Faham, S., Yang, D., Bare, E., Yohannan, S., Whitelegge, J.P., Bowie, J.U. **2004**. Side-chain contributions to membrane protein structure and stability. *J. Mol. Biol. 335*, 297–305.

45 Zhou, Y., Bowie, J.U. **2000**. Building a thermostable membrane protein. *J. Biol. Chem. 275*, 6975–6979.

46 Lu, H., Marti, T., Booth, P.J. **2001**. Proline residues in transmembrane α helices affect the folding of bacteriorhodopsin. *J. Mol. Biol. 308*, 437–446.

47 Kahn, T.W., Engelman, D.M. **1992**. Bacteriorhodopsin can be refolded from two independently stable transmembrane helices and the complementary five-helix fragment. *Biochemistry 31*, 6144–6151.

48 Kimura, Y., Vassylyev, D.G., Miyazawa, A., Kidera, A., Matsushima, M., Mitsuoka, K., Murata, K., Hira, T., Fujiyoshi, Y. **1997**. Surface of bacteriorhodopsin revealed by high resolution electron crystallography. *Nature 389*, 206–211.

49 Mitsuoka, K., Hirai, T., Murata, K., Miyazawa, A., Kidera, A., Kimura, Y., Fugiyoshi, Y. **1999**. The structure of bacteriorhodopsin at 3.0 angstrom resolution based on electron crystallography: implication of the charge distribution. *J. Mol. Biol. 286*, 861–882.

50 Subramaniam, S. **1999**. The structure of bacteriorhodopsin: an emerging consensus. *Curr. Opin. Struct. Biol. 9*, 462–468.

51 Allen, S.J., Kim, J.-M., Khorana, H.G., Lu, H., Booth, P.J. **2001**. Structure and function in bacteriorhodopsin: the role of the interhelical loops in folding and stability of bacteriorhodopsin. *J. Mol. Biol. 308*, 423–435.

52 Oesterhelt, F., Oesterhelt, D., Pfeiffer, M., Engel, A., Gaub, H.E., Müller, D.J. **2000**. Unfolding pathways of individual bacteriorhodopsins. *Science 288*, 143–146.

53 Merkel, R., Nassoy, P., Leung, A., Ritchie, K., Evans, E. **1999**. Energy landscapes of receptor–ligand bonds explored with dynamic force spectroscopy. *Nature 397*, 50–53.

54 Rief, M., Gautel, M., Oesterhelt, F., Fernandez, J.M., Gaub, H.E. **1997**. Reversible unfolding of individual titin immunoglobulin domains by AFM. *Science 276*, 1109–1112.

55 Bustamante, C., Chemla, Y.R., Forde, N.R., Izhaky, D. **2004**. Mechanical processes in biochemistry. *Annu. Rev. Biochem. 73*, 705–748.

56 Clausen-Schaumann, H., Seitz, M., Krautbauer, R., Gaub, H.E. **2000**. Force spectroscopy with single bio-molecules. *Curr. Opin. Chem. Biol. 4*, 524–530.

57 Janovjak, H., Struckmeier, J., Hubain, M., Kedrov, A., Kessler, M., Muller, D.J. **2004**. Probing the energy landscape of the membrane protein bacteriorhodopsin. *Structure (Camb.) 12*, 871–879.

58 Mueller, D.J., Kessler, B., Oesterhelt, F., Moeller, C., Oesterhelt, D., Gaub, H. **2002**. Stability of bacteriorhrodopsin alpha helices and loops analyzed by single-molecular force spectroscopy. *Biophys.J. 83*, 3578–3588.

59 Kedrov, A., Ziegler, C., Janovjak, H., Kuhlbrandt, W., Muller, D.J. **2004**. Controlled unfolding and refolding of a single sodium-proton antiporter using atomic force microscopy. *J. Mol. Biol. 340*, 1143–1152.

60 Krebs, M.P., Isenbarger, T.A. **2000**. Structural determinants of purple membrane assembly. *Biochim. Biophys. Acta 1460*, 15–26.

61 Oesterhelt, D., Stoeckenius, W. **1974**. Isolation of the cell membrane of *Halobacterium halobium* and its fractionation into red and purple membrane. *Methods Enzymol. 31*, 667–679.

62 Oesterhelt, D., Meentzen, M., Schumann, L. **1973**. Reversible dissociation of the purple complex in bacteriorhodopsin and identification of 13-*cis* and all-*trans*-retinal as its chromophores. *Eur. J. Biochem. 40*, 453–463.

63 Schreckenbach, T., Walckhoff, B., Oesterhelt, D. **1977**. Studies on the retinal–protein interaction in bacteriorhodopsin. *Eur. J. Biochem. 76*, 499–511.

64 Schreckenbach, T., Walckhoff, B., Oesterhelt, D. **1978**. Specificity of the retinal binding site of bacteriorhodopsin: chemical and stereochemical requirements for the binding of retinol and retinal. *Biochemistry 17*, 5353–5359.

65 Schweiger, U., Tittor, J., Oesterhelt, D. **1994**. Bacteriorhodopsin can function without a covalent linkage between retinal and protein. *Biochemistry 33*, 535–541.

66 Gärtner, W., Towner, P., Hopf, H., Oesterhelt, D. **1983**. Removal of methyl groups from retinal controls the activity of bacteriorhodopsin. *Biochemistry 22*, 2637–2644.

67 Fischer, U.C., Oesterhelt, D. **1980**. Changes in the protonation state of bacterio-opsin during reconstitution of bacteriorhodopsin. *Biophys. J. 31*, 139–146.

68 Khorana, H.G. **1994**. Adventures in light-transducing systems: bacterial rhodopsin and mammalian rhodopsin. In *Structural Biology: The State of the Art* (R.H. Sarma and M.H. Sarma, eds). New York: Adenine Press.

69 Khorana, H.G. **1993**. Two light-transducing membrane proteins: bacteriorhodopsin and the mammalian rhodopsin. *Proc. Natl Acad. Sci. USA 90*, 1166–1171.

70 Booth, P.J., Flitsch, S.L., Stern, L.J., Greenhalgh, D.A., Kim, P.S., Khorana, H.G. **1995**. Intermediates in the folding of the membrane protein bacteriorhodopsin. *Nat. Struct. Biol. 2*, 139–143.

71 Dale, H., Angevine, C.M., Krebs, M.P. **2000**. Ordered membrane insertion of an archaeal opsin *in vivo*. *Proc. Natl Acad. Sci. USA 97*, 7847–7852.

72 Dale, H., Krebs, M.P. **1999**. Membrane insertion kinetics of a protein domain *in vivo*. The bacterioopsin N-terminus inserts cotranslationally. *J. Biol. Chem. 274*, 22693–22698.

73 Oesterhelt, D., Schuhmann, L. **1974**. Reconstitution of bacteriorhodopsin. *FEBS Lett. 44*, 262–265.

74 Draheim, J.E., Gibson, N.J., Cassim, J.Y. **1991**. Dramatic in situ conformational dynamics of the transmembrane protein bacteriorhodopsin. *Biophys. J. 60*, 89–100.

75 Kollbach, G., Steinmüller, S., Berndsen, T., Buss, V., Gärtner, W. **1998**. The chromophore induces a correct folding of the polypeptide-chain of bacteriorhodopsin. *Biochemistry 37*, 8227–8232.

76 Curran, A.R., Templer, R.H., Booth, P.J. **1999**. Modulation of folding and assembly of the membrane protein bacteriorhodopsin by intermolecular forces within the lipid bilayer. *Biochemistry 38*, 9328–9336.

77 Lu, H., Booth, P.J. **2000**. The final stages of folding of the membrane protein bacteriorhodopsin occur by kinetically indistinguishable parallel folding paths that are mediated by pH. *J. Mol. Biol. 299*, 233–243.

78 Booth, P.J., Farooq, A., Flitsch, S.L. **1996**. Retinal binding during folding and assembly of the membrane protein bacteriorhodopsin. *Biochemistry 35*, 5902–5909.

79 Booth, P.J., Farooq, A. **1997**. Transient intermediates in the regeneration of bacteriorhodopsin investigated by time-resolved absorption spectroscopy. *Eur. J. Biochem. 246*, 674–680.

80 Booth, P. J., Curran, A. R. **1999**. Membrane protein folding. *Curr. Opin. Struct. Biol. 9*, 115–121.

81 Allen, S. J., Curran, A. R., Templer, R. H., Meijberg, W., Booth, P. J. **2004**. Controlling the folding efficiency of an integral membrane protein. *J. Mol. Biol. 342*, 1293–1304.

82 Booth, P. J., Curran, A. R., Templer, R. H., Lu, H., Meijberg, W. **2001**. Manipulating the folding of membrane proteins: using the bilayer to our advantage. *Biochem. Soc. Symp. 68*, 27–33.

83 Meijberg, W., Booth, P. J. **2002**. The activation energy for insertion of transmembrane alpha-helices is dependent on membrane composition. *J. Mol. Biol. 319*, 839–853.

84 Anfinsen, C. B., Redfield, R. R., Choate, W. L., Page, J., Carroll, W. R. **1954**. Studies on the gross structure, cross-linkages, and terminal sequences in ribonuclease. *J. Biol. Chem. 207*, 201–210.

85 Anfinsen, C. B. **1973**. Principles that govern the folding of protein chains. *Science 181*, 223.

86 Booth, P. J., Paulsen, H. **1996**. Assembly of the light harvesting chlorophyll *a/b* complex *in vitro*. Time-resolved fluorescence measurements. *Biochemistry 35*, 5103–5108.

87 Reinsberg, D., Booth, P. J., Khoo, B. J., Jegerschold, C., Paulsen, H. **2000**. Folding, assembly and stability of the major light harvesting complex of higher plants, LHCII, in the presence of native lipids. *Biochemistry 39*, 14305–14313.

88 Reinsberg, D., Ottman, K., Booth, P. J., Paulsen, H. **2001**. Effects of chlorophyll *a*, chlorophyll *b* and xanthophylls on the *in vitro* assembly of the major light-harvesting chlorophyll *a/b* complex, LHCIIb. *J. Mol. Biol. 308*, 59–67.

89 Yang, C., Horn, R., Paulsen, H. **2003**. The light-harvesting chlorophyll *a/b* complex can be reconstituted *in vitro* from its completely unfolded apoprotein. *Biochemistry 42*, 4527–4533.

90 Otzen, D. **2003**. Folding of DsbB in mixed micelles: a kinetic analysis of the stability of a bacterial membrane protein. *J. Mol. Biol. 330*, 641–649.

91 Sanders II, C. R., Czerski, L., Vinogradova, Badola, P., Song, D., Smith, S. O. **1996**. *Escherichia coli* diacylglycerol kinase is an *α*-helical polytopic membrane protein and can spontaneously insert into preformed lipid vesicles. *Biochemistry 35*, 8610–8618.

92 Nagy, J. K., Lonzer, W. L., Sanders, C. R. **2001**. Kinetic study of folding and misfolding of diacylglycerol kinase in model membranes. *Biochemistry 40*, 8971–8980.

93 Gorzelle, B. M., Nagy, J. K., Oxenoid, K., Lonzer, W. L., Cafiso, D. S., Sanders, C. R. **1999**. Reconstitutive refolding of diacylglycerol kinase, an integral membrane protein. *Biochemistry 38*, 16373–16382.

94 Lorch, M., Booth, P. J. **2004**. Insertion kinetics of a denatured alpha helical membrane protein into phospholipid bilayer vesicles. *J. Mol. Biol. 344*, 1109–1121.

95 Anukanth, A., Khorana, H. G. **1994**. Structure and function in rhodopsin. Requirements of a specific structure for the intradiscal domain. *J. Biol. Chem. 269*, 19738–19744.

96 Hwa, J., Garriga, P., Liu, X., Khorana, H. G. **1997**. Structure and function in rhodopsin: packing of the helices in the transmembrane domain and folding to a tertiary structure in the intradiscal domain are coupled. *Proc. Natl Acad. Sci. USA 94*, 10571–10576.

97 Hwa, J., Reeves, P., Klein-Seetharaman, J., Davidson, F., Khorana, H. **1999**. Structure and function in rhodopsin: further elucidation of the role of the intradiscal cysteines, Cys-110, -185 and -187 in rhodopsin folding and function. *Proc. Natl Acad. Sci. USA 96*, 1932–1935.

98 Karnik, S. S., Sakmar, T. P., Chen, H. B., Khorana, H. G. **1998**. Cysteine residues 110 and 187 are essential for the formation of correct structure in bovine rhodopsin. *Proc. Natl Acad. Sci. USA 85*, 8459–8463.

99 Karnik, S. S. K., H. G. **1990**. Assembly of functional rhodopsin requires a disulfide bond between cysteine residues 110 and 187. *J. Biol. Chem. 265*, 17520–17524.

100 Hwa, J., Klein-Seetharaman, J., Khorana, H. G. **2001**. Structure and function in rhodopsin: mass spectrometric identification of the abnormal intradiscal disulfide bond in misfolded retinitis pigmentosa mutants. *Proc. Natl Acad. Sci. USA 98*, 4872–4876.

101 Kaushel, S., Khorana, H. G. **1994**. Structure and function in rhodopsin. 7. Point Mutations associated with autosomal dominant retinitis pigmentosa. *Biochemistry 33*, 6121–6128.

102 Curnow, P., Lorch, M., Charalambous, K., Booth, P. J. **2004**. The reconstitution and activity of the small multidrug transporter EmrE is modulated by non-bilayer lipid composition. *J. Mol. Biol. 343*, 213–222.

103 Rapoport, T. A., Goder, V., Heinrich, S. U., Matlack, K. E. **2004**. Membrane-protein integration and the role of the translocation channel. *Trends Cell Biol., 14*, 568–575.

104 Alder, N. N., Johnson, A. E. **2004**. Cotranslational membrane protein biogenesis at the endoplasmic reticulum. *J. Biol. Chem. 279*, 22787–22790.

4
Post-integration Misassembly of Membrane Proteins and Disease

Charles R. Sanders

4.1
Introduction

While estimates indicate that 15–30% of all proteins are integral membrane proteins (IMPs), more than 50% of existing drugs target IMPs [1]. It is therefore not surprising that a host of IMPs play critical roles in human diseases. This is exemplified by the fact that many phenotypes of common inherited diseases are caused by mutations in multispan IMPs, including retinitis pigmentosa, cystic fibrosis, Charcot-Marie-Tooth disease and polycystic kidney disease. As of October 2004, 37% of the 1800 proteins in the SwissProt database that are linked to human disorders were IMPs [2]. Here, we focus primarily upon inherited mutations that lead to "simple" diseases (caused by a single genetic lesion). However, as predisposing genetic factors are uncovered for complex (multifactorial) diseases such as diabetes mellitus, many factors will turn out to be mutations in membrane protein-encoding genes. Moreover, non-genetic contributing factors to disease such as unhealthy diet, aging or environment may also commonly involve IMPs as targets for toxic agents.

The goal of this chapter is to summarize what is known about how perturbations in human membrane protein assembly result in disease phenotypes. This work complements another review from this laboratory [3] by focusing less on the cellular context of IMP misassembly and more on the related proteins. As previously, we use the term "misassembly" to broadly describe the failure of a membrane protein to achieve a properly folded state. This is in preference to the term "misfolding", which tends to imply that the defective protein is kinetically trapped in an aberrant conformational state. There is evidence that many proteins misassemble in the cell and are degraded without ever actually adopting a stable incorrect structure [3].

This chapter neglects the relationship of membranes and the secretory pathway to amyloid formation and related diseases. This very important topic merits

separate treatment elsewhere (e.g. [4–6]). The same is true for IMP misassembly that is derived from problems that arise during membrane integration via the translocon, such as incorrect topology of transmembrane segments [7–9]. While such "early-stage" misassembly may be disease-relevant, this step of cellular IMP assembly is beyond the scope of this review. Instead, we focus on misassembly that is staged by protein that has been properly integrated into the membrane and that has (usually) been subjected to immature *N*-glycosylation, but for which tertiary and quaternary structure has not yet been completed. This point in cellular IMP assembly may generally be characterized by protein structural properties that roughly correspond to the unfolded state present in stage 1 of Popot and Engelman's Two-Stage Model for membrane protein folding [10, 11]. We realize that there is evidence that some tertiary structural contacts may be established in concert with membrane integration (cf. [12]). It is also recognized that the propensity for a host of resident endoplasmic reticulum (ER) proteins to form complexes with other protein components of the early secretory pathway is so extensive that various stages of membrane protein assembly may be difficult to resolve, both spatially and in terms of the subsets of proteins involved. Nevertheless, there is a variety of evidence (see below) that supports the notion that much disease-related IMP misassembly takes place at a post-integration stage of trafficking through the ER.

For a majority of the literally tens of thousands of documented disease-linked missense mutations, no follow-up cellular biological or biochemical analysis has been conducted to ascertain the affect of the mutation upon the encoded protein. However, for several multispan membrane proteins including rhodopsin, the vasopressin V2 receptor and peripheral myelin protein 22, cell trafficking studies have been conducted on dozens of different disease mutant forms [13–25]. For these proteins it is clear that the most common result of disease-linked mutation is protein misassembly rather than "active-site" functional perturbations within otherwise properly folded proteins. Whether this observation can be broadly extrapolated throughout IMP/disease-relationship space is not yet certain, but seems probable. In passing, it is important to note that other factors besides mutations can trigger IMP misassembly [26], although establishing relationships to specific disease phenotypes is a formidable challenge [27].

4.2
A Given IMP May be Subject to Numerous Disease-linked Mutations

For a particular disorder, any of many different mutations in a single protein can lead to disease phenotypes. For example, there are hundreds of known disease-linked recessive mutations in the gene encoding the cystic fibrosis transmembrane regulator (CFTR), any one of which is sufficient to cause cystic fibrosis [28]. The CFTR sites for which mutations can cause disease are rather evenly distributed throughout all intra- and extramembrane domains of the full length of the protein (see [3]). The same observation can be made for a number of

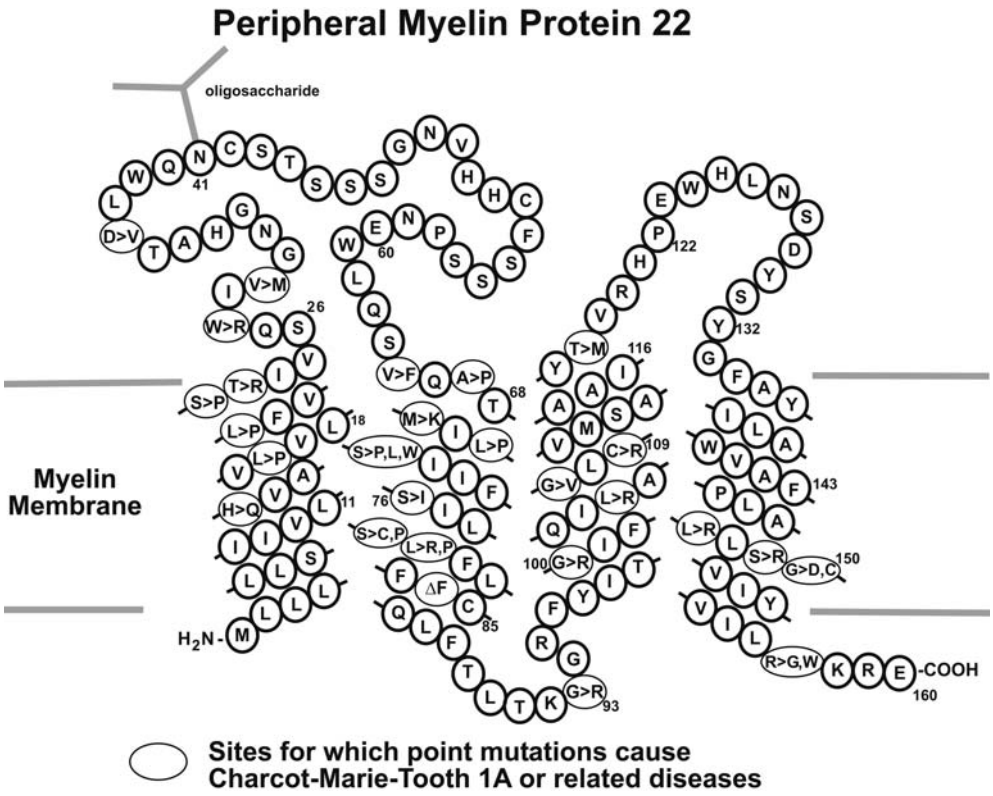

Fig. 4.1 Membrane topology of human myelin protein 22 and summary of disease-linked amino acid replacements due to mutations (usually autosomal dominant) of its encoding gene. A review of the misassembly of this protein can be found elsewhere [103]. In this figure, the notation X > Y,Z means amino acid X in the wild-type protein is mutated to either residues Y or Z in known disease phenotypes. The ΔF mutation involves deletion of this residue.

other IMPs, PMP22 (Fig. 4.1), the vasopressin V2 receptor, connexins [29, 30], and rhodopsin (Fig. 4.2). As noted above, it appears that a majority of these mutations lead to protein misassembly. The fact that so many different mutations within a single protein are often able to disrupt proper folding and trafficking suggests that protein folding in the cell is not always robust. Rather, single amino acid changes sometimes significantly tip the balance between assembly and misassembly. This notion is supported by evidence that even for wild-type proteins, measured efficiencies of assembly are often much less than 100% (review in [3]). Experimental measurements of folding efficiency are not without controversy because some have been conducted under conditions where the protein of interest is being expressed at much higher levels than occurs under physiological conditions. This leads to the objection that observed inefficiency may reflect artificial oversaturation of the cellular folding/quality control systems. However,

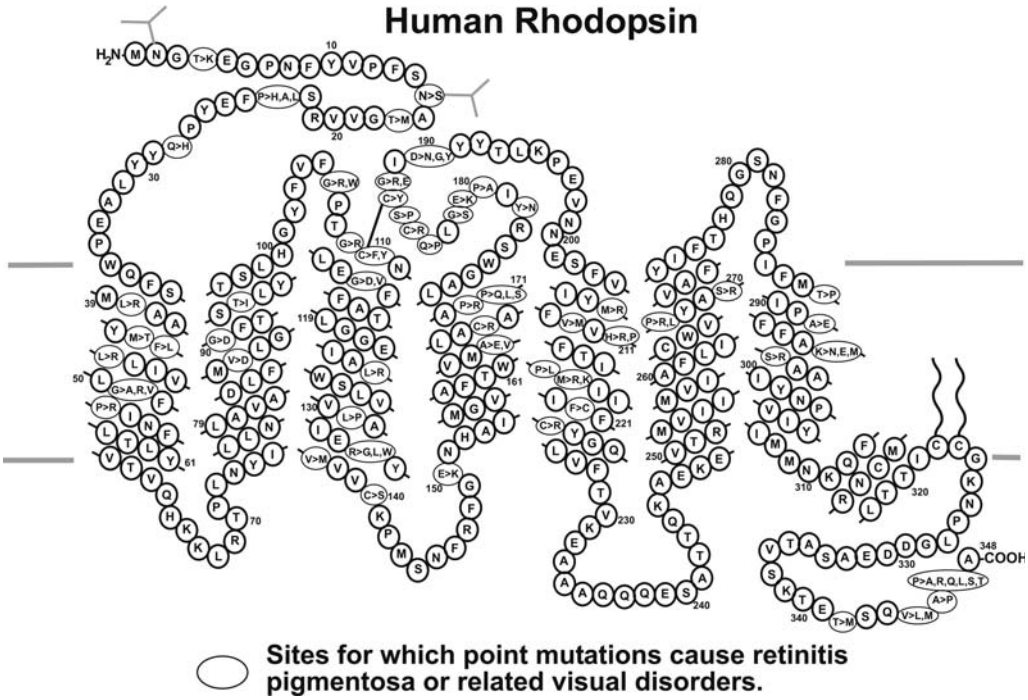

Fig. 4.2 Membrane topology of human rhodopsin and summary of disease-linked amino acid replacements due to mutations (usually autosomal dominant) of its encoding gene.

this concern cannot be raised for all such studies (cf. [31]) and the idea that even wild-type protein folding in the cell is not always robust provides an energetically satisfying rationale for how each of so many different mutations within a single protein can result in disease. It is possible that protein folding in higher organisms may, in general, be less efficient than protein folding occurring in free-living prokaryotes [32, 33]. This may reflect an evolutionary adaptation within small-population, multicellular species by which requirements for high folding efficiency are relaxed in favor of elaboration of quality control systems dedicated to *managing* protein folding and misassembly.

4.3
Ligand Rescue of Misassembly-prone Membrane Proteins: Implications

While the final conformational state of a properly folded membrane protein may usually be determined solely by amino acid sequence, the pathway taken by a nascent membrane protein to reach the properly folded state in the cell typically involves a series of protein–protein interactions involving the ribosome,

the translocon pore complex of the ER and some of the many protein components of protein folding quality control [34–37]. Proteins that are judged to be hopelessly folding-defective by quality control are targeted for degradation. We have argued elsewhere that such proteins need not necessarily have reached kinetically trapped misfolded states [3]. Rather, it is the failure to complete folding promptly that may be the primary determinant for degradation.

For a protein with a critical cellular function, if a large enough fraction of that protein is targeted for degradation as a result of mutations or other misassembly-promoting factors, loss-of-function disease phenotypes may result. Other folding-defective proteins may be able to escape the surveillance of quality control and degradation, leading to accumulation of misfolded protein. In such cases, loss-of-function contributions to disease phenotypes may be compounded by "gain-of-function" toxicity caused by accumulated protein. Examples of both loss- and gain-of-function disorders are compiled elsewhere [38, 39].

Despite the number of distinct protein–protein interactions in which a new protein may participate en route to a properly folded state, it appears that partitioning of a particular protein between pathways leading to proper assembly versus misassembly/degradation may often be governed by relatively simple principles. Particularly compelling evidence that this is the case is provided by numerous observations that membrane proteins that would otherwise be judged "defective" by quality control and targeted for degradation can be rescued by the presence of ligands that specifically recognize and bind to the protein in the ER [19, 40–45]. Such "pharmacological chaperones" can lead to dramatic enhancement in the efficiency of correct protein assembly and trafficking. This represents the basis for a new paradigm in rational drug development.

Ligand-based rescue of misfolding-prone membrane proteins offers important insight into disease-related protein misassembly. First, the fact that a single ligand can often rescue multiple mutant forms of a protein (cf. [44]) suggests that some mutants must share common defects, all correctable through a single ligand binding event. From a clinical standpoint, this is fortuitous since it implies that a series of disease phenotypes based on distinct mutations within a protein may sometimes be treated by a single drug. Moreover, it has been observed that sites in IMPs that are subject to disease-linked mutations are often conserved in related IMPs, where they are sometimes also subject to disease-linked mutations. We have described the relationship between the conserved disease-linked sites as being "phenotologous" [104]. Rescue of one set of mutants by a ligand specific to one protein implies that the defects for the corresponding set of phenologs in another protein should also be correctable by ligand rescue.

While it is conceivable that ligands bind directly to folding intermediates, leading to enhanced folding efficiency relative to degradation, we have argued in support of a model that ligands generally act to enhance folding efficiency by favorably perturbing a two-state quasi-equilibrium in the ER (Fig. 4.3) [3]. The first state involves folding intermediates from which irreversible targeting for degradation can be staged. This state most likely involves protein that is prop-

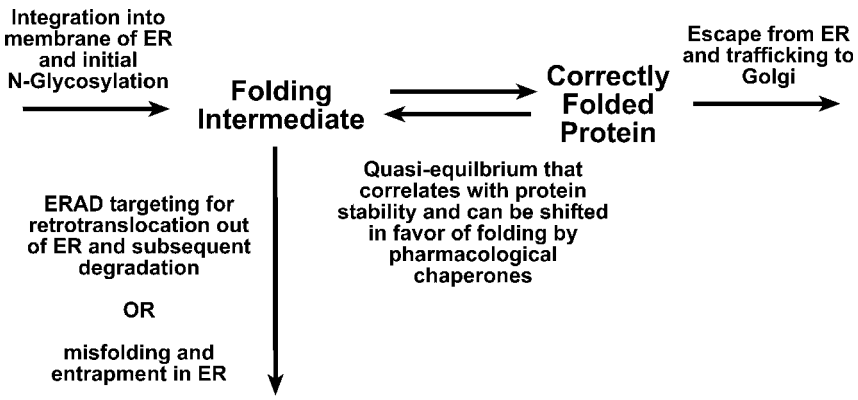

Fig. 4.3 Minimal kinetic scheme to account for partitioning of nascent IMPs between pathways leading to correct folding/trafficking and those leading to irreversible misfolding or degradation. In reality, some steps depicted in this scheme may combine several reversible and/or irreversible steps in the cell. These include the addition and removal of sugars from the immature *N*-linked oligosaccharides and the engagement of the nascent proteins by chaperones and folding sensors [36, 96–102].

erly membrane integrated, but has immature tertiary/quaternary structure. The second state is the folded form of the same protein – a form that is competent for trafficking beyond the ER. By selectively binding to only the completely folded form, ligands shift this quasi-equilibrium in favor of folding, thus promoting escape from possible degradation. The notion that ligands recognize the folded form of the protein is supported by the fact that many "pharmacological chaperones" discovered to date are functionally related to the protein they rescue. For example, a number of the cell permeable ligands found to be effective in rescuing defective G-protein-coupled receptors were originally discovered because they acted either as agonists or antagonists to receptor signaling at the cell surface (cf. [42]).

Characteristics of the folding intermediates from which degradation can be staged have been reviewed previously [3], although it must be pointed out that most results to date have been for water soluble secretory proteins or for extramembrane domains of IMPs. The detailed mechanisms by which folding intermediates are recognized by quality control as being "not yet folded" remain largely unknown – particularly for IMPs which do not have large extramembrane domains. Even the basic identities of some key protein components of membrane protein quality control/degradation systems are still in the process of being discovered (cf. [46–51]).

4.4
What IMP Properties Affect Folding Efficiency in the Cell?

As implied by the ability of cognate ligands to enhance folding efficiency in the cell, it is quite possible that *in vivo* folding efficiency of IMPs will be found to correlate closely with a protein's thermodynamic stability, particularly across a series of mutant forms of a single protein. There is already some direct evidence that this is the case for soluble proteins that pass through the secretory pathway, where they are subject to some of the same quality control mechanisms as IMPs (see review in [3]). This correlation may also apply to cytoplasmic proteins (cf. [52]). Available evidence that this is the case for membrane proteins is less direct, but is supported by the phenomenon of ligand rescue and by observations that factors that generally lead to enhanced IMP stability often lead to an increase in folding efficiency in the cell. These factors include lower-than-physiological culture temperatures and the presence of cell permeable osmolytes (see review in [43]). Other evidence for a tight stability/folding efficiency correlation has been provided by a recent computational analysis by Klein-Seetharaman et al. of the crystal structure of rhodopsin [53]. Their effort led to the proposal that there is a set of around 50 residues in this receptor that are particularly critical for maintaining rhodopsin's stability. About 80% of these sites have previously been subjected to mutagenesis and for the vast majority of these sites (35 out of 39), there is experimental evidence that mutation results in protein misassembly in model cell lines. Indeed, 26 of these sites are linked to retinitis pigmentosa (RP; see Fig. 4.2 for a listing of known RP amino acid replacements). The destabilizing nature of some RP mutants of rhodopsin have also been examined by Hwa et al. [16, 54]. In the same vein, Wang et al. observed that over half of the approximately 30 different glycogen storage disease-linked mutations in the glucose-6-phosphate transporter are predicted to destabilize the protein [55]. This prediction is based on the location of those sites within a homology-based structural model for this human transporter developed using the crystal structure of the *Escherichia coli* glycerol 3-phosphate transporter as a template. Furthermore, as anecdotally illustrated in Fig. 4.4 and discussed in the next section, there is evidence that the majority of disease-linked IMP mutations in transmembrane domains involve specific amino acid replacements that might well be expected to result in protein destabilization based on simple physical chemical principles.

The evidence cited above suggests thermodynamic stability may be a reliable predictor of changes in cellular folding efficiency that occur as a result of mutations in a given IMP. This highlights the importance of continuing efforts (see other chapters in this book) to develop and apply methods for characterizing membrane protein stability – still a frontier area even for purified IMPs in model membranes. Yet, why should the cell care about perturbations in protein stability that would have little affect on the amount of folded protein, if indeed folding reaches equilibrium? Consider the following paradox. An amino acid mutation might lower a protein's thermodynamic stability from 7 to 4.5 kcal mol^{-1}. Assuming folding reaches equilibrium in both cases, this means that, on average, only

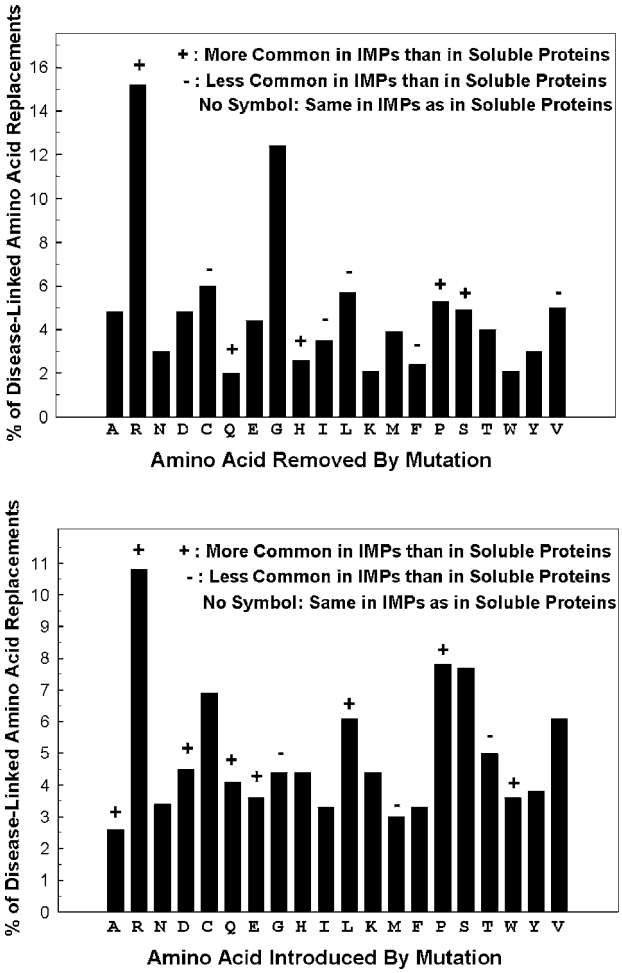

Fig. 4.4 Ranking of each amino acid type in terms of probability of being mutated into or out of proteins (both soluble and membrane) in a disease-linked fashion. This graph was compiled using data found at the Human Disease Mutation Database website (http://www.hgmd.org/) [57]. Also illustrated by "+" or "–" notations are substitutions that were observed by Partridge et al. to be more or less common in disease-linked membrane proteins than in soluble proteins [61].

1 : 100 000 wild-type molecules will be unfolded at any given moment, compared to 1 : 10 000 molecules of the mutant. In both cases, the vast majority of the protein would be functionally competent. Nevertheless, mutations involving such modest changes in stability are often linked to misassembly-related disease. These considerations suggest that the cell is not so much concerned with stability itself, as it is with some other property that closely *correlates* with stability. We have summarized evidence elsewhere that the critical factor determining IMP folding efficiency in

the cell may be the folding *rate* in the cell [3]. While an unstable protein does not have to be a slow folder, kinetics and thermodynamics are linked, such that destabilized proteins often fold more slowly than more stable forms of the same proteins. There is evidence that post-integration/translocation protein folding quality control in the ER is attuned to monitor the *rate* of protein folding, with the result being that proteins which fail to promptly complete folding are targeted for degradation [35, 36, 56].

It will be fortuitous if additional experimental data confirms a strong correlation between IMP stability and *in vivo* folding efficiency. In general, stability measurements can be more easily carried out than folding kinetic measurements – particularly within a cellular context. Moreover, measurements using purified proteins and model membranes are likely reflect thermodynamic stability under cellular conditions, whereas kinetic measurements made under these two sets of conditions are less likely to be in accord.

4.5 Common Mutations in Transmembrane Domains That Lead to Misassembly and Disease

Figure 4.4 illustrates the frequencies for amino acid mutations leading to disease for all proteins (soluble and membrane) extracted from a late 2004 database of around 23,000 documented mutations [57]. In addition to the data in Fig. 4.4, we note that the 10 most common disease-linked amino acid substitutions account for 27% of all missense mutation-based amino acid substitutions, which are: G → R, L → P, R → C, R → W, R → Q, R → H, E → K, P → L, G → D and C → Y. When considering these mutations and the data of Fig. 4.4 it should, of course, be kept in mind that many amino acid substitutions are not possible based only on single missense mutations, and also that there are nucleic acid chemical and structural factors which dictate that some mutation-based codon changes are much more probable than others [58–60]. Moreover, the mutations summarized in Fig. 4.4 do not include mutations which are so devastating that they are embryonic-lethal. With these caveats in mind it can be observed that most common mutations involve the substitution of amino acids exhibiting extremes in terms of physical chemical properties.

Deber et al. conducted a careful analysis of disease-linked mutations for sites in predicted transmembrane domains of 240 IMPs [61]. They compared the frequencies of particular substitutions in membrane proteins to those for disease-linked soluble proteins. Some of their results are summarized in Fig. 4.4. They observed that both the insertion and removal of polar residues play an especially frequent role in IMP-related disease mechanisms. Wild-type polar residues in transmembrane domains usually play critical roles in protein function and may participate in very strong electrostatic interactions or hydrogen bonds, such that it is not surprising that they are often indispensable. The introduction of a polar residue might be expected to disrupt membrane protein stability and/or folding

kinetics, either of which would be expected to lead to quality control-based degradation. There is also the possibility that an introduced polar residue may find another intramembrane polar residue with which to form a very strong hydrogen bond or salt bridge (see reviews in [62, 63]). This could have important functional consequences and may also lead to structures that are kinetically or thermodynamically trapped in a misfolded conformation. Such stable structures may evade degradation by quality control and persist as misfolded structures in the cell, possibly leading to toxic gain-of-function effects.

Based on current interest in glycine-based sequence motifs in membrane proteins [62, 64, 65], it is also interesting to note that Deber et al. found that mutations of wild-type glycine residues in transmembrane segments are no more likely to be related to disease in membrane proteins than in soluble proteins, a fact that highlights the general importance of Gly residues in folding and stability for *both* classes of proteins. However, the introduction of transmembrane Gly into IMPs was observed to be less frequently disease-linked in membrane proteins than in water-soluble proteins.

4.6 Correlating Biophysical, Cell-biological and Biomedical Measurements

There has been a recent and continuing acceleration in the pace at which high-resolution structures of IMPs are being determined [66]. In conjunction with homology-based modeling and other computational methods, the possible affects of disease-linked mutations upon the stability, structure, and function of membrane proteins can now, in many cases, be predicted (cf. [44, 53, 55, 67]). Progress in membrane protein expression, purification and reconstitution is reaching the stage where it is feasible to biochemically and biophysically characterize the affects of disease-linked mutations upon full-length human membrane proteins under well-controlled model membrane conditions [68–74]. Such work will build upon previous studies of the folding and stability of human IMP fragments and model membrane proteins/polypeptides [10, 62, 75–84]. The possibility of making quantitative measurements of protein stability and folding rates in cells or cell-free microsomes is enabled by a variety of technologies (cf. [85–89]). Moreover, it is clear that there is now great potential for quantitatively coupling cellular measurements of membrane protein folding rates and efficiencies to structural biophysical measurements using purified proteins and model membranes (cf. [90, 91]). Much is already known regarding the identities of the molecular components and mechanisms of eukaryotic membrane protein biosynthesis and membrane integration [92–95]. While there are major gaps in our knowledge, even of the key protein components of post-integration IMP quality control, great progress is being made [36, 96–102]. That almost nothing is known about interactions of membrane protein with the relevant components of ER quality control offers opportunities for exploration that are so exciting that rapid settlement of this frontier is predictable.

The initial discovery and continued development of pharmacological chaperones highlights the very positive impact that even rudimentary knowledge of the mechanisms of protein folding and trafficking in the cell can have upon biomedicine. This impact will grow, perhaps exponentially, as the structural biophysical basis for membrane protein folding, misassembly and quality control in the cell is elaborated by continued research. Moreover, as the non-genetic factors that can cause IMP misassembly are characterized and as the role of misassembly in complex and sporadic diseases are unveiled, the fruits of collaboration between membrane protein cell biologists, structural biophysicists and biochemists should be fully manifest.

Acknowledgments

The author thanks Lukas Tamm, Jeff Myers and Chuck Ellis for their comments on a draft version of this manuscript, as well as Anthony Partridge, Charlie Deber and Judith Klein-Seetharaman for providing access to their bioinformatic data. Support of this work by US NIH grants RO1 GM 47485 and R21 NS48573 is gratefully acknowledged.

References

1 A. L. Hopkins, C. R. Groom, *Nat. Rev. Drug Discov.* **2002**, *1*, 727–730.
2 SwissProt/TrEMBL Database and Annotations. Available: http://ca.expasy.org/sprot/.
3 C. R. Sanders, J. K. Myers, *Annu. Rev. Biophys. Biomol. Struct.* **2004**, *33*, 25–51.
4 M. E. Huff, W. E. Balch, J. W. Kelly, *Curr. Opin. Struct. Biol.* **2003**, *13*, 674–682.
5 J. Johansson, *Biochem. Soc. Trans.* **2001**, *29*, 601–606.
6 J. Johansson, T. E. Weaver, L. O. Tjernberg, *Cell Mol. Life Sci.* **2004**, *61*, 326–335.
7 C. G. Levine, D. Mitra, A. Sharma, C. L. Smith, R. S. Hegde, *Mol. Biol. Cell* **2004**.
8 S. J. Kim, R. S. Hegde, *Mol. Biol. Cell* **2002**, *13*, 3775–3786.
9 V. R. Lingappa, D. T. Rutkowski, R. S. Hegde, O. S. Andersen, *BioEssays* **2002**, *24*, 741–748.
10 D. M. Engelman, Y. Chen, C. N. Chin, A. R. Curran, A. M. Dixon, A. D. Dupuy, A. S. Lee, U. Lehnert, E. E. Matthews, Y. K. Reshetnyak, A. Senes, J. L. Popot, *FEBS Lett.* **2003**, *555*, 122–125.
11 J. L. Popot, D. M. Engelman, *Biochemistry* **1990**, *29*, 4031–4037.
12 M. Hermansson, G. von Heijne, *J. Mol. Biol.* **2003**, *334*, 803–809.
13 A. Andres, A. Kosoy, P. Garriga, J. Manyosa, *Eur. J. Biochem.* **2001**, *268*, 5696–5704.
14 S. Kaushal, H. G. Khorana, *Biochemistry* **1994**, *33*, 6121–6128.
15 R. S. Saliba, P. M. Munro, P. J. Luthert, M. E. Cheetham, *J. Cell Sci.* **2002**, *115*, 2907–2918.
16 A. Stojanovic, J. Hwa, *Receptors Channels* **2002**, *8*, 33–50.
17 J. Colby, R. Nicholson, K. M. Dickson, W. Orfali, R. Naef, U. Suter, G. J. Snipes, *Neurobiol. Dis.* **2000**, *7*, 561–573.
18 S. W. Edwards, C. M. Tan, L. E. Limbird, *Trends Pharmacol. Sci.* **2000**, *21*, 304–308.
19 J. P. Morello, A. Salahpour, A. Laperriere, V. Bernier, M. F. Arthus, M. Lonergan, U. Petaja-Repo, S. Angers, D. Morin, D. G. Bichet, M. Bouvier, *J. Clin. Invest* **2000**, *105*, 887–895.
20 J. P. Morello, A. Salahpour, U. E. Petaja-Repo, A. Laperriere, M. Lonergan, M. F. Arthus, I. R. Nabi, D. G. Bichet, M. Bouvier, *Biochemistry* **2001**, *40*, 6766–6775.

21 R. Naef, U. Suter, *Neurobiol. Dis.* **1999**, *6*, 1–14.

22 R. Hermosilla, M. Oueslati, U. Donalies, E. Schonenberger, E. Krause, A. Oksche, W. Rosenthal, R. Schulein, *Traffic* **2004**, *5*, 993–1005.

23 N. Marr, D.G. Bichet, S. Hoefs, P.J. Savelkoul, I.B. Konings, F. de Mattia, M.P. Graat, M.F. Arthus, M. Lonergan, T.M. Fujiwara, N.V. Knoers, D. Landau, W.J. Balfe, A. Oksche, W. Rosenthal, D. Muller, C.H. van Os, P.M. Deen, *J. Am. Soc. Nephrol.* **2002**, *13*, 2267–2277.

24 N. Marr, D.G. Bichet, M. Lonergan, M.F. Arthus, N. Jeck, H.W. Seyberth, W. Rosenthal, C.H. van Os, A. Oksche, P.M. Deen, *Hum. Mol. Genet.* **2002**, *11*, 779–789.

25 J.P. Taylor, R.A. Metcalfe, P.F. Watson, A.P. Weetman, R.C. Trembath, *J. Clin. Endocrinol. Metab.* **2002**, *87*, 1778–1784.

26 C. Reiss, T. Lesnik, H. Parvez, S. Parvez, R. Ehrlich, *Toxicology* **2000**, *153*, 115–121.

27 S. Ghosh, F.S. Collins, *Annu. Rev. Med.* **1996**, *47*, 333–353.

28 L.-C. Tsui, E. Wong, Cystic Fibrosis Mutation Database. Available: http://www.genet.sickkids.on.ca/.

29 C.K. Abrams, S. Oh, Y. Ri, T.A. Bargiello, *Brain Res. Rev.* **2000**, *32*, 203–214.

30 R. Rabionet, P. Gasparini, X. Estivill, *Hum. Mutat.* **2000**, *16*, 190–202.

31 U. Schubert, L.C. Anton, J. Gibbs, C.C. Norbury, J.W. Yewdell, J.R. Bennink, *Nature* **2000**, *404*, 770–774.

32 U. Bastolla, A. Moya, E. Viguera, R.C. van Ham, *J. Mol. Biol.* **2004**, *343*, 1451–1466.

33 R.C. van Ham, J. Kamerbeek, C. Palacios, C. Rausell, F. Abascal, U. Bastolla, J.M. Fernandez, L. Jimenez, M. Postigo, F.J. Silva, J. Tamames, E. Viguera, A. Latorre, A. Valencia, F. Moran, A. Moya, *Proc. Natl Acad. Sci. USA* **2003**, *100*, 581–586.

34 J.L. Brodsky, A.A. McCracken, *Semin. Cell Dev. Biol.* **1999**, *10*, 507–513.

35 L. Ellgaard, A. Helenius, *Curr. Opin. Cell Biol.* **2001**, *13*, 431–437.

36 L. Ellgaard, A. Helenius, *Nat. Rev. Mol. Cell Biol.* **2003**, *4*, 181–191.

37 S.W. Fewell, K.J. Travers, J.S. Weissman, J.L. Brodsky, *Annu. Rev. Genet.* **2001**, *35*, 149–191.

38 M. Aridor, L.A. Hannan, *Traffic* **2000**, *1*, 836–851.

39 M. Aridor, L.A. Hannan, *Traffic* **2002**, *3*, 781–790.

40 M.S. Gelman, R.R. Kopito, *J. Clin. Invest* **2002**, *110*, 1591–1597.

41 T.W. Loo, D.M. Clarke, *J. Biol. Chem.* **1997**, *272*, 709–712.

42 S.M. Noorwez, R. Malhotra, J.H. McDowell, K.A. Smith, M.P. Krebs, S. Kaushal, *J. Biol. Chem.* **2004**, *279*, 16278–16284.

43 A. Ulloa-Aguirre, J.A. Janovick, S.P. Brothers, P.M. Conn, *Traffic* **2004**, *5*, 821–837.

44 S. Wuller, B. Wiesner, A. Loffler, J. Furkert, G. Krause, R. Hermosilla, M. Schaefer, R. Schulein, W. Rosenthal, A. Oksche, *J. Biol. Chem.* **2004**, *279*, 47254–47263.

45 J.P. Morello, U.E. Petaja-Repo, D.G. Bichet, M. Bouvier, *Trends Pharmacol. Sci.* **2000**, *21*, 466–469.

46 K.K. Eriksson, R. Vago, V. Calanca, C. Galli, P. Paganetti, M. Molinari, *J. Biol. Chem.* **2004**, *279*, 44600–44605.

47 B.N. Lilley, D. Tortorella, H.L. Ploegh, *Mol. Biol. Cell* **2003**, *14*, 3690–3698.

48 B.N. Lilley, H.L. Ploegh, *Nature* **2004**, *429*, 834–840.

49 Y. Oda, N. Hosokawa, I. Wada, K. Nagata, *Science* **2003**, *299*, 1394–1397.

50 E. Swanton, S. High, P. Woodman, *EMBO J.* **2003**, *22*, 2948–2958.

51 S. Vashist, D.T. Ng, *J. Cell Biol.* **2004**, *165*, 41–52.

52 Z. Wang, J. Moult, *Hum. Mutat.* **2001**, *17*, 263–270.

53 A.J. Rader, G. Anderson, B. Isin, H.G. Khorana, I. Bahar, J. Klein-Seetharaman, *Proc. Natl Acad. Sci. USA* **2004**, *101*, 7246–7251.

54 A. Stojanovic, I. Hwang, H.G. Khorana, J. Hwa, *J. Biol. Chem.* **2003**, *278*, 39020–39028.

55 J. Almqvist, Y. Huang, S. Hovmoller, D.N. Wang, *Biochemistry* **2004**, *43*, 9289–9297.

56 Y. Wu, M. T. Swulius, K. W. Moremen, R. N. Sifers, *Proc. Natl Acad. Sci. USA* **2003**, *100*, 8229–8234.

57 P. D. Stenson, E. V. Ball, M. Mort, A. D. Phillips, J. A. Shiel, N. S. Thomas, S. Abeysinghe, M. Krawczak, D. N. Cooper, *Hum. Mutat.* **2003**, *21*, 577–581.

58 D. N. Cooper, M. Krawczak, *Hum. Genet.* **1990**, *85*, 55–74.

59 M. Krawczak, E. V. Ball, D. N. Cooper, *Am. J. Hum. Genet.* **1998**, *63*, 474–488.

60 T. Lindahl, *Nature* **1993**, *362*, 709–715.

61 A. W. Partridge, A. G. Therien, C. M. Deber, *Proteins* **2004**, *54*, 648–656.

62 A. Senes, D. E. Engel, W. F. DeGrado, *Curr. Opin. Struct. Biol.* **2004**, *14*, 465–479.

63 A. W. Partridge, A. G. Therien, C. M. Deber, *Biopolymers* **2002**, *66*, 350–358.

64 R. A. Melnyk, S. Kim, A. R. Curran, D. M. Engelman, J. U. Bowie, C. M. Deber, *J. Biol. Chem.* **2004**, *279*, 16591–16597.

65 W. P. Russ, D. M. Engelman, *J. Mol. Biol.* **2000**, *296*, 911–919.

66 S. H. White, *Protein Sci.* **2004**, *13*, 1948–1949.

67 H. A. Lewis, S. G. Buchanan, S. K. Burley, K. Conners, M. Dickey, M. Dorwart, R. Fowler, X. Gao, W. B. Guggino, W. A. Hendrickson, J. F. Hunt, M. C. Kearins, D. Lorimer, P. C. Maloney, K. W. Post, K. R. Rajashankar, M. E. Rutter, J. M. Sauder, S. Shriver, P. H. Thibodeau, P. J. Thomas, M. Zhang, X. Zhao, S. Emtage, *EMBO J.* **2004**, *23*, 282–293.

68 J. L. Baneres, A. Martin, P. Hullot, J. P. Girard, J. C. Rossi, J. Parello, *J. Mol. Biol.* **2003**, *329*, 801–814.

69 C. Berrier, K. H. Park, S. Abes, A. Bibonne, J. M. Betton, A. Ghazi, *Biochemistry* **2004**, *43*, 12585–12591.

70 K. Lundstrom, *Biochim. Biophys. Acta* **2003**, *1610*, 90–96.

71 P. J. Reeves, R. L. Thurmond, H. G. Khorana, *Proc. Natl Acad. Sci. USA* **1996**, *93*, 11487–11492.

72 V. Sarramegna, F. Talmont, P. Demange, A. Milon, *Cell Mol. Life Sci.* **2003**, *60*, 1529–1546.

73 D. N. Wang, M. Safferling, M. J. Lemieux, H. Griffith, Y. Chen, X. D. Li, *Biochim. Biophys. Acta* **2003**, *1610*, 23–36.

74 J. F. White, L. B. Trinh, J. Shiloach, R. Grisshammer, *FEBS Lett.* **2004**, *564*, 289–293.

75 P. J. Booth, R. H. Templer, W. Meijberg, S. J. Allen, A. R. Curran, M. Lorch, *Crit. Rev. Biochem. Mol. Biol.* **2001**, *36*, 501–603.

76 A. K. Chamberlain, S. Faham, S. Yohannan, J. U. Bowie, *Adv. Protein Chem.* **2003**, *63*, 19–46.

77 M. Y. Choi, L. Cardarelli, A. G. Therien, C. M. Deber, *Biochemistry* **2004**, *43*, 8077–8083.

78 K. G. Fleming, *J. Mol. Biol.* **2002**, *323*, 563–571.

79 J. Liang, *Curr. Opin. Chem. Biol.* **2002**, *6*, 878–884.

80 A. L. Lomize, I. D. Pogozheva, H. I. Mosberg, *Protein Sci.* **2004**, *13*, 2600–2612.

81 S. H. White, W. C. Wimley, *Annu. Rev. Biophys. Biomol. Struct.* **1999**, *28*, 319–365.

82 S. H. White, *FEBS Lett.* **2003**, *555*, 116–121.

83 J. K. Nagy, C. R. Sanders, *Biochemistry* **2004**, *43*, 19–25.

84 L. K. Tamm, H. Hong, B. Liang, *Biochim. Biophys. Acta* **2004**, *1666*, 250–263.

85 H. Dale, M. P. Krebs, *J. Biol. Chem.* **1999**, *274*, 22693–22698.

86 H. Dale, C. M. Angevine, M. P. Krebs, *Proc. Natl Acad. Sci. USA* **2000**, *97*, 7847–7852.

87 J. Oberdorf, W. R. Skach, *Methods Mol. Med.* **2002**, *70*, 295–310.

88 J. Lippincott-Schwartz, T. H. Roberts, K. Hirschberg, *Annu. Rev. Cell Dev. Biol.* **2000**, *16*, 557–589.

89 J. Lippincott-Schwartz, E. Snapp, A. Kenworthy, *Nat. Rev. Mol. Cell Biol.* **2001**, *2*, 444–456.

90 W. C. Wigley, M. J. Corboy, T. D. Cutler, P. H. Thibodeau, J. Oldan, M. G. Lee, J. Rizo, J. F. Hunt, P. J. Thomas, *Nat. Struct. Biol.* **2002**, *9*, 381–388.

91 M. F. Princiotta, D. Finzi, S. B. Qian, J. Gibbs, S. Schuchmann, F. Buttgereit, J. R. Bennink, J. W. Yewdell, *Immunity* **2003**, *18*, 343–354.

92 R. E. Dalbey, G. v. Heijne, *Protein Targeting, Transport and Translocation*, Academic Press, Amsterdam, **2002**.

93 M. Higy, T. Junne, M. Spiess, *Biochemistry* **2004**, *43*, 12716–12722.

94 S. Saksena, Y. Shao, S. C. Braunagel, M. D. Summers, A. E. Johnson, *Proc. Natl Acad. Sci. USA* **2004**, *101*, 12537–12542.

95 S. H. White, *FEBS Lett.* **2003**, *555*, 116–121.

96 A. Ahner, J. L. Brodsky, *Trends Cell Biol.* **2004**, *14*, 474–478.

97 S. Dejgaard, J. Nicolay, M. Taheri, D. Y. Thomas, J. J. Bergeron, *Curr. Issues Mol. Biol.* **2004**, *6*, 29–42.

98 A. Helenius, M. Aebi, *Annu. Rev. Biochem.* **2004**, *73*, 1019–1049.

99 A. A. McCracken, J. L. Brodsky, *BioEssays* **2003**, *25*, 868–877.

100 R. Schulein, *Rev. Physiol Biochem. Pharmacol.* **2004**, *151*, 45–91.

101 R. Sitia, I. Braakman, *Nature* **2003**, *426*, 891–894.

102 E. S. Trombetta, A. J. Parodi, *Annu. Rev. Cell Dev. Biol.* **2003**, *19*, 649–676.

103 C. R. Sanders, F. Ismail-Beigi, M. W. McEnery, *Biochemistry* **2001**, *40*, 9453–9459.

104 J. K. Myers, L. A. Beihoffer, C. R. Sanders, *Hum. Mutat.* **2004**, *25*, 90–97.

Part 2
How Proteins Shape Lipids

5
A Census of Ordered Lipids and Detergents in X-ray Crystal Structures of Integral Membrane Proteins

Michael C. Wiener

5.1
Introduction

The most well-established and robust method for the determination of macromolecular structure is X-ray crystallography. The structures obtained with this method present the long-time and large-number average structure of the components in the asymmetric unit of the crystallographic unit cell. These components will be visible as electron density; this electron density is interpreted and the specific molecule or molecular fragment is built into the electron density. In addition to the "primary" macromolecule (e.g. the protein), the locations and structures of other molecules that occupy well-defined well-ordered positions will also be determined. These other molecules can include waters, ions, cofactors, ligands, etc. Solutions of purified integral membrane proteins used for three-dimensional crystallization contain lipids and/or lipid-mimetic molecules such as detergents. These can be present as native lipids that remain with the protein during purification and crystallization or they can be added during the purification process to maintain protein solubility. With nearly no exception, the entity that is crystallized is the protein–detergent complex (PDC) – the membrane protein surrounded by a torus of detergent or detergent–lipid mixture. If the lipids or detergents exist in well-defined average positions and possess well-defined average structures, then their structures will be determined along with that of the membrane protein.

According to the website "Membrane Proteins of Known 3D Structure" (http://blanco.biomol.uci.edu/Membrane_Proteins_xtal.html), there are 88 unique proteins and 165 coordinate sets deposited in the Protein Data Bank (PDB; http://www.rcsb.org) as of April 2005. Membrane protein structure determination is proceeding at an exponential rate that is rather similar to that of soluble proteins, although the number of membrane protein structures today is like that of soluble proteins approximately 30 years ago [1]. There are 50 different membrane protein structures with coordinate sets that include lipids and/or detergents. The purpose of

this "2005 Census" is to perform a first examination of these structures en masse and to seek to elucidate any aspects of lipid–protein interactions that emerge from these structures. The integral membrane proteins in the website "Membrane Proteins of Known 3D Structure" and their PDB entries were examined individually. Those entries containing lipids, detergents and related molecules were then examined graphically (Quanta, Accelrys). All amino acids within 5 Å of lipids, detergents and related molecules were noted, and used for subsequent analysis. Figures were made with PyMOL [2].

5.2 Results

The 50 proteins utilized in this analysis are listed in Table 5.1. Bound lipids, detergents and related molecules are placed into several categories. NL refers to native lipids; these are present in the membrane of the organism in which the protein is expressed, and remain bound to the protein through solubilization, purification and crystallization. There are 78 NL molecules in the set of structures examined. D refers to detergents, added for solubilization and purification; there are 173 detergent molecules in the set of structures examined. SA refers to small amphiphiles. Small amphiphiles (such as heptane-triol and benzamidine) have been used with success to improve the quality of membrane protein crystals [3]. They partition into the detergent portion of the PDC, causing a decrease in the number of detergent molecules in the PDC along with a decrease in the size of the detergent region [4]. This reduction in size enables the more ready formation of stable protein–protein crystal contacts. There are 11 small amphiphile molecules in the set of structures examined. The set of structures also includes one cross-linked lipid (XL) and three palmitoyl moieties attached to amino acids post-translationally (PTM). While the vast preponderance of integral membrane protein structures are obtained from crystals grown in the "classical fashion" (i.e. vapor diffusion crystallization with purified membrane proteins present in PDCs), crystallization via the lipidic cubic phase (LCP) [5] has been uniquely successful for heptahelical archaebacterial membrane proteins (i.e. bacteriorhodopsin [6, 7], sensory rhodopsin [8–10] and halorhodopsin [11]). Two coordinate sets of proteins crystallized using the LCP contain lipids, either cubic-phase-forming lipids (LCP) added for LCP or native lipids (NL).

A total of 2541 amino acids are within 5 Å of these lipid and detergent molecules. Note that an amino acid was counted if any part of it was within the 5 Å distance; therefore, it is possible for a side-chain to be pointing away from the lipid but it will be included if any backbone atoms are within the 5 Å distance. The distribution of amino acid species is shown in Table 5.2. Aliphatic amino acids (A, L, G, V and I) comprise nearly half (47.0%) of the set, with leucine being the most common (15.1%) of both the aliphatics and all other amino acids. The second most-abundant residue is phenylalanine (10.2%), which is more commonly found than the other aromatics (tyrosine 7.1% and tryptophan

Table 5.1 Membrane protein structures included in analysis

Protein	PDB accession no.	Lipids, detergents	Reference
Squalene-hopene cyclase	2SQC	**D** C8E4 (3)	12
Bacteriorhodopsin (bR)	1QHJ	**NL** PHYT (8)	6
Bacteriorhodopsin (bR)	1C3W	**NL** PHYT (4 whole, 9 partial), **NL** SQ (1)	7
Bacteriorhodopsin (bR) (not LCP)	1BRR	**NL** PHYT (2 whole, 5 partial), **D** OG (1)	13
Halorhodopsin (hR)	1E12	**LCP** MO (10), **NL** C16 (1)	11
Sensory rhodopsin (sR) (*Natronobacterium pharaonis)*	1JGJ	**D** OG (1)	8
Sensory rhodopsin (sR) [*Anabaena* (Nostoc) sp. PCC7120]	1XIO	**LCP** and/or **NL** PE (13)	9
Sensory rhodopsin (sR)–transducer complex (*N. pharaonis*)	1H2S	**D** OG (1)	10
Rhodopsin	1HZX	**D** NG (7), **SA** HPT (6), **PTM** palmitoyl (3)	14
Rhodopsin	1GZM	**D** C8E4 (12), **D** LDAO (3), **NL** DPPE (2), **NL** C16 (2)	15
Porin (*Rhodobacter blastica*)	1PRN	**D** C8E4 (3)	16
Porin (*Klebsiella pneumoniae*)	1OSM	**D** C8HES and/or C8Em (9)	17
Porin (OmpF)	2OMF	**D** C8E4 (12)	18
BtuB	1NQE	**D** C8E4 (7)	19
BtuB/E-colicin complex	1UJW	**NL** LPS (2), **D** C8E4 (7)	20
OmpA	1BXW	**D** C8E4 (1)	21
OmpT	1I78	**D** OG (4)	22
OmpX	1QJ8	**D** C8E4 (1)	23
OmpLA (monomer)	1QD5	**D** OG (5, 3 partial, 2 full)	24
OmpLA (dimer)	1QD6	**XL** 1-hexadecanosulfonic acid (2)	24
OpcA	1K24	**D** C10E5 (2 partial)	25
NspA	1P4T	**D** C10E5 (5 partial)	26
NalP	1UYN	**D** C10E5 (1 whole)	27
PagP	1THQ	**D** LDAO (5)	28

Table 5.1 (continued)

Protein	PDB accession no.	Lipids, detergents	Reference
FadL	1T16	**D** C8E4 (3), **D** LDAO (4)	29
FhuA	1BY5	**D** C8HES (8)	30
FhuA	2FCP	**NL** LPS (1)	31
FecA	1KMO	**D** LDAO (17), **SA** HPT (2)	32
KcsA	1K4C	**NL** DAG (1 partial), **NL** 9C (1 partial)	33
ClC	1KPL	**D** OM (1 partial), **NL** C15 (1 partial)	34
AQP0	1TM8	**D** NG (2)	35
AQP1	1J4N	**D** NG (3)	36
AQPZ	1RC2	**D** OG (4)	37
GlpF	1FX8	**D** OG (3)	38
AmtB	1U7G	**D** OG (1)	39
PSRC (*Rhodopseudomonas viridis*)	1PRC	**D** LDAO (2)	40
PSRC (*Thermochromatium tepidum*)	1EYS	**NL** DPPE (1), **D** OG (6), **D** LDAO (1)	41
LH2 (*Rhodopseudomonas acidophila*)	1NKZ	**D** OG (6), **SA** BEN (3)	42
LHC-II	1RWT	**NL** DPPG (1), **D** NG (1), **AL** digalactosyl diacylglycerol (DGD) (1)	43
PS-I (*Thermosynechococcus elongates*)	1JB0	**NL** DPPG (3), **NL** distearoyl monogalactosyl diglyceride (1)	44
PS-I (*T. elongates*)	1S5L	**D** DDM (1)	45
Cytochrome b_6f (*Chlamydomonas reinhardtii*)	1Q90	**NL** C20 (1), **NL** distearoyl monogalactosyl diglyceride (2), **NL** sulphoquinovosyldiacyl-glycerol (SQDG) (1)	46
Fumerate reductase (*Escherichia coli*)	1L0V	**D** C12E8 (4)	47
Fumerate reductase (*Wolinella succinogenes*)	1QLA	**D** DDM (1)	48

Table 5.1 (continued)

Protein	PDB accession no.	Lipids, detergents	Reference
Succinate dehydrogenase	1NEN	**NL** cardiolipin (1), **NL** POPE (1)	49
Nitrate reductase	1Q16	**NL** 1,2-diacylglycerol phosphate (1), **NL** AGA (1)	50
Mitochondrial ADP/ATP carrier	1OKC	**NL** Cardiolipin (3), **D** LDM (2), **NL** DSPC (4)	51
Cytochrome *c* oxidase (*Paracoccus denitrificans*)	1AR1	**D** LDAO (9)	52
Cytochrome *c* oxidase (*Thermus thermophilus*)	1EHK	**D** NG (3)	53
Cytochrome *c* oxidase (chicken)	1BCC	**D** OG (1), **NL** PE (2)	54

D = detergent; NL = native lipid; SA = small amphiphile; PTM = post-translational modification; XL = cross-linked lipid; AL = added lipid; C8E4 = octyltetraoxyethylene; PHYT = phytanyl lipid; SQ = squalene; OG = octylglucoside; MO = mono-olein; 16C = 16-carbon chain; PE = phosphatidylethanolamine; NG = nonylglucoside; HPT = heptane-triol; LDAO = lauryldimethylamine-*N*-oxide; DPPE = dipalmitoylphosphatidylcholine; C8HES = 2-hydroxyethyloctylsulfoxide; C8Em = octyl-polyoxyethylene; LPS = lipopolysaccharide; C10E5 = decylpentaoxyethylene; DAG = diacylglycerol; OM = octylmaltoside; C15 = 15-carbon chain; DPPG = dipalmitoylphosphatidylglycerol; DDM = dodecylmaltoside; C12E8 = dodecyloctaoxyethylene; POPE = palmitoyl-oleoyl-phosphatidylethanolamine; AGA = 2,3-dihydroxypropyl-oxyhydroxyphosphoryloxy-1-pentanoyloxy-methylethyl-octanoate; LDM = 3-laurylamido-dimethylpropylamine-oxide; DSPC = distearoylphosphatidylethanolamine.

5.5%). As would be expected, charged and polar residues are less common. Interestingly, basic residues (lysine 2.1% and arginine 3.0%) are more common than acidic residues (glutamate 1.3% and aspartate 1.7%).

Do the propensities of amino acids to be in proximity to ordered lipids or detergents in membrane protein crystal structures have any relation to the thermodynamics of their partitioning into bilayers or other hydrophobic environments? A variety of hydrophobicity scales exist. Two of the more-utilized scales are those for whole-residue partitioning into lipid bilayers [55] and into octanol [56]. Figure 5.1 plots the frequency of occurrence of amino acids (Table 5.2) versus these two hydrophobicity scales. A correlation exists between the free energy of partitioning ΔG and the frequency of occurrence of these amino acids. Specifically, those residues with an unfavorable energetic cost for partitioning into a lipid bilayer interface or into octanol are more rarely found in the proximity of ordered lipid and detergent molecules than are those residues with less unfavorable or favorable energies of transfer ΔG. The most noticeable outlier from this trend is tryptophan, which possesses a ΔG of approximately -2 kcal mol^{-1}. Among all of the amino acids, this is the most favorable ΔG for partitioning

Table 5.2 Distribution of amino acids within 5 Å of ordered lipids or detergents

Amino acid	*N* (%)	Amino acid	*N* (%)
Alanine (A)	212 (8.3)	Arginine (R)	76 (3.0)
Glutamate (E)	32 (1.3)	Threonine (T)	128 (5.0)
Glutamine (Q)	48 (1.9)	Proline (P)	88 (3.5)
Aspartate (D)	42 (1.7)	Isoleucine (I)	221 (8.7)
Asparagine (N)	50 (2.0)	Methionine (M)	84 (3.3)
Leucine (L)	383 (15.1)	Phenylalanine (F)	260 (10.2)
Glycine (G)	152 (6.0)	Tyrosine (Y))	180 (7.1)
Lysine (K)	53 (2.1)	Cysteine (C)	33 (1.3)
Serine (S)	96 (3.8)	Tryptophan (W)	141 (5.5)
Valine (V)	226 (8.9)	Histidine (H)	36 (1.4)

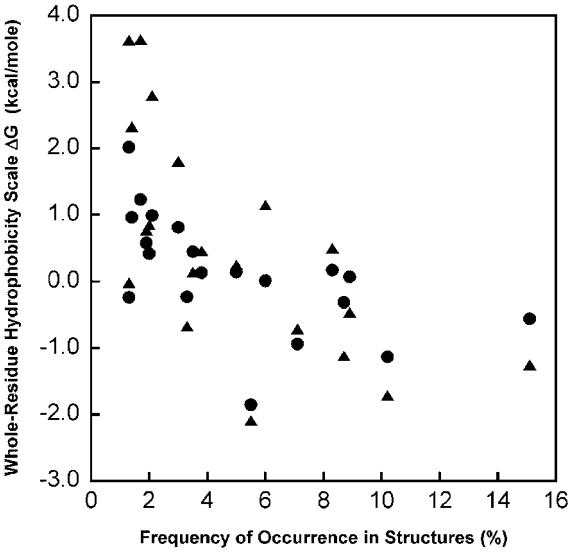

Fig. 5.1 Relationship between the frequency of occurrence of amino acids within 5 Å of ordered lipids and detergents in crystal structures and whole-residue hydrophobicity scales. The frequency of occurrence values are from Table 5.2. The filled circles are whole-residue free energies of transfer ΔG from aqueous to octanol phases [56]; the filled triangles are whole-residue free energies of transfer ΔG from an aqueous phase to a lipid bilayer interface [55].

into the membrane interface or into the bilayer interior. Therefore, based solely upon this, one would predict that tryptophan would be the most common amino acid in this population, but it is not. Analogously, leucine is "over-represented" with respect to its ΔG value. One can perhaps rationalize these outliers by considering steric/packing effects. Tryptophan, possessing the largest side-chain volume, may not easily pack well against lipids. Leucine, with its two δ

carbons symmetrically attached to the γ carbon, may be better able to pack against a wide number of lipid conformations. It is useful to note that these thermodynamic partitioning data were obtained in unstructured host–guest peptide systems, i.e. the amino acid residue was not in an ordered α-helical or β-strand structural element. In the context of a transmembrane helix or strand, thermodynamic parameters could vary. Also, those lipids that are observed in crystal structures both possess well-defined energetically favorable average conformations and occupy positions that can essentially be considered to be lipid-binding sites on the protein surface. As such, they are neither necessarily representative of all of the lipids in a bilayer nor of all of the "boundary" lipids that are adjacent to proteins in membranes. Specifically, steric factors involved in packing amino acid side-chains and lipids together could be affected by neighboring residues on the face of the helix or strand. The possible conformations of an amino acid residue when it is in a secondary-structure element, when that element is positioned within the membrane within a specific range of orientations, could be quite different from possible conformations by the same residue in an unordered region of polypeptide chain.

5.3
Illustrative Examples of Selected Bound Lipids, Detergents and Related Molecules

The remainder of this chapter will consist of a descriptive examination of a series of structures of integral membrane proteins with ordered bound lipids, detergents and related molecules. These structures exemplify a variety of characteristics of the interactions of lipids (and related molecules) with integral membrane proteins. The example structures will be presented in multiple-panel figures; the first figure will show a ribbon diagram of the protein or protein complex with bound lipids, detergents and related molecules shown in stick representation. The following figures for a specific protein will depict specific bound lipids, detergents and related molecules with amino acid side-chains that are in close proximity.

5.3.1
Integral Membrane Protein Structures Contain Ordered Native Lipids

The preparation of membrane proteins for three-dimensional crystallization entails purification of the protein. This purification typically consists of a detergent solubilization of the membrane in which the expressed protein is embedded, followed by multiple chromatographic steps (all in the presence of detergent at a concentration above its critical micelle concentration). The initial detergent solubilization step is usually performed at an even higher detergent concentration. Therefore, those lipids that remain and are seen as well-ordered interpretable electron density are those that are most tightly bound to the protein. Examples of bound native lipids are shown in Figs. 5.2 to 5.4. Figure 5.2 depicts the

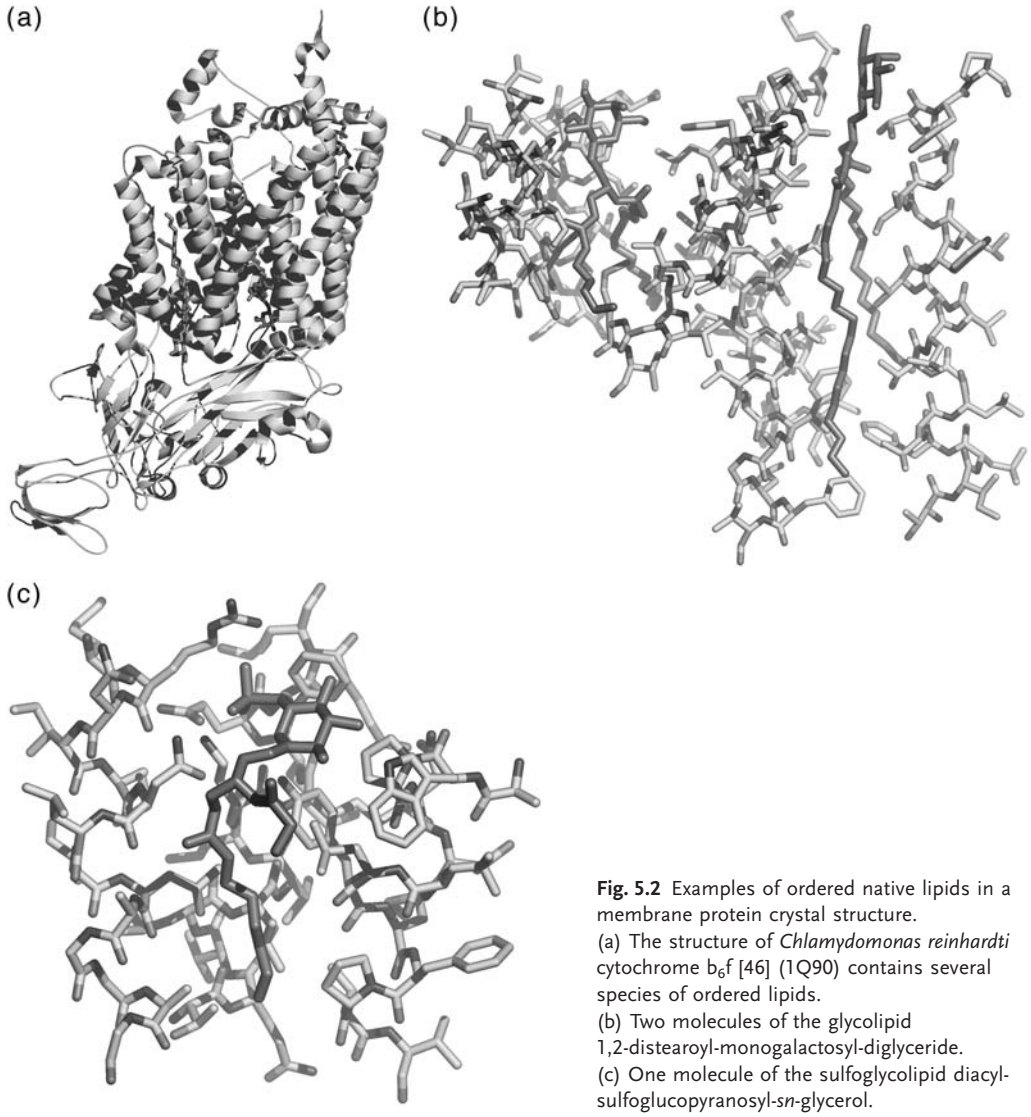

Fig. 5.2 Examples of ordered native lipids in a membrane protein crystal structure.
(a) The structure of *Chlamydomonas reinhardti* cytochrome b_6f [46] (1Q90) contains several species of ordered lipids.
(b) Two molecules of the glycolipid 1,2-distearoyl-monogalactosyl-diglyceride.
(c) One molecule of the sulfoglycolipid diacyl-sulfoglucopyranosyl-*sn*-glycerol.

structure of cytochrome b_6f from *C. reinhardii* [46]. Two different types of native lipids are found in the structure, the glycolipid 1,2-distearoyl-monogalactosyl-diglyceride (two of them, Fig. 5.2 b) and a sulfoglycolipid, diacyl-sulfoglucopyranosyl-*sn*-glycerol (Fig. 5.2 c). Examples of a more common phospholipid, phosphatidylethanolamine (PE), are shown in Fig. 5.3. Two ordered PE molecules are observed in the structure of the chicken cytochrome bc_1 complex [54]. Figure 5.3 a and b indicates that phospholipid acyl chains can take on multiple conformations in crystal structures. In other words, it is unlikely that three-dimen-

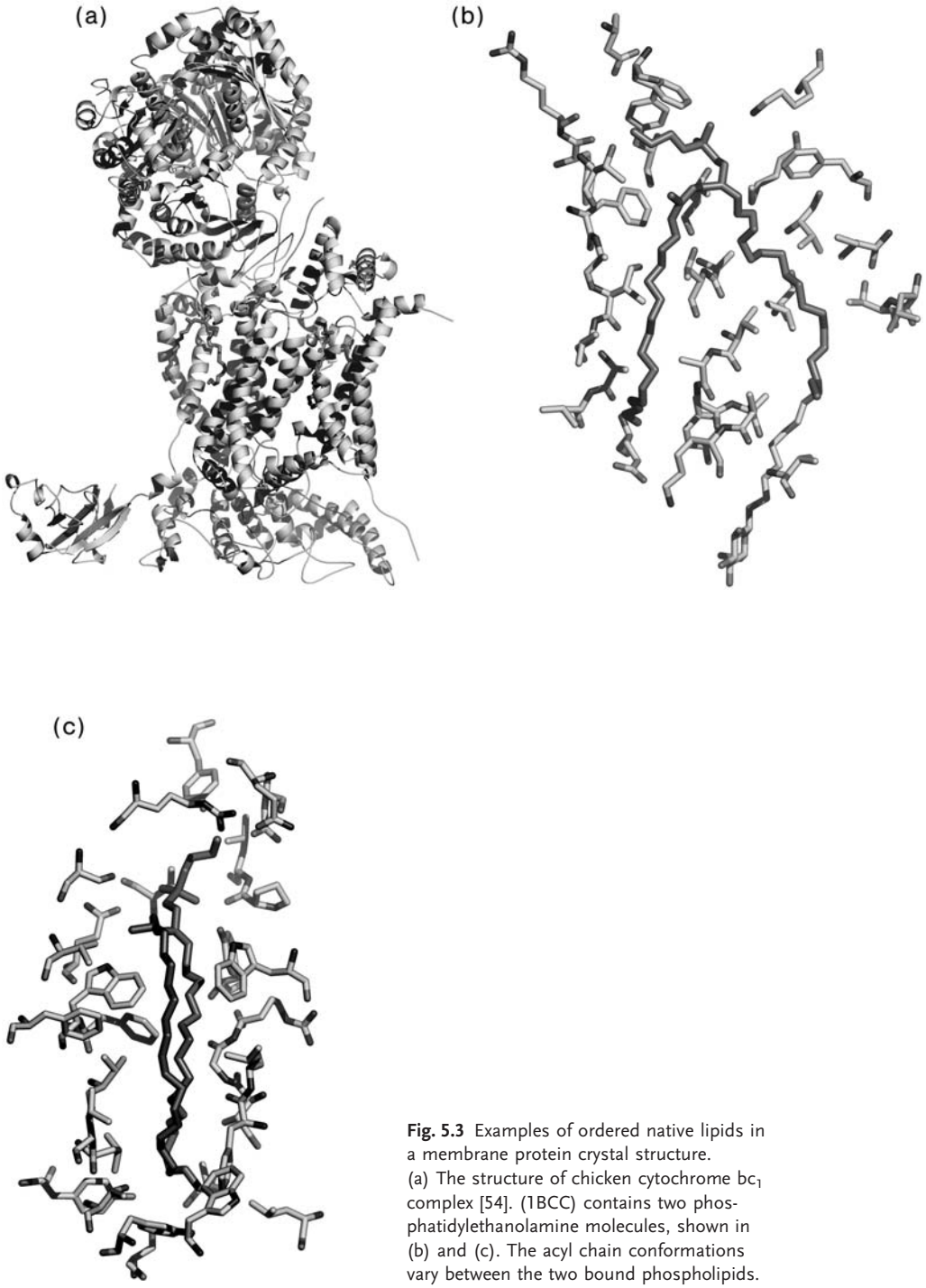

Fig. 5.3 Examples of ordered native lipids in a membrane protein crystal structure. (a) The structure of chicken cytochrome bc_1 complex [54]. (1BCC) contains two phosphatidylethanolamine molecules, shown in (b) and (c). The acyl chain conformations vary between the two bound phospholipids.

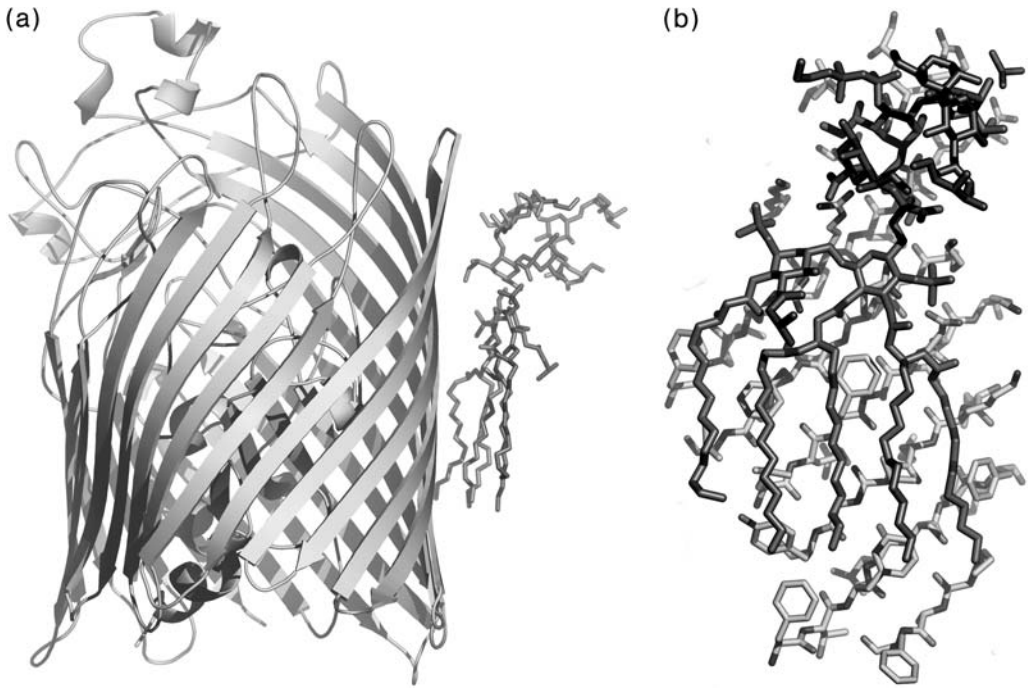

Fig. 5.4 Examples of ordered native lipids in a membrane protein crystal structure. (a) The structure of the *Escherichia coli* outer membrane iron-siderophore transporter FhuA [31]. (2FCP) contains a lipopolysaccharide molecule, shown in (b).

sional crystallization *per se* drives lipids to a single average conformation. Another aspect of these, and of other lipids, detergents and related molecules in crystal structures, is that the only portions of these molecules (or of any other molecules in crystal structures for that matter) that can be modeled into electron density are those molecules or portions of molecules for which statistically significant electron density exists. It is often the case that only a portion of a molecule can be built into density, making its specific identity ambiguous. In particular, if portions of the acyl chains of a lipid are highly disordered, those parts will not be seen in electron density. There are many examples where partial molecules are built into density, just as there are many protein structures where highly flexible termini or loops are absent from the structure. The outer membranes of Gram-negative bacteria (such as *E. coli*) are not "standard" lipid bilayers; the outer leaflet is composed of lipopolysaccharide (LPS). Partial LPS molecules are present in several membrane protein structures and the most complete LPS structure is found in a structure of the iron siderophore transporter FhuA [31] (Fig. 5.4).

5.3.2

Structures of Lipids in Membrane Protein Co-crystals Differ from Those in Pure Lipid Crystals

As seen in Table 5.1 and stated previously, there are 78 native lipids present in complex with integral membrane proteins in X-ray crystal structures. Although the amphipathic nature of lipids has made them a challenging target for small-molecule crystallography, a number of phospholipid structures have been determined (and this literature has been reviewed [57]). How do the structures of lipids found in complex with integral membrane protein structures compare to structures of "pure" lipids? An illustrative example is shown in Fig. 5.5. Figure 5.5a depicts the refined structure of dilauroylphosphatidylethanolamine (DLPE) determined by small-molecule crystallography [58]. Three PE molecules found in membrane protein crystal structures are shown in the other figure panels; Fig. 5.5b depicts a dipalmitoylphosphatidylethanolamine (DPPE) molecule located in the structure of the photosynthetic reaction center of *T. tepidum* [41]; and Fig. 5.5c and d depicts two different diheptadecanoylphosphatidylethanolamine (DHPE) molecules located in the crystal structure of chicken cytochrome *c* oxidase [54]. The most striking difference between the lipid small-molecule structure and those from the membrane protein complexes is the acyl chain conformation. The acyl chain conformation in structures of neat lipids is all-*trans*, while *trans–gauche* isomerization occurs in the acyl chains of lipids bound to membrane proteins. So, although the presence of well-defined lipid structures in membrane protein complexes implies (by definition) a long time-average and large number-average structure, the presence of *gauche* rotamers in

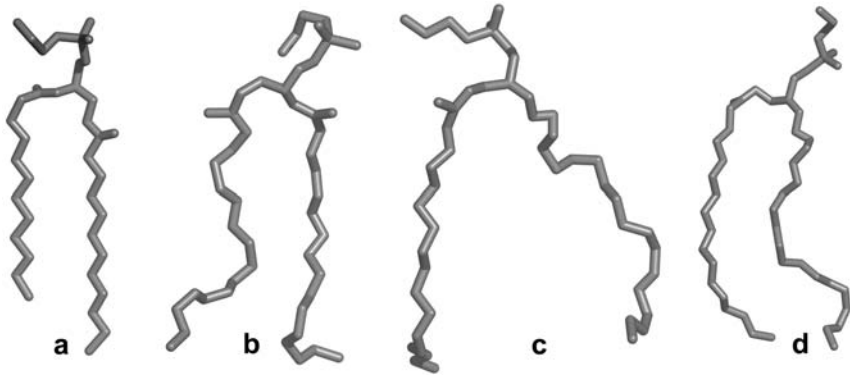

Fig. 5.5 A comparison between lipid structures in a pure phospholipid crystal and in complex with membrane proteins.
(a) Dilauroylphosphatidylethanolamine (DLPE) determined by small-molecule crystallography [58]. The acyl chains are all-*trans*.
(b) Dipalmitoylphosphatidylethanolamine (DPPE), located in the structure of the photosynthetic reaction center of *T. tepidum* [41] (1EYS).
(c, d) Two different diheptadecanoylphosphatidylethanolamine (DHPE) molecules located in the crystal structure of chicken cytochrome c oxidase [54] (1BCC).

these average structure indicates that structures less well-ordered than all-*trans* conformers are stabilized and energetically favorable. The PE headgroup and glycerol backbone conformations also differ. In addition to the obvious presence of the lipid–protein interface in membrane protein crystal structures (versus its absence in lipid small-molecule structures), the amount of water in the two crystalline systems also varies significantly. Membrane protein crystals, like other macromolecular crystals, contain substantial amounts of water; in membrane protein crystals, detergent and water make up 50–80% of the unit-cell volume. Water plays a critical role at the membrane interface, and induces conformational flexibility of acyl chains. In contrast, crystals of pure phospholipids contain little or no water and have typically been crystallized from organic solvents or acid solutions containing little or no water.

5.3.3
Native Lipids can Stabilize and Preserve Protein–Protein Interfaces

The lipids in Figs. 5.2 b and 5.3 b and c are located between subunits of two multiprotein complexes. Frequently, excessive or complete delipidation leads to dissociation or inactivation of membrane protein complexes. A direct structural indication of the importance of lipids in protein–protein interaction and stability is illustrated in these two examples. In a practical sense, maintenance of membrane protein stability and function will likely frequently require the proper amount of native lipid to be present, necessitating the mildest possible solubilization and purification conditions (along with performing functional assays). However, the presence of lipid increases the size of the detergent/lipid region that surrounds the protein (this comprises the PDC that is the entity that is crystallized). Since nearly all productive lattice contacts in three-dimensional membrane protein crystals are made through the protein regions that extend out of the detergent/lipid region, enlarging this region can sterically prevent crystal contacts from forming. Therefore, preparation of membrane protein samples for three-dimensional crystallization presents a challenge to form the smallest PDC that maintains membrane protein function and stability. Interested readers can refer to a recent review on membrane protein crystallization [59].

5.3.4
Multiple Acyl Chain Conformations Exist for Efficient Packing with Protein Interfaces

The substantial conformational flexibility of lipid acyl chains (e.g. *gauche* and *trans* rotamers) permits lipids to pack efficiently against the lipid-facing portions of membrane proteins. Conversely, a wide range of lipid conformers would imply that the amino acids in the transmembrane regions of membrane proteins that face the lipid should not need to be very strongly conserved in sequence. This feature has been previously noted, i.e. the amino acids facing lipid are less conserved than those involved in protein–protein interactions [60]. The two PE

molecules in Fig. 5.3 b and c illustrate two widely disparate acyl chain conformations of the same lipid species located at two different protein interfaces in the same protein complex.

5.3.5
Lipid Acyl Chains Interact Primarily with Aliphatic and Aromatic Amino Acid Side-chains

As shown in Table 5.2, aliphatic and aromatic amino acids are most commonly observed in the proximity of lipids, detergents and related molecules in membrane protein structures. An example of these interactions is shown in Fig. 5.6. Two bound nonylglucoside molecules are observed in the structure of the water channel bovine aquaporin-1 (bAQP1) [36]. Fig. 5.6 b illustrates interactions that are almost completely mediated through aliphatic side-chains; Fig. 5.6 c illustrates interactions that are almost completely mediated through aromatic side-chains. Commonly, a mixture of aliphatic and aromatic side-chains is observed to interact with a specific lipid or lipid-like molecule.

5.3.6
Unusual Lipid/Detergent Conformations Occur at the Protein–Lipid Interface

In addition to acyl chain flexibility, lipid bilayers (especially in the fluid phase) possess an extraordinary range of accessible conformations. In particular, the interfacial region between the more hydrophobic membrane interior and the hydrophilic aqueous milieu beyond the headgroup region has been described as a region of "tumultuous chemical heterogeneity" [61]. The polarity of the membrane can be affected significantly by the composition of lipids (e.g. unsaturated lipids are less non-polar than saturated lipids). Also, the presence of water that penetrates into the membrane interface or that solvates the side-chains of amino acids that are in the membrane interior can make the physical properties and structure of the membrane very different from the canonical bilayer structure. The structure of the membrane certainly plays a role in determining the structures of proteins that are embedded within it (see Chapters 1–3). In X-ray crystal structures of integral membrane proteins, there are examples of detergent conformations at the protein interface that are highly unusual. While one must realize that detergents and lipids are not equivalent, the existence of these conformations should provide some indication that many things are possible at the lipid–protein interface. A structure of rhodopsin [15], shown in Fig. 5.7 a, contains a plethora of ordered lipids and detergents (e.g. 12 C8E4 and three LDAO detergent molecules, as well as two DPPE and two 16-carbon chain native lipids). One C8E4 molecule, highlighted in Fig. 5.7 b, has a "corkscrew" conformation. Other "corkscrew" and "horseshoe" conformations of detergents exist in various X-ray crystal structures. The photosynthetic light-harvesting complex LH2 from *Rps acidophila* [42] is depicted in Fig. 5.8. Six OG detergent molecules and three benzamidine molecules (serving as small amphiphiles to improve

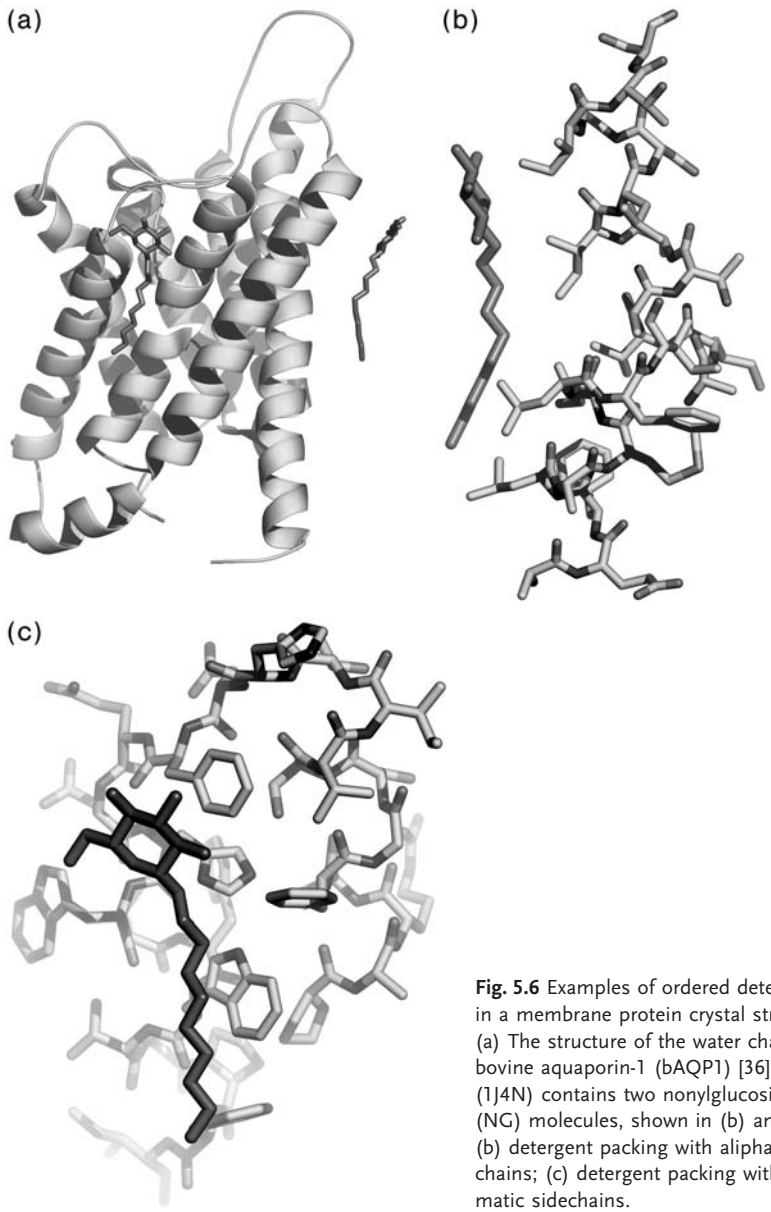

Fig. 5.6 Examples of ordered detergents in a membrane protein crystal structure. (a) The structure of the water channel bovine aquaporin-1 (bAQP1) [36]. (1J4N) contains two nonylglucoside (NG) molecules, shown in (b) and (c); (b) detergent packing with aliphatic sidechains; (c) detergent packing with aromatic sidechains.

crystal quality [3]) are observed in the structure of LH2 (Fig. 5.8 b). The six OG molecules comprise a structure mimicking a bilayer. However, remarkably, one layer of three OG molecules has its glucoside headgroups at a position corresponding to the membrane interior while the other layer has its glucoside headgroups at the "expected" position of the bilayer interface. The three benzamidine

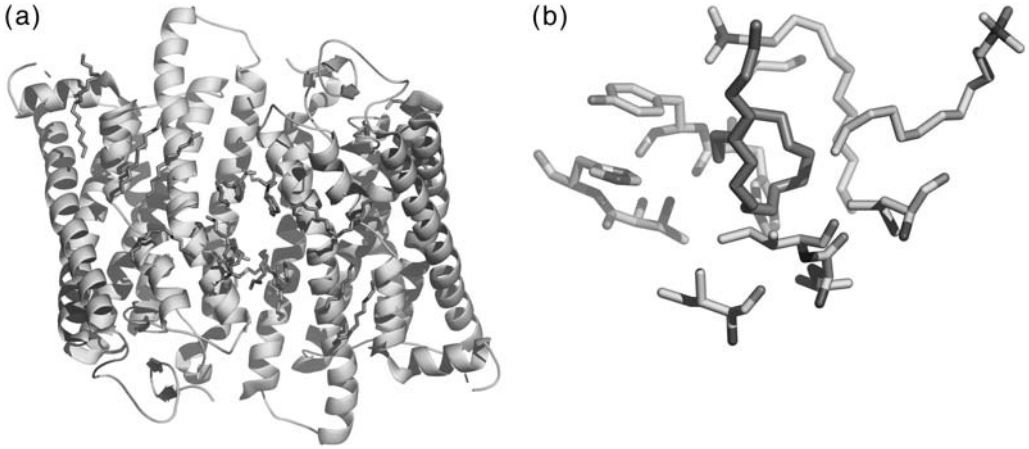

Fig. 5.7 Examples of ordered detergents (in unusual conformations) in a membrane protein crystal structure. (a) The structure of bovine rhodopsin [15] (1GZM) contains four different species of bound lipid or detergent. (b) The structure of an octyltetraoxyethylene molecule (C8E4) that possesses a 'corkscrew' acyl chain.

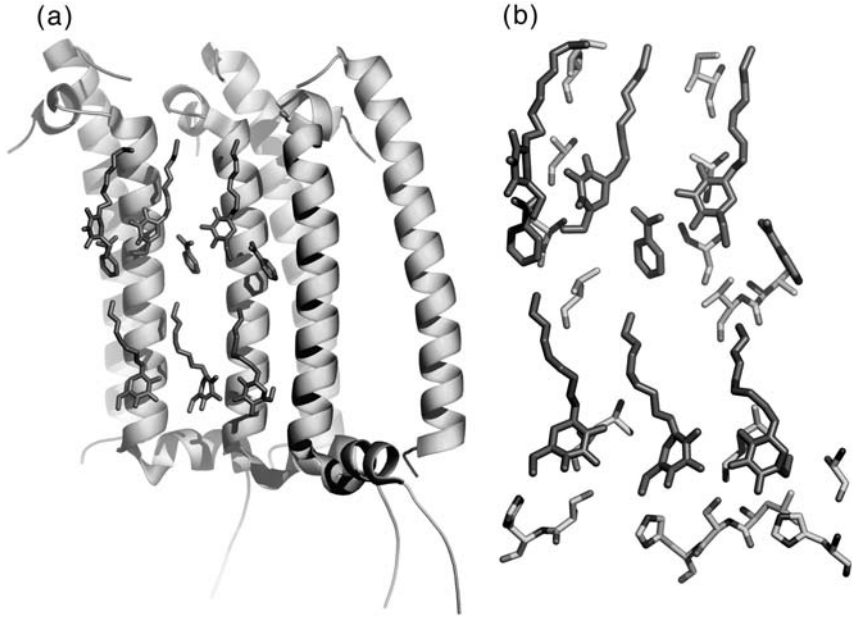

Fig. 5.8 Examples of ordered detergents (in unusual conformations) in a membrane protein crystal structure. (a) The photosynthetic light-harvesting complex LH2 from *Rps. acidophila* [42] (1NKZ) contains a 'bilayer' structure of two layers of octylglucoside (OG) interleaved with three benzamidine molecules. (b) The OG headgroups in the bilayer are asymmetrical; one row of headgroups is in the region corresponding to the membrane interior, and the other row is at the position of the membrane interface.

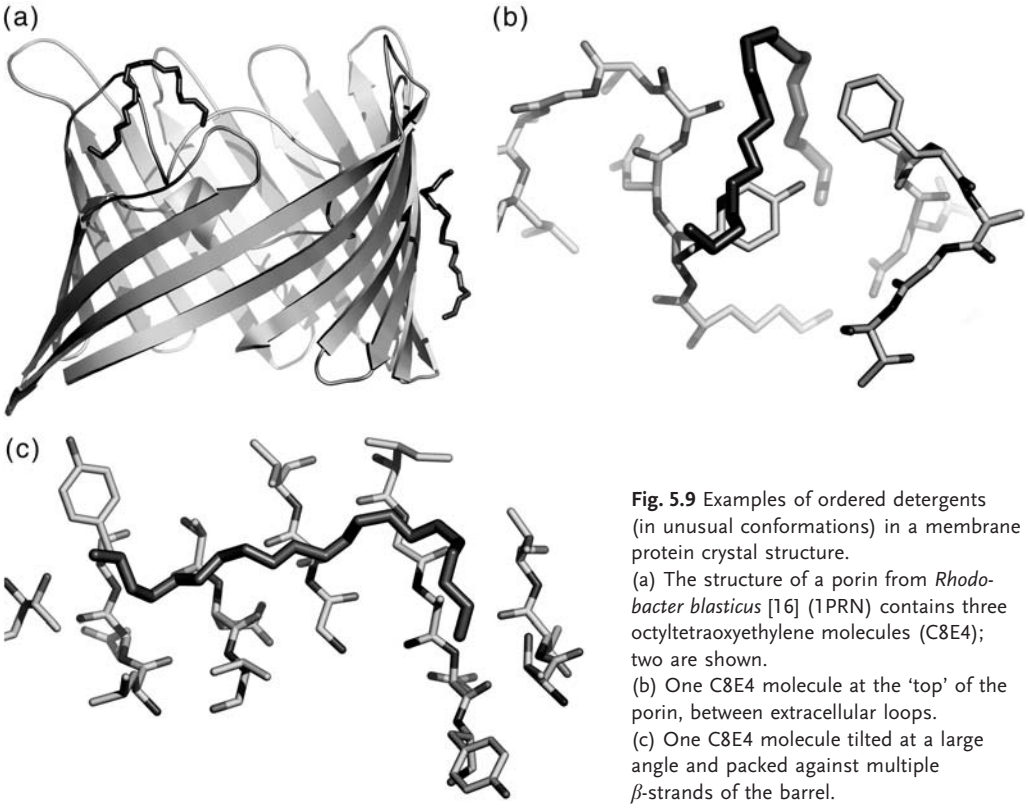

Fig. 5.9 Examples of ordered detergents (in unusual conformations) in a membrane protein crystal structure.
(a) The structure of a porin from *Rhodobacter blasticus* [16] (1PRN) contains three octyltetraoxyethylene molecules (C8E4); two are shown.
(b) One C8E4 molecule at the 'top' of the porin, between extracellular loops.
(c) One C8E4 molecule tilted at a large angle and packed against multiple β-strands of the barrel.

molecules, near the center of the bilayer, are arrayed between the two OG layers. Lastly, the structure of a porin from *R. blasticus* [16] is shown in Fig. 5.9. Two (of the three) ordered C8E4 detergent molecules are shown in Fig. 5.9a. One of these C8E4 molecules is at the "top" of the protein, between extracellular loops (Fig. 5.9b). The other C8E4 molecule, instead of being approximately normal to the membrane surface (or being slightly tilted with respect to the membrane normal) is tilted at a large angle and packs against multiple β-strands of the barrel (Fig. 5.9c).

5.3.7
A Bilayer Structure is Present in Crystals Grown from the LCP

An interesting aspect of the LCP is that, essentially, the bilayer structure is recreated within the crystal lattice. This bilayer may consist of the cubic-phase-forming lipids utilized during crystallization, native lipids present in the protein sample or a combination of the two. An example of this is shown in a structure of the light-driven proton pump bacteriorhodopsin [7] (Fig. 5.10). Thirteen phytanyl-lipids, native to the archaebacterial purple membrane, were built into the

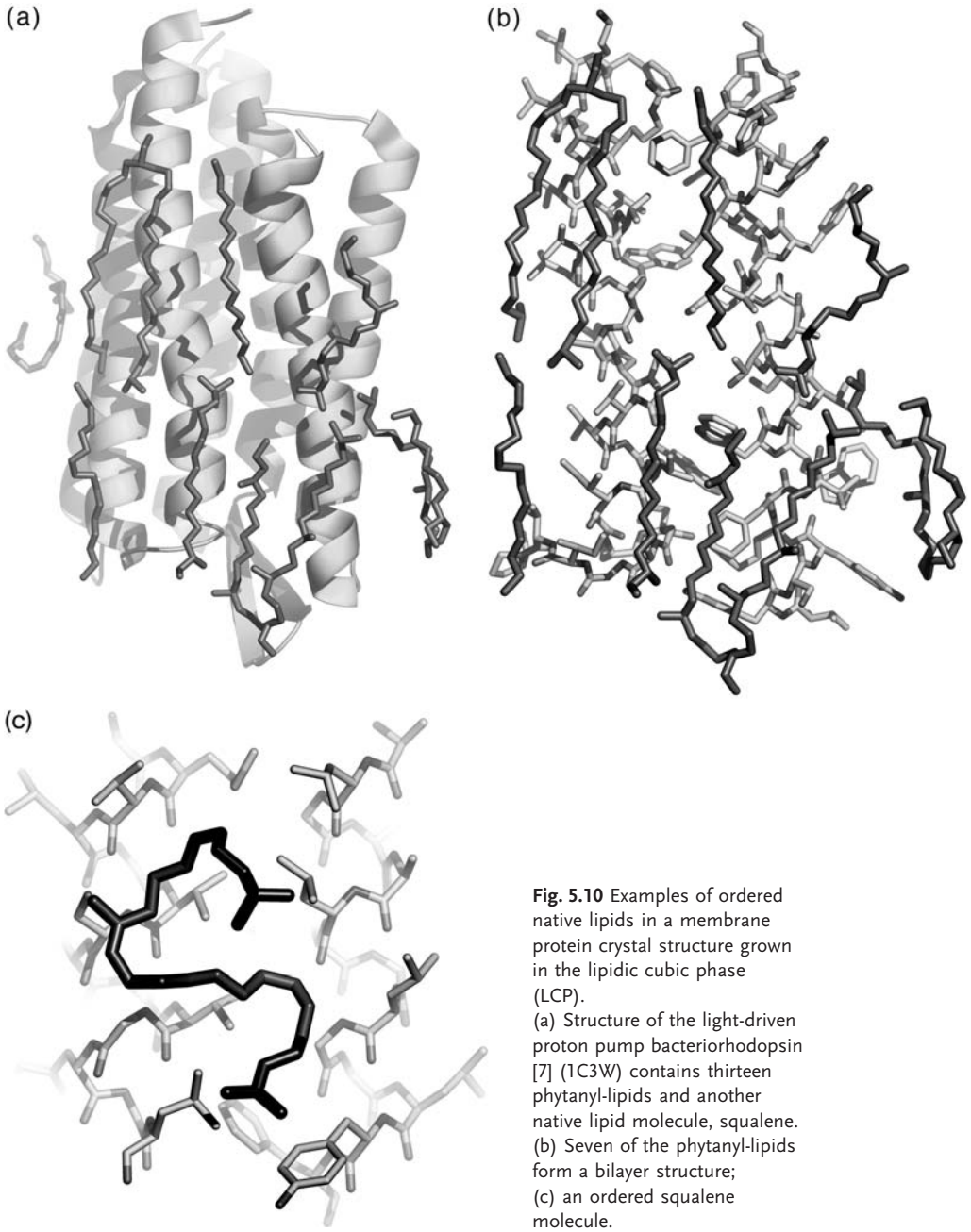

Fig. 5.10 Examples of ordered native lipids in a membrane protein crystal structure grown in the lipidic cubic phase (LCP).
(a) Structure of the light-driven proton pump bacteriorhodopsin [7] (1C3W) contains thirteen phytanyl-lipids and another native lipid molecule, squalene.
(b) Seven of the phytanyl-lipids form a bilayer structure;
(c) an ordered squalene molecule.

structure as whole molecules or fragments. Seven of these lipids form a bilayer structure (Fig. 5.10b). In addition, another native lipid, squalene, is present in the structure (Fig. 5.10c).

5.4 Conclusion

An initial census of bound lipids, detergents and related molecules in the X-ray crystal structures of integral membrane proteins reveals a number of characteristics that are relevant to the general issue of lipid–protein interactions. Further and more detailed bioinformatic analysis of this aspect of X-ray crystal structures will likely yield more quantitative information that may be of predictive utility. This descriptive chapter is intended to be only an initial step in such analyses. It should be emphasized that the ordered lipid and detergent molecules "queried" in this census are only a small fraction of the total number of lipids and detergents that comprise the lipid–protein interface in the protein–detergent complexes that comprise three-dimensional crystals. The presence of ordered lipids and detergents can be viewed as strong evidence for the existence of locations at the protein surface that function very much like high or moderate affinity binding sites for lipids. The majority of the protein surface is likely of a broader and lower-affinity nature, where in the milieu of the membrane interactions with lipids are highly dynamic and are not selective for an induced fit of a specific lipid conformation. In this context, methods (such as nuclear magnetic resonance and molecular dynamics) that investigate both structure and dynamics will be especially useful. The absence of a larger number or frequency of ordered lipids in crystal structures does not necessarily imply their paucity *in vivo*; rather, it implies that they are not present over the large number and time average of a macroscopic crystallography experiment.

Acknowledgments
Research in my laboratory is supported by funding from the National Institutes of Health. Additional past support from the National Aeronautics and Space Administration and from the American Heart Association is also acknowledged. This review is dedicated to A. S.

References

1 White, S. H. The progress of membrane protein structure determination. *Protein Sci. 13*, 1948–1949, **2004**.

2 DeLano, W. L. *The PyMOL Molecular Graphics System*. DeLano Scientific, San Carlos, CA, **2002**.

3 Michel, H. Crystallization of membrane proteins. *Trends Biol. Sci. 8*, 56–59, **1983**.

4 Gast, P., Hemelrijk, P., Hoff, A. J. Determination of the number of detergent molecules associated with the reaction center protein isolated from the photosynthetic bacterium *Rhodopseudomonas viridis*. Effects of the amphiphilic molecule 1,2,3-heptanetriol. *FEBS Lett. 337*, 39–42, **1994**.

5 Landau, E. M., Rosenbusch, J. P. Lipidic cubic phases: a novel concept for the crystallization of membrane proteins. *Proc. Natl Acad. Sci. USA 93*, 14532–14535, **1996**.

6 Belrhali, H. et al. Protein, lipid and water organization in bacteriorhodopsin crystals: a molecular view of the purple membrane at 1.9 Å resolution. *Structure 7*, 909–917, **1999**.

7 Luecke, H., Schobert, B., Richter, H. T., Cartailler, J. P., Lamyi, J. K. Structure of bacteriorhodopsin at 1.55 Å resolution. *J. Mol. Biol. 291*, 899–911, **1999**.

8 Luecke, H., Schobert, B., Lanyi, J. K., Spudich, E. N., Spudich, J. L. Crystal structure of sensory rhodopsin II at 2.4 angstroms: insights into color tuning and transducer interaction. *Science 293*, 1499–1503, **2001**.

9 Vogeley, L. et al. Anabaena sensory rhodopsin: a photochromic color sensor at 2.0 Å. *Science 306*, 1390–1393, **2004**.

10 Gordeliy, V. I. et al. Molecular basis of transmembrane signaling by sensory rhodopsin II–transducer complex. *Nature 419*, 484–487, **2002**.

11 Kolbe, M., Besir, H., Essen, L. O., Oesterhelt, D. Structure of the light-driven chloride pump halorhodopsin at 1.8 Å resolution. *Science 288*, 1390–1396, **2000**.

12 Wendt, K. U., Lenhart, A., Schulz, G. E. The structure of the membrane protein squalene-hopene cyclase at 2.0 Å resolution. *J. Mol. Biol. 286*, 175–187, **1999**.

13 Essen, L., Siegert, R., Lehmann, W. D., Oesterhelt, D. Lipid patches in membrane protein oligomers: crystal structure of the bacteriorhodopsin-lipid complex. *Proc. Natl Acad. Sci. USA 95*, 11673–11678, **1998**.

14 Teller, D. C., Okada, T., Behnke, C. A., Palczewski, K., Stenkamp, R. E. Advances in determination of a high-resolution three-dimensional structure of rhodopsin, a model of G-protein-coupled receptors (GPCRs). *Biochemistry 40*, 7761–7772, **2001**.

15 Li, J., Edwards, P. C., Burghammer, M., Villa, C., Schertler, G. F. Structure of bovine rhodopsin in a trigonal crystal form. *J. Mol. Biol. 343*, 1409–1438, **2004**.

16 Kreusch, A., Neubuser, A., Schiltz, E., Weckesser, J., Schulz, G. E. Structure of the membrane channel porin from *Rhodopseudomonas blastica* at 2.0 Å resolution. *Protein Sci. 3*, 58–63, **1994**.

17 Dutzler, R. et al. Crystal structure and functional characterization of OmpK*36*, the osmoporin of *Klebsiella pneumoniae*. *Structure 7*, 425–434, **1999**.

18 Cowan, S. W. et al. Crystal structures explain functional properties of two E. coli porins. *Nature 358*, 727–733, **1992**.

19 Chimento, D. P., Mohanty, A. K., Kadner, R. J., Wiener, M. C. Substrate-induced transmembrane signaling in the cobalamin transporter BtuB. *Nat. Struct. Biol. 10*, 394–401, **2003**.

20 Kurisu, G. et al. The structure of BtuB with bound colicin E3 R-domain implies a translocon. *Nat. Struct. Biol. 10*, 948–954, **2003**.

21 Pautsch, A., Schulz, G. E. Structure of the outer membrane protein A transmembrane domain. *Nat. Struct. Biol. 5*, 1013–1017, **1998**.

22 Vandeputte-Rutten, L. et al. Crystal structure of the outer membrane protease OmpT from *Escherichia coli* suggests a novel catalytic site. *EMBO J. 20*, 5033–5039, **2001**.

23 Vogt, J., Schulz, G. E. The structure of the outer membrane OmpX from *Escherichia coli* reveals possible mecha-

nisms of virulence. *Structure 7*, 1301–1309, **1999**.

24 Snijder, H. J. et al. Structural evidence for dimerization-regulated activation of an integral membrane phospholipase. *Nature 401*, 717–721, **1999**.

25 Prince, S. M., Achtman, M., Derrick, J. P. Crystal structure of the OpcA integral membrane adhesin from *Neisseria meningitidis*. *Proc. Natl. Acad. Sci. USA 99*, 3417–3421, **2002**.

26 Vandeputte-Rutten, L., Bos, M. P., Tommassen, J., Gros, P. Crystal structure of Neisserial surface protein A (NspA), a conserved membrane protein with vaccine potential. *J. Biol. Chem. 278*, 24825–24830, **2003**.

27 Oomen, C. J. et al. Structure of the translocator domain of a bacterial autotransporter. *EMBO J. 23*, 1257–1266, **2004**.

28 Ahn, V. E. et al. A hydrocarbon ruler measures palmitate in the enzymatic acylation of endotoxin. *EMBO J. 23*, 2931–2941, **2004**.

29 van den Berg, B., Black, P. N., Clemons, W. M., Jr, Rapoport, T. A. Crystal structure of the long-chain fatty acid transporter FadL. *Science 304*, 1506–1509, **2004**.

30 Locher, K. P. et al. Transmembrane signaling across the ligand-gated FhuA receptor: crystal structures of free and ferrichrome-bound states reveal allosteric changes. *Cell 95*, 771–778, **1998**.

31 Ferguson, A. D., Hofmann, E., Coulton, J. W., Diederichs, K., Welte, W. Siderophore-mediated iron transport: crystal structure of FhuA with bound lipopolysaccharide. *Science 282*, 2215–2220, **1998**.

32 Ferguson, A. D. et al. Structural basis of gating by the outer membrane transporter FecA. *Science 295*, 1715–1719, **2002**.

33 Zhou, Y., Morais-Cabral, J. H., Kaufman, A., MacKinnon, R. Chemistry of ion coordination and hydration revealed by a K^+ channel–Fab complex at 2.0 Å resolution. *Nature 414*, 43–48, **2001**.

34 Dutzler, R., Campbell, E. B., Cadene, M., Chait, B. T., MacKinnon, R. X-ray structure of a ClC chloride channel at 3.0 Å reveals the molecular basis of anion selectivity. *Nature 415*, 287–294, **2002**.

35 Harries, W. E., Akhavan, D., Miercke, L. J., Khademi, S., Stroud, R. M. The channel architecture of aquaporin 0 at a 2.2-Å resolution. *Proc. Natl. Acad. Sci. USA 101*, 14045–14050, **2004**.

36 Sui, H., Han, B. G., Lee, J. K., Walian, P., Jap, B. K. Structural basis of water-specific transport through the AQP1 water channel. *Nature 414*, 872–878, **2001**.

37 Savage, D. F., Egea, P. F., Robles-Colmenares, Y., O'Connell, J. D. Jr., Stroud, R. M. Architecture and selectivity in aquaporins: 2.5 Å X-ray structure of aquaporin Z. *PLoS Biol. 1*, 334–340, **2003**.

38 Fu, D. et al. Structure of a glycerol-conducting channel and the basis for its selectivity. *Science 290*, 481–486, **2000**.

39 Khademi, S. et al. Mechanism of ammonia transport by Amt/MEP/Rh: structure of AmtB at 1.35 Å. *Science 305*, 1587–1594, **2004**.

40 Deisenhofer, J., Epp, O., Sinning, I., Michel, H. Crystallographic refinement at 2.3 Å resolution and refined model of the photosynthetic reaction center from *Rhodopseudomonas viridis*. *J. Mol. Biol. 246*, 429–457, **1995**.

41 Nogi, T., Fathir, I., Kobayashi, M., Nozawa, T., Miki, K. Crystal structures of photosynthetic reaction center and high-potential iron-sulfur protein from *Thermochromatium tepidum*: thermostability and electron transfer. *Proc. Natl. Acad. Sci. USA 97*, 13561–13566, **2000**.

42 Papiz, M. Z., Prince, S. M., Howard, T., Cogdell, R. J., Isaacs, N. W. The structure and thermal motion of the B800–850 LH2 complex from *Rps. acidophila* at 2.0 Å resolution and 100 K: new structural features and functionally relevant motions. *J. Mol. Biol. 326*, 1523–1538, **2003**.

43 Liu, Z. et al. Crystal structure of spinach light-harvesting complex at 2.72 Å resolution. *Nature 428*, 287–292, **2004**.

44 Jordan, P. et al. Three-dimensional structure of cyanobacterial photosystem I at 2.5 Å resolution. *Nature 411*, 909–917, **2001**.

45 Ferreira, K. N., Iverson, T. M., Maghlaoui, K., Barber, J., Iwata, S. Architecture of the photosynthetic oxygen-evolving center. *Science 303*, 1831–1838, **2004**.

46 Stroebel, D., Choquet, Y., Popot, J.L., Picot, D. An atypical haem in the cytochrome b_6f complex. *Nature 426*, 413–418, **2003**.

47 Iverson, T.M., Luna-Chavez, C., Cecchini, G., Rees, D.C. Structure of the *Escherichia coli* fumerate reductase respiratory complex. *Science 284*, 1961–1966, **1999**.

48 Lancaster, C.R., Kroger, A., Auer, M., Michel, H. Structure of fumerate reductase from *Wolinella succinogenes* at 2.2 Å resolution. *Nature 402*, 377–385, **1999**.

49 Yankovskaya, V. et al. Architecture of succinate dehydrogenase and reactive oxygen species generation. *Science 299*, 700–704, **2003**.

50 Bertero, M.G. et al. Insights into the respiratory electron transfer pathway from the structure of nitrate reductase A. *Nat. Struct. Biol. 10*, 681–687, **2003**.

51 Pebay-Peyroula, E. et al. Structure of mitochondrial ADP/ATP carrier in complex with carboxyatractyloside. *Nature 426*, 39–44, **2003**.

52 Iwata, S., Ostermeier, C., Ludwig, B., Michel, H. Structure at 2.8 Å resolution of cytochrome *c* oxidase from *Paracoccus denitrificans*. *Nature 376*, 660–669, **1995**.

53 Soulimane, T. et al. Structure and mechanism of the aberrant ba_3-cytochrome *c* oxidase from *Thermus thermophilus*. *EMBO J. 19*, 1766–1776, **2000**.

54 Zhang, Z. et al. Electron transfer by domain movement in cytochrome bc1. *Nature 392*, 677–684, **1998**.

55 Wimley, W.C., White, S.H. Experimentally determined hydrophobicity scale for proteins at membrane interfaces. *Nat. Struct. Biol. 3*, 842–848, **1996**.

56 Wimley, W.C., Creamer, T.P., White, S.H. Solvation energies of amino acid side chains and backbone in a family of host–guest pentapeptides. *Biochemistry 35*, 5109–5124, **1996**.

57 Shipley, G.G. In *The Physical Chemistry of Lipids: From Alkanes to Phospholipids*, Small, D.M. (ed.). Plenum Press, New York, **1986**, pp. 97–147.

58 Elder, M., Hitchcock, P., Mason, R., Shipley, G.G. A refinement analysis of the crystallography of the phospholipid, 1,2-dilauroyl-DL-phosphatidylethanolamine, and some remarks on lipid–lipid and lipid–protein interactions. *Proc. R. Soc. Lond. A 354*, 157–170, **1977**.

59 Wiener, M.C. A pedestrian guide to membrane protein crystallization. *Methods 34*, 364–372, **2004**.

60 Donnelly, D., Overington, J.P., Ruffle, S.V., Nugent, J.H.A., Blundell, T.L. Modeling α-helical transmembrane domains: the calculation and use of substitution tables for lipid-facing residues. *Protein Sci. 2*, 55–70, **1993**.

61 Wiener, M.C., White, S.H. Structure of a fluid dioleoylphosphatidylcholine bilayer determined by joint refinement of X-ray and neutron diffraction data. III. Complete structure. *Biophys. J. 61*, 437–447, **1992**.

6
Lipid and Detergent Interactions with Membrane Proteins Derived from Solution Nuclear Magnetic Resonance

Ashish Arora

6.1
Introduction

Approximately 30% of all genes in a genome code for integral membrane proteins, which are involved in a wide range of functional activities essential for the cell [1]. Membrane proteins, including ion channels and receptors, are the known targets for around 50% of the existing drugs [2]. Despite their functional significance, high-resolution structures of only about 50 proteins have been determined so far [3]. It would be fair to suggest that our current understanding of the structurally and functionally vast class of membrane proteins is limited to a very small fraction. Development of approaches that push the boundaries of existing techniques for structure determination of membrane proteins is therefore of great interest. In the last few years, interest in structural studies of membrane proteins has been fuelled by successful determination of structures of membrane proteins in crystals, micellar solutions and membranes by the use of X-ray crystallography, and solution and solid-state nuclear magnetic resonance (NMR) spectroscopy, respectively.

Most structures of membrane proteins have been determined by X-ray crystallography. However, in spite of the great success in solving crystal structures of fairly large and complex membrane proteins, such as the glycerol facilitator [4] or the ClC chloride channel [5], the uncertainty in obtaining diffraction-quality crystals is still quite high. Crystallization of membrane proteins is a tedious process because the inclusion of detergents, which are necessary for maintaining membrane proteins in soluble and native form, adds another dimension and additional difficulties to crystallization trials. However, there is no doubt that X-ray crystallography will dominate in determination of structures of membrane proteins and will remain the only technique capable of determining atomic-resolution structures of large membrane proteins. A few membrane protein structures have been solved by electron crystallography of two-dimensional crystals to a resolution of about 3 Å in the best cases [6]. The structures of a few small mem-

brane proteins that were uniformly labeled and incorporated in oriented multibilayers have been studied by polarization inversion with spin exchange at the magic angle (PISEMA) and other solid-state NMR techniques [7–9].

Recently, the structures of a few membrane proteins have been determined in solution in the presence of detergent micelles using high-resolution NMR spectroscopy [10–16]. Determination of structures using NMR methods, in particular using the high-resolution solution NMR methods, is very important because the technique provides information not only about the atomic coordinates of the structures, but also dynamic motions of the backbone and side-chains of proteins in a biologically relevant environment. X-ray crystallography often requires (almost) complete delipidation of membrane proteins and their subsequent suspension in detergents that are often structurally only distantly related to membrane lipids. In contrast, solution NMR requires and allows one to solubilize the membrane proteins in a large excess of mild detergents, such as dodecyl phosphocholine (DPC) or 1,2-dihexanoyl-*sn*-glycero-3-phosphocholine (DHPC), that structurally closely resemble membrane lipids, and thus preserve the native structures and functions of membrane proteins in a near-natural environment. In addition, NMR offers unique opportunities to study the interactions of the membrane proteins with disordered lipids and detergents in fluid states. The goal of this chapter is to review measurements of these interactions that have been or potentially could be achieved using solution NMR techniques.

6.2 Heteronuclear Solution NMR of Protein/Detergent Complexes

Until a few years ago, the application of solution NMR spectroscopy was limited to relatively small membrane peptides (10–20 residues) bound to or inserted into sodium dodecyl sulfate (SDS) or DPC micelles. The reason, of course, was that the size of pure detergent micelle (around 25–30 kDa), that would add to the size of the protein under investigation, was itself large for early NMR standards. More recently, new NMR techniques, especially transverse relaxation optimized NMR spectroscopy (TROSY) [17], have been developed to tackle ever-larger sizes of proteins, including membrane proteins in detergent micelles. TROSY results in a substantial reduction of the ^{15}N relaxation rates of the ^{15}N–^{1}H moieties during coherence transfer steps by constructive use of the interference between the ^{15}N and ^{1}H dipolar–dipolar coupling and ^{15}N-chemical shift anisotropy. TROSY is advantageous for protein complexes of 50 kDa and higher at high magnetic fields, especially when the proteins are uniformly deuterated. TROSY has been implemented in the standard triple-resonance experiments for sequential assignments of proteins [18], in three-dimensional ^{15}N-edited nuclear Overhauser effect spectroscopy (NOESY) experiments, and in ^{15}N T_1, T_2 and $\{^{1}H\}^{15}N$-NOE relaxation experiments [19].

Membrane proteins fall into two families. Membrane proteins of the eukaryotic cell or plasma membrane and the inner membrane of prokaryotes belong to the α-helix bundle family. Membrane proteins of the outer membranes of Gram-negative

bacteria, and of chloroplasts and mitochondria, belong to the β-barrel family. Backbone structures of three β-barrel membrane proteins (16–19 kDa) [10–12] have been determined by heteronuclear solution NMR spectroscopy. TROSY methods and uniform deuteration with back-exchange of amide protons were used in most cases. For outer membrane protein A transmembrane domain residues 1–176 (OmpA) and outer membrane protein X (OmpX), use of samples with methyl protonation of δ-methyls of valine, leucine and isoleucine in an otherwise uniformly deuterated background has been made [20–23]. For helical proteins, structures of only small peptides with one or two transmembrane helices (around 4–10 kDa) have so far been determined by NMR spectroscopy [13–15], although resonance assignments for the α-helical 40-kDa trimeric protein diacylglycerol kinase (DAGK) [20] and the three-dimensional structure of the 13-kDa membrane integrating protein Mistic in *N*,*N*-dimethyldodecylamine *N*-oxide (LDAO) [16] have been determined very recently. This is because NMR poses different problems for the two classes of membrane proteins. Sequential assignments are easier to obtain for the β-barrel membrane proteins because of the relatively good chemical shift dispersion of resonances in β-sheets, and the alternating nature of hydrophilic and hydrophobic residues in this class of proteins. In addition, a good number of long-range NOEs are available which, together with implementation of interstrand hydrogen bonds, allow calculation of the backbone fold to high accuracy. The sequential assignments are harder for α-helical membrane proteins, because of the smaller dispersion of the shifts of many consecutive aliphatic and other apolar residues that typically occur in this class of proteins. However, although the larger number of sequential HN–HN NOEs in the helix can be helpful to some extent, it has proven extremely difficult to find enough long-range NOEs that are sufficient to pack helices against each other and thus fold the tertiary structure of helical bundle membrane proteins.

The approaches commonly used for structural refinement of soluble proteins have also been adapted for membrane proteins. Significant improvement in the quality of the structure of OmpX has been achieved by including additional NOEs between the protons of the amide group and the δ-methyl groups of Val, Leu, Ile-methyl protonated and otherwise uniformly ^{2}H,^{13}C,^{15}N-labeled OmpX [21–25]. Residual dipolar couplings (RDC) [26–28] offer an alternative route for structure calculation and refinement. RDCs provide angular constraints based on the orientation of internuclear vectors relative to the magnetic field, which can be used for improving structural accuracy. However, for the measurement of RDCs, weak alignment of the protein molecules is required. The success for magnetic alignment of membrane proteins has been very limited so far because a suitable medium for magnetic alignment was lacking. 1,2-dimyristoyl-*sn*-glycero-3-phosphocholine (DMPC)/DHPC or DMPC/3-[(3-cholamidopropyl)-dimethylammonio]-1-propanesulfonate (CHAPS) bicelles are not suitable for alignment of integral membrane proteins. Filamentous phage pf1 is also not stable in the presence of detergents, especially at high experimental temperatures. The high-concentration of polyacrylamide necessary for mechanical stability of polyacrylamide hydrogels leads to reduced rotational diffusion and extensive broadening of NMR signals and, therefore, the use of polyacrylamide gels

was successful only for relatively small peptides [7, 29–31]. Very recently, a useful degree of alignment has been achieved for OmpA in DPC micelles in negatively and positively charged copolymer gels [32]. Negatively charged copolymer gels were prepared from a 1:1 mixture of acrylamide and either acrylic acid or 2-acrylamido-2-methyl-1-propanesulfonic acid (AMPS). Positively charged copolymer gels were prepared from a mixture of 1:1 acrylamide and *N*-(2-acryloamidoethyl)triethylammonium chloride (APTMAC) [33, 34]. Compressed gels in shigimi tubes having a copolymer concentration of 3–4% gave alignment of OmpA characterized by $^{1}D_{HN}$ in the range between –22 and +25, –10 and +20, and –10 and +25 Hz, for AMPS, acrylic acid and APTMAC copolymers, respectively. In all cases, very good agreement, with a quality factor of around 24%, was obtained between the experimental RDCs and those calculated from the 1.65-Å crystal structure of the OmpA transmembrane (TM) domain [35].

Very recently, the high-resolution structure of a four-helix bundle membrane integrating protein Mistic (110 residues, 13 kDa) has been determined in LDAO micelles [16]. While routine NMR measurements enabled the assignment of secondary structure, the fold of the protein could not be determined. In order to obtain long-range distance constraints necessary for the determination of the three-dimensional fold, the strategy used was to incorporate site-directed spin-labels individually at five different positions along the sequence of Mistic. Distance-dependent line broadening perturbations, caused by the site-directed spin-labels on the amide resonances in the ^{15}N–^{1}H-TROSY spectra of Mistic, were translated into long-range distance constraints. The long-range distance constraints aided in the determination of a preliminary fold, which was refined through an iterative process by collecting long- and medium-range NOEs and refining calibration of the spin-label restraints. The final structure calculation was performed with 573 NOE distance restraints, 346 angle restraints from chemical shifts and NOEs, and 478 distance restraints from the spin-label experiments. In summary, the methodologies described in this section may prove to be of great value in the calculation and refinement of structures of relatively large membrane proteins; in particular, α-helical proteins having many transmembrane segments.

6.3 Choice of Detergents

Solution NMR studies are carried out by solubilizing the proteins in detergent micelles. While this may not reflect the exact same environment as the lipid bilayer of a membrane, extensive biochemical and biophysical characterizations of membrane proteins in non-denaturing detergent micelles lend strong credibility to studying membrane proteins in such environments. In any case, during the course of purification, membrane proteins are solubilized either in detergent micelles or detergent/phospholipid mixed micelles, or denaturing agents such as 8 M urea or 6 M guanidine hydrochloride, or mixtures of organic solvents

like methanol and chloroform. Solubilization in detergents, especially the non-ionic detergents, is the mildest in terms of perturbation of protein structure in comparison to the alternatives mentioned above. Solubilization in detergent micelles is also a prerequisite for crystallization of membrane proteins. For crystallization, the detergent concentration is minimized and maintained only slightly above their critical micelle concentration (CMC) in order to maximize protein–protein contacts. However, for solution NMR studies, detergent concentrations are kept high enough to minimize protein–protein contacts that would degrade the quality of NMR spectra. This is usually achieved by taking the micelles in 2- to 8-fold molar excess over the protein.

DPC is most commonly used as a detergent for structural studies of membrane proteins by solution NMR. OmpA, PhoPQ activated gene product (PagP), DAGK, glycophorin transmembrane domain (GphTM), phospholamban and others have been studied in DPC [10, 12, 13, 20, 36]. DPC has a low CMC (1.5 mM) and an aggregation number of 70–80 at 25 °C in 50 mM NaCl, which

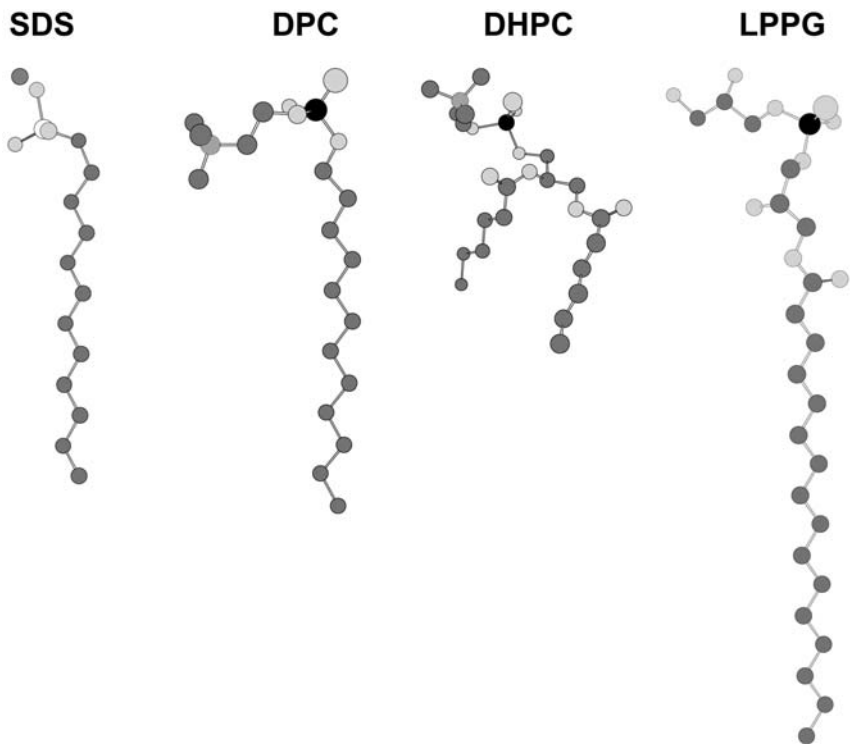

Fig. 6.1 Schematic representation of the chemical structures of some commonly used detergents used for solubilizing membrane proteins for NMR spectroscopy. SDS = sodium dodecyl sulfate; DPC = dodecylphosphocholine, DHPC = 1,2-dihexanoyl-*sn*-glycero-3-phosphocholine; LPPG = 1-palmitoyl-2-hydroxy-*sn*-glycero-3-[phospho-RAC-(1-glycerol)].

translates into an apparent molecular mass of around 26 kDa [24]. Therefore, incorporation of a monomeric or oligomeric protein of total molecular mass up to 50 kDa is manageable for study with modern solution NMR techniques. The other detergents that have been used are DHPC (OmpX), *n*-octyl-*β*-D-glucoside (*β*-OG) (PagP), SDS (M13 coat protein), lyso-myristoyl-PG (Ike coat protein) and LDAO (Mistic) [10, 11, 16, 37, 38]. Schematic representations of the chemical structures of some commonly used detergents are shown in Fig. 6.1. Recently, Krueger-Koplin et al. have conducted an extensive evaluation of detergents for NMR structural studies of small *α*-helical membrane proteins of 4–10 kDa and having two to four TM segments [39]. They have found lyso-palmitoyl-PG to be most suitable for obtaining samples that have a long lifetime and yield high quality NMR spectra.

Detergent concentration needs to be standardized carefully by counting the number and also line-widths at half height of the peaks in the heteronuclear single quantum correlation (HSQC) spectra of proteins. For DPC, detergent concentrations from 300 to 600 mM have been used [40]. In most of the reported studies, use of perdeuterated detergent has been made. However, based on the fast dynamics and exchange of individual detergent molecules, it would appear that perdeuteration of detergent is not necessary. Most of the NMR studies have been conducted at temperatures between 40 and 50 °C, except for OmpX in DHPC micelles for which the temperature was 30 °C. In the presence of certain detergents, the NMR sample can solidify at ambient temperature, leading sometimes to irreversible changes in the sample state [39].

6.4 Size and Shape of Pure Detergent Micelles and Detergent/Protein Complexes

Detergents cooperatively assemble above their CMC in aqueous solutions to form micelles. The CMCs for SDS, DPC and DHPC are 2.2, 1.5 and 15.2 mM, respectively. Above the CMC, the micellar form of detergent is in equilibrium with monomeric detergent. The size of the micelle is described in terms of the number of monomers forming the aggregate, i.e. the "aggregation number". The aggregation number depends on the volume of the hydrated polar region and that of the apolar alkyl region. The aggregation numbers for SDS, DPC and DHPC are around 70, 80 and 35, respectively, corresponding to aggregate molecular masses of around 25, 28 and 16 kDa, respectively. Detergent micelles are usually depicted as idealized spherical structures. Indeed, molecular dynamics (MD) simulations of pure DPC micelles with either 56 or 65 detergent molecules have revealed almost spherical structures with a ratio of the principle moments of inertia of 1.2 : 1.1 : 1 [41]. However, when membrane proteins are solubilized in detergent micelles, the number of detergent molecules associated with the protein would be determined by the hydrophobic surface of the protein that needs to be coated with the hydrophobic alkyl chains of the detergent molecules. The OmpX/DHPC and OmpA/DPC complexes both have apparent molec-

ular masses of around 50 kDa and around 80 detergent molecules associated with the protein.

A variety of techniques, e.g. analytical ultracentrifugation, dynamic light scattering, gel-exclusion chromatography and NMR gradient spin-echo diffusion have been used to determine the sizes of the detergent/protein aggregates. An indirect estimate of the size of the detergent/protein complex can also be derived from the rotational correlation time and global diffusion tensor by analysis of the amide ^{15}N T_1, T_2 and heteronuclear NOE relaxation parameters. The eight-stranded β-barrel proteins have all been found to have rotational correlation times of 20–22 ns corresponding to apparent molecular masses of the detergent/protein complexes of around 50–60 kDa [10–12, 42]. These values are in close agreement with the dynamic light scattering measurements and significantly lower than the molecular mass estimated from NMR gradient diffusion experiments (OmpX).

Consensus is building on the arrangement of detergent molecules around the protein. Analysis of relaxation parameters of OmpA in detergent micelles, MD simulations of OmpA in DPC micelles, intermolecular NOEs in the OmpX/DHPC system [23] and relaxation parameters from a few small α-helical bundle proteins [39] all point towards arrangement of detergent molecules as an oblate ellipsoid around the long axis of protein molecule, covering the cylindrical hydrophobic surface area of the proteins. A schematic representation of a DPC/OmpA micelle is shown in Fig. 6.2. The detergent/protein interface also appears to be slippery, such that the protein can rotate within the confines of the micelle. For OmpX/DHPC, the intermolecular NOEs between protein backbone amide protons and detergent protons were negative, indicating that the lifetime of the individual DHPC molecules on the protein surface were longer than around 0.3 ns. Furthermore, the association of detergent molecules with the protein is dynamic. Detergent molecules exchange between the protein/detergent complex, free monomeric detergent and detergent-only micelles on a submillisecond timescale [23].

6.5 Sample Preparation for Solution NMR Measurements

The β-barrel proteins for which NMR structures have been determined are all expressed into inclusion bodies. The inclusion bodies are solubilized either into 8 M urea (OmpA) or 6 M guanidinium hydrochloride (OmpX, PagP). For NMR studies, the proteins are refolded by diluting the urea or guanidinium hydrochloride solution into buffer containing detergent micelles. For the OmpA TM domain, refolding was carried out by slowly diluting the protein solution in 15 mM Tris buffer, pH 8.5, containing 8 M urea into more than 10-fold excess of 20 mM borate buffer, pH 10.0, containing 150 mM NaCl, 1 mM EDTA and 20 mM DPC. After overnight refolding, the solution was concentrated through Amicon PM10 or YM1 membranes. The dilution–concentration step was repeated twice with

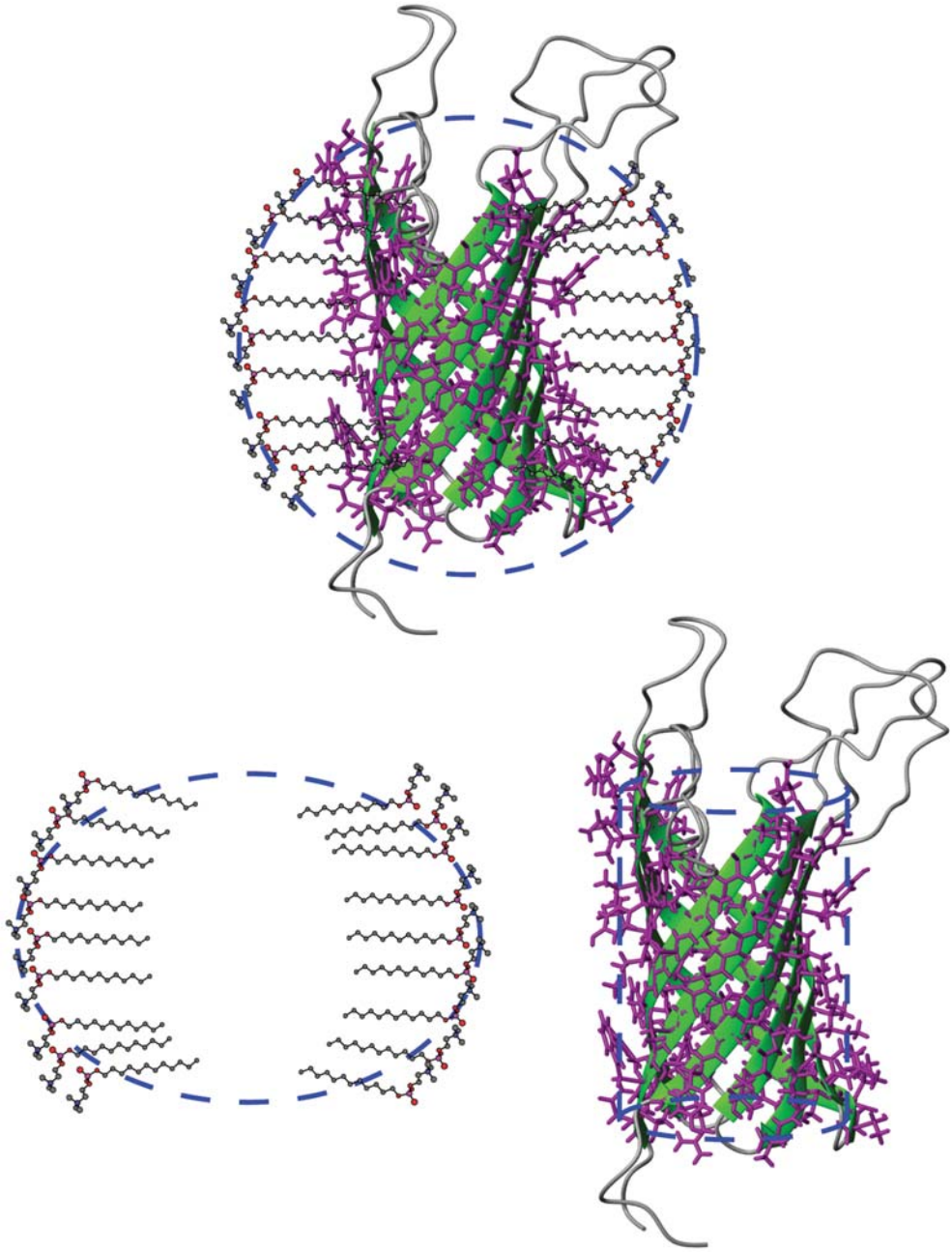

Fig. 6.2 Schematic representation of the spherical OmpA/DPC micelle shown as a combination of DPC molecules arranged as an oblate ellipsoid and a cylindrical molecule of OmpA.

NMR buffer (20 mM sodium phosphate, 50 mM NaCl, 0.1% NaN_3) to give a final concentration of 1 mM protein and around 600 mM DPC [12].

PagP was refolded from 6 M GdmCl solution into phosphate buffer containing DPC, pH 6.0, using a procedure similar to that described above for OmpA. However, for the refolding of PagP in *β*-OG, precipitated PagP was dissolved in 1 ml of 5% perdeuterated SDS and dialyzed for 5 days through a membrane with molecular weight cutoff of 6.5 kDa, against 50 mM sodium phosphate buffer, pH 6.0; 32 mg of *β*-OG was slowly dissolved and then d5-ethanol was added to 1%. The sample was concentrated to yield a 1 mM PagP NMR sample in around 200 mM *β*-OG. Both SDS and ethanol were required for 100% refolding [10].

OmpX was solubilized in 6 M GdmCl in 20 mM Tris buffer (20 mM Tris and 5 mM EDTA), pH 8.5. Solubilization and reconstitution of OmpX was preformed by slowly diluting the protein solution in 6 M GdmCl into a 6-fold excess of refolding buffer containing 3% DHPC, 20 mM Tris, 5 mM EDTA, 0.6 M arginine, pH 8.5, at 4 °C. The OmpX/DHPC solution was then dialyzed against 2.5 l of 20 mM Tris buffer, pH 8.5, having 5 mM EDTA and 100 mM NaCl, at 4 °C for 20 min to remove residual GdmCl and L-arginine. The sample was concentrated to a volume of 300 µl. The final protein concentration was about 2 mM and the detergent concentration was adjusted to 300 mM by adding solid DHPC to the solution [11].

Sample preparation protocols have to be worked out more carefully for *α*-helical membrane proteins. Sample preparation has been described for this category of membrane proteins starting from solid-phase peptide synthesis to overexpression in *Escherichia coli* membranes. Several membrane peptides synthesized through solid-phase synthesis can be lyophilized and dissolved in buffer having the appropriate detergent. Lyophilized pardaxin (33 residues) and phospholamban (50 residues) were dissolved in 20 mM phosphate buffered saline, pH 6.5, containing 300 and 600 mM DPC, respectively. The sample pH was adjusted to pH 4.5 with NaOH for NMR experiments [36, 43]. Other small membrane peptides, e.g. *E. coli* and *Bacillus pseudofirmus* OF4 ATP synthase c subunits, have been expressed in bacterial cells and extracted with organic solvents. The peptides were reconstituted by mixing detergent and peptide in 3 : 1 chloroform : methanol and drying to a thin, clear film under a stream of argon for up to 12 h. Detergent/protein films were then dissolved in 1–50 mM aqueous potassium phosphate buffer, pH 4.5–8, for NMR experiments [39].

A more specialized protocol of reconstitutive refolding was followed for the preparation of an NMR sample for the multihelix membrane-spanning protein DAGK. The protein that was obtained after purification in DPC micelles was inactive. In order to get active protein, DAGK/DPC micelles were mixed with POPC to generate DAGK/DPC/POPC mixed micelles. DPC was removed by extensive dialysis to yield POPC lipid vesicles containing DAGK at 1 : 100 DAGK : POPC mol : mol ratio in refolding buffer (pH 7.8 buffer containing 10 mM imidazole and 0.05 mM EDTA). The membrane preparation was resolubilized in DPC micelles and POPC was removed to recover DAGK/DPC micelles with DAGK in its active form [44].

6.6 Protein/Detergent Interactions Monitored by NMR Spectroscopy

The complementarities of X-ray crystallography and NMR spectroscopy approaches are most apparent when one tries to piece together information for visualizing the detergent/protein complex. The lipid and water molecules observed in the crystal structures of membrane proteins are those frozen in an ordered manner during the crystallization process. On the other hand, by virtue of their chemical structures, water, detergent and protein all contain NMR-active nuclei that are observable only in their dynamic state in solution by NMR spectroscopy. The simplest case is differentiation of regions of the peptide backbone exposed to and protected from the solvent by virtue of the micelle. Solvent exchange experiments using the solvent-exposed amides with TROSY (SEA-TROSY) technique [45] on the backbone amide protons of OmpA in DPC micelles indicate that the amide protons in the loops and turns are fully solvent exposed (having very low protection factors), whereas the amides of the β-strand residues are highly shielded from the solvent H_2O (unpublished results). These results suggest that the detergent is "wrapped" as a belt around the barrel of OmpA with the loops and turns extending into the solvent.

Distinct ^{1}H chemical shifts of the various groups of protons of the detergent can be used to determine the proximity of these moieties to the assigned backbone and side-chain protons of the protein in the protein/detergent micelle, either by designing suitable saturation transfer difference (STD) NMR experiments or through measurement of intermolecular NOEs. Protein detergent interactions have been characterized in great detail for the OmpX/DHPC system using the V,L,I-δ-methyl protonated-^{2}H,^{13}C,^{15}N-labeled protein, utilizing the previously determined backbone and protonated methyl group sequence-specific assignments [23]. The distribution of DHPC molecules on the surface of the proteins was analyzed in terms of intermolecular NOEs between the protein methyl groups and DHPC, and between backbone amide protons and DHPC. The headgroup and alkyl chains resonances of DHPC were assigned from ^{1}H–^{1}H, and ^{1}H–^{13}C correlation experiments. All DHPC molecules were considered to form a continuous hydrophobic phase surrounding the protein, where individual DHPC molecules cannot be distinguished. However, in spite of the large size (around 50–60 kDa) of the mixed OmpX/DHPC micelle, spin diffusion between the headgroup choline methyl group and the alkyl chain methyl or methylene groups were not observed allowing clear distinction for the orientation of detergent molecules relative to the protein surface. For all of the 13 Val, Leu and Ile residues located on the outside hydrophobic surface of the barrel, strong intermolecular NOEs were observed between the protein methyl groups and the alkyl protons of DHPC. For Val, Leu or Ile residues located on the extracellular loops or having side-chains pointing towards the core of the barrel, weak or very weak NOEs to DHPC were observed.

Intermolecular NOEs between the amide protons of OmpX and the hydrophobic ends of DHPC were also observed. The intensities of these NOEs were largest for residues located centrally on the barrel surface and decreased towards

the edges of the barrel. No amide proton-detergent NOEs were detected in the polypeptide segments corresponding to the loops and turns. Intermolecular NOEs between the backbone amide protons and DHPC cover the surface of OmpX over a range of approximately 28 Å centered about the middle of the β-barrel, which coincides with the hydrophobic surface of OmpX. This precludes the arrangement of a bilayer of DHPC molecules in the form of a torus around OmpX, because of the thermodynamically unfavorable "hydrophobic mismatch" between the bilayer thickness of fully extended hydrophobic chains of DHPC (16 Å) and the hydrophobic surface of OmpX (28 Å). Alternatively, an arrangement of DHPC molecules on the hydrophobic protein surface with the detergent molecules oriented perpendicular to the protein surface forming a cylindrical belt around the hydrophobic surface can account both for the intermolecular NOEs and the hydrophobic length of OmpX. The approximate molecular mass of the OmpX/DHPC micelles is known to be in the range 50–70 kDa. Calculations based on approximating the surface of OmpX to a cylinder with a diameter and height of 25 and 28 Å, respectively, and a diameter of 4 Å for each of the two hydrophobic tails of DHPC, yields the number of DHPC molecules in contact with OmpX to be about 80. From the molecular weight of 453 Da of DHPC and 16 384 Da for OmpX, the micelle size comes to about 52 kDa.

The organization of DHPC molecules around OmpX has also been studied by monitoring the differential relaxation effects of water-soluble and lipophilic paramagnetic relaxation agents on the resonances of the detergent and the protein [46]. The paramagnetic relaxation agents chosen were Gd(DOTA) (Gd^{3+} chelated with 1,4,7,10-tetraazocyclododecane-*N*,*N*′,*N*″,*N*‴-tetraacetic acid), 16-doxylstearing acid (16-DSA) and 5-doxylstearic acid (5-DSA). Gd(DOTA) is water soluble and does not penetrate into the micelle interior. On the other hand, 16-DSA and 5-DSA are incorporated into the DHPC micelles. Relaxation effects of titration with paramagnetic relaxation agents were monitored in terms of decrease in the intensity of peaks in the ^{15}N–^{1}H-TROSY spectrum for OmpX, and line broadening of the headgroup $N(CH_3)_3$ group and the alkyl chain terminal CH_3 group for DHPC. Gd(DOTA) affected mostly the $N(CH_3)_3$ resonances of DHPC and the residues located in the extracellular loops L1–L4 of OmpX. The effect of Gd(DOTA) on the residues located in the periplasmic turn was smaller than that for the loops, while the β-strands showed almost no effect. In contrast, 16-DSA exerted a maximal effect on the alkyl chain terminal CH_3 resonances of DHPC and residues located in only the central parts of the β-strands. The effect of 5-DSA was very interesting. While the relaxation effect of 5-DSA was also most pronounced for the alkyl chain terminal CH_3 resonances of DHPC, its magnitude was lower than that caused by 16-DSA. At the same time, 5-DSA affected a larger area of the protein surface than 16-DSA. In fact, two narrow bands around the β-barrel near the ends of each β-strand, which could represent the residues located in the interfacial region in lipid membranes, were affected only by 5-DSA and not by 16-DSA or Gd(DOTA). For this region of the OmpX surface, intermolecular NOEs from the protein to the $N(CH_3)_3$ groups of DHPC were also observed. Thus, while intermolecular NOEs between OmpX and

DHPC were not able to differentiate between the central hydrophobic region and the interfacial region of OmpX, this distinction was made possible by the use of 16-DSA and 5-DSA [46].

Detergent/protein intermolecular NOEs and the relaxation effects of paramagnetic probes that selectively partition to hydrophilic and hydrophobic environments were measured for the four-helix bundle membrane integrating protein Mistic/LDAO micelle system [16]. The results are consistent with an arrangement of the detergent molecules as a concentric ring around the helical bundle. The global rotational correlation time of Mistic in LDAO micelles was found to be 11 ns, which corresponds to a molecular mass of around 22 kDa, suggesting an association of 40–50 LDAO molecules around every molecule of Mistic.

6.7 Dynamics and Conformational Transitions of Membrane Proteins in Detergent Micelles

NMR offers the unique advantage of measuring dynamical properties of proteins and macromolecular complexes. In the last few years, the study of membrane proteins in detergent micelles by NMR spectroscopy has led to the realization of fundamentally new concepts about the dynamic behavior of membrane proteins. Existence of a flexibility gradient was first determined from $\{^1H\}^{15}N$-NOE measurements on OmpA in DPC micelles. The central portion of the β-barrel was found to be very rigid, with flexibility increasing towards the two ends. Similar results were obtained for OmpX and PagP in detergent micelles, suggesting that this may be a common feature of membrane proteins. Detailed NMR dynamics measurements are based on the analysis of amide ^{15}N longitudinal (T_1) and transverse (T_2) relaxation times and heteronuclear nuclear Overhauser enhancement ($\{^1H\}^{15}N$-NOE) which can characterize motions of the protein on timescales ranging from picoseconds to milliseconds. Dynamic analysis of the polypeptide backbone has revealed motions on three time scales for the OmpA/DPC system. The residues of the β-barrel exhibit fast motions on a picosecond timescale. The extracellular loops on the other hand experience picosecond motions and also collective motions on a nanosecond timescale. Eighteen residues mostly in the center of the β-barrel have been found to be involved in conformational exchange on the micro- to millisecond timescale. While experimentally it has been demonstrated that OmpA can form an ion conducting pore in planar lipid bilayers, the static picture offered by the crystal structure does not support or explain this finding. In the X-ray crystal structure, the lumen of the OmpA pore is obstructed primarily by a salt-bridge formed by the side-chains of residues Arg138 and Glu52. Based on MD simulations it has been proposed that the closing and opening of the pore could be linked to switching of salt-bridge formation of Arg138 with either Glu52 or Glu128, respectively. In strong support of this hypothesis it has been found that Arg138 is one of the residues involved in conformational exchange, and although Glu52

does not show conformational exchange itself, its nearest neighbor Met 53 does (Tamm et al., unpublished results).

Another important example of the application of dynamics to explain the function of a membrane protein is that of PagP. PagP is an eight-stranded β-barrel outer membrane enzyme that catalyzes the transfer of a palmitate chain from phospholipids to the lipid A moiety of lipopolysaccharide. The putative catalytic site of PagP is located on the highly mobile extracellular L1 loop that connects strands A and B. The X-ray crystal structure of PagP in LDAO shows one bound detergent molecule in the center of the β-barrel, the position of which corresponds to the binding site for the *sn*-1 palmitate of the phospholipid substrate [47]. The extracellular loop L1 is not seen in the X-ray structure. PagP is functionally inactive in LDAO, DPC and β-OG, perhaps because the detergent molecules occupy the binding site and compete with the phospholipid substrate. PagP is active in CYFOS-7, i.e. a detergent, which has a cyclohexyl ring at the end of its alkyl chain and therefore cannot penetrate into the β-barrel. Interestingly, two distinct sets of peaks for the amide residues are seen in the HSQC spectrum of PagP in CYFOS-7 micelles at 25 °C. Based on the chemical shifts of the L1 loop region, the major conformer has been designated to represent the relaxed or "R" form, while the minor conformer has been assigned to represent the tense or "T" form. Structural differences between the two forms are localized mainly to the L1 loop, the β-bulge of strand A, and the adjacent region on strand H. The $R \rightarrow T$ and $T \rightarrow R$ conversion rates at 25 °C have been found to be 2.8 ± 0.5 and $6.5 \pm 0.9\ s^{-1}$, respectively, from $^{15}N_{ZZ}$ exchange spectroscopy, based on which the proportion of the minor conformer was determined to be around 30%. The choice of detergent and temperature are both important for the observation of the minor component. At 45 °C, the population of minor conformer is only around 10% in CYFOS-7, whereas in DPC and β-OG, the minor conformer is not observed at all. Existence of the two conformers and interchange between them in CYFOS-7 is thought to reflect the functioning of this protein in its native membrane environment with the R form facilitating substrate entry and the T form facilitating substrate catalysis [48].

6.8 MD Simulations of Protein/Detergent Complexes

Substantial advancement in MD simulations of membrane proteins in detergent micelles and lipid bilayers has been achieved in the last few years. MD simulation studies offer a means to integrate the experimental NMR results into computational models of membrane protein/detergent complexes. The mixed micelle models can then be extended through MD simulations to lipid bilayer model membranes. By taking this route, one can garner a finer understanding of the behavior of membrane proteins in membranes than is possible through experiments only on these systems. A vast number of MD simulations on pure micelles and a few on micelles with small peptides have been performed [49–60].

MD simulations of adrenocorticotropin hormone (ACTH) fragment (1–10) offer a convenient case study for MD simulations of small peptides in micelles [59, 60]. MD simulations of ACTH (1–10) have been performed in SDS and DPC micelles. ACTH (1–10) binds to the surface of the micelle, but does not insert into the hydrophobic core because of its amphipathic character. MD simulations can detect small differences in conformation of the peptide in the presence of SDS or DPC micelles. In SDS, the segment Met4 to Phe7 adopts a turn conformation, while in DPC the same segment is part of a helix. The segment between Glu5 and Trp9 of the peptide interacts strongly with the head group of SDS, whereas in DPC such interactions are absent. These results are consistent with the observation of more extensive intramolecular NOEs in DPC than in SDS micelles and, therefore, this study nicely demonstrates excellent agreements between the simulation and experimental NMR results for this peptide in two different micelle environments.

Recently, 10-ns MD simulation studies on pure DPC micelles, DPC/OmpA mixed micelles and a DMPC/OmpA bilayer system have been performed [61]. This offers direct comparison of the structural dynamics of OmpA in DPC micelles determined from NMR spectroscopy, with the DPC/OmpA simulation, and further a comparison of the DPC/OmpA and DMPC/OmpA simulations. Starting from the X-ray structure of OmpA, the DPC/OmpA micelle was modeled as an "expanded micelle-like torus" around the barrel domain of OmpA, with detergent molecules radiating like spokes from the protein surface. In the 10-ms OmpA/DPC simulation, the root mean square displacement drifts of the Cα positions in the β-barrel, extracellular loops, and periplasmic turns was 0.1, 7 and 2 Å, respectively. The simulation results in the loss of a few strand residues towards the extracellular ends of the strands β2–β6 and an opening of the extracellular loops, which is consistent with the dynamic NMR structure of OmpA [12]. $\{^1H\}^{15}N$-heteronuclear NOEs of OmpA in DPC micelles have indicated a dynamic gradient of flexibility for the barrel, with the barrel center being most rigid and flexibility increasing towards both the ends. A similar flexibility gradient is observed for the OmpA barrel in both the micelle and bilayer simulation. This gradient of protein flexibility directly counters the fluidity gradient of the alkyl chains of the lipid bilayer.

An analysis of the micelle geometry indicates that both the pure DPC micelle and the DPC/OmpA mixed micelle are roughly spherical with a ratio of the principle moments of inertia equal to 1.2 : 1.1 : 1, and an eccentricity parameter, η, of around 0.1 (a perfectly spherical object has $\eta = 0$). In contrast, the shape of the detergent part only of the mixed OmpA/DPC micelle resembles an oblate ellipsoid with a ratio of 1.5 : 1.3 : 1 and $\eta = 0.21$ (see Fig. 6.2). Thus, the MD simulations are overall in excellent agreement with the results obtained from NMR studies on protein/detergent system, including the detection of minor changes in secondary structure, large-scale motions of the loop regions, and a dynamic gradient of flexibility along the barrel axis and membrane normal. A comparison of the simulation of the pure DPC micelle with the DPC/OmpA micelle suggests that the presence of OmpA loosens the detergent head group packing

in comparison with the pure micelles. At the same time, the hydrophobic tails of DPC molecules pack rather tightly against the protein surface in the core of the micelle. The presence of the protein renders the hydrophobic tail conformations of the micelle more bilayer-like with reduced gauche defects.

When the DPC/OmpA and DMPC/OmpA simulations are compared, the largest differences are seen in the extracellular loops. High mobility of the loops allows them to drift freely in the micelle simulation, thus optimizing the number of favorable interactions with detergent. In contrast, the loops are far less mobile in the bilayer simulation, due to the surrounding relatively rigid lattice of the lipid bilayer. Interestingly, except for the residues at the ends of the β-strands, the structural deviations between β-barrel residues in the micelle and membrane environments are small. Yet, subtle static and dynamical differences between the detergents in DPC micelles and the phospholipids in DMPC bilayers result in a slightly larger pore expansion and a correspondingly higher mobility of water molecules within the pore of OmpA when embedded in the micelle, in comparison to these parameters in the lipid bilayer. In fact, in the DPC/OmpA simulation, one water molecule is actually able to traverse the entire length of the pore, by passing through the proposed Arg138–Glu52 salt-bridge "gate". Over the last 8 ns of DPC/OmpA simulation, the Cβ–Cγ–Cδ–Nε dihedral angle of the Arg138 side-chain is mostly in the *trans* state, so that the Arg138 N–H vector points directly towards the carboxylate group of Glu128, leading to an arrangement in which Arg138 is partially salt-bridged to both Glu52 and Glu128. This picture is very similar to the one suggested on the basis of conformational exchange observed for the Arg138 backbone amide. Interestingly, the Cβ–Cγ–Cδ–Nε dihedral angle of the Arg138 side-chain is mostly in the *gauche*(–) or *gauche*(+) state in the DMPC/OmpA simulation and no water-crossing events occur past the Arg138–Glu52 salt-bridge "gate" during the time of this simulation.

6.9 Implications on the Structure and Function of Membrane Proteins in Biological Membranes

A combination of NMR spectroscopy and MD simulations offers a deep insight into the structures of membrane proteins in micellar environments, the organization of detergent molecules around hydrophobic surface of membrane proteins, and the dynamics of these proteins and protein/detergent complexes. The results show that micelles, in particular DPC micelles, provide excellent substitutes for the lipid bilayer environment of real membranes for the structure determination of membrane proteins by solution NMR. The structural differences between membrane proteins in micelles and bilayers can be expected to be largest at the polar ends and near the interfacial region of the protein. However, subtle differences in dynamics of some side-chains, which could have a bearing on differences in the functioning of membrane proteins in micelle or bilayer

environments, could come from an increased lateral pressure in lipid bilayers, decreased head-group packing, and increased rates of translational diffusion of detergent molecules in detergent and lipid micelles.

References

1 Wallin E, von Heijne G. Genome-wide analysis of integral membrane proteins from eubacterial, archaean, and eukaryotic organisms. *Protein Sci.* **1998**, *7*, 1029–1038.

2 Terstappen GC, Reggiani A. *In silico* research in drug discovery. *Trends Pharmacol. Sci.* **2001**, *22*, 23–26.

3 *Membrane Proteins of Known 3D Structure*. Available: http://blanco.biomol.uci.edu/Membrane_Proteins_xtal.html.

4 Fu D, Libson A, Miercke LJ, Weitzman C, Nollert P, Krucinski J, Stroud RM. Structure of a glycerol-conducting channel and the basis for its selectivity. *Science* **2000**, *290*, 481–486.

5 Dutzler R, Campbell EB, Cadene M, Chait BT, MacKinnon R. X-ray structure of a ClC chloride channel at 3.0 Å reveals the molecular basis of anion selectivity. *Nature* **2002**, *415*, 287–294.

6 Kimura Y, Vassylyev DG, Miyazawa A, Kidera A, Matsushima M, Mitsuoka K, Murata K, Hirai T, Fujiyoshi Y. Surface of bacteriorhodopsin revealed by high-resolution electron crystallography. *Nature* **1997**, *389*, 206–211.

7 Park SH, Mrse AA, Nevzorov AA, Mesleh MF, Oblatt-Montal M, Montal M, Opella SJ. Three-dimensional structure of the channel-forming trans-membrane domain of virus protein "u" (Vpu) from HIV-1. *J. Mol. Biol.* **2003**, *333*, 409–424.

8 Thiriot DS, Nevzorov AA, Zagyanskiy L, Wu CH, Opella SJ. Structure of the coat protein in Pf1 bacteriophage determined by solid state NMR spectroscopy. *J. Mol. Biol.* **2004**, *341*, 869–879.

9 Nishimura K, Kim S, Zhang L, Cross TA. The closed state of a H^+ channel helical bundle combining precise orientational and distance restraints from solid state NMR. *Biochemistry* **2002**, *41*, 13170–13177.

10 Hwang PM, Choy WY, Lo EI, Chen L, Forman-Kay JD, Raetz CR, Prive GG, Bishop RE, Kay LE. Solution structure and dynamics of the outer membrane enzyme PagP by NMR. *Proc. Natl Acad. Sci. USA* **2002**, *99*, 13560–13565.

11 Fernandez C, Adeishvili K, Wuthrich K. Transverse relaxation-optimized NMR spectroscopy with the outer membrane protein OmpX in dihexanoyl phosphatidylcholine micelles. *Proc. Natl Acad. Sci. USA* **2001**, *98*, 2358–2363.

12 Arora A, Abildgaard F, Bushweller JH, Tamm LK. Structure of outer membrane protein A transmembrane domain by NMR spectroscopy. *Nat. Struct. Biol.* **2001**, *8*, 334–338.

13 MacKenzie KR, Prestegard JH, Engelman DM. A transmembrane helix dimer: structure and implications. *Science* **1997**, *276*, 131–133.

14 Rastogi VK, Girvin ME. Structural changes linked to proton translocation by subunit c of the ATP synthase. *Nature* **1999**, *402*, 263–268.

15 Mesleh MF, Lee S, Veglia G, Thiriot DS, Marassi FM, Opella SJ. Dipolar waves map the structure and topology of helices in membrane proteins. *J. Am. Chem. Soc.* **2003**,*125*, 8928–8935.

16 Roosild TP, Greenwald J, Vega M, Castronovo S, Riek R, Choe S. NMR structure of Mistic, a membrane-integrating protein for membrane protein expression. *Science* **2005**, *307*, 1317–1321.

17 Pervushin K, Riek R, Wider G, Wuthrich K. Attenuated T2 relaxation by mutual cancellation of dipole–dipole coupling and chemical shift anisotropy indicates an avenue to NMR structures of very large biological macromolecules in solution. *Proc. Natl Acad. Sci. USA* **1997**, 94, 12366–12371.

18 Salzmann M, Pervushin K, Wider G, Senn H, Wuthrich K. TROSY in triple-

resonance experiments: new perspectives for sequential NMR assignment of large proteins. *Proc. Natl Acad. Sci. USA* 1998, 95, 13585–13590.

19 Zhu G, Xia Y, Lin D, Gao X. TROSY-based NMR experiments for the study of macromolecular dynamics and hydrogen bonding. *Methods Mol. Biol.* **2004**, *278*, 161–184.

20 Oxenoid K, Kim HJ, Jacob J, Sonnichsen FD, Sanders CR. NMR assignments for a helical 40 kDa membrane protein. *J. Am. Chem. Soc.* **2004**, *126*, 5048–5049.

21 Gardner KH, Rosen MK, Kay LE. Global folds of highly deuterated, methyl-protonated proteins by multidimensional NMR. *Biochemistry* **1997**, *36*, 1389–1401.

22 Hilty C, Wider G, Fernandez C, Wuthrich K. Stereospecific assignments of the isopropyl methyl groups of the membrane protein OmpX in DHPC micelles. *J. Biomol. NMR* **2003**, *27*, 377–382.

23 Fernandez C, Hilty C, Wider G, Wuthrich K. Lipid–protein interactions in DHPC micelles containing the integral membrane protein OmpX investigated by NMR spectroscopy. *Proc. Natl Acad. Sci. USA* **2002**, *99*, 13533–13537.

24 Arora A, Tamm LK Biophysical approaches to membrane protein structure determination *Curr. Opin. Struct. Biol.* **2001**, *11*, 540–547.

25 Fernandez C, Hilty C, Wider G, Guntert P, Wuthrich K. NMR structure of the integral membrane protein OmpX. *J. Mol. Biol.* **2004**, *336*, 1211–1221.

26 Prestegard JH, al-Hashimi HM, Tolman JR. NMR structures of biomolecules using field oriented media and residual dipolar couplings. *Q. Rev. Biophys.* **2000**, *33*, 371–424.

27 Bax A. Weak alignment offers new NMR opportunities to study protein structure and dynamics. *Protein Sci.* **2003**, *12*, 1–16.

28 de Alba E, Tjandra N. Residual dipolar couplings in protein structure determination. *Methods Mol. Biol.* **2004**, *278*, 89–106.

29 Chou JJ, Kaufman JD, Stahl SJ, Wingfield PT, Bax A. Micelle-induced curvature in a water-insoluble HIV-1 Env peptide revealed by NMR dipolar coupling measurement in stretched polyacrylamide gel. *J. Am. Chem. Soc.* **2002**, *124*, 2450–2451.

30 Lee S, Mesleh MF, Opella SJ. Structure and dynamics of a membrane protein in micelles from three solution NMR experiments. *J. Biomol. NMR* **2003**, *26*, 327–334.

31 Mascioni A, Eggimann BL, Veglia G. Determination of helical membrane protein topology using residual dipolar couplings and exhaustive search algorithm: application to phospholamban. *Chem. Phys. Lipids* **2004**, *132*, 133–44.

32 Cierpicki T, Bushweller JH. Charged gels as orienting media for measurement of residual dipolar couplings in soluble and integral membrane proteins. *J. Am. Chem. Soc.* **2004**, *126*, 16259–16266.

33 Meier S, Haussinger D, Grzesiek S. Charged acrylamide copolymer gels as media for weak alignment. *J. Biomol. NMR* **2002**, *24*, 351–356.

34 Ulmer TS, Ramirez BE, Delaglio F, Bax A. Evaluation of backbone proton positions and dynamics in a small protein by liquid crystal NMR spectroscopy. *J. Am. Chem. Soc.* **2003**, *125*, 9179–9191.

35 Pautsch A, Schulz GE. High-resolution structure of the OmpA membrane domain. *J. Mol. Biol.* **2000**, *298*, 273–282.

36 Zamoon J, Mascioni A, Thomas DD, Veglia G. NMR solution structure and topological orientation of monomeric phospholamban in dodecylphosphocholine micelles. *Biophys. J.* **2003**, *85*, 2589–2598.

37 Henry GD, Sykes BD. Assignment of amide ^{1}H and ^{15}N NMR resonances in detergent-solubilized M13 coat protein: a model for the coat protein dimer. *Biochemistry* **1992**, *31*, 5284–5297.

38 Williams KA, Farrow NA, Deber CM, Kay LE. Structure and dynamics of bacteriophage IKe major coat protein in MPG micelles by solution NMR. *Biochemistry* **1996**, *35*, 5145–5157.

39 Krueger-Koplin RD, Sorgen PL, Krueger-Koplin ST, Rivera-Torres IO, Cahill SM, Hicks DB, Grinius L, Krulwich TA, Girvin ME. An evaluation of detergents for NMR structural studies of membrane proteins. *J. Biomol. NMR* **2004**, *28*, 43–57.

40 Mcdonnell PA, Opella SK. Effect of detergent concentration on multidimensional solution NMR spectra of membrane proteins in micelles. *J. Mag. Reson. B* **1993**, *102*, 120–125.

41 Tieleman DP, van der Spoel D, Berendsen HJ. Molecular dynamics simulations of dodecylphosphocholine micelles at three different aggregate sizes: micellar structure and chain relaxation. *J. Phys. Chem. B* **2000**, *104*, 6380–388.

42 Tamm LK, Abildgaard F, Arora A, Blad H, Bushweller JH. Structure, dynamics and function of the outer membrane protein A (OmpA) and influenza hemagglutinin fusion domain in detergent micelles by solution NMR. *FEBS Lett.* **2003**, *555*, 139–143.

43 Porcelli F, Buck B, Lee DK, Hallock KJ, Ramamoorthy A, Veglia G. Structure and orientation of pardaxin determined by NMR experiments in model membranes. *J. Biol. Chem.* **2004**, *279*, 45815–45823.

44 Gorzelle BM, Nagy JK, Oxenoid K, Lonzer WL, Cafiso DS, Sanders CR. Reconstitutive refolding of diacylglycerol kinase, an integral membrane protein. *Biochemistry* **1999**, *38*, 16373–16382.

45 Pellecchia M, Meininger D, Shen AL, Jack R, Kasper CB, Sem DS. SEA-TROSY (solvent exposed amides with TROSY): a method to resolve the problem of spectral overlap in very large proteins. *J. Am. Chem. Soc.* **2001**, *123*, 4633–4634.

46 Hilty C, Wider G, Fernandez C, Wuthrich K. Membrane protein–lipid interactions in mixed micelles studied by NMR spectroscopy with the use of paramagnetic reagents. *ChemBiochem* **2004**, *5*, 467–473.

47 Ahn VE, Lo EI, Engel CK, Chen L, Hwang PM, Kay LE, Bishop RE, Prive GG. A hydrocarbon ruler measures palmitate in the enzymatic acylation of endotoxin. *EMBO J.* **2004**, *23*, 2931–2941.

48 Hwang PM, Bishop RE, Kay LE. The integral membrane enzyme PagP alternates between two dynamically distinct states. *Proc. Natl Acad. Sci. USA* **2004**, *101*, 9618–9623.

49 MacKerell AD. Molecular dynamics simulation analysis of a sodium dodecyl sulfate micelle in aqueous solution: decreased fluidity of the micelle hydrocarbon interior. *J. Phys. Chem.* **1995**, *99*, 1846–1855.

50 Bruce CD, Berkowitz ML, Perera L, Forbes MDE. Molecular dynamics simulation of sodium dodecyl sulfate micelle in water: micellar structural characteristics and counterion distribution. *J. Phys. Chem. B* **2002**, *106*, 3788–3793.

51 Boecker J, Brickmann J, Bopp P. Molecular dynamics simulation study of an n-decyltrimethylammonium chloride micelle in water. *J. Phys. Chem.* **1994**, *98*, 712–717.

52 Bogusz S, Venable RM, Pastor RW. Molecular dynamics simulations of octyl glucoside micelles: structural properties. *J. Phys. Chem. B* **2000**, *104*, 5462–5470.

53 Bogusz S, Venable RM, Pastor RW. Molecular dynamics simulations of octyl glucoside micelles: dynamic properties. *J. Phys. Chem. B* **2001**, *105*, 8312–8321.

54 Wendoloski JJ, Kimatian SJ, Schutt CE, Salemme FR. Molecular dynamics simulation of a phospholipid micelle. *Science* **1989**, *243*, 636–638.

55 Schuler LD, Walde P, Luisi PL, van Gunsteren WF. Molecular dynamics simulation of *n*-dodecyl phosphate aggregate structures. *Eur. Biophys. J.* **2001**, *30*, 330–343.

56 Wymore T, Gao, XF, Wong TC. Molecular dynamics simulations of the structure and dynamics of a dodecylphosphocholine micelle in aqueous solution. *J. Mol. Struct.* **1999**, *486*, 195–210.

57 Vasudevan SV, Balaji PV. Conformation, orientation and dynamics of dodecylphosphocholine in micellar aggregate: a 3.2 ns molecular dynamics simulation study Indian. *J. Biochem. Biophys.* **2002**, *39*, 87–92.

58 Wong TC, Kamath S. Molecular dynamics simulations of adrenocorticotropin (1–24) peptide in a solvated dodecylphosphocholine (DPC) micelle and in a dimyristoylphosphatidylcholine (DMPC) bilayer. *J. Biomol. Struct. Dyn.* **2002**, *20*, 39–57.

59 Gao X, Wong TC. Molecular dynamics simulation of adrenocorticotropin (1–10) peptide in a solvated dodecylphosphocholine micelle. *Biopolymers* **2001**, *58*, 643–659.

60 Wymore T, Wong TC. The structure and dynamics of ACTH (1–10) on the surface of a sodium dodecylsulfate (SDS) micelle: a molecular dynamics simulation study. *J. Biomol. Struct. Dyn.* **2000**, *18*, 461–476.

61 Bond PJ, Sansom MS. Membrane protein dynamics versus environment: simulations of OmpA in a micelle and in a bilayer. *J. Mol. Biol.* **2003**, *329*, 1035–1053.

Part 3
Membrane Penetration by Toxins

7
Lipid Interactions of α-Helical Protein Toxins

Gregor Anderluh and Jeremy H. Lakey

7.1
Introduction

The two major forms of secondary structure, i.e. the α-helix and β-sheet, confer very different properties on the otherwise similar amino acid sequences that form them. Bearing this in mind, it is interesting to see that membrane-active protein toxins can be largely divided into α- or β-rich structures. This is not simply a division upon architectural lines since it has profound consequences upon the toxin's mode of action and, in the context of this chapter, their interaction with the membrane lipids themselves. Here, we will concentrate on the two families of toxins which we have studied over several years – the actinoporins and the pore-forming colicins. These provide representatives of proteins that are, respectively, partially and wholly α-helical (Fig. 7.1). The mechanism of action of these proteins will be compared with those of other families of toxins and membrane-penetrating proteins. Since the secondary structure is going to be a theme of this chapter we will, therefore, without covering material to be found in other chapters, examine the fundamental differences imposed by the choice of α or β topology.

7.1.1
The Two Secondary Structures Compared

First and foremost, the α-helix can fold as an independent unit typified in membrane systems by the Type I helical membrane proteins which are embedded in the lipid bilayer by a single hydrophobic helix. This is not to dismiss the fact that many helices only fold stably because of their local context (Minor and Kim 1996), but the hydrogen-bonding pattern which defines the secondary structure (Kabsch and Sander 1983) is entirely within each helix. The β-strand, on the other hand, cannot exist as a single unit since by definition it needs at least one partner strand to form the definitive hydrogen bonds (Fig. 7.2). The requirement of these secondary structures for a stable hydrogen bond network is well known, but it assumes greater importance in the low dielectric constant envi-

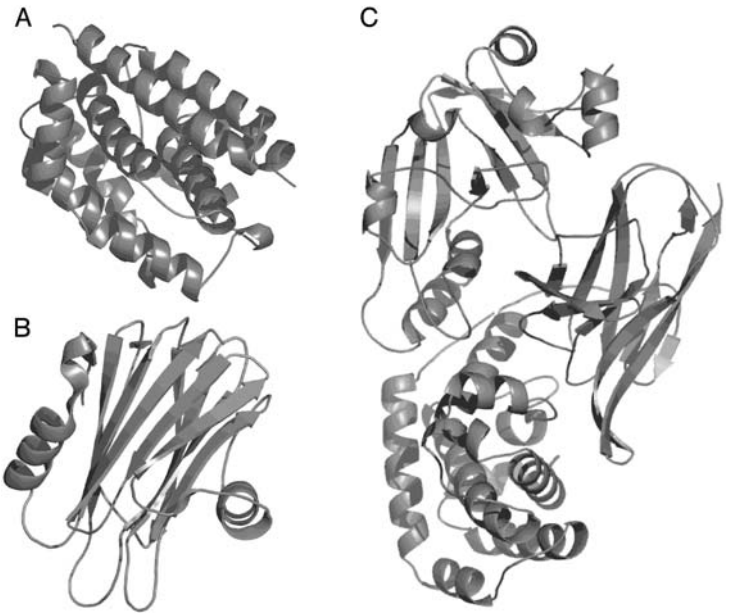

Fig. 7.1 Three-dimensional structures of some representative examples of α-helical pore-forming toxins.
(A) Colicin A pore-forming domain (PDB code 1COL) (Parker et al. 1992); here the membrane-penetrating helical hairpin is shown sandwiched between two layers of amphiphilic helices.
(B) EqtII (1IAZ) (Athanasiadis et al. 2001); the N-terminal membrane-penetrating helix is at the left side.
(C) DT (1MDT) (Choe et al. 1992); the membrane-inserting helical B domain is at the bottom, with buried membrane penetrating helices.

ronment of the membrane interior (Deechongkit et al. 2004). Here, the stabilization energy of the bond is greater than elsewhere since unpaired bonding partners, the backbone carbonyl and amide groups from the peptide bond, incur a heavy energetic cost in a hydrophobic environment (Popot and Engelman 2000). The size of this increase compared to hydrogen bonds in globular soluble proteins has only been understood recently, but it only serves to strengthen the original helical hairpin hypothesis of Englemann and Steiz (1981). This paper describes the advantage of inserting a preformed hydrophobic helical hairpin into a membrane compared to the energetic cost of forcing unfolded (and therefore weakly hydrogen bonded) peptides into the membrane where they would then form helices due to the constraints outlined above. Although it was initially aimed at explaining how integral membrane proteins fold, it is, in its treatment of an isolated protein transferring from water into the membrane, probably more applicable to α-helical toxins. This is because most helical membrane proteins insert cotranslationally and rarely exist in a water-soluble state. The simple model emphasizes two points which will be common to the toxins described in this chapter: (1) that helices are invariably preformed and (2) the importance of the hydrophobic membrane core.

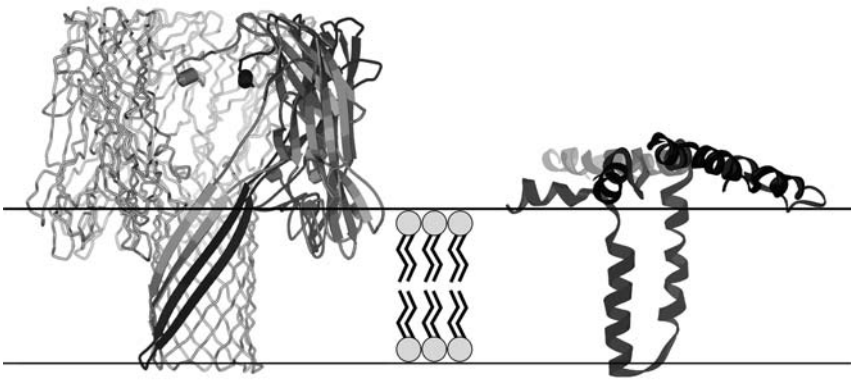

Fig. 7.2 A comparison of the known membrane structure of a β-barrel pore-forming toxin (α-hemolysin) (Song et al. 1996) and a *proposed* conformation for the membrane-bound structure of an α-helical toxin (colicin) (Parker et al. 1989). The β-structure requires clear and stable interactions between the separate secondary structural elements which are provided by separate subunits of the heptameric toxin. Each donates a β-hairpin to the 14-stranded barrel as shown by the shading. The α-structure requires no specific interaction within the α-hairpin and the separate elements can move easily with respect to one another. This model is closest to the closed-channel state, and, when membrane potential opens the pore, it is clear that large rearrangements and translocations of protein into and across the membrane take place (Qiu et al. 1996).

We have yet to discover helical protein toxins which create significant amounts of new helix upon membrane insertion. This is certainly possible with the amphipathic helices found in lytic peptides such as melittin (Bechinger 2004; Shai 2002) but the toxins described here are helical before insertion (by spectroscopy and X-ray structures) and similarly helical (by spectroscopy and other methods) after insertion. That is not to say that the exact structural elements are conserved; we cannot judge that at the moment, but creation of helical segments from previously unfolded or β-strand segments is not a common theme. Thus, we shall see that the transition from the water-soluble state to the membrane-bound form usually involves the transfer of existing helices into the hydrophobic membrane core.

The classical view of the membrane arises from the fluid mosaic model of Singer and Nicholson (1972) which has for 30 years been able to provide an explanation for most relevant experimental observations. More recent discoveries such as the identification of lipid domains or rafts have required updating of the model, but it is still the basis for any model of membrane function. It provides two fundamental ways by which lipids can present toxins with unique interactions – via the interface and via the hydrophobic core. Helices which are amphipathic can readily sit at the interface and satisfy the Janus-like environment it promotes (Parker and Pattus 1993), whereas the more hydrophobic helices can, as in the hairpin model, be stabilized by the 30-Å deep hydrophobic core. As will be seen in this chapter, the pure fluid mosaic model may not be

appropriate in all conditions of toxin insertion as it is being increasingly found not to account for all the observed behavior. Disruption of the lipid bilayer may accompany the action of several toxins.

Briefly comparing the α-helical toxins to the mainly β structures, we notice that in the latter the concept of a non-inserted pre-pore is common. All β-strand toxins form membrane-inserted states composed of several subunits which each contribute a pair ("hairpin") of strands to the membrane-inserted pore. Here the pre-pore, a stable association of subunits, often at the surface of the membrane, provides the exact context for the β-hairpins to penetrate into the membrane, with the necessarily concurrent formation of hydrogen bonds with adjacent partner strands (Fang et al. 1997; Heuck et al. 2003; Miller et al. 1999; Vecsey-Semjen et al. 1999). The essential result of this is that a β-barrel is formed which leaves no free non-hydrogen-bonded edge exposed to the non-polar core (Fig. 7.2). This is analogous to the insertion of β-barrel proteins into the outer membrane of Gram-negative bacteria as they too move from a water-soluble state to the membrane-bound one (Jansen et al. 2000).

So if β structures are apparently rigid structures (Vecsey-Semjen et al. 1999) then helical toxins share a characteristic of mobility since the interactions between the helices are much weaker than those found between strands. Transmembrane helices are not necessarily mobile and specific stabilizing interactions have been demonstrated in some intrinsic membrane proteins (Dawson et al. 2002). The mobility of toxin helices is probably the reason why we have no high-resolution three-dimensional structures of membrane inserted α-helical toxins, but two examples of β-sheet versions (Parker et al. 1994; Song et al. 1996). Therefore, the models described in this chapter commonly benefit from good structural data on the soluble toxin coupled with extensive and varied indirect evidence for the membrane-bound state. The models of the membrane form are thus rearrangements of the soluble form using experimental data and theoretical constraints. These constraints consist of the number of residues in a α-helical conformation needed to cross the membrane (more than 20), the number of helices needed to form an ion channel (more than three) and the required hydrophobicity of helices able to enter the membrane. The contrast here with β is especially interesting since only nine β-strand residues are needed to cross the membrane core, at least 12 strands are needed to make a pore and most notably the primary sequence of these strands need not be strongly hydrophobic. The last point is because only alternate residues in a transmembrane β-strand point towards the membrane core (Jeanteur et al. 1994). Thus, in a nine-residue strand only four need be non-polar, a ratio that could be easily found in soluble proteins. When considering that the β pore formers are also characterized by having large extracellular domains, this small region of membrane-penetrating structure can simply be incorporated into the soluble structure. After the complex oligomerization step, the β proteins can easily manage the water-soluble to membrane transition by a relatively small rearrangement.

To dissolve a single hydrophobic helix into the membrane requires that most of 20 residues are hydrophobic. Such a sequence would severely limit the aqueous

solubility of a protein and it will be noticed that such helices are packaged in the water-soluble structure (Fig. 7.1). Since the majority of these toxins form ion channels or pores in the membrane, the needs of these structures also define the composition of the helical regions. Four helices could, by model building, make a pore, but this requires that each helix is amphipathic, i.e. the cylindrical form of the helix presents a face that contains polar residues. If every third or fourth residue is polar, then one face of the helix can form the wall of the pore, and allow ion and water movement. This is not enough to render the helix individually water soluble, so in solution such helices are found on the surface of the toxin with the non-polar face buried within the globular structure. Many such water-soluble structures are known and the challenge is to understand how these are rearranged to create the membrane-bound channel-forming structure. As will become clear from reading this chapter, many of our ideas are probably too simplistic to describe the actual membrane-bound forms and thus the roles of lipids in defining these structures has moved to center stage.

7.1.2
Lessons from a Potassium Channel

As pore formation is a common theme in these toxins it is useful to see how resolution of the first helical ion channel structure changed ideas in that field. Prior to the publication of the KcsA potassium channel structure (Doyle et al. 1998) the models of these tetramers consisted of four sets of transmembrane helices in which one was suitably amphipathic to form one-quarter of the wall of a cylindrical ion channel which traversed the membrane core. Ions could dehydrate by interaction with polar side-chains and travel easily through the membrane. The structure of the channel determined by X-ray crystallography to 3.2 Å resolution revealed a narrow pore that only stretches partly across the membrane, some helices that are similarly short, some that cross it at such an angle that they are much longer than envisaged and, finally, that the pore itself is made from loop structures of no defined secondary structure that use their backbone hydrogen bonding C=O groups to interact with the positive ions. The tetrameric protein also binds a negatively charged lipid molecule which appears to be essential for folding and ion conduction (Valiyaveetil et al. 2002). Such surprises from a relatively static well-defined protein indicate that, should we ever accurately determine their membrane pore structure, we are likely to discover equally surprising results with helical pore-forming toxins.

7.2
Pore-forming Colicins

Colicins take their name from their "host" organism *Escherichia coli* and very similar bacteriocins are to be found in other gram negative bacteria [pyocin = *Pseudomonas* (Kageyama et al. 1996), pesticin = *Yersinia pestis* (Rakin et al. 1996;

Vollmer et al. 1997), etc.]. They are plasmid-encoded toxins that enable their hosts to kill related bacteria whilst remaining immune to the toxin themselves. They form two groups named after their toxic activity – the nuclease colicins, which kill by digesting host nucleic acids, and the pore-forming toxins, which create ion channels in their victims inner membrane. The biology of colicins is fascinating and readers are strongly advised to consult recent reviews (James et al. 1996; Lakey and Slatin 2001; Riley and Wertz 2002; Zakharov and Cramer 2002).

Colicins are three-domain proteins consisting of the translocation domain, the receptor-binding domain and the pore-forming domain. These enable it to span one membrane and form a pore in the second.

There are currently three high-resolution structures known for pore-forming colicins (Hilsenbeck et al. 2004; Vetter et al. 1998; Wiener et al. 1997) and two more of just the pore-forming domains (Elkins et al. 1997; Parker et al. 1992) (Fig. 7.1). The first to be determined was the pore-domain of colicin A (Parker et al. 1989, 1990, 1992). This was a seminal discovery since it revealed for the first time the pattern of how membrane-inserting toxins are packaged to allow them to remain water soluble until contact with the membrane is achieved. The pore-forming domain consists of 10 α-helices arranged in three layers. Buried within the helical structure is a pair of hydrophobic helices (numbers 8 and 9). These resemble the central helices of both the diphtheria toxin (DT) B subunit (Choe et al. 1992) (Fig. 7.1), the *Bacillus thuringiensis* toxins (Li et al. 1991, 1996) and the Bcl/Bax family of apoptosis regulators (Muchmore et al. 1996). This motif of a very hydrophobic core surrounded by (and solubilized by) an outer shell of amphipathic helices thus became a recurring theme in helical proteins which undergo a soluble to membrane-bound transition (Parker and Pattus 1993). The colicin pore-forming domains all share a clear homology of sequence and size, thus it was not unexpected that the other colicins have very similar three-dimensional structures. Colicin Ia [and the later colicin E1 pore-domain structure (Elkins et al. 1997)] has a shorter hydrophobic hairpin than A or colicin N, but in essence they all conform to the pattern first revealed in colicin A.

7.2.1 Outer Membrane Interactions

The first lipid interaction of colicins is likely to be with the outer surface of the bacterial envelope, although lipid may be released along with colicins during their release from the producing cells. The bacterial surface is a structure which is asymmetric in its lipid component with solely lipopolysaccharide (LPS) on the outer surface and only phospholipids on the inner leaflet. The LPS has shorter carbon chains (six to eight carbons) compared to phospholipids and is composed of a long, water-soluble O antigen attached to the membrane lipid A structure via the core antigen. It is interesting to note that smooth strains of *E. coli* (those with long O antigen chains) are relatively resistant to colicins compared to the rough strains that are commonly used in laboratories, and which express only the lipid A and core antigen. Little is known of the specific involvement of LPS. It has been

shown to be important in maturation and folding of outer membrane proteins such as OmpF (Fourel et al. 1994), and it also promotes the interaction between colicin N and OmpF (which is its outer membrane receptor protein) (Dover et al. 2000). Since the colicin probably spans the outer membrane (Benedetti et al. 1992) some helical segments are likely to be at a complex junction between LPS (in the outer leaflet), phosphatidylethanolamine (in the inner leaflet) and the OmpF. There is still debate as to whether the colicin uses the OmpF channel to cross the outer membrane (Bainbridge et al. 1998; Cao and Klebba 2002). The helices which span the outer membrane are very likely to be the first two or three of the pore-forming domain since these are not required for pore formation (Vetter et al. 1996) and have been shown to be required for colicin N–OmpF complex formation (J. H. Lakey, unpublished data). The complex is also stabilized by SDS, enabling it to be observed on polyacrylamide gels (Dover et al. 2000), a behavior it shares with the observed complex between OmpF and TolA (Derouiche et al. 1996). Although the OmpF crystal structure does not reveal the presence of LPS, its affinity for this lipid been clearly demonstrated (Fourel et al. 1994; Holzenburg et al. 1989) and the specific binding of LPS has been shown in other high-resolution structures of outer membrane proteins (Ferguson et al. 1998; Kurisu et al. 2003). As is usually the case, there is no evidence of phospholipid in the structures of any of the outer membrane proteins, their place being taken by the chains of detergent molecules. Nevertheless, the role of lipids in the interfacial interaction of the colicin with inner membrane has been investigated biochemically for colicin A.

7.2.2
Colicin A Requires Acidic Lipids

Acidic lipids and low pH increase the efficiency of colicin A insertion into model membranes [a common theme amongst helical toxins from DT to *Pasteurella multocida* toxin (Baldwin et al. 2004; van der Goot et al. 1992)]. This was correlated with the appearance of an acidic molten globule state (van der Goot et al. 1991) which consists of the same helical content of the fully folded protein, but with much reduced tertiary interactions (Bychkova et al. 1988). This is not a general feature of colicins and only two, A and B, have been shown to form an acidic molten globule. This correlates with their p*I* since these are the only acidic pore-forming domains, the rest being strongly basic (Evans et al. 1996). For example, the colicin N pore domain is structurally very similar but has a high p*I* and is pH insensitive. Whatever causes these other colicins to unfold and insert into membranes, it is not low pH. Amongst proteins in general, colicin A is very unusual in that it is stabilized by surface negative charges and when these are lost, by mutagenesis or protonation at low pH, the domain unfolds (Fridd and Lakey 2002). The periplasm is not a low pH environment and so the influence of acidic lipids was tested. *E. coli* strains which do not produce acidic lipids were treated with colicins A or N and the results compared with cells containing these lipids. The results showed clearly that colicin A is depen-

dent upon acidic lipids in the cytoplasmic membrane and that colicin N is unaffected by this loss (Letellier et al. 1994; van der Goot et al. 1993). Hence the surface charge caused by acidic lipids was shown to cause the formation of an insertion intermediate and the role of the acidic sensitivity was explained. This is a clear demonstration of the role of specific lipids in a protein's function.

7.2.3 The Open Channel

The initial insertion of pore-forming colicins into the membrane may only be at the interface. The hydrophobic hairpin is short and not proven to span the bilayer in this closed channel state. The open channel state requires the application of a transmembrane potential difference and the channels can be measured in artificial bilayer lipid membranes (BLMs). Here they can be studied free of any of the cellular proteins with which they may interact *in vivo* and also appear not to be affected by the type of lipid present (Kienker et al. 1996; Martinez et al. 1983; Nogueira and Varanda 1988; Pattus et al. 1983; Schein et al. 1978). The membrane potential has been shown to cause a transmembrane translocation of large segments of the protein (Qiu et al. 1996; Slatin et al. 1994) and the hairpin can be seen to reach across the membrane (Figs. 7.2 and 7.3). Charged lipids affect interfacial potential, and may alter gating behavior and ion selectivity measurements, but generally the ion channels are of similar size and activity in a range of lipids. The evidence from many experiments is that the channel is formed from one monomer and that less than 130 of the 200 amino acids are needed. This has serious consequences for models of channel structure (Lakey and Slatin 2001). The conductance of the channel is small and usually pH dependent. Typical values in 1 M KCl at pH 7 range from 15 pS for colicin A to about 60 pS for colicin Ia. The conductances are smaller than many well-characterized and highly selective, eukaryotic channels, such as many sodium and potassium channels. Despite its small conductance, the lumen of the channel appears to have a substantial diameter and several approaches agree that the lumen is large, comparable to, say, the acetylcholine receptor channel, which is, however, formed by a pentamer of a total molecular weight of approximately 300 kDa. However the data suggests that colicins build a stable, 9-Å pore from a single peptide of no more than about 100 residues. This is not the only difficulty – recent work has shown the colicin pore domain to be able to translocate large charged segments of its own and, even more perplexing, inserted segments from other proteins (Jakes et al. 1998). Thus this small domain not only allows ions to move freely across the lipid core, but also charged amino acid residues which theory would suggest cost far more in free energy than is provided by a 50–100 mV membrane potential which drives the process (Fig. 7.3). One answer to this problem is to discard the fluid mosaic model in the vicinity of the toxin and allow for some other structure of lipid and protein. This possibility will arise again in this chapter, but we lack evidence for any such structure.

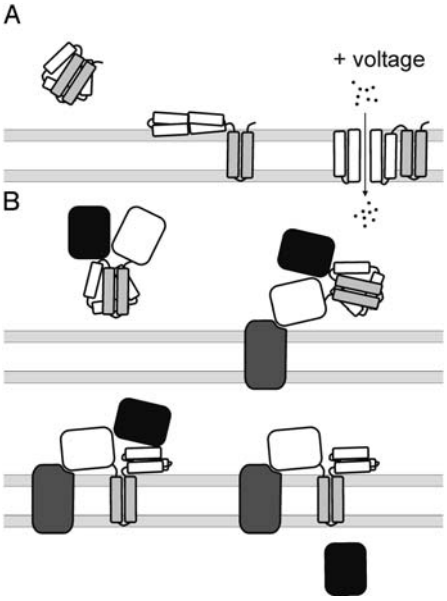

Fig. 7.3 α-Helices are used for pore formation or translocation of toxic molecules into cell.
(A) In colicin, the shaded hydrophobic helices are packaged within the helical bundle and insert into the membrane. They are too short to span the membrane and may not traverse the bilayer as shown. The remaining amphipathic helices reside at the interface, but penetrate the membrane when a transmembrane voltage is applied and the pore opens.
(B) In DT, the hydrophobic helices are used to insert protein toxin into membranes and subsequent translocation of enzymatic domain into the cell. After receptor-mediated endocytosis the grey helices insert into the membrane of the acidic endosome. The lower panel represents the translocation of the A subunit (black) by the B subunit of DT and creation of a pathway for protein translocation which also behaves as an ion channel *in vitro*.

7.2.4
The Colicin–Phospholipid Complex

One way to address the structure of the protein–lipid complex is to move to the other extreme from a few channels in the BLM and investigate the interaction at high protein to lipid ratios. When colicin A pore-forming domain was added to short chain saturated lipids such as L-α-1,2-dimyristoylphosphatidylcholine (DMPC) this caused the formation of stable complexes containing nine proteins and about 250–300 lipids (Massotte et al. 1989). The ratios varied with lipid type, but excess lipid caused a progression to free proteins in lipid vesicles. These complexes were observable by electron microscopy as flattened disks (Massotte et al. 1989) and were studied by neutron scattering (Jeanteur et al. 1994). The neutron scattering contrast between the background water and protein or lipid can be altered by different H_2O/D_2O ratios allowing the distribu-

tion of each to be separately defined. The results hinted at a model in which protein lays upon the central surface of a discoid lipid micelle and this may reflect the behavior of the protein in BLM. Finally, it should be remembered that colicins A and N have, like many lytic peptides, been shown to provoke fusion of lipid vesicles (Massotte and Pattus 1989), a process which by definition must involve non-bilayer behavior. The possible non-bilayer behavior may suggest an involvement of phosphatidylethanolamine, the predominant *E. coli* lipid, but its addition to BLMs does not change colicin channel behavior.

7.2.5
Other Similar Proteins

Colicins are structurally related to the Bcl family of apoptosis regulators (Schendel et al. 1998). These interact with the mitochondrial membrane to promote or prevent apoptosis. Bcl-2, an anti-apoptotic version, can form channels in BLMs whilst the pro-apoptotic Bax oligomerizes to provoke the release of cytochrome *c*. Several domains have been identified which correlate with the various activities, but the lipid interactions are not clear. Recently is has been proposed that Bax and the tBid combine to form pores via non-bilayer structures (Terrones et al. 2004).

DT is important in the virulence of *Corynebacterium diphtheria* and is the basis of the thankfully effective vaccine which has all but eliminated this dreadful disease from immunized groups. It shows a similar packing motif to colicins, although, in this case, the mode of action is not pore formation, but protein translocation (Choe et al. 1992) (Fig. 7.1). DT, like colicin, is a three-domain protein, one domain of which is a bundle of 10 α-helices which forms channels in planar bilayers. It is also likely to form channels as a monomer (Huynh et al. 1997), although it is clear that the channel is formed by only two helices, the equivalent to the hydrophobic hairpin of the colicins (Silverman et al. 1994). The mode of action is for the pore-forming domain to translocate the enzymatic domain (Fig. 7.3). The protein first attaches to the cell surface, then undergoes receptor-mediated endocytosis. In the acidic endosome the channel domain forms a molten globule and inserts into the membrane. It then translocates the entire enzymatic domain, along with a substantial portion of itself into the cytoplasm of the host. This was shown to occur in BLMs in the absence of any another proteinaceous components (Oh et al. 1999; Senzel et al. 1998). Once inside the cell the A domain dissociates from the channel-forming domain by reduction of the disulfide bridge that links them. It then glycosylates a specific residue on elongation factor Tu, permanently terminating protein synthesis and causing cell death. Thus, the lipids do not create the low pH environment, but their role in translocation is again a mystery. Here we have another short protein sequence with duties of pore formation and protein translocation which seem to onerous considering its size and our present knowledge.

The packaging motif of buried hydrophobic helices found in colicins, DT and Bcl is shared by the Bt toxins or δ-endotoxins from *Bacillus thuringiensis*. These

are insecticidal toxins of great commercial importance which contain two structural families. The Cyt toxins which unlike the colicins consist of a single domain comprising two outer layers of α-helix hairpins wrapped around a mixed β-sheet (Li et al. 1996) and the three domain Cry toxins which contain a β-sheet receptor binding domain and α-helical bundle (Li et al. 1991) (Fig. 7.1). This helical bundle contains a hidden hydrophobic helix which inserts into the epithelial cell membrane of the insect midgut at high pH and kills by pore formation. Hence, structural rearrangement of a helical packaging motif is also a feature of this toxin. The Cyt toxin may form a β-barrel pore, but it is interesting to note that the hydrophobic β-sheet core is packaged by a helical hairpin pair which may unfold onto the lipid surface during membrane binding and others which may assist in oligomerization (Gazit et al. 1997; Li et al. 1996).

Finally, there is at least one pore-forming helical toxin that does not rearrange its structure upon pore formation as revealed by the recently solved structure of the *Entamoeba histolytica* Amoebapore A. This is a 77-residue protein, which lyses both bacterial and eukaryotic cells, and is important in the pathogenesis of this organism. The five-helix fold is stabilized by disulfide bonds and no evidence exists for its rearrangement during pore formation. Instead the interaction with membranes is provoked by a pH- and histidine-dependent dimerization which then leads to a probable hexameric pore composed of subunits similar in structure to the water-soluble form (Hecht et al. 2004).

7.3 Actinoporins

Actinoporins are an extremely conserved family of potent pore-forming proteins from sea anemones. They have been thoroughly studied in recent years due to their potency and particular mechanism of membrane permeabilization, although they do not represent a particular threat to humans or marine vertebrates. The family includes more than 30 members from 20 different sea anemones (Anderluh and Macek 2002). Two most studied representatives are equinatoxin II (EqtII) from *Actinia equina* and sticholysin I (StI) from *Stichodactyla helianthus*. All members of this family are 20-kDa cysteine-free proteins with high isoelectric points, with the exception of one acidic member described just recently (Jiang et al. 2002). They share high sequence similarity, i.e. EqtII and StI are by sequence most dissimilar, but they still share more than 60% identical residues. It is amazing that this family is currently restricted solely to the sea anemones. There is only one protein, described from marine gastropod *Monoplex echo*, that shows any significant sequence similarity (Kawashima et al. 2003).

Actinoporins exhibit a variety of pharmacological effects. They are lethal to crabs, fish and mammals (i.v. LD_{50} for mice is 35 $\mu g\, kg^{-1}$ for EqtII) (Anderluh and Macek 2002). They were shown to cause platelet aggregation (Teng et al. 1988), pulmonary edema (Lafranconi et al. 1984) and are cardiotoxic (Bunc et al. 1999). All this variety of pharmacological effects can be at least partly be ex-

plained by increased permeability for Na^+, K^+, Ca^{2+} and other smaller solutes in the targeted membranes (Zorec et al. 1990). This also causes the lysis of erythrocytes as the result of the colloid-osmotic shock (Macek and Lebez 1981; Zorec et al. 1990). Actinoporins are one of the most potent group of hemolysins, effective at nanomolar concentrations, and the formation of pores in natural or model lipid membranes is the most studied effect (Belmonte et al. 1993; De los Rios et al. 1998; Tejuca et al. 1996; Zorec et al. 1990). Actinoporins are sphingomyelin dependent (Anderluh and Macek 2002). However, this specificity is not yet explained in full. It is not clear whether the toxin recognizes the sphingomyelin headgroup or whether the higher permeabilization is due to physical properties of sphingomyelin-containing membranes. In addition, it was shown that in some conditions cholesterol enhances lytic activity (Barlic et al. 2004; De los Rios et al. 1998), and in this respect a recent paper proposes that Eqt preferentially binds to borders of lipid domains consisting of sphingomyelin and cholesterol (Barlic et al. 2004). Significant progress has been made in the last few years in the understanding of molecular mechanism of actinoporin pore formation (Anderluh et al. 2003; Hong et al. 2002; Malovrh et al. 2003; Mancheno et al. 2003). It is clear now that actinoporin pore formation is a multistep process that involves distinct toxin conformations in each step (Fig. 7.4 A).

7.3.1 Initial Lipid Binding

The high-resolution three-dimensional structures of EqtII and StI are available (Fig. 7.1) (Athanasiadis et al. 2001; Hinds et al. 2002; Mancheno et al. 2003). They are very similar, indicating that the same fold is conserved throughout the actinoporin family. The structure consists of a tightly folded β-sandwich composed of two β-sheets, each containing five strands. The sandwich is flanked on two sites by α-helices that are placed approximately perpendicularly to each other. One side of the molecule is flattened (termed here as the top), while the other side (bottom) is formed by two broad loops that carry some of the functionally important residues (Anderluh et al. 1999, 2000; Kristan et al. 2004). The C-terminal helix is attached to the sandwich on both sides and does not exhibit structural rearrangements during pore formation (Kristan et al. 2004). The amphipathic N-terminal helix is part of a segment that is connected to the β-sandwich by a short loop and is the only part of the protein that can be dislocated from the β-sandwich without disrupting the general fold of the molecule. Unlike the Amoebapore, it is hard to imagine efficient pore formation without rearrangements of at least part of the structure. The longest axis of the molecule is approximately 4 nm, which is slightly less than the thickness of the membrane. In one suggestion for creating a transmembrane pore, the whole body forms part of the conductive channel. This requires insertion of the whole molecule in the lipid membrane. However, this possibility was soon excluded when low-resolution cysteine scanning mutagenesis was performed (Anderluh et al. 1999). Nineteen single cysteine mutants were generated throughout the molecule and

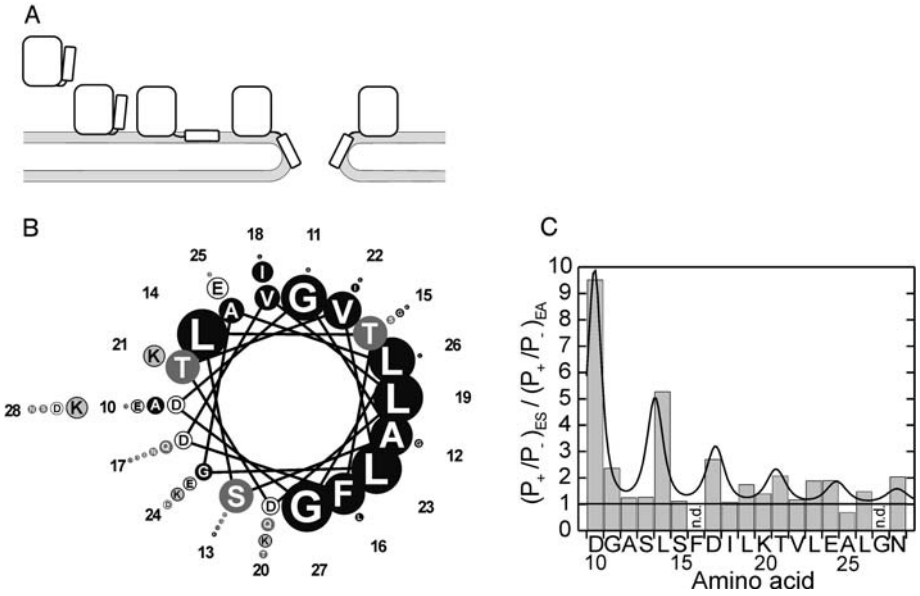

Fig. 7.4 Pore formation of actinoporins is performed with the amphipathic N-terminal region.
(A) Amphipathic helices are used to perforate lipid membranes. A nice example is the actinoporins – pore-forming toxins from sea anemones. The mechanism of membrane permeabilization by actinoporins involves at least three distinct membrane-bound conformational states of the toxin: surface-attached protein, form with translocated N-terminal region and final pore state, where the conductive channel is formed by amphipathic helices.
(B) Conservational helical wheel presentation of crucial amphipathic region 10–28. The size of the circle corresponds to the degree of conservation of that particular amino acid at that position in the actinoporin family, i.e. residues Leu14, Leu19, Leu23 and Gly26 are 100% conserved in the family. Black = hydrophobic residues (L, I, V, F, G, A); dark grey = polar residues (S, T, N, Q), light grey = positively charged residues (K, R); white = negatively charged residues (D, R).
(C) The contribution of the N-terminal amphipathic region to the pore properties. Single cysteine mutants were chemically modified with methanethiosulfonate reagents introducing additional negative or positive charge. Ion selectivity of pores produced by modified mutants was measured and summarized as the ratio of selectivities when negative charge was compared to that with the positive one. Positions oriented towards the lipid bilayer did not contribute to selectivity of the pore and the ratio was approximately 1. The most exposed mutants underwent large changes in selectivity. The periodicity of approximately three to four residues was observed from Asp10 towards the N-terminal part of the region. Also, the effect diminished from Asp10, indicating that the helix is tilted. (Adapted with permission from Malovrh et al., 2003).

labeled with the environment-specific fluorescent probe acrylodan, and additionally used in topological studies by using biotin–avidin system. Only two parts of the molecule were shown to interact with the lipid bilayer: the N-terminal segment 13–20 and mutants around the tryptophan-rich region in the middle of the polypeptide chain (Fig. 7.4). Additionally, according to two-dimensional crys-

tals of StI on lipid monolayers, the majority of the molecule remains on the surface of the membrane (Mancheno et al. 2003) and quenching of tryptophan fluorescence of EqtII indicated that of five tryptophans only exposed W112 and W116 from the aromatic-rich region are transferred to the lipid bilayer (Hong et al. 2002; Malovrh et al. 2000). This region is located at the bottom of the molecule. It also contains buried tryptophan 117 that contributes to the stability of the β-sandwich (Kristan et al. 2004). There are also additional tyrosines (at positions 108 from the broad loop, and 133, 137 and 138 from the C-terminal helix) that contribute to an aromatic-rich surface. As aromatic residues are important in anchoring proteins to the lipid–membrane interface, it was tempting to suggest that these are responsible for the initial binding to the membrane. In fact, it was shown by site-directed mutagenesis that most critical were tryptophans 112 and 116 (Hong et al. 2002; Malovrh et al. 2000). In addition, very close to this region is located the so-called phosphorylcholine-binding site that was recently defined for StI (Mancheno et al. 2003). It is located behind the aromatic-rich region and its probable role is in additional stabilization of the toxin during the membrane attachment. Since phosphatidylcholine and sphingomyelin have the same headgroup, some further part of the toxin, that still needs to be determined, must be responsible for the observed lipid selectivity. It is interesting to note that a similar structural domain is used for membrane attachment by cholesterol-dependant cytolysins (CDC) from Gram-positive bacteria (Tweten et al. 2001). These toxins are approximately three times larger than actinoporins and are composed of four domains (Rossjohn et al. 1997). Domain 4 is a β-sandwich that contains exposed tryptophans shown to interact with membranes in a first shallow binding step (Ramachandran et al. 2002). Despite this similarity in the membrane attachment step, the final outcome is much different for both groups of toxins. In CDC, a huge β-barrel is formed, each monomer contributing two β-hairpins. A huge pore that is permeable to larger molecules is formed from more than 40 monomers. In actinoporins, on the contrary, the pore is formed by α-helices by four monomers only and pores are permeable only to small solutes, i.e. divalent cations.

7.3.2 Helix Insertion

The next step in the formation of the actinoporin transmembrane pore is translocation of residues 1–30 into the lipid membrane (Fig. 7.4). The N-terminal segment 10–28 (including the N-terminal α-helix at position 16–24) shares weak sequence similarity to honey bee venom melittin, an amphipathic peptide that readily creates pores in lipid membranes (Belmonte et al. 1994; Dempsey 1990). The conservation of the hydrophobic face of this region is almost complete within the family, while residues on the polar face are less conserved (Fig. 7.4). What is important, however, is that the most conserved amino acids are negatively charged at positions 10, 17 and 24. These are important for weak cation selectivity exhibited by actinoporins (Belmonte et al. 1993; Malovrh et al. 2003;

Tejuca et al. 1996). Due to its "surface-seeking" properties and considering structural properties of actinoporins, this segment was soon proposed to be the one involved in the binding to membranes and forming at least part of the functional pore (Athanasiadis et al. 2001; Belmonte et al. 1994). This was confirmed with single cysteine mutants of segment 10–28 (Malovrh et al. 2003). First, it was shown that this segment is transferred into the lipid–water interface upon binding, in such a way that the hydrophobic face is oriented towards acyl lipid chains and polar side is facing the aqueous environment. The same position was shown for melittin by using X-ray diffraction (Hristova et al. 1999). Second, by using the same set of mutants in a planar lipid membrane experiment, it was shown that the ion selectivity could be modulated by chemical modification of the introduced thiol group. In particular residues from the polar face were affected, while ones from the hydrophobic face were not (Fig. 7.4). The most influential was residue 10 and the effects diminished towards residue 28, indicating that helices are placed in a tilt to the membrane normal. The tilt angle, estimated by two different methods (Anderluh et al. 2003; Malovrh et al. 2003), was approximately 21° (Fig. 7.4).

7.3.3 The Oligomeric Pore

The final actinoporin pore is not structurally stable and has not yet been directly visualized. The diameter and arrangement of monomers in the pore was deduced from biochemical studies. It was shown that pores of 2 nm in diameter are composed of three or, more likely, four monomers (Belmonte et al. 1993; Macek et al. 1994; Tejuca et al. 1996, 2001). Pores of such a diameter cannot be simply formed by a cluster of four helices. Either other parts of the molecule contribute to the final oligomeric conductive pore or the pore is composed partially of lipid molecules from the bilayer. The first possibility requires considerable unfolding of the β-sandwich and its rearrangements in such a way that remaining space between helices is filled with the polypeptide chain. According to StI structural properties (Mancheno et al. 2003) and mutagenesis of EqtII (Kristan et al. 2004) this is not likely. StI oligomeric structures were visualized by electron microscopy on lipid monolayers and tetrameric assemblies were observed. The electron density could be simply fitted into the StI solution structure solely by slightly rotating the N-terminal segment from the β-sandwich. An excellent fit was obtained for the remaining sandwich that apparently did not undergo gross unfolding. It is tempting to suggest that these assemblies were an intermediate state of the toxin that could correspond to the membrane-bound state with translocated helix described above. In addition, just recently Kristan et al. (2004) showed with double cysteine scanning mutagenesis that conformational changes are restricted solely to the N-terminal region of EqtII, and that the β-sandwich and C-terminal helix do not undergo structural rearrangements. Unfolding of β-sandwich on the membranes can, therefore, be excluded and instead it was proposed that lipid molecules fill the remaining space

between helices (Anderluh et al. 2003). Protein–lipid membrane pores are becoming a common theme in α-helical pore-forming peptides, proteins or toxins. The toroidal pore concept was first proposed for small helical peptides melittin and magainin (Yang et al. 2001). Protein–lipid pores are also responsible for release of cytochrome *c* and other high-molecular-weight molecules from mitochondria by the pro-apoptotic Bcl-2 family (Basanez et al. 2002; Kuwana et al. 2002; Terrones et al. 2004). As stated above this family consists of proteins with an α-helical-rich fold similar to the colicin pore-forming domain. There are already some indications that actinoporins form toroidal pores, i.e. StI more efficiently permeabilizes vesicles that include lipids that promote negative curvature and, furthermore, increased flip-flop of vesicles was observed in the presence of StI (Valcarcel et al. 2001). It was further shown that cation selectivity for EqtII increases if negatively charged lipids were included in the membrane (Anderluh et al. 2003). Finally, an isotropic component was observed using ^{31}P-NMR that could be the consequence of non-bilayer membrane structure in toroidal pores (Anderluh et al. 2003; Bonev et al. 2003).

Actinoporins thus represent an interesting example of a molecular chimera. A β-sandwich is used to specifically attach toxin to membranes containing sphingomyelin, while the final steps of pore formation are performed by an amphipathic helix – a concept widely used by small amphipathic antimicrobial peptides.

7.4 Conclusion

Whilst specific lipid headgroup interactions are uncommon in these toxins, their ability to insert into and create pores in BLMs indicates a very specific interaction with the structures formed by phospholipids. The lack of high-resolution information about the structures that are formed in the membrane means that models based upon biophysics, biochemistry and the solution structures are currently the best we can do. The structures formed by helices appear to have great flexibility and the overall impression is that the pores cannot be easily created by pure protein structures spanning the bilayer core leaving the lipids unaffected in serried ranks. Whether the proteolipid pore is the answer or whether it is the "last refuge of the intellectually bankrupt" (Qiu et al. 1996) makes understanding the roles of lipids and proteins in these pores the major challenge in this field.

References

Anderluh, G., Maček, P. **2002**. Cytolytic peptide and protein toxins from sea anemones (Anthozoa: Actiniaria). *Toxicon 40*, 111–124.

Anderluh, G., Barlič, A., Podlesek, Z., Maček, P., Pungerčar, J., Gubenšek, F., Zecchini, M.L., Dalla Serra, M., Menestrina, G. **1999**. Cysteine-scanning mutagenesis of an eukaryotic pore-forming toxin from sea anemone – topology in lipid membranes. *Eur. J. Biochem. 263*, 128–136.

Anderluh, G., Barlič, A., Potrich, C., Maček, P., Menestrina, G. **2000**. Lysine 77 is a key residue in aggregation of equinatoxin II, a pore-forming toxin from sea anemone *Actinia equina*. *J. Membr. Biol. 173*, 47–55.

Anderluh, G., Dalla Serra, M., Viero, G., Guella, G., Maček, P., Menestrina, G. **2003**. Pore formation by equinatoxin II, a eukaryotic protein toxin, occurs by induction of nonlamellar lipid structures. *J. Biol. Chem. 278*, 45216–45223.

Athanasiadis, A., Anderluh, G., Maček, P., Turk, D. **2001**. Crystal structure of the soluble form of equinatoxin II, a pore-forming toxin from the sea anemone *Actinia equina*. *Structure 9*, 341–346.

Bainbridge, G., Armstrong, G.A., Dover, L.G., Whelan, K.F., Lakey, J.H. **1998**. Displacement of OmpF loop 3 is not required for the membrane translocation of colicins N and A *in vivo*. *FEBS Lett. 432*, 117–122.

Baldwin, M.R., Lakey, J.H., Lax, A.J. **2004**. Identification and characterization of the *Pasteurella multocida* toxin translocation domain. *Mol. Microbiol. 54*, 239–250.

Barlič, A., Gutierrez-Aguirre, I., Caaveiro, J.M., Cruz, A., Ruiz-Arguello, M.B., Perez-Gil, J., Gonzalez-Manas, J. **2004**. Lipid phase coexistence favors membrane insertion of equinatoxin-II, a pore-forming toxin from *Actinia equina*. *J. Biol. Chem. 279*, 34209–34216.

Basanez, G., Sharpe, J.C., Galanis, J., Brandt, T.B., Hardwick, J.M., Zimmerberg, J. **2002**. Bax-type apoptotic proteins porate pure lipid bilayers through a mechanism sensitive to intrinsic monolayer curvature. *J. Biol. Chem. 277*, 49360–49365.

Bechinger, B. **2004**. Structure and function of membrane-lytic peptides. *Crit. Rev. Plant Sci. 23*, 271–292.

Belmonte, G., Pederzolli, C., Maček, P., Menestrina, G. **1993**. Pore formation by the sea anemone cytolysin equinatoxin-II in red blood cells and model lipid membranes. *J. Membr. Biol. 131*, 11–22.

Belmonte, G., Menestrina, G., Pederzolli, C., Križaj, I., Gubenšek, F., Turk, T., Maček, P. **1994**. Primary and secondary structure of a pore-forming toxin from the sea anemone, *Actinia equina* L, and its association with lipid vesicles. *Biochim. Biophys. Acta Biomembr. 1192*, 197–204.

Benedetti, H., Lloubes, R., Lazdunski, C., Letellier, L. **1992**. Colicin A unfolds during its translocation in *Escherichia coli* cells and spans the whole cell envelope when its pore has formed. *EMBO J. 11*, 441–447.

Bonev, B.B., Lam, Y.H., Anderluh, G., Watts, A., Norton, R.S., Separovic, F. **2003**. Effects of the eukaryotic pore-forming cytolysin equinatoxin II on lipid membranes and the role of sphingomyelin. *Biophys. J. 84*, 2382–2392.

Bunc, M., Drevenšek, G., Budihna, M., Šuput, D. **1999**. Effects of equinatoxin II from *Actinia equina* (L.) on isolated rat heart: the role of direct cardiotoxic effects in equinatoxin II lethality. *Toxicon 37*, 109–123.

Bychkova, V.E., Pain, R.H., Ptitsyn, O.B. **1988**. The molten globule state is involved in the translocation of proteins across membranes. *FEBS Lett. 238*, 231–234.

Cao, Z., Klebba, P.E. **2002**. Mechanisms of colicin binding and transport through outer membrane porins. *Biochimie 84*, 399–412.

Choe, S., Bennett, M.J., Fujii, G., Curmi, P.M.G., Kantardjeff, K.A., Collier, R.J., Eisenberg, D. **1992**. The crystal structure of diphtheria toxin. *Nature 357*, 216–222.

Dawson, J.P., Weinger, J.S., Engelman, D.M. **2002**. Motifs of serine and threonine can drive association of transmembrane helices. *J. Mol. Biol. 316*, 799–805.

De los Rios, V., Mancheno, J. M., Lanio, M. E., Onaderra, M., Gavilanes, J. G. **1998**. Mechanism of the leakage induced on lipid model membranes by the hemolytic protein sticholysin II from the sea anemone *Stichodactyla helianthus*. *Eur. J. Biochem. 252*, 284–289.

Deechongkit, S., Nguyen, H., Powers, E. T., Dawson, P. E., Gruebele, M., Kelly, J. W. **2004**. Context-dependent contributions of backbone hydrogen bonding to beta-sheet folding energetics. *Nature 430*, 101–105.

Dempsey, C. E. **1990**. The actions of melittin on membranes. *Biochim. Biophys. Acta 1031*, 143–161.

Derouiche, R., Gavioli, M., Benedetti, H., Prilipov, A., Lazdunski, C., Lloubes, R. **1996**. TolA central domain interacts with *Escherichia coli* porins. *EMBO J. 15*, 6408–6415.

Dover, L. G., Evans, L. J., Fridd, S. L., Bainbridge, G., Raggett, E. M., Lakey, J. H. **2000**. Colicin pore-forming domains bind to *Escherichia coli* trimeric porins. *Biochemistry 39*, 8632–8637.

Doyle, D. A., Cabral, J. M., Pfuetzner, R. A., Kuo, A. L., Gulbis, J. M., Cohen, S. L., Chait, B. T., MacKinnon, R. **1998**. The structure of the potassium channel: Molecular basis of K^+ conduction and selectivity. *Science 280*, 69–77.

Elkins, P., Bunker, A., Cramer, W. A., Stauffacher, C. V. **1997**. A mechanism for toxin insertion into membranes is suggested by the crystal structure of the channel-forming domain of colicin E1. *Structure 5*, 443–458.

Engelman, D. M., Steitz, T. A. **1981**. The spontaneous insertion of proteins into and across membranes. The helical hairpin hypothesis. *Cell 23*, 411–422.

Evans, L. J. A., Goble, M. L., Hales, K., Lakey, J. H. **1996**. Different sensitivities to acid denaturation within a family of proteins; Implications for acid unfolding and membrane translocation. *Biochemistry 35*, 13180–13185.

Fang, Y., Cheley, S., Bayley, H., Yang, J. **1997**. The heptameric prepore of a Staphylococcal alpha-hemolysin mutant in lipid bilayers imaged by atomic force microscopy. *Biochemistry 36*, 9518–9522.

Ferguson, A. D., Hofmann, E., Coulton, J. W., Diederichs, K., Welte, W. **1998**. Siderophore-mediated iron transport: crystal structure of FhuA with bound lipopolysaccharide. *Science 282*, 2215–2220.

Fourel, D., Bernadac, A., Pages, J. M. **1994**. Involvement of exposed polypeptide loops in trimeric stability and membrane insertion of *Escherichia coli* ompf porin. *Eur. J. Biochem. 222*, 625–630.

Fridd, S. L., Lakey, J. H. **2002**. Surface aspartate residues are essential for the stability of colicin A P-domain: a mechanism for the formation of an acidic molten-globule. *Biochemistry 41*, 1579–1586.

Gazit, E., Burshtein, N., Ellar, D. J., Sawyer, T., Shai, Y. **1997**. *Bacillus thuringiensis* cytolytic toxin associates specifically with its synthetic helices A and C in the membrane bound state. Implications for the assembly of oligomeric transmembrane pores. *Biochemistry 36*, 15546–15554.

Hecht, O., van Nuland, N. A., Schleinkofer, K., Dingley, A. J., Bruhn, H., Leippe, M., Grotzinger, J. **2004**. Solution structure of the pore-forming protein of *Entamoeba histolytica*. *J. Biol. Chem. 279*, 17834–17841.

Heuck, A. P., Tweten, R. K., Johnson, A. E. **2003**. Assembly and topography of the prepore complex in cholesterol-dependent cytolysins. *J. Biol. Chem. 278*, 31218–31225.

Hilsenbeck, J. L., Park, H., Chen, G., Youn, B., Postle, K., Kang, C. H. **2004**. Crystal structure of the cytotoxic bacterial protein colicin B at 2.5 angstrom resolution. *Mol. Microbiol. 51*, 711–720.

Hinds, M. G., Zhang, W., Anderluh, G., Hansen, P. E., Norton, R. S. **2002**. Solution structure of the eukaryotic pore-forming cytolysin equinatoxin II: implications for pore formation. *J. Mol. Biol. 315*, 1219–1229.

Holzenburg, A., Engel, A., Kessler, R., Manz, H. J., Lustig, A., Aebi, U. **1989**. Rapid isolation of Ompf porin LPS complexes suitable for structure–function studies. *Biochemistry 28*, 4187–4193.

Hong, Q., Gutierrez-Aguirre, I., Barlič, A., Malovrh, P., Kristan, K., Podlesek, Z., Maček, P., Turk, D., Gonzalez-Manas, J. M., Lakey, J. H., Anderluh, G. **2002**. Two-step membrane binding by equinatoxin II,

a pore-forming toxin from the sea anemone, involves an exposed aromatic cluster and a flexible helix. *J. Biol. Chem. 277*, 41916–41924.

Hristova, K., Wimley, W.C., Mishra, V.K., Anantharamiah, G.M., Segrest, J.P., White, S.H. **1999**. An amphipathic alpha-helix at a membrane interface: a structural study using a novel X-ray diffraction method. *J. Mol. Biol. 290*, 99–117.

Huynh, P.D., Cui, C., Zhan, H.J., Oh, K.J., Collier, R.J., Finkelstein, A. **1997**. Probing the structure of the diphtheria toxin channel – reactivity in planar lipid bilayer membranes of cysteine-substituted mutant channels with methanethiosulfonate derivatives. *J. Gen. Physiol. 110*, 229–242.

Jakes, K.S., Kienker, P.K., Slatin, S.L., Finkelstein, A. **1998**. Translocation of inserted foreign epitopes by a channel-forming protein. *Proc. Natl Acad. Sci. USA 95*, 4321–4326.

James, R., Kleanthous, C., Moore, G.R. **1996**. The biology of E colicins: paradigms and paradoxes. *Microbiology UK 142*, 1569–1580.

Jansen, C., Heutink, M., Tommassen, J., de Cock, H. **2000**. The assembly pathway of outer membrane protein PhoE of *Escherichia coli*. *Eur. J. Biochem. 267*, 3792–3800.

Jeanteur, D., Pattus, F., Timmins, P.A. **1994**. Membrane-bound form of the pore-forming domain of colicin A – a neutron-scattering study. *J. Mol. Biol. 235*, 898–907.

Jiang, X.Y., Yang, W.L., Chen, H.P., Tu, H.B., Wu, W.Y., Wei, J.W., Wang, J., Liu, W.H., Xu, A.L. **2002**. Cloning and characterization of an acidic cytolysin cDNA from sea anemone *Sagartia rosea*. *Toxicon 40*, 1563–1569.

Kabsch, W., Sander, C. **1983**. Dictionary of protein secondary structure – pattern-recognition of hydrogen-bonded and geometrical features. *Biopolymers 22*, 2577–2637.

Kageyama, M., Kobayashi, M., Sano, Y., Masaki, H. **1996**. Construction and characterization of pyocin–colicin chimeric proteins. *J. Bacteriol. 178*, 103–110.

Kawashima, Y., Nagai, H., Ishida, M., Nagashima, Y., Shiomi, K. **2003**. Primary structure of echotoxin 2, an actinoporin-like hemolytic toxin from the salivary gland of the marine gastropod *Monoplex echo*. *Toxicon 42*, 491–497.

Kienker, P., Qiu, X.Q., Nassi, S., Slatin, S., Finkelstein, A., Jakes, K. **1996**. Orientation of the hydrophobic hairpin in the colicin Ia channel. *Biophys. J. 70*, MAMM6.

Kristan, K., Podlesek, Z., Hojnik, V., Gutierrez-Aguirre, I., Gunčar, G., Turk, D., Gonzalez-Manas, J., Lakey, J.H., Maček, P., Anderluh, G. **2004**. Pore formation by equinatoxin, an eukaryotic pore-forming toxin, requires a flexible N-terminal region and a stable *β*-sandwich. *J. Biol. Chem. 279*, 46509–46517.

Kurisu, G., Zakharov, S.D., Zhalnina, M.V., Bano, S., Eroukova, V.Y., Rokitskaya, T.I., Antonenko, Y.N., Wiener, M.C., Cramer, W.A. **2003**. The structure of BtuB with bound colicin E3 R-domain implies a translocon. *Nat. Struct. Biol. 10*, 948–954.

Kuwana, T., Mackey, M.R., Perkins, G., Ellisman, M.H., Latterich, M., Schneiter, R., Green, D.R., Newmeyer, D.D. **2002**. Bid, Bax, and lipids cooperate to form supramolecular openings in the outer mitochondrial membrane. *Cell 111*, 331–342.

Lafranconi, W.M., Ferlan, I., Russell, F.E., Huxtable, R.J. **1984**. The action of equinatoxin, a peptide from the venom of the sea anemone, *Actinia equina*, on the isolated lung. *Toxicon 22*, 347–352.

Lakey, J.H., Slatin, S.L. **2001**. Pore-forming colicins and their relatives, vol. *257*. In *Pore-forming Toxins*, van der Goot, F.G. (ed.). Springer, Heidelberg, pp. 131–161.

Letellier, L., van der Goot, F.G., Gonzalez-Manas, J.-M., Lakey, J.H., Dowhan, W., Pattus, F. **1994**. Role of negatively charged phospholipids in the mode of action of negatively charged colicins: an attempt to relate *in vitro* to *in vivo* studies. In *Phosphate in Microorganisms: Cellular and Molecular Biology*, Torriani-Gorini, A., Yagil, E., Silver, S. (eds). American Society for Microbiology, Washington, DC, pp. 239–244.

Li, J., Carroll, J., Ellar, D.J. **1991**. Crystal-structure of insecticidal delta-endotoxin from *Bacillus thuringiensis* at 2.5-Å resolution. *Nature 353*, 815–821.

Li, J., Koni, P.A., Ellar, D.J. **1996**. Structure of the mosquitocidal delta-endotoxin CytB from *Bacillus thuringiensis* sp kyushuensis and implications for membrane pore formation. *J. Mol. Biol. 257*, 129–152.

Maček, P., Lebez, D. **1981**. Kinetics of hemolysis induced by equinatoxin, a cytolytic toxin from the sea-anemone *Actinia equina* – effect of some ions and pH. *Toxicon 19*, 233–240.

Maček, P., Belmonte, G., Pederzolli, C., Menestrina, G. **1994**. Mechanism of action of equinatoxin-II, a cytolysin from the sea-anemone *Actinia equina* L belonging to the family of actinoporins. *Toxicology 87*, 205–227.

Malovrh, P., Barlič, A., Podlesek, Z., Maček, P., Menestrina, G., Anderluh, G. **2000**. Structure-function studies of tryptophan mutants of equinatoxin II, a sea anemone pore-forming protein. *Biochem. J. 346*, 223–232.

Malovrh, P., Viero, G., Dalla Serra, M., Podlesek, Z., Lakey, J. H., Maček, P., Menestrina, G., Anderluh, G. **2003**. A novel mechanism of pore formation – membrane penetration by the N-terminal amphipathic region of equinatoxin. *J. Biol. Chem. 278*, 22678–22685.

Mancheno, J. M., Martin-Benito, J., Martinez-Ripoll, M., Gavilanes, J. G., Hermoso, J. A. **2003**. Crystal and electron microscopy structures of sticholysin II actinoporin reveal insights into the mechanism of membrane pore formation. *Structure 11*, 1319–1328.

Martinez, M. C., Lazdunski, C., Pattus, F. **1983**. Isolation, molecular and functional properties of the C-terminal domain of colicin A. *EMBO J. 2*, 1501–1507.

Massotte, D., Pattus, F. **1989**. Colicin N and its thermolytic fragment induce phospholipid vesicle fusion. *FEBS Lett. 257*, 447–450.

Massotte, D., Dasseux, J. L., Sauve, P., Cyrklaff, M., Leonard, K., Pattus, F. **1989**. Interaction of the pore-forming domain of colicin A with phospholipid vesicles. *Biochemistry 28*, 7713–7719.

Miller, C. J., Elliott, J. L., Collier, R. J. **1999**. Anthrax protective antigen: prepore-to-pore conversion. *Biochemistry 38*, 10432–10441.

Minor, D. L., Kim, P. S. **1996**. Context-dependent secondary structure formation of a designed protein sequence. *Nature 380*, 730–734.

Muchmore, S. W., Sattler, M., Liang, H., Meadows, R. P., Harlan, J. E., Yoon, H. S., Nettesheim, D., Chang, B. S., Thompson, C. B., Wong, S. L., Ng, S. C., Fesik, S. W. **1996**. X-ray and NMR structure of human bcl-x_L, an inhibitor of programmed cell-death. *Nature 381*, 335–341.

Nogueira, R. A., Varanda, W. A. **1988**. Gating properties of channels formed by Colicin Ia in planar lipid bilayer membranes. *J. Membr. Biol. 105*, 143–153.

Oh, K. J., Senzel, L., Collier, R. J., Finkelstein, A. **1999**. Translocation of the catalytic domain of diphtheria toxin across planar phospholipid bilayers by its own T domain. *Proc. Natl Acad. Sci. USA 96*, 8467–8470.

Parker, M. W., Pattus, F. **1993**. Rendering a membrane-protein soluble in water – a common packing motif in bacterial protein toxins. *Trends Biochem. Sci.* 391–395.

Parker, M. W., Pattus, F., Tucker, A. D., Tsernoglou, D. **1989**. Structure of the membrane-pore-forming fragment of colicin A. *Nature 337*, 93–96.

Parker, M. W., Tucker, A. D., Tsernoglou, D., Pattus, F. **1990**. Insights into membrane insertion based on studies of colicins. *Trends Biochem. Sci. 15*, 126–129.

Parker, M. W., Postma, J. P., Pattus, F., Tucker, A. D., Tsernoglou, D. **1992**. Refined structure of the pore-forming domain of colicin A at 2.4 Å resolution. *J. Mol. Biol. 224*, 639–657.

Parker, M. W., Buckley, J. T., Postma, J., Tucker, A. D., Leonard, K., Pattus, F., Tsernoglou, D. **1994**. Structure of the aeromonas toxin proaerolysin in its water-soluble and membrane-channel states. *Nature 367*, 292–295.

Pattus, F., Cavard, D., Verger, R., Lazdunski, C., Rosenbusch, J., Schindler, H. **1983**. Formation of voltage dependent pores in planar bilayers by colicin A. In *Physical Chemistry of Transmembrane Ion Motions*, Spach, G. (ed.). Elsevier, Amsterdam, pp. 407–413.

Popot, J. L., Engelman, D. M. **2000**. Helical membrane protein folding, stability, and evolution. *Annu. Rev. Biochem. 69*, 881–922.

Qiu, X.Q., Jakes, K.S., Kienker, P.K., Finkelstein, A., Slatin, S.L. **1996**. Major transmembrane movement associated with colicin Ia channel gating. *J. Gen. Physiol. 107*, 313–328.

Rakin, A., Boolgakowa, E., Heesemann, J. **1996**. Structural and functional organization of the *Yersinia pestis* bacteriocin pesticin gene cluster. *Microbiology UK 142*, 3415–3424.

Ramachandran, R., Heuck, A.P., Tweten, R.K., Johnson, A.E. **2002**. Structural insights into the membrane-anchoring mechanism of a cholesterol-dependent cytolysin. *Nat. Struct. Biol.9*, 823–827.

Riley, M.A., Wertz, J.E. **2002**. Bacteriocins: evolution, ecology, and application. *Annu. Rev. Microbiol. 56*, 117–137.

Rossjohn, J., Feil, S.C., McKinstry, W.J., Tweten, R.K., Parker, M.W. **1997**. Structure of a cholesterol-binding, thiol-activated cytolysin and a model of its membrane form. *Cell 89*, 685–692.

Schein, S.J., Kagan, B.L., Finkelstein, A. **1978**. Colicin K acts by forming voltage-dependent channels in phospholipid bilayer membranes. *Nature 276*, 159–163.

Schendel, S.L., Montal, M., Reed, J.C. **1998**. Bcl-2 family proteins as ion-channels. *Cell Death Differ. 5*, 372–380.

Senzel, L., Huynh, P.D., Jakes, K.S., Collier, R.J., Finkelstein, A. **1998**. The diphtheria toxin channel-forming T domain translocates its own NH_2-terminal region across planar bilayers. *J. Gen. Physiol. 112*, 317–324.

Shai, Y. **2002**. Mode of action of membrane active antimicrobial peptides. *Biopolymers 66*, 236–248.

Silverman, J.A., Mindell, J.A., Zhan, H., Finkelstein, A., Collier, R.J. **1994**. Structure–function relationships in diphtheria toxin channels. 1. Determining a minimal channel-forming domain. *J. Membr. Biol. 137*, 17–28.

Singer, S., Nicolson, G. **1972**. The fluid mosaic model of cell membranes. *Science 175*, 720–731.

Slatin, S.L., Qiu, X.Q., Jakes, K.S., Finkelstein, A. **1994**. Identification of a translocated protein segment in a voltage-dependent channel. *Nature 371*, 158–161.

Song, L.Z., Hobaugh, M.R., Shustak, C., Cheley, S., Bayley, H., Gouaux, J.E. **1996**. Structure of staphylococcal alpha-hemolysin, a heptameric transmembrane pore. *Science 274*, 1859–1866.

Tejuca, M., Serra, M.D., Ferreras, M., Lanio, M.E., Menestrina, G. **1996**. Mechanism of membrane permeabilization by sticholysin I, a cytolysin isolated from the venom of the sea anemone *Stichodactyla helianthus*. *Biochemistry 35*, 14947–14957.

Tejuca, M., Dalla Serra, M., Potrich, C., Alvarez, C., Menestrina, G. **2001**. Sizing the radius of the pore formed in erythrocytes and lipid vesicles by the toxin sticholysin I from the sea anemone *Stichodactyla helianthus*. *J. Membr. Biol. 183*, 125–135.

Teng, C.M., Lee, L.G., Lee, C.Y., Ferlan, I. **1988**. Platelet-aggregation induced by equinatoxin. *Thromb. Res. 52*, 401–411.

Terrones, O., Antonsson, B., Yamaguchi, H., Wang, H.G., Liu, J.H., Lee, R.M., Herrmann, A., Basanez, G. **2004**. Lipidic pore formation by the concerted action of proapoptotic BAX and tBID. *J. Biol. Chem. 279*, 30081–30091.

Tweten, R.K., Parker, M.W., Johnson, A.E. **2001**. The cholesterol-dependent cytolysins. In *Pore-forming Toxins*, van der Goot, F.G. (ed.). Springer, Heidelberg, vol. *257*, pp. 15–33.

Valcarcel, C.A., Dalla Serra, M., Potrich, C., Bernhart, I., Tejuca, M., Martinez, D., Pazos, F., Lanio, M.E., Menestrina, G. **2001**. Effects of lipid composition on membrane permeabilization by sticholysin I and II, two cytolysins of the sea anemone *Stichodactyla helianthus*. *Biophys. J. 80*, 2761–2774.

Valiyaveetil, F.I., Zhou, Y.F., Mackinnon, R. **2002**. Lipids in the structure, folding, and function of the KcsA K^+ channel. *Biochemistry 41*, 10771–10777.

van der Goot, F.G., González-Mañas, J.M., Lakey, J.H., Pattus, F. **1991**. A "molten-globule" membrane-insertion intermediate of the pore-forming domain of colicin A. *Nature 354*, 408–410.

van der Goot, F.G., Lakey, J.H., Pattus, F. **1992**. The molten globule intermediate for protein insertion or translocation through membranes. *Trends Cell Biol. 2*, 343–348.

van der Goot, F.G., Didat, N., Pattus, F., Dowhan, W., Letellier, L. **1993**. Role of acidic lipids in the translocation and channel activity of colicins A and N in *Escherichia coli* cells. *Eur. J. Biochem. 213*, 217–221.

Vecsey-Semjen, B., Knapp, S., Mollby, R., van der Goot, F.G. **1999**. The staphylococcal alpha-toxin pore has a flexible conformation. *Biochemistry 38*, 4296–4302.

Vetter, I.R., Parker, M.W., Pattus, F., Tsernoglou, D. **1996**. Insights into membrane insertion based on studies of colicins. In *Protein Toxin Structure*, Parker, M.W. (ed.). Landes, Austin, TX, pp. 5–24.

Vetter, I.R., Parker, M.W., Tucker, A.D., Lakey, J.H., Pattus, F., Tsernoglou, D. **1998**. Crystal structure of a colicin N fragment suggests a model for toxicity. *Structure 6*, 863–874.

Vollmer, W., Pilsl, H., Hantke, K., Holtje, J.V., Braun, V. **1997**. Pesticin displays muramidase activity. *J. Bacteriol. 179*, 1580–1583.

Wiener, M., Freymann, D., Ghosh, P., Stroud, R.M. **1997**. Crystal structure of colicin Ia. *Nature 385*, 461–464.

Yang, L., Harroun, T.A., Weiss, T.M., Ding, L., Huang, H.W. **2001**. Barrel-stave model or toroidal model? A case study on melittin pores. *Biophys. J. 81*, 1475–1485.

Zakharov, S.D., Cramer, W.A. **2002**. Colicin crystal structures: pathways and mechanisms for colicin insertion into membranes. *Biochim. Biophys. Acta Biomembr. 1565*, 333–346.

Zorec, R., Tester, M., Maček, P., Mason, W.T. **1990**. Cytotoxicity of equinatoxin-II from the sea-anemone *Actinia equina* involves ion channel formation and an increase in intracellular calcium activity. *J. Membr. Biol. 118*, 243–249.

8
Membrane Recognition and Pore Formation by Bacterial Pore-forming Toxins

Alejandro P. Heuck and Arthur E. Johnson

8.1
Introduction

Many bacteria secrete polypeptides with intrinsic properties that generate a remarkably wide range of stable structural states designed to accomplish a single function – forming a hole in a cellular membrane. These polypeptides can exist either as a water-soluble monomer or, after bilayer insertion, as a multimeric integral membrane protein. Furthermore, the ability to convert from a stable folded state in water to a different stable folded state inside a membrane is also an intrinsic property of such polypeptides. This conversion is spontaneous and, although it is triggered by an interaction with a specific lipid, protein and/or carbohydrate at the membrane surface, the insertion of the polypeptide into the membrane proceeds without the assistance of other proteins as chaperones or energy transducers. Protein biochemists, protein folders, structural biologists, lipid biochemists and others are therefore intrigued by the structural dimorphism of these polypeptides, while clinicians, microbiologists and others are focused on the functional ramifications of these interesting structural properties. These proteins are the bacterial pore-forming toxins (PFTs), and their purpose is to damage or infiltrate mammalian cells and interfere with their function.

8.2
Classification of Bacterial PFTs

It is almost impossible to find a unique classification for all known bacterial PFTs. We can classify them according to the structural similarity of the water-soluble forms, by the number of monomers in the membrane-inserted state, by the mechanism of cell target recognition, by the secondary/tertiary structure that perforates the membrane, by the activation mechanism, etc. However, these

classifications are arbitrary and are beneficial primarily for the purpose of simplifying the analysis of a particular property of the toxins. Since the purpose here is to describe our current knowledge of how the different bacterial toxins penetrate and form pores in the membrane of their target cell, a reasonable classification is one that uses the structural features of the formed channel to classify the different bacterial PFTs. To date, it appears that bacteria create transmembrane pores using one of two structural motifs: either amphipathic α-helices or amphipathic β-hairpins [1–4]. More importantly, a common mechanism of pore formation is used by most of the toxins that employ a particular motif (see Section 8.3).

Using this criterion, a PFT is classified as an α-PFT if it forms transmembrane pores by the insertion of amphipathic α-helices such as pore-forming colicins and diphtheria toxin (DT). If the toxins form pores by the insertion of amphipathic β-hairpins into the membrane to create a transmembrane β-barrel, PFTs are classified as β-PFT [e.g. *Staphylococcus aureus* α-hemolysin (α-HL), streptolysin O (SLO), anthrax protective antigen (anthrax PA) and aerolysin].

One drawback of this classification is that it is difficult to include valuable data obtained for toxins which cannot be classified in either of these two categories because their structural and/or mechanistic information is unavailable (e.g. *Vibrio cholerae* cytolysin [5], RTX toxins [6], *Helicobacter pylori* vacuolating toxin [7] and *Clostridium perfringens* ε-toxin [8]). In addition, some of these PFTs have an additional translocation function (e.g. DT, anthrax PA and colicins; see [9]). In the case of the pore-forming colicins, it is ultimately the formed pore that kills the cell; however, in the case of DT and anthrax PA, it is the translocation function that is biologically relevant. How the pore-forming properties contribute (or not) to the translocation function of these toxins is still under investigation.

8.2.1 α-PFTs

In general, α-PFTs tend to be highly α-helical, and the pore-forming domains of colicins define the archetypal structure of the class that also includes the DT T subunit and the *Bacillus thuringiensis* insecticidal δ-endotoxins [10]. The first high-resolution structure of a member of this family of toxins was the pore-forming domain of colicin A [11]. This was an influential discovery since it revealed for the first time the folding pattern that allowed a membrane-inserting toxin to remain water soluble. The pore-forming domain consists of a pair of hydrophobic helices surrounded by an outer shell of amphipathic α-helices (Fig. 8.1a). Upon interacting with the membrane, the hydrophobic helical hairpin is thought to spontaneously penetrate the bilayer, while the amphipathic helices lie on the surface (or the interface) of the membrane with the hydrophobic sides of the helices oriented towards the core of the bilayer. Application of a negative transmembrane potential then leads to the formation of the open channel. Unfortunately, the structure of the membrane-inserted version of this class of toxins is far from being understood [12–14].

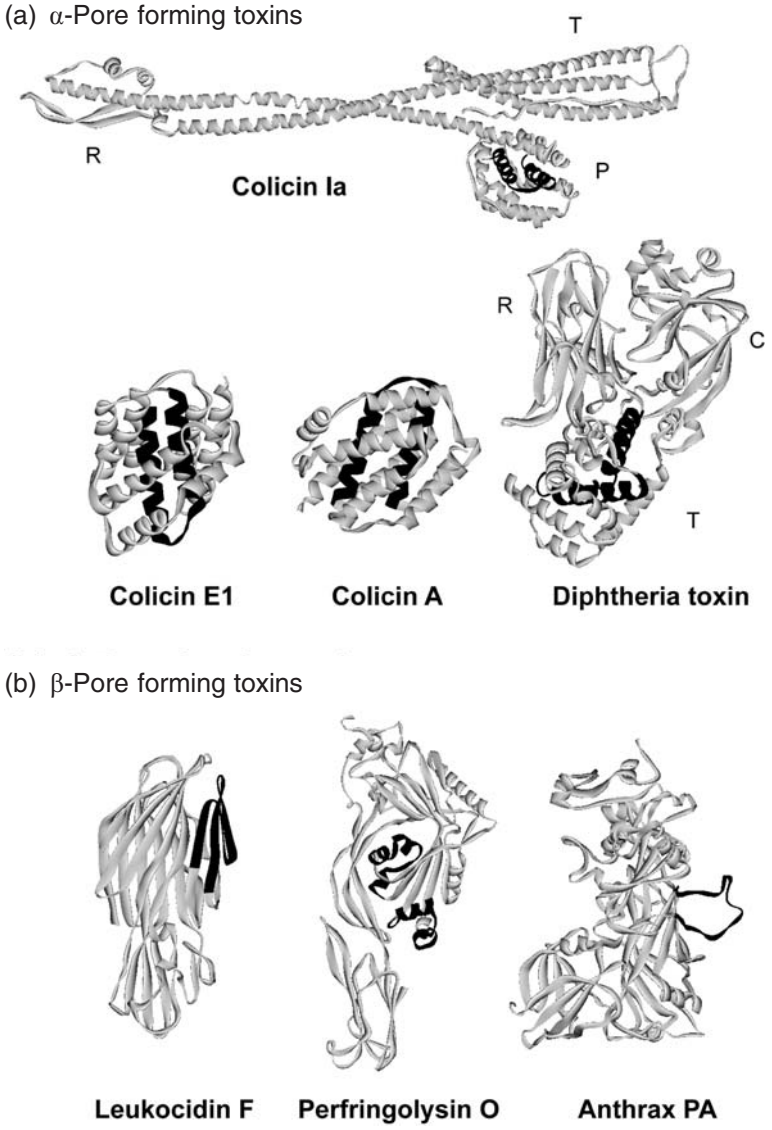

Fig. 8.1 Ribbon representations of the three-dimensional structures of representative bacterial PFTs. The regions thought to form transmembrane regions in the membrane-inserted conformation of each protein are highlighted in black.
(a) α-PFTs. The putative hydrophobic α-helices are surrounded and hidden from water by other amphipathic α-helices in the globular domain. For colicin E1 and colicin A, only the pore-forming domain is shown. R = receptor-binding domain, T = translocation domain, C = catalytic domain and P = pore-forming domain.
(b) β-PFTs. The amphipathic transmembrane β-hairpins are folded in the water-soluble monomeric form as β-strands (LukF), α-helices (PFO) or as an unstructured loop (anthrax PA). The structure of anthrax PA shown corresponds to a monomer in the pre-pore complex [35].

Interestingly, it has been proposed recently that a group of PFT secreted by sea anemones, the actinoporins (e.g. equinatoxin II, sticholysin II), creates a transmembrane pore by the insertion of amphipathic α-helices. However, in contrast to the colicin-related α-PFTs, the monomeric water-soluble form of equinatoxin is rich in β-structure and oligomerizes on the membrane surface to form a tetrameric complex. These particular toxins seem to share some features and properties characteristic of both bacterial PFT families [15, 16].

8.2.2 *β*-PFTs

β-PFT proteins are predicted to penetrate the target membrane by forming a β-barrel, and, in general, the water-soluble monomers tend to be rich in β-structure (Fig. 8.1 b). This group of toxins represents a growing family of proteins involved in bacterial pathogenesis, and several reviews on β-PFTs have been published [3, 17–19]. Most β-PFT pores are formed by heptameric oligomers and are 15–35 Å in diameter (e.g. α-HL [20], aerolysin [21] and anthrax PA [22]). In general, most of these toxins contribute one amphipathic β-hairpin per protein to the oligomeric barrel. A subset of these β-PFTs is formed by the cholesterol-dependent cytolysins (CDCs) that form pores as large as 300 Å in diameter by the oligomerization of 40–50 monomers [23, 24]. In this case, each monomer contributes at least two amphipathic β-hairpins to the oligomeric β-barrel [25, 26].

Whereas most of the β-PFTs form homo-oligomeric complexes, the bicomponent leukotoxins, a group of toxins also secreted by *S. aureus* and structurally related to α-HL, have the unique characteristic of forming oligomers composed of two different water-soluble proteins (class S and class F). This group consists of the staphylococcal γ-hemolysin (Hlg), leukocidin (Luk) and Panton-Valentine leukocidin (PVL). For this group of toxins, oligomers containing six to eight monomers have been described [27, 28].

8.3 A General Mechanism of Pore Formation?

After secretion from the bacterial cell, bacterial PFTs fold into a stable water-soluble intermediate state that may be very long-lived. However, upon encountering the appropriate cell membrane, the proteins convert spontaneously into a membrane-inserted conformation that punctures the membrane of the target cell. In most cases, if not all, multiple copies of a protein are required to form a pore.

Each α-PFT that shares the colicin-like insertion/translocation motif appears to operate using a similar multistep mechanism. In the initial step, the toxin recognizes the target cell's membrane by binding to a receptor. After binding, the toxin inserts into/translocates across the membrane to express its toxic activity.

The molecular mechanism of pore formation for α-PFTs is poorly understood and controversial. The conversion from a water-soluble to a membrane-inserted

form necessitates a large change in conformation. It has been proposed that conversion into the membrane-inserted conformation involves a molten globule intermediate that would lower the energy barrier of the conversion [29]. Changes in the pH or in the temperature of the medium can trigger the putative transition to the more flexible molten globule state and thereby increase the accessibility of the hydrophobic core of the insertion domain, leading to its exposure within the membrane. A precursor to the open channel state has been described, and consists of the hydrophobic helical hairpin inserting into the membrane and the amphipathic α-helices spreading onto the membrane surface (for reviews, see [14, 30, 31]).

It has been claimed for colicins that a single molecule is able to form the pore by the insertion of a three- or four-helix bundle [12]. This would require the movement of surface-bound helices into the membrane. However, a pore comprised of a four-helix bundle is expected to be far too small to account for the ions that are known to permeate colicin [32], implying that the structure is something other than a bundle of transmembrane helices. For DT it has been proposed that the toxin forms oligomers with a variable stoichiometry and that the pore size depends on the oligomerization state [33]. However, the mechanism by which the size of the pore influences the translocation process is uncertain.

In contrast, it is clear for β-PFTs that several monomers are needed to create a pore and β-PFTs seem to follow a common mechanism of pore formation that is independent of pore size [3, 26, 34]. In general, the secreted monomeric β-PFTs diffuse toward the target membrane and bind via specific interactions with the host surface molecules. These can be lipids, carbohydrates or proteins. The surface-bound monomeric toxin becomes competent for oligomerization by the exposure of hidden polypeptides after proteolytic activation and/or upon membrane-binding-dependent conformational changes. The "activated" monomer then diffuses in the two-dimensional space of the membrane until it encounters other monomers and forms a ring-like structure known as the pre-pore complex. Only after the formation of these pre-pore complexes is a transmembrane β-barrel created by the insertion of amphipathic β-hairpins into the bilayer (Fig. 8.2).

A breakthrough in our understanding of pore formation by β-PFTs was provided by the determination of the crystal structure of the oligomeric complex of *S. aureus* α-HL [20]. With a shape resembling that of a mushroom, the α-HL heptamer measures approximately 100 Å in height and up to 100 Å in diameter. A solvent-filled channel parallels the seven-fold axis and ranges from around 15 to around 46 Å in diameter. The stem domain, a 14-strand antiparallel β-barrel, constitutes the transmembrane pore. The cap domain protrudes from the extracellular surface to form a large hydrophilic domain, while the seven rim domains define the underside of the cap at the interface of the inner leaflet of the cell membrane (Fig. 8.2 a).

The crystal structure of the α-HL oligomer was important because it revealed the structural basis for the formation of an aqueous pore through the phospholipid bilayer: a β-barrel that spanned the membrane and that was created by β-hairpins contributed by seven α-HL polypeptides. As the first crystal structure

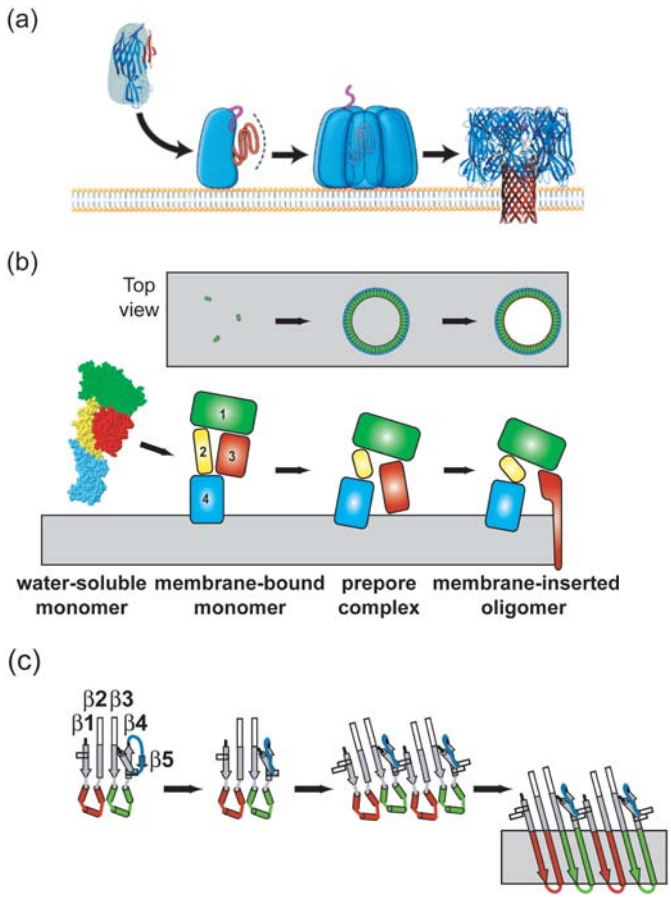

Fig. 8.2 General pore formation mechanism for β-PFTs. Secreted as water-soluble proteins, the toxins bind to the target membrane and oligomerize into a ring-like structure called the pre-pore complex. An as-yet poorly understood conformational change then leads to the insertion of the transmembrane region into the bilayer to form the aqueous pore.
(a) Mechanism of assembly for α-HL. The ribbon representation for the structure of LukF was used as a model for the water-soluble monomer. The membrane-bound monomer and pre-pore complex are depicted as cartoons because their structures are unknown. The assembled and inserted heptamer is drawn in ribbon representation. The amino latches are shown in pink and the polypeptide that contains the transmembrane hairpin is shown in red. (Adapted from [19] with permission)
(b) Stages of PFO pore formation. The domains of PFO are color coded as indicated. The membrane bilayer is depicted in grey. To simplify the figure, only a single PFO polypeptide is shown in the side view (lower panel). The upper panel shows a schematic top view (perpendicular to the plane of the membrane) for each stage of pore formation. (Adapted from [3] with permission.)
(c) Conformational changes in domain 3 of PFO required for monomer–monomer association and β-barrel formation. Each stage corresponds to a stage shown in (b). The transmembrane hairpin 1 is shown in red and the transmembrane hairpin 2 in green. The small β5 strand is shown in blue. The aromatic residues involved in the alignment of the β-strands are shown as open rectangles. (Adapted from [80])

of a β-PFT oligomer, this structure established a paradigm that has guided subsequent thinking about β-PFT structure and function.

For many putative β-PFTs that appear to oligomerize forming complexes of six to eight monomers, the adoption of the α-HL oligomeric structure as a paradigm seems reasonable. For example, the crystallographic structure of the heptameric anthrax PA pre-pore is available at 3.6-Å resolution and it has a shape similar to that of the heptameric oligomer of α-HL [35]. Low-resolution structures of the aerolysin complex have shown that this toxin also forms a heptamer with a mushroom-like shape. In this complex, the stem has an external diameter of 46 Å and encircles a water-filled pore that is 17 Å in diameter. The disk-like cap has a diameter of about 140 Å, a thickness of about 30–40 Å and is thought to reside at a distance of about 20 Å above the membrane surface [21].

Whereas several X-ray crystal structures for the water-soluble form of β-PFTs have been solved, only one high-resolution structure that resembles a membrane-inserted complex is available to date [36]. This scarcity of high-resolution structural information for membrane-inserted oligomers is not surprising because obtaining crystals of membrane proteins is rather difficult and because the size of the oligomers exceeds what can currently be successfully analyzed using nuclear magnetic resonance (NMR) methods. Given the difficulties associated with membrane protein structural analysis by crystallography and NMR, other experimental approaches have been required to obtain residue-specific structural information about β-PFTs inserted into membranes [37].

8.4 Membrane Recognition

The essential first step in the cytolytic action of many PFTs is binding to specific molecules (receptors) on the target cell surface. Among the variety of PFTs secreted by bacteria, few act against other bacteria. Those that do clearly differ in one respect from the toxins that are directed against eukaryotic cells: they generally attack similar species and thus are involved in competition for resources rather than the provision of the resources themselves. One group of these toxins, the pore-forming colicins, exhibits a particularly well-developed and complex mechanism of membrane recognition and pore formation [12]. Pore-forming colicins are composed of three domains – the receptor binding domain, the translocation domain and the pore-formation domain (Fig. 8.1 a). The receptor domain is involved in the recognition of the Gram-negative target cell, the translocation domain is involved in translocation through the outer membrane and periplasm, and the C-terminal domain is responsible for pore formation. It has been suggested that outer membrane β-barrel proteins such as OmpF, BtuB, FepA and FhuA are the first receptors contacted by the colicin molecule [12]. Translocation through the outer membrane exposes the colicin pore-forming domain to the phospholipid bilayer of the inner membrane. This colicin domain then binds to and permeabilizes the bacterial cytoplasmic membrane, thereby causing cell death.

Since colicins are produced to attack similar species, mechanisms have evolved to avoid self-injury after secretion. An appropriate immunity protein is expressed by the cell that produces the colicin molecule. The immunity protein is a three to four transmembrane helix protein inserted into the inner membrane which binds to the closed form of the inserted pore-forming colicin, thus preventing toxicity [38, 39].

To direct toxins to specific eukaryotic cells, bacteria employ different mechanisms for targeting a toxin to a particular membrane. Some toxins specifically recognize certain lipids (e.g. cholesterol) or particular proteins anchored in the plasma membrane of the target cell [e.g. glycosylphosphatidylinositol (GPI)-anchored proteins]. In addition to recognition of the appropriate cell membrane, receptor binding may facilitate the concentration of monomers on the membrane surface and could trigger conformational changes that initiate the transition to convert the toxin to an oligomerization-competent form.

8.4.1 Recognition of Specific Membrane Lipids

Among the different lipids that shape the vast variety of cell membranes, cholesterol is a distinguishing feature of mammalian membranes. Some bacterial PFTs have evolved to take advantage of this feature of mammalian cells. For example, the CDCs secreted by several Gram-positive bacteria absolutely require cholesterol in the target membrane to create a pore.

This specificity for cholesterol led researchers to postulate that the receptor for the CDCs was indeed the cholesterol molecule. However, in artificial membranes containing only phosphatidylcholine and cholesterol, more than 40 mol% cholesterol was required for CDCs such as tetanolysin [40], SLO [41] and perfringolysin O (PFO, [42]), to bind and create a pore in the bilayer. For PFO, no binding at all is detected when the cholesterol concentration in the liposomal membrane is less than around 40 mol% of the total lipids (Fig. 8.3). If cholesterol acts solely as a receptor and, hence, as a ligand for PFO binding, reducing the cholesterol concentration in the bilayer should only affect the kinetics of the cytolytic process. Therefore, lowering the amount of cholesterol in the membrane should result in a longer time required for PFO to form a transmembrane pore. However, the sharp transition observed in the binding isotherm of PFO suggests that the basis of this recognition is more complex than a simple encounter frequency between PFO and individual cholesterol molecules [42].

Interestingly, it has been shown that SLO is able to bind to cholesterol microcrystals and form oligomeric complexes similar to the ones observed in natural and synthetic membranes [43]. We have also observed that PFO is able to bind to pure cholesterol aggregates in an aqueous solution (Heuck and Johnson, unpublished data). This observation suggests the interesting possibility that PFO may bind only to cholesterol aggregates and that the sharp transition observed in the binding isotherm (Fig. 8.3) may reflect the appearance of a new lipid phase that is rich in cholesterol [44–46]. Consistent with this view, PFO has

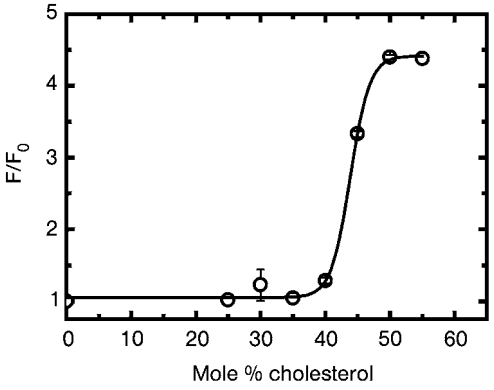

Fig. 8.3 Cholesterol-dependent PFO membrane recognition. The cysteine-less derivative of PFO in which Cys459 was replaced by alanine was used and prepared as described elsewhere [97]. The change in tryptophan fluorescence intensity that coincides with $PFO^{Cys459Ala}$ binding to membranes is shown as a function of the cholesterol content of liposomes. As noted in the text, PFO only binds to liposomes containing more than 40 mol% cholesterol [42].

been reported to bind to cholesterol-rich microdomains in mammalian cells [47]. If true, PFO and SLO would only bind, oligomerize and form a pore when this cholesterol-rich phase is present in the membrane, and not when phospholipids are the primary component of the bilayer.

V. cholerae cytolysin exhibits specificity for membranes containing cholesterol and ceramides, two components prevalent in its natural target membrane [48]. Interestingly, like SLO, *V. cholerae* cytolysin can bind to and oligomerize on cholesterol microcrystals [49].

Unless the function of the toxin is to indiscriminately create pores with the possible purpose of releasing nutrients or killing the host cell, phospholipids and cholesterol are not by themselves good candidates for specific receptor molecules since they are present in almost every membrane. However, the possibility that PFO would create pores only in membranes containing cholesterol aggregates (or with high cholesterol chemical activity) could provide certain specificity to a PFT, limiting its toxin activity to membranes that contain only a high cholesterol level.

Studies on other members of the CDC family suggest that the role of cholesterol in toxin pore formation may sometimes involve something other than initial binding of the toxin monomer to the bilayer. The CDC from *Streptococcus intermedius*, intermedilysin, exhibits an exquisite specificity for human cells, over other mammalian cells [50]. Since cholesterol is present in all mammalian cells, membrane recognition by intermedilysin must be dictated by some other component of the membrane. Yet pore formation by intermedilysin is still sensitive to the presence of sufficient cholesterol [50] and this observation led Tweten et al. [51] to analyze the role of cholesterol on different steps of the cytolytic mech-

anism of various CDCs. In the case of intermedilysin, they found that a high concentration of cholesterol in erythrocyte membranes was required for the conversion of the membrane-bound pre-pore complex to the membrane-inserted complex, but not for membrane binding [51]. They suggested that a low cholesterol concentration in erythrocyte membranes abrogates the cytolytic activity of intermedilysin by preventing membrane insertion of the transmembrane β-barrel of the pre-pore complex. Moreover, based on these observations they were able to identify a membrane protein receptor for intermedilysin, the human CD59 [127]. Thus, cholesterol mediates the binding of some, but not all CDCs to the membrane.

It is not yet clear if the presence of protein receptors is a general requirement for the cytolytic activity of all the PFTs *in vivo* or if only some of these toxins have evolved to take advantage of a more precise cell recognition mechanism. Nevertheless, it is clear that certain lipids present in mammalian cells, like cholesterol and/or ceramides, play an important role in the mechanism of pore formation of toxins like the CDCs and the *V. cholerae* cytolysin.

8.4.2 Recognition of Membrane-anchored Proteins or Carbohydrates

The recognition of a membrane component like cholesterol is important for the bacteria to avoid self-injury after secretion of the toxin. However, as noted in Section 8.4.1, this recognition mechanism provides poor toxin specificity because cholesterol is present in all mammalian cells. In general, PFTs bind to receptors expressed exclusively in a certain type of cells, thereby providing the specificity necessary to recognize not only different mammalian species, but also different tissues or cell types in the target organism.

For example, α-HL and *V. cholerae* cytolysin are 1000 times more sensitive towards rabbit erythrocytes than to human erythrocytes, suggesting that rabbit erythrocytes possess specific receptors for these toxins, although they have not been conclusively identified [48, 52]. Of the α-HL-related bicomponent leukotoxins, Hlg effectively lyses erythrocytes from human and other mammalian species, Luk is cytolytic toward human and rabbit polymorphonuclear leukocytes and rabbit erythrocytes (but not hemolytic toward human erythrocytes), and PVL shows cytolytic activity with a high cell specificity to leukocytes [27]. Of the two secreted components, classes S and F, the class S proteins are the ones that recognize a specific membrane receptor [53].

When some PFTs are involved in the translocation of the catalytic domain of the toxin into the cytosol of the target cell, as in the cases of DT and anthrax toxin, the toxins are internalized by receptor-mediated endocytosis. The DT receptor has been identified, isolated, and cloned, and is identical to the cell surface-expressed precursor form of the heparin-binding epidermal growth factor-like growth factor [54].

It has been recently shown that the anthrax PA binds to two closely related host cell receptors, the tumor endothelial marker 8 and the capillary morphogenesis

protein 2 (CMG2) [55, 56]. Each is a single peptide chain consisting of an extracellular domain, a membrane-spanning region and a cytoplasmic tail. In the extracellular domain, there is a von Willebrand type A (VWA) domain of about 200 residues that has 60% amino acid identity between the two proteins. The VWA domain fold is found in many cell adhesion proteins and it generally promotes protein–protein interactions. The recently solved crystal structure of the complex between the anthrax PA and its host receptor CMG2 constitutes the first high-resolution structure determined for a PFT bound to its receptor [35, 57]. Interestingly, the analysis of the crystal structure indicates that by binding to two adjacent domains of anthrax PA, CMG2 may restrain the conformational changes that lead to membrane insertion by stabilizing the pre-pore conformation at neutral pH. The authors suggest that the receptor may act as a brace to prevent premature membrane insertion on the cell surface before endocytosis.

A different strategy has been adopted by aerolysin, which does not recognize a specific polypeptide chain at the surface of the mammalian host, but instead recognizes a post-translational modification, a GPI anchor [58]. This anchor is added in the endoplasmic reticulum to the C-terminus of newly synthesized proteins that contain the signal for the GPI modification and the GPI-anchored proteins are then targeted to the plasma membrane [59, 60]. Cells that lack GPI-anchored proteins are 1000 times less sensitive to aerolysin, indicating the crucial role of the receptors [60].

The aerolysin-related cytolysin, the *Clostridium septicum* α-toxin, also binds to cells via GPI-anchored protein receptors [61], although aerolysin appears to bind to some receptors that are not recognized by the *C. septicum* α-toxin and vice versa. The difference seen in receptor specificity of the two PFTs appears to be linked to the presence of an N-terminal polypeptide of aerolysin that is not conserved in *C. septicum* α-toxin [62]. This polypeptide (or domain) contributes to the high binding affinity of aerolysin for the *N*-glycan core of the GPI-anchored receptor.

As a result, the recognition of specific membrane-anchored proteins or carbohydrates as receptors on the cellular cell surface not only provides bacterial toxins with high specificity towards the target cells, but it could also offer mechanistic advantages such as (1) triggering conformational changes necessary for proteolytic activation or oligomerization, (2) orienting of the toxin molecule on the membrane surface to optimize insertion, (3) stabilizing the pre-pore state to avoid premature insertion; and (4) concentrating the toxins at certain region of the membrane to maximize efficiency.

8.4.3 The Role of Membrane Lipid Domains

It has recently become apparent that the interactions between bacteria or toxins and their target host cells do not occur randomly at the plasma membrane, but rather localize in well-defined areas or microdomains [63]. Therefore, an understanding of the origin and characteristics of these microdomains is essential to comprehend how different pathogens direct the secreted PFTs to the target cell.

Our view of the structure of the plasma membrane has also improved considerably since the original "fluid mosaic" model proposed by Singer and Nicolson in 1972 [64]. It has become clear that the membrane is a dynamic combination of heterogeneous membrane domains, each with a selective protein–lipid composition and defined functions ([65] and references therein).

These domains originate primarily from the phase separation of membrane lipids that results from their different physical and chemical properties [46]. The most abundant lipids in the plasma membrane of eukaryotic cells are glycerophospholipids, sterols and sphingolipids. Sphingolipids are based on ceramide and have either a phosphocholine head group (sphingomyelin) or one of a range of carbohydrate structures (sphingoglycolipids). They further differ from the glycerophospholipids in that both acyl chains are often saturated, and also that the ceramide backbone contains both hydrogen bond donors and acceptors. The sterols consist of a four-ring hydrocarbon structure, with some amphipathic character provided by a hydroxyl group located at one end of the ring system. The principal sterol found in the vertebrate's cell membrane is cholesterol.

Studies with model systems have shown that cholesterol can promote phase separation between a low transition temperature (T_m) lipid and a high T_m lipid at an intermediate temperature when the fraction of one lipid is too low to create a separate phase in the absence of cholesterol [66–68]. When the concentration of cholesterol increases, the bilayer tends to form a single phase, but a phase separation can persist above the T_m of both lipids. The rationalization presented for these phenomena is a preferential interaction of cholesterol with (mostly) saturated lipids [69]. Above a certain threshold level of cholesterol, two different phases can co-exist in a single bilayer, one rich in cholesterol and saturated lipids (termed liquid ordered phase or l_o), and another poor in cholesterol (termed liquid disordered or l_d). The amount of the l_o phase increases with the cholesterol level until there is a continuous l_o phase. It has been also reported that the membrane sterols in excess of the phospholipids have a high chemical potential [70]. The physical state of the excess sterol is not known; it could be a bilayer solution of monomers [66] or self-associated [71].

Transmembrane proteins in a lipid bilayer would either reside in, or be excluded from, a membrane domain depending on partitioning characteristics imparted by the physical properties of the transmembrane domains [65, 72]. In the case of the outer leaflet of the bilayer, it is suggested that a major resident of cholesterol-rich microdomains are proteins attached to the bilayer by covalent linkage to GPI lipid anchors.

In conclusion, there is not a consensus on the shape, size, and lifetime of membrane microdomains *in vivo* [65, 72]. However, is well accepted that biological membranes are not homogeneous mixtures of lipids, and also that bacterial pathogens may take advantage of these membrane properties to infect host cells and promote their propagation [73].

8.5
Oligomerization on the Membrane Surface

After successful recognition of the target membrane, most β-PFTs oligomerize on the membrane surface and form a membrane-bound pre-pore complex prior to pore formation (e.g. [74]). Since this requires lateral toxin movement on the surface, the lipid composition and structure of the cell membrane plays a critical role in the association of toxin monomers. First, the monomers need to find each other on the membrane surface. These encounters will be affected by the membrane fluidity, as well as by any compartmentalization of the membrane surface [72].

It is still unclear if the pore-forming colicins form oligomers or not and it is also not known how the oligomerization state of DT affects the translocation of the C domain. For these reasons we will not discuss the α-PFTs in the present section.

Membrane fluidity, understood here as a measure of the resistance to movement of the membrane-bound monomers or the receptor-bound monomers, will be altered by changes in temperature, pressure, cholesterol content, phospholipid composition, etc. In general, it has been difficult to distinguish how fluidity differentially affects oligomerization and membrane insertion, because it has been difficult to isolate intermediate states (i.e. pre-pore complex) and thereby separate the two processes. Oligomerization can sometimes be monitored by sodium dodecylsulfate (SDS)–gel electrophoresis because the oligomers sometimes are resistant to SDS and can be observed directly on a gel. However, at least in the case of the β-PFTs, the toxin complexes are very resistant to detergent solubilization only after membrane insertion (i.e. formation of the transmembrane β-barrel) and not after pre-pore complex formation [75, 76]. Apparently, the stability of the complex is enhanced by the multiple hydrogen bonds formed between adjacent β-strands in a transmembrane β-barrel. Recently, the rational design of genetically engineered disulfide bonds to trap the toxins in the pre-pore state (i.e. avoiding pore formation) has allowed researchers to isolate various intermediates of the pore formation mechanism [42, 77–80]. These intermediates will allow researchers to analyze how fluidity affects oligomerization independently of pore formation and will enhance our understanding of how membranes with different lipid compositions affect the association of toxin monomers.

Although oligomerization has been observed in the absence of membranes for certain toxins (e.g. pneumolysin [81] and aerolysin [82]), it only occurs when the toxin concentration is relatively high (in the micromolar range or higher) compared to the concentration needed for efficient oligomerization when incubated with natural membranes. The difference in efficiency between oligomerization in solution and at the surface of a cell membrane suggests that the cells promote in some way the association of toxin monomers. Membrane binding reduces the dimensionality from three to two and this certainly contributes to an increase in the local concentration of the toxin. It has been proposed that the localization of toxin receptors (e.g. GPI-anchored proteins) in certain mem-

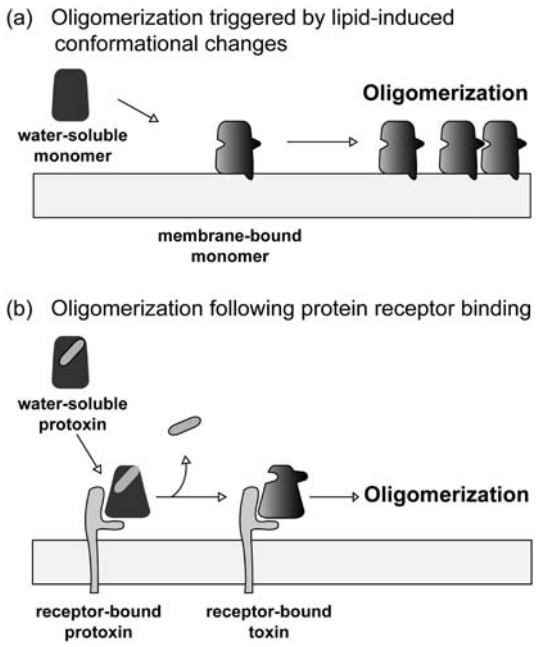

Fig. 8.4 Examples of mechanisms for β-PFT oligomerization on the surface of a target membrane.
(a) Binding of the toxin monomer to the membrane bilayer triggers a conformational change that transforms the toxin into an oligomerization-competent form (e.g. α-HL and PFO).
(b) Protein receptor recognition and binding is followed in some cases by proteolytic activation. In the case shown, the release of a peptide transforms the toxin into an oligomerization-competent form (e.g. aerolysin). In other cases, such as observed for the CDC intermedilysin, only the binding to the human CD59 receptor is required [127].

brane domains would further promote the cell surface oligomerization of aerolysin [83]. These domains appear to act as concentration platforms at the cell surface, due to their ability to recruit certain toxin receptors.

In general, oligomerization requires the exposure of hidden polypeptide regions involved in the monomer–monomer interaction. This process is triggered by conformational changes induced by protein–lipid interactions (e.g. α-HL and PFO) and/or preceded by proteolytic activation of the bacterial toxin (e.g. anthrax PA and aerolysin) (Fig. 8.4).

8.5.1 Oligomerization Triggered by Lipid-induced Conformational Changes

It is well documented that the interaction of some toxin monomers with lipids in the target membrane triggers conformational changes in the protein [42, 84–87]. However, little information is available to date that identifies the specific interactions between the lipids and the PFTs at the membrane surface. In general,

lipid–protein interactions involve a combination of ionic interactions between the protein and the lipid head groups and van der Waals interactions between the lipid tails and the electroneutral surface of the protein exposed to the non-polar core of the bilayer. In the head group region, ionic interactions involve the polar atoms of the protein backbone and bound water molecules. In the non-polar core of the membrane, any irregular non-polar surface of the protein packs with the hydrophobic hydrocarbon lipid tails.

S. aureus α-HL preferentially assembles on membranes composed of cholesterol and phosphatidylcholine or sphingomyelin. Liposomes composed of phosphatidylethanolamine, phosphatidylserine, phosphatidylglycerol or phosphatidylinositol are resistant to toxin action [88], suggesting a specific interaction of the toxin with the choline moiety of the phospholipid. The high-resolution structures of the heptameric complex of α-HL revealed a binding site for glycerophosphocholine and di-propanoyl phosphatidylcholine [89]. These results showed that the phosphocholine molecules bind primarily through cation–π interactions between the quaternary ammonium group of the phosphatidylcholine head group and the indole ring of Trp179, as well as a water-mediated hydrogen bonding between Arg200 and the phosphatidylcholine phosphate group. The critical role of Arg200 in binding of α-HL to an erythrocyte membrane was directly assessed by cysteine-scanning mutagenesis and targeted chemical modification [90]. With respect to the Trp–headgroup interaction, it is clear that upon membrane binding and oligomerization, α-HL undergoes a conformational change that leads to a rearrangement of the Trp side-chain environment [84]. However, it is not clear if the observed conformational changes are related to the binding of the choline moiety or if the interaction of α-HL with the phospholipid headgroup observed in the high-resolution crystal structure occurs after the conformational changes have taken place.

What regions of the α-HL molecule are involved in these membrane dependent conformational changes? When the water-soluble LukF monomer and the α-HL oligomer are compared, the only regions that show dramatically different conformations are the amino latch (Ala1–Val20 in α-HL) and the stem region (Lys110–Tyr148 in α-HL) [20, 91, 92]. In the monomer, the two segments are packed against the core of the molecule. In the oligomer, both segments have undergone a major conformational change and they are now in close contact with their respective counterparts of the neighboring subunits (Fig. 8.2 a). Mutations in either the N-terminal amino latch or the transmembrane hairpin region can markedly alter the efficiency of pore formation (see, e.g. [93–95]) and structural coupling of these two different regions may also be linked to the regions of α-HL that interact directly with the membrane [93, 96].

Oligomerization of PFO does not occur in solution and therefore the binding of the PFO molecule to the target membrane must somehow trigger the oligomerization process. Ramachandran et al. [80] have shown that in the water-soluble form of the toxin, oligomerization is prevented by blocking access to one edge of a core β-sheet in the monomer, thereby preventing its association with the edge of the core β-sheet in the neighboring monomer, to form an extended

β-sheet (Fig. 8.2c). Specifically, premature association of PFO molecules (before they bind to the appropriate membrane surface) is prevented by the presence of β5, a short polypeptide loop that hydrogen bonds to β4 in the monomer, and thereby prevents its interaction with the β1 strand in the adjacent monomer. The binding of the tip of domain 4 to the membrane surface immediately elicits a conformational change in domain 3, more than 70 Å above the membrane [42, 97, 128]. This conformational change rotates β5 away from β4 and thereby exposes β4 to the aqueous medium where it can associate with the always-exposed β1 strand of another PFO molecule to initiate and promote oligomerization.

Based on these two examples, it appears that the structural changes associated with converting a β-PFT from a water-soluble monomer to a membrane-inserted oligomer extend through much of the molecule, not just the membrane-interacting domains. Such an extensive network of structural linkages within a β-PFT protein can be advantageous because it reduces the chances of prematurely undergoing a structural transition that exposes a transmembrane β-hairpin. By allosterically linking different domains or regions of the protein, the system can couple separate interactions (e.g. binding to the membrane and binding to another subunit) and thereby ensure that pore formation proceeds only when the necessary criteria are met.

When a PFT forms hetero-oligomers, as in the case of the leukotoxins, it appears that membrane binding strengthens the initial side-by-side interaction between two different subunits to form a heterodimer [98]. The authors suggest that dimer–dimer association is the major pathway for the formation of tetramers, where dimerization on the membrane surface triggers structural changes at the interaction sides of their subunits for further cooperative tetramerization. Even though the molecular details of these conformational changes are still unknown, it is clear that the formation of hetero-oligomers requires a more tightly regulated mechanism of oligomerization to ensure that the complex has the proper subunit stoichiometry.

8.5.2
Oligomerization Following Proteolytic Activation of Toxins

Certain bacterial toxins like aerolysin and anthrax PA are secreted in an inactive form and require proteolytic activation before oligomerizing to form a pre-pore complex on the membrane surface, and ultimately forming a pore (Fig. 8.4b).

Proteolytic activation of pro-aerolysin involves a proteolytic cleavage within a flexible loop located in the C-terminal domain of the toxin [99]. This activation can occur in solution or when the toxin is bound to its receptor on the membrane surface. However, oligomerization only occurs in solution when the concentration of the toxin is higher than around 10 μM; therefore, there is little chance that oligomers will form if activation occurs before membrane binding. The cleavage of the approximately 40-amino-acid peptide from the C-terminus of the toxin triggers subtle conformational changes [100] that presumably pro-

mote oligomerization. The cleaved peptide dissociates from the rest of the toxin molecule spontaneously and plays no role in the remaining steps of pore formation [101]. In contrast, in the aerolysin homolog *C. septicum* α-toxin, the corresponding activation peptide appears to remain associated with the rest of the protein and to act as a molecular chaperone [102].

When activated, aerolysin can oligomerize and the resulting heptamer will expose hydrophobic patches at its surface. Therefore, if oligomerization occurs in the absence of a membrane, aerolysin is prone to aggregation and precipitation [103]. When bound to a receptor, the oligomers will be situated close to the bilayer and therefore insert into the membrane to form a pore. Thus, the activation process in aerolysin not only helps the bacteria avoid self-injury, but also guarantees an effective membrane insertion.

Similarly, when bound to its cellular receptor, anthrax PA is activated by a member of the furin family of cellular proteases that cleaves the toxin into two fragments: PA_{20} and PA_{63} [104]. PA_{20} slowly dissociates from PA_{63} and diffuses into the surrounding medium, leaving PA_{63} bound to the receptor. Receptor-bound PA_{63} spontaneously self-associates to form a ring-shaped heptameric oligomer. For PA_{20} to separate from PA_{63}, a β-sheet must be ruptured and a large hydrophobic surface on PA_{63} must separate from the complementary surface of PA_{20} [22]. The function of PA_{20} is therefore to maintain PA as a soluble monomer by preventing premature self-association while the protein diffuses from the bacteria to the host cells. Thus, by limiting proteolytic activation of the toxins at the membrane surface, oligomerization and pre-pore complex assembly are both restricted to the appropriate target membrane and precisely regulated chronologically.

8.6 Membrane Penetration and Pore Formation

PFTs insert amphipathic polypeptides into membranes to form protein-lined pores of various sizes depending on the toxin involved. In these pores, the hydrophobic surfaces of the transmembrane domains are exposed to the non-polar lipid core of the membrane bilayer and the hydrophilic surfaces face the aqueous pore.

Both the identities of the individual transmembrane segments that define the pore of α-PFTs and also the stoichiometries of the inserted complexes are still being debated. Therefore, it is difficult to discuss the role of protein–lipid interactions on membrane insertion for this subclass of bacterial toxins. In general, membrane penetration by colicins is favored in fluid membranes that contain anionic phospholipids at low pH and have a surface potential [105]. However, because of the lack of consensus about the mechanism, we will focus our discussion instead on the better characterized subclass of β-PFTs.

For the β-PFT that form aqueous pores by the insertion of a transmembrane β-barrel, the insertion of a single amphipathic β-hairpin into a membrane is not

energetically favored. In a hydrophobic environment that lacks hydrogen bond donors or acceptors, isolated β-hairpins cannot achieve the hydrogen-bond formation necessary to lower the thermodynamic cost of transferring the polar atoms of the polypeptide backbone into the hydrocarbon interior [106]. However, this energetic barrier is circumvented if the β-strands are inserted as β-sheets and form closed structures such as the β-barrel.

For monomeric β-barrel membrane proteins such as OmpA, a concerted folding mechanism has been observed *in vitro* in which the hydrogen bonds formed between adjacent β-chains presumably favor the insertion of the β-barrel into the membrane [107, 108]. Similarly, the formation of a β-PFT pre-pore complex may be required to allow the concerted, and perhaps simultaneous, insertion of the β-hairpins from individual monomers, thereby avoiding the energetic barrier of inserting non-hydrogen-bonded β-strands into the membrane. It is therefore of interest that co-expression of two complementary fragments of OmpA still results in the assembly of a functional protein [109]. Also, the complementary combination of several truncation mutants on the transmembrane β-hairpins of α-HL were analyzed and only complementary fragments separated within a β-hairpin loop were able to form pores with a hemolytic activity approaching that of the wild-type toxin [110]. Thus, these results are consistent with the idea that insertion of a β-strand into the membrane is energetically unfavorable unless the polypeptide is completely hydrogen bonded to adjacent polypeptides in a β-conformation.

In addition, the lipid composition of the target membrane plays a critical role on pore formation. We envision that a membrane composed of highly packed saturated phospholipids will be very difficult to perforate by a PFT. For example, it was shown that α-HL was able to bind to membranes composed solely by saturated phospholipids [111], but was unable to penetrate to these membranes. Pore formation was observed only in membranes containing unsaturated phospholipid [112, 113]. In addition, the susceptibility to α-HL of liposomes containing phosphatidylcholine or sphingomyelin is augmented by an increase in the cholesterol content of the liposomes. However, the presence of cholesterol was not essential for membrane binding. Taken together, these results suggest that the presence of elements which increase membrane fluidity and/or decrease membrane packing favors the insertion of transmembrane β-hairpins and the formation of a transmembrane pore by some, if not all, PFTs.

Interestingly, the presence of membrane cholesterol has also been found to enhance pore formation for other PFTs, including aerolysin [82], *V. cholerae* cytolysin [114, 115] and the CDCs [40–42]. However, the role that cholesterol plays in each of the different steps of the mechanism of pore formation is still poorly understood [116].

It has also been reported that the presence in the membrane of cone-shaped lipids such as phosphatidylethanolamine, diacylglycerol and ceramides augmented membrane permeabilization by toxins like aerolysin [82], as well as *V. cholerae* cytolysin and SLO [115]. Alonso et al. [82] proposed that for aerolysin, hexagonal phase lipids may promote pore formation by facilitating the localized

and transient generation of non-bilayer structures as the oligomeric amphipathic barrel enters the membrane. In contrast, for SLO and *V. cholerae* cytolysin, which require cholesterol in the target membrane, Zitzer et al. [115] proposed that lipids having a conical molecular shape appear to effect a change in the energetic state of membrane cholesterol that in turn augments the interaction of the sterol with the cholesterol-specific cytolysin.

An additional energetic constraint for the insertion of a β-hairpin into the membrane is the exposure of the hydrophilic surface of a single amphipathic β-hairpin to the non-polar interior of the bilayer after insertion. The insertion of a single such hydrophilic surface into the membrane would be thermodynamically unfavorable. However, if the hairpins are inserted in a concerted process, the hydrophilic edges of the hairpins could remain in contact with the aqueous medium. Such a concerted insertion would require the displacement of lipids as the aqueous pore is formed in the bilayer. Since the cross-sectional area occupied by an inserted α-HL heptamer is about 950 $Å^2$ (assuming an outer radius of 17.5 Å) and since a phospholipid occupies about 70 $Å^2$ of surface area [117], about 14 phospholipid molecules in each leaflet need to be moved to allow space for the α-HL β-barrel.

Whereas the lateral displacement of such a relatively low number of lipid molecules does not seem to create a major energetic barrier, lipid displacement during CDC pore formation is a completely different matter. The creation of a CDC hole with an outer radius near 150 Å requires the displacement of about 1000 phospholipid molecules in each leaflet (or about 800 phospholipids plus 800 cholesterol molecules because the average surface area occupied by one phospholipid molecule plus one cholesterol molecule is about 90 $Å^2$ in a 1:1 phospholipid/cholesterol mixture [118]). Using a method that determines the rate of formation of pores of different sizes, it appears that all of these lipid molecules leave the pore formed by the CDC PFO at the same time [119], although not all agree [120]. However, there is little information available about how this occurs. Thus, the mechanism by which lipids are eliminated from a CDC pore remains one of the most obscure aspects of pore formation.

8.7 Unresolved Issues

Our knowledge of the structure, function, assembly and regulation of the large number of PFTs is spotty, and focused primarily on only a few members of each of the subclasses considered in this chapter, the α-PFTs and β-PFTs. Although it is sometimes difficult, and perhaps even dangerous, to extrapolate from fragmentary information to the general principles of PFT structure and function, the available data at least provide us with working models that can be further tested experimentally.

Complete understanding the mechanism of pore formation at a molecular level would require high-resolution structures of the initial (water-soluble mono-

meric form), the final (membrane-inserted complex), and any intermediate states that occur during the pore formation process. Although more high-resolution X-ray crystal structures for different PFTs are becoming available, the reality is that membrane-inserted PFT structure determinations are difficult to achieve. This is especially true for toxins such as the CDCs that form oligomers that are very large both in size and in number of subunits. Thus, other experimental approaches will have to be used to characterize toxin structure, function, assembly and regulation. For example multiple independent fluorescence techniques have proven to be very valuable in such characterization [37], especially in the case of PFO (e.g. [25, 42, 80, 86, 97, 119, 121]). A particular advantage of using such techniques is the ability to monitor the spectral signal as a function of time, thereby allowing the kinetics of the different steps of the pore formation mechanism to be determined (e.g. [42, 80, 119, 122, 123]). The kinetic aspect of pore formation has not been well characterized, but since it cannot be determined or inferred from crystal structures, spectral techniques will have to be used more frequently to fully characterize the mechanism of pore formation.

The introduction of engineered disulfide bonds into the tertiary structure of different PFTs has been shown to be an effective method of isolating intermediate states and characterizing the individual steps of pore formation [42, 77–80, 124–126].

The involvement of lipids in the targeting of PFT to membranes is poorly understood at the molecular level, as well as the role, if any, of lipids in the oligomerization and insertion phases of pore formation. A detailed understanding of the structure and dynamics of lipids microdomains, as well as the thermodynamics that govern the protein–membrane interactions, will undoubtedly assist our efforts to understand how PFT interacts and penetrates the membrane of the target cell. Yet the apparent heterogeneity of natural membranes makes such studies difficult to interpret under the best circumstances.

An especially pertinent aspect of pore formation in this regard is the involvement of the protein receptors for toxin molecules, most of which have yet to be identified. Do such receptors actively participate in pre-pore complex formation or toxin insertion into the membrane? Do receptors serve only as binding targets and/or anchors of toxins? When do toxins release from their receptors, if at all? Do all receptors function stoichiometrically (e.g. one toxin molecule binds to one receptor molecule) or do receptors function catalytically in facilitating the addition of individual toxin molecules to the pre-pore complex? Clearly, we have much yet to learn about this and most other aspects of toxin binding to membranes and pore formation.

Acknowledgments

Work in the authors' laboratory was supported by grant AI 37657 from the National Institutes of Health (USA) and by the Robert A. Welch Foundation. We thank Dr Greg Caputo for critically reading this chapter.

References

1 E. Gouaux, *Curr. Opin. Struct. Biol.* **1997**, *7*, 566–573.
2 D. B. Lacy, R. C. Stevens, *Curr. Opin. Struct. Biol.* **1998**, *8*, 778–784.
3 A. P. Heuck, R. K. Tweten, A. E. Johnson, *Biochemistry* **2001**, *40*, 9065–9073.
4 E. Gouaux, *J. Struct. Biol.* **1998**, *121*, 110–122.
5 R. Olson, E. Gouaux, *Protein Sci.* **2003**, *12*, 379–383.
6 R. A. Welch, *Curr. Topics Microbiol. Immunol.* **2001**, *257*, 85–111.
7 C. Montecucco, M. De Bernard, E. Papini, M. Zoratti, *Curr. Topics Microbiol. Immunol.* **2001**, *257*, 113–129.
8 A. R. Cole, M. Gibert, M. Popoff, D. S. Moss, R. W. Titball, A. K. Basak, *Nat. Struct. Mol. Biol.* **2004**, *11*, 797–798.
9 V. Cabiaux, C. Wolff, J.-M. Ruysschaert, *Int. J. Biol. Macromol.* **1997**, *21*, 285–298.
10 M. W. Parker, F. Pattus, *Trends Biochem. Sci.* **1993**, *18*, 391–395.
11 M. W. Parker, F. Pattus, A. D. Tucker, D. Tsernoglou, *Nature* **1989**, *337*, 93–96.
12 J. H. Lakey, S. L. Slatin, *Curr. Topics Microbiol. Immunol.* **2001**, *257*, 131–161.
13 R. J. Collier, *Toxicon* **2001**, *39*, 1793–1803.
14 S. D. Zakharov, W. A. Cramer, *Biochim. Biophys. Acta* **2002**, *1565*, 333–346.
15 G. Anderluh, P. Macek. In *Cellular and Molecular Mechanisms of Toxin Action. Pore-forming peptides and protein toxins*, Menestrina, G., Serra, M. D., Lazarovici, P. (eds). Taylor & Francis, New York, **2003**, pp. 132–147.
16 P. Malovrh, G. Viero, M. D. Serra, Z. Podlesek, J. H. Lakey, P. Macek, G. Menestrina, G. Anderluh, *J. Biol. Chem.* **2003**, *278*, 22678–22685.
17 J. Rossjohn, S. C. Feil, W. J. McKinstry, D. Tsernoglou, F. G. van der Goot, J. T. Buckley, M. W. Parker, *J. Struct. Biol.* **1998**, *121*, 92–100.
18 G. Menestrina, M. D. Serra, G. Prévost, *Toxicon* **2001**, *39*, 1661–1672.
19 M. Montoya, E. Gouaux, *Biochim. Biophys. Acta* **2003**, *1609*, 19–27.
20 L. Song, M. R. Hobaugh, C. Shustak, S. Cheley, H. Bayley, J. E. Gouaux, *Science* **1996**, *274*, 1859–1866.
21 M. W. Parker, J. T. Buckley, J. P. M. Postma, A. D. Tucker, K. Leonard, F. Pattus, D. Tsernoglou, *Nature* **1994**, *367*, 292–295.
22 C. Petosa, R. J. Collier, K. R. Klimpel, S. H. Leppla, R. C. Liddington, *Nature* **1997**, *385*, 833–838.
23 J. L. Duncan, R. Schlegel, *J. Cell. Biol.* **1975**, *67*, 160–173.
24 A. Olofsson, H. Hebert, M. Thelestam, *FEBS Lett.* **1993**, *319*, 125–127.
25 O. Shatursky, A. P. Heuck, L. A. Shepard, J. Rossjohn, M. W. Parker, A. E. Johnson, R. K. Tweten, *Cell* **1999**, *99*, 293–299.
26 R. K. Tweten, M. W. Parker, A. E. Johnson, *Curr. Topics Microbiol. Immunol.* **2001**, *257*, 15–33.
27 G. Prévost, L. Mourey, D. A. Colin, G. Menestrina, *Curr. Topics Microbiol. Immunol.* **2001**, *257*, 53–83.
28 G. Menestrina, M. D. Serra, M. Comai, M. Coraiola, G. Viero, S. Werner, D. A. Colin, G. Prévost, *FEBS Lett.* **2003**, *552*, 54–60.
29 F. G. van der Goot, J.-M. González-Mañas, J. H. Lakey, F. Pattus, *Nature* **1991**, *354*, 408–410.
30 M. W. Parker, A. D. Tucker, D. Tsernoglou, F. Pattus, *Trends Biochem. Sci.* **1990**, *15*, 126–129.
31 R. M. Stroud, K. Reiling, M. Wiener, D. Freymann, *Curr. Opin. Struct. Biol.* **1998**, *8*, 525–533.
32 J. D. Lear, Z. R. Wasserman, W. F. DeGrado, *Science* **1988**, *240*, 1177–1181.
33 J. C. Sharpe, E. London, *J. Membrane Biol.* **1999**, *171*, 209–221.
34 F. G. van der Goot. In *Bacterial Protein Toxins*, Burns, D. L., Barbieri, J. T., Iglewski, B. H., Rappuoli, R. (eds). American Society for Microbiology, Washington, DC, **2003**, pp. 189–202.
35 D. B. Lacy, D. J. Wigelsworth, R. A. Melnyk, S. C. Harrison, R. J. Collier, *Proc. Natl Acad. Sci. USA* **2004**, *101*, 13147–13151.
36 M. W. Parker, *Toxicon* **2003**, *42*, 1–6.
37 A. P. Heuck, A. E. Johnson, *Cell Biochem. Biophys.* **2002**, *36*, 89–102.
38 V. Geli, D. Baty, F. Pattus, C. Lazdunski, *Mol. Microbiol.* **1989**, *3*, 679–687.

39 D. Espesset, D. Duche, D. Baty, V. Geli, *EMBO J*. **1996**, *15*, 2356–2364.

40 C.R. Alving, W.H. Habig, K.A. Urban, M.C. Hardegree, *Biochim. Biophys. Acta* **1979**, *551*, 224–228.

41 E. Rosenqvist, T.E. Michaelsen, A.I. Vistnes, *Biochim. Biophys. Acta* **1980**, *600*, 91–102.

42 A.P. Heuck, E.M. Hotze, R.K. Tweten, A.E. Johnson, *Mol. Cell* **2000**, *6*, 1233–1242.

43 J.R. Harris, M. Adrian, S. Bhakdi, M. Palmer, *J. Struct. Biol*. **1998**, *121*, 343–355.

44 R.P. Mason, T.N. Tulenko, R.F. Jacob, *Biochim. Biophys. Acta* **2003**, *1610*, 198–207.

45 D. Bach, E. Wachtel, *Biochim. Biophys. Acta* **2003**, *1610*, 187–197.

46 H.M. McConnell, M. Vrljic, *Annu. Rev. Biophys. Biomol. Struct*. **2003**, *32*, 469–492.

47 A. Waheed, Y. Shimada, H.F.G. Heijnen, M. Nakamura, M. Inomata, M. Hayashi, S. Iwashita, J.W. Slot, Y. Ohno-Iwashita, *Proc. Natl Acad. Sci. USA* **2001**, *98*, 4926–4931.

48 A. Zitzer, O. Zitzer, S. Bhakdi, M. Palmer, *J. Biol. Chem*. **1999**, *274*, 1375–1380.

49 J.R. Harris, S. Bhakdi, U. Meissner, D. Scheffler, R. Bittman, G. Li, A. Zitzer, M. Palmer, *J. Struct. Biol*. **2002**, *139*, 122–135.

50 H. Nagamune, C. Ohnishi, A. Katsuura, K. Fushitani, R.A. Whiley, A. Tsuji, Y. Matsuda, *Infect. Immun*. **1996**, *64*, 3093–3100.

51 K.S. Giddings, A.E. Johnson, R.K. Tweten, *Proc. Natl Acad. Sci. USA* **2003**, *100*, 11315–11320.

52 A. Hildebrand, M. Pohl, S. Bhakdi, *J. Biol. Chem*. **1991**, *266*, 17195–17200.

53 D.A. Colin, I. Mazurier, S. Sire, V. Finck-Barbançon, *Infect. Immun*. **1994**, *62*, 3184–3188.

54 J.G. Naglich, J.E. Metherall, D.W. Russell, L. Eidels, *Cell* **1992**, *69*, 1051–1061.

55 H.M. Scobie, G.J. Rainey, K.A. Bradley, J.A. Young, *Proc. Natl Acad. Sci., USA* **2003**, *100*, 5170–5174.

56 K.A. Bradley, J. Mogridge, M. Mourez, R.J. Collier, J.A.T. Young, *Nature* **2001**, *414*, 225–233.

57 E. Santelli, L.A. Bankston, S.H. Leppla, R.C. Liddington, *Nature* **2004**, *430*, 905–908.

58 L. Abrami, M. Fivaz, F.G. van der Goot, *Trends Microbiol*. **2000**, *8*, 168–172.

59 D.B. Diep, K.L. Nelson, S.M. Raja, E.N. Pleshak, J.T. Buckley, *J. Biol. Chem*. **1998**, *273*, 2355–2360.

60 L. Abrami, M.-C. Velluz, Y. Hong, K. Ohishi, A. Mehlert, M. Ferguson, T. Kino, F.G. van der Goot, *FEBS Lett*. **2002**, *512*, 249–254.

61 V.M. Gordon, K.L. Nelson, J.T. Buckley, V.L. Stevens, R.K. Tweten, P.C. Elwood, S.H. Leppla, *J. Biol. Chem*. **1999**, *274*, 27274–27280.

62 D.B. Diep, K.L. Nelson, T.S. Lawrence, B.R. Sellman, R.K. Tweten, J.T. Buckley, *Mol. Microbiol*. **1999**, *31*, 785–794.

63 F. Lafont, L. Abrami, F.G. van der Goot, *Curr. Opin. Microbiol*. **2004**, *7*, 4–10.

64 S.J. Singer, G.L. Nicolson, *Science* **1972**, *175*, 720–731.

65 S. Munro, *Cell* **2003**, *115*, 377–388.

66 H.M. McConnell, A. Radhakrishnan, *Biochim. Biophys. Acta* **2003**, *1610*, 159–173.

67 J.R. Silvius, *Biochim. Biophys. Acta* **2003**, *1610*, 174–183.

68 J.M. Crane, L.K. Tamm, *Biophys. J*. **2004**, *86*, 2965–2979.

69 H. Ohvo-Rekilä, B. Ramstedt, P. Leppimäki, J.P. Slotte, *Prog. Lipid Res*. **2002**, *41*, 66–97.

70 A. Radhakrishnan, H.M. McConnell, *Biochemistry* **2000**, *39*, 8119–8124.

71 J. Huang, G.W. Feigenson, *Biophys. J*. **1999**, *76*, 2142–2157.

72 P.H.M. Lommerse, H.P. Spaink, T. Schmidt, *Biochim. Biophys. Acta Biomembr*. **2004**, *1664*, 119–131.

73 F.G. van der Goot, T. Harder, *Immunology* **2001**, *13*, 89–97.

74 L.A. Shepard, O. Shatursky, A.E. Johnson, R.K. Tweten, *Biochemistry* **2000**, *39*, 10284–10293.

75 A. Valeva, M. Palmer, S. Bhakdi, *Biochemistry* **1997**, *36*, 13298–13304.

76 E.M. Hotze, A.P. Heuck, D.M. Czajkowsky, Z. Shao, A.E. Johnson, R.K. Tweten, *J. Biol. Chem.* **2002**, *277*, 11597–11605.

77 E.M. Hotze, E.M. Wilson-Kubalek, J. Rossjohn, M.W. Parker, A.E. Johnson, R.K. Tweten, *J. Biol. Chem.* **2001**, *276*, 8261–8268.

78 V.T. Nguyen, H. Higuchi, Y. Kamio, *Mol. Microbiol.* **2002**, *45*, 1485–1498.

79 T. Kawate, E. Gouaux, *Protein Sci.* **2003**, *12*, 997–1006.

80 R. Ramachandran, R.K. Tweten, A.E. Johnson, *Nat. Struct. Mol. Biol.* **2004**, *11*, 697–705.

81 R.J.C. Gilbert, J. Rossjohn, M.W. Parker, R.K. Tweten, P.J. Morgan, T.J. Mitchell, N. Errington, A.J. Rowe, P.W. Andrew, O. Byron, *J. Mol. Biol.* **1998**, *284*, 1223–1237.

82 A. Alonso, F.M. Goñi, J.T. Buckley, *Biochemistry* **2000**, *39*, 14019–14024.

83 M. Fivaz, L. Abrami, Y. Tsitrin, F.G. van der Goot, *Curr. Topics Microbiol. Immunol.* **2001**, *257*, 35–52.

84 B. Vecsey-Semjen, C. Lesieur, R. Mollby, F.G. van der Goot, *J. Biol. Chem.* **1997**, *272*, 5709–5717.

85 R.K. Bortoleto, A.H.C. de Oliveira, R. Ruller, R.K. Arni, R.J. Ward, *Arch. Biochem. Biophys.* **1998**, *351*, 47–52.

86 M. Nakamura, N. Sekino, M. Iwamoto, Y. Ohno-Iwashita, *Biochemistry* **1995**, *34*, 6513–6520.

87 E.M. Abdel-Ghani, S. Weis, I. Walev, M. Kehoe, S. Bhakdi, M. Palmer, *Biochemistry* **1999**, *38*, 15204–15211.

88 M. Watanabe, T. Tomita, T. Yasuda, *Biochim. Biophys. Acta* **1987**, *898*, 257–265.

89 S. Galdiero, E. Gouaux, *Protein Sci.* **2004**, *13*, 1503–1511.

90 B. Walker, H. Bayley, *J. Biol. Chem.* **1995**, *270*, 23065–23071.

91 R. Olson, H. Nariya, K. Yokota, Y. Kamio, E. Gouaux, *Nat. Struct. Biol.* **1999**, *6*, 134–140.

92 J.-D. Pedelacq, L. Maveyraud, G. Prevost, L. Baba-Moussa, A. Gonzalez, E. Courcelle, W. Shepard, H. Monteil, J.-P. Samama, L. Mourey, *Structure* **1999**, *7*, 277–287.

93 B. Walker, M. Krishnasastry, L. Zorn, H. Bayley, *J. Biol. Chem.* **1992**, *267*, 21782–21786.

94 R.G. Panchal, H. Bayley, *J. Biol. Chem.* **1995**, *270*, 23072–23076.

95 S. Vandana, M. Raje, M.V. Krishnasastry, *J. Biol. Chem.* **1997**, *272*, 24858–24863.

96 A. Valeva, R. Schnabel, I. Walev, F. Boukhallouk, S. Bhakdi, M. Palmer, *J. Biol. Chem.* **2001**, *276*, 14835–14841.

97 R. Ramachandran, A.P. Heuck, R.K. Tweten, A.E. Johnson, *Nat. Struct. Biol.* **2002**, *9*, 823–827.

98 V.T. Nguyen, Y. Kamio, H. Higuchi, *EMBO J.* **2003**, *22*, 4968–4979.

99 S.P. Howard, J.T. Buckley, *J. Bacteriol.* **1985**, *163*, 336–340.

100 V. Cabiaux, J.T. Buckley, R. Wattiez, J.-M. Ruysschaert, M.W. Parker, F.G. van der Goot, *Biochemistry* **1997**, *36*, 15224–15232.

101 F.G. van der Goot, K.R. Hardie, M.W. Parker, J.T. Buckley, *J. Biol. Chem.* **1994**, *269*, 30496–30501.

102 B.R. Sellman, B.L. Kagan, R.K. Tweten, *Mol. Microbiol.* **1997**, *23*, 551–558.

103 Y. Tsitrin, C.J. Morton, C. El Bez, P. Paumard, M.-C. Velluz, M. Adrian, J. Dubochet, M.W. Parker, S. Lanzavecchia, F.G. van der Goot, *Nat. Struct. Biol.* **2002**, *9*, 729–733.

104 K.R. Klimpel, S.S. Molloy, G. Thomas, S.H. Leppla, *Proc. Natl Acad. Sci. USA* **1992**, *89*, 10277–10281.

105 S.D. Zakharov, E.A. Kotova, Y.N. Antonenko, W.A. Cramer, *Biochim. Biophys. Acta* **2004**, *1666*, 239–249.

106 S.H. White, W.C. Wimley, *Annu. Rev. Biophys. Biomol. Struct.* **1999**, *28*, 319–365.

107 J.H. Kleinschmidt, L.K. Tamm, *Biochemistry* **1999**, *38*, 4996–5005.

108 L.K. Tamm, H. Hong, B. Liang, *Biochim. Biophys. Acta* **2004**, *1666*, 250–263.

109 R. Koebnik, *EMBO J.* **1996**, *15*, 3529–3537.

110 B. Walker, M. Krishnasastry, H. Bayley, *J. Biol. Chem.* **1993**, *268*, 5285–5292.

111 H. Ikigai, T. Nakae, *J. Biol. Chem.* **1987**, *262*, 2156–2160.

112 T. Tomita, M. Watanabe, T. Yasuda, *Biochim. Biophys. Acta* **1992**, *1104*, 325–330.

113 T. Tomita, M. Watanabe, T. Yasuda, *J. Biol. Chem.* **1992**, *267*, 13391–13397.

114 H. Ikigai, A. Akatsuka, H. Tsujiyama, T. Nakae, T. Shimamura, *Infect. Immun.* **1996**, *64*, 2968–2973.

115 A. Zitzer, R. Bittman, C. A. Verbicky, R. K. Erukulla, S. Bhakdi, S. Weis, A. Valeva, M. Palmer, *J. Biol. Chem.* **2001**, *276*, 14628–14633.

116 M. Palmer, *FEMS Microbiol. Lett.* **2004**, *238*, 281–289.

117 J. F. Nagle, S. Tristram-Nagle, *Curr. Opin. Struct. Biol.* **2000**, *10*, 474–480.

118 H. Lecuyer, D. G. Dervichian, *J. Mol. Biol.* **1969**, *45*, 39–57.

119 A. P. Heuck, R. K. Tweten, A. E. Johnson, *J. Biol. Chem.* **2003**, *278*, 31218–31225.

120 M. Palmer, R. Harris, C. Freytag, M. Kehoe, J. Tranum-Jensen, S. Bhakdi, *EMBO J.* **1998**, *17*, 1598–1605.

121 R. W. Harris, P. J. Sims, R. K. Tweten, *J. Biol. Chem.* **1991**, *266*, 6936–6941.

122 S. D. Zakharov, M. Lindeberg, W. A. Cramer, *Biochemistry* **1999**, *38*, 11325–11332.

123 D. J. Wigelsworth, B. A. Krantz, K. A. Christensen, D. B. Lacy, S. J. Juris, R. J. Collier, *J. Biol. Chem.* **2004**, *279*, 23349–23356.

124 D. Duché, M. W. Parker, J.-M. González-Mañas, F. Pattus, D. Baty, *J. Biol. Chem.* **1994**, *269*, 6332–6339.

125 J. Rossjohn, S. M. Raja, K. L. Nelson, S. C. Feil, F. G. van der Goot, M. W. Parker, J. T. Buckley, *Biochemistry* **1998**, *37*, 741–746.

126 D. M. Czajkowsky, E. M. Hotze, Z. Shao, R. K. Tweten, *EMBO J.* **2004**, *23*, 3206–3215.

127 K. S. Giddings, J. Zhao, P. J. Sims, R. K. Tweten, *Nat. Struct. Mol. Biol.* **2004**, *11*, 1173–1178.

128 R. Ramachandran, R. K. Tweten, A. E. Johnson, *Proc. Natl. Acad. Sci.* **2005**, *102*, 7139–7144.

9
Mechanism of Membrane Permeation and Pore Formation by Antimicrobial Peptides

Yechiel Shai

9.1
Introduction

Antimicrobial peptides are a large group within the water/membrane-soluble proteins and peptide toxins used in the defense and offense systems of all organisms. They represent ancient host defense effectors present virtually in every kingdom and phylum across the evolutionary spectrum, ranging from prokaryotes to humans [1–8]. They vary significantly in their length, secondary structure, tertiary structure and the presence or absence of disulfide bridges. Their size varies from around 9 to 100 amino acids (mostly common L-amino acids) and most of them share three properties: (1) they are composed of more than 50% hydrophobic amino acids, (2) they have a net positive charge and (3) they undergo a major conformational change upon their transfer from water to phospholipids membranes. The membrane-soluble form has a linear or cyclic amphipathic structure (i.e. the hydrophilic and the hydrophobic side-chains of the amino acids are segregated at opposite faces), which can be α-helix, β-sheet or any other structure [1, 9–13]. During the past years thousands of antimicrobial peptides have been either isolated or synthetically prepared (the reader is referred to http://www.bbcm.univ.trieste.it/~tossi/search.htm for an updated list).

Antimicrobial peptides vary in their spectrum of activity irrespective of whether they share high homology and similar structures. Based on their activities they can be classified into several groups:

1. Peptides that are highly toxic to microorganisms, but are not active or have low toxicity toward normal mammalian cells. This group includes peptides that are selective to different types of bacteria, e.g. cecropins isolated from the cecropia moth, which are active mainly on Gram-positive bacteria [14]. Others are active on both Gram-positive and Gram-negative bacteria, e.g. magainins [15] and dermaseptins [16] (both isolated from the skin of frogs), cathelicidins [4, 17], and many others. This family also includes peptides that are active to-

ward bacteria and fungi or active solely on fungi and not on other targets [18].

2. Peptides that are toxic to microorganisms and mammalian cells, such as the bee venom melittin [19], the Moses sole fish (*Pardachirus marmoratus*) venom pardaxin [20, 21], and to some extent the human cecropin-like LL-37 (the first amphipathic α-helical peptide isolated from human), and other cathelicidins [22, 23] and defensins [24].

The reader is referred to many studies in the field for more examples.

Understanding the mode of action of antimicrobial peptides and the parameters involved in their target cell specificity were the subject of intense studies in recent years. This is mainly because of the increasing resistance of bacteria to conventional antibiotics, which urged the search for new antibiotics with new modes of action. Bacterial resistance to available drugs is developed rapidly because these drugs do not cause physical damage to the bacteria, but instead penetrate into the cytoplasm and act on specific targets, which cause, for example, blockage of cell division, blockage of cell wall peptidoglycan biosynthesis in growing cells, triggering of intrinsic autolysins and breakage of double-stranded DNA due to inhibition of DNA gyrase, etc. [25]. In contrast to available antibiotics, most antimicrobial peptides cause physical damage to the microorganism by disrupting and increasing the permeability of its cytoplasmic membrane, damage hard to fix [2, 3, 5, 26–29]. Further support for the difficulties encountered by bacteria to become resistant to antimicrobial peptides is the fact that antimicrobial peptides are ancient components of all species of life, and their induction pathways in all organisms, including insects and plants, are conserved, and yet they are active for millions of years. The long list of natural antimicrobial peptides isolated so far, as well as the synthetic peptides, makes it hard to review most of them. Therefore, this chapter will focus only on a few representative peptides.

9.2 The Cell Membrane is the Major Binding Site for Most Cationic Antimicrobial Peptides

Among the large number of antimicrobial peptides isolated and *de novo* synthesized so far, only some of them were studied extensively in order to fully understand how they select and kill their target cell. Most known antimicrobial peptides are believed to use the microorganisms' cytoplasmic membrane as their final and lethal target, although recent studies pointed out that they have other targets inside the cell as well [30, 31]. Lehrer et al. [32] were the first to demonstrate a membrane permeabilization mechanism in intact bacteria. They showed that human neutrophil peptide defensin (HNP)-mediated bactericidal activity against *Escherichia coli* is associated with sequential permeabilization of the outer and inner membranes, and that inner membrane permeabilization appears

to be the lethal event. For this study they utilized the ability of the normally impermeable substrate *o*-nitrophenyl galactoside (ONPG) to be hydrolyzed by a cytoplasmic enzyme L-galactosidase as a test of increased permeability. Since the main constituents of these membranes are phospholipids, many studies were conducted on the interaction of antimicrobial peptides with model phospholipid membranes [11, 33–36]. Note, however, that the peptides need to transverse first the outer wall of the cell before they can reach the cytoplasmic membrane. The importance of this barrier in determining the mode of action of antimicrobial peptides will be elaborated later on. The following sections will focus on several questions including:

1. What are the binding sites for antimicrobial peptides?
2. What is the molecular mechanism by which antimicrobial peptides recognize and increase the permeability of phospholipid membranes?
3. Is there a direct correlation between the activity of antimicrobial peptides on model membranes mimicking the membranes of different microorganisms and their corresponding biological function on these organisms?
4. Is there a need for a specific peptide sequence and structure to gain potent antimicrobial activity?

It is interesting to note that most antimicrobial peptides, irrespective of their size, charge and secondary structure, are active *in vitro* at micromolar concentrations, which is their biological concentration at the sites of infections [10]. These concentrations can reach very high levels not found with most biologically active molecules. In insects, for example, antimicrobial peptides are secreted mainly from the fat body into the hemolymph where they can reach up to 100 μM concentration [37]. These high concentrations support the notion that most of the antimicrobial peptides have a similar non-receptor binding site and therefore it is more likely that they kill microorganisms through a non-receptor-mediated mechanism. Only a few of them act by binding to a receptor, which in turn increases their activity to the nanomolar concentrations [10]. Overall, accumulating data suggest two modes of binding used by most antimicrobial peptides: one is a non-receptor-mediated process and the other a receptor-mediated process. Note, however, that in both cases the lethal step includes the permeation of the cytoplasmic membrane of the target pathogen. The following sections will elaborate on these two modes of bindings.

9.2.1
Non-receptor-mediated Interaction of Antimicrobial Peptides with their Target Cells

The first support for a non-receptor-mediated mode of action of antimicrobial peptides came from studies with synthetic peptides. These studies showed that enantiomers of antimicrobial peptides (composed solely of D-amino acids) preserved the same biological function of their all L-amino acid parental native peptides. If a receptor-mediated binding process was involved, one would expect a chirality-dependent activity. The chirality independent binding of antimicrobial

peptides to microorganisms was demonstrated with several antimicrobial peptides. Enantiomeric peptide analogs were synthesized for melittin (a non-cell-selective α-helical lytic peptide), cecropin (a non-hemolytic α-helical peptide active mainly on Gram-positive bacteria), magainin (a non-hemolytic α-helical peptide active on both Gram-positive and Gram-negative bacteria), androctonin (a non-hemolytic β-sheeted peptide containing cysteine) and others [38–41]. The amphipathic structure of the enantiomeric antimicrobial peptides was preserved, but as the mirror image of the parental peptides. These studies and the fact that most antimicrobial peptides isolated so far were found to have an amphipathic structure in the form of either an α-helix or β-sheet led to the proposal that a peptide's amphipathic structure is crucial for antimicrobial activity. Based on this assumption many studies focused on improving the amphipathic structure in order to gain better biological activity. However, a drawback in the increased amphipathicity is a decrease in cell specificity and peptides can become more hemolytic. Further support for the importance of peptide amphipathicity came from studies on the effect of replacement of a single L-amino acid in the antimicrobial peptide magainin with its D-amino acid enantiomer, which resulted in a loss of its antibacterial activity [42]. Very interestingly, in contrast to this study, it was shown that diastereomeric analogs (containing both L- and D-amino acids) of potent non-cell-selective lytic peptides that kill both bacteria and mammalian cells preserved their antimicrobial activity, whereas their lytic activity toward mammalian cells was abolished. This has been shown with diastereomers of pardaxin, a channel-forming peptide isolated from the *P. marmoratus*, the bee venom melittin, and *de novo* designed lytic peptides composed of leucine and lysines [21, 43–47]. The structure of the diastereomers is different from that of their parental all L-amino acid peptides and, therefore, a similar receptor should not recognize equally all the L-amino acids and the diastereomeric forms. Furthermore, a similar amphipathic structure for the parental peptides was also not preserved, suggesting that this structure is not a prerequisite for antimicrobial activity. Other studies further demonstrated the advantages of incorporating D-amino acids into membrane-active and antimicrobial peptides [48, 49].

Overall, all of these studies suggest that antimicrobial peptides have a general and common target. This target is believed to be the bacterial cell wall and the cytoplasmic membrane, which are negatively charged [50] compared with zwitterionic mammalian membranes [51], as will be discussed in the following sections. The net positive charge, which is the most preserved property of antimicrobial peptides, allows preferential binding to the negatively charged constituents of the bacterial wall (reviewed in [11, 12, 36, 52–54]). Note, however, that most studies use erythrocytes, in which the outer leaflet is zwitterionic, to mimic normal mammalian cells. Nevertheless, some cells, such as epithelial cells, are enriched with negatively charged phospholipids and therefore are potential targets for antimicrobial peptides.

9.2.2
A Receptor-mediated Interaction of Antimicrobial Peptides with their Target Cells

Recent studies confirmed that some peptides use receptors for their interaction with the bacteria cell wall. Peptides belonging to this group are produced mainly by bacteria, they are active at nanomolar concentrations and have a narrow spectrum of activity. They are composed of two regions: a receptor-binding domain and a membrane-binding domain. The receptor helps to increase their affinity to the membrane and, as a consequence, they can reach a high concentration of membrane-bound peptides which induces an increase in membrane permeability. The first identified peptide within this group was nisin Z, which uses the membrane-anchored cell wall precursor Lipid II as a receptor [10]. Nisin combines high affinity for Lipid II with pore-forming ability, causing the peptide to be highly active. It is not clear, however, how the pore-forming domain permeates the target membrane. It has been also shown that Lipid II is not only the receptor for nisin, but an intrinsic component of the pore formed by nisin, and that the stoichiometry between nisin and lipid II is 1:1 [55]. Furthermore, Wiedemann [56] performed single-channel experiments in the absence of lipid II and found that a constant voltage of 100 mV had to be applied in order to obtain a strong current. However, when the membrane was doped with 1 mol% lipid II, only 5 mV was sufficient to produce regular patterns of membrane conductance, corresponding to an average pore diameter of 2–2.5 nm. Bacteriocins are another group of antimicrobial peptides with a receptor-mediated activity. They are composed of 37–44 amino acids, ribosomally synthesized by lactic acid bacteria [57, 58]. These peptides show potent activity toward a narrow spectrum of potential Gram-positive food spoilage and pathogenic bacteria, e.g. *Listeria*. They display no toxicity toward humans or other eukaryotes [59]. An enantiomer of leuA, a member of this family composed of only D-amino acids, was completely inactive against bacteria, thereby demonstrating that a chiral interaction is required at the target cell surface for bacteriocin to display its effects [60]. This is in contrast to enantiomers of other antimicrobial peptides (e.g. mellitin and magainin) that do not use chiral interaction with a receptor molecule and preserve full biological activity (discussed in the previous section). Recently, a mannose phosphotransferase system (PTS) permease (EII_t^{Man}) has been proposed to be a target molecule for mesentericin Y105 and leuA [61, 62]. Structural studies with mutated peptides confirmed the importance of maintaining the structural integrity of an α-helical region in the C-terminus for optimal activity and molecular recognition by the target receptor [63]. Removal of the receptor-binding domain in members of this group resulted in a loss of bacteria-specific selectivity. The resultant analogs became active toward other bacteria at a micromolar range.

Since most of the antimicrobial peptides isolated so far do not use receptors for their function, the following sections will focus on a non-receptor-mediated killing mechanism of antimicrobial peptides.

9.3
Parameters Involved in the Selection of Target Cells by Antimicrobial Peptides

Antimicrobial peptides vary considerably in their spectrum of activity. Some are highly active on microorganisms, but are not active or have low potency against normal mammalian cells. Furthermore, there are also significant variations in their activities against microorganisms; most of them are active toward both Gram-positive and Gram-negative bacteria, whereas others are active solely on Gram-negative bacteria, e.g. cecropins isolated from the cecropia moth [14]. Furthermore, several are active toward bacteria and fungi or solely on fungi and not on other types of cells [18]. Antimicrobial peptides also selectively kill specific stains from the same bacteria and not others. Fig. 9.1 shows an example list of antimicrobial peptides, all of which have been shown to form a stable amphipathic α-helical structure in a hydrophobic environment (envisioned schematically in the wheel structure [64] also shown in Fig. 9.1). However, as indicated in Fig. 9.1, some kill specifically bacteria and others are active also against eukaryotic cells. These intriguing properties led to a fundamental question – what are the parameters that are involved in their activities toward a particular target? Obviously these

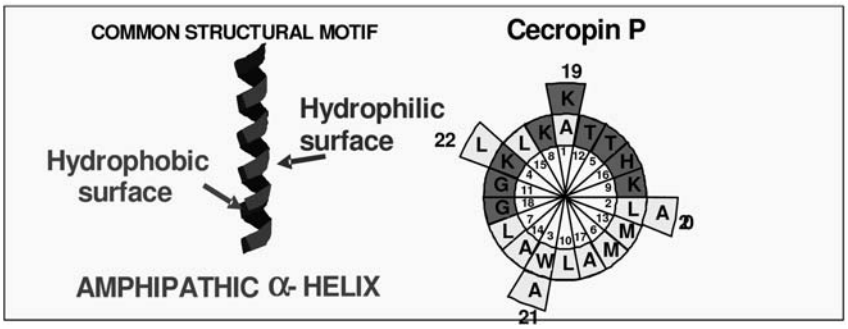

Fig. 9.1 A list containing examples of cell-selective and non-cell-selective lytic peptides, all of which adopt an amphipathic α-helical structure as envisioned by the wheel projection [64] and determined experimentally by several groups.

parameters should be dependent on the properties of both the peptide and the target cell. With respect to properties of the peptides, these have been shown to include peptide length, structure, net charge, hydrophobicity, and ability to oligomerize in solution and/or in the membrane. Regarding the target cell, these include the charge of the outer surface of the cell, the composition of the cytoplasmic membrane, and the thickness and composition of the cell wall.

9.3.1 The Role of the Composition of the Cell Wall and the Cytoplasmic Membrane

Most antimicrobial peptides which are able to increase the permeability of the bacterial membrane share two major properties – they have a high net cationic charge contributed by a large number of positively-charged amino acids (mostly lysine and arginine) and they are composed of approximately 50% hydrophobic amino acids (reviewed in [11, 12, 54, 65–69]). However, there are exceptions such as temporins, 13-amino-acid antimicrobial peptides isolated from the skin of frogs, which contain only one positively charged amino acid [70, 71]. Note, however, that some of these peptides can also bind strongly and increase the permeability of non-bacterial cells. Overall, there are several significant differences between the phospholipids of the cytoplasmic membranes of different cells, as well as between the compositions of the outer wall/layer of various target cells, through which the peptides need to traverse. The outer surface of Gram-negative bacteria contains lipopolysaccharides (LPS) and that of Gram-positive bacteria contains acidic polysaccharides (teichoic acids), conferring a net negative charge to the surface of both Gram-positive and Gram-negative bacteria [50]. Furthermore, the phospholipids of the inner membrane of Gram-negative bacteria and the single membrane of Gram-positive bacteria are negatively charged and composed predominantly of phosphatidylglycerol (PG) and phosphatidylethanolamine (PE). In addition, Gram-negative bacteria have a thinner cell wall peptidoglycan layer compared with Gram-positive bacteria. In contrast to bacteria, the distribution of phospholipids in normal mammalian cells is asymmetric; the outer leaflet is composed predominantly of zwitterionic phosphatidylcholine (PC) and sphingomyelin, whereas the inner leaflet is composed of negatively charged phosphatidylserine (PS) [51]. However, they also contain a large number of highly negatively charged sialic acid-containing carbohydrate moieties in the form of glycoproteins and glycosphingolipids, which form the glycocalix layer. Similarly, the outer surface of fungi is composed of PC and ergosterol instead of cholesterol found in mammalian cells. It should be noted also that the outer surface of many cancer cells is slightly more negatively charged compared with normal cells because (1) they are slightly enriched with PS in their outer surface compared with normal cells and (2) they are enriched with *O*-glycosylated mucines, high molecular weight glycoproteins comprised of a backbone protein, to which oligosaccharides are attached via the hydroxylic groups of serine or threonine [72]. This might explain why some antimicrobial peptides lyse efficiently also cancer cells [73–76].

9.3.2 The Role of the Peptide Chain and Its Organization

Antimicrobial peptides that adopt similar structures can differ markedly in their target cell specificity, whereas others with different structures can have a similar specificity toward target cells. Furthermore, it is possible to substitute more than 60% of the amino acids in a particular antimicrobial peptide without affecting its biological function, while in others, minor changes in their primary sequences strongly affect the spectrum of activity of the resulting peptide analogs. The following sections will shed light into these interesting observations.

9.3.2.1 The Extent of Hydrophobicity and Distribution of Positively-charged Amino Acids Along the Peptide Chain

Accumulating data revealed that most antimicrobial peptides which have their positively charged amino acids spread along the peptide chain act better toward bacteria compared with mammalian cells. Examples include magainin [67], cecropins [14, 77, 78], dermaseptins [16, 79] and others [12, 69]. In contrast, antimicrobial peptides that are toxic to a variety of target cells, e.g. bacteria, fungi and mammalian cells, have either a low number of positive charges or, alternatively, most of their positively charged amino acids are segregated at the termini of the peptides. Examples include melittin [80, 81], pardaxin analogs [82], indolicidin [83] and bombinins [84]. Although this rule seems to hold in most cases, there are exceptions. Several highly potent antifungal antimicrobial peptides do not have their positively charged amino acids segregated at the peptide termini. Examples include defensins [6], dermaseptins [85, 86], cathelicidines [87], the human-like cecropin, LL-37 [22, 88], tachystatin [89], bovine lactoferricin [90], etc. Note that peptides which are active against fungi are in most cases also more hemolytic. This is because the predominant component of the outer leaflet of the membranes of both mammalian and fungal cells is zwitterionic (PC phospholipids), although those of fungi are slightly more acidic due to the presence of PI. However, a few native positively charged antimicrobial peptides and lipopeptides are sensitive to this mild difference in lipid composition and therefore act on fungi at concentrations which do not lyse mammalian cells. These include dermaseptin, LL-37 and *de novo* designed short (12mer) fatty-acid-conjugated diastereomeric peptides [91, 92]. Loss of cell specificity can also result if the peptide hydrophobicity is increased, concomitant with a reduction in the number of positively charged amino acids [93, 94].

9.3.2.2 The Stability of the Amphipathic Structure

An amphipathic structure is formed when the hydrophobic and hydrophilic sidechains of the amino acids are distributed at opposite faces of α-helix or β-sheet structures. Therefore, peptides with a stable amphipathic structure can expose their hydrophobic face to the hydrophobic constituents of the target cell mem-

brane. This should permit strong interactions with the cell membrane, driven by hydrophobic interactions rather than by electrostatic interactions. As a consequence, they are active against a broad range of microorganisms and eukaryotic cells. This group also includes peptides in which their positively charged amino acids are spread along the peptide backbone. However, in this case their overall hydrophobicity is high enough to initiate strong hydrophobic interactions, which results in a stable α-helix structure in the membrane. The bee venom melittin serves as a good example. Melittin is a non-cell-selective lytic peptide which adopts around 80% α-helical structure when bound to phospholipid membranes. A diastereomeric analog of melittin was synthesized by substituting four L-amino acids along the helical chain with their D-enantiomers. The diastereomeric melittin bound strongly and destabilized only negatively charged phospholipid vesicles, in contrast to native melittin, which bound strongly also zwitterionic phospholipids. As a result, this diastereomer was not active against erythrocytes, but preserved activity toward bacteria [21]. The structure of the diastereomer was determined by nuclear magnetic resonance (NMR) in water, as well as in three different membrane-mimicking environment, 40% 2,2,2-trifluoroethanol (TFE)/water, methanol and dodecylphosphocholine/phosphatidylglycerol (DPC/DMPG) micelles [81]. The NMR data revealed an amphipathic α-helix only in the C-terminal region of the diastereomer in TFE/water and methanol solutions and in DPC/DMPG micelles. In solution, native melittin forms tetramers which stabilize its α-helix [95]. However, the diastereomer is completely unstructured and exists as monomers in solution. This structural alteration affects the free energy of binding and insertion into membranes. The free energy cost of inserting unfolded peptides into both negatively charged and zwitterionic phospholipids membranes include the hydrophobic interactions between the non-polar amino acids and the phospholipid hydrocarbon layer and the cost of partitioning the polar amino acids and the peptide bond (CONH) into a non-polar environment [96]. Electrostatic interactions appear to play an important role in the initial binding of the diastereomer to negatively charged membranes [97]. When bound to negatively charged membranes, the positive charges of the diastereomer are partially neutralized by the negative charges of the phospholipid headgroups, thus reducing the energy cost of adsorbing the peptide into the membrane. Subsequently, it allows the hydrophobic forces to manifest themselves following the formation of a stable α-helical structure in the C-terminal of the peptide, thus driving the peptide further into the interface, leading to membrane lysis. In the case of zwitterionic phospholipids, the rate-limiting step in the insertion and membrane lysis appears to be the initial binding of the diastereomer to the surface, which is very low; two to three orders of magnitude less than that of native melittin [97, 98].

9.3.2.3 **The Ability of a Peptide to Self-associate in Solution and/or in Membranes**

Self-association of antimicrobial peptides has been shown to be an important parameter which affects their selectivity toward different cells. Self-association is driven either by a hydrophobic N- or C-terminus, or by specific amino acids in

the peptide sequence, resulting in the formation of α-helical bundles that could initiate strong hydrophobic binding to zwitterionic membranes [85, 86, 88]. The role of self-association of antimicrobial peptides in their selective binding to target cells is elaborated in the following subsections.

Self-association of Antimicrobial Peptides Resulting from Backbone Mutations The effects of peptide self-association on the function of antimicrobial peptides have been demonstrated in several studies: (1) Dermaseptins are antimicrobial peptides isolated from the skin of the *Phyllomedusa* frog [99]. A member of this family, dermaseptin S, is active predominantly toward bacteria, whereas another one, dermaseptin B, is also hemolytic and has potent antifungal activities. This is despite the fact that both analogs are almost identical and adopt a similar amphipathic α-helical structure in hydrophobic environments [79, 85, 100]. Their primary sequence shows that Thr at the fifth position in dermaseptin S is substituted with Asp in dermaseptin B. Similar to most non-hemolytic antimicrobial peptides, dermaseptin S binds weakly and permeates zwitterionic membranes, but has a high affinity and permeating activity toward negatively charged membranes [79]. Mode-of-action studies revealed that it binds both types of membranes in a monomeric form. In contrast, dermaseptin B oligomerizes in its membrane-bound state, and efficiently binds and permeates both zwitterionic and negatively charged membranes [85]. The high affinity of dermaseptin B toward zwitterionic PC phospholipid membranes (despite its high net positive charge) suggests a major role for hydrophobic interactions between the peptide and the membrane. Since the N-terminal of dermaseptin B is highly hydrophobic and the peptide binds to the membrane as an oligomer, a bundle of hydrophobic N-termini regions could facilitate binding to zwitterionic membranes. The assembly of dermaseptin B could be driven by the additional negative charge (Asp at the fifth position) in an otherwise basic peptide, therefore reducing repulsion forces. (2) Dermaseptin S3 (DS3) and dermaseptin S4 (DS4) are highly homologous, and both of them are cytotoxic toward human erythrocytes infected by the malaria parasite *Plasmodium falciparum*, by inhibiting the parasite's ability to incorporate [^{3}H]hypoxanthine [86]. However, while DS4 was toxic toward both the parasite and the host erythrocyte, DS3 was toxic only toward the intra-erythrocytic parasite. Studies with fluorescently labeled peptides revealed that in *Plasmodium*-infected cells the peptides interacted directly with the intracellular parasite, in contrast to non-infected cells, where the peptides remained bound to the erythrocyte plasma membrane. Binding experiments to phospholipid membranes revealed that DS3 and DS4 had similar binding characteristics. Membrane permeation studies indicated that the peptides were equally potent in permeating PS/PC vesicles, whereas DS4 was more active in increasing the permeation of zwitterionic PC vesicles. The major difference between the two peptides is that DS4 forms larger aggregates in aqueous solution compared with DS3. (3) Several analogs of dermaseptin S4 were investigated with respect to molecular organization in solution, binding properties to model phospholipid membranes and cytotoxic properties [101]. Native dermaseptin S4

displayed high aggregation in solution and high binding affinity. These properties correlated with its high cytotoxicity toward erythrocytes. Yet, potency was progressively limited when facing cells whose plasma membrane was surrounded by increasingly complex barriers. The C-terminal hydrophobic domain was found responsible for binding to membranes but not for their disruption. (4) The role of peptide oligomerization in selective lytic activity was addressed also with the human cecropin-like LL-37, which is cytotoxic to both bacteria and normal eukaryotic cells. However, its N-terminal truncated form, FF-33, preserved the antimicrobial activity of the parental LL-37 but was devoid of hemolytic activity. Using fluorescently labeled peptides, it was found that LL-37, but not FF-33, exists in equilibrium between monomers and oligomers in solution at very low concentrations [23]. (5) Peptide oligomerization has been shown to play a significant role in the biological function of all L-amino acid lytic peptides compared with their diastereomeric versions (containing both L- and D-amino acids). A series of model amphipathic all L-amino acid peptides and their diastereomers were synthesized. The template for the sequence was $KX_3KWX_2KX_2K$, where X = Gly, Ala, Val, Ile or Leu. The effect of these amino acids on the biological activity, binding, structure, membrane localization and mode of action of these peptides was investigated [102]. This study demonstrated that most of the L-amino acid peptides oligomerized and adopted distinct structures (random coil, α-helix or β-sheet) in solution and in a membrane mimetic environment. Among this group, only the Leu-containing peptide was active on both bacteria and human erythrocytes, while its diastereomer, which did not oligomerize in solution, was active only on bacteria. In contrast, the Val- and Ile-containing L-amino acid peptides were hemolytic, but inactive towards most bacteria tested; their diastereomers were monomeric and unstructured in solution, but they adopted distinct structures upon membrane binding. While the hemolytic activity of the diastereomers was drastically reduced, the spectrum of their antibacterial activity was preserved or increased compared with the all L-amino acid wild-type peptides. Studies on their oligomeric states revealed that whereas the Leu-containing peptide was predominantly dimer in sodium dodecylsulfate-polyacrylamide gel electrophoresis (SDS-PAGE), the Ile- and the Val-containing peptides formed high-order oligomers. The large size of these oligomers probably prevented them from penetrating into the bacterial phospholipid membrane and, therefore, their all L-amino acid parental peptides were practically inactive [102].

Self-association of Antimicrobial Peptides Induced by the Attachment of Fatty Acids

Increasing the peptides' hydrophobicity and ability to self-associate, without altering the properties of the peptide chain, has been achieved by attaching fatty acids of different lengths to the N-terminus of magainin [103]. Previous studies reported that magainin adopts a monomeric unordered structure in aqueous solution and a highly α-helical structure in the membrane-bound state [104]. When fatty acids with different lengths were attached to the N-terminal of magainin they affected its organization in solution in a length-dependent manner.

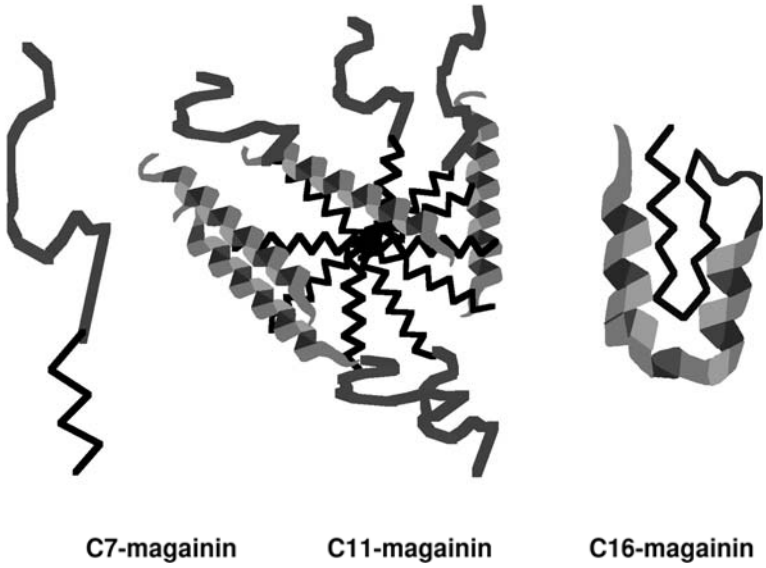

Fig. 9.2 A cartoon illustrating possible organizations of three lipophilic magainin analogs in solution. Thick lines and helices represent the peptides, and thin lines represent the fatty acid moieties (modified from [103]).

The attachment of heptanoic (C7), undecanoic (C11), and palmitic (C16) acids results in lipopeptides with three distinct structures and oligomeric states in solution, at their minimal inhibitory concentration (MIC). (1) The attachment of heptanoic acid resulted in a monomeric, unordered structure, (2) the attachment of undecanoic acid yielded concentration-dependent oligomers of α-helices and (3) the attachment of palmitic acid yields concentration-independent α-helical monomers, a novel lipopeptide structure, which is resistant to proteolytic digestion. A cartoon illustrating possible organizations of the three lipopeptides studied is shown in Fig. 9.2. Attenuated total reflectance Fourier transform IR spectroscopy (ATR-FTIR) revealed that the attachment of the fatty acids did not affect the structure of magainin in the membrane-bound state. As expected, the increase in hydrophobicity and oligomeric state of magainin analogs increased its activity toward cells expressing zwitterionic membranes in their outer leaflet. Indeed, a direct correlation was found between oligomerization of the lipopeptides in solution and hemolytic and antifungal activity. Similar results were obtained with fatty acid-conjugated 12mer diastereomeric antimicrobial peptides [91].

Covalently Linking Antimicrobial Peptides Forming Undissociatable Oligomers The role of the peptide length and preassembly on the ability of antimicrobial peptides to discriminate between bacteria, erythrocytes and fungal cells was investigated by using diastereomeric (containing both L- and D-amino acids) cationic antimicro-

bial peptides with variable lengths (13, 16 and 19 amino acids long) and their covalently linked pentameric bundles [105]. Functional studies revealed that the monomeric 13mer was practically devoid of antimicrobial activity, in contrast with the pentameric form, which was highly active on bacteria and yeast (*Cryptococcus neoformans*). The activity of the 13mer bundle was similar to that of the 16mer and 19mer bundles (MIC = 0.2–0.3 μM), despite the fact that both monomeric 16mer and 19mer were active, and the monomeric 13mer not. Hemolytic activity was also observed at concentrations higher than those required for antifungal activity. Binding experiments revealed that the 19mer monomer binds around 300-fold better than the 13mer monomer to zwitterionic [egg PC/egg sphingomyelin (SM)/cholesterol] vesicles. However, all the monomeric peptides displayed similar high affinity to negatively charged (*E. coli* PE/egg PG) vesicles regardless of their length and antimicrobial activity. In contrast, irrespective of the size of the monomeric subunit, all the bundles bind irreversibly and strongly disrupt both PC/SM/cholesterol and PE/PG membranes. ATR-FTIR revealed that peptide assembly has also an effect on the structure of the peptides. This has been demonstrated by the increase in the α-helical and β-sheet contents of the oligomers in membranes, concomitant with enhanced acyl chain disruption in the case of PC/cholesterol. Overall, there was a correlation between the antibacterial activity of the peptides and their ability to depolarize the transmembrane potential of *E. coli* spheroplasts, as well as the ability to induce calcein release from vesicles. This supports the notion that the bacterial membrane is their target.

Cyclization of Linear Lytic Peptides Decreases Assembly and Increases Selectivity Towards Bacteria Cyclization of linear amphipathic α-helical peptides has been shown to reduce the extent of the α-helical structure of these peptides, and as a consequence their organization in solution and in membranes, which in turn affected their biological function. Cyclic forms of magainin 2 and melittin were synthesized by incorporation of cysteins at both the N- and C-termini of the peptides [103]. Cyclization of magainin markedly reduced its cytolytic activity toward both erythrocytes and bacteria. In contrast to magainin, cyclization of the melittin analog significantly reduced its hemolytic activity, but preserved or increased activity toward bacteria. The reduction in hemolytic activity of both peptides upon cyclization was correlated with a reduction in their binding and the ability to increase the permeability of PC/cholesterol membranes, the major component of the outer leaflet of red blood cells. Most importantly, at similar molar ratios of bound peptide : lipid, both linear and cyclic magainin analogs showed similar membrane permeation activity with both zwitterionic and negatively charged phospholipid membranes, indicating that the linearity of this peptide is not required for membrane binding and permeation. However, the finding that cyclic magainin is much less active than linear magainin in the killing of bacteria points to the role of linearity in reaching the bacterial inner phospholipid membrane. To reach this membrane, peptides must cross several barriers. Cyclic magainin should have a larger volume and less flexibility compared with the linear version. Therefore, it is probably more difficult for the cyclic analog to cross these barriers

compared with the linear magainin. Interestingly, however, this is not the case with cyclic melittin, which is active in both the linear and the cyclic forms. This can be explained by the difference in the distribution of the positive charges between magainin and melittin. The 22-amino-acid N-terminal of melittin analog is highly hydrophobic, and is followed by four consecutive positively charged amino acids and two glutamines. Upon cyclization, all the charges, including the N-terminal-free amine, remain on a small portion of the ring and most of the ring is hydrophobic. In contrast, the five positively charged amino acids in magainin are distributed along its amphipathic helix. Upon cyclization, all the positive charges, including the N-terminal-free amine, are distributed throughout the ring and the peptide thus becomes less helical. These changes can induce more efficient binding of the cyclic magainin analog to the negatively charged cell wall components and hence make it more difficult for the cyclic form to diffuse into the inner target phospholipid membrane.

9.3.2.4 Fatty Acid Modification can Compensate for the Hydrophobicity and Amphipathicity of the Peptide Chain

Recent studies have shown that aliphatic acid conjugation to non-membrane-active peptides bestowed them with antimicrobial activities [91, 92]. A new group of lipopeptides with potent antifungal or both antibacterial and antifungal activities was developed by conjugation of palmitic acid to short positively charged peptides, which are devoid of biological activity. The parental peptides also do not have the threshold hydrophobicity required for membrane binding and permeation. This study demonstrated that palmitic acid conjugated to the N-terminus of inactive peptides can compensate for the hydrophobicity of the peptide chain. More specifically, a group of diastereomeric peptides with a general sequence K_4X_7W (X = Gly, Ala, Val or Leu) were palmitoylated at their N-terminus. Most importantly, palmitoylated K_4G_7W and K_4A_7W gained potent antibacterial and antifungal activity with low hemolytic activity, despite the fact that both parental peptides were completely devoid of any activity toward microorganisms and model phospholipid membranes. In contrast, palmitoylated K_4L_7W lost the potent antibacterial activity of the parental peptide, but preserved antifungal activity albeit with different selectivities. Interestingly, both K_4V_7W and its palmitoylated analog were inactive toward bacteria, and only the palmitoylated peptides were highly potent toward yeast. Both the Leu- and Val-derived lipopeptides were also endowed with hemolytic activity. Mode-of-action studies were performed by using tryptophan fluorescence, ATR-FTIR and circular dichroism spectroscopy, as well as the transmembrane depolarization assay with bacteria and fungi. The data suggested that this group of lipopeptides acts by increasing the permeability of the cell membrane, and that differences in their potencies and target specificities are the result of differences in their oligomeric state and ability to dissociate and insert through the cell wall into the cytoplasmic membrane. Most importantly, self-assembly of non-membrane-interacting peptides can endow them with both antibacterial and antifungal activity.

9.4 The Lethal Event Caused by Antimicrobial Peptides

All the studies described above pointed out the cell membrane as the major target of antimicrobial peptides. However, it is still not clear whether the actual killing event is the result of one of two processes: (1) The peptides cause damage to the bacterial membrane in the form of pores or membrane disintegration, which results in the collapse of the transmembrane electrochemical gradients (for reviews, see, e.g. [3, 11, 12, 25, 28, 33, 35, 54, 100, 106–108]). Upon electrochemical gradient collapse, microorganisms lose their source of energy, allowing increased water and ion flow across the membrane, which results in cell swelling and osmolysis. (2) The peptides act via a multi-hit mechanism that involves the action on more than one anionic target located in the cytoplasm or the cell surface [28]. In support of this, recent studies on a number of cationic peptides suggest that they traverse the bacterial phospholipid membrane to interact with internal targets (reviewed in [25]). For example, cecropin P1 [109] and PR-39 [110] are two antibacterial peptides isolated from the upper part of the small intestine of the pig. PR-39 belongs to a group of proline-rich antimicrobial peptides isolated from mammals and invertebrates, and is characterized by a high content of proline residues (up to 50%). In contrast to cecropin P1 which is believed to kill bacteria by membrane lysis [111], members of the proline-rich family kill bacteria by a non-lytic mechanism. These peptides enter the cells without membrane lysis and, once in the cytoplasm, bind to and inhibit the activity of specific molecular targets essential to bacterial growth, thereby causing cell death (reviewed in [112]).

In another study, Hancock et al. [36] investigated the interaction of a series of peptides with model membranes and the cytoplasmic membrane of *E. coli*, in order to test whether permeation of the inner bacterial membrane is indeed the killing step for all of these peptides. The list included 12 peptides representing four structural classes of antimicrobial peptides. Planar lipid bilayer studies indicated that there was considerable variance in the interactions of the peptides with model phospholipid membranes, but generally both high concentrations of peptide and high transmembrane voltages (usually –180 mV) were required to induce conductance events (channels). The channels observed for most peptides varied widely in magnitude and duration. They also demonstrated that individual peptides varied widely in their ability to depolarize the cytoplasmic membrane potential of *E. coli*, with certain peptides such as the loop peptide bactenecin and the α-helical peptide CP26 being unable to cause depolarization at the MIC, and others like gramicidin S causing maximal depolarization below the MIC. These studies indicate that the lethal step of some membrane-active antimicrobial peptides takes place before the permeation of the cytoplasmic membrane.

An opposite case was described for temporins, 13-amino-acid cyclic antimicrobial peptides isolated from the skin secretion of the frog *Rana temporaria*. The authors used a triple-staining method based on the fluorochromes 5-cyano-2,3-ditolyl tetrazolium chloride, 4′,6-diamidino-2-phenylindole and fluorescein iso-

thiocyanate. This technique enabled the identification, in the same sample, of both living and total cells, as well as bacteria with altered membrane permeability. It was found that temporins increase the permeability of the bacterial inner membrane in a dose-dependent manner without destroying the cell's integrity. The interesting observation was that at low peptide concentrations, the inner membrane became permeable to small molecules without killing of the bacteria. However, at high peptide concentrations, larger molecules, but not DNA, leaked out, which resulted in cell death. Furthermore, in contrast to many antimicrobial peptides, temporins did not lyse *E. coli* cells, but rather formed ghost-like bacteria, as observed by scanning and transmission electron microscopy.

9.5
How do Antimicrobial Peptides Damage the Integrity of the Target Cell Membrane?

9.5.1
Membrane-imposed Amphipathic Structure

In order to interact and insert into the target membrane, antimicrobial peptides must undergo substantial conformational changes. In water, their overall exposed surface needs to be hydrophilic. However, upon interaction with membranes they must expose a hydrophobic region to the lipid constituent of the membrane. This can be achieved via two general ways: (1) a monomeric peptide that adopts a random structure in solution gains an amphipathic structure upon its interaction with the membrane, and (2) the peptide forms oligomers in solution such that the hydrophobic regions are buried in the lumen of the oligomer and the hydrophilic regions are exposed to the solution. Upon reaching the membrane the oligomers undergo a substantial organization depending upon their mode of action: (1) the peptide oligomerizes and the oligomers insert into the membrane such that the hydrophobic faces are exposed to the lipid constituents of the membrane and the hydrophilic regions are segregated in the lumen of the oligomer as described in the "barrel–stave" mechanism (see Fig. 9.4, discussed below) and (2) the peptide bound onto the surface with the hydrophilic face exposed to the solution and the hydrophobic face toward the lipid layer as described in the "carpet" mechanism (see Fig. 9.5, discussed below).

Interestingly, an amphipathic structure can be formed in the membrane even when D-amino acids are incorporated along the peptide chain [81, 113] or when the linear amphipathic helix is cyclized [114]. This has been demonstrated in three cases: (1) NMR studies on a diastereomer of melittin ([D]-$V^{5,8}$,I^{17},K^{21}-melittins, in which the indicated amino acids are in the D-form) reveal a random structure in water [81], in agreement with observations for native melittin [115]. However, the diastereomer adopted an amphipathic α-helix in its C-terminal region in TFE/water and methanol solutions and in DPC/DMPG micelles. In methanol, the helix extends from residue Leu13 to Gln26, similar to the C-terminal helix of native melittin in methanol [116]. A similar result was obtained

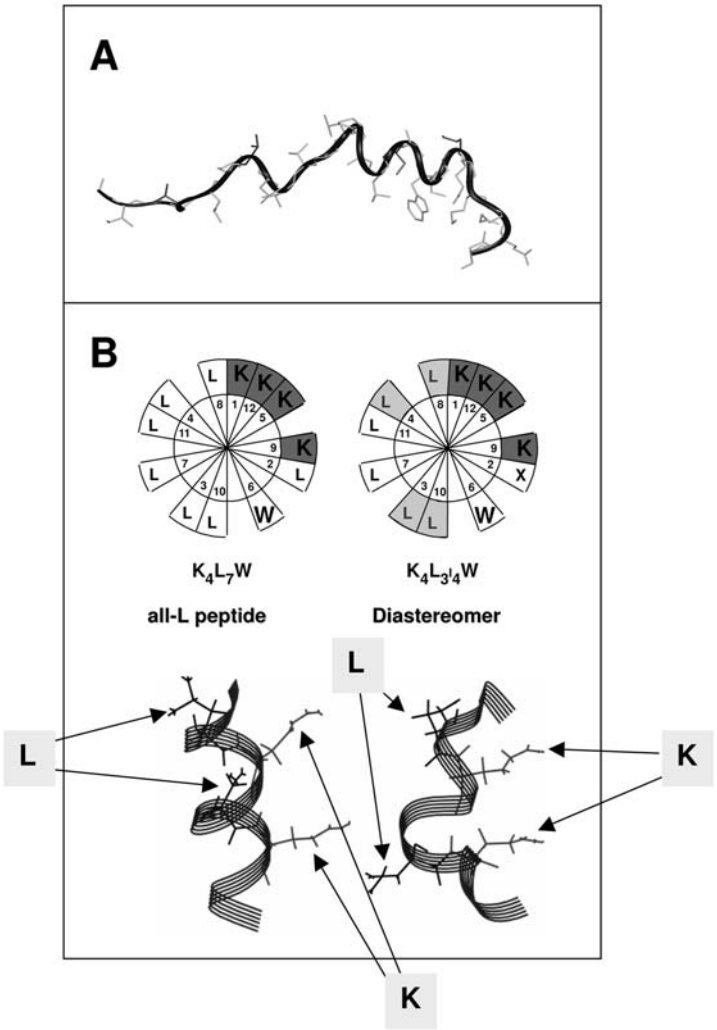

Fig. 9.3 (A) The NMR structure of [D]-$V^{5,8}$,I^{17},K^{21}-melittin in DPC/DMPG micelles [81]. (B) Wheel structure and calculated average structures of diastereomeric peptides composed of Lys and Leu, showing the orientation of residues Leu4, Leu8, Lys5 and Lys9 in DPC micelles [113].

in DPC/DMPG micelles, where the helix is extended from residue 13 to 24. The apparent disorder of the N-terminal reflects the flexibility of this region (see Fig. 9.3A). (2) A NMR study was conducted to determine the structure of an amphipathic α-helical peptide KLLLKWLLKLLK-NH_2 (K_4L_7W) and its diastereomer K*LLL*KWL*LK*LLK-NH_2 (D-$L^{3,4,8,10}K_4L_7W$) (where underlined letters indicate D-amino acids) in hydrophobic environments [113]. The structures in

DPC micelles of and D-$L^{3,4,8,10}K_4L_7W$ shown in Fig. 9.3 (B, left and right side, respectively) display the relative positions of the two central lysine residues (Lys5 and Lys9) and adjacent leucines (Leu4 and Leu8). Interestingly, an α-helix was clearly observed for K_4L_7W in the DPC micelles and a less defined, although somewhat helical structure was observed for D-$L^{3,4,8,10}K_4L_7W$. This is despite the incorporation of around 30% D-amino acids within its sequence. Importantly, the positions of the leucine and lysine side-chains illustrate the amphipathic organization of the peptides. The relative side-chain orientations depicted in Fig. 9.3 B clearly reveal segregation between charged (lysine side-chains) and hydrophobic (leucine side-chains) interfaces within the membrane-associated peptides. (3) K_4L_7W and its diastereomers were cyclized after the introduction of cysteines at both the N- and C-termini of the peptides [114]. ATR-FTIR studies revealed that linear K4L7W has a high tendency to form an α-helical structure in both zwitterionic and negatively charged membranes. Incorporation of D-amino acids and cyclization increased the flexibility of the α-helical structure, when bound to negatively charged PE/PG membranes. However, a pronounced α-helical structure was preserved. These results indicate that, in the presence of membranes, a helical structure will remain without appreciable disturbance, despite the presence of D-amino acids and cyclization in a segment with a high tendency to form a helical conformation.

9.5.2 Molecular Mechanisms of Membrane Permeation

The details of the actual membrane permeation pathways for most antimicrobial peptides are still not clear. However, although several models were proposed in recent years, practically all of them suggest that the membrane permeation process takes place via two major consecutive steps: (1) peptides bind onto the surface of the membrane until a threshold local concentration occurs and (2) peptides organize to form a permeation pathway [8].

9.5.2.1 Pore Formation via the Barrel–Stave Model

The barrel–stave mechanism was originally proposed to describe the formation of transmembrane channels/pores by bundles of amphipathic α-helical peptides [117]. Peptides which act via this mechanism are inserted into the membrane such that their hydrophobic surfaces interact with the lipid core of the membrane and their hydrophilic surfaces point inward producing an aqueous pore (Fig. 9.4). Amphipathic α-helical lytic peptides which act on a specific or several types of cells, including bacteria, fungi and mammalian cells, were among the first to be discovered and therefore used as models for extensive mode-of-action studies. It has been suggested that following binding, linear amphipathic α-helical lytic peptides independent of their specific biological target cell, would form transmembrane pores, presumably via a "barrel–stave" mechanism [117] (Fig. 9.4). The experimental evidence for this model was predominantly the

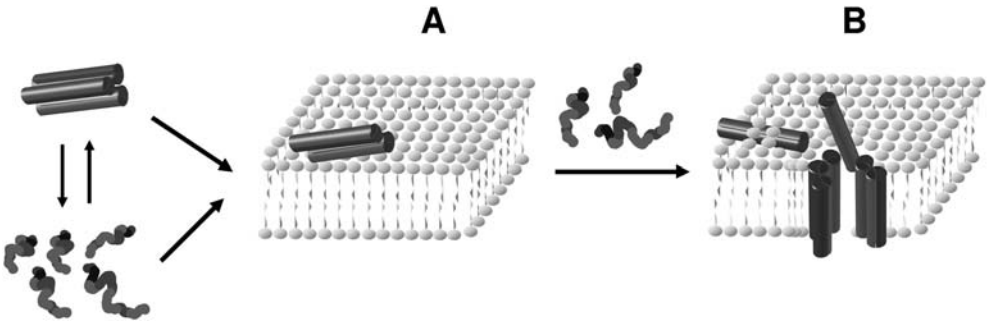

Fig. 9.4 A cartoon illustrating the formation of channels/pores via the barrel–stave model. Peptides reach the membrane either as monomers or oligomers and assemble on the surface of the membrane (step A). In the next step they insert into the lipid core of the membrane following recruitment of additional monomers (step B).

ability of many of these peptides to induce single channels in planar lipid membranes [118–121]. Peptides that act via the barrel–stave mechanism need to insert into the hydrophobic lipid core of the membrane and, therefore, their interaction with the target membrane is governed predominantly by hydrophobic interactions. The following steps are involved in the barrel–stave mechanism: (1) the peptides bind onto the surface of the membrane and self-associate, (2) as soon as a bundle is formed, it inserts into the membrane to form a transmembrane pore, (3) the pore increases due to the recurrent of more monomers and (4) a minimal length of around 22 amino acids is required for a peptide to transverse the lipid bilayers if it adopts an α-helical structure or around 8 amino acids if the peptide adopts a β-sheeted structure. Extensive mode-of-action studies demonstrated that only a few lytic amphipathic peptides act via the barrel–stave mechanism. All of these peptides bind to membranes via hydrophobic interactions and are usually very toxic to any types of cells including bacteria, mammalian cells and fungi. Examples include alamethicin [122, 123], melittin [124–127], pardaxin [128–130] and the helix α5 of δ-endotoxin [131, 132]. As only a few transmembrane pores are required to induce the dissipation of the transmembrane potential in cells, the MIC of the peptides should be at the nanomolar concentrations. In comparison, peptides that are active at the micromolar concentration fully cover the outer surface of the bacterial membrane [133].

9.5.2.2 **The Carpet Model**

Extensive mode-of-action studies were performed to understand why most antimicrobial peptides kill predominantly bacteria in contrast to other membrane-active peptides which are toxic to various cells, independent of the charge of the head groups of their phospholipid membranes. These studies revealed that the

barrel–stave mechanism is used by the non-cell-selective lytic peptides but not by those peptides that are selectively active on bacteria [85, 128–130, 132, 134, 135]. Based on these studies an alternative model termed the "carpet" model or a detergent-like model was proposed for antimicrobial peptides [111, 134, 136]. Major differences between the carpet and barrel–stave models are: (1) the carpet model does not require recognition between membrane-bound peptide monomers, (2) in the carpet model peptides do not insert into the hydrophobic core of the membrane and (3) the carpet model does not require a specific peptide structure. Based on the above, a major advantage of the carpet mechanism is that many peptides can fall within the criteria required, which indeed explains why thousands of peptides have antimicrobial activity regardless of their length, sequence and secondary structure.

The steps presumably involved in the carpet mechanism are shown in Fig. 9.5. (1) Positively charged lytic peptides in a monomeric or oligomeric form bind onto the surface of the negatively charged target membrane and cover it in a "carpet"-like manner. Before reaching the bacterial phospholipid membrane, peptides need to transverse the outer wall of Gram-negative bacteria, which contains LPS, or the outer surface of the single wall of Gram-positive bacteria, which contains acidic polysaccharides (teichoic acids) [50]. (2) The peptides reorient themselves such that their hydrophobic face is toward the lipids and the hydrophilic face toward the phospholipid head groups. (3) The peptides reach a threshold concentration. (4) The peptides permeate/disintegrate the membrane by disrupting the bilayer curvature. According to the carpet model, peptides are in contact with the phospholipid head group throughout the entire process of membrane permeation. An early step before the collapse of the membrane packing may include the formation of transient holes in the membrane. Such holes were described in the torodial model for pore formation or in the two-state model, in which the lipid bends back on itself like the inside of a torus (described in detail in the following section [137–140].

The carpet mechanism described the mode of action of other antimicrobial peptides, such as dermaseptin natural analogs [85, 86, 141], cecropins [77, 111, 142], the human antimicrobial peptide LL-37 [88], caerin 1.1 [143], trichogin GA IV [144], androctonin [41], diastereomers of lytic peptides [43, 44, 49, 81, 88, 114], Kassinatuerin-1 [145], melittin in anionic lipids [127, 146], mastoparan X [147] and apomyoglobin 56–131 peptide [148] (also reviewed in [8, 12, 35, 106, 149, 150–152]). Note, however, that the carpet model is not characteristics only for antimicrobial peptides, because short lytic peptides which are highly hydrophobic and are toxic to erythrocytes and fungi also act via the carpet mechanism [44, 88, 101].

In support of the membrane disintegration step, studies on the morphology of bacteria after treatment with antimicrobial peptides that act via the carpet mechanism demonstrated the breakage of the bacterial membrane [21, 23, 43, 44, 114]. Fig. 9.6 shows an example of electron micrographs of negatively stained *E. coli* untreated and treated with a diastereomeric peptide and cecropin B.

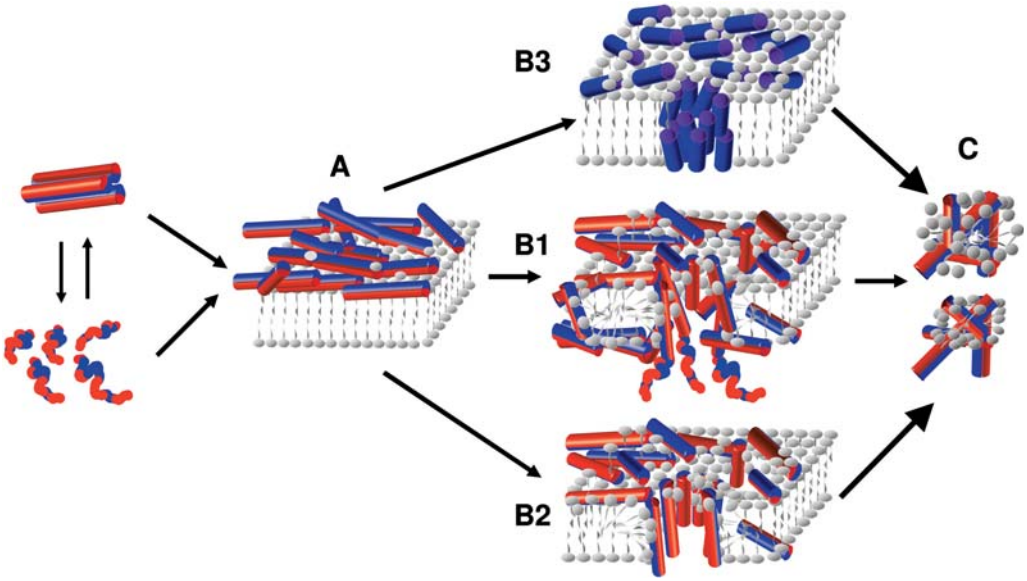

Fig. 9.5 A cartoon illustrating the carpet model suggested for membrane permeation. The peptides reach the membrane as monomers or oligomers, followed by binding to the surface of the membrane with their hydrophobic surfaces facing the membrane and their hydrophilic surfaces facing the solvent (step A). After a threshold concentration of peptide monomers has been reached, the peptides permeate the membrane. This can be achieved by different ways, e.g. a detergent-like effect via the formation of a non-organized transient pore (step B1), formation of organized transient or permanent toroidal pores (step B2) or hydrophobic pores/channel aggregates (step B3) when the peptide is very hydrophobic. The final stage in all cases could be membrane disintegration (step C).

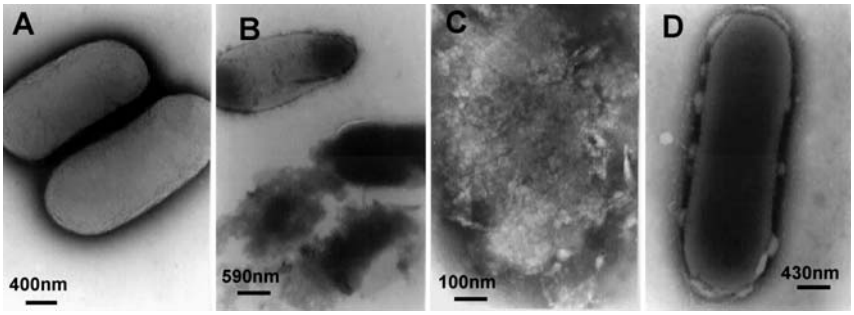

Fig. 9.6 Electron micrographs of negatively stained *E. coli* untreated and treated with antimicrobial peptides. (A) C control. (B) After treatment of the bacteria with a diastereomeric antimicrobial peptide $K_4L_3l_4W$ (l designates the D-isomer of Leu, as shown in Fig. 9.3) at a concentration of 80% the MIC. (C) The bacteria treated with the diastereomer at the MIC concentration. (D) The bacteria treated with cecropin B at a concentration of 80% of the MIC.

9.5.3 The Molecular Architecture of the Permeation Pathway

An intermediate step in the mode of action of many antimicrobial peptides prior to membrane rupture is assumed to be the formation of transient pores. The architecture of these pores should depend upon the properties of the peptides, i.e. length, amphipathicity, amino acid composition and structure. This points toward a general mechanism which can include different types of pores. However, a specific architecture for these pores is not a prerequisite for their antimicrobial activity. This strongly supports the carpet mechanism as a general and efficient mechanism for bacteria killing.

9.5.3.1 Toroidal Pores

Toroidal pores were described by Huang et al. for magainin, protegrin and melittin by using neutron diffraction [153, 154]. The proposed structure of these pores is elucidated in Fig. 9.5 (B2). In order to investigate whether the formation of these organized pores is a crucial step in the killing mechanism of these particular peptides, both magainin and melittin were synthesized in their cyclic form and compared with their linear parental peptides regarding their structure, biological function and interaction with model membranes [155]. Interestingly, it was found that at similar bound peptide : lipid molar ratios, both linear and cyclic analogs of magainin and melittin preserved their high potency to permeate model phospholipid membranes. It is reasonable to assume that the cyclic forms of magainin and melittin cannot form the toroidal pore structure similarly to their linear parental peptides. This supports the notion that the formation of organized pores by these two peptides is the consequence of their specific structure, but these pores are not a prerequisite for bacteria killing. Instead, the extent of hydrophobicity, net positive charge and ability to form a kind of amphipathic structure are sufficient for activities.

9.5.3.2 Channel Aggregates/Hydrophobic Pores

A NMR study of indolicidin, a short 13-amino-acid linear peptide with an extended structure, revealed an interesting fold consisting of a hydrophobic core flanked by two dispersed, positively charged regions. Due to its central hydrophobic core, it was suggested that indolicidin inserts into the hydrophobic core of the membrane and forms channel aggregates [156]. In another study, ranacyclin, a 17-amino-acid cyclic peptide lacking of an amphipathic secondary structure, has been shown to insert into the hydrophobic core of the membrane. As a consequence, the peptide increased the permeability of model membranes. Interestingly, in contrast to many other antimicrobial peptides, ranacyclin increased the permeability of the cytoplasmic membrane of bacteria without disrupting the integrity of the bacteria. Furthermore, the peptide inserted into the hydrophobic core of the membrane and disrupted the acyl chain order similarly

to pore forming peptides, such as melittin [81] and the α5 helix of δ-endotoxin [157], as revealed by ATR-FTIR spectroscopy [11]. In addition, the peptide could bind similarly to zwitterionic and negatively charged membranes, indicating a major contribution of the hydrophobic core of the membrane to the binding process, compared with the electrostatic interaction between most antimicrobial peptides and the lipid head groups. Further studies indicated that the peptide binds first to the outer leaflet followed by insertion into the bilayers to form pores. Importantly, these pores are formed only after a threshold concentration of bound peptide has been reached, similarly to what has been described in the "carpet" mechanism. However, since ranacyclin is too short to span the membrane, such hydrophobic pores could be formed by segregation of several monomers until they span the entire hydrophobic region. Fig. 9.5 (B3) illustrates a possible architecture for these pores.

9.6 Summary and Conclusions

Antimicrobial peptides are a major subgroup within a large repertoire of membrane-active lytic peptides which kill various cells, including bacteria, fungi and mammalian cells. Mode-of-action studies revealed that an appropriate balance between hydrophobicity and a net positive charge is sufficient to endow the peptides with biological function, mainly antibacterial activity. However, cell specificity depends also on other parameters, such as the volume of the molecule, its aggregation state in solution and the membrane, and its ability to co-assemble in the membrane-bound state. These parameters also affect the mode of action of the peptides. However, in contrast to a few known lytic peptides with a specific structure which act via the barrel–stave mechanism (mostly killing mammalian cells and fungi), there are thousands of antimicrobial peptides with variable lengths and sequences. The finding that these antimicrobial peptides are active at similar micromolar concentrations suggests a general detergent-like (or carpet) mechanism for the killing of bacteria, rather than a specific mode of action. Overall, the carpet model was successful because it allowed the development of a novel family of diastereomeric antibacterial peptides. The unique properties of this family, such as controlled enzymatic degradation, stability in serum and in whole blood, and the drastic changes that can be made to their sequences, make them promising candidates for systemic treatment of infectious diseases and cancer [76, 158, 159].

Finally, although many studies suggest that the lethal event is the damage to the bacterial membrane, some studies point to a multi-hit mechanism in which the peptide binds to targets in the cytoplasmic region of the bacteria [25].

Acknowledgments

The studies described were supported by the Israel Science Foundation, the Prostate Cancer Foundation (former CapCure), the Israel Cancer Association and the Israel Cancer Research Foundation.

References

1 Boman, H.G. **1995**. Peptide antibiotics and their role in innate immunity. *Annu. Rev. Immun. 13*, 61–92.
2 Boman, H.G. **1991**. Antibacterial peptides: key components needed in immunity. *Cell 65*, 205–207.
3 Lehrer, R.I., Ganz, T. **1999**. Antimicrobial peptides in mammalian and insect host defence. *Curr. Opin. Immunol. 11*, 23–27.
4 Lehrer, R.I., Ganz, T. **2002**. Cathelicidins: a family of endogenous antimicrobial peptides. *Curr. Opin. Hematol. 9*, 18–22.
5 Hoffmann, J.A., Kafatos, F.C., Janeway, C.A., Ezekowitz, R.A. **1999**. Phylogenetic perspectives in innate immunity. *Science 284*, 1313–1318.
6 Hoffmann, J.A., Reichhart, J.M. **2002**. *Drosophila* innate immunity: an evolutionary perspective. *Nat. Immunol. 3*, 121–126.
7 Devine, D.A., Hancock, R.E. **2002**. Cationic peptides: distribution and mechanisms of resistance. *Curr. Pharm. Des. 8*, 703–714.
8 Zasloff, M. **2002**. Antimicrobial peptides of multicellular organisms. *Nature 415*, 389–395.
9 Dimarcq, J.L., Bulet, P., Hetru, C., Hoffmann, J. **1998**. Cysteine-rich antimicrobial peptides in invertebrates. *Biopolymers 47*, 465–477.
10 Breukink, E., Wiedemann, I., van Kraaij, C., Kuipers, O.P., Sahl, H., de Kruijff, B. **1999**. Use of the cell wall precursor lipid II by a pore-forming peptide antibiotic. *Science 286*, 2361–2364.
11 Shai, Y. **1999**. Mechanism of the binding, insertion and destabilization of phospholipid bilayer membranes by alpha-helical antimicrobial and cell nonselective membrane-lytic peptides. *Biochim. Biophys. Acta. 1462*, 55–70.
12 Tossi, A., Sandri, L., Giangaspero, A. **2000**. Amphipathic, alpha-helical antimicrobial peptides. *Biopolymers 55*, 4–30.
13 Brotz, H., Sahl, H.G. **2000**. New insights into the mechanism of action of lantibiotics-diverse biological effects by binding to the same molecular target. *J. Antimicrob. Chemother. 46*, 1–6.
14 Steiner, H., Hultmark, D., Engstrom, A., Bennich, H., Boman, H.G. **1981**. Sequence and specificity of two antibacterial proteins involved in insect immunity. *Nature 292*, 246–248.
15 Zasloff, M. **1987**. Magainins, a class of antimicrobial peptides from Xenopus skin: isolation, characterization of two active forms, and partial cDNA sequence of a precursor. *Proc. Natl Acad. Sci. USA 84*, 5449–5453.
16 Mor, A., Nguyen, V.H., Delfour, A., Migliore-Samour, D., Nicolas, P. **1991**. Isolation, amino acid sequence, and synthesis of dermaseptin, a novel antimicrobial peptide of amphibian skin. *Biochemistry 30*, 8824–8830.
17 Zanetti, M., Gennaro, R., Skerlavaj, B., Tomasinsig, L., Circo, R. **2002**. Cathelicidin peptides as candidates for a novel class of antimicrobials. *Curr. Pharm. Des. 8*, 779–793.
18 Landon, C., Sodano, P., Hetru, C., Hoffmann, J., Ptak, M. **1997**. Solution structure of drosomycin, the first inducible antifungal protein from insects. *Protein Sci. 6*, 1878–1884.
19 Habermann, E., Jentsch, J. **1967**. *Hoppe Seyler's Z. Physiol. Chem. 348*, 37–50.
20 Shai, Y., Fox, J., Caratsch, C., Shih, Y.L., Edwards, C., Lazarovici, P. **1988**. Sequencing and synthesis of pardaxin, a polypeptide from the Red Sea Moses sole with ionophore activity. *FEBS Lett. 242*, 161–166.

21 Oren, Z., Shai, Y. **1996**. Selective lysis of bacteria but not mammalian cells by diastereomers of melittin: structure–function study. *Biochemistry 36*, 1826–1835.

22 Johansson, J., Gudmundsson, G. H., Rottenberg, M. E., Berndt, K. D., Agerberth, B. **1998**. Conformation-dependent antibacterial activity of the naturally-occurring human peptide LL-37. *J. Biol. Chem. 273*, 3718–3724.

23 Oren, Z., Lerman, J. C., Gudmundsson, G. H., Agerberth, B., Shai, Y. **1999**. Structure and organization of the human antimicrobial peptide LL-37 in phospholipid membranes: relevance to the molecular basis for its non-cell selective activity. *Biochem. J. 341*, 501–513.

24 Lehrer, R. I., Lichtenstein, A. K., Ganz, T. **1993**. Defensins – antimicrobial and cytotoxic peptides of mammalian cells. *Annu. Rev. Immunol. 11*, 105–128.

25 Hancock, R. E., Rozek, A. **2002**. Role of membranes in the activities of antimicrobial cationic peptides. *FEMS Microbiol. Lett. 206*, 143–149.

26 Zasloff, M. **1992**. Antibiotic peptides as mediators of innate immunity. *Curr. Opin. Immunol. 4*, 3–7.

27 Nicolas, P., Mor, A. **1995**. Peptides as weapons against microorganisms in the chemical defense system of vertebrates. *Annu. Rev. Microbiol. 49*, 277–304.

28 Hancock, R. E., Diamond, G. **2000**. The role of cationic antimicrobial peptides in innate host defences. *Trends Microbiol. 8*, 402–410.

29 Guder, A., Wiedemann, I., Sahl, H. G. **2000**. Posttranslationally modified bacteriocins – the lantibiotics. *Biopolymers 55*, 62–73.

30 Bowdish, D. M., Davidson, D. J., Speert, D. P., Hancock, R. E. **2004**. The human cationic peptide LL-37 induces activation of the extracellular signal-regulated kinase and p38 kinase pathways in primary human monocytes. *J. Immunol. 172*, 3758–3765.

31 Davidson, D. J., Currie, A. J., Reid, G. S., Bowdish, D. M., MacDonald, K. L., Ma, R. C., Hancock, R. E., Speert, D. P. **2004**. The cationic antimicrobial peptide LL-37 modulates dendritic cell differentiation and dendritic cell-induced T cell polarization. *J. Immunol. 172*, 1146–1156.

32 Lehrer, R. I., Barton, A., Daher, K. A., Harwig, S. S., Ganz, T., Selsted, M. E. **1989**. Interaction of human defensins with *Escherichia coli*. Mechanism of bactericidal activity. *J. Clin. Invest. 84*, 553–561.

33 Matsuzaki, K. **1999**. Why and how are peptide–lipid interactions utilized for self-defense? Magainins and tachyplesins as archetypes. *Biochim. Biophys. Acta 1462*, 1–10.

34 Wieprecht, T., Apostolov, O., Beyermann, M., Seelig, J. **2000**. Membrane binding and pore formation of the antibacterial peptide PGLa: thermodynamic and mechanistic aspects. *Biochemistry 39*, 442–452.

35 Bechinger, B. **1999**. The structure, dynamics and orientation of antimicrobial peptides in membranes by multidimensional solid-state NMR spectroscopy. *Biochim. Biophys. Acta 1462*, 157–183.

36 Wu, M., Maier, E., Benz, R., Hancock, R. E. **1999**. Mechanism of interaction of different classes of cationic antimicrobial peptides with planar bilayers and with the cytoplasmic membrane of *Escherichia coli*. *Biochemistry 38*, 7235–7242.

37 Lee, W. J., Brey, P. T. **1994**. Isolation and identification of cecropin antibacterial peptides from the extracellular matrix of the insect integument. *Anal. Biochem. 217*, 231–235.

38 Wade, D., Boman, A., Wahlin, B., Drain, C. M., Andreu, D., Boman, H. G., Merrifield, R. B. **1990**. All-D-amino acid-containing channel-forming antibiotic peptides. *Proc. Natl Acad. Sci. USA 87*, 4761–4765.

39 Bessalle, R., Kapitkovsky, A., Gorea, A., Shalit, I., Fridkin, M. **1990**. All-D-magainin: chirality, antimicrobial activity and proteolytic resistance. *FEBS Lett. 274*, 151–155.

40 Merrifield, R. B., Juvvadi, P., Andreu, D., Ubach, J., Boman, A., Boman, H. G. **1995**. Retro and retroenantio analogs of cecropin-melittin hybrids. *Proc. Natl Acad. Sci. USA 92*, 3449–3453.

41 Hetru, C., Letellier, L., Oren, Z., Hoffmann, J. A., Shai, Y. **2000**. Androctonin,

a hydrophilic disulphide-bridged non-haemolytic anti-microbial peptide: a plausible mode of action. *Biochem. J. 345*, 653–664.

42 Chen, H.C., Brown, J.H., Morell, J.L., Huang, C.M. **1988**. Synthetic magainin analogues with improved antimicrobial activity. *FEBS Lett. 236*, 462–466.

43 Shai, Y., Oren, Z. **1996**. Diastereoisomers of cytolysins, a novel class of potent antibacterial peptides. *J. Biol. Chem. 271*, 7305–7308.

44 Oren, Z., Hong, J., Shai, Y. **1997**. A repertoire of novel antibacterial diastereomeric peptides with selective cytolytic activity. *J. Biol. Chem. 272*, 14643–14649.

45 Hong, J., Oren, Z., Shai, Y. **1999**. The structure and organization of hemolytic and nonhemolytic diastereomers of antimicrobial peptides in membranes. *Biochemistry 38*, 16963–16973.

46 Kondejewski, L.H., Jelokhani-Niaraki, M., Farmer, S.W., Lix, B., Kay, C.M., Sykes, B.D., Hancock, R.E., Hodges, R.S. **1999**. Dissociation of antimicrobial and hemolytic activities in cyclic peptide diastereomers by systematic alterations in amphipathicity. *J. Biol. Chem. 274*, 13181–13192.

47 Avrahami, D., Oren, Z., Shai, Y. **2001**. Effect of multiple aliphatic amino acids substitutions on the structure, function, and mode of action of diastereomeric membrane active peptides. *Biochemistry 40*, 12591–12603.

48 Jelokhani-Niaraki, M., Kondejewski, L.H., Farmer, S.W., Hancock, R.E., Kay, C.M., Hodges, R.S. **2000**. Diastereoisomeric analogues of gramicidin S: structure, biological activity and interaction with lipid bilayers. *Biochem. J. 349*, 747–755.

49 Fernandez-Lopez, S., Kim, H.S., Choi, E.C., Delgado, M., Granja, J.R., Khasanov, A., Kraehenbuehl, K., Long, G., Weinberger, D.A., Wilcoxen, K.M., Ghadiri, M.R. **2001**. Antibacterial agents based on the cyclic D,L-alpha-peptide architecture. *Nature 412*, 452–455.

50 Brock, T.D. **1974**. *Biology of Microorganism*, 2nd edn. Prentice-Hall, Englewood Cliffs, NJ.

51 Verkleij, A.J., Zwaal, R.F., Roelofsen, B., Comfurius, P., Kastelijn, D., Deenen, L.V. **1973**. The asymmetric distribution of phospholipids in the human red cell membrane. A combined study using phospholipases and freeze-etch electron microscopy. *Biochim. Biophys. Acta 323*, 178–193.

52 Matsuzaki, K., Sugishita, K., Ishibe, N., Ueha, M., Nakata, S., Miyajima, K., Epand, R.M. **1998**. Relationship of membrane curvature to the formation of pores by magainin 2. *Biochemistry 37*, 11856–11863.

53 Oren, Z., Shai, Y. **1998**. Mode of action of linear amphipathic alpha-helical antimicrobial peptides. *Biopolymers 47*, 451–463.

54 Bulet, P., Hetru, C., Dimarcq, J.L., Hoffmann, D. **1999**. Antimicrobial peptides in insects; structure and function. *Dev. Comp. Immunol. 23*, 329–344.

55 Breukink, E., van Heusden, H.E., Vollmerhaus, P.J., Swiezewska, E., Brunner, L., Walker, S., Heck, A.J., de Kruijff, B. **2003**. Lipid II is an intrinsic component of the pore induced by nisin in bacterial membranes. *J. Biol. Chem. 278*, 19898–19903.

56 Wiedemann, I., Benz, R., Sahl, H.G. **2004**. Lipid II-mediated pore formation by the peptide antibiotic nisin: a black lipid membrane study. *J. Bacteriol. 186*, 3259–3261.

57 Marugg, J.D., Gonzalez, C.F., Kunka, B.S., Ledeboer, A.M., Pucci, M.J., Toonen, M.Y., Walker, S.A., Zoetmulder, L.C., Vandenbergh, P.A. **1992**. Cloning, expression, and nucleotide sequence of genes involved in production of pediocin PA-1, and bacteriocin from *Pediococcus acidilactici* PAC1.0. *Appl. Environ. Microbiol. 58*, 2360–2367.

58 Fleury, Y., Dayem, M.A., Montagne, J.J., Chaboisseau, E., Le Caer, J.P., Nicolas, P., Delfour, A. **1996**. Covalent structure, synthesis, and structure–function studies of mesentericin Y 105(37), a defensive peptide from gram-positive bacteria *Leuconostoc mesenteroides*. *J. Biol. Chem. 271*, 14421–14429.

59 Ennahar, S., Sashihara, T., Sonomoto, K., Ishizaki, A. **2000**. Class IIa bacteriocins:

biosynthesis, structure and activity. *FEMS Microbiol. Rev. 24*, 85–106.

60 Yan, L. Z., Gibbs, A. C., Stiles, M. E., Wishart, D. S., Vederas, J. C. **2000**. Analogues of bacteriocins: antimicrobial specificity and interactions of leucocin A with its enantiomer, carnobacteriocin B2, and truncated derivatives. *J. Med. Chem. 43*, 4579–4581.

61 Ramnath, M., Beukes, M., Tamura, K., Hastings, J. W. **2000**. Absence of a putative mannose-specific phosphotransferase system enzyme IIAB component in a leucocin A-resistant strain of *Listeria monocytogenes*, as shown by two-dimensional sodium dodecyl sulfate-polyacrylamide gel electrophoresis. *Appl. Environ. Microbiol. 66*, 3098–3101.

62 Hechard, Y., Pelletier, C., Cenatiempo, Y., Frere, J. **2001**. Analysis of sigma$_{54}$-dependent genes in *Enterococcus faecalis*: a mannose PTS permease (EII^{Man}) is involved in sensitivity to a bacteriocin, mesentericin Y105. *Microbiology 147*, 1575–1580.

63 Kaur, K., Andrew, L. C., Wishart, D. S., Vederas, J. C. **2004**. Dynamic relationships among type IIa bacteriocins: temperature effects on antimicrobial activity and on structure of the C-terminal amphipathic alpha helix as a receptor-binding region. *Biochemistry 43*, 9009–9020.

64 Schiffer, M., Edmundson, A. B. **1967**. Use of helical wheels to represent the structures of protein and to identify segments with helical potential. *Biophys. J. 7*, 121–135.

65 Saberwal, G., Nagaraj, R. **1994**. Cell-lytic and antibacterial peptides that act by perturbing the barrier function of membranes: facets of their conformational features, structure–function correlations and membrane-perturbing abilities. *Biochim. Biophys. Acta 1197*, 109–131.

66 Oren, Z., Shai, Y. **1998**. Mode of action of linear amphipathic alpha-helical antimicrobial peptides. *Biopolymers 47*, 451–463.

67 Matsuzaki, K. **1998**. Magainins as paradigm for the mode of action of pore forming polypeptides. *Biochim. Biophys. Acta. 1376*, 391–400.

68 Hwang, P. M., Vogel, H. J. **1998**. Structure–function relationships of antimicrobial peptides. *Biochem. Cell Biol. 76*, 235–246.

69 Andreu, D., Rivas, L. **1998**. Animal antimicrobial peptides: an overview. *Biopolymers 47*, 415–433.

70 Simmaco, M., Mignogna, G., Canofeni, S., Miele, R., Mangoni, M. L., Barra, D. **1996**. Temporins, antimicrobial peptides from the European red frog *Rana temporaria*. *Eur. J. Biochem. 242*, 788–792.

71 Mangoni, M. L., Papo, N., Barra, D., Simmaco, M., Bozzi, A., Di Giulio, A., Rinaldi, A. C. **2004**. Effects of the antimicrobial peptide temporin L on cell morphology, membrane permeability and viability of *Escherichia coli*. *Biochem. J. 380*, 859–865.

72 Cappelli, G., Paladini, S., D'Agata, A. **1999**. Tumor markers in the diagnosis of pancreatic cancer. *Tumori 85*, S19–21.

73 Ohsaki, Y., Gazdar, A. F., Chen, H. C., Johnson, B. E. **1992**. Antitumor activity of magainin analogues against human lung cancer cell lines. *Cancer Res. 52*, 3534–3538.

74 Baker, M. A., Maloy, W. L., Zasloff, M., Jacob, L. S. **1993**. Anticancer efficacy of Magainin2 and analogue peptides. *Cancer Res. 53*, 3052–3057.

75 Papo, N., Shahar, M., Eisenbach, L., Shai, Y. **2003**. A novel lytic peptide composed of DL-amino acids selectively kills cancer cells in culture and in mice. *J. Biol. Chem. 278*, 21018–21023.

76 Papo, N., Shai, Y. **2003**. New lytic peptides based on the D,L-amphipathic helix motif preferentially kill tumor cells compared to normal cells. *Biochemistry 42*, 9346–9354.

77 Gazit, E., Lee, W. J., Brey, P. T., Shai, Y. **1994**. Mode of action of the antibacterial cecropin B2: a spectrofluorometric study. *Biochemistry 33*, 10681–10692.

78 Bechinger, B. **1997**. Structure and functions of channel-forming peptides: magainins, cecropins, melittin and alamethicin. *J. Membr. Biol. 156*, 197–211.

79 Pouny, Y., Rapaport, D., Mor, A., Nicolas, P., Shai, Y. **1992**. Interaction of antimicrobial dermaseptin and its fluorescently labeled analogues with phospholipid

membranes. *Biochemistry 31*, 12416–12423.

80 Blondelle, S.E., Houghten, R.A. **1991**. Hemolytic and antimicrobial activities of the twenty-four individual omission analogues of melittin. *Biochemistry 30*, 4671–4678.

81 Sharon, M., Oren, Z., Shai, Y., Anglister, J. **1999**. 2D-NMR and ATR-FTIR study of the structure of a cell-selective diastereomer of melittin and its orientation in phospholipids. *Biochemistry 38*, 15305–15316.

82 Oren, Z., Shai, Y. **1996**. A class of highly potent antibacterial peptides derived from pardaxin, a pore-forming peptide isolated from Moses sole fish *Pardachirus marmoratus*. *Eur. J. Biochem. 237*, 303–310.

83 Selsted, M.E., Novotny, M.J., Morris, W.L., Tang, Y.Q., Smith, W., Cullor, J.S. **1992**. Indolicidin, a novel bactericidal tridecapeptide amide from neutrophils. *J. Biol. Chem. 267*, 4292–4295.

84 Mignogna, G., Simmaco, M., Kreil, G., Barra, D. **1993**. Antibacterial and haemolytic peptides containing D-alloisoleucine from the skin of *Bombina variegata*. *EMBO J. 12*, 4829–4832.

85 Strahilevitz, J., Mor, A., Nicolas, P., Shai, Y. **1994**. Spectrum of antimicrobial activity and assembly of dermaseptin-b and its precursor form in phospholipid membranes. *Biochemistry 33*, 10951–10960.

86 Ghosh, J.K., Shaool, D., Guillaud, P., Ciceron, L., Mazier, D., Kustanovich, I., Shai, Y., Mor, A. **1997**. Selective cytotoxicity of dermaseptin S3 toward intraerythrocytic *Plasmodium falciparum* and the underlying molecular basis. *J. Biol. Chem. 272*, 31609–31616.

87 Zanetti, M., Gennaro, R., Romeo, D. **1997**. The cathelicidin family of antimicrobial peptide precursors: a component of the oxygen-independent defense mechanisms of neutrophils. *Ann. NY Acad. Sci. 832*, 147–162.

88 Oren, Z., Hong, J., Shai, Y. **1999**. A comparative study on the structure and function of a cytolytic alpha-helical peptide and its antimicrobial beta-sheet diastereomer. *Eur. J. Biochem. 259*, 360–369.

89 Osaki, T., Omotezako, M., Nagayama, R., Hirata, M., Iwanaga, S., Kasahara, J., Hattori, J., Ito, I., Sugiyama, H., Kawabata, S. **1999**. Horseshoe crab hemocyte-derived antimicrobial polypeptides, tachystatins, with sequence similarity to spider neurotoxins. *J. Biol. Chem. 274*, 26172–26178.

90 Vogel, H.J., Schibli, D.J., Jing, W., Lohmeier-Vogel, E.M., Epand, R.F., Epand, R.M. **2002**. Towards a structure–function analysis of bovine lactoferricin and related tryptophan- and arginine-containing peptides. *Biochem. Cell Biol. 80*, 49–63.

91 Avrahami, D., Shai, Y. **2003**. Bestowing antifungal and antibacterial activities by lipophilic acid conjugation to D,L-amino acid-containing antimicrobial peptides: a plausible mode of action. *Biochemistry 42*, 14946–14956.

92 Avrahami, D., Shai, Y. **2004**. A new group of antifungal and antibacterial lipopeptides derived from non-membrane active peptides conjugated to palmitic acid. *J. Biol. Chem. 279*, 12277–12285.

93 Hong, S.Y., Oh, J.E., Lee, K.H. **1999**. Effect of D-amino acid substitution on the stability, the secondary structure, and the activity of membrane-active peptide. *Biochem. Pharmacol. 58*, 1775–1780.

94 Oren, Z., Shai, Y. **1997**. Selective lysis of bacteria but not mammalian cells by diastereomers of melittin: structure–function study. *Biochemistry 36*, 1826–1835.

95 Terwilliger, T.C., Eisenberg, D. **1982**. The structure of melittin. *J. Biol. Chem. 257*, 6016–6022.

96 Wimley, W.C., White, S.H. **1996**. Experimentally determined hydrophobicity scale for proteins at membrane interfaces. *Nat. Struct. Biol. 3*, 842–848.

97 Papo, N., Shai, Y. **2003**. Exploring peptide membrane interaction using surface plasmon resonance: differentiation between pore formation versus membrane disruption by lytic peptides. *Biochemistry 42*, 458–466.

98 Ladokhin, A.S., White, S.H. **1999**. Folding of amphiphatic alpha-helices on membranes: energetics of helix formation by melittin. *J. Mol. Biol. 285*, 1363–1369.

99 Mor, A., Hani, K., Nicolas, P. **1994**. The vertebrate peptide antibiotics dermaseptins have overlapping structural features but target specific microorganisms. *J. Biol. Chem. 269*, 31635–31641.

100 Amiche, M., Seon, A.A., Pierre, T.N., Nicolas, P. **1999**. The dermaseptin precursors: a protein family with a common preproregion and a variable C-terminal antimicrobial domain. *FEBS Lett. 456*, 352–356.

101 Kustanovich, I., Shalev, D.E., Mikhlin, M., Gaidukov, L., Mor, A. **2002**. Structural requirements for potent versus selective cytotoxicity for antimicrobial dermaseptin S4 derivatives. *J. Biol. Chem. 277*, 16941–16951.

102 Avrahami, D., Oren, Z., Shai, Y. **2001**. The effect of multiple aliphatic amino acids substitutions on the structure, function and mode of action of diastereomeric membrane active peptides. *Biochemistry 40*, 12591–12603.

103 Avrahami, D., Shai, Y. **2002**. Conjugation of a magainin analogue with lipophilic acids controls hydrophobicity, solution assembly, and cell selectivity. *Biochemistry 41*, 2254–2263.

104 Jackson, M., Mantsch, H.H., Spencer, J.H. **1992**. Conformation of magainin-2 and related peptides in aqueous solution and membrane environments probed by Fourier transform infrared spectroscopy. *Biochemistry 31*, 7289–7293.

105 Sal-Man, N., Oren, Z., Shai, Y. **2002**. Preassembly of membrane-active peptides is an important factor in their selectivity toward target cells. *Biochemistry 41*, 11921–11930.

106 Dathe, M., Wieprecht, T. **1999**. Structural features of helical antimicrobial peptides: their potential to modulate activity on model membranes and biological cells. *Biochim. Biophys. Acta 1462*, 71–87.

107 Gennaro, R., Zanetti, M. **2000**. Structural features and biological activities of the cathelicidin-derived antimicrobial peptides. *Biopolymers 55*, 31–49.

108 Shai, Y. **2002**. From innate immunity to *de-novo* designed antimicrobial peptides. *Curr. Pharm. Des. 8*, 715–725.

109 Lee, J.Y., Boman, A., Sun, C.X., Andersson, M., Jornvall, H., Mutt, V., Boman, H.G. **1989**. Antibacterial peptides from pig intestine: isolation of a mammalian cecropin. *Proc. Natl Acad. Sci. USA 86*, 9159–9162.

110 Agerberth, B., Lee, J.Y., Bergman, T., Carlquist, M., Boman, H.G., Mutt, V., Jornvall, H. **1991**. Amino acid sequence of PR-39. Isolation from pig intestine of a new member of the family of proline-arginine-rich antibacterial peptides. *Eur. J. Biochem. 202*, 849–854.

111 Gazit, E., Boman, A., Boman, H.G., Shai, Y. **1995**. Mechanism of Interaction of the mammalian antibacterial peptide cecropin P1 with phospholipid vesicles. *Biochemistry 34*, 11479–11488.

112 Gennaro, R., Zanetti, M., Benincasa, M., Podda, E., Miani, M. **2002**. Pro-rich antimicrobial peptides from animals: structure, biological functions and mechanism of action. *Curr. Pharm. Des. 8*, 763–778.

113 Oren, Z., Ramesh, J., Avrahami, D., Suryaprakash, N., Shai, Y., Jelinek, R. **2002**. Structures and mode of membrane interaction of a short α-helical lytic peptide and its diastereomer determined by NMR, FTIR, and fluorescence spectroscopy. *Eur. J. Biochem. 269*, 3869–3880.

114 Oren, Z., Shai, Y. **2000**. Cyclization of a cytolytic amphipathic alpha-helical peptide and its diastereomer: effect on structure, interaction with model membranes, and biological function. *Biochemistry 39*, 6103–6114.

115 Lauterwein, J., Brown, L.R., Wuthrich, K. **1980**. High-resolution ^{1}H-NMR studies of monomeric melittin in aqueous solution. *Biochim. Biophys. Acta 622*, 219–230.

116 Bazzo, R., Tappin, M.J., Pastore, A., Harvey, T.S., Carver, J.A., Campbell, I.D. **1988**. The structure of melittin. A ^{1}H-NMR study in methanol. *Eur. J. Biochem. 173*, 139–146.

117 Ehrenstein, G., Lecar, H. **1977**. Electrically gated ionic channels in lipid bilayers. *Q. Rev. Biophys. 10*, 1–34.

118 Christensen, B., Fink, J., Merrifield, R.B., Mauzerall, D. **1988**. Channel-

forming properties of cecropins and related model compounds incorporated into planar lipid membranes. *Proc. Natl Acad. Sci. USA 85*, 5072–5076.

119 Westerhoff, H.V., Juretic, D., Hendler, R.W., Zasloff, M. **1989**. Magainins and the disruption of membrane-linked free-energy transduction. *Proc. Natl Acad. Sci. USA 86*, 6597–6601.

120 Duclohier, H., Molle, G., Spach, G. **1989**. Antimicrobial peptide magainin I from *Xenopus* skin forms anion-permeable channels in planar lipid bilayers. *Biophys. J. 56*, 1017–1021.

121 Matsuzaki, K., Harada, M., Funakoshi, S., Fujii, N., Miyajima, K. **1991**. Physicochemical determinants for the interactions of magainins 1 and 2 with acidic lipid bilayers. *Biochim. Biophys. Acta 1063*, 162–170.

122 Sansom, M.S. **1993**. Alamethicin and related peptaibols – model ion channels. *Eur. Biophys. J. 22*, 105–124.

123 Rizzo, V., Stankowski, S., Schwarz, G. **1987**. Alamethicin incorporation in lipid bilayers: a thermodynamic study. *Biochemistry 26*, 2751–2759.

124 DeGrado, W.F., Musso, G.F., Lieber, M., Kaiser, E.T., Kezdy, F.J. **1982**. Kinetics and mechanism of hemolysis induced by melittin and by a synthetic melittin analogue. *Biophys. J. 37*, 329–338.

125 Vogel, H., Jahnig, F., Hoffmann, V., Stumpel, J. **1983**. The orientation of melittin in lipid membranes. A polarized infrared spectroscopy study. *Biochim. Biophys. Acta 733*, 201–209.

126 Dempsey, C.E., Butler, G.S. **1992**. Helical structure and orientation of melittin in dispersed phospholipid membranes from amide exchange analysis *in situ*. *Biochemistry 31*, 11973–11977.

127 Ladokhin, A.S., White, S.H. **2001**. "Detergent-like" permeabilization of anionic lipid vesicles by melittin. *Biochim. Biophys. Acta 1514*, 253–260.

128 Shai, Y., Bach, D., Yanovsky, A. **1990**. Channel formation properties of synthetic pardaxin and analogues. *J. Biol. Chem. 265*, 20202–20209.

129 Rapaport, D., Shai, Y. **1991**. Interaction of fluorescently labeled pardaxin and its analogues with lipid bilayers. *J. Biol. Chem. 266*, 23769–23775.

130 Rapaport, D., Shai, Y. **1992**. Aggregation and organization of pardaxin in phospholipid membranes. A fluorescence energy transfer study. *J. Biol. Chem. 267*, 6502–6509.

131 Gazit, E., Shai, Y. **1993**. Structural and functional characterization of the α-5 segment of *Bacillus thuringiensis* δ-endotoxin. *Biochemistry 32*, 3429–3436.

132 Gazit, E., Bach, D., Kerr, I.D., Sansom, M.S., Chejanovsky, N., Shai, Y. **1994**. The alpha-5 segment of *Bacillus thuringiensis* delta-endotoxin: *in vitro* activity, ion channel formation and molecular modelling. *Biochem. J. 304*, 895–902.

133 Steiner, H., Andreu, D., Merrifield, R.B. **1988**. Binding and action of cecropin and cecropin analogues: antibacterial peptides from insects. *Biochim. Biophys. Acta 939*, 260–266.

134 Pouny, Y., Shai, Y. **1992**. Interaction of D-amino acid incorporated analogues of pardaxin with membranes. *Biochemistry 31*, 9482–9490.

135 Shai, Y. **1994**. Pardaxin: channel formation by a shark repellant peptide from fish. *Toxicology 87*, 109–129.

136 Shai, Y. **1995**. Molecular recognition between membrane-spanning polypeptides. *Trends. Biochem. Sci. 20*, 460–464.

137 Matsuzaki, K., Murase, O., Miyajima, K. **1995**. Kinetics of pore formation by an antimicrobial peptide, magainin *2*, in phospholipid bilayers. *Biochemistry 34*, 12553–12559.

138 Ludtke, S.J., He, K., Heller, W.T., Harroun, T.A., Yang, L., Huang, H.W. **1996**. Membrane pores induced by magainin. *Biochemistry 35*, 13723–13728.

139 Heller, W.T., Waring, A.J., Lehrer, R.I., Huang, H.W. **1998**. Multiple states of beta-sheet peptide protegrin in lipid bilayers. *Biochemistry 37*, 17331–17338.

140 Huang, H.W. **2000**. Action of antimicrobial peptides: two-state model. *Biochemistry 39*, 8347–8352.

141 La Rocca, P., Biggin, P.C., Tieleman, D.P., Sansom, M.S. **1999**. Simulation studies of the interaction of antimicrobial peptides and lipid bilayers. *Biochim. Biophys. Acta 1462*, 185–200.

142 Gazit, E., Miller, I.R., Biggin, P.C., Sansom, M.S.P., Shai, Y. **1996**. Structure and orientation of the mammalian antibacterial peptide cecropin P1 within phospholipid membranes. *J. Mol. Biol. 258*, 860–870.

143 Wong, H., Bowie, J.H., Carver, J.A. **1997**. The solution structure and activity of caerin 1.1, an antimicrobial peptide from the Australian green tree frog, *Litoria splendida. Eur. J. Biochem. 247*, 545–557.

144 Monaco, V., Formaggio, F., Crisma, M., Toniolo, C., Hanson, P., Millhauser, G.L. **1999**. Orientation and immersion depth of a helical lipopeptaibol in membranes using TOAC as an ESR probe. *Biopolymers 50*, 239–253.

145 Mattute, B., Knoop, F.C., Conlon, J.M. **2000**. Kassinatuerin-1: a peptide with broad-spectrum antimicrobial activity isolated from the skin of the hyperoliid frog, *Kassina senegalensis. Biochem. Biophys. Res. Commun. 268*, 433–436.

146 Steinem, C., Galla, H., Janshoff, A. **2000**. Interaction of melittin with solid supported membranes. *Phys. Chem. Chem. Phys. 2*, 4580–4585.

147 Whiles, J.A., Brasseur, R., Glover, K.J., Melacini, G., Komives, E.A., Vold, R.R. **2001**. Orientation and effects of mastoparan X on phospholipid bicelles. *Biophys. J. 80*, 280–293.

148 Mak, P., Szewczyk, A., Mickowska, B., Kicinska, A., Dubin, A. **2001**. Effect of antimicrobial apomyoglobin 56–131 peptide on liposomes and planar lipid bilayer membrane. *Int. J. Antimicrob. Agents 17*, 137–142.

149 Lohner, K., Prenner, E.J. **1999**. Differential scanning calorimetry and X-ray diffraction studies of the specificity of the interaction of antimicrobial peptides with membrane-mimetic systems. *Biochim. Biophys. Acta 1462*, 141–156.

150 Epand, R.M., Vogel, H.J. **1999**. Diversity of antimicrobial peptides and their mechanisms of action. *Biochim. Biophys. Acta 1462*, 11–28.

151 Sitaram, N., Nagaraj, R. **1999**. Interaction of antimicrobial peptides with biological and model membranes: structural and charge requirements for activity. *Biochim. Biophys. Acta 1462*, 29–54.

152 Mor, A. **2000**. Peptide-based antibiotics: a potential answer to raging antimicrobial resistance. *Drug Dev. Res. 50*, 440–447.

153 Yang, L., Weiss, T.M., Lehrer, R.I., Huang, H.W. **2000**. Crystallization of antimicrobial pores in membranes: magainin and protegrin. *Biophys. J. 79*, 2002–2009.

154 Yang, L., Harroun, T.A., Weiss, T.M., Ding, L., Huang, H.W. **2001**. Barrel–stave model or toroidal model? A case study on melittin pores. *Biophys. J. 81*, 1475–1485.

155 Unger, T., Oren, Z., Shai, Y. **2001**. The effect of cyclization of magainin 2 and melittin analogues on structure, function, and model membrane interactions: implication to their mode of action. *Biochemistry 40*, 6388–6397.

156 Rozek, A., Friedrich, C.L., Hancock, R.E. **2000**. Structure of the bovine antimicrobial peptide indolicidin bound to dodecylphosphocholine and sodium dodecyl sulfate micelles. *Biochemistry 39*, 15765–15774.

157 Gazit, E., La Rocca, P., Sansom, M.S., Shai, Y. **1998**. The structure and organization within the membrane of the helices composing the pore-forming domain of *Bacillus thuringiensis* delta-endotoxin are consistent with an "umbrella-like" structure of the pore. *Proc. Natl Acad. Sci. USA 95*, 12289–12294.

158 Braunstein, A., Papo, N., Shai, Y. **2004**. In vitro activity and potency of an intravenously injected antimicrobial peptide and its DL amino acid analog in mice infected with bacteria. *Antimicrob. Ag. Chemother. 48*, 3127–3129.

159 Papo, N., Braunstein, A., Eshhar, Z., Shai, Y. **2004**. Suppression of human prostate tumor growth in mice by a cytolytic D-, L-amino acid peptide: membrane lysis, increased necrosis, and inhibition of prostate-specific antigen secretion. *Cancer Res. 64*, 5779–5786.

Part 4
Mechanisms of Membrane Fusion

10
Cell Fusion in Development and Disease

Benjamin Podbilewicz and Leonid V. Chernomordik

10.1
Introduction

Cell fusion is a key stage of many fundamental developmental processes. In humans cell fusion is essential in fertilization, placentation, myogenesis and osteogenesis. Here we discuss different developmental fusions with special emphasis on muscle and epithelial fusion in *Drosophila* and in *Caenorhabditis elegans*. We then describe the emerging understanding of membrane fusion in simpler fusion reactions, highlighting cell fusion mediated by viral glycoproteins. While developmental cell fusion is an example of fusion in normal cell physiology, viral fusion represents an example of a fusion-based pathological process. In the last section we discuss lessons from the developmental cell fusion field to viral membrane fusion and vice versa. First, we analyze approaches to separate expression of a candidate developmental cell fusion protein from its activation (if any) at the time of fusion. Second, we review approaches to block developmental fusion at different stages and to uncouple local fusion events from subsequent stages of fusion pore expansion. Third, we discuss the importance of dividing the role of cell adhesion mechanisms from the machinery that mediates actual fusion.

10.2
Developmental Cell Fusion for Health

While most cells in a multicellular organism will not fuse during normal development, cell fusion plays a central function as part of the differentiation of specific cells at determined times during development. Currently, for most cell fusion events it is not known what makes a particular cell membrane fusogenic, while most cell membranes will never fuse. This is in contrast to the highly fusogenic intracellular membranes that are constantly fusing during exocytic and endocytic transport events.

From fertilization to organogenesis, cell fusion has important developmental functions. Little is known about the molecular and cellular mechanisms that prevent most cells from fusing, and how membrane fusion is triggered, executed and completed in certain cells. Healthy individuals require normal sperm–egg fusion to procreate and defective fertilization may identify the proteins required during sperm–egg fusion. In addition, lack of homotypic fusion between myoblasts, pre-osteoclasts or trophoblasts will certainly result in lethality or major diseases. However, human diseases where any cell fusion is clearly defective have not been characterized, probably due to early embryonic lethality or severe placentation defects. Candidate diseases where cell fusion may be compromised include infertility, muscle diseases with small or immature muscle fibers, cancers with giant multinucleated cells, preclampsia and placental implantation defects.

While many cell adhesion molecules have been implicated in binding between gametes of opposite sexes from yeast to vertebrates [1–7], there is little evidence for these molecules being responsible for post-binding membrane merger activities. Members of the ADAM family of type I membrane glycoproteins with metalloprotease and disintegrin domains have been considered as candidate fusion proteins (fusogens or fusases) for sperm–egg and myoblast–myoblast fusion in vertebrates [8–11]. However, homologs in invertebrates do not appear to participate in cell fusion [12–18] and recent studies in vertebrates have not demonstrated a direct role for ADAM proteins in cell membrane merger [19–23]. Recently, tetraspanin surface receptors have been implicated in sperm–egg interactions [24–26]; however, studies in phagocytes suggest that CD9 and CD81 tetraspanins may prevent and not promote cell fusion [27]. Other adhesion membrane glycoproteins, including CD47 and CD44, have been implicated in cell–cell interactions required for mononuclear pre-osteoclasts binding and cell fusion in bones [28–31]. Here, we will further discuss and compare the process of cell fusion in the formation of muscles and epithelial organs in vertebrates and invertebrates.

10.2.1 Muscles

10.2.1.1 Vertebrates

During embryonic development stem cells differentiate into muscle cells that will form muscle fibers. These muscle fibers cannot proliferate, so the number of fibers is determined embryonically in vertebrates. In the first stage of muscle development, embryonic muscle cells fuse to form primary fibers. In the second stage of fetal development, several secondary fibers grow on each primary fiber [32]. Muscle fibers are formed by the fusion of myoblasts and each muscle fiber is a syncytial cell containing thousands of nuclei. In humans, each skeletal muscle contains many long and tubular muscle fibers. Each muscle fiber ranges in size from only about 1 mm to a few centimeters in length and their diameters vary from ten to a few hundred micrometers. While muscle fibers cannot

divide, in times of muscle growth and increased protein synthesis, additional nuclei are provided by cell fusion of muscle satellite cells formed during embryogenesis. Thus, post-embryonic cell fusion appears to be a strategy to increase the size of differentiated muscle fibers that cannot proliferate and this process is believed to occur during hypertrophy (e.g. exercise), in degenerative muscular diseases and in injuries [32].

Many studies in vertebrate muscle cells in tissue culture have identified numerous adhesion molecules, proteases, kinases, phospholipases, channels, growth factors and signaling molecules implicated in myoblast fusion [9, 33–43]. It remains to be determined whether any of these *in vitro* studies are applicable to *in vivo* model systems [44–46].

10.2.1.2 *Drosophila*

In the fruit fly, muscle formation can be studied *in vivo* and many mutations that affect myoblast fusion have been identified [44, 46–49]. The muscle fibers in *Drosophila* are smaller syncytial cells that contain fewer nuclei than in vertebrates, and its development takes hours compared to days and weeks in vertebrates [46]. Based on elegant molecular genetic studies combined with ultrastructural analyses of wild-type and mutants in *Drosophila* (Fig. 10.1), researchers have proposed a path-

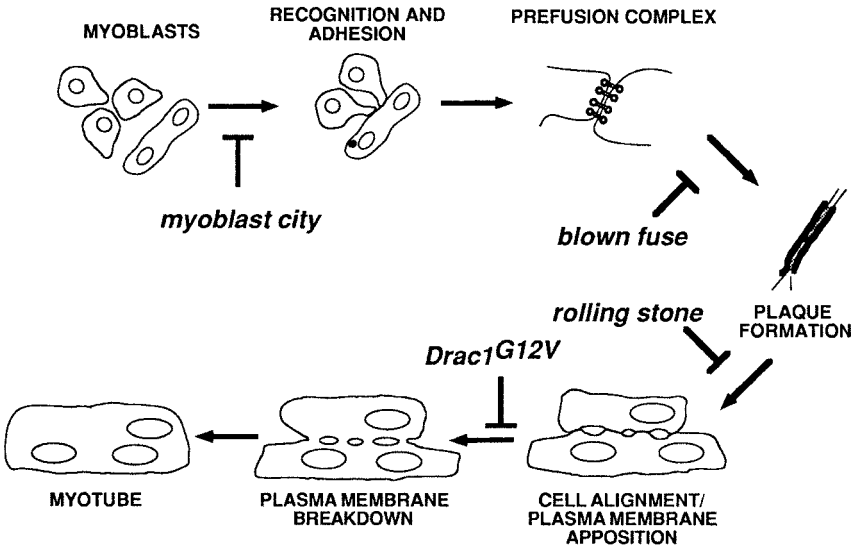

Fig. 10.1 Model of intermediate steps in myoblast fusion in *Drosophila*. Proposed schematic of the steps of myoblast fusion at the ultrastructural level, indicating the action point of each mutant. (Reprinted from [50], © 1997 with permission from Rockefeller University Press).

way that includes recognition, adhesion and transduction of putative fusion signals from the cell surface to the cytoskeleton [46, 50, 51].

Myoblast Fate Determination, Attraction, Recognition and Adhesion Two populations of myoblasts have been characterized in *Drosophila*: muscle founder/pioneer cells and fusion-competent cells [44–46, 52]. Determination of the fate of the fusion-competent cells and the founder cells depends on the activities of transcription factors and cell–cell interactions [44–46, 52]. Founder cells expressing specific identity or selector genes attract fusion-competent cells using membrane receptors containing immunoglobulin superfamily (IgSF) domains [53, 54]. In turn, fusion-competent cells expressing different IgSF receptors [55–57] migrate extending filopodia, recognize and adhere to the founder cell forming the contact zone (CZ) [50]. It has been shown that cell–cell recognition and adhesion is mediated by specific IgSF receptors [47, 57]. Interestingly, formation of multinucleated osteoclasts in vertebrates, involves transmembrane glycoproteins that also belong to the IgSF [29].

Vesicle Pairs in a Pre-fusion Complex The next step in myogenesis is the formation of a characteristic pre-fusion complex containing pairs of vesicles of around 40 nm diameter containing electron dense "coats" (Fig. 10.2 A–C). These pairs of coated vesicles appear symmetrically aligned along the juxtaposed cell membranes [50].

Myoblast city, a cytoplasmic protein with Src homology (SH3), Crk and Docker domains and homologous to the vertebrate Dock180 and the *C. elegans* protein CED-5 required for phagocytosis of cell corpses, appears to have a function in this stage [44, 58]. Other activities that are required in the early pre-fusion stages involve the intracellular protein Antisocial/Rolling pebbles expressed in the founder cell and containing a lipolytic domain, ATP- and GTP-binding sites, ankyrin repeats, and coiled-coil domains [59, 60].

Formation of an Electron-dense Plaque or Junctional Complex The next morphological intermediate appears to be the formation of a 10-nm thick and around 500-nm long electron-dense plaque extending along the cytoplasmic face of the apposed plasma membranes in the CZ with diffuse electron-dense material also present in the extracellular space (Figs. 10.1 and 10.2 D) [50]. It is not known what the molecular components of this electron-dense plaque are, but it is tempting to speculate that the IgSF membrane receptors, other adhesion molecules and cytoskeletal components may be associated to these structures.

This step requires the activity of Blown fuse, a cytoplasmic protein with a plexin homology (PH) domain [50]. The involvement of the intracellular proteins Blown fuse and Antisocial in the pre-fusion complex formation as well as other cytoskeletal (D-Titin and Paramyosin) and signal transduction components such as Loner, a founder cell-specific ADP-ribosylation factor GDP-exchange protein (ARF-GEP) and three different GTPases (Drac1, Drac2 and dARF6) suggests that there are signal transduction pathways linked to myoblast fusion [51, 61]. In particular, it

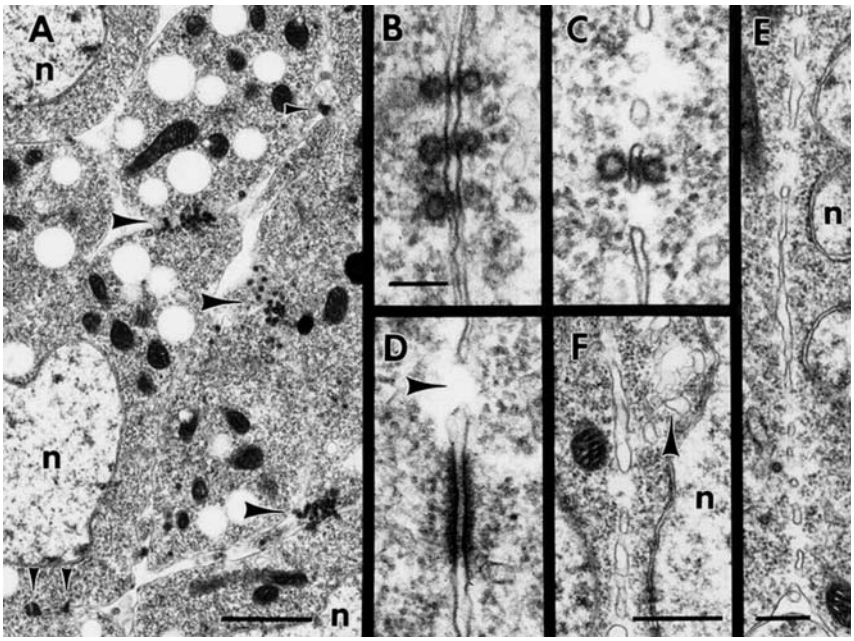

Fig. 10.2 Ultrastructure of intermediate steps in myoblast fusion in *Drosophila*. Electron micrographs of wild-type myoblast fusion in early stage 13 embryos. All the stages of the fusion process occur simultaneously in various parts of the developing musculature.
(A) Myoblasts in early stage of fusion. Note pre-fusion complexes at points of cell–cell contact (arrowheads); n = myoblast nuclei.
(B) Three sets of paired vesicles. Note electron-dense material in the extracellular space between pairs of vesicles.
(C) Paired vesicles oriented across a vesiculating pair of plasma membranes.
(D) An electron-dense plaque near a region of actively fusing membrane; note fusion pore (arrow).
(E) Fusion pores in a vesiculating plasma membrane.
(F) Later-stage vesiculating plasma membrane. The membrane sacs have increased in width and a group of irregular clear vesicles is present (arrowhead).
Bars: (A) 1 µm; (B–D) 100 nm; (E) 250 nm; (F) 500 nm.
(Reprinted from [50], © 1997 with permission from Rockefeller University Press).

appears that Antisocial and Loner are recruited independently to the sites of fusion by one of the IgSF receptors [51]. The presence of a lipolytic enzyme signature sequence in Antisocial suggests that a cytoplasmic lipase could modify the inner leaflet, catalyzing fusion from the opposite side of the plasma membranes. In summary, the proposed signaling pathway would be initiated in the IgSF membrane receptors through adaptors and intracellular signals that would be transduced to the cytoskeleton [46]. Cytoskeleton modifications may be required for plaque formation and/or for the next steps in the process.

Cell Alignment, Plasma Membrane Apposition and Pore Formation After or during the formation of the plaques, the cells align longitudinally closely apposing their cell membranes in the CZ. This is followed by the formation of multiple small pores or microfusions that appear to have a diameter between 20 and 50 nm by transmission electron microscopy (TEM) (Fig. 10.2 C–D). From three-dimensional reconstructions of serial sections it is not clear whether the pores are circular in cross-section. It is conceivable that the pores are connected or that each pore originated from an independent membrane fusion event [50].

In *rolling stone/rost* mutant embryos, there is accumulation of extensive electron-dense plaques and the plasma membranes between aligned myoblasts appear closer than in wild-type with little fusion detected [50]. It is proposed that removal of membrane glycoproteins from the CZ is required before close apposition of the membranes. This could be accomplished by proteolysis or by movement of the proteins outside the CZ. In *rost* mutants the removal of the proteins in the CZ may be eventually completed, explaining the closer than normal distance between the membranes after disappearance of the plaques [50]. *rost* molecular identity is not clear [49, 62, 63] and, based on the phenotypes observed by TEM, *rost* may be involved in removal of the electron dense plaques or in membrane merger [50].

In *drac1* dominant-negative mutant embryos [61], the plaques appear to form, elongate and align normally (Fig. 10.1). However, the juxtaposed cell membranes in the CZ have abnormal morphology with few or no pores and it was estimated that fusion failed in 90% of the myoblasts. It was proposed that Drac1 is required for a late step in plasma membrane pore formation [50].

Vesiculation: Microfusion Expansion to Macrofusion The next step is vesiculation (also called plasma membrane breakdown; Fig. 10.2 C, E and F). The plasma membranes form vesicles along their shared lengths, and the plasma membrane remnants are probably recycled resulting in vesicles and the formation of a myotube [50]. Candidate mutations affecting this stage have not been described.

Later in development, additional mononucleated fusion-competent cells extend filopodia towards multinucleated muscle precursors initiating a second wave of cell fusion that results in growth of syncytial myotubes [46, 52].

10.2.2 *C. elegans*

C. elegans, a free-living nematode worm, is a robust genetic system to analyze developmental cell fusion because it has a high number of invariant epithelial and myoepithelial cell fusions [64]. Three hundred somatic cell fusion events occur during different stages of development in distinct tissues from the mouth to the tail [64–73]. While in *Drosophila* cell fusion has been described in muscles and in humans cell fusions have been confirmed in only three organs, i.e. skeletal muscles, placenta and bones, in *C. elegans* one-third of all somatic cells

reproducibly fuse in muscles, gland and epithelia of the pharynx, epidermis (hypodermis), uterus, vulva, excretory gland, and male tail. Interestingly, the body wall muscle cells responsible for locomotion are not syncytial and only a few pharyngeal muscles fuse in *C. elegans*. Both epithelial and muscle developmental cell fusion in *C. elegans*, as in other organisms, has been divided in the following steps: (1) proliferation, cell fate determination and differentiation; (2) cell migration; (3) cell–cell recognition and adhesion; (4) membrane fusion; and (5) mixing of cytoplasmic contents and rearrangement of the cytoskeleton. For the purpose of this chapter we will concentrate on the last two steps.

10.2.2.1 **Epithelial Cell Fusion Assay in *C. elegans***

Most developmental fusions in *C. elegans* are between cells that first differentiate into components of polarized epithelial tissues. There are apical junctions (AJ) marking the apical borders between epithelial cells [74]. After cell–cell fusion the AJ between any two cells disassembles, indicating the fusion of the juxtaposing membranes. TEM of cells before and after fusion has demonstrated that disappearance of AJ correlates with membrane fusion. The dynamic behavior of AJs during cell fusion has been well documented [64, 69, 70, 75–81].

10.2.2.2 **Control of Cell Fusion**

As in *Drosophila* and vertebrates, a number of transcription factors and signaling pathways are known that control epithelial and muscle differentiation and distinct cell fusion events in *C. elegans* [82–101]. Signaling pathways active upstream of cell membrane fusion will not be discussed. The identified cell-specific regulators of cell fusion affect a few restricted events resulting in hyperfusion when there is loss of function of the regulator. However, until recently no proteins involved in the actual membrane merger event had been identified. The prediction is that knocking down any gene required for cell fusion will result in hypofusion or complete fusion failure.

10.2.2.3 **Developmental Genetics of Cell Fusion in *C. elegans***

Screens using mutagenized transgenic *C. elegans* strains expressing AJM-1::GFP were designed to identify mutants in which epithelial cells are properly differentiated and patterned but fail to fuse. Two such mutants, *eff-1(oj55)* and *eff-1(hy21)*, were isolated in independent screens and failed to complement each other. Mutant *eff-1(oj55)* was isolated by Bill Mohler and John White in a screen for embryonic epidermal fusion defects, while *eff-1(hy21)* was isolated by Gidi Shemer in a distinct conditional screen for vulva morphogenesis and cell fusion defects. Both mutations result in subviable worms that have deformed bodies and behavioral defects associated with cell fusion failure [102]. Additional alleles of *eff-1* have been recently isolated in different screens (Gattegno, Assaf and Podbilewicz, unpublished results).

10.2.2.4 *eff-1* Mutant Epidermal Cells do not Initiate Cell Membrane Fusion

eff-1 mutant embryos have a specific block in all epidermal cell fusion events. In both wild-type and *eff-1* mutant embryos the epidermal cells are born, and undergo normal migration and patterning events forming an epidermal monolayer. However, all of the 43 cells that would normally fuse to form eight syncytia containing between two to 23 nuclei remain distinct in *eff-1*, failing to fuse as the embryo elongates.

Mixing of cytoplasm between Green Fluorescent Protein (GFP)-labeled and unlabeled cells in live embryos can be followed in wild-type cells as cell fusion progresses. In contrast, in *eff-1* mutant embryos cytoplasmic GFP remains contained within single epidermal cells, demonstrating that cell fusion was blocked after recognition, AJ formation and tight adhesion in the CZ, but before membrane merger and cytoplasmic content mixing [102].

To determine whether the effects of *eff-1(hy21)* on larval epidermal cells were specific to the process of cell fusion, the behavior of cells and their AJs in larvae at different stages of development was studied. These epithelial cells were generated at the right stages of development, exhibited their appropriate cell lineage division patterns and interacted normally within the epithelium, making the correct cell contacts and migrations. However, the cells failed to fuse and abnormal ectopic extensions connect all regions of the epidermis. Thus, failures in cell fusion and syncytium formation result in the presence of "unfused" cells in the epidermis of *eff-1(hy21)* worms. Unfused seam cells produce defective cuticular structures, and ectopic cell junctions persist between the progeny of the seam cells and ventral cells even in the adult. In summary, the morphology and behavior of the unfused epithelial cells by light microscopy appears normal, except that the plasma membranes, CZs and cell junctional complexes remain intact and unfused cells send processes that abnormally link epidermal cells [88, 102, 103].

TEM of mutant *eff-1(hy21)* L4 grown at the restrictive temperature shows normal ultrastructure of the hypodermal membranes (Fig. 10.3 A). The extra seam cells that failed to fuse form multilayered stratified epithelia that are not seen in wild-type animals containing the characteristic epithelial monolayer. Higher magnification of the unfused epithelial cells shows that the distance between two plasma membranes in the CZs that failed to fuse is, as in wild-type, between 9 and 13 nm. The ultrastructure of the AJ and membranes appear normal except for the appearance of autophagocytic organelles that may be a way in which cells try to dispose excess membranes [103].

10.2.2.5 *eff-1*-mediated Cell Fusion is Essential for Healthy Organogenesis

Widespread, but precise, cell fusion failure in epidermal, tail and vulval cells is consistent with the interpretation that a block in cell fusion may prevent normal morphogenesis in these organs. The general anatomy and behavior are also compromised since *eff-1* animals are deformed, dumpy and uncoordinated, suggesting that *eff-1* activity is also required for normal growth, organ morphology and movement [73, 88, 102, 103].

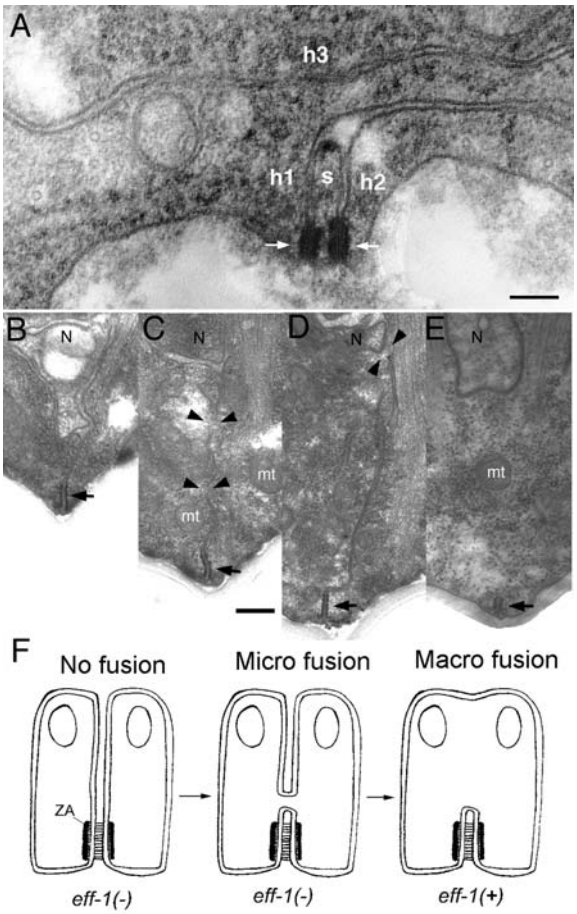

Fig. 10.3 TEM of unfused epidermal and muscle cells.
(A) Transverse thin section of mutant *eff-1(hy21)* L4 grown at the restrictive temperature shows normal ultrastructure of the hypodermal membranes, where the separation between apposing plasma membranes that failed to fuse is generally between 9 and 13 nm as in wild-type. The ultrastructure of the AJs (arrows) and membranes appears normal. Here a seam cell process (s) narrows and three neighboring hypodermal cells (h1, h2, h3) remain unfused along the lateral body wall. The lateral cuticle lies along the bottom edge of the panel.
(B–F) TEM of pharyngeal muscle pairs shows variable fusion failure in a mutant *eff-1(hy21)* adult grown at the restrictive temperature or successful fusion in wild-type cells.
(B) Two cells have failed to fuse, leaving a persistent cell border running from the neuron process (N) to the AJ (arrows).
(C and D) Two pairs of cells have formed microfusions (arrowheads) above the AJ, which are so small that no mitochondria (mt) could pass.
(E) Two wild-type cells have fully fused below the neuron process (N), leaving behind a complete AJ on the plasma membrane of the fused cell pair.
(F) Model showing a pathway for pharyngeal muscle homotypic fusion based on TEM intermediates. ZA, zonula adherens is a component of the AJ [74] (B–E).
Scale bars: 100 nm.
(Reprinted from [103], © 2004 with permission from Elsevier).

10.2.2.6 *eff-1* Encodes Novel Type I Membrane and Secreted Proteins

eff-1 was cloned to study its molecular activity in epithelial cell fusion using transformation rescue, RNA interference and sequencing of mutant alleles compared to wild-type [102]. *eff-1* encodes four alternatively spliced isoforms – two predicted type-I membrane proteins and two secreted proteins (WormBase 2003; http://www.wormbase.org). Homologs of *eff-1* were identified in the closely related free-living nematode *C. briggsae* and in a variety of animal and plant parasitic nematodes [88]. The EFF-1 predicted membrane proteins in *C. elegans* and *C. briggsae* share a single transmembrane domain and a large N-terminal ectodomain. This ectodomain contains cysteines that may form disulfide bonds, potential glycosylation sites and a 22-amino-acid internal putative fusion peptide [104]. A predicted coiled-coil domain characteristic of viral class I fusogens [105] was not found in neither of the predicted EFF-1 isoforms. Sequencing the coding regions from homozygous *eff-1* mutant worms revealed mutations of the putative proteins: from Pro183 to Leu in *eff-1(hy21)* and from Ser441 to Leu in *eff-1(oj55)* [102].

EFF-1 isoforms in *C. elegans* and in *C. briggsae* contain a predicted consensus phospholipase A_2 (PLA_2) aspartic acid active site. Although they lack other domains required for catalytic activity [106], the presence of the PLA_2 consensus raises two functional possibilities: (1) that EFF-1 may associate with another protein to reconstitute PLA_2 activity and (2) that this domain could act by interacting with phospholipids within membranes.

10.2.2.7 *eff-1* is Highly Expressed in Epidermal Cells Ready to Fuse

Expression of *eff-1p::gfp* was visualized in wild-type embryos and worms by confocal microscopy, and three- and four-dimensional reconstruction [73, 88, 102, 103, 107]. *eff-1p::gfp* expression was silent throughout the first third of embryogenesis, first appearing about 4 h after fertilization in a subset of epidermal precursor cells. Over the next 3 h, these and additional fluorescent cells were observed to migrate over the ventral and dorsal surfaces of the embryo, and most of the GFP-positive cells fused to form the hyp6 and hyp7 syncytia. Mononucleated epithelial cells remained non-fluorescent until shortly before initiation of cell fusion. Expression was seen in epithelial and non-epithelial organs known to fuse [102].

10.2.2.8 *eff-1* is Sufficient for Cell Membrane Fusion *in vivo*

It was shown that *eff-1* is required for cell fusion in *C. elegans*. To test whether *eff-1* is also sufficient to promote cell fusion, *eff-1* was ectopically expressed in wild-type and *eff-1* mutant animals using a heat-shock promoter. Less than 1 h after heat shock, epithelial seam cells ectopically fused to the epidermis, resulting in discontinuities in the anterior–posterior rows of lateral cells and confirmed by ectopic cytoplasmic content mixing between cells that do not normally fuse. This ectopic fusion was also apparent in the ventral epithelia as vul-

val precursor cells fused ectopically to the epidermis, resulting in aberrant vulvae. Thus, *eff-1* ectopic expression promotes ectopic fusion in normally non-fusogenic cells [103].

In summary, *eff-1* is not only necessary, but it is also sufficient to promote epithelial fusion *in vivo*. These experiments, together with evidence showing that different mutations in the Hox gene *lin-39/deformed/hoxD4* and other homeobox containing genes prevent downregulation of *eff-1* expression and suppression of specific epithelial cells fusions during restricted stages in development [73, 88, 107], strongly suggest that many epithelial cells are fusion competent and *eff-1* expression is sufficient to fuse cells [103].

10.2.2.9 **Tissue-specific Fusogenic Activity of *eff-1* in Pharyngeal Muscles**

In *C. elegans*, strong *eff-1* mutations block cytoplasmic content mixing, initiation of pore formation and plasma membrane breakdown in epithelial and myoepithelial cells (Fig. 10.3 A and B) [103]. Surprisingly, multiple stable 20- to 50-nm microfusions have been characterized in *eff-1* conditional mutants at the semi-restrictive temperature in pharyngeal muscles (myoepithelial cells; Fig. 10.3 C and D), but not in epidermal cells [103]. Thus, *eff-1* is required to initiate and expand cell–cell fusion in the muscles (Fig. 10.3 F). The mechanism of fusion pore expansion from a microfusion, that is not large enough to allow the free passage of mitochondria, to a completed macrofusion in myotubes or syncytial hypodermal cells is not known (see Fig. 10.5). It is interesting that the dense plaque (AJ) disappears during syncytia formation in epithelial cells of *C. elegans* as also occurs with the dense plaques in *Drosophila* myoblasts. However, in wild-type pharyngeal muscles of *C. elegans*, the AJ plaques remain even in the adult, marking the positions where the plasma membranes used to be before syncytia formation (Fig. 10.3 E and F).

Finally, there is tissue specificity in the fusogenic activity of this gene. While *eff-1* is essential and sufficient to initiate and complete cell fusion in epidermal and vulval cells, *eff-1* is not essential for the fusion of the gonadal anchor cell to uterine cells [103].

10.2.3
Comparison between Cell Fusion in a Worm, a Fly and Vertebrates

The major steps of developmental cell fusion are conserved in worms, flies and humans, and include differentiation, recognition, adhesion, alignment, membrane fusion and rearrangement of the cytoskeleton.

In human skeletal muscles each syncytial fiber contains thousands of nuclei, compared to around 30 nuclei in an insect muscle cell and exactly two, four, or 139 nuclei in each specific epithelial or myoepithelial syncytia in *C. elegans*. Something unique about cell fusion in worms is that the identity, number, position and behavior of the cells that fuse are invariant.

Pairing of vesicles in the CZ before cell membrane fusion is distinctive for *Drosophila* myoblasts [50]. While in *C. elegans* coated vesicles along the cytoplasmic domains of the plasma membranes have not been observed [70, 102, 103], in the muscle cell line L6 [108] and in primary cultures of quail myoblasts [109] vesicles with electron-dense materials have been observed and associated with myoblast fusion. It is not known what is the molecular and subcellular nature of the paired vesicles in the pre-fusion complex. It has been hypothesized that the symmetry of the paired vesicles may be due to the mechanics of homotypic cell fusion [50].

The electron-dense plaques formed in *Drosophila* prior to myoblast cell fusion are similar to plaques previously described in vertebrate myoblasts [110]. Interestingly, in *C. elegans* pharyngeal muscles, there is an AJ containing AJM-1 and other proteins characteristic of the zonula adherens forming an electron-dense plaque that is present before, during and after cell fusion [67, 103]. In contrast, in the epithelial cell fusions in *C. elegans*, the AJ disappears as the membrane fusion site expands from microfusion (25–50 nm) detected in electron micrographs to expanding macrofusion (250–20 000 nm) detected by confocal microscopy (Fig. 10.3) [70, 79, 81, 102, 103].

It is believed that specific membrane proteins are required to maintain cells in close proximity in the CZ before fusogenic proteins can act. In *blown fuse* mutants, electron-dense paired vesicles lining the cell border accumulate in *Drosophila* myoblasts. In *rolling stone* mutants, electron-dense plaques between unfused myoblasts accumulate to abnormally high levels. In *myoblast city* all membrane-associated pre-fusion complexes are absent [50]. These symmetrical junctional structures are postulated to be part of the pre-fusion complex in *Drosophila* myoblasts, perhaps delivering or holding fusogenic molecules in place on both membranes prior to fusion [50]. Similarly, gap junctions have been reported to be a necessary precursor to a fusion event in some vertebrate myoblasts and specific channel blockers can inhibit cell fusions [42, 111, 112]. These dense plaques are similar to adherens junctions and may be required at some sites of cell fusion, apparently to localize signaling or fusogenic molecules [50]. It has been proposed that adherens junctions provide such a function in the tail tip cells [70]. Unlike *Drosophila* myoblast fusions, no obvious pre-fusion complexes or vesicles participate in initiating cell fusions in the embryo or on the tail tip of *C. elegans*. Thus, in both the tail tip and the embryonic cell fusions, the fusing membranes appear to be maintained closely together by an adherens plaque or AJ, with fusion pore formation occurring at or very near the AJ [70, 79]. However, during the embryonic fusions but not in the tail tip, the AJs do not immediately disappear, but retreat away from the apical side toward more basal portions of the cell border, leading a front of fusions between adjacent cells beginning apically and progressing basally. In addition, vesiculation in the *C. elegans* embryonic hypodermal syncytia result in irregular 20- to 50-nm vesicles or tubules along the area formerly covered by the apposed plasma membranes similar to the vesicles observed in *Drosophila* myoblasts [50, 79]. However, in the tail tip, larger vesicles appear in the fusing cells, but not only where the apposed fusing membranes were localized [70].

Microfusions, also called fusion pores, ranging from 25 to 50 nm have been observed in *Drosophila* [50] and vertebrate myoblasts [40]. In *Drosophila*, a dominant-negative mutation in *drac1* appears to block pore formation. Interestingly, in *C. elegans* pharyngeal muscles, a complete block in *eff-1* activity results in a total failure in the initiation of cell fusion with no apparent discontinuities in the apposed plasma membranes [103]. However, partial loss of function in *eff-1* blocks cell fusion in a microfusion stage showing multiple 25- to 50-nm pores, very similar to the ones observed in myoblasts from *Drosophila* and vertebrates (Figs. 10.1–10.3). It is conceivable that the same protein, EFF-1, may be essential to initiate membrane merger and/or microfusion formation and also to expand these microfusions to a macrofusion in a syncytium.

After the cell membranes fuse there is a change in syncytial cell shapes within muscle fibers, epidermal syncytia, osteoclasts and syncytial trophoblasts [71–73], and in some cases there are simultaneous nuclear migrations within the newly formed syncytia [70]. These changes in syncytia shape must be accompanied by active changes in the cytoskeleton in these cells. The changes in cell shape may result from a migratory behavior, similar to other cell migrations involving a blunt leading edge or filopodia with the cell nucleus pressed close to the front and with thinner processes trailing behind the cells [70, 113]. In addition, the cell shape changes upon fusion may involve redistribution of large amounts of membranes from the site of fusion to a different domain of the newly formed syncytial cell [71, 72].

10.3 Cell Fusion in Diseases

Infertility, cancer, preeclampsia, muscle diseases, and parasitic, bacterial and viral infections are some of the diseases that may involve cell–cell fusion defects as part of their pathogenesis [104, 105, 114–117]. Here, we will discuss how enveloped viruses cause cell fusion.

10.3.1 Cell Fusion Mediated by Enveloped Viruses

Arguably, fusion mediated by viral glycoproteins remains the best-characterized example of a fusion reaction. Recent years have brought new experimental approaches to dissecting pathways of membrane and protein rearrangements in fusion. New findings indicate that fusion proteins drive the entire reaction and that completion of the fusion reaction is a harder job than the initiation of fusion.

Membrane fusion is an important stage of enveloped virus infection (see Chapter 12). While some viruses (e.g. influenza) first enter the cell by endocytosis and then fuse their envelope with the endosomal membrane upon acidification of the endosome, other viruses (e.g. HIV, measles and mumps) fuse direct-

ly with the plasma membrane. During replication of the viruses such as measles and mumps, expression of the fusion protein at the cell membrane can result in the fusion of neighboring cells, and the formation of multinucleated cells or syncytia that might be important for viral cell–cell spread and pathogenicity. Since several of the fusogenic envelope glycoproteins [e.g. influenza hemagglutinin (HA), HIV gp120/41 protein and E1 of Semliki Forrest virus] are among the best-characterized membrane proteins, exploration of viral fusion reactions is important not only for developing new antivirals but also as a model for ubiquitous biological fusion.

10.3.1.1 **Dissection of Viral Membrane Fusion**

Viral fusion is usually studied *in vitro* where the virus fuses with liposomes or target cells. In an alternative and widely used approach, viral fusion proteins are expressed in cells. Fusion of virus protein-expressing cells with target cells or with lipid bilayers is assayed as redistribution of membrane and aqueous content probes using fluorescence microscopy, spectrofluorimetry and electrophysiology. In many studies on the dissection of the viral fusion pathway, cell–cell fusion was slowed down or blocked at different stages by lowering temperature, modifying fusogenic proteins, decreasing their numbers, blocking their conformational changes by specific peptides and/or altering lipid composition to that unsuitable for fusion [118–128]. These studies suggest that viral fusion proceeds through a hemifusion intermediate (fusion of contacting membrane monolayers without merger of the inner monolayers), similar to those identified for fusion of protein-free lipid bilayers (for review, see [123]). HA-mediated hemifusion requires only a fraction of all HAs needed for complete fusion. Additional activated HAs stabilize the hemifusion connection and then expand it to allow lipid redistribution through it. HAs in still greater numbers advance the reaction beyond hemifusion to an opening and then irreversible expansion of a fusion pore connecting two aqueous volumes initially separated by the membranes. In brief, local merger of membranes into hemifusion and then fusion pore connections appear to be much less energy intensive than the subsequent stage of fusion pore expansion, still driven by the fusion proteins. The emerging pathway of viral fusion and the notion of the fusion pore expansion as the most demanding job for fusion proteins are further substantiated by studies on cell fusion mediated by HIV env proteins [129, 130] and on fusion mediated by retroviral envelope glycoproteins [128, 131, 132].

10.3.1.2 **Initiation and Expansion of Membrane Fusion**

Neither the mechanism(s) by which viral envelope glycoproteins form early fusion intermediates nor the mechanism(s) by which the proteins drive fusion pore expansion are known. However, while the former have been the subject of several hypotheses, the latter remain almost unexplored. Recent work on the mechanisms of protein-driven pore expansion was based on contrasting fusion with another

kind of membrane remodeling, i.e. fission of one membrane into two. Analysis of the best-characterized biological processes that involve membrane budding-off and fission emphasizes the critical role of protein coats. Formation of vesicles out of a plasma membrane and *trans*-Golgi membranes, trafficking of membrane vesicles between the endoplasmic reticulum, *cis*-Golgi and the Golgi cisternae, and budding of and release of enveloped viruses at the latest stages of viral morphogenesis all involve self-assembly of the coat proteins at the membrane surface. The protein coat spontaneously acquires a strongly curved shape, bends the membrane into a bud with a constricted neck and, finally, mediates lipid bilayer fission either on its own or with involvement of additional proteins. Since local fusion/expansion of the fusion pore and budding/fission rearrangements involve similar topological stages organized in the opposite order, a recent study suggests that an interconnected coat formed by membrane-bound activated fusion proteins generates the driving force for fusion [133].

10.3.1.3 **Protein–Protein and Protein–Lipid Interactions in Membrane Fusion**

The protein coat model of membrane fusion [133] assumes that activated fusion proteins form a dense interconnected protein coat (Fig. 10.4). This coat surrounds the developing fusion site and has an intrinsic shape, which is strongly curved in the direction opposite to that of the coat driving membrane budding and fission. The bending of the protein coat deforms the underlying lipid bi-

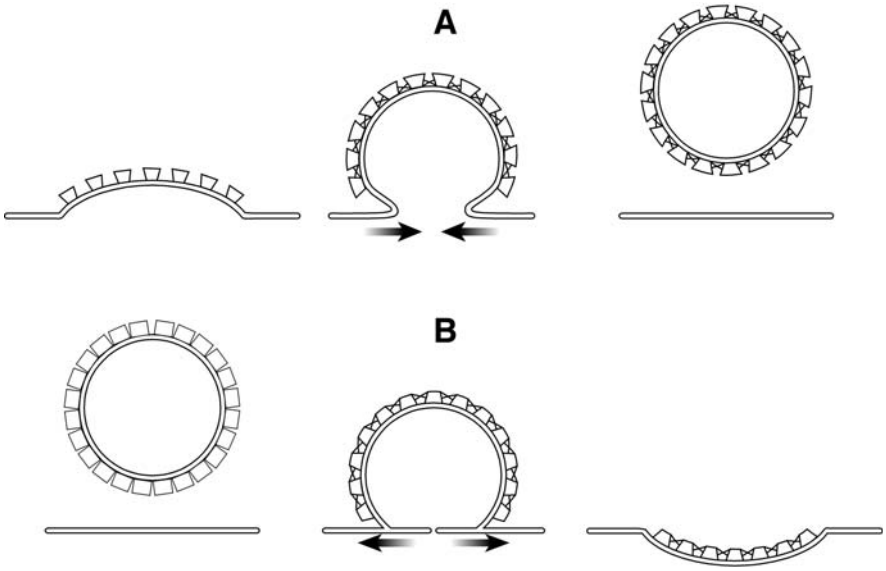

Fig. 10.4 Coat mechanism for membrane remodeling.
(A) Budding – fission. (B) Fusion – expansion of the fusion pore.
(Reprinted from [123] with permission from Annual Reviews).

layer, and produces tension that drives fusion and expands the fusion pore. In contrast to the models that describe only the earliest fusion stages that might yield local fusion intermediates, the protein coat model accounts for the force driving the fusion pore expansion until it reaches the dimension of the coat itself. For a virus, whose surface is completely covered by the coat, this means a complete insertion of the viral membrane into the target one.

10.3.1.4 **The Role of Fusion Proteins Outside the Fusion Site**

One of the most unexpected predictions of the fusion coat hypothesis is the possible functional role suggested for fusion proteins located outside of the fusion site. Based on the literature, it appears that proteins driving membrane merger in fusion and fission do it in radically different ways. Fission can and likely is mediated by proteins, which are not located between merging membranes [134, 135]. In contrast, fusion has been generally believed to result from the local action of only those fusion proteins, which are located in the CZ between the membranes and interact directly with the target membrane [136–140]. However, until recently the role of the fusion proteins outside of the CZ had not been tested.

The role of the "outsider" fusion proteins was studied for HA-mediated fusion in a recent study [141]. While both outsiders and insiders undergo similar restructuring at the pH of fusion [142], the inter-membrane contact in the CZ involves only a fragment of the viral or HA expressing cell surface, so that only some of the HAs, referred to as "insiders", are situated inside the CZ, while the rest – the "outsiders" – cannot directly interact with the target membrane. To differentiate between the fusogenic actions of the insider and the outsider HAs, different agents that inhibit or promote HA fusogeneity were conjugated to polystyrene beads too large to enter very tight and extended CZs between HA cells and bound red blood cells. Bead-conjugated antibodies that bind to HA, and proteases that cleave HA, specifically target HA outsiders, but leave HA insiders intact. The results in this experimental system indicate that changes in the fusogenic properties of HA outsiders have significant effects on fusion with the latest fusion stage of a fusion pore expansion being most sensitive [141].

10.3.1.5 **HA Insiders Initiate Hemifusion and HA Outsiders Expand Fusion Pores**

The mechanisms by which the proteins that at the time of the activation are located outside of the CZ directly influence the most energy-intensive stages of fusion leading to opening and expansion of a fusion pore remain to be understood. Since early fusion intermediates are not affected by the HA outsider-targeting agents, fusion might involve two radically different activities of the same fusion protein HA. First, local action of HA insiders generates local hemifusion. In contrast, the subsequent transition from hemifusion to the expanding fusion pore might be driven by HAs located outside of the initial fusion site. The achieved fusion phenotype might depend on the total number of activated HAs including both insiders and outsiders. At the highest HA densities, only the most advanced

fusion stage, an expansion of the fusion pore, depends on HA outsiders and is inhibited by the bead-conjugated agents. For lower density of activated HAs, outsiders are required even for lipid mixing. While the discovered involvement of HA outsiders in fusion can be readily explained by the fusion coat mechanism, it is also possible that HA-mediated fusion develops along the circumference rather than in the central region of the CZ, allowing HA outsiders located in the immediate proximity to the CZ circumference to significantly affect fusion. The functional role of fusion proteins located outside of the CZ strengthens a tempting hypothesis that the oppositely directed processes of membrane fusion and fission work according to a common principle: the proteins drive membrane remodeling from outside of the zone of the actual membrane rearrangement.

Clearly, opening of an initial fusion pore of around 0.5 nm is only the beginning of the fusion reaction [143]. Even after reaching 15 nm in diameter, fusion pores can still close [144]. The transition from an initial flickering pore to an irreversibly expanding fusion pore depends on having sufficient number of activated fusion proteins (see above) and on the structure of the fusion proteins. Mutations and deletions in different regions of viral envelope glycoproteins, i.e. fusion peptide [145], transmembrane domain [127, 146] and cytoplasmic region [125, 147, 148], block fusion pore dilation. In addition, fusion pore expansion versus pore resealing depends on the lipid composition of the membranes. For instance, the incorporation of cholesterol into the target lipid bilayer greatly decreases the number of flickers and the first pore formed usually irreversibly expands [149].

10.3.1.6 **Models for Final Expansion of Fusion Pores**

Even when fusion connections become irreversible and the fusion pore reaches the largest size resolvable by electrophysiological assays, and by following redistribution of usual aqueous probes (e.g. 6-nm diameter, 70-kDa dextran [150]) with fluorescence microscopy, further enlargement is required for successful completion of the fusion reaction. The characteristic size of a rod-shaped influenza virus ribonucleoprotein that is delivered into cytosol of the infected cell by endosome/envelope fusion is around 10–20 nm in diameter and 20–80 nm in length [151]. Syncytia formation involves the enlargement of a cytoplasmic bridge between cells to the cell-size scale of many microns.

The mechanisms that underlie these late fusion stages and their dependence on the proteins that initiated fusion remain almost unexplored. In general, the final enlargement of an aqueous connection between fusing membranes can proceed by four radically different scenarios (Fig. 10.5). First, it can be a radial expansion of a single fusion pore formed in the central part of the CZ. Second, the enlargement of the cytoplasmic bridge might involve excising of a CZ disk by a pore(s) that form(s) at and grow(s) along the CZ edge. This unexpected pathway was discovered for vacuole fusion, where proteins that regulate docking and fusion accumulate at the edge of the CZ [152]. The third scenario suggests that after earlier fusion stages, two membranes in the CZ are connected by multiple expanding fusion pores. Further development of these pores is topolog-

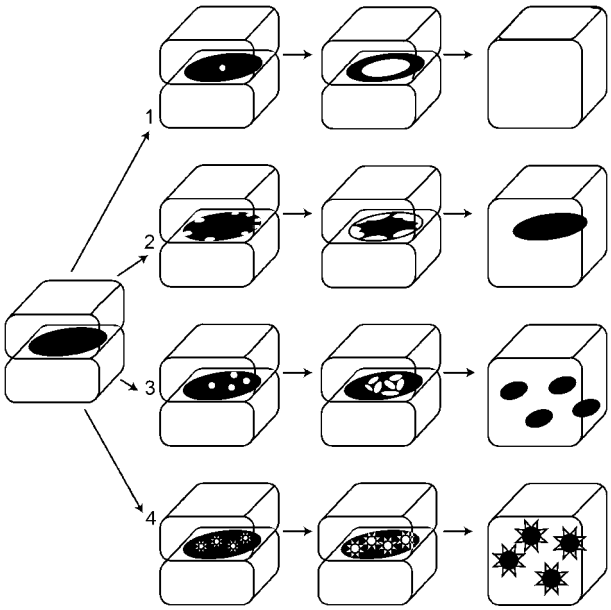

Fig. 10.5 Models of the final enlargement of fusion pores. We show here four different pathways by which two contacting cells at the left (the tight CZ is shown in black) can completely join their volumes in a final syncytium at the right. (1) Opening of a single pore within a CZ is followed by its radial expansion over the entire CZ. (2) Initial pores are formed only along the edge of the CZ. Enlargement of the pores proceeds along the edge and finally excises a CZ membrane disk released into the volume of the fused cell as a membrane vesicle. (3) Expansion of multiple fusion pores formed within CZ results in its breakdown into vesicles. (4) Vesiculation of the CZ is controlled and catalyzed by cell protein machinery shown as triangular shapes surrounding pores and then vesicles.

ically impossible and subsequent widening of the cytoplasmic bridge involves spontaneous vesiculation of the CZ [153]. While the fourth scenario also suggests vesiculation of the CZ, in this case the vesiculation is controlled and catalyzed by the cell machinery that might include dynamin, actin and other proteins involved in intracellular processes of membrane fission. Note that resealing of wounds in the plasma membrane, a process analogous to membrane vesiculation, but oppositely directed, is driven by the intracellular fusion machinery [154]. The CZ disassembly by cell-controlled vesiculation might be triggered by opening of a single or multiple fusion pores.

The specific mechanisms of the late fusion stages, including the nature of the driving force, and the involvement of the cytoskeleton and membrane trafficking machinery of the cell, in the generation and control of this force remain to be understood. For syncytia formation, late fusion stages most likely involve dynamic changes in cytoskeletal structures. As shown for cell fusion induced by an electric field [155, 156], a few minutes after fusion initiation bundles of microtubules be-

gin to extend into the cytoplasmic bridges between the cells, establishing connection between cytoskeletal networks of two cells. Actin bundles condensed at cell edges might widen the bridges by lamellipodial extension. In contrast to electrofusion initiation that can be achieved at 4 °C, the cytoskeleton-dependent stages of syncytia formation downstream of local fusion proceed only upon raising the temperature to 37 °C [157]. This interesting finding along with a recent discovery of long-living intercellular connections between cells of 50–200 nm diameter [158] indicate that both stabilization and widening of these connections might be controlled by the cellular machinery. Thus, late stages of cell fusion likely involve proteins different from the fusion machinery that generated the fusion pores.

10.4 Dissection of Developmental Fusion Based on Viral Fusion Analogies

In this section we will discuss different strategies already tested in viral systems that can be applied to study more complex developmental cell fusion systems.

10.4.1 Activation of a Developmental Fusogen

EFF-1 is a unique candidate for a developmental cell fusogen or fusase. This is because (1) *eff-1* mutants block cell fusion at a stage that is after recognition and adhesion, (2) cell fusion fails before early membrane fusion events, prior to microfusion (pore formation) as detected by TEM and prior to cytoplasmic content mixing as detected by fluorescence microscopy, (3) *eff-1* is expressed in cells prior to cell fusion, and (4) ectopic expression of EFF-1 proteins in cells that do not normally fuse induces ectopic fusion, thus *eff-1* is both necessary and sufficient for cell fusion in *C. elegans*. To test whether EFF-1 needs to be activated at the time of fusion it will be necessary to identify the trigger. The trigger could be a certain threshold concentration of protons or calcium. Alternatively, binding to an unknown EFF-1 receptor could trigger activation of the candidate fusogen. In addition, it is conceivable that a certain concentration of EFF-1 in the membrane is necessary to initiate the fusion reaction.

10.4.2 Dissection of Developmental Cell Fusion

To separate the process of developmental cell fusion into additional stages it would be useful to describe the kinetics of the process and change conditions that will block or slow down the rates of initiation of cell fusion, microfusion (pore formation) and macrofusion (pore expansion). This can be accomplished using different temperatures, additional mutations, changing the concentrations of EFF-1, changing the lipid composition of the membranes and other treatments that have been extensively used for viral fusion reactions.

10.4.3
Direct Cell Fusion Promotion or Indirect Relaxation of Fusion Blocks

It is conceivable that cells fuse when a fusogen is expressed and activated as occurs in viral-induced membrane fusion. Alternatively, the fusogen could be lifting mechanisms that prevent cell fusion by maintaining the plasma membranes separated. Interestingly, in *Drosophila* several adhesion molecules from the IgSF have been found to participate in the recognition and adhesion between myoblasts. It is conceivable that if the adhesion is too strong and stable, it will prevent cells from fusing. Different mutations and concentrations of adhesion receptors and fusion inducers may play a role in maintaining the cells separate or triggering cell–cell fusion. Finally, the apparent morphological similarity between the myoblast–myoblast electron-dense plaques in vertebrates and *Drosophila* compared to the electron-dense AJs in *C. elegans* myoepithelial pharyngeal muscles and epithelial cells suggests a simple mechanistic similarity with the coat hypothesis of membrane fusion and fission. Microfusions of 20–50 nm diameter appear near or at the electron-dense plaques (Fig. 10.2C and D), from this region the pore(s) expand, and it is tempting to hypothesize that the coat of electron-dense material may have an active role in the expansion of the fusion pore during developmental and viral induced cell fusions.

10.5
Concluding Remarks

Undoubtedly the mechanisms of most important developmental fusion reactions remain obscure at present. However, recent advances in the characterization of specific developmental fusion reactions along with methodology and mechanistic motifs emerging from the work on simpler examples of cell fusion suggest that this research field is ready for rapid progress. Cross-fertilization between developmental systems that have identified numerous pre-fusion molecules involved in recognition, binding, signal transduction and cytoskeletal reorganization (e.g. *Drosophila*) could help other systems where the pre-fusion genes have not been identified (e.g. *C. elegans*), but where a strong candidate for a fusion protein has been identified. Finally, all of the developmental systems will benefit from using the expertise generated over several decades on the studies of viral fusogens. Clearly, in all complex and simpler systems the late stages of cell membrane fusion deserve more attention because initiating membrane fusion reactions is not sufficient to complete the formation of a syncytial cell.

Acknowledgments
We thank Elizabeth Chen for discussions and advice on *Drosophila* myoblast fusion. We thank our past and current collaborators for enjoyable discussions. Supported by grants from the Israel Science Foundation, Binational Science Foundation, Fund for the Promotion of Research at the Technion and HFSP to B. P.

References

1 A. Singson, K.B. Mercer, S.W. L'Hernault, *Cell* **1998**, *93*, 71–79.
2 B.D. Shur, M.A. Ensslin, C. Rodeheffer, *Curr. Opin. Cell Biol.* **2004**, *16*, 477–485.
3 J. Trueheart, G.R. Fink, *Proc. Natl Acad. Sci. USA* **1989**, *86*, 9916–9920.
4 M.G. Heiman, P. Walter, *J. Cell Biol.* **2000**, *3*, 719–730.
5 P. Primakoff, D.G. Myles, *Science* **2002**, *296*, 2183–2185.
6 X.Z. Xu, P.W. Sternberg, *Cell* **2003**, *114*, 285–297.
7 P.M. Wassarman, L. Jovine, E.S. Litscher, *Nat. Cell Biol.* **2001**, *3*, E59–64.
8 T.G. Wolfsberg, J.M. White, *Dev. Biol.* **1996**, *180*, 389–401.
9 T. Yagami-Hiromasa, T. Sato, T. Kurisaki, K. Kamijo, Y.-i. Nabeshima, A. Fujisawa-Sehara, *Nature* **1995**, *377*, 652–656.
10 A.-P. Huovila, E.A. Almedia, J.M. White, *Curr. Opin. Cell Biol.* **1996**, *8*, 692–699.
11 C.P. Blobel, T.G. Wolfsberg, C.W. Turck, D.G. Myles, P. Primakoff, J.M. White, *Nature* **1992**, *356*, 248–252.
12 B. Podbilewicz, *Mol. Biol. Cell* **1996**, *7*, 1877–1893.
13 X. Huang, P. Huang, M.K. Robinson, M.J. Stern, Y. Jin, *Development* **2003**, *130*, 3147–61.
14 M. Doron, C. Valansi, B. Podbilewicz. Presented at *Int.* C. elegans *Meeting*, Los Angeles, CA, **2001**, abstr. 716,
15 C. Wen, M.M. Metzstein, I. Greenwald, *Development* **1997**, *124*, 4759–4767.
16 R. Blelloch, J. Kimble, *Nature* **1999**, *399*, 586–590.
17 H. Qi, M.D. Rand, X. Wu, N. Sestan, W. Wang, P. Rakic, T. Xu, S. Artavanis-Tsakonas, *Science* **1999**, *283*, 91–94.
18 K. Nishiwaki, N. Hisamoto, K. Matsumoto, *Science* **2000**, *288*, 2205–2208.
19 C. Cho, D.O. Bunch, J.E. Faure, E.H. Goulding, E.M. Eddy, P. Primakoff, D.G. Myles, *Science* **1998**, *281*, 1857–1859.
20 C. Cho, G. Haiyan, D. Branciforte, P. Primakoff, D.G. Myles, *Dev. Biol.* **2000**, *222*, 289–295.
21 K. Shirakabe, S. Wakatsuki, T. Kurisaki, A. Fujisawa-Sehara, *J. Biol. Chem* **2001**, *276*, 9352–9358.
22 D. Nath, P.M. Slocombe, A. Webster, P.E. Stephens, A.J. Docherty, G. Murphy, *J. Cell Sci.* **2000**, *113*, 2319–2328.
23 N. Kawaguchi, X. Xu, R. Tajima, P. Kronqvist, C. Sundberg, F. Loechel, R. Albrechtsen, U.M. Wewer, *Am. J. Pathol.* **2002**, *160*, 1895–1903.
24 M. Chen, K. Tung, S. Coonrod, Y. Takahashi, D. Bigler, A. Chang, Y. Yamashita, P. Kincade, J. Herr, J. White, *Proc. Natl Acad. Sci. USA* **1999**, *96*, 11830–11835.
25 K. Kaji, S. Oda, S. Miyazaki, A. Kudo, *Dev. Biol.* **2002**, *247*, 327–334.
26 F. Le Naour, E. Rubinstein, C. Jasmin, M. Prenant, C. Boucheix, *Science* **2000**, *287*, 319–321.
27 Y. Takeda, I. Tachibana, K. Miyado, M. Kobayashi, T. Miyazaki, T. Funakoshi, H. Kimura, H. Yamane, Y. Saito, H. Goto, T. Yoneda, M. Yoshida, T. Kumagai, T. Osaki, S. Hayashi, I. Kawase, E. Mekada, *J. Cell Biol.* **2003**, *161*, 945–956.
28 A. Vignery, *Int. J. Exp. Pathol.* **2000**, *81*, 291–304.
29 X. Han, H. Sterling, Y. Chen, C. Saginario, E.J. Brown, W.A. Frazier, F.P. Lindberg, A. Vignery, *J. Biol. Chem.* **2000**, *275*, 37984–37992.
30 H. Sterling, C. Saginario, A. Vignery, *J. Cell Biol.* **1998**, *143*, 837–847.
31 C. Saginario, H.-Y. Qian, A. Vignery, *Proc. Natl Acad. Sci. USA* **1995**, *92*, 12210–12214.
32 M.J. Rennie, H. Wackerhage, E.E. Spangenburg, F.W. Booth, *Annu. Rev. Physiol.* **2004**, *66*, 799–828.
33 A. Entwistle, R.J. Zalin, A.E. Warner, S. Bevan, *J. Cell Biol.* **1988**, *106*, 1703–1712.
34 M.J. Wakelam, in *Current Topics in Membranes and Transport*, Duzgunes, N., Bronner, F. (eds). Academic Press, Orlando, FL, **1988**.
35 H. Li, S.K. Choudhary, D.J. Milner, M.I. Munir, I.R. Kuisk, Y. Capetanaki, *J. Cell Biol.* **1994**, *124*, 827–841.
36 M.J.O. Wakelam, *Biochem. J.* **1985**, *228*, 1–12.
37 S. Barnoy, T. Glaser, N.S. Kosower, *Biochem. Biophys. Res. Commun.* **1996**, *220*, 933–938.

38 K. A. Knudsen, A. F. Horwitz, *Dev. Biol.* **1977**, *58*, 328–338.
39 K. A. Knudsen, *J. Cell Biol.* **1985**, *101*, 891–897.
40 N. Kalderon, N. B. Gilula, *J. Cell Biol.* **1979**, *81*, 411–425.
41 C. B. Couch, W. J. Strittmatter, *Cell* **1983**, *32*, 257–265.
42 R. M. Mege, D. Goudou, C. Giaume, M. Nicolet, F. Rieger, *Cell Adhes. Commun.* **1994**, *2*, 329–343.
43 C. A. Charlton, W. A. Mohler, G. L. Radice, R. O. Hynes, H. M. Blau, *J. Cell Biol.* **1997**, *138*, 331–336.
44 S. M. Abmayr, L. Balagopalan, B. J. Galletta, S. J. Hong, *Int. Rev. Cytol* **2003**, *225*, 33–89.
45 M. V. Taylor, *Curr. Biol.* **2000**, *10*, 646–648.
46 E. H. Chen, E. N. Olson, *Trends Cell Biol.* **2004**, *14*, 452–460.
47 H. A. Dworak, H. Sink, *BioEssays* **2002**, *24*, 591–601.
48 M. Frasch, M. Leptin, *Cell* **2000**, *102*, 127–129.
49 A. Paululat, A. Holz, R. Renkawitz-Pohl, *Mech. Dev.* **1999**, *83*, 17–26.
50 S. K. Doberstein, R. D. Fetter, A. Y. Mehta, C. S. Goodman, *J. Cell Biol.* **1997**, *136*, 1249–1261.
51 E. H. Chen, B. A. Pryce, J. A. Tzeng, G. A. Gonzalez, E. N. Olson, *Cell* **2003**, *114*, 751–762.
52 M. Bate, *Development* **1990**, *110*, 781–804.
53 M. Ruiz-Gomez, N. Coutts, A. Price, M. V. Taylor, M. Bate, *Cell* **2000**, *102*, 189–198.
54 M. Strunkelnberg, B. Bonengel, L. M. Moda, A. Hertenstein, H. G. de Couet, R. G. P. Ramos, K. F. Fischbach, *Development* **2001**, *128*, 4429–4439.
55 B. A. Bour, M. Chakravati, J. M. West, A. M. Abmayr, *Genes Dev.* **2000**, *14*, 1498–1511.
56 R. D. Artero, I. Castanon, M. K. Baylies, *Development* **2001**, *128*, 4251–4264.
57 H. A. Dworak, M. A. Charles, L. B. Pellerano, H. Sink, *Development* **2001**, *128*, 4265–4276.
58 E. Rushton, R. Drysdale, S. M. Abmayr, A. M. Michelson, M. Bate, *Development* **1995**, *121*, 1979–1988.
59 E. H. Chen, E. N. Olson, *Dev. Cell* **2001**, *1*, 705–715.
60 S. D. Menon, W. Chia, *Dev. Cell* **2001**, *1*, 691–703.
61 L. Luo, L. Y. Joyce, J. L. Yeh, J. Y. Nung, *Genes Dev.* **1994**, *8*, 1787–1802.
62 A. Paululat, A. Goubeaud, C. Damm, S. Knirr, S. Burchard, R. Renkawitz-Pohl, *J. Cell Biol.* **1997**, *138*, 337–348.
63 A. Paululat, S. Burchard, R. Renkawitz-Pohl, *Development* **1995**, *121*, 2611–2620.
64 B. Podbilewicz, J. G. White, *Dev. Biol.* **1994**, *161*, 408–424.
65 J. E. Sulston, H. R. Horvitz, *Dev. Biol.* **1977**, *56*, 110–156.
66 J. E. Sulston, E. Schierenberg, J. G. White, J. N. Thomson, *Dev. Biol.* **1983**, *100*, 64–119.
67 D. G. Albertson, J. N. Thomson, *Philos. Trans. R. Soc. Lond. B Biol. Sci.* **1976**, *275*, 299–325.
68 E. M. Hedgecock, J. G. White, *Dev. Biol.* **1985**, *107*, 128–138.
69 A. P. Newman, J. G. White, P. W. Sternberg, *Development* **1996**, *122*, 3617–3626.
70 C. Q. Nguyen, D. H. Hall, Y. Yang, D. H. A. Fitch, *Dev. Biol.* **1999**, *207*, 86–106.
71 B. Podbilewicz, *Nematology* **2000**, *2*, 99–111.
72 G. Shemer, B. Podbilewicz, *Dev. Dyn.* **2000**, *218*, 30–51.
73 G. Shemer, B. Podbilewicz, *BioEssays* **2003**, *25*, 672–682.
74 E. Knust, O. Bossinger, *Science* **2002**, *298*, 1955–1959.
75 S. E. Baird, D. A. Fitch, I. A. A. Kassem, S. W. Emmons, *Development* **1991**, *113*, 515–526.
76 B. B. Wang, M. M. Muller-Immergluck, J. Austin, N. T. Robinson, A. Chisholm, C. Kenyon, *Cell* **1993**, *74*, 29–42.
77 R. J. Sommer, *Development* **1997**, *124*, 243–251.
78 R. Sharma-Kishore, J. G. White, E. Southgate, B. Podbilewicz, *Development* **1999**, *126*, 691–699.
79 W. A. Mohler, J. S. Simske, E. M. Williams-Masson, J. D. Hardin, J. G. White, *Curr. Biol.* **1998**, *8*, 1087–1090.
80 G. Shemer, R. Kishore, B. Podbilewicz, *Dev. Biol.* **2000**, *221*, 233–248.

81 M. Koppen, J. S. Simske, P. A. Sims, B. L. Firestein, D. H. Hall, A. D. Radice, C. Rongo, J. D. Hardin, *Nat. Cell Biol.* **2001**, *3*, 983–991.

82 S. G. Clark, A. D. Chisholm, H. R. Horvitz, *Cell* **1993**, *74*, 43–55.

83 S. Alper, C. Kenyon, *Development* **2001**, *128*, 1793–1804.

84 Q. Ch'ng, C. Kenyon, *Development* **1999**, *126*, 3303–3312.

85 K. Koh, J. H. Rothman, *Development* **2001**, *128*, 2867–2880.

86 Z. Chen, M. Han, *Curr. Biol.* **2001**, *11*, 1874–1879.

87 K. Koh, S. M. Peyrot, C. G. Wood, J. A. Wagmaister, M. F. Maduro, D. M. Eisenmann, J. H. Rothman, *Development* **2002**, *129*, 5171–5180.

88 G. Shemer. *PhD Thesis*, Technion – Israel Institute for Technology, Haifa **2002**.

89 S. Alper, C. Kenyon, *Development* **2002**, *129*, 3335–3348.

90 L. Chen, M. Krause, M. Sepanski, A. Fire, *Development* **1994**, *120*, 1631–1641.

91 M. Krause, *BioEssays* **1995**, *17*, 219–228.

92 H. R. Horvitz, P. W. Sternberg, *Nature* **1991**, *351*, 535–541.

93 J. E. Gleason, H. C. Korswagen, D. M. Eisenmann, *Genes Dev.* **2002**, *16*, 1281–1290.

94 M. Wang, P. W. Sternberg, *Curr. Topics Dev. Biol.* **2001**, *51*, 189–220.

95 T. von Zelewsky, F. Palladino, K. Brunschwig, H. Tobler, A. Hajnal, F. Muller, *Development* **2000**, *127*, 5277–5284.

96 L. Nilsson, X. Li, T. Tiensuu, R. Auty, I. Greenwald, S. Tuck, *Development* **1998**, *125*, 4809–4819.

97 J. N. Maloof, C. Kenyon, *Development* **1998**, *125*, 181–190.

98 D. M. Eisenmann, J. N. Maloof, J. S. Simske, C. Kenyon, S. K. Kim, *Development* **1998**, *125*, 3667–3680.

99 K. Kornfeld, *Trends Genet.* **1997**, *13*, 55–61.

100 I. Greenwald, in C. elegans *II*, Riddle, D. L., Blumenthal, T., Meyer, B. J., Priess, J. R. (eds.). Cold Spring Harbor Laboratory Press, Cold Spring Harbor, NY, **1997**.

101 M. Labouesse, S. Mango, *Trends Genet.* **1999**, *15*, 307–313.

102 W. A. Mohler, G. Shemer, J. del Campo, C. Valansi, E. Opoku-Serebuoh, V. Scranton, N. Assaf, J. G. White, B. Podbilewicz, *Dev. Cell* **2002**, *2*, 355–362.

103 G. Shemer, M. Suissa, I. Kolotuev, K. C. Q. Nguyen, D. H. Hall, B. Podbilewicz, *Curr. Biol.* **2004**, *14*, 1587–1591.

104 L. D. Hernandez, L. R. Hoffman, T. G. Wolfsberg, J. M. White, *Annu. Rev. Cell Dev. Biol.* **1996**, *12*, 627–661.

105 R. Blumenthal, M. J. Clague, S. R. Durell, R. M. Epand, *Chem. Rev.* **2003**, *103*, 53–69.

106 A. Dessen, J. Tang, H. Schmidt, M. Stahl, J. D. Clark, J. Seehra, W. S. Somers, *Cell* **1999**, *97*, 349–360.

107 G. Shemer, B. Podbilewicz, *Genes Dev.* **2002**, *16*, 3136–3141.

108 L. C. Engel, M. W. Egar, R. J. Przybylski, *Eur. J. Cell Biol.* **1986**, *39*, 360–365.

109 B. H. Lipton, I. R. Konigsberg, *J. Cell Biol.* **1972**, *53*, 348–364.

110 J. E. Rash, D. Fambrough, *Dev. Biol.* **1973**, *30*, 166–186.

111 A. A. Proulx, Z. X. Lin, C. C. Naus, *Cell Growth. Differ.* **1997**, *8*, 533–540.

112 A. Proulx, P. A. Merrifield, C. C. Naus, *Dev. Genet.* **1997**, *20*, 133–144.

113 E. M. Hedgecock, J. G. Culotti, D. H. Hall, B. D. Stern, *Development* **1987**, *100*, 365–382.

114 J. S. Sutton, L. Weiss, *J. Cell Biol.* **1966**, *28*, 303–332.

115 T. A. Robertson, J. M. Papadimitriou, M. D. Grounds, *Neuropath. Appl. Neurobiol.* **1993**, *19*, 350–358.

116 D. Duelli, Y. Lazebnik, *Cancer Cell* **2003**, *3*, 445–448.

117 A. J. Mighell, P. A. Robinson, W. J. Hume, *J. Oral. Pathol. Med.* **1996**, 25–29.

118 L. V. Chernomordik, V. A. Frolov, E. Leikina, P. Bronk, J. Zimmerberg, *J. Cell Biol.* **1998**, *140*, 1369–1382.

119 E. Leikina, L. V. Chernomordik, *Mol. Biol. Cell* **2000**, *11*, 2359–2371.

120 G. B. Melikyan, H. Jin, R. A. Lamb, F. S. Cohen, *Virology* **1997**, *235*, 118–128.

121 G. B. Melikyan, R. M. Markosyan, H. Hemmati, M. K. Delmedico, D. M. Lambert, F. S. Cohen, *J. Cell Biol.* **2000**, *151*, 413–423.

122 G. B. Melikyan, J. M. White, F. S. Cohen, *J. Cell Biol.* **1995**, *131*, 679–691.

123 L. V. Chernomordik, M. M. Kozlov, *Annu. Rev. Biochem.* **2003**, *72*, 175–207.

124 C. J. Russell, T. S. Jardetzky, R. A. Lamb, *EMBO J* **2001**, *20*, 4024–4034.

125 R. E. Dutch, R. A. Lamb, *J. Virol.* **2001**, *75*, 5363–5369.

126 G. W. Kemble, T. Danieli, J. M. White, *Cell* **1994**, *76*, 383–391.

127 R. T. Armstrong, A. S. Kushnir, J. M. White, *J. Cell Biol.* **2000**, *151*, 425–438.

128 G. B. Melikyan, R. J. Barnard, R. M. Markosyan, J. A. Young, F. S. Cohen, *J. Virol.* **2004**, *78*, 3753–3762.

129 R. M. Markosyan, F. S. Cohen, G. B. Melikyan, *Mol. Biol. Cell* **2003**, *14*, 926–938.

130 F. S. Cohen, G. B. Melikyan, *J. Membr. Biol.* 2004 **199**, 1–14.

131 R. M. Markosyan, P. Bates, F. S. Cohen, G. B. Melikyan, *Biophys. J.* 2004.

132 S. Matsuyama, S. E. Delos, J. M. White, *J. Virol.* **2004**, *78*, 8201–8209.

133 M. M. Kozlov, L. V. Chernomordik, *Traffic* **2002**, *3*, 256–267.

134 K. N. Burger, *Traffic* **2000**, *1*, 605–613.

135 D. Corda, C. Hidalgo Carcedo, M. Bonazzi, A. Luini, S. Spano, *Cell Mol. Life Sci.* **2002**, *59*, 1819–32.

136 L. K. Tamm, J. Crane, V. Kiessling, *Curr. Opin. Struct. Biol.* **2003**, *13*, 453–466.

137 W. Weissenhorn, A. Dessen, S. C. Harrison, J. J. Skehel, D. C. Wiley, *Nature* **1997**, *387*, 426–430.

138 D. L. Gibbons, M. C. Vaney, A. Roussel, A. Vigouroux, B. Reilly, J. Lepault, M. Kielian, F. A. Rey, *Nature* **2004**, *427*, 320–325.

139 M. M. Kozlov, L. V. Chernomordik, *Biophys. J.* **1998**, *75*, 1384–1396.

140 J. Bentz, *Biophys. J.* **2000**, *78*, 886–900.

141 E. Leikina, A. Mittal, M. S. Cho, K. Melikov, M. M. Kozlov, L. V. Chernomordik, *J. Biol. Chem.* **2004**, *279*, 26526–26532.

142 D. C. Wiley, J. J. Skehel, *Annu. Rev. Biochem.* **1987**, *56*, 365–394.

143 G. B. Melikyan, L. V. Chernomordik, *Trends Microbiol.* **1997**, *5*, 349–355.

144 G. B. Melikyan, W. D. Niles, V. A. Ratinov, M. Karhanek, J. Zimmerberg, F. S. Cohen, *J. Gen. Physiol.* **1995**, *106*, 803–819.

145 C. Schoch, R. Blumenthal, *J. Biol. Chem.* **1993**, *268*, 9267–9274.

146 G. B. Melikyan, R. M. Markosyan, M. G. Roth, F. S. Cohen, *Mol. Biol. Cell* **2000**, *11*, 3765–3775.

147 C. Kozerski, E. Ponimaskin, B. Schroth-Diez, M. F. Schmidt, A. Herrmann, *J. Virol.* **2000**, *74*, 7529–7537.

148 G. B. Melikyan, S. Lin, M. G. Roth, F. S. Cohen, *Mol. Biol. Cell* **1999**, *10*, 1821–1836.

149 V. I. Razinkov, F. S. Cohen, *Biochemistry* **2000**, *39*, 13462–13468.

150 J. K. Jaiswal, S. Chakrabarti, N. W. Andrews, S. M. Simon, *PLoS Biol.* **2004**, *2*, E233.

151 G. R. Whittaker, M. Kann, A. Helenius, *Annu. Rev. Cell Dev. Biol.* **2000**, *16*, 627–651.

152 L. Wang, E. S. Seeley, W. Wickner, A. J. Merz, *Cell* **2002**, *108*, 357–369.

153 L. V. Chernomordik, A. E. Sowers, *Biophys. J.* **1991**, *60*, 1026–1037.

154 P. L. McNeil, R. A. Steinhardt, *Annu. Rev. Cell Dev. Biol.* **2003**, *19*, 697–731.

155 Q. A. Zheng, D. C. Chang, *Cell Motil. Cytoskeleton* **1990**, *17*, 345–355.

156 Q. Zheng, D. Chang, *J. Cell Sci.* **1991**, *100*, 431–442.

157 J. Teissie, M. P. Rols, C. Blangero, in *Electroporation and Electrofusion in Cell Biology*, Neumann, E., Sowers, A. E., Jordan, C. A. (eds). Plenum Press, New York, **1989**.

158 A. Rustom, R. Saffrich, I. Markovic, P. Walther, H. H. Gerdes, *Science* **2004**, *303*, 1007–1010.

11
Molecular Mechanisms of Intracellular Membrane Fusion

Olga Vites and Reinhard Jahn

11.1
Introduction

Eukaryotic cells are compartmentalized into organelles that are surrounded by phospholipid membranes. Both organellar membranes and the surrounding plasma membrane remain intact during the lifetime of the cell. However, membranes are highly dynamic structures that undergo continuous turnover by means of budding and fusion reactions.

With the exception of the mitochondria, chloroplasts and probably the peroxisomes, all intracellular membranes are derived from the ER (see full list of Abbreviations at the end of the chapter). The ER is the major site for *de novo* synthesis of membrane lipids and it is the origin of transport vesicles (or specialized cisternae) that serve as prime precursors for all intracellular membranes, including the plasma membrane. Originating from the ER, highly ordered membrane trafficking pathways connect the main intracellular organelles including the Golgi apparatus, the plasma membrane, early and late endosomes, and lysosomes. They also account for the generation and consumption of tissue- and cell-type-specific organelles such as secretory granules, synaptic vesicles and phagosomes. Together, these pathways are collectively referred to as the secretory pathway, although it should be borne in mind that they are not confined to secreting macromolecules produced inside the cell. In the secretory pathway, each trafficking step exhibits a high (but not absolute) degree of specificity. For instance, a transport vesicle originating from the ER will not fuse directly with the plasma membrane and a secretory vesicle destined to fuse with the plasma membrane will not fuse with another membrane. This specificity is an intrinsic feature of the organelles themselves that is encoded by specific proteins and controlled by several layers of regulation.

In this chapter we discuss molecular mechanisms of intracellular fusion events, with a special emphasis on the SNARE proteins that have emerged as

the leading candidates for the fusion catalysts in the secretory pathway. The reader is also referred to several recent reviews that provide in-depth coverage of aspects that can be only briefly discussed here (Bai and Chapman 2004; Bonifacino and Glick 2004; Dietrich et al. 2003; Fasshauer 2003; Jahn et al. 2003; Segev 2001; Sørensen 2004; Whyte and Munro 2002).

11.2 Intracellular Fusion Reactions – An Overview

What is needed for intracellular membranes to fuse successfully? First, the membranes need to "know" that a potential fusion partner is nearby, requiring signaling between the membranes. Second, some kind of "proofreading" of the partner membrane is needed to ensure that it is an appropriate fusion partner. Third, a firm physical contact must be established at the prospective fusion site, often referred to as docking. Finally, bilayer fusion is executed.

In the secretory pathway, fusion reactions are mediated by dynamic supramolecular complexes that are assembled before or during membrane contact and that are dissociated when fusion is completed. Although fusion events show enormous diversity with respect to speed and structure of the fusing membranes, many of the participating proteins belong to evolutionarily conserved protein families, suggesting common underlying mechanisms. Protein families involved in all fusion events include small GTPases of the Rab/Ypt family, the SNARE proteins and SM proteins. Rab GTPases cycle between GTP- and GDP-bound forms, and probably orchestrate the initial assembly of docking complexes. SNAREs are small membrane proteins that undergo assembly–disassembly cycles associated with large changes in energy and that probably catalyze membrane merger. SM proteins interact both with SNAREs and with other proteins, and probably provide scaffolds for the assembly of fusion-competent SNAREs. Rab proteins, SM proteins and SNAREs interact with a multitude of additional proteins. Some of the interacting proteins are shared between all fusion reactions including those involved in re-generating active Rabs and SNAREs such as GDI and NSF. Other proteins, however, only operate in a subset of intracellular fusion reactions or may even be confined to a specific cell type such as neurons. As far as is known, only the SNAREs and the regulatory synaptotagmins are integral membrane proteins. All other proteins are recruited to the membrane from cytoplasmic pools.

In recent years, it has become apparent that mitochondria possess their own fusion apparatus that is completely different from that of the secretory pathway (Westermann 2003). Mitochondria readily fuse with each other and split up again. They are surrounded by two membranes – an outer and an inner membrane – that need to fuse consecutively.

Genetic screens revealed that only one outer membrane protein is required for mitochondrial fusion (Dimmer et al. 2002). This protein, termed Fzo (the name is derived from the phenotype "fuzzy onions") forms a complex with the

GTPase Mgm1 that resides in the intermembrane space. In yeast these two proteins are linked into a complex by another outer membrane protein termed Ugo1p (Sesaki and Jensen 2004). Fzo protein contains an N-terminal GTPase domain and a C-terminal domain consisting of coiled-coil-like sequences separated by two transmembrane domains. Recently it has been shown that the C-terminal coiled-coil sequence forms antiparallel *trans*-dimers connecting the outer membrane of adjacent mitochondria and leaving a space of 10 nm between them (Koshiba et al. 2004). GTP hydrolysis performed by the N-terminal domain of Fzo was required for the subsequent fusion step. The newly developed mitochondrial fusion assay (Meeusen et al. 2004) revealed that no additional cytosolic factors are required for fusion. Fusion, however, is dependent on the proton electrochemical gradient across the inner mitochondrial membrane.

11.3 Tethering and Docking

Very little is known about the initial reactions. Recent advances in life cell imaging using fluorescently tagged proteins have shown that not only transport vesicles but also tubulo-vesicular structures dynamically move in cells, frequently making contact and spontaneously fusing with each other (Lippincott-Schwartz et al. 2000; Toomre et al. 2000). It is conceivable that (with the exception of regulated fusion events) physical contact between membranes suffices to trigger a reaction cascade leading to fusion, i.e. that membranes are constitutively competent for fusion. Physical contact allows for short-range signalling between the membranes, e.g. by "*trans*" interaction of certain proteins that then orchestrate the subsequent steps. Indeed, large proteins with elongated coiled-coil domains, capable of homomeric and heteromeric interactions, are involved in some fusion reactions where they may serve as long-range tethering factors. Examples include EEA1 that is involved in the fusion of early endosomes and p115 together with GM130 participating in the fusion within the Golgi apparatus (Christoforidis et al. 1999; Dumas et al. 2001; Nakamura et al. 1995; Sönnichsen et al. 1998). Pairing specificity might constitute a first proofreading step. In other fusion reactions, such factors have not been found, and it is thus unclear whether they are needed in all fusion reactions.

Rab proteins are essential factors in the assembly of the initial protein complexes at the fusion site (Zerial and McBride 2001). They operate as molecular switches that shuttle between an active GTP-bound and an inactive GDP-bound form. Interconversion is mediated by regulatory proteins termed GAPs and GEFs. Rab proteins contain long hydrophobic modifications (geranylgeranyl chains) attached to the C-terminus that mediate membrane attachment. The GDP–GTP cycle is accompanied by a membrane dissociation–rebinding cycle that again requires specific proteins for assistance (Seabra and Wasmeier 2004). GDI serves as a universal dissociation cofactor that appears to act upon all GDP-Rabs and extracts them from the membrane. Rebinding of Rab proteins is

assisted in some cases by proteins of the Yip/Pra1 family, which displace GDI from the complex with Rab-GDP and are called GDFs. Dissociation–association allows for removal of the Rab protein after the task is completed and re-insertion in the precursor membrane, thus avoiding complex recycling pathways as needed for the SNAREs (see below).

A vast number of diverse proteins are known to bind to active Rab proteins. Originally, it was assumed that each of the 60 known mammalian Rab proteins has its own set of binding partners (termed effectors). However, it is becoming apparent that some effectors and GEFs may be shared between multiple Rabs, e.g. rabaptin, the TRAPP complex and mss4 (Segev 2001). At present, there is no common denominator emerging between the effectors of different Rab proteins. Often Rab effectors form complexes with corresponding GEFs. In this manner they promote their own recruitment, keeping the Rab protein in an active state. Furthermore, some of the tethering factors discussed above are Rab effectors suggesting that they are recruited to the membrane in consequence of the activation of the respective Rab protein. Interestingly, Rab effectors include phosphatidylinositol-3-kinases and proteins containing FYVE or PX domains that bind to specific polyphosphoinositides. Polyphosphoinositides are central players in vesicle budding and fusion along the secretory pathway (Roth 2004), and it is thus likely that they operate in conjunction with Rab proteins.

Many Rab effectors are part of multiprotein complexes that are recruited to the prospective fusion site. These complexes include the exocyst (first characterized in yeast exocytosis), GARP, COG and TRAPP complexes that are involved in Golgi trafficking, and the HOPS/VpsC complex functioning in yeast vacuole fusion (Whyte and Munro 2002). In many cases the subunits of the tethering complexes provide a link to the fusion apparatus, e.g. by interacting directly with SNARE proteins as has been shown for the HOPS complex. The function of these multiprotein complexes is largely unknown. It is unlikely that they solely function as tethering factors. Their protein constituents are rather diverse. In some cases, they appear to be involved in forming links to the cytoskeleton (exocyst), in others they directly interact with SNAREs (HOPS/VpsC), but so far no common principles have emerged.

Little is known about the processes taking place between vesicle attachment and SNARE pairing. A tentative sequence of events involving several additional proteins in regulated association–dissociation cycles has been worked out for yeast vacuolar fusion (Wickner 2002; Wickner and Haas 2000). Similarly, assembly and disassembly of multiprotein complexes appears to be involved in yeast exocytosis (Hsu et al. 2004), but it is not known to which extent these findings can be extended to other intracellular fusion reactions.

11.4
SNARE Proteins – The Fusion Catalysts?

11.4.1
Assembly–Disassembly Cycle of SNARE Proteins

SNARE proteins comprise a superfamily of small proteins with 24 members in the yeast *Saccharomyces cerevisiae*, 23 members in *Caenorhabditis elegans*, 54 members in *Arabidopsis thaliana* (Uemura et al. 2004) and at least 35 members in mammals (Bock et al. 2001). Their molecular masses range from 10 to 35 kDa, with some notable exceptions of larger size. A characteristic feature of all SNAREs is a homologous stretch of 60–70 amino acids arranged in heptad repeats, referred to as the SNARE motif. Most SNAREs contain a single transmembrane domain at the C-terminal end that is connected to the SNARE motif by a short linker. Exceptions include the SNARE SNAP-25 and its relatives SNAP-23 and SNAP-29 in mammals, and Sec9p and Spo20 in yeast, which contain two SNARE motifs. These SNAREs lack a transmembrane domain, but (except SNAP-29) contain post-translationally added palmitoyl side-chains that serve as membrane anchor. Other exceptions include splicing variants of syntaxin 1c and the yeast SNARE Vam7p that contain single SNARE motifs and lack membrane anchor domains altogether. In addition, many SNAREs contain separately folded N-terminal domains (see Section 11.4.2; for review, see Chen and Scheller 2001; Fasshauer 2003; Jahn et al. 2003; Rizo and Südhof 2002).

Key to the understanding of SNARE proteins was the discovery of an assembly–disassembly cycle that is mediated by the SNARE motifs and that is associated with major conformational changes. Monomeric SNARE motifs are unstructured in solution. However, when appropriate SNAREs are combined, they spontaneously form α-helical bundles of extraordinary stability, referred to as core complexes (Fasshauer et al. 1997 b). The crystal structures of two only distantly related SNARE complexes revealed that core complexes are coiled-coils and contain four different α-helices (Antonin et al. 2002 b; Sutton et al. 1998). The core of the helical bundle contains 16 stacked layers of interacting side-chains that are mostly hydrophobic and highly conserved. In the center a "0" layer is formed by four polar residues (one arginine and three glutamines) that are almost completely conserved among the entire SNARE superfamily. Accordingly, the SNAREs are classified into four different subfamilies designated as Qa-SNAREs (syntaxins), Qb-SNAREs, Qc-SNAREs and R-SNAREs (Fasshauer et al. 1998). Each core complex contains one SNARE motif of each subfamily (QaQbQcR) that occupies a specific position in the complex. The division into these four subfamilies is strongly supported by features within the primary structure.

Assembled SNARE complexes are heat resistant. They only melt at temperatures above 75 °C. Alternatively, they require very strong denaturants (5 M guanidinium chloride) for dissociation. Interestingly, the unfolding–refolding transitions do not overlap, resulting in a profound hysteresis, with both reaction paths being essentially irreversible.

Disassembly of SNARE complexes is mediated by the ATPase NSF (Söllner et al. 1993a). On its own, NSF cannot interact with SNAREs, it requires cofactors (termed SNAPs) to first interact with core complexes. There are three isoforms of SNAP in mammalian cells termed α-, β- and γ-SNAP, with α-SNAP being the ubiquitous isoform. Three SNAPs bind to one SNARE core complex, and in turn NSF is recruited, resulting in a complex referred to as the 20S complex. Despite limited sequence homology between SNAREs, particularly with respect to residues exposed on the outer surface of the helical bundle, α-SNAP binds to all known SNARE complexes. In Sec17p, the yeast homolog of α-SNAP whose crystal structure is solved (Rice and Brunger 1999), two regions can be discerned – an N-terminal region in which nine α-helices are packed against each other in an antiparallel fashion, resulting in a bent sheet, and a C-terminal, more globular region that is primarily also composed of α-helices. Recently it has been shown that SNARE binding involves the concave surface of the N-terminal sheet and is mediated primarily by ionic interactions with side-chains in the middle region (i.e. around the "0" layer) of the SNARE complex (Marz et al. 2003). α-SNAP is aligned along the SNARE complex in an antiparallel fashion, with its N-terminus near the membrane and the C-terminus pointing outward. The C-terminal part is responsible for recruiting NSF. Mutations in the C-terminal region α-SNAP that exhibit impaired NSF binding, but display normal binding to SNAREs, are dominant inhibitors of membrane fusion.

NSF is a hexameric ATPase belonging to the AAA-ATPase superfamily (Whiteheart et al. 2001). AAA-ATPases are often operating as "unfoldases", i.e. they dissociate or unfold tightly packed proteins or protein aggregates (Lupas and Martin 2002). Each monomer consists of two homologous C-terminal domains, referred to as the D1 and D2 domain, respectively, that contain canonical ATP binding sites, and an N-terminal N domain (Wilson et al. 1989). NSF forms a double-barrel structure in which the D2 domain is responsible for oligomerization and is catalytically inactive, the D1 domain carries out ATP hydrolysis, and the N domains do the work by binding to the α-SNAP–SNARE complex and then undergoing major conformational changes upon ATP cleavage (Furst et al. 2003; Hanson et al. 1997). NSF only binds to α-SNAP when bound to SNARE complexes or when α-SNAP is artificially oligomerized or adsorbed to plastic. α-SNAP binding stimulates the ATPase activity of NSF. How exactly NSF dissociates the SNARE complex is still not clear. Apparently, the "0" layer is important for disassembly since its substitution by hydrophobic amino acids impairs disassembly (Scales et al. 2001). It is indeed fascinating how this enzyme, under physiological conditions, manages to rip apart a helical bundle so stable that it tolerates temperatures up to 80°C without denaturing. A full catalytic cycle of NSF involves cleavage of no less then six ATP units, certainly sufficient energy for the job. Without NSF, SNARE complexes cannot be dissociated, core complexes pile up and intracellular fusion reactions are blocked, as has been shown for temperature-sensitive NSF mutants both in yeast (Novick and Schekman 1979) and *Drosophila* (Littleton et al. 1998).

Although the role of NSF as a disassembly chaperone for SNARE complexes is well established, NSF has also been reported to bind to other proteins (White-

heart and Matveeva 2004) such as the glutamate receptor GluR2, the β_2-adrenergic receptor and protein complexes involved in trafficking (e.g. LMA-1, GATE-16, Rab effectors). SNAP proteins are apparently not required for these interactions. The functional significance of these interactions remains to be clarified, particularly with respect to the ATPase activity of NSF.

11.4.2 N-terminal Domains of SNAREs – Recruiting Proteins or Regulating SNARE Function?

The N-termini of SNARE proteins are more variable. Whereas some SNAREs, including a subgroup of R-SNAREs and some SNAP-25 homologs, possess only a few amino acids beyond the SNARE motif, others contain independently folded domains that are connected to the SNARE motif by linkers of varying size.

The most common domain is represented by an antiparallel three-helix bundle of variable length (Dulubova et al. 2001; Fernandez et al. 1998; Munson et al. 2000). This fold appears to be shared among all Qa-SNAREs. In addition, it appears to be present in at least some Qb- and Qc-SNAREs (Antonin et al. 2002a; Misura et al. 2002). Despite an astonishingly high degree of structural conservation (Dietrich et al. 2003), no hints for a common function have yet emerged. For instance, in yeast Sso1p the N-terminal domain is essential for fusion (Munson et al. 2000; Y. Wang et al. 2001) whereas in yeast Vam3p it is not (Laage and Ungermann 2001). In some Qa-SNAREs, including syntaxin 1, syntaxin 7 and Sso1/2p, the three-helix bundle is capable of forming an intramolecular complex with its own SNARE motif. No SNARE complexes can be formed when the Qa-SNARE is in this "closed" conformation, and mutations that prevent formation of the closed conformation accelerate SNARE binding and affect fusion (Margittai et al. 2003; Nicholson et al. 1998). However, other Qa-SNAREs such as Vam3p are incapable of forming such a closed conformation, rendering it unlikely that inhibiting SNARE motifs is the conserved function of these domains (Dulubova et al. 2001). Furthermore, the N-terminal domain of many Qa-SNAREs binds to SM proteins but again the mechanism of binding is not conserved (see Section 11.5). Thus it remains to be established whether the three helix bundles serve as tethering domains for the recruitment of other proteins to fusion sites and/or whether they are directly involved in regulating SNARE activity.

A separate fold, referred to as the longin domain, has been discovered in certain R-SNAREs including ykt6, VAMP7/Ti-VAMP, Sec22 and most plant R-SNAREs (Filippini et al. 2001; Gonzalez et al. 2001; Tochio et al. 2001). This globular fold is also present in other proteins such as profilins. Some data suggest that longin domains may also form intramolecular complexes with the SNARE motifs, but again this feature appears not to be shared by all subfamily members (Hasegawa et al. 2004; Martinez-Arca et al. 2003). Again, the molecular role of the longin domain remains to be established.

In addition to these common folds, certain SNAREs possess divergent N-termini. For instance, the Qc-SNARE Vam7p contains a PX domain that interacts with

specific polyphosphoinositides. Vam7p cycles off and on the membrane during vacuolar fusion, a feature for which the PX domain is essential (Boeddinghaus et al. 2002). Other examples include yeast Sec9p and Spo20p, two SNAP-25 homologs that possess large N-terminal extensions of unknown structure.

Finally, it should be mentioned that some large soluble proteins possess C-terminal SNARE motifs including tomosyn and amisyn. It has been suggested that these proteins regulate SNARE function by competing with genuine SNAREs (Hatsuzawa et al. 2003; Scales et al. 2002). For instance, the SNARE motif of tomosyn forms stable complexes *in vivo* and *in vitro* with neuronal SNAREs by substituting for synaptobrevin, resulting in a core complex of very similar structure (Pobbati et al. 2004).

11.4.3 "Zippering" Model for SNARE-mediated Membrane Fusion

The central role of SNARE proteins in all eukaryotic fusion reactions was established in the beginning of the 1990s by three independent lines of evidence: the interaction of neuronal SNAREs with NSF and α-SNAP, known to be essential components of intracellular fusion reactions, the identification of genes homologous to mammalian SNAREs as being responsible for defects in secretory pathway of yeast, and the discovery that all three neuronal SNARE proteins are specific targets of botulinum and tetanus neurotoxins, strong inhibitors of neuronal exocytosis (Ferro-Novick and Jahn 1994). Initially, it was assumed that SNAREs align in an antiparallel orientation, with NSF/SNAPs catalyzing membrane merger by means of injecting conformational energy (Söllner et al. 1993a). However, it was recognized early on that the SNAREs themselves may operate as the actual catalysts (Pelham et al. 1995; Südhof et al. 1993), particularly when it became apparent that NSF is not required in the final steps leading up to fusion (Hanson et al. 1997; Mayer et al. 1996). The discovery that after assembly all SNAREs are aligned in parallel, with their transmembrane domains grouped at one end of the complex, then led to the proposal of the "zippering" model (Hanson et al. 1997; Jahn and Hanson 1998; Lin and Scheller 1997) that is presently largely accepted. According to this model, it is the spontaneous assembly of SNARE proteins that drives membrane fusion. SNARE proteins facing each other on opposed membranes are thought to "zipper up" from the N-termini of the SNARE motifs towards their membrane associated C-termini, with the energy released during assembly being used to overcome the energy barrier for fusion. During fusion, the SNAREs are converted from a strained *trans*-configuration into a relaxed *cis*-configuration, with all SNAREs of the complex being aligned in one membrane. Regeneration of active SNAREs is then mediated by the action of the NSF disassembly machinery.

A large body of experimental evidence strongly supports this model. First, deletion or impairment of many SNAREs in yeast, mice, flies and worms results in massive defects of the respective fusion steps (Broadie et al. 1995; Nonet et al. 1998; Novick and Schekman 1979; Saifee et al. 1998; Schoch et al. 2001;

Washbourne et al. 2002). Second, many spontaneously generated SNARE mutants that were discovered because of fusion defects carry amino acid substitutions in the central layers (Fasshauer et al. 1998). Inappropriate packing during the zippering reaction is responsible for the defect although it cannot be excluded that the substitutions also affect other parts of the SNARE cycle such as disassembly (see below). Furthermore, defects caused by replacing one of the glutamines in the central "0" layer with an arginine can be rescued by converting the R-SNARE- arginine into a glutamine, documenting that appropriate assembly of the "0" layer is essential for fusion (Katz and Brennwald 2000; Ossig et al. 2000). Third, in an elegant study Hu et al. (Hu et al. 2003) showed that SNARE proteins that have been engineered to have the SNARE motifs facing outside instead of towards the cytoplasm are capable of fusing cells. Fourth, interference with SNAREs in cell-free fusion assays using antibodies, clostridial neurotoxins and competition by soluble SNARE motifs invariably blocks fusion (Antonin et al. 2000a; Ungermann and Wickner 1998). Finally, liposomes reconstituted with appropriate sets of SNAREs spontaneously fuse with each other in a reaction that is dependent on the formation of SNARE core complexes (Schütte et al. 2004; Weber et al. 1998).

While the zippering model invoking sequential zippering of the central layers of the complex is very attractive in its intuitive beauty, direct experimental evidence for this mechanism is still scarce. Recently, both exocytosis in cracked PC12 cells and SNARE-complex formation *in vitro* have been found to be inhibited by N-terminal, but not C-terminal, portions of SNARE motifs (Fasshauer and Margittai 2004; Matos et al. 2003), in agreement with the notion that N-terminal assembly precedes that of the C-terminal parts. On the other hand, Zhang et al. failed to detect a kinetic difference between assembly of the N- versus C-terminal positions but the time resolution of these experiments was not high (Zhang et al. 2004).

11.4.4
Trans-complexes – Intermediates in the Fusion Pathway?

Regulated exocytosis requires that one of the steps in the sequence of events leading to fusion is inhibited unless triggered by a second messenger (normally calcium ions). In neurons, the delay time between calcium influx and the onset of exocytosis is below 1 ms (Schneggenburger and Neher 2000), raising the question at which step precisely the control is exerted. With respect to the SNAREs, the question is whether a metastable intermediate state can exist for some time in which the SNAREs are partially zippered, connecting the membranes in *trans*-configuration, and if so how further zippering is regulated by other proteins.

Evidence for such metastable intermediates is primarily derived from studies on chromaffin cells. Here, exocytosis can be measured with high time resolution using capacitance patch-clamping (which monitors membrane surface changes associated with exocytosis) and carbon fiber amperometry (which mea-

sures release of transmitter by an electrochemical procedure) (for reviews, see Neher 1998; Rettig and Neher 2002). Chromaffin granules exist in distinct pools that differ in their kinetic behavior in exocytosis. At least four pools have been described: a cytoplasmic depot pool, a reserve pool representing unprimed but membrane-attached vesicles and two pools of primed vesicles that are released within seconds upon Ca^{2+} stimulation, referred to as the SRP and RRP, respectively. Each of the pools exhibits a characteristic time constant for exocytosis. Extensive studies by Neher et al. have shown that these pools are in dynamic equilibria with each other, with the reserve pool feeding into the SRP, and the SRP feeding into the RRP. When exocytosis is triggered by a jump in intracellular calcium, the RRP is depleted first, followed by the SRP. Then a sustained phase of exocytosis is observed which is thought to represent refilling of the releasable pools from the pool of docked vesicles.

In recent years, exocytosis of chromaffin cells has served as a powerful model to study intermediates in SNARE assembly. In particular, the role of the Qbc-SNARE SNAP-25 has been intensely studied because (1) due to its lack of transmembrane domains overexpression does not require elaborate membrane trafficking, resulting in efficient incorporation into the plasma membrane upon overexpression, and (2) chromaffin cells from transgenic mice lacking SNAP-25 are available, allowing for gain-of-function mutagenesis in a genetically clean background (Nagy et al. 2002, 2004; Sørensen et al. 2002, 2003).

Injection of monoclonal antibodies that differentiate between free and complexed SNAP-25 resulted in reduction of both the RRP and the reserve pool, whereas the SRP remained largely unaffected. These data were interpreted as evidence that the SRP is characterized by a "loosely" zippered intermediate whereas the RRP represents a more tightly packed intermediate (Xu et al. 1999). Pre-fusion arrest at the level of partially assembled SNARE complexes was also inferred from experiments on the crayfish neuromuscular junction (Hua and Charlton 1999). Here, it was shown that inhibition of exocytosis by tetanus toxin and botulinum neurotoxin D, that both require a free N-terminus of synaptobrevin for binding, was stimulation dependent. In contrast, inhibition by botulinum neurotoxin B, that binds synaptobrevin at the C-terminal end of the SNARE motif, was not dependent on stimulation, indicating that in a resting terminal the N-terminal, but not the C-terminal, part of synaptobrevin is engaged in a pre-fusion complex.

Interestingly, overexpression of a SNAP-25 variant containing a hydrophobic side-chain in the "0" layer caused no changes in the burst phase, but reduced the sustained phase and the response after repetitive stimulation, indicating a defect in the refilling of the exocytotic vesicles pool rather than during zippering of the SNAREs (Wei et al. 2000). However, it cannot be excluded that the defect is primarily caused by a defect in NSF-driven disassembly after fusion, particularly since "0" layer mutations have been shown to interfere with NSF-driven disassembly *in vitro* (Scales et al. 2001).

Partially zippered SNARE complexes may provide enough energy to keep membranes in close apposition, but other proteins probably regulate progres-

sion to full fusion. For neuronal exocytosis, prime candidates for those regulatory proteins are synaptotagmin, the Ca^{2+} sensor (Rizo and Südhof 1998), and complexin, a small cytosolic protein that binds to the surface of SNARE complexes and is proposed to stabilize the C-terminal part of the *trans*-SNARE complex (Marz and Hanson 2002). For synaptotagmin, two alternative mechanisms are currently under discussion which explain how it exerts its action (Bai and Chapman 2004): either through calcium-dependent binding to the *trans*-SNARE complex that is thought to trigger the completion of the zippering reaction or through interaction with phospholipids in the opposite membrane, resulting in the generation of a local bilayer defect that may further lower the energy barrier for fusion. Numerous studies (whose full discussion is beyond the scope of this chapter) have provided evidence that the calcium-binding modules of synaptotagmin (termed C2 domains) bind both to SNAREs and to acidic phospholipid in a calcium-dependent manner. Genetic deletion of synaptotagmin I leads to a massive loss of calcium-dependent exocytosis while leaving calcium-independent constitutive exocytosis unaffected (Geppert et al. 1994). Interestingly, the phenotype of complexin deletion is very similar to that of synaptotagmin I deletion, albeit with milder manifestations (Reim et al. 2001). These findings suggest that both proteins operate at the same step, i.e. regulation of partially zippered *trans*-complexes.

For the final fusion reaction it is assumed that a pulling force is exerted from the assembled SNARE complex on the transmembrane domains. Accordingly, one would expect that the linker between the assembled complex and the transmembrane domain is stiff. An insertion of three to five amino acids into the linker reduces fusion efficiency in liposome reconstitution assays (McNew et al. 1999; Y. Wang et al. 2001), suggesting that interference with the linker structure negatively affects force transduction. Computational analysis of the syntaxin linker using molecular dynamics supports the view that linker stiffness may substantially reduce the activation energy barrier for fusion. In contrast, spin labeling of the linkers of syntaxin (Kim et al. 2002) and synaptobrevin (Kweon et al. 2003) suggests that the linkers are tilted, with the side-chains partially penetrating into the membrane whereas a preformed ternary SNARE complex containing syntaxin 1, SNAP-25, and synaptobrevin 2 is "upright", i.e. perpendicular to the membrane plane (Kiessling and Tamm 2003).

Despite the central importance of the transmembrane domains for the proposed fusion mechanism, only few studies are available. The transmembrane domains of synaptobrevin and syntaxin 1 were shown to form of homo- and hetero-oligomers (Laage and Langosch 1997; Margittai et al. 1999). Whether this oligomerization is an *in vitro* artifact or related to function, e.g. by forming local clusters, is still unclear (Han et al. 2004; Roy et al. 2004). Furthermore, peptides corresponding to the transmembrane domains of synaptobrevin and syntaxin (Langosch et al. 2001) readily fuse liposomes. It is thus conceivable that the transmembrane domains, in addition to forming oligomers and transmitting mechanical force, also destabilize bilayer structure, thus lowering the activation energy for fusion.

11.4.5 Acceptor Complexes, Topology and Specificity

11.4.5.1 SNARE Acceptor Complexes

As discussed in Section 11.4.1, monomeric SNARE motifs are unstructured in solution, but they spontaneously assemble into core complexes, a reaction associated with a large drop in potential energy. However, assembly kinetics in solution is exceedingly slow, requiring many hours for completion (Fasshauer and Margittai 2004; Margittai et al. 2003; Nicholson et al. 1998). Furthermore, fusion of SNARE-containing liposomes is several orders of magnitude slower than biological fusion reactions (Weber et al. 1998) even when the liposomes are artificially docked before fusion (Schütte et al. 2004). For these reasons it is important to understand the assembly pathway, particularly if intermediates are conformationally arrested or if SNARE motifs are grouped into acceptor complexes of defined structure before the zippering reaction.

Detailed studies of SNARE assembly *in vitro* have revealed the presence of intermediates that have major impact on the overall reaction. The neuronal Q-SNAREs syntaxin 1 and SNAP-25 form a binary complex with a 2:1 stoichiometry (Fasshauer et al. 1997a). This complex also forms a four-helix bundle that is, however, less stable than the core complex, with the second syntaxin probably occupying the slot of synaptobrevin in the complex. For synaptobrevin to bind, one of the syntaxin molecules needs to be displaced. This replacement reaction may be rate limiting under *in vitro* conditions. Furthermore, evidence for an unstable intermediate containing partially folded syntaxin and SNAP-25 at a 1:1 stoichiometry has recently been obtained (Fasshauer and Margittai 2004). This intermediate may be the "real" acceptor, with synaptobrevin binding occurring at a much faster kinetics than to the binary 2:1 complex. Accordingly, the thermodynamically favored formation of a 2:1 complex would be viewed as a biological "dead-end" reaction, requiring the NSF-chaperone system for reactivation. Other intermediates have been observed such as homo-oligomers of SNARE motifs of syntaxin alone (Misura et al. 2001b), of syntaxin with the N-terminal SNARE motif of SNAP-25 (Misura et al. 2001a) or even of a complete SNARE complex in which synaptobrevin is aligned in antiparallel orientation (Weninger et al. 2003). Whether these reactions have any biological relevance remains to be seen, but they certainly have a major impact on the kinetics of *in vitro* assembly and fusion reactions involving purified SNAREs. Intriguingly, the corresponding yeast SNAREs Sso1p (syntaxin) and Sec9p (SNAP-25) also form a binary complex that, however, appears to be stable at a 1:1 stoichiometry (Fiebig et al. 1999; Nicholson et al. 1998). No interactions were observed between synaptobrevin and either syntaxin or SNAP-25 alone, i.e. synaptobrevin can only bind when both SNAP-25 and syntaxin are present.

The idea that SNAREs need to be grouped into acceptor complexes for efficient fusion is supported by studies addressing SNARE distribution and reactivity in native membranes. In plasma membranes, SNAREs are not uniformly distributed, but rather concentrated in microdomains that require cholesterol

for stabilization (Chamberlain et al. 2001; Lang et al. 2001). SNARE concentration in these domains is very high and fusion appears to take place exclusively at such domains. Furthermore, evidence for a syntaxin/SNAP-25 acceptor complex has been obtained with properties resembling that of the unstable 1:1 complex observed in *in vitro* studies. Intriguingly, SNAREs in freshly prepared native membrane are active, i.e. they readily bind recombinant partner SNAREs but in the absence of the NSF/SNAP disassembly system they inactivate over time due to the formation of endogenous SNARE complexes (Lang et al. 2002).

There are two take-home messages from these studies: (1) Formation of acceptor complexes consisting of, for instance, QaQbQc-SNAREs appears to constitute an essential intermediate step in fusion. It is conceivable that formation of such acceptor complexes is assisted by other proteins and that this activity comprises a crucial step in regulating SNARE activity. (2) It appears that SNAREs in native membranes are constitutively active although modulation of activity by mechanisms such as regulating closed versus open conformations (see above) cannot be excluded at present.

11.4.5.2 **Topology of SNAREs**

The zippering model of SNARE-mediated fusion requires that each of the membranes destined to fuse carries at least one SNARE with a transmembrane domain. The SNAREs involved in neuronal exocytosis were the first to be characterized, with the R-SNARE synaptobrevin being localized to the synaptic vesicle, and the Q-SNAREs syntaxin 1 (Qa) and SNAP-25 (Qbc) on the plasma membrane. This topology was originally used to classify SNAREs into v-SNAREs (for SNAREs present on transport vesicles) and t-SNAREs (for SNAREs present on the target membrane) (Söllner et al. 1993b). Indeed, in many cases of "heterotypic" fusion the transport vesicle contains the R-SNARE whereas the target membrane contains the Q-SNAREs. However, there are some notable exceptions that led to major confusions. For instance, in the fusion of ER-derived transport vesicles with the *cis*-Golgi in yeast, the transport vesicle contains three SNAREs [Sec22p (R), Bos1p (Qb) and Bet1p (Qc)], whereas the target membrane provides the Qa-SNARE (Sed5p). As result, the v-SNARE/t-SNARE classification does not correspond to the structurally defined subclasses, and groups SNAREs together that are biochemically and functionally non-equivalent. As a result, structurally erroneous combinations of SNAREs that violate the QabcR rule were used in liposome fusion assays (McNew et al. 2000; Parlati et al. 2000; Paumet et al. 2001). Similarly, the classification into SNARE "heavy" and "light" chains (Fukuda et al. 2000) does not follow structure-based subclasses. Recently, certain SNAREs operating in the Golgi complex have been analyzed for their ability to inhibit liposome fusion reactions when co-reconstituted with fusogenic SNAREs, resulting in the proposal of an inhibitory class of SNAREs termed i-SNAREs (Varlamov et al. 2004). Again, however, these results are easily explainable when the correct classification is used. In most cases, inhibition was observed when one of the membranes contained SNAREs of all four sub-

classes (QabcR), resulting in the formation of stable and non-fusogenic *cis*-core complexes as frequently observed between non-cognate SNAREs (see below).

Whereas the examples discussed above already show that the topology of SNAREs allowing for functional *trans*-interactions may be more variable, it remains to be established whether all combinations are functional or whether only certain combinations are possible. Again, liposome fusion experiments suggest that only one type of topology results in fusion. However, in yeast there is an increasing body of evidence suggesting that some SNAREs can participate in fusion reactions with different topology. For instance, the above-mentioned R-SNARE Sec22p is joined by the Qb SNARE Bos1p and the Qc-SNARE Bet1p on transport vesicles in anterograde traffic, resulting in a topology R/Qb/Qc (donor)–Qa (Sed5p, acceptor) (Hardwick and Pelham 1992; Newman et al. 1990). In retrograde traffic from the Golgi to the ER, the topology is likely to be R (Sec22p, donor)–QaQbQc (Ufe1p, Sec20p, Use1p, acceptor) (Dilcher et al. 2003). Presently it is unclear whether such "unusual" combinations are more widespread. In homotypic fusion reactions (i.e. fusion between equivalent organelles) both fusion partners contain a full complement of all SNAREs, making it difficult to discern which donor–acceptor combinations result in functional *trans*-complexes. Furthermore, SNAREs lacking a genuine transmembrane domain cannot operate as the sole SNARE in one of the partner membranes since force transduction as required by the model would be insufficient. Such SNAREs are found among Qb and Qc-SNAREs, such as Vam7 and SNAP-25 with its relatives, and also among R-SNAREs, such as Ykt6.

11.4.5.3 **Specificity of SNAREs**

After the discovery of the SNAREs it was proposed that the specificity of membrane fusion reactions is encoded by the SNAREs themselves (McNew et al. 2000; Söllner et al. 1993a). In other words, it was assumed that only appropriate SNAREs would interact with each other and fuse membranes. However, control of specificity must include other factors as the SNAREs cannot be solely responsible for the following reasons. First, *in vitro* studies revealed that SNAREs form complexes with each other rather promiscuously as long as one SNARE of each subclass is present, with little preference for cognate versus non-cognate SNAREs (Fasshauer et al. 1999; Yang et al. 1999). From liposome fusion experiments, a higher degree of specificity was postulated, but because the QabcR rule was violated most of the conclusions are not correct (McNew et al. 2000; Parlati et al. 2000; Paumet et al. 2001). In a way, such promiscuity is not surprising because the structure of SNARE complexes is conserved to an extraordinary degree, particularly with respect to the interacting amino acid sidechains. Second, it is becoming apparent that under certain conditions cognate SNAREs may be functionally substituted by non-cognate SNAREs of the same subclass, although the resulting fusion is often less efficient. For instance, the C-terminal part of SNAP-23 could completely rescue exocytosis in permeabilized botulinum neurotoxin E-treated PC12 cells. SNAP-29 was much less efficient,

although stable non-cognate complexes have been observed *in vitro* (Scales et al. 2000). Furthermore, Ykt6p is capable of substituting for Sec22p in anterograde traffic between the ER and the Golgi (Liu and Barlowe 2002), and SNAP-23 can substitute for SNAP-25 in chromaffin granule exocytosis (Sørensen et al. 2003). Third, as already mentioned in the previous section, certain SNAREs are involved in multiple trafficking steps. Well-characterized examples include the yeast SNAREs Vti1p, Sec22p, Sed5p and Ykt6p. As far known, the SNARE partners involved in these different fusion reactions are not identical.

The question then arises whether a given SNARE complex (i.e. the full complement of QabcR-SNAREs) can operate in more than one fusion step. Apparently, this is not the case although the identity of many functionally interacting SNARE complexes has not been clarified with certainty. A second problem is how it is decided which SNAREs are to be used in a certain fusion step and which SNAREs need to be kept inactive. This problem is particularly relevant in pathways involving membrane recycling. As integral membrane proteins, SNAREs can only be returned to their "home" resident membrane by means of membrane traffic and appropriate sorting. During trafficking, they pass through other compartments involving fusion steps in which they do not participate. For instance, in neuroendocrine cells exocytosis involves the neuronal SNAREs synaptobrevin, syntaxin 1 and SNAP-25. After endocytosis by clathrin-coated vesicles and decoating, the endocytosed vesicles undergo at least one fusion step (endosome fusion) before being returned to the secretory vesicle pool (Maxfield and McGraw 2004). The SNAREs involved in this step probably include syntaxin 13 or 16, syntaxin 6, vti1a and VAMP-4 (Kreykenbohm et al. 2002). Endosomes from neuroendocrine cells, however, appear to contain all SNAREs functioning in exocytosis. Conversely, highly purified synaptic vesicles contain vti1a in a fully assembled SNARE core complex that is different from the neuronal complex (Antonin et al. 2000b). The need for recycling explains why the subcellular distribution of many SNAREs is rather widespread and why subcellular localization alone cannot be used to identify the compartment in which a certain SNARE functions. Indeed, most membranes of the secretory pathway are likely containing several sets of SNAREs, and it is presently not clear how the appropriate set is "selected" for an upcoming fusion step.

11.4.6 Challenges of the SNARE Hypothesis

As discussed above, an almost overwhelming body of evidence documents that SNARE proteins are intimately involved in intracellular fusion reactions. However, it is still not universally accepted that SNAREs operate as fusion catalysts that mediate membrane merger. These challenges are primarily based upon three strands of evidence that are discussed in the following subsections.

11.4.6.1 Persistence of Fusion in Spite of SNARE Deletions

In the yeast *Saccharomyces cerevisiae*, most SNAREs are essential genes, i.e. no viable cells are obtained when these genes are deleted. However, genetic ablation of some SNAREs (particularly R-SNAREs) results in viable cells and surprisingly mild phenotypes. For instance, deletion of Sec22p, an R-SNARE operating in both anterograde and retrograde traffic between the ER and the Golgi apparatus (Dilcher et al. 2003; Hardwick and Pelham 1992; Newman et al. 1990), results in viable cells (Liu and Barlowe 2002). Similarly, Snc1p and Snc2p, R-SNAREs involved in exocytosis, are not required for survival, although cells lacking these genes are rather sick (Protopopov et al. 1993). Interestingly, the latter phenotype can be rescued by overexpression of ELO2 and ELO3, two genes involved in the elongation of very long fatty acids (David et al. 1998).

In both *Drosophila* and mice, deletion of neuronal synaptobrevin results in almost complete block of regulated exocytosis, but miniature endplate potentials persist, indicating that constitutive fusion of synaptic vesicles is functioning normally (Schoch et al. 2001; Sweeney et al. 1995). Similarly, SNAP-25 is essential for evoked release, but is not required for nerve growth or stimulus-independent exocytosis. Deletion of the vti1b in mice, a Qb-SNARE involved in the fusion of late endosomes and lysosomes, yields surprisingly mild phenotypes, with the mice growing to adulthood (Atlashkin et al. 2003). Interestingly, the partner Qc-SNARE syntaxin 8 is also downregulated, suggesting that both SNAREs need to interact to maintain stable expression.

In none of these cases, however, can it be excluded that another SNARE of the same subfamily is substituting for the deleted protein. For instance, the R-SNARE Ykt6p has recently been shown to be responsible for maintaining forward traffic from the ER to the Golgi apparatus in Sec22p knockout strains (Liu and Barlowe 2002). In neurons it is conceivable that another R-SNARE is present that normally operates in constitutive exocytosis. Indeed, it has recently been shown that synaptic vesicles contain a full set of SNAREs in addition to those functioning in regulated exocytosis (Antonin et al. 2000b), but their identities are only partially known.

11.4.6.2 Late-acting Factors Uncovered in Yeast Vacuolar Fusion

Pioneered by W. B. Wickner and his colleagues, homotypic fusion of yeast vacuoles is presently one of the most powerful model systems for studying the biochemistry of intracellular fusion reactions. Vacuolar fusion is not essential for survival and sophisticated genetic screens were introduced to identify genes involved in fusion. A simple *in vitro* assay, based on genetically introduced markers, is available, thus allowing for combining biochemistry with genetics. This assay is capable, at least to a certain extent, to discern between different steps (e.g. docking, priming and fusion) in the fusion pathway (Wickner 2002; Wickner and Haas 2000).

During the last decade, many novel gene products involved in fusion have been identified in this system and most of them have been tentatively assigned

to distinct steps in the fusion pathway. Using antibody inhibition, SNARE assembly was shown to be required rather early during or after docking. Furthermore, *trans*-complexes were reported to form before fusion. Importantly, these complexes were dissociated when fusion was blocked by interfering with late-acting factors and they were not required anymore when fusion was subsequently initiated by removal of the block (Ungermann et al. 1998). These late-acting factors were suggested to include calmodulin (Peters and Mayer 1998), protein phosphatase 1 (Peters et al. 1999) and the Vo subunit of the vacuolar proton ATPase (Peters et al. 2001). Along the same lines, formation of *trans*-complexes has recently been shown to cause release of calcium from the vacuoles, which in turn is required to trigger fusion (Merz and Wickner 2004).

A problem with the assignment of SNAREs to an earlier step relates to the fact that there are no reliable tools for effectively and selectively blocking their activity. In vacuolar fusion, SNAREs are inhibited either by antibodies or by excess amounts of soluble SNARE motifs acting as competitive inhibitors. Antibody binding to unrelated proteins, however, has been shown to block fusion by steric hindrance (Antonin et al. 2000a) even when Fab fragments are used (Schierding and Jahn, unpublished observations). Soluble SNARE motifs are disassembled by NSF, requiring careful titrations to show the specificity of the effect. Finally, it should be noted that there is presently no reliable method for directly measuring SNARE *trans*-complexes. All procedures involve at some point detergent solubilization of the membrane. Under these conditions, all *trans*-complexes either convert to *cis*-complexes or dissociate, questioning the validity of the conclusions.

Of the late-acting factors, the Vo subunit of the vacuolar proton ATPase has gained some prominence since it was proposed to function as a fusion pore by forming connexon-like *trans*-complexes between membranes (Bayer et al. 2003; Peters et al. 2001). The vacuolar ATPase is a highly conserved enzyme with many structural similarities to the mitochondrial FoF1-ATPase (Sun-Wada et al. 2004; Wilkens et al. 2004). Both enzymes contain a head, a stalk referred to as stator and a ring of integral membrane proteins. ATP hydrolysis in the head domain drives rotation of the stalk and the proteolipid ring, but unlike the FoF1 ATPase the V-ATPase cannot synthesize ATP (Capaldi and Aggeler 2002; Weber and Senior 2003). Postulating that the membrane-embedded proteolipid ring, a highly specialized biological nanomachine, has a "second life" by functioning as a fusion pore in the secretory pathway is hard to reconcile with biological common sense. In particular, such a fusion mechanism not only requires reversible association of proteolipid rings in *trans* (i.e. head-to-head), but also dissociation of the ring subunits after fusion for allowing the fusion pore to grow (see Section 11.6). Clearly, more direct evidence and independent confirmation by other laboratories is required to strengthen this interesting speculation.

11.4.6.3 Exocytosis of Cortical Granules in Sea Urchin Oocytes

Oocytes contain large subcortical granules that undergo calcium-dependent exocytosis upon fertilization. A fertilization envelope is formed around the oocyte that prevents fertilization by additional spermatoids.

Oocytes of the sea urchin provide a powerful model system for monitoring exocytosis. Cortical granules are large in size, allowing on-line monitoring of exocytosis using standard microscopes. Furthermore, inverted lawns of oocyte membranes, with their granules still attached, were the first cell-free system developed for the study of membrane fusion (Vacquier 1975). Although cortical granules contain SNAREs, fusion appears to require only proteins in the granule membrane and is triggered by calcium, with no other factors being required. Indeed, cortical granules were shown to undergo calcium-dependent exocytosis with protein-free liposomes (Vogel et al. 1992), thus challenging the idea that the presence of SNAREs in both membranes is a prerequisite for exocytosis (Avery et al. 1999; Szule and Coorssen 2003).

Presently, this system must be considered as the most serious challenge to the SNARE theory as there is clear evidence for protein-mediated and calcium-dependent fusion of a eukaryotic trafficking organelle with artificial membranes. However, it must be borne in mind that this fusion requires harsh conditions (centrifugation of the granules onto the membranes), resulting in membrane contact areas exceeding that of a normal trafficking vesicle more than 1000-fold. Furthermore, fusion of artificial membranes can be induced by numerous amphiphilic agents, including peptides and certain proteins (including NSF!) that are clearly not involved in biological fusion reactions (Jahn et al. 2003). The fusogenic activity observed in these assays is due to such non-specific side-activity. It is thus too early to count out SNARE proteins as the physiological fusogens in cortical granule exocytosis.

11.5 SM Proteins and Other Regulators

Considering the pivotal role of SNAREs in membrane fusion, it is not surprising that many laboratories are searching for control proteins that regulate SNARE activity. It is beyond the scope of this chapter to discuss regulation of SNAREs by proteins such as synaptotagmins (Bai and Chapman 2004; Rizo and Südhof 1998), complexins (McMahon et al. 1995; Pabst et al. 2002; Reim et al. 2001), Munc13 (Augustin et al. 1999; Junge et al. 2004; Rhee et al. 2002) and Rab effectors (Segev 2001; Zerial and McBride 2001). In each of these cases, there are several lines of evidence that not only invoke these proteins in the control of fusion (mostly exocytosis), but also suggest that the control is exerted by regulating SNAREs. However, with the possible exception of complexins it is not known how this control is exerted at the molecular level.

In addition to these well-characterized molecules, a large number of proteins have been suggested to bind to SNAREs and to control SNARE activity, either

directly by interfering with the SNARE conformational cycle or indirectly by recruiting ion channels and receptors to fusion sites. For instance, there has been an almost inflationary increase in "specific" syntaxin 1-binding proteins (more than 40 published, many of them in leading journals), including an extensive list of ion channels, neurotransmitter receptors, and other membrane and soluble proteins. In most cases, however, these interactions are only documented by crude and qualitative methods such as non-quantitative co-immunoprecipitations, pull-down experiments and yeast two-hybrid scans, with little or no information about specificity, affinity, stoichiometry or structural properties. Considering that syntaxin 1 and SNAP-25 are not only the most abundant neuronal membrane proteins [at least 1% each of total protein in brain (Walch-Solimena et al. 1995)], but also partially unstructured and thus "sticky", it remains to be seen which of these interactions will survive scrutiny (see, e.g. Vites et al. 2004).

11.5.1 SM Proteins

SM proteins are arch-shaped soluble molecules that are essential for fusion and that interact with SNAREs. There are fewer SM proteins than SNAREs (four in yeast and seven in mammals). The crystal structure of two only distantly related SM proteins (yeast Sly1p and mammalian/squid Munc18) revealed that the overall structure of these proteins is well conserved (for review, see Gallwitz and Jahn 2003; Toonen and Verhage 2003).

SM proteins bind to SNAREs. However, despite the structural conservation there is a bewildering variety of SM protein/SNARE interactions that are difficult to integrate into a coherent picture. The first type of interaction is exemplified by mammalian Munc18 that binds to syntaxin 1. Syntaxin 1 can adopt an open and a closed conformation that are in rapid equilibrium with each other (Dulubova et al. 1999; Margittai et al. 2003), depending of whether the N-terminal three-helix bundle is folded back onto the SNARE motif. In the closed conformation syntaxin is unable to enter SNARE complexes. Munc18 only binds to the closed conformation and stabilizes it, with numerous crystal contacts between both the N-terminal domain and the SNARE motif of syntaxin and the arch-shaped cavity of Munc18 (Misura et al. 2000). Consequently, Munc18 is unable to bind to assembled SNARE complexes (Hata et al. 1993). In stark contrast, the SM proteins Sly1p and Vps45p only bind to the N-terminal tip of the respective SNAREs Sec5p and Tlg2p (Dulubova et al. 2002), with the binding site being on the outer surface of Sly1p rather than in the arch-shaped cleft (Bracher and Weissenhorn 2002). Thus, these proteins bind to the corresponding syntaxins irrespective of whether they are free or whether they are part of an assembled SNARE complex. To further add to the confusion, it appears that Sec1p, an SM protein operating in yeast exocytosis, only binds to the respective SNARE complex when the complex is fully assembled (Carr et al. 1999). Finally, the SM protein Vps33p does not bind to SNAREs directly, but is part of a multiprotein complex (termed HOPS or the VpsC complex) that interacts with the

corresponding Qa-SNARE only in its assembled form (Sato et al. 2000). Interestingly, binding does not require the N-terminal domain, but rather depends on the SNARE motif of the Qa-SNARE Vam3p (Dulubova et al. 2001).

How can these seemingly contradictive findings be integrated? An important clue has recently been provided by Peng and Gallwitz (2004) who show that Sly1p mutants that are defective in Sed5p binding are fully functional. Furthermore, the mutants defective in binding showed increased binding to some of the SNARE partners of Sed5p but they were unable to bind to fully assembled SNARE complexes. Thus, it is conceivable that binding to the N-terminal regions of Qa-SNAREs is merely a recruiting mechanism that is not essential for function. Rather, SM proteins may provide a scaffold for SNARE complex formation, e.g. by loosely grouping sets of SNAREs into acceptor complexes to which *trans*-binding of the SNARE(s) in the partner membrane is thus facilitated. Indeed, the relevance of such acceptor complexes for efficient SNARE assembly has recently been shown for the neuronal SNARE complex (Fasshauer and Margittai 2004; also see above). Apparently, formation of such acceptor complexes is critical as in all studied cases fusion is absolutely dependent on SM proteins.

Although most evidence suggests that SM proteins regulate SNAREs, SM proteins are known to interact with other proteins whose functional significance is less well understood. For instance, Munc18 binds to two membrane-associated proteins Doc2 and Mint (each represented by two family members) that are enriched in synapses, and likely play a role in synaptic transmission. Other SM interactions include Mso1p with Sec1p and Unc18 with Unc13 (for review, see Toonen and Verhage 2003). Last not least, genetic interactions were detected between an SM protein (Sly1) and a Rab protein (Ypt1), which originally led to the discovery of the first SM protein (Dascher et al. 1991).

11.6 Fusion Pores

Membrane fusion involves transient non-bilayer intermediates that culminate with the opening of an aqueous connection between the distal sides of the fusing membranes (fusion pores). More than 10 years ago, two alternative models for the structure of biological fusion pores were proposed (Almers and Tse 1990; Monck and Fernandez 1992). They represent extreme opposite views that continue to be controversially discussed. According to the first model, the transition states and the initial pore are primarily proteinaceous. In its simplest form, it assumes that protein rings are formed within each membrane that span the membrane and connect in "*trans*". Opening of the fusion pore would therefore be reminiscent of the opening of gap junction channels (Breckenridge and Almers 1987a) but fusion pore expansion requires subunit separation by invading membrane lipids and ultimately breakup of the *trans*-connections. The second model assumes that the transition states and the fusion pore are primarily governed by lipid physics, involving stalk-like non-bilayer intermediates. Accord-

ing to this model, the proteins involved in fusion influence transition state energies, e.g. by stabilizing energetically unfavorable (curved) intermediates or by overcoming electrostatic repulsion between the proximal monolayers, but they are not part of the fusion pore structure (Jahn and Grubmüller 2002).

11.6.1 Measuring Fusion Pore Opening and Closure

The kinetics of exocytotic fusion pores can be studied by capacitance patch-clamping, carbon fiber amperometry and dye unloading. With capacitance patch-clamping, currents can be monitored upon fusion pore opening that charge the vesicle membrane, providing highly sensitive measurements of fusion pore conductances. Amperometry measures the release of oxidizable secretory products such as monoamines with high time resolution. Although signals are dampened by diffusion and gradually approach zero upon vesicle emptying, initial efflux kinetics is governed by diffusional constraints caused by fusion pores ("foot signals"), providing an indirect albeit transient readout for fusion pore dynamics. Dye unloading, particularly when lipophilic dyes such as FM dyes are used, is also dependent on diffusion and, in addition, is governed by the kinetics of dye dissociation from the membrane. Finally, expression of pH-sensitive fluorescent proteins in the vesicle lumen has recently emerged as a new tool in studying fusion pore opening and endocytosis (for review, see Lindau and Alvarez de Toledo 2003).

Using capacitance patch-clamping on a mast cell variant with giant vesicles, Breckenridge and Almers (1987b) were the first to show that fusion is preceded by rapid sequences of fusion pore opening and closing (also referred to as "flickering"). Since then, many studies addressed the question whether fusion pores open transiently ("kiss-and-run"), which may result in partial content release, or whether it involves complete fusion followed by separately controlled endocytosis. In particular, "kiss-and-run" of synaptic vesicles in fast synapses has been intensely studied by leading neuroscientists using sophisticated methods. Although this field continues to enjoy the attention of our leading journals, the major issues are still controversial (see, e.g. Gandhi and Stevens 2003; Rizzoli and Betz 2004; Ryan 2003; Staal et al. 2004; Stevens and Williams 2000; Zenisek et al. 2002). While a discussion of the pros and cons is beyond the scope of this chapter, it is generally agreed that (1) fusion pores open abruptly (with time constants of less than 50 μs, (2) fusion pores can undergo rapid cycles of opening and closing ("flickering"), although it remains to be clarified whether flickering is physiologically relevant, and (3) secretory organelles can, at least occasionally and under certain experimental conditions, undergo "transient" fusion, i.e. these organelles retain their identity while maintaining an open fusion pore, and they are subsequently retrieved at the site of exocytosis without complete membrane mixing (Holroyd et al. 2002; Thorn et al. 2004).

The major unresolved question is whether the "reversibility" of fusion pore opening is due to a reversibility of the underlying molecular reactions or whether it is

due to a tight spatial and temporal coupling of biochemically distinct molecular processes. In neurons fusion pores were suggested to remain open for only few ms (Aravanis et al. 2003; Stevens and Williams 2000) indicating a reversible mechanism. Furthermore, flickering involves repetitive opening and closing events, which is difficult to reconcile with biologically irreversible reactions. Flickering, however, is also observed during the fusion of protein-free artificial membranes (Chanturiya et al. 1997) and thus may reflect a metastable transition state instead of being the signature of a protein complex operating in an ion-channel like fashion. At least in neuroendocrine cells exocytosis and re-capture involve different proteins (Holroyd et al. 2002; Palfrey and Artalejo 2003; Tsuboi et al. 2004). Here, exocytosis of secretory vesicles is clearly SNARE-dependent whereas re-capture requires dynamin, a GTPase involved in severing the neck of budding vesicles (Präfcke and McMahon 2004). This is in line with the emerging concept that fusion and fission are carried out by completely different protein complexes, thus guaranteeing the vectoriality of intracellular trafficking pathways (Bonifacino and Glick 2004).

11.6.2
The Role of Proteins in Controlling Fusion Pore Opening

The model described above suggests that the SNAREs are primarily responsible for membrane merger. Accordingly, it is tempting to speculate that fusion pores are surrounded by SNARE complexes in transition from the *trans*- to *cis*-configuration. Titration experiments involving soluble SNARE fragments suggest that at least three SNARE complexes must cooperate for membrane fusion to occur (Hua and Scheller 2001). In recent years, major efforts have been made to find out whether manipulation of either SNAREs themselves or of proteins known to bind to SNAREs *in vitro* affect fusion pore kinetics. Thus, mutations and/or introduction of protein fragments were used in combination with carbon fiber amperometry to find out which protein may be involved in regulating fusion pore opening and/or closing. Proteins thus invoked in the control of fusion pore kinetics include syntaxin 1 (Han et al. 2004), synaptotagmin I (Bai et al. 2004; C.T. Wang et al. 2001, 2003), synaptotagmin VII (Jaiswal et al. 2004) synaptotagmin IV (C.T. Wang et al. 2001), complexin (Archer et al. 2002), and Munc18 (Barclay et al. 2004; Fisher et al. 2001).

In most of these studies, the data were interpreted as evidence for a direct involvement of the manipulated proteins in the fusion reaction, e.g. by tweaking the SNAREs or by directly participating in the structure of the fusion pore. However, it needs to be borne in mind that it is principally not possible to prove such an involvement from kinetic data. First, most of the studies involve overexpression of mutant proteins against the background of endogenous wild-type variants, making it difficult to exclude experimental artifacts. Second, it cannot be excluded that effects on fusion pores are exerted "at a distance", e.g. by changing the elastic properties of the membrane (Kozlov and Chernomordik 2002). In this context it is interesting to note that, with the exception of the study of Han et al. (2004), ma-

nipulations of the SNAREs, e.g. by mutagenesis or by gradual cleavage using clostridial neurotoxins, does not appear to alter fusion pore kinetics. Thus, it remains to be resolved whether SNAREs or other proteins line the fusion pore and whether the initial pore is primarily lipidic or proteinaceous.

11.7 Concluding Remarks

During the last decade, we have witnessed an almost explosive growth in our understanding of intracellular membrane fusions. However, we are just beginning to appreciate the molecular complexity of these fusion reactions. For instance, a comprehensive screen for non-essential genes involved in yeast vacuolar fusion revealed no less than 137 genes that are thought to be directly involved in fusion and an additional 700 genes that indirectly influenced the fusion pathway (Seeley et al. 2002). Furthermore, with the exception of the SNAREs and, to some extent, of the Rab proteins, very little is known about the molecular mechanisms and the associated conformational changes. In particular, the mechanisms of vesicle attachment and the reactions taking place between vesicle attachment and bilayer fusion are mostly unclear. Fusion sites are dynamic biological nanomachines, i.e. they operate at a size and time scale that is difficult to access experimentally. Recent developments in high-resolution physical techniques such as single-molecule spectroscopy and imaging, in addition to advances in structural biology, raise the hope that a refined understanding of these reactions and of the molecular basis of fusion pore opening and enlargement will be achieved in the coming years.

List of Abbreviations

AAA	ATPase family associated with various cellular activities
ATP	adenosine 5′-triphosphate
COG	conserved oligomeric Golgi
EEA1	early endosomal antigen 1
ER	endoplasmic reticulum
FYVE	zinc-finger domain found originally in Fab1p, YOTB, Vac1p, EEA1
FM	dye family of amphiphilic fluorescent dyes developed by Fei Mao
Fzo	fuzzy onion
GAP	GTPase-activating protein
GARP	Golgi-associated retrograde protein
GDF	GDI displacement factors
GDI	GDP dissociation inhibitor
GDP	guanosine 5′-diphosphate
GEF	guanine nucleotide exchange factor
GTP	guanosine 5′-triphosphate

HOPS	homotypic vacuole fusion and protein sorting
Munc18	mammalian homolog of the unc18 gene
NSF	*N*-ethylmaleimide-sensitive factor
PX	phox homology
Rab	ras-like protein from brain
RRP	rapidly releasable pool
Sec	secretory pathway protein
SM	sec/Munc18-like
SNAP	soluble NSF attachment protein
SNAP-25	synaptosomal-associated protein of 25 kDa
SNARE	SNAP receptor
SRP	slowly releasable pool
TRAPP	transport protein particle
VAMP	vesicle associated membrane protein
Vps	vacuolar protein sorting
Yip	ypt-interacting protein

References

Almers, W., Tse, F. W. **1990**. Transmitter release from synapses: does a preassembled fusion pore initiate exocytosis? *Neuron 4*, 813–818.

Antonin, W., Holroyd, C., Tikkanen, R., Höning, S., Jahn, R. **2000a**. The R-SNARE endobrevin/VAMP-8 mediates homotypic fusion of early endosomes and late endosomes. *Mol. Biol. Cell 11*, 3289–3298.

Antonin, W., Riedel, D., von Mollard, G. F. **2000b**. The SNARE Vti1a-beta is localized to small synaptic vesicles and participates in a novel SNARE complex. *J. Neurosci. 20*, 5724–5732.

Antonin, W., Dulubova, I., Arac, D., Pabst, S., Plitzner, J., Rizo, J., Jahn, R. **2002a**. The N-terminal domains of syntaxin 7 and Vti1b form three-helix bundles that differ in their ability to regulate SNARE complex assembly. *J. Biol. Chem. 277*, 36449–36456.

Antonin, W., Fasshauer, D., Becker, S., Jahn, R., Schneider, T. R. **2002b**. Crystal structure of the endosomal SNARE complex reveals common structural principles of all SNAREs. *Nat. Struct. Biol. 9*, 107–111.

Aravanis, A. M., Pyle, J. L., Tsien, R. W. **2003**. Single synaptic vesicles fusing transiently and successively without loss of identity. *Nature 423*, 643–647.

Archer, D. A., Graham, M. E., Burgoyne, R. D. **2002**. Complexin regulates the closure of the fusion pore during regulated vesicle exocytosis. *J. Biol. Chem. 277*, 18249–18252.

Atlashkin, V., Kreykenbohm, V., Eskelinen, E. L., Wenzel, D., Fayyazi, A., Fischer von Mollard, G. **2003**. Deletion of the SNARE vti1b in mice results in the loss of a single SNARE partner, syntaxin 8. *Mol. Cell Biol. 23*, 5198–5207.

Augustin, I., Rosenmund, C., Südhof, T. C., Brose, N. **1999**. Munc13-1 is essential for fusion competence of glutamatergic synaptic vesicles. *Nature 400*, 457–461.

Avery, J., Jahn, R., Edwardson, J. M. **1999**. Reconstitution of regulated exocytosis in cell-free systems: a critical appraisal. *Annu. Rev. Physiol. 61*, 777–807.

Bai, J., Chapman, E. R. **2004**. The C2 domains of synaptotagmin – partners in exocytosis. *Trends Biochem. Sci. 29*, 143–151.

Bai, J., Wang, C. T., Richards, D. A., Jackson, M. B., Chapman, E. R. **2004**. Fusion pore dynamics are regulated by synaptotagmin*t-SNARE interactions. *Neuron 41*, 929–942.

Barclay, J. W., Aldea, M., Craig, T. J., Morgan, A., Burgoyne, R. D. **2004**. Regulation of

the fusion pore conductance during exocytosis by cyclin-dependent kinase 5. *J. Biol. Chem. 279*, 41495–41503.

Bayer, M.J., Reese, C., Buhler, S., Peters, C., Mayer, A. **2003**. Vacuole membrane fusion: V0 functions after *trans*-SNARE pairing and is coupled to the Ca^{2+}-releasing channel. *J. Cell Biol. 162*, 211–222.

Bock, J.B., Matern, H.T., Peden, A.A., Scheller, R.H. **2001**. A genomic perspective on membrane compartment organization. *Nature 409*, 839–841.

Böddinghaus, C., Merz, A.J., Laage, R., Ungermann, C. **2002**. A cycle of Vam7p release from and PtdIns 3-P-dependent rebinding to the yeast vacuole is required for homotypic vacuole fusion. *J. Cell Biol. 157*, 79–89.

Bonifacino, J.S., Glick, B.S. **2004**. The mechanisms of vesicle budding and fusion. *Cell 116*, 153–166.

Bracher, A., Weissenhorn, W. **2002**. Structural basis for the Golgi membrane recruitment of Sly1p by Sed5p. *EMBO J. 21*, 6114–6124.

Breckenridge, L.J., Almers, W. **1987a**. Currents through the fusion pore that forms during exocytosis of a secretory vesicle. *Nature 328*, 814–817.

Breckenridge, L.J., Almers, W. **1987b**. Final steps in exocytosis observed in a cell with giant secretory granules. *Proc. Natl Acad. Sci. USA 84*, 1945–1949.

Broadie, K., Prokop, A., Bellen, H.J., O'Kane, C.J., Schulze, K.L., Sweeney, S.T. **1995**. Syntaxin and synaptobrevin function downstream of vesicle docking in *Drosophila*. *Neuron 15*, 663–673.

Capaldi, R.A., Aggeler, R. **2002**. Mechanism of the F_1F_0-type ATP synthase, a biological rotary motor. *Trends Biochem. Sci. 27*, 154–160.

Carr, C.M., Grote, E., Munson, M., Hughson, F.M., Novick, P.J. **1999**. Sec1p binds to SNARE complexes and concentrates at sites of secretion. *J. Cell Biol. 146*, 333–344.

Chamberlain, L.H., Burgoyne, R.D., Gould, G.W. **2001**. SNARE proteins are highly enriched in lipid rafts in PC12 cells: implications for the spatial control of exocytosis. *Proc. Natl Acad. Sci. USA 98*, 5619–5624.

Chanturiya, A., Chernomordik, L.V., Zimmerberg, J. **1997**. Flickering fusion pores comparable with initial exocytotic pores occur in protein-free phospholipid bilayers. *Proc. Natl Acad. Sci. USA 94*, 14423–14428.

Chen, Y.A., Scheller, R.H. **2001**. SNARE-mediated membrane fusion. *Nat. Rev. Mol. Cell Biol. 2*, 98–106.

Christoforidis, S., McBride, H.M., Burgoyne, R.D., Zerial, M. **1999**. The Rab5 effector EEA1 is a core component of endosome docking. *Nature 397*, 621–625.

Dascher, C., Ossig, R., Gallwitz, D., Schmitt, H.D. **1991**. Identification and structure of four yeast genes (SLY) that are able to suppress the functional loss of YPT1, a member of the RAS superfamily. *Mol. Cell Biol. 11*, 872–885.

David, D., Sundararababu, S., Gerst, J.E. **1998**. Involvement of long chain fatty acid elongation in the trafficking of secretory vesicles in yeast. *J. Cell Biol. 143*, 1167–1182.

Dietrich, L.E., Boeddinghaus, C., LaGrassa, T.J., Ungermann, C. **2003**. Control of eukaryotic membrane fusion by N-terminal domains of SNARE proteins. *Biochim. Biophys. Acta 1641*, 111–119.

Dilcher, M., Veith, B., Chidambaram, S., Hartmann, E., Schmitt, H.D., Fischer von Mollard, G. **2003**. Use1p is a yeast SNARE protein required for retrograde traffic to the ER. *EMBO J. 22*, 3664–3674.

Dimmer, K.S., Fritz, S., Fuchs, F., Messerschmitt, M., Weinbach, N., Neupert, W., Westermann, B. **2002**. Genetic basis of mitochondrial function and morphology in *Saccharomyces cerevisiae*. *Mol. Biol. Cell 13*, 847–853.

Dulubova, I., Sugita, S., Hill, S., Hosaka, M., Fernandez, I., Südhof, T.C., Rizo, J. **1999**. A conformational switch in syntaxin during exocytosis: role of munc18. *EMBO J. 18*, 4372–4382.

Dulubova, I., Yamaguchi, T., Wang, Y., Südhof, T.C., Rizo, J. **2001**. Vam3p structure reveals conserved and divergent properties of syntaxins. *Nat. Struct. Biol. 8*, 258–264.

Dulubova, I., Yamaguchi, T., Gao, Y., Min, S.W., Huryeva, I., Südhof, T.C., Rizo, J. **2002**. How Tlg2p/syntaxin 16 "snares" Vps45. *EMBO J. 21*, 3620–3631.

Dumas, J.J., Merithew, E., Sudharshan, E., Rajamani, D., Hayes, S., Lawe, D., Corvera, S., Lambright, D.G. **2001**. Multivalent endosome targeting by homodimeric EEA1. *Mol. Cell 8*, 947–958.

Fasshauer, D. **2003**. Structural insights into the SNARE mechanism. *Biochim. Biophys. Acta 1641*, 87–97.

Fasshauer, D., Margittai, M. **2004**. A transient N-terminal interaction of SNAP-25 and syntaxin nucleates SNARE assembly. *J. Biol. Chem. 279*, 7613–7621.

Fasshauer, D., Bruns, D., Shen, B., Jahn, R., Brunger, A.T. **1997a**. A structural change occurs upon binding of syntaxin to SNAP-25. *J. Biol. Chem. 272*, 4582–4590.

Fasshauer, D., Otto, H., Eliason, W.K., Jahn, R., Brunger, A.T. **1997b**. Structural changes are associated with soluble *N*-ethylmaleimide-sensitive fusion protein attachment protein receptor complex formation. *J. Biol. Chem. 272*, 28036–28041.

Fasshauer, D., Sutton, R.B., Brunger, A.T., Jahn, R. **1998**. Conserved structural features of the synaptic fusion complex: SNARE proteins reclassified as Q- and R-SNAREs. *Proc. Natl Acad. Sci. USA 95*, 15781–15786.

Fasshauer, D., Antonin, W., Margittai, M., Pabst, S., Jahn, R. **1999**. Mixed and noncognate SNARE complexes. Characterization of assembly and biophysical properties. *J. Biol. Chem. 274*, 15440–15446.

Fernandez, I., Ubach, J., Dulubova, I., Zhang, X., Südhof, T.C., Rizo, J. **1998**. Three-dimensional structure of an evolutionarily conserved N-terminal domain of syntaxin 1A. *Cell 94*, 841–849.

Ferro-Novick, S., Jahn, R. **1994**. Vesicle fusion from yeast to man. *Nature 370*, 191–193.

Fiebig, K.M., Rice, L.M., Pollock, E., Brunger, A.T. **1999**. Folding intermediates of SNARE complex assembly. *Nat. Struct. Biol. 6*, 117–123.

Filippini, F., Rossi, V., Galli, T., Budillon, A., D'Urso, M., D'Esposito, M. **2001**. Longins: a new evolutionary conserved VAMP family sharing a novel SNARE domain. *Trends Biochem. Sci. 26*, 407–409.

Fisher, R.J., Pevsner, J., Burgoyne, R.D. **2001**. Control of fusion pore dynamics during exocytosis by Munc18. *Science 291*, 875–878.

Fukuda, R., McNew, J.A., Weber, T., Parlati, F., Engel, T., Nickel, W., Rothman, J.E., Söllner, T.H. **2000**. Functional architecture of an intracellular membrane t-SNARE. *Nature 407*, 198–202.

Furst, J., Sutton, R.B., Chen, J., Brunger, A.T., Grigorieff, N. **2003**. Electron cryomicroscopy structure of *N*-ethyl maleimide sensitive factor at 11 Å resolution. *EMBO J. 22*, 4365–4374.

Gallwitz, D., Jahn, R. **2003**. The riddle of the Sec1/Munc-18 proteins – new twists added to their interactions with SNAREs. *Trends Biochem. Sci. 28*, 113–116.

Gandhi, S.P., Stevens, C.F. **2003**. Three modes of synaptic vesicular recycling revealed by single-vesicle imaging. *Nature 423*, 607–613.

Geppert, M., Goda, Y., Hammer, R.E., Li, C., Rosahl, T.W., Stevens, C.F., Südhof, T.C. **1994**. Synaptotagmin I: a major Ca^{2+} sensor for transmitter release at a central synapse. *Cell 79*, 717–727.

Gonzalez, L.C., Jr, Weis, W.I., Scheller, R.H. **2001**. A novel snare N-terminal domain revealed by the crystal structure of Sec22b. *J. Biol. Chem. 276*, 24203–24211.

Han, X., Wang, C.T., Bai, J., Chapman, E.R., Jackson, M.B. **2004**. Transmembrane segments of syntaxin line the fusion pore of Ca^{2+}-triggered exocytosis. *Science 304*, 289–292.

Hanson, P.I., Roth, R., Morisaki, H., Jahn, R., Heuser, J.E. **1997**. Structure and conformational changes in NSF and its membrane receptor complexes visualized by quick-freeze/deep-etch electron microscopy. *Cell 90*, 523–535.

Hardwick, K.G., Pelham, H.R. **1992**. SED5 encodes a 39-kD integral membrane protein required for vesicular transport between the ER and the Golgi complex. *J. Cell Biol. 119*, 513–521.

Hasegawa, H., Yang, Z., Oltedal, L., Davanger, S., Hay, J.C. **2004**. Intramolecular protein–protein and protein–lipid interactions control the conformation and subcellular targeting of neuronal Ykt6. *J. Cell Sci. 117*, 4495–4508.

Hata, Y., Slaughter, C. A., Südhof, T. C. **1993**. Synaptic vesicle fusion complex contains unc-18 homologue bound to syntaxin. *Nature 366*, 347–351.

Hatsuzawa, K., Lang, T., Fasshauer, D., Bruns, D., Jahn, R. **2003**. The R-SNARE motif of tomosyn forms SNARE core complexes with syntaxin 1 and SNAP-25 and down-regulates exocytosis. *J. Biol. Chem. 278*, 31159–31166.

Holroyd, P., Lang, T., Wenzel, D., De Camilli, P., Jahn, R. **2002**. Imaging direct, dynamin-dependent recapture of fusing secretory granules on plasma membrane lawns from PC12 cells. *Proc. Natl Acad. Sci. USA 99*, 16806–16811.

Hsu, S. C., TerBush, D., Abraham, M., Guo, W. **2004**. The exocyst complex in polarized exocytosis. *Int. Rev. Cytol. 233*, 243–265.

Hu, C., Ahmed, M., Melia, T. J., Söllner, T. H., Mayer, T., Rothman, J. E. **2003**. Fusion of cells by flipped SNAREs. *Science 300*, 1745–1749.

Hua, S. Y., Charlton, M. P. **1999**. Activity-dependent changes in partial VAMP complexes during neurotransmitter release. *Nat. Neurosci. 2*, 1078–1083.

Hua, Y., Scheller, R. H. **2001**. Three SNARE complexes cooperate to mediate membrane fusion. *Proc. Natl Acad. Sci. USA 98*, 8065–8070.

Jahn, R., Grubmüller, H. **2002**. Membrane fusion. *Curr. Opin. Cell Biol. 14*, 488–495.

Jahn, R., Hanson, P. I. **1998**. Membrane fusion. SNAREs line up in new environment. *Nature 393*, 14–15.

Jahn, R., Lang, T., Südhof, T. C. **2003**. Membrane fusion. *Cell 112*, 519–533.

Jaiswal, J. K., Chakrabarti, S., Andrews, N. W., Simon, S. M. **2004**. Synaptotagmin VII restricts fusion pore expansion during lysosomal exocytosis. *PLoS Biol. 2*, E233.

Junge, H. J., Rhee, J. S., Jahn, O., Varoqueaux, F., Spiess, J., Waxham, M. N., Rosenmund, C., Brose, N. **2004**. Calmodulin and Munc13 form a Ca^{2+} sensor/effector complex that controls short-term synaptic plasticity. *Cell 118*, 389–401.

Katz, L., Brennwald, P. **2000**. Testing the 3Q:1R "rule": mutational analysis of the ionic "zero" layer in the yeast exocytic SNARE complex reveals no requirement for arginine. *Mol. Biol. Cell 11*, 3849–3858.

Kiessling, V., Tamm, L. K. **2003**. Measuring distances in supported bilayers by fluorescence interference-contrast microscopy: polymer supports and SNARE proteins. *Biophys. J. 84*, 408–418.

Kim, C. S., Kweon, D. H., Shin, Y. K. **2002**. Membrane topologies of neuronal SNARE folding intermediates. *Biochemistry 41*, 10928–10933.

Koshiba, T., Detmer, S. A., Kaiser, J. T., Chen, H., McCaffery, J. M., Chan, D. C. **2004**. Structural basis of mitochondrial tethering by mitofusin complexes. *Science 305*, 858–862.

Kozlov, M. M., Chernomordik, L. V. **2002**. The protein coat in membrane fusion: lessons from fission. *Traffic 3*, 256–267.

Kreykenbohm, V., Wenzel, D., Antonin, W., Atlachkine, V., von Mollard, G. F. **2002**. The SNAREs vti1a and vti1b have distinct localization and SNARE complex partners. *Eur. J. Cell Biol. 81*, 273–280.

Kweon, D. H., Kim, C. S., Shin, Y. K. **2003**. Regulation of neuronal SNARE assembly by the membrane. *Nat. Struct. Biol. 10*, 440–447.

Laage, R., Langosch, D. **1997**. Dimerization of the synaptic vesicle protein synaptobrevin (vesicle-associated membrane protein) II depends on specific residues within the transmembrane segment. *Eur. J. Biochem. 249*, 540–546.

Laage, R., Ungermann, C. **2001**. The N-terminal domain of the t-SNARE Vam3p coordinates priming and docking in yeast vacuole fusion. *Mol. Biol. Cell 12*, 3375–3385.

Lang, T., Bruns, D., Wenzel, D., Riedel, D., Holroyd, P., Thiele, C., Jahn, R. **2001**. SNAREs are concentrated in cholesterol-dependent clusters that define docking and fusion sites for exocytosis. *EMBO J. 20*, 2202–2213.

Lang, T., Margittai, M., Hölzler, H., Jahn, R. **2002**. SNAREs in native plasma membranes are active and readily form core complexes with endogenous and exogenous SNAREs. *J. Cell Biol. 158*, 751–760.

Langosch, D., Crane, J. M., Brosig, B., Hellwig, A., Tamm, L. K., Reed, J. **2001**. Peptide mimics of SNARE transmembrane segments drive membrane fusion depending on their conformational plasticity. *J. Mol. Biol. 311*, 709–721.

Lin, R. C., Scheller, R. H. **1997**. Structural organization of the synaptic exocytosis core complex. *Neuron 19*, 1087–1094.

Lindau, M., Alvarez de Toledo, G. **2003**. The fusion pore. *Biochim. Biophys. Acta 1641*, 167–173.

Lippincott-Schwartz, J., Roberts, T. H., Hirschberg, K. **2000**. Secretory protein trafficking and organelle dynamics in living cells. *Annu. Rev. Cell Dev. Biol. 16*, 557–589.

Littleton, J. T., Chapman, E. R., Kreber, R., Garment, M. B., Carlson, S. D., Ganetzky, B. **1998**. Temperature-sensitive paralytic mutations demonstrate that synaptic exocytosis requires SNARE complex assembly and disassembly. *Neuron 21*, 401–413.

Liu, Y., Barlowe, C. **2002**. Analysis of Sec22p in endoplasmic reticulum/Golgi transport reveals cellular redundancy in SNARE protein function. *Mol. Biol. Cell 13*, 3314–3324.

Lupas, A. N., Martin, J. **2002**. AAA proteins. *Curr. Opin. Struct. Biol. 12*, 746–753.

Margittai, M., Otto, H., Jahn, R. **1999**. A stable interaction between syntaxin 1a and synaptobrevin 2 mediated by their transmembrane domains. *FEBS Lett. 446*, 40–44.

Margittai, M., Widengren, J., Schweinberger, E., Schröder, G. F., Felekyan, S., Haustein, E., König, M., Fasshauer, D., Grubmüller, H., Jahn, R., Seidel, C. A. **2003**. Single-molecule fluorescence resonance energy transfer reveals a dynamic equilibrium between closed and open conformations of syntaxin 1. *Proc. Natl Acad. Sci. USA 100*, 15516–15521.

Martinez-Arca, S., Rudge, R., Vacca, M., Raposo, G., Camonis, J., Proux-Gillardeaux, V., Daviet, L., Formstecher, E., Hamburger, A., Filippini, F., et al. **2003**. A dual mechanism controlling the localization and function of exocytic v-SNAREs. *Proc. Natl Acad. Sci. USA 100*, 9011–9016.

Marz, K. E., Hanson, P. I. **2002**. Sealed with a twist: complexin and the synaptic SNARE complex. *Trends Neurosci. 25*, 381–383.

Marz, K. E., Lauer, J. M., Hanson, P. I. **2003**. Defining the SNARE complex binding surface of alpha-SNAP: implications for SNARE complex disassembly. *J. Biol. Chem. 278*, 27000–27008.

Matos, M. F., Mukherjee, K., Chen, X., Rizo, J., Südhof, T. C. **2003**. Evidence for SNARE zippering during Ca^{2+}-triggered exocytosis in PC12 cells. *Neuropharmacology 45*, 777–786.

Maxfield, F. R., McGraw, T. E. **2004**. Endocytic recycling. *Nat. Rev. Mol. Cell Biol. 5*, 121–132.

Mayer, A., Wickner, W., Haas, A. **1996**. Sec18p (NSF)-driven release of Sec17p (alpha-SNAP) can precede docking and fusion of yeast vacuoles. *Cell 85*, 83–94.

McMahon, H. T., Missler, M., Li, C., Südhof, T. C. **1995**. Complexins: cytosolic proteins that regulate SNAP receptor function. *Cell 83*, 111–119.

McNew, J. A., Weber, T., Engelman, D. M., Söllner, T. H., Rothman, J. E. **1999**. The length of the flexible SNAREpin juxtamembrane region is a critical determinant of SNARE-dependent fusion. *Mol. Cell 4*, 415–421.

McNew, J. A., Parlati, F., Fukuda, R., Johnston, R. J., Paz, K., Paumet, F., Söllner, T. H., Rothman, J. E. **2000**. Compartmental specificity of cellular membrane fusion encoded in SNARE proteins. *Nature 407*, 153–159.

Meeusen, S., McCaffery, J. M., Nunnari, J. **2004**. Mitochondrial fusion intermediates revealed *in vitro*. *Science 305*, 1747–1752.

Misura, K. M., Scheller, R. H., Weis, W. I. **2000**. Three-dimensional structure of the neuronal-Sec1-syntaxin 1a complex. *Nature 404*, 355–362.

Misura, K. M., Gonzalez, L. C., Jr, May, A. P., Scheller, R. H., Weis, W. I. **2001 a**. Crystal structure and biophysical properties of a complex between the N-terminal SNARE region of SNAP25 and syntaxin 1a. *J. Biol. Chem. 276*, 41301–41309.

Misura, K. M., Scheller, R. H., Weis, W. I. **2001 b**. Self-association of the H3 region of syntaxin 1A. Implications for intermediates in SNARE complex assembly. *J. Biol. Chem. 276*, 13273–13282.

Misura, K. M., Bock, J. B., Gonzalez, L. C., Jr, Scheller, R. H., Weis, W. I. **2002**. Three-dimensional structure of the amino-terminal domain of syntaxin 6, a SNAP-25 C homo-

log. *Proc. Natl Acad. Sci. USA 99*, 9184–9189.

Monck, J.R., Fernandez, J.M. **1992**. The exocytotic fusion pore. *J. Cell Biol. 119*, 1395–1404.

Munson, M., Chen, X., Cocina, A.E., Schultz, S.M., Hughson, F.M. **2000**. Interactions within the yeast t-SNARE Sso1p that control SNARE complex assembly. *Nat. Struct. Biol. 7*, 894–902.

Nagy, G., Matti, U., Nehring, R.B., Binz, T., Rettig, J., Neher, E., Sørensen, J.B. **2002**. Protein kinase C-dependent phosphorylation of synaptosome-associated protein of 25 kDa at Ser187 potentiates vesicle recruitment. *J. Neurosci. 22*, 9278–9286.

Nagy, G., Reim, K., Matti, U., Brose, N., Binz, T., Rettig, J., Neher, E., Sørensen, J.B. **2004**. Regulation of releasable vesicle pool sizes by protein kinase A-dependent phosphorylation of SNAP-25. *Neuron 41*, 417–429.

Nakamura, N., Rabouille, C., Watson, R., Nilsson, T., Hui, N., Slusarewicz, P., Kreis, T.E., Warren, G. **1995**. Characterization of a *cis*-Golgi matrix protein, GM130. *J. Cell Biol. 131*, 1715–1726.

Neher, E. **1998**. Vesicle pools and Ca^{2+} microdomains: new tools for understanding their roles in neurotransmitter release. *Neuron 20*, 389–399.

Newman, A.P., Shim, J., Ferro-Novick, S. **1990**. BET1, BOS1, and SEC22 are members of a group of interacting yeast genes required for transport from the endoplasmic reticulum to the Golgi complex. *Mol. Cell Biol. 10*, 3405–3414.

Nicholson, K.L., Munson, M., Miller, R.B., Filip, T.J., Fairman, R., Hughson, F.M. **1998**. Regulation of SNARE complex assembly by an N-terminal domain of the t-SNARE Sso1p. *Nat. Struct. Biol. 5*, 793–802.

Nonet, M.L., Saifee, O., Zhao, H., Rand, J.B., Wei, L. **1998**. Synaptic transmission deficits in *Caenorhabditis elegans* synaptobrevin mutants. *J. Neurosci. 18*, 70–80.

Novick, P., Schekman, R. **1979**. Secretion and cell-surface growth are blocked in a temperature-sensitive mutant of *Saccharomyces cerevisiae*. *Proc. Natl Acad. Sci. USA 76*, 1858–1862.

Ossig, R., Schmitt, H.D., de Groot, B., Riedel, D., Keranen, S., Ronne, H., Grubmüller, H., Jahn, R. **2000**. Exocytosis requires asymmetry in the central layer of the SNARE complex. *EMBO J. 19*, 6000–6010.

Pabst, S., Margittai, M., Vainius, D., Langen, R., Jahn, R., Fasshauer, D. **2002**. Rapid and selective binding to the synaptic SNARE complex suggests a modulatory role of complexins in neuroexocytosis. *J. Biol. Chem. 277*, 7838–7848.

Palfrey, H.C., Artalejo, C.R. **2003**. Secretion: kiss and run caught on film. *Curr. Biol. 13*, R397–R399.

Parlati, F., McNew, J.A., Fukuda, R., Miller, R., Söllner, T.H., Rothman, J.E. **2000**. Topological restriction of SNARE-dependent membrane fusion. *Nature 407*, 194–198.

Paumet, F., Brügger, B., Parlati, F., McNew, J.A., Söllner, T.H., Rothman, J.E. **2001**. A t-SNARE of the endocytic pathway must be activated for fusion. *J. Cell Biol. 155*, 961–968.

Pelham, H.R., Banfield, D.K., Lewis, M.J. **1995**. SNAREs involved in traffic through the Golgi complex. *Cold Spring Harbor Symp. Quant. Biol. 60*, 105–111.

Peng, R., Gallwitz, D. **2004**. Multiple SNARE interactions of an SM protein: Sed5p/Sly1p binding is dispensable for transport. *EMBO J. 23*, 3939–3949.

Peters, C., Mayer, A. **1998**. Ca^{2+}/calmodulin signals the completion of docking and triggers a late step of vacuole fusion. *Nature 396*, 575–580.

Peters, C., Andrews, P.D., Stark, M.J., Cesaro-Tadic, S., Glatz, A., Podtelejnikov, A., Mann, M., Mayer, A. **1999**. Control of the terminal step of intracellular membrane fusion by protein phosphatase 1. *Science 285*, 1084–1087.

Peters, C., Bayer, M.J., Buhler, S., Andersen, J.S., Mann, M., Mayer, A. **2001**. *Trans*-complex formation by proteolipid channels in the terminal phase of membrane fusion. *Nature 409*, 581–588.

Pobbati, A., Razeto, A., Böddener, M., Becker, S., Fasshauer, D. **2004**. Structural basis for the inhibitory role of tomosyn in exocytosis. *J. Biol. Chem. 279*, 47192–47200.

Praefcke, G. J., McMahon, H. T. **2004**. The dynamin superfamily: universal membrane tubulation and fission molecules? *Nat. Rev. Mol. Cell Biol. 5*, 133–147.

Protopopov, V., Govindan, B., Novick, P., Gerst, J. E. **1993**. Homologs of the synaptobrevin/VAMP family of synaptic vesicle proteins function on the late secretory pathway in *S. cerevisiae*. *Cell 74*, 855–861.

Reim, K., Mansour, M., Varoqueaux, F., McMahon, H. T., Südhof, T. C., Brose, N., Rosenmund, C. **2001**. Complexins regulate a late step in Ca^{2+}-dependent neurotransmitter release. *Cell 104*, 71–81.

Rettig, J., Neher, E. **2002**. Emerging roles of presynaptic proteins in Ca^{2+}-triggered exocytosis. *Science 298*, 781–785.

Rhee, J. S., Betz, A., Pyott, S., Reim, K., Varoqueaux, F., Augustin, I., Hesse, D., Südhof, T. C., Takahashi, M., Rosenmund, C., Brose, N. **2002**. Beta phorbol ester- and diacylglycerol-induced augmentation of transmitter release is mediated by Munc13s and not by PKCs. *Cell 108*, 121–133.

Rice, L. M., Brunger, A. T. **1999**. Crystal structure of the vesicular transport protein Sec17: implications for SNAP function in SNARE complex disassembly. *Mol. Cell 4*, 85–95.

Rizo, J., Südhof, T. C. **1998**. C2-domains, structure and function of a universal Ca^{2+}-binding domain. *J. Biol. Chem. 273*, 15879–15882.

Rizo, J., Südhof, T. C. **2002**. Snares and Munc18 in synaptic vesicle fusion. *Nat. Rev. Neurosci. 3*, 641–653.

Rizzoli, S. O., Betz, W. J. **2004**. The structural organization of the readily releasable pool of synaptic vesicles. *Science 303*, 2037–2039.

Roth, M. G. **2004**. Phosphoinositides in constitutive membrane traffic. *Physiol. Rev. 84*, 699–730.

Roy, R., Laage, R., Langosch, D. **2004**. Synaptobrevin transmembrane domain dimerization-revisited. *Biochemistry 43*, 4964–4970.

Ryan, T. A. **2003**. Kiss-and-run, fuse-pinch-and-linger, fuse-and-collapse: the life and times of a neurosecretory granule. *Proc. Natl Acad. Sci. USA 100*, 2171–2173.

Saifee, O., Wei, L., Nonet, M. L. **1998**. The *Caenorhabditis elegans* unc-64 locus encodes a syntaxin that interacts genetically with synaptobrevin. *Mol. Biol. Cell 9*, 1235–1252.

Sato, T. K., Rehling, P., Peterson, M. R., Emr, S. D. **2000**. Class C Vps protein complex regulates vacuolar SNARE pairing and is required for vesicle docking/fusion. *Mol. Cell 6*, 661–671.

Scales, S. J., Chen, Y. A., Yoo, B. Y., Patel, S. M., Doung, Y. C., Scheller, R. H. **2000**. SNAREs contribute to the specificity of membrane fusion. *Neuron 26*, 457–464.

Scales, S. J., Yoo, B. Y., Scheller, R. H. **2001**. The ionic layer is required for efficient dissociation of the SNARE complex by alpha-SNAP and NSF. *Proc. Natl Acad. Sci. USA 98*, 14262–14267.

Scales, S. J., Hesser, B. A., Masuda, E. S., Scheller, R. H. **2002**. Amisyn, a novel syntaxin-binding protein that may regulate SNARE complex assembly. *J. Biol. Chem. 277*, 28271–28279.

Schneggenburger, R., Neher, E. **2000**. Intracellular calcium dependence of transmitter release rates at a fast central synapse. *Nature 406*, 889–893.

Schoch, S., Deak, F., Königstorfer, A., Mozhayeva, M., Sara, Y., Südhof, T. C., Kavalali, E. T. **2001**. SNARE function analyzed in synaptobrevin/VAMP knockout mice. *Science 294*, 1117–1122.

Schütte, C. G., Hatsuzawa, K., Margittai, M., Stein, A., Riedel, D., Küster, P., König, M., Seidel, C., Jahn, R. **2004**. Determinants of liposome fusion mediated by synaptic SNARE proteins. *Proc. Natl Acad. Sci. USA 101*, 2858–2863.

Seabra, M. C., Wasmeier, C. **2004**. Controlling the location and activation of Rab GTPases. *Curr. Opin. Cell Biol. 16*, 451–457.

Seeley, E. S., Kato, M., Margolis, N., Wickner, W., Eitzen, G. **2002**. The genomics of homotypic vacuole fusion. *Mol. Biol. Cell 13*, 782–794.

Segev, N. **2001**. Ypt/rab gtpases: regulators of protein trafficking. *Sci STKE 2001*, RE11.

Sesaki, H., Jensen, R. E. **2004**. Ugo1p links the Fzo1p and Mgm1p GTPases for mitochondrial fusion. *J. Biol. Chem. 279*, 28298–28303.

Söllner, T., Bennett, M. K., Whiteheart, S. W., Scheller, R. H., Rothman, J. E. **1993 a**. A protein assembly–disassembly pathway *in vitro* that may correspond to sequential steps of synaptic vesicle docking, activation, and fusion. *Cell 75*, 409–418.

Söllner, T., Whiteheart, S. W., Brunner, M., Erdjument-Bromage, H., Geromanos, S., Tempst, P., Rothman, J. E. **1993 b**. SNAP receptors implicated in vesicle targeting and fusion. *Nature 362*, 318–324.

Sönnichsen, B., Lowe, M., Levine, T., Jamsa, E., Dirac-Svejstrup, B., Warren, G. **1998**. A role for giantin in docking COPI vesicles to Golgi membranes. *J. Cell Biol. 140*, 1013–1021.

Sørensen, J. B. **2004**. Formation, stabilisation and fusion of the readily releasable pool of secretory vesicles. *Pflugers Arch. 448*, 347–362.

Sørensen, J. B., Matti, U., Wei, S. H., Nehring, R. B., Voets, T., Ashery, U., Binz, T., Neher, E., Rettig, J. **2002**. The SNARE protein SNAP-25 is linked to fast calcium triggering of exocytosis. *Proc. Natl Acad. Sci. USA 99*, 1627–1632.

Sørensen, J. B., Nagy, G., Varoqueaux, F., Nehring, R. B., Brose, N., Wilson, M. C., Neher, E. **2003**. Differential control of the releasable vesicle pools by SNAP-25 splice variants and SNAP-23. *Cell 114*, 75–86.

Staal, R. G., Mosharov, E. V., Sulzer, D. **2004**. Dopamine neurons release transmitter via a flickering fusion pore. *Nat. Neurosci. 7*, 341–346.

Stevens, C. F., Williams, J. H. **2000**. "Kiss and run" exocytosis at hippocampal synapses. *Proc. Natl Acad. Sci. USA 97*, 12828–12833.

Südhof, T. C., De Camilli, P., Niemann, H., Jahn, R. **1993**. Membrane fusion machinery: insights from synaptic proteins. *Cell 75*, 1–4.

Sun-Wada, G. H., Wada, Y., Futai, M. **2004**. Diverse and essential roles of mammalian vacuolar-type proton pump ATPase: toward the physiological understanding of inside acidic compartments. *Biochim. Biophys. Acta 1658*, 106–114.

Sutton, R. B., Fasshauer, D., Jahn, R., Brunger, A. T. **1998**. Crystal structure of a SNARE complex involved in synaptic exocytosis at 2.4 Å resolution. *Nature 395*, 347–353.

Sweeney, S. T., Broadie, K., Keane, J., Niemann, H., O'Kane, C. J. **1995**. Targeted expression of tetanus toxin light chain in Drosophila specifically eliminates synaptic transmission and causes behavioral defects. *Neuron 14*, 341–351.

Szule, J. A., Coorssen, J. R. **2003**. Revisiting the role of SNAREs in exocytosis and membrane fusion. *Biochim. Biophys. Acta 1641*, 121–135.

Thorn, P., Fogarty, K. E., Parker, I. **2004**. Zymogen granule exocytosis is characterized by long fusion pore openings and preservation of vesicle lipid identity. *Proc. Natl Acad. Sci. USA 101*, 6774–6779.

Tochio, H., Tsui, M. M., Banfield, D. K., Zhang, M. **2001**. An autoinhibitory mechanism for nonsyntaxin SNARE proteins revealed by the structure of Ykt6p. *Science 293*, 698–702.

Toomre, D., Steyer, J. A., Keller, P., Almers, W., Simons, K. **2000**. Fusion of constitutive membrane traffic with the cell surface observed by evanescent wave microscopy. *J. Cell Biol. 149*, 33–40.

Toonen, R. F., Verhage, M. **2003**. Vesicle trafficking: pleasure and pain from SM genes. *Trends Cell Biol. 13*, 177–186.

Tsuboi, T., McMahon, H. T., Rutter, G. A. **2004**. Mechanisms of dense core vesicle recapture following "kiss and run" ("cavicapture") exocytosis in insulin-secreting cells. *J. Biol. Chem. 279*, 47115–47124.

Uemura, T., Ueda, T., Ohniwa, R. L., Nakano, A., Takeyasu, K., Sato, M. H. **2004**. Systematic analysis of SNARE molecules in arabidopsis: dissection of the post-Golgi network in plant cells. *Cell Struct. Funct. 29*, 49–65.

Ungermann, C., Sato, K., Wickner, W. **1998**. Defining the functions of *trans*-SNARE pairs. *Nature 396*, 543–548.

Ungermann, C., Wickner, W. **1998**. Vam7p, a vacuolar SNAP-25 homolog, is required for SNARE complex integrity and vacuole docking and fusion. *EMBO J. 17*, 3269–3276.

Vacquier, V. D. **1975**. The isolation of intact cortical granules from sea urchin eggs: calcium lons trigger granule discharge. *Dev. Biol. 43*, 62–74.

Varlamov, O., Volchuk, A., Rahimian, V., Doege, C. A., Paumet, F., Eng, W. S., Arango, N., Parlati, F., Ravazzola, M., Orci, L., et al. **2004**. i-SNAREs: inhibitory SNAREs that fine-tune the specificity of membrane fusion. *J. Cell Biol. 164*, 79–88.

Vites, O., Rhee, J. S., Schwarz, M., Rosenmund, C., Jahn, R. **2004**. Reinvestigation of the role of snapin in neurotransmitter release. *J. Biol. Chem. 279*, 26251–26256.

Vogel, S. S., Chernomordik, L. V., Zimmerberg, J. **1992**. Calcium-triggered fusion of exocytotic granules requires proteins in only one membrane. *J. Biol. Chem. 267*, 25640–25643.

Walch-Solimena, C., Blasi, J., Edelmann, L., Chapman, E. R., von Mollard, G. F., Jahn, R. **1995**. The t-SNAREs syntaxin 1 and SNAP-25 are present on organelles that participate in synaptic vesicle recycling. *J. Cell Biol. 128*, 637–645.

Wang, C. T., Grishanin, R., Earles, C. A., Chang, P. Y., Martin, T. F., Chapman, E. R., Jackson, M. B. **2001**. Synaptotagmin modulation of fusion pore kinetics in regulated exocytosis of dense-core vesicles. *Science 294*, 1111–1115.

Wang, C. T., Lu, J. C., Bai, J., Chang, P. Y., Martin, T. F., Chapman, E. R., Jackson, M. B. **2003**. Different domains of synaptotagmin control the choice between kiss-and-run and full fusion. *Nature 424*, 943–947.

Wang, Y., Dulubova, I., Rizo, J., Südhof, T. C. **2001**. Functional analysis of conserved structural elements in yeast syntaxin Vam3p. *J. Biol. Chem. 276*, 28598–28605.

Washbourne, P., Thompson, P. M., Carta, M., Costa, E. T., Mathews, J. R., Lopez-Bendito, G., Molnar, Z., Becher, M. W., Valenzuela, C. F., Partridge, L. D., Wilson, M. C. **2002**. Genetic ablation of the t-SNARE SNAP-25 distinguishes mechanisms of neuroexocytosis. *Nat. Neurosci. 5*, 19–26.

Weber, J., Senior, A. E. **2003**. ATP synthesis driven by proton transport in F_1F_0-ATP synthase. *FEBS Lett. 545*, 61–70.

Weber, T., Zemelman, B. V., McNew, J. A., Westermann, B., Gmachl, M., Parlati, F., Söllner, T. H., Rothman, J. E. **1998**. SNAREpins: minimal machinery for membrane fusion. *Cell 92*, 759–772.

Wei, S., Xu, T., Ashery, U., Kollewe, A., Matti, U., Antonin, W., Rettig, J., Neher, E. **2000**. Exocytotic mechanism studied by truncated and zero layer mutants of the C-terminus of SNAP-25. *EMBO J. 19*, 1279–1289.

Weninger, K., Bowen, M. E., Chu, S., Brunger, A. T. **2003**. Single-molecule studies of SNARE complex assembly reveal parallel and antiparallel configurations. *Proc. Natl Acad. Sci. USA 100*, 14800–14805.

Westermann, B. **2003**. Mitochondrial membrane fusion. *Biochim. Biophys. Acta 1641*, 195–202.

Whiteheart, S. W., Matveeva, E. A. **2004**. Multiple binding proteins suggest diverse functions for the N-ethylmaleimide sensitive factor. *J. Struct. Biol. 146*, 32–43.

Whiteheart, S. W., Schraw, T., Matveeva, E. A. **2001**. *N*-ethylmaleimide sensitive factor (NSF) structure and function. *Int. Rev. Cytol. 207*, 71–112.

Whyte, J. R., Munro, S. **2002**. Vesicle tethering complexes in membrane traffic. *J. Cell Sci. 115*, 2627–2637.

Wickner, W. **2002**. Yeast vacuoles and membrane fusion pathways. *EMBO J. 21*, 1241–1247.

Wickner, W., Haas, A. **2000**. Yeast homotypic vacuole fusion: a window on organelle trafficking mechanisms. *Annu. Rev. Biochem. 69*, 247–275.

Wilkens, S., Inoue, T., Forgac, M. **2004**. Three-dimensional structure of the vacuolar ATPase: localization of subunit H by difference imaging and chemical cross-linking. *J. Biol. Chem. 279*, 41942–41949.

Wilson, D. W., Wilcox, C. A., Flynn, G. C., Chen, E., Kuang, W. J., Henzel, W. J., Block, M. R., Ullrich, A., Rothman, J. E. **1989**. A fusion protein required for vesicle-mediated transport in both mammalian cells and yeast. *Nature 339*, 355–359.

Xu, T., Rammner, B., Margittai, M., Artalejo, A. R., Neher, E., Jahn, R. **1999**. Inhibition of SNARE complex assembly differentially affects kinetic components of exocytosis. *Cell 99*, 713–722.

Yang, B., Gonzalez, L., Jr, Prekeris, R., Steegmaier, M., Advani, R. J., Scheller, R. H. **1999**. SNARE interactions are not selective. Implications for membrane fusion specificity. *J. Biol. Chem. 274*, 5649–5653.

Zenisek, D., Steyer, J. A., Feldman, M. E., Almers, W. **2002**. A membrane marker leaves synaptic vesicles in milliseconds after exocytosis in retinal bipolar cells. *Neuron 35*, 1085–1097.

Zerial, M., McBride, H. **2001**. Rab proteins as membrane organizers. *Nat. Rev. Mol. Cell Biol. 2*, 107–117.

Zhang, F., Chen, Y., Su, Z., Shin, Y. K. **2004**. SNARE assembly and membrane fusion: a kinetic analysis. *J. Biol. Chem.* 279, 38668–38672.

12
Interplay of Proteins and Lipids in Virus Entry by Membrane Fusion

Alex L. Lai, Yinling Li, and Lukas K. Tamm

12.1
Introduction

A large number of animal viruses are enveloped by lipid bilayer membranes. Since enveloped viruses bud during biogenesis from specialized areas of the host cell surface, viral membrane envelopes are also highly specialized in terms of their lipid and protein compositions. Like the cell membranes from which they derive, they are enriched in sphingomyelin, phosphatidylcholine (PC) and cholesterol in the outer leaflet, and phosphatidylethanolamine (PE) and various negatively charged lipids in the inner leaflet. Viral membrane envelopes contain only a very small number, typically one to three, different integral membrane proteins. Most viral membrane envelope proteins are glycosylated and appear as elongated projections or spikes in electron micrographs of these viruses. The different viral spike glycoproteins have a number of specific tasks in viral cell entry. One function is to attach viruses to receptors on the surface of target cells. A second major function is to promote the fusion of viral and target cell membranes, either directly at the cell surface or after endocytosis with the endosomal membrane in a reaction that proceeds only at the lower pH that prevails in the endosome. In some viruses, both functions are packaged into a single protein, whereas in other viruses they are distributed between two different proteins. The atomic structures of the ectodomains of several viral spike glycoproteins have been solved by X-ray crystallography. According to these structures, viral membrane fusion proteins are generally grouped into two classes. Class I viral fusion proteins are elongated proteins characterized by trimeric bundles of helical hairpins with coiled-coil α-helical cores. In contrast, class II viral fusion proteins consist of three β-sheet domains that pair into dimers and form relatively flat lattices on the viral membrane surfaces (Fig. 12.1).

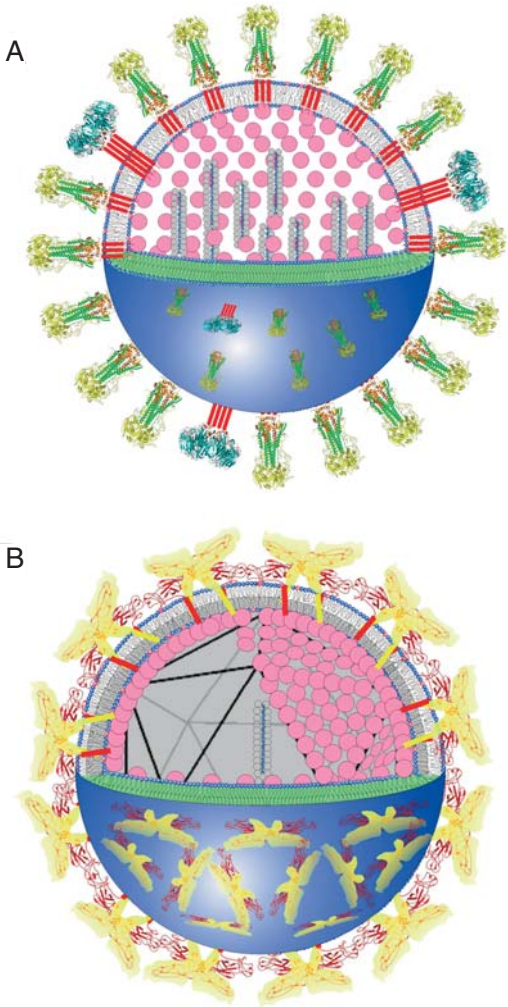

Fig. 12.1 Diagrams of representative membrane-enveloped viruses with type I and type II fusion proteins.
(A) Influenza virus. The type I fusion spike glycoprotein is HA, which is a trimer consisting of three identical subunits. Each subunit is composed of HA1 and HA2 chains. The coiled-coil structures (green) in the stem are formed by the HA2 chains and the globular domains (yellow) at the tip of the molecule are formed by the HA1 chains. The virus also contains the matrix M1 protein (pink) and eight segments of single (–) strand RNA (blue) that together with the nucleocapsid protein NP (grey) form ribonucleoprotein complexes. The envelope also contains neuraminidase NA (blue) and the proton channel M2 protein (not shown) in relatively small copy numbers.
(B) Semliki Forest virus. The type II fusion glycoprotein is the E1 protein (red) that forms together with the receptor binding protein E2 (yellow) a $T=4$ icosahedral lattice on the membrane surface. The nucleocapsid consists of 240 copies of the capsid protein C (pink). A single (+) strand RNA (blue) contains the entire genome of this alphavirus. The envelope also contains the small soluble E3 protein in stoichiometric amounts (not shown).

12.2
Fusion of Pure Lipid Bilayers

Pure lipid bilayers do not spontaneously fuse. The headgroups of phospholipids are highly hydrated and hydration repulsion prevents the spontaneous fusion of uncharged lipid bilayers. If bilayers are negatively charged, charge repulsion adds to the repulsive energy between lipid bilayers. At equilibrium, fluid-phase PC binds about 34 molecules of water and PE binds about eight waters per lipid [1]. Therefore, the equilibrium distance measured from headgroup phosphate to headgroup phosphate between two fluid-phase lipid bilayers is about 30 Å for PC bilayers and about 10 Å for PE bilayers. The hydration of negatively charged phosphatidylserine (PS) is similar or slightly larger than that of PC [2]. This hydration barrier must be overcome en route to membrane fusion. There are a few different views of how this could happen. These will be briefly discussed in the following.

It has been postulated as early as in the late 1970s and early 1980s that membrane fusion may proceed through "point defects" [3, 4]. The nature of these point defects, however, was not so clear. Markin et al. proposed in a theoretical study that membrane fusion could proceed through an hourglass-shaped "lipid stalk" intermediate [5]. Since lipid stalks are thought to be transient structures that may exist only briefly, these structures have never been observed experimentally in membrane fusion. However, arrays of lipid stalks have recently been observed in X-ray diffraction experiments of aligned stacks of membranes at submaximal hydration [6, 7]. Under specialized experimental conditions, pure lipid bilayers can also be observed to form "hemifusion" diaphragms when they are closely apposed to each other. In hemifusion, the two distal leaflets of two approaching bilayers join to form a single bilayer in the central hemifused region. Depending on the experimental set-up, hemifusion diaphragms may be quite extended. Hemifusion has been observed electrophysiologically in planar bilayer experiments [8, 9] and in the surface forces apparatus when two mica-supported lipid bilayers are mechanically pushed together [10, 11]. The combination of electrophysiological and theoretical studies on pure lipid bilayer fusion led to the "stalk–pore" model of membrane fusion (reviewed in [12]). In this model, lipid stalks radially expand until the two distal monolayers contact each other to form a hemifusion diaphragm. The hemifusion diaphragm is thought to break at some point to form an initial fusion pore. The stalk and initial pore intermediates have different curvatures, whose energies have been calculated in numerous theoretical studies. The effect of lipid additives that alter the spontaneous curvature of lipid bilayers are consistent with the stalk–pore model. For example, lyso-PC (induces positive curvature) added to the proximal monolayers and oleic acid (induces negative curvature) added to the distal monolayers promote fusion, whereas lyso-PC added to the distal monolayers and oleic acid added to the proximal monolayers inhibit fusion [12]. These and a multitude of similar studies on many different reconstituted and biological fusion systems are often taken as direct evidence for the stalk–pore model of membrane fusion. However, the reader should be cautioned: neither theoretical calculations of en-

ergies of stalks nor the correlation between the effect of curvature agents on the calculated energy of stalks and membrane fusion prove that neatly organized stalks actually exist as intermediates in fusion. They just prove that calculated energies with sometimes somewhat arbitrarily chosen boundary conditions are compatible with certain non-bilayer lipid structures and that certain lipophilic agents produce membrane situations (curvature, hydration, defects, etc.) that are conducive/inhibitory to membrane fusion. It is important to make this distinction because the stalk–pore model has become so popular recently that many take it for a fact rather than a model. One should also be aware that it is virtually impossible to distinguish experimentally between different stalk and hemifusion intermediates in fusion of biological membranes because, by definition, lipids can exchange freely between the two membranes through all hemifusion intermediates. If well-organized stalks exist, they are probably short-lived transient intermediates that according to the newer models progress directly to fusion pre-pores without the need for a transmonolayer contact hemifusion intermediate [13]. Extended hemifusion diaphragms may occur rather as off-pathway side-products under suboptimal conditions in biological membrane fusion [14–18].

Lentz et al. developed sophisticated methods to monitor many important details of the kinetics of fusion between pure lipid bilayers [19]. In this work, small unilamellar vesicles were induced to fuse by the addition of 5–20% polyethylene glycol of molecular weight 8000. Polyethylene glycol aggregates the vesicles by reducing the activity of water. It has been found that bilayers composed of PC, PE, sphingomyelin and cholesterol at a molar ratio of 35 : 30 : 15 : 20 fuse quite efficiently and in a non-leaky fashion [20]. The kinetics of outer leaflet lipid mixing (fast), transbilayer lipid movement (intermediate), inner leaflet mixing (intermediate) and contents mixing (slow) have been resolved [21]. Clearly, outer leaflet lipid mixing (around 0.5 min) and pore formation (4–6 min) are two distinct kinetic processes in these well-defined pure lipid bilayer model systems. A "problem" of the original stalk–pore model for membrane fusion is that hydrophobic "voids", i.e. volumes of hydrophobic mismatch are created in the stalk, which may be energetically very costly [22, 23]. Different authors have tried to get around this problem by different means. Newer calculations have simply eliminated the voids by assuming intermediate structures with tilted lipids [13, 24] or reduced their effects by relaxing the geometry of the stalk [25]. In another effort to rescue the original stalk model, it has been postulated that the "voids" have to be filled by hydrophobic substances that reduce the high energy of the stalk and make it a viable intermediate in lipid bilayer fusion. Indeed, when small amounts of very long-chain lipids or alkanes were added to the lipid mixtures, the rates of fusion (contents mixing), but not hemifusion (lipid mixing) of pure lipid bilayers were increased up to about 2-fold [26]. This rate increase was additional to that achieved by negative curvature inducing lipids. Even if the rates are increased by these lipid additions, these experiments do not explain why bilayers in their absence are still able to fuse at fairly rapid rates. Finally self-consistent field theory of flexible amphiphilic chains has been used to model the formation of traditional lipid stalks [27]. The energetic bar-

rier to forming a stalk derived from this theory was significantly smaller than that derived from the phenomenological continuum theories, but a large energetic barrier, which depended on the spontaneous intrinsic curvature of the amphiphile, was associated with the radial expansion of the stalk into a hemifusion diaphragm.

Coarse-grained molecular simulations have been used recently to provide more insight into the microscopic details of transitions at lipid bilayer fusion junctions. In one study, lipids were modeled as amphiphilic three-segment rods and studied by Brownian dynamics [28]. In another set of studies, the amphiphiles were modeled as flexible co-polymer chains in a hydrophilic polymer solvent and their transformation from bilayers into fusion intermediates was studied by Monte-Carlo lattice simulations [29, 30]. Interestingly, the outcome of both approaches was similar and suggested a new fusion mechanism, which was different from the classical stalk–pore mechanism. After formation of an initial quite disordered lipid stalk between two closely apposed bilayers, a hole appeared in either one or both parent membranes next to the stalk and the stalk then grew asymmetrically around these holes to form the initial fusion pore. These initial small holes appear in the bilayer because the line tension is high near disorganized lipid stalks. Coarse-grained molecular dynamics simulations revealed a few additional new aspects of microscopic details in the evolution of lipid stalks and fusion pores [31, 32]. In one study [31], the stalk was initiated by the displacement of a few lipid molecules from their normal position in one of the two bilayers. Fusion could then proceed through the classical stalk–pore or the new stalk–hole mechanism. Which mechanism prevailed depended on the headgroup composition of the bilayers with negative curvature-inducing lipids favoring the stalk–pore and bilayer-forming lipids favoring the stalk–hole mechanism. In the other study [32], the lipid molecules became tilted and eventually splayed their aliphatic tails such that each chain was resident in different opposing leaflets. The nucleus of the initial stalk formed by lipid tail splaying was again seen to expand asymmetrically in a circle to gradually enclose an initial fusion pore. Whether specific details of each of these mechanisms will hold up for bilayers made of "real" phospholipids (i.e. not coarse-grained models) remains to be seen. However, the fact that so many different oversimplified models and methods of simulation independently led to very similar general results is very promising. Perhaps the recently observed spurious leakage in influenza hemagglutinin (HA)-mediated membrane fusion is a reflection of hole formation in the new stalk–hole model of membrane fusion and thus may provide experimental support for this mechanism [33]. New details of how fusion between pure lipid bilayers proceeds at the microscopic level will almost certainly emerge as computational simulation methods continue to be further refined and as computer power increases year-by-year.

12.3
Viral Protein Sequences that Mediate Lipid Bilayer Fusion

12.3.1
Fusion Peptides

Photoaffinity labeling studies have shown that the major regions of viral spike glycoproteins that interact with lipid bilayers are domains called "fusion peptides" as well as the transmembrane anchors of the viral spike glycoproteins. While the transmembrane anchor domains are permanently inserted into the viral lipid bilayer, the fusion peptides interact with the lipid bilayer of target (and/or viral) membranes only upon activation of the fusion process. Although fusion peptides are quite hydrophobic, these polypeptide sequences are protected by other parts of the viral spike glycoproteins and therefore do not interact with membranes in their resting state. Many fusion peptides like those of the influenza and human immunodeficiency viruses are located at the extreme N-terminus of the fusion

Virus	*Class*	*Sequence*	*Gly*	*Ala*
		N-terminal		
Influenza HA2:	Class I	GLFGAIAGFI ENGWEGMIDG WYGF	29%	8%
HIV-1 gp41:	Class I	AVGIGALFLG FLGAAGSTMG AASMTLTVQA	20%	23%
Sendai F1:	Class I	FFGAVIGTIA LGVATSAQIT AGIALA	15%	27%
Respir. Syn. F1:	Class I	FLGFLLGVGS AIASGVAVSK VLHL	17%	12%
		internal		
Ebola GP:	Class I	GAAIGLAWIP YFGPAA	19%	31%
ASLV gp37:	Class I	IFASILAPGV AAAQAL	6%	38%
Dengue E:	Class II	DRGWGNGCGL FGKGGIVTCA	35%	5%
TBE E:	Class II	DRGWGNHCGL FGKGSIVA	28%	6%
SFV E1:	Class II	DYQCKVYTGV YPFMWGGAYC FCD	13%	4%

Fig. 12.2 Sequences of class I and II N-terminal and internal fusion peptides. Glycines and alanines, which are frequent in these sequences are highlighted. Bulky aromatic residues are underlined and hydrophilic residues are marked with a dot. HIV, human immunodeficiency virus; ASLV, avian sarcoma leukemia virus; TBE, tick-borne encephalitis virus; SFV, Semliki Forest virus.

subunit of the viral spike glycoproteins. Others such as those of Ebola or Dengue virus are internal sequences of the respective fusion proteins. A list of a few selected fusion peptides is shown in Fig. 12.2 (see also [34, 35]).

The sequences of fusion peptides are extremely well conserved within each family of viruses, but not between different families. There are, however, some general features that are common between fusion peptides of the different virus families: the propensities of glycines and alanines are high, large bulky aromatic residues are frequently found, and hydrophilic residues are found interspersed towards the C-terminal end of N-terminal fusion peptides and towards both ends of internal fusion peptides. Although it is not always totally clear where a fusion peptide sequence begins and ends, site-directed mutagenesis has shown that quite dramatic fusion phenotype changes are found with some only relatively mild single amino acid changes in the fusion peptide region. Most evidence for this comes from work with influenza virus [36–40], whose fusion protein HA contains a receptor binding subunit (HA1) and a fusion subunit (HA2). Glycines 1 and 4 of HA2 are particularly susceptible to fusion defects. For example, the G1S mutant causes hemifusion, whereas a G1V replacement is completely defective in fusion [39]. Large bulky hydrophobic residues can be replaced with other large bulky hydrophobic residues, but not with glycines [40]. It appears that a proper balance and spacing of glycines and large bulky hydrophobic residues in the fusion peptide is important to confer fusion activity to influenza HA2. Even a deletion of the first glycine is not tolerated in this fusion protein [41].

12.3.2
Transmembrane Domains

A first indication that the transmembrane domain is also very important for fusion and not just for anchoring the fusion protein in the viral membrane came from a study in which the transmembrane domain of influenza HA2 was replaced with a glycosylphosphatidylinositol anchor [14]. This construct was able to induce hemifusion between HA expressing and red blood cells, but it was unable to complete the reaction to develop a full fusion pore. Subsequent studies in several laboratories established that there was little requirement on the actual sequence of the transmembrane domain, but that its length mattered. For example, HA constructs with only the N- or C-terminal half of the transmembrane domain present mediated hemifusion, but not full fusion, and full fusion was gradually recovered as the domain length was increased to its full length [42].

12.3.3
Other Regions of the Fusion Protein

Some fusion proteins with N-terminal fusion peptides contain other segments of the ectodomain that may interact with lipids in the process of membrane fusion. For example, the kink region of the ectodomain of influenza HA2 (resi-

dues 106–112) that connects the inner and outer layer α-helices in the pH5 structure has been proposed to contribute to membrane fusion [43] either by pH-dependent lipid interactions [44] or protein–protein interactions [45]. Similarly, it has been suggested that paramyxoviruses contain an internal membrane-interactive segment in addition to the N-terminal fusion peptide [46]. This putative internal secondary fusion peptide, which comprises residues 208–229 of the Sendai virus F protein is located in between the N- and C-terminal heptad repeats that form coiled coils in the post-fusion structure [47]. This sequence also maps to the C-terminal end of the N-terminal heptad repeat and a short helix (N1) that is part of the neck in the pre-fusion structure of the F protein of the related Newcastle disease virus [48].

It has been reported that a tryptophan-rich region just N-terminal to the transmembrane domain of HIV gp41 contributes to membrane fusion [49, 50]. This segment has been predicted to lie in the interface of the external leaflet of the viral membrane. A similar interfacial juxta-membrane domain has been predicted to exist in Ebola virus [51]. It is interesting to note that juxta-membrane domains have also been implicated to contribute to fusion in the SNARE proteins syntaxin 1a and synaptobrevin 2, and that the aromatic residues of this segment may serve an important structural and functional role in this process (see also Chapter 11) [52].

Finally, HIV and other lenti- and retroviruses contain three consecutive helices on the cytoplasmic or inner side of the viral membrane that exhibit large hydrophobic moments that promote strong interactions with the inner surfaces of the viral membranes. However, rather than contributing to fusion, the predominant roles of these amphipathic helices appear to direct the intracellular targeting of the Env glycoproteins in virus assembly and their targeting to the perinuclear envelope after host cell entry [53]. In the case of influenza HA2, the cytoplasmic domain comprises only 13 residues, three of which are palmitoylated cysteines. Palmitoylation appears to be particularly important in intracellular vesicle traffic for correctly targeting HAs to the apical membrane and for subsequent virus assembly [54, 55]. However, a minor modulatory role in fusion pore opening has also been ascribed to the palmitoylated cytoplasmic tail of influenza HA2 [56].

12.4 Interactions of Fusion Peptides with Lipid Bilayers

N-terminal fusion peptides likely form independent folding units in membranes and, therefore, are sometimes also called fusion domains. The reason for this contention is that the linkers between fusion peptides and the structured ectodomains (1) contain several glycines, (2) are not ordered in crystal structures even if the residues are present, and (3) are susceptible to protease digestion. Moreover, the lipid bilayer and its interface constitutes a very different folding environment for membrane proteins or inserted peptides than the aqueous environment, in which ectodomains fold [57]. However, to obtain meaningful folding units of fusion peptide models in lipid bilayers, it is important to choose peptides that comprise the

full length of the membrane-interactive fusion domain. Peptides can be quite polymorphic in membrane environments and different conformations and molecular properties may be expressed if shorter than full-length peptide models are chosen. This has been a particular problem in studies of the HIV envelope glycoprotein gp41 fusion peptide in lipid bilayers, where different authors have found quite diverging results. As seen in Fig. 12.2, this fusion peptide is quite long, but several studies have used relatively short model peptides to study the interactions with lipid bilayers. The hydrophobicity of the full-length HIV gp41 fusion peptide also makes it quite prone to aggregation in solution and in membranes, which adds further difficulties in its handling and potential reasons for differences in results that have been reported for this peptide. Therefore, choosing a certain length of a fusion peptide model often represents a trade-off between a short sequence that is more easily handled and a long sequence that may better represent the membrane-bound structure of the full-length protein, but may form non-physiological aggregates before it is incorporated into the membrane. The results that are summarized below should be judged in the light of this background.

12.4.1 HIV Fusion Peptide–Bilayer Interactions

Some of the earliest studies on the HIV gp41 fusion peptide reported that the 16 most N-terminal residues inserted as an oblique α-helix into lipid bilayers [58, 59]. The oblique insertion correlated with the fusion activity because mutations with reduced activity inserted more parallel to the membrane surface as determined by polarized Fourier transform infrared (FTIR) spectroscopy. This finding was in agreement with a prediction from computer models of several viral fusion peptides that a tilted insertion into membranes might be a common feature of many viral fusion peptides [60]. The N-terminal segment of the simian immunodeficiency virus (SIV) fusion peptide analog was also found by neutron diffraction to insert as an oblique α-helix into lipid bilayers [61]. The first 23 residues of the HIV fusion peptide were also predominantly α-helical at low concentrations in membranes, but adopted an extended β-structure at higher concentrations [62, 63]. A still longer HIV fusion peptide analog (first 33 residues) was found by circular dichroism (CD) and FTIR spectroscopy to consist of about 30% α-helical and 50% β-structures [64]. Solution-state nuclear magnetic resonance (NMR) studies of the first 23-residue peptide revealed that these segments adopted predominantly α-helical structures in sodium dodecylsulfate (SDS) [65] and dodecylphosphocholine (DPC) micelles [66], but solid-state NMR found the first 23 residues of the HIV fusion peptide in parallel and antiparallel laterally associated β-sheet conformations when bound to lipid bilayer membranes [67–69]. Combining site-directed ^{13}C-FTIR spectroscopy and molecular modeling, Gordon et al. [70] suggested that the first 16 residues of the HIV fusion peptide are α-helical and the next seven residues extended under dilute conditions in lipid bilayers. In solution and at higher loading on membranes, the same peptide assembles into antiparallel β-sheets [71].

12.4.2 Influenza Fusion Peptide Structure

CD and FTIR spectroscopy showed that the fusion peptide of influenza virus HA2 adopts about 50% helix in lipid bilayers [72–74]. This has been confirmed with 23-residue models of the HA fusion peptides [75]. Several critical single site mutations in positions 1, 5 and 7 induce larger amounts of β-structure, when these peptides are incorporated into lipid bilayers [75, 76]. The relative proportion of β-structure is roughly anti-correlated with fusion activity when the same mutation is introduced into the full-length HA and fusion is measured between HA-expressing cells. The fusion activity is not so easily measured with the peptide models themselves because generally only lipid mixing, but not contents mixing, are observed in liposome fusion assays with peptides. In contrast to their full-length analogs, fusion peptides cause contents leakage, i.e. pore formation, when added to lipid bilayers [77, 78]. Short of testing the effect of mutations in full-length fusion proteins, the best correlation between fusion-active and inactive peptide models is their ability to cause hemolysis in red blood cells [74, 76]. Why hemolysis induced by mutant fusion peptides is a better indicator for fusion activity of the full-length protein with the same mutation than lipid mixing and leakage assays of peptides with liposomes is not entirely clear.

The influenza HA2 fusion peptide models discussed so far were all only poorly soluble in water and had to be added to liposomes from dimethylsulfoxide or combined with lipids in organic solvents for structural and functional measurements. To eliminate potential artifacts that might arise from solvent exposure of the peptides, we designed a new generation of fusion peptide models which had a very polar carrier peptide appended to the C-terminus of the fusion peptide via a flexible, i.e. glycine-rich, linker. The polar carrier peptide in a sense replaces the ectodomain of the fusion protein in these models. This strategy generates fusion peptides that are highly soluble in water or buffer, while retaining their ability to bind and insert into lipid bilayers with high affinity [79]. The solubilized 20-residue fusion peptide of influenza HA2 is largely random coil in solution, but adopts about 50% α-helical structure when bound to lipid bilayers as do the first-generation fusion peptides [79]. At very high surface concentrations on lipid bilayers, a fraction of the peptide is converted to extended self-associated β-structures at the membrane surface [80]. The new peptide design has permitted their atomic structures to be solved by solution NMR in DPC detergent micelle solutions at pH 7 and 5 [81]. The pH 5 structure is the physiologically relevant structure when influenza HA interacts with target membranes in the endosome, but the pH 7 structure is also informative because the differences between the two pH structures explain why influenza virus requires a low pH not only for releasing the fusion peptide by the conformational change of its ectodomain, but also for membrane fusion. Both structures are characterized by a well-defined N-terminal α-helix that extends to glutamate 11 (Fig. 12.3). Residues 11–13 form a turn and redirect the polypeptide chain so that it forms a “V” or “boomerang” with an opening angle of about

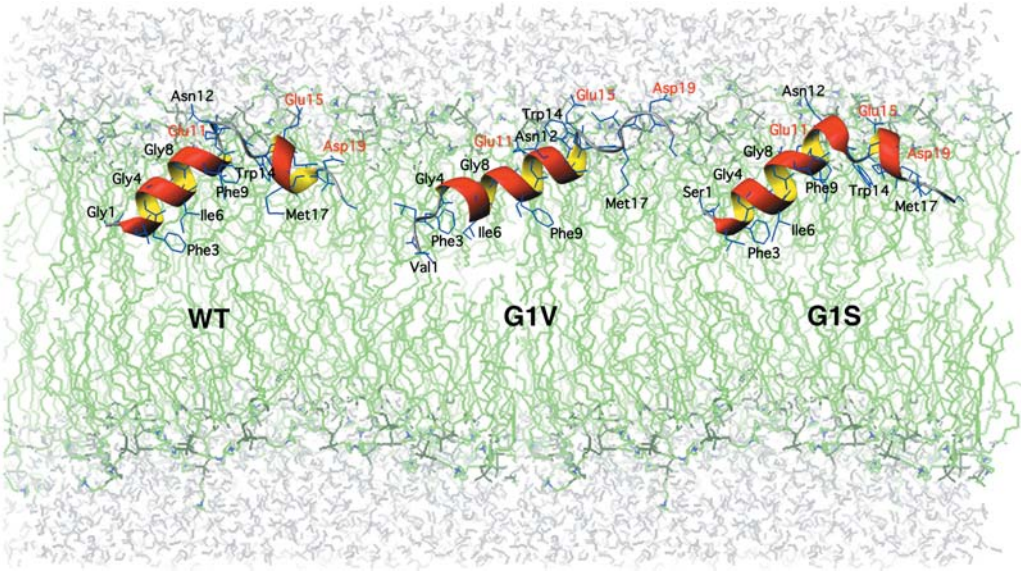

Fig. 12.3 Structures of the influenza HA fusion peptide in a lipid bilayer membrane at pH 5. The atomic structures of the wild-type, the glycine1-to-valine mutant (which causes a complete fusion defect), and the glycine1-to-serine mutant (which causes hemifusion) fusion peptides are shown. All structures were determined by NMR in DPC micelles and their dispositions in lipid bilayers were measured by site-directed spin-labeling (adapted from [81, 86]).

105°. The C-terminal arm does not form a regular secondary structure at pH 7, but residues 14–18 form a 3_{10}-helix at pH 5. The inner volume of the boomerang is filled with bulky hydrophobic residues, a ridge of conserved glycines lines the N-terminal outer face and polar residues characterize the C-terminal outer face of the boomerang at pH 5, but not at pH 7. Therefore, folding of the C-terminal arm at pH 5 likely drives the N-terminal arm deeper into the membrane. These structures determined in detergent micelles by NMR have been confirmed by site-directed spin-labeling in lipid bilayers [81]. The spin-label electron paramagnetic resonance (EPR) measurements also determine the angle between the N-terminal α-helix and the membrane plane (23° at pH 7 and 38° at pH 5) and the depth of membrane penetration of the fusion peptide. These studies confirmed and substantially refined earlier spin-label studies on a HA2 construct with the fusion peptide and a differently designed fusion peptide [82, 83]. Fig. 12.3 shows that the Cα of Asn 12, which forms the apex of the boomerang, is located in the phosphate plane of a fluid lipid bilayer. The N-terminal arm penetrates to about the mid-plane of the lipid bilayer at pH 5, but to a shallower depth at pH 7. Two NMR structures of a different influenza HA2 fusion peptide analog are also available [84, 85]. Since two of the conserved glycines were replaced with glutamates (to make the peptides more soluble) and since in one study the peptide was bound to highly negatively charged SDS micelles, it

is not surprising that many details of the structures are quite different, although some general aspects of the wild-type structure of Fig. 12.3 are preserved.

12.4.3 Influenza Fusion Peptide Mutants

The structures of the hemifusion-inducing fusion peptide mutant G1S and the fusion-blocking mutant G1V have also been determined recently by NMR in DPC micelles using the polar C-terminal carrier peptide approach [86]. The NMR structure of G1S is very similar to that of the wild-type (Fig. 12.3). It also forms an amphipathic boomerang with all bulky hydrophobic residues sequestered into the hydrophobic pocket of the structure. Only the glycine ridge on the N-terminal outer edge is disrupted. In contrast, G1V forms an irregular approximately linear amphipathic helix (Fig. 12.3). Site-directed spin-labeling shows that this helix is oriented more parallel to the membrane surface. Apparently, an angled and deeply membrane inserted boomerang structure is necessary to promote hemifusion, but a preserved glycine ridge is further required to drive the hemifusion intermediate into a full fusion product.

12.4.4 Binding of Fusion Peptides to Lipid Bilayers

The binding of the solubilized fusion peptides to lipid bilayers has been measured by fluorescence spectroscopy and isothermal titration calorimetry [79, 80, 87]. The free energy of partitioning of the wild-type influenza HA2 fusion peptide into fluid lipid bilayers is –7.6 kcal mol^{-1}. In small unilamellar vesicles, this interaction is driven by enthalpy (–18.0 kcal mol^{-1}) and opposed by entropy (10.4 kcal mol^{-1}). Apparently, there is a real energetic affinity of the fusion peptide for highly curved membrane interfaces, rather than a classical hydrophobic effect-driven peptide association with the lipid bilayer. The entropy loss (–34.8 kcal mol^{-1}) could be due to a combination of folding of the peptide and its partial immobilization (reduction of dimensionality of degrees of motional freedom) upon membrane binding. Interestingly, the enthalpy of binding of G1V is much reduced (–9.2 kcal mol^{-1}), but that of G1S is similar to that of the wild-type fusion peptide (–15.9 kcal mol^{-1}). Recent results from our laboratory show that measurements of binding enthalpy are more sensitive than measurements of free energy to discriminate between active and inactive fusion peptides (A. L. Lai and L. K. Tamm, unpublished results).

12.4.5 Sendai, Measles and Ebola Fusion Peptide–Bilayer Interactions

The secondary structures and lipid interactions of the N-terminal fusion peptides of the F proteins of two paramyxoviruses, Sendai and measles virus, have also been studied. The fusion peptide of Sendai virus is about 50% α-helical in

lipid bilayers [88], but that of measles virus exhibited only weak membrane interactions, which is surprising given its close sequence similarity with the Sendai fusion peptide [89]. A study of the internal fusion peptide of the Ebola virus glycoprotein revealed only a limited amount of secondary structure, but attributed an important structural role to the central conserved proline [90]. A peptide corresponding to the putative secondary internal fusion peptide of Sendai virus (see Section 12.3.3) is helical in membrane mimetic environments and promotes lipid mixing between liposomes [46]. A similar internal secondary fusion peptide has been postulated to exist in the F protein of measles virus and its interactions with lipid bilayers have been found to be stronger than those of the N-terminal fusion peptide [89]. This anomalous result may be explained if the more hydrophobic N-terminal fusion peptide was not adequately solubilized prior to membrane binding in these experiments. Whether the internal secondary "fusion peptides" of the F proteins of paramyxoviruses really contribute to fusion by lipid interactions in the context of the full-length proteins is not yet known. Even for the primary internal fusion peptides, such as those shown in Fig. 12.2, it is presently not clear how well peptide models represent their true structures in the context of the membrane-bound forms of the entire fusion proteins. It may be possible to design looped peptide models with appropriately constrained distances between the ends of the loops in the cases of class II fusion proteins, for which the atomic structures of the post-fusion conformations of the entire ectodomains are known from X-ray crystallography such as, for example, for Semliki Forest and Dengue viruses (see Figs. 12.1 and 12.4) [91, 92].

12.4.6
Perturbation of Bilayer Structure by Fusion Peptides

How do fusion peptides alter the structure of lipid bilayers? How do they induce non-bilayer structures in lipid bilayers, which must occur in some form at intermediate stages of membrane fusion? These are questions of much current debate with few definite answers mostly because it is difficult to trap lipid–protein fusion intermediates for structural studies. A frequently held notion is that fusion peptides alter membrane curvature and make it more negative as required in the stalk–pore model of membrane fusion. For example, 20-residue models of the influenza HA2 fusion peptide decrease the transition temperature from bilayer to curved hexagonal phases and thus stabilize the negatively curved lipid phase [93]. The same result has been observed for the interaction of the 12-residue SIV gp32 fusion peptide with lipid bilayers that are prone to hexagonal phase formation [94]. Given the structure and position of the fusion peptide shown in Fig. 12.3, it is difficult to envisage how this structure could promote negative curvature in lipid bilayers. If anything, it is expected to promote positive curvature. The experimentally observed depression of the bilayer-to-hexagonal phase transition temperature may be explained if the hydrophobic peptides escaped into the interstitial spaces in the hexagonal phases, which they could not do if they were attached to polar ectodomains that must tie the fusion pep-

tides to the membrane surface. Influenza HA2 fusion peptides have also been found to alter the hydration properties of bilayers at the level of the lipid ester carbonyl groups as measured by FTIR spectroscopy [75, 76]. It is likely that the observed lipid signals reflect a partial dehydration of the membrane surface by the peptides because they also induce more order in the lipid acyl chains [75, 76], which is a common consequence of headgroup dehydration in lipid bilayers. As discussed in Section 12.2, lipid dehydration could lead to rather disorganized lipid stalks connecting two bilayers. Such dynamically disorganized stalks may exhibit quite different structures than the lipid stalks with neatly curved surfaces that have been proposed in the standard stalk–pore mechanism of membrane fusion. In addition to changing lipid hydration, fusion peptides also decrease the rupture tension of lipid bilayers as has been demonstrated with the influenza HA2 fusion peptide [95]. A trimeric version of the HA2 fusion peptide is more effective in rupturing membranes than its monomeric version [96]. Similarly, a trimeric HIV gp41 fusion peptide construct induced more rapid lipid mixing than a fusion peptide dimer, which in turn was more active than the monomer [97].

It may be expected that further microscopic detail about fusion peptide–lipid interactions will be learned from molecular dynamics simulations, particularly those that are run for long enough times and large enough systems to allow for extended membrane transformations. Encouraging first steps in this direction have been taken by several groups. Kamath and Wong [98] have simulated the 16-residue HIV gp41 fusion peptide as an α-helix in a POPE bilayer. The peptide maintained an α-helical structure and became tilted in the bilayer during the 1.5 ns of the simulation. The fusion peptide increased the thickness of the proximal leaflet of the bilayer, but left the distal monolayer unperturbed. Huang et al. [99] performed an 18-ns simulation of the 20-residue influenza HA2 fusion peptide in a DMPC bilayer. Although they started from a helical rod structure, the peptide adopted a kinked and tilted helical structure in the bilayer similar to that observed by NMR and EPR spectroscopy [81]. In this study, the lipids of the proximal layer and closest to the N-terminus of the peptide were compressed in both leaflets of the bilayer relative to lipids in unperturbed bilayers or farther away from the N-terminus. Vaccaro et al. [100] started from the NMR structure of the influenza HA2 fusion peptide and simulated it for 5 ns in a POPC bilayer. The kinked tilted α-helical structure was maintained throughout the simulation and the order parameters of the lipid acyl chains were decreased leading to bilayer thinning. No differences between proximal and distal lipids have been reported in this study.

12.5
Interactions of Transmembrane Domains with Lipid Bilayers

Numerous mutagenesis studies indicate that the transmembrane domains of viral spike glycoproteins are more than just simple anchoring devices to attach

these proteins to the viral membrane surfaces. A first indication for this comes from studies on expressed influenza HA, in which the transmembrane domain, i.e. a single α-helix, has been replaced with a glycosylphosphatidylinositol lipid anchor [14]. Cells expressing this mutant are arrested at the hemifusion stage in fusion assays with red blood cells. A similar result has been found for the parainfluenza type 2 fusion protein [101]. Since a deletion of the 12-residue cytoplasmic tail of HA2 still promotes membrane fusion [102], it is clear that the transmembrane domain contributes to the fusion reaction in a major way. This is true even if the cytoplasmic tail influences details of fusion pore opening, which are not yet completely understood [56]. The transmembrane domain must span both leaflets of the lipid bilayer because versions that span only half of the lipid bilayer cause hemifusion just as do the lipid-anchored HAs [42]. Despite the requirement for a near full-length transmembrane domain, there may be no specific sequence requirement of the influenza HA2 transmembrane domain to support membrane fusion [42]. However, some sequence requirements in this domain and appropriate acylations of three cysteines in the short cytoplasmic domain must be met to correctly target influenza HA to cholesterol/sphingomyelin-rich domains in the apical membrane during the biogenesis of influenza virus particles [54, 55]. In retroviruses, a conserved arginine or lysine in the middle of the transmembrane domain of the envelope glycoprotein appears to be important for folding and assembly of the protein in the membrane [103, 104] and/or its ability to support membrane fusion [105, 106]. Similarly, the murine leukemia virus envelope glycoprotein requires a proline [107] and the vesicular stomatitis virus (VSV) G glycoprotein requires two glycines in the middle of the transmembrane domain in order to support the transition from the hemifusion intermediate to the full fusion product [108]. Perhaps, flexibility or kinks are necessary in the transmembrane domains of some fusion proteins for the completion of full membrane fusion.

The transmembrane domain of influenza virus HA2 by itself is α-helical and oriented at an angle of 15° or less from the membrane normal [109]. It forms oligomers (dimers, trimers and tetramers) in SDS micelles and readily exchanges amide hydrogens when embedded in lipid bilayers. Therefore, it may form a small partially water-accessible helical bundle in membranes. Helical contacts and perhaps water accessibility may be mediated by three conserved serines (or two serines and a cysteine in some strains) that occur in heptad repeats in the central part of the transmembrane domain. Interestingly, the synthetic transmembrane domains of influenza HA2 also increase the lipid chain order parameters [109], which could be a consequence of a partial dehydration at the membrane surface as discussed above in the context of fusion peptide-membrane interactions. Lipid interactions of the tryptophan-rich juxta-membrane domains of HIV gp41 have also been examined. Peptides corresponding to this domain insert into membranes as amphipathic helices parallel to the membrane surface and competitively inhibit fusion promoted by full-length gp41 [110, 111].

12.6
Structure–Function (Fusion) Relationships of Membrane-interactive Viral Fusion Protein Domains

12.6.1
Fusion Peptide Mutants

Studies establishing correlations between the structures of membrane-interactive segments of fusion proteins in membranes and their ability to support membrane fusion are only in their beginning stages. The first residue, a glycine, of the influenza HA2 fusion peptide appears to be particularly important for supporting fusion. If glycine 1 is missing, fusion and viral infectivity is completely aborted [40, 41]. Molecular dynamics simulations indicate that the fusion peptide lacking the first glycine is more linear in structure and lies more parallel to the membrane surface compared to the wild-type fusion peptide structure [100]. This mutant also has a higher tendency to self-associate into β-structures on membrane surfaces than the wild-type fusion peptide [75]. If glycine 1 is substituted with a valine, fusion is also completely blocked [39]. This functional defect correlates with a more linear and more surface-located structure of the G1V fusion peptide in lipid bilayers ([86, 87], see also Fig. 12.3). The defective G1V fusion peptide also has an increased propensity for self-association on membrane surfaces. Substitution of glycine 1 with a serine causes a milder fusion phenotype: fusion can proceed to hemifusion, but not to full fusion [39]. Structural analysis reveals that the G1S fusion peptide still forms a kinked boomerang structure in lipid bilayers similar to that of the wild-type fusion peptide, but that the glycine ridge on the upper face of the N-terminal arm of the V-shaped molecule is disrupted ([86, 87], see also Fig. 12.3). Very recent data show that mutation of tryptophan 14 to an alanine also completely blocks fusion and that peptides with the W14A substitution are very flexible and lack a fixed angle between the two arms of the boomerang structure of the wild-type (A. Lai et al., unpublished results). Therefore, it appears that a deep insertion into the bilayer at a fixed oblique angle as accomplished by the boomerang structure is required to promote the initial joining of two bilayers (hemifusion), but that an intact glycine ridge may be additionally required to proceed to the formation and expansion of the fusion pore. Further experiments are needed to examine whether or not an intact glycine ridge on the N-terminal arm of the boomerang is an absolute structural requirement for influenza HA-mediated full membrane fusion.

Glycine residues in the fusion peptide of HIV gp41 also appear to be critically important to support the fusion activity of the expressed fusion protein and infectivity of the virus [112]. The highly conserved glycines 10 and 13 are particularly sensitive to mutation, whereas the less conserved glycines 3 and 5 are more permissive to substitutions. Substitution of the bulky aliphatic side-chains of valine 2 and leucine 9 with the charged residues glutamate and arginine, respectively, also reduces the fusion activity of gp41 and the infectivity of HIV par-

ticles bearing these mutations [113]. The V2E substitution is particularly severe, whereas the L9R and A15E substitutions are milder and reduce syncytium formation to about 50%. The relatively conservative mutation of phenylalanine 11 to a tyrosine blocks syncytium formation of HIV gp41 expressing cells almost completely [114]. The V2E, L9R and F11Y mutations have been introduced into peptide models [115]. All three mutant peptides induced decreased levels of hemolysis of red blood cells compared to hemolysis induced by the wild-type gp41 fusion peptide. The V2E, L9R and F11Y mutant fusion peptides also exhibit significantly decreased contents of α-helix and increased contents of β-structure in lipid bilayers when compared to the wild-type fusion peptide [115]. Molecular dynamics simulations indicate that the V2E and L9R peptides may lie parallel on the membrane surface whereas the wild-type fusion peptide inserts as an oblique helix into lipid bilayers [98]. Therefore, it appears that some general structure-function relationships described for the influenza HA fusion peptide are recapitulated in the HIV gp41 fusion peptide.

12.6.2 Transmembrane Domain Mutants

As discussed above, the structural requirements on the transmembrane domain are likely less stringent than those on the fusion peptides. It appears that in some cases a full-length transmembrane domain of an almost generic sequence is sufficient to support fusion. However, there may be requirements for some flexibility in the middle of the transmembrane domain and perhaps the presence of some polar/apolar residues in heptad repeats to allow for appropriate homotypic and heterotypic helix–helix interactions. An alignment of the sequences of the transmembrane domains of fourteen different subtype strains of influenza virus HAs shows that the N-terminal half of the domain is more conserved than the C-terminal half [109]. A heptad repeat with the conserved motif ILsIYSsbssSL or ILWISFsbssFL (s = small semipolar, i.e. G, A, S, T or C; b = branched aliphatic, i.e. I or V; underlines denote heptad repeats of apolar residues) is found in the N-terminal half, i.e. the half that resides in the outer leaflet of the viral lipid bilayer, in all fourteen strains. A conserved glycine or alanine is found eight or seven residues, respectively, downstream from these motifs in all strains. The C-terminal half of the transmembrane domain that resides in the inner leaflet of the viral lipid bilayer is otherwise highly variable between the strains and does not show features that distinguishes it from any generic transmembrane domain. Despite their good conservation, a few point mutations (e.g. W3 → A or s9 → L) in the above motifs did not affect fusion, nor did deletion of the first five residues of this motif [42]. As noted above, tryptophan 3 is not totally conserved and is a "s" in the other motif. Significant lipid–protein mismatch may occur in the deletion mutant and thereby destabilize the viral membrane and induce fusion in an unusual manner. The insensitivity of the G9L mutation in an H3 subtype HA is significant and interesting [42]. In contrast, changing glycine 10 into a leucine in an H2 subtype HA leads to a

hemifusion phenotype [116, 117]. Apparently, a single glycine-to-leucine substitution in this region with several s residues is sufficient in some, but not in all, cases to reduce full fusion to hemifusion phenotypes. The high conservation of unusual motifs in the N-terminal half of the transmembrane domain of influenza HA remains intriguing and more drastic motif changes may lead to interesting new fusion mutants. Transmembrane domain glycines also seem to be important for fusion mediated by the VSV G protein. Two critical glycine substitutions in the transmembrane domain of this fusion protein block the transition from hemifusion to full fusion [108]. In the case of HIV gp41 and some other retroviruses, a conserved arginine or lysine residue in the center of the transmembrane domain appears to be important for fusion and viral infection [103–106].

12.7 Possible Mechanisms for Initiating the Formation of Viral Fusion Pores

Fusion is initiated by quite dramatic conformational changes in the ectodomains of the viral fusion proteins. These conformational changes are triggered by low pH in the endosome after receptor-mediated endocytosis for some viruses or by a receptor-mediated activation mechanism in other cases. Two examples for possible intermediate and final fusion structures of a class I and a class II fusion protein are shown in Fig. 12.4. These structures and their lateral organization in between two fusing membranes should be compared to the dramatically different resting structures that are present on the viral membrane surfaces and that are depicted in Fig. 12.1. In class I proteins, exemplified by influenza HA2, the coiled coils refold by executing large jack-knife motions (see, e.g. Fig. 2 in [118]). The pH 7 structure of influenza HA2 is metastable. Energy is gained when HA2 assumes the pH 5 structure, which is why this conformational change has been characterized as “spring loaded” [119]. An important feature of the conformational change of class I fusion proteins is that the hydrophobic fusion peptide, which is protected in a hydrophobic pocket in the resting structure, becomes exposed and available for interaction with the target membrane upon fusion activation. In influenza HA2, for which most structural information is available, the conformational change is thought to occur in two steps: the core coiled-coils of HA2 extend in the N-terminal direction and thereby translocate the fusion peptides towards the top of the molecule where they become available for interaction with the target membrane (see, e.g. Fig. 6 in [120]). Next, the outer layer helices refold to form helical hairpins with the core helices and thereby redirect the C-terminal ends with the attached transmembrane domains toward the N-terminal ends with the attached fusion peptides. These are the states shown in Fig. 12.4 on the left. Interestingly, the N- and C-terminal ends of the ectodomains form a tight cap structure [121] and disruption of this cap by mutagenesis also disrupts fusion and, therefore, is functionally important [122]. This is clear evidence that, at least in the case of influenza

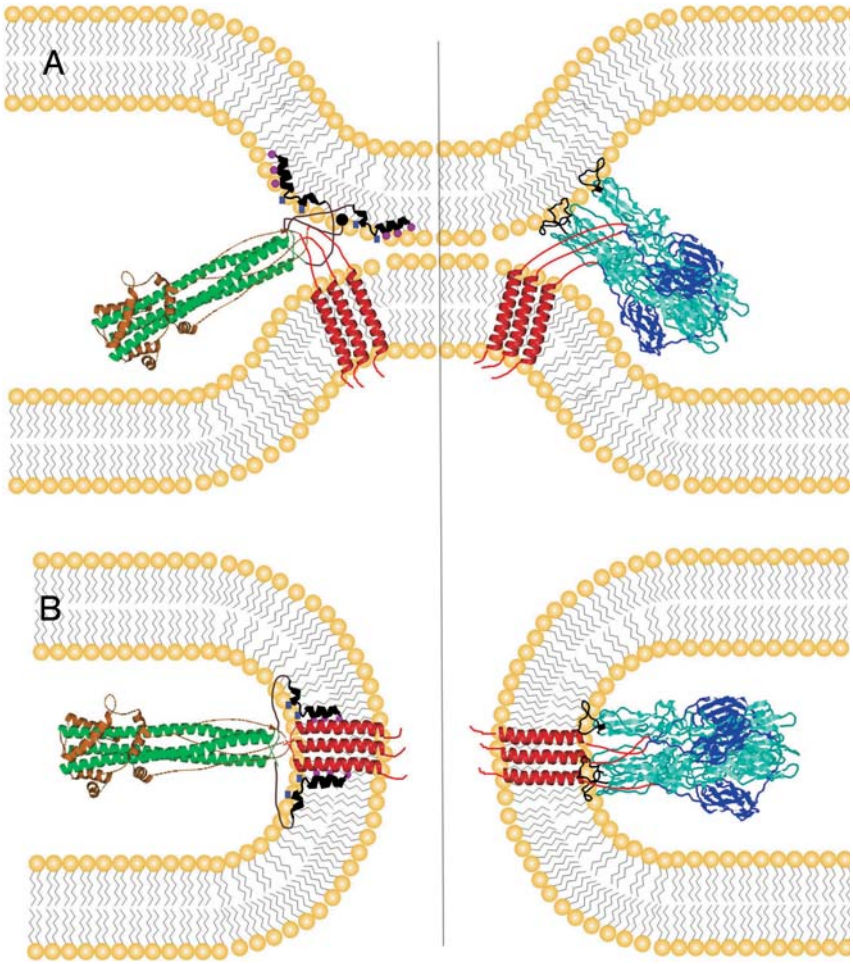

Fig. 12.4 Structures of influenza virus HA (left) and Semliki Forest virus E1 protein (right) in their post-fusion state modeled into a possible fusion intermediate (A) and into a fusion pore (B). The membrane-inserted fusion peptides are shown in black and the transmembrane domains in red. Note the large conformational changes of both proteins when compared to their prefusion structures depicted on the virus surfaces in Fig. 12.1. The pink dots in the influenza HA fusion peptide structure denote glycines that may mediate helix interactions and the blue squares denote glutamates that may be responsible for the pH-dependence of the fusion peptide penetration into lipid bilayers.

HA2, the fusion peptide and transmembrane domain, which each are only about nine residues away from the cap, end up inserted into the fused membranes in very close proximity to each other (Fig. 12.4, bottom left).

Although not quite as much information is yet available on class II proteins, the final situation upon completion of fusion is likely very similar in class I and

II fusion proteins [91, 92]. Class II proteins start out as lattices of dimers that lie almost flat on the viral membrane surface (Fig. 12.1). The dimer contacts and/or the receptor protein (E2 in the case of Semliki Forest virus) protect the fusion peptide loops from hydrophobic exposure. Each subunit in the dimer consists of four domains, i.e. a N-terminal domain, a middle domain that contains the fusion peptide at its tip, a C-terminal domain and the most C-terminal transmembrane domain. Upon activation, the N-terminal and middle domains re-associate into a trimer with the fusion peptide loops exposed close to each other on the tip of the pear-shaped molecule (Fig. 12.4, top right). The C-terminal domains become redirected and pack into the grooves between neighboring subunits at the base of the trimer. The C-terminal ends of the ectodomain, to which the transmembrane domains are attached, are not visible in the crystal structures, but likely pack into the upper parts of the grooves and thereby position the transmembrane domains very close to the fusion peptides (Fig. 12.4, bottom right). Therefore, a major purpose of the refolding of the ectodomains of class I and II viral membrane fusion proteins appears to be a mechanical device to (1) insert the fusion peptides into the target membrane, and (2) bring the viral membrane-inserted transmembrane domains into close proximity of the target membrane-inserted fusion peptides and thereby induce a merger of the two membranes.

In the following, we briefly discuss protein–lipid and protein–protein interactions that may lead to hemifused and fully fused states similar to those depicted in Fig. 12.4. It is clear that the ectodomains with attached highly specific fusion peptides are sufficient to proceed to hemifusion, at least in the case of influenza HA-mediated membrane fusion. A specific transmembrane domain is not required and a simple lipid anchor suffices to bring the two membranes into hemifusion contact, presumably by inducing "nipples" in one or both membranes and tilting the ectodomains. Nipple membrane protrusions have been observed by electron microscopy [123], and a tilting of the influenza HA ectodomains relative to the viral and target membranes has been measured by polarized IR spectroscopy under fusion conditions [124–126]. We do not believe that the boomerang-shaped structure of the fusion peptide is compatible with the membrane curvature required to induce a classical hourglass-shaped lipid stalk structure. We rather believe that a high concentration of fusion peptides in the contact zone between two membranes perturbs the bilayer structure by removing water molecules from this region. Therefore, the lipid stalk may be much more dynamic than previously thought and may resemble a "lipid mixer" rather than a highly organized fluid ordered structure. A cartoon of such a dynamic lipid ("mixer") stalk is depicted in Fig. 12.5 for the case of influenza HA [127]. Perhaps the fusion loops of class II viral fusion proteins create similar perturbations of the lipids in between the two membranes that are about to fuse.

We have postulated that the fusion peptides of class I viral fusion proteins may adopt a full transmembrane orientation and interact directly (presumably as continuous α-helices) with the transmembrane domains [118, 120]. This postulate is based on circumstantial evidence and direct evidence for a direct inter-

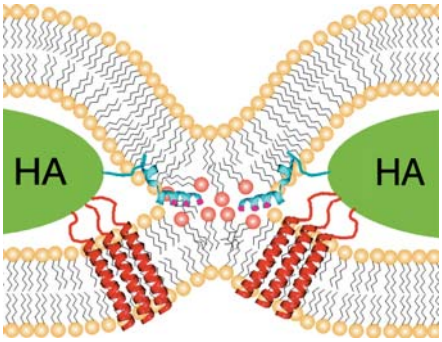

Fig. 12.5 Dynamic lipid mixer stalk that may be responsible for the hemifusion intermediate in influenza HA-mediated membrane fusion (adapted from [127]). The glycines in the fusion peptide structures are indicated with small dots. The larger spheres in the center are the headgroups of perturbed lipids whose apolar sidechains may rapidly flip between the upper and lower membranes.

action of the fusion peptides and transmembrane domains in membranes is still lacking as is a detailed structure of the fusion pore. Proteinaceous pores of fusion proteins have been previously suggested for fusion mediated by influenza HA [128] and SNARE proteins [129]. The fundamental difference between the model suggested here and these earlier "gap junction-type" models is that in our model the different transmembrane segments are postulated to interact laterally in the same membrane and not in *trans* across two different membranes. Obviously, lateral helix association models cannot explain full fusion of type II viral fusion proteins. It appears that in this case, insertion of the fusion loops into the membrane interface must suffice to attract the transmembrane domains to this destabilized membrane region. However, heteromeric lateral helix associations may still occur in class II fusion proteins because many of these proteins have other transmembrane domains in their vicinity in stoichiometric amounts, i.e. those of the receptor subunits – E2 in the case of Semliki Forest virus. The discussion about the structures that lead to the opening of fusion pores and the dilation of these pores to complete the membrane fusion reaction is reminiscent of a similar vivid discussion on the action of lytic peptides (see Chapter 9). Some antimicrobial peptides induce purely proteinaceous pores (barrel stave model), whereas others induce pores with more loosely arranged peptides with many interspersed lipids (carpet model). Clearly, more work needs to be done to define how exactly class I and II fusion proteins work on membranes and creative new combinations of structural and biophysical experimentation will be needed to establish what exact structures lead to membrane fusion in both classes of viral fusion proteins.

Acknowledgments

We thank the many members of the Tamm laboratory, present and past, who have contributed to our current understanding of the mechanisms of membrane fusion. This work was funded in part by grants from the National Institutes of Health.

References

1 J. F. Nagle, S. Tristram-Nagle, *Biochim. Biophys. Acta* **2000**, *1469*, 159–195.
2 H. I. Petrache, S. Tristram-Nagle, K. Gawrisch, D. Harries, V. A. Parsegian, J. F. Nagle, *Biophys. J.* **2004**, *86*, 1574–1586.
3 D. Gingell, I. Ginsberg, in *Membrane Fusion*, Poste, G. (ed.), Elsevier, Amsterdam, **1978**.
4 S. W. Hui, T. P. Stewart, L. T. Boni, P. L. Yeagle, *Science* **1981**, *212*, 921–923.
5 V. S. Markin, M. M. Kozlov, V. L. Borovjagin, *Gen. Physiol. Biophys.* **1984**, *3*, 361–377.
6 L. Yang, H. W. Huang, *Science* **2002**, *297*, 1877–1879.
7 L. Yang, L. Ding, H. W. Huang, *Biochemistry* **2003**, *42*, 6631–6635.
8 L. V. Chernomordik, G. B. Melikyan, I. G. Abidor, V. S. Markin, Y. A. Chizmadzhev, *Biochim. Biophys. Acta* **1985**, *812*, 643–655.
9 L. V. Chernomordik, G. B. Melikyan, Y. A. Chizmadzhev, *Biochim. Biophys. Acta* **1987**, *906*, 309–352.
10 C. A. Helm, J. N. Israelachvili, P. M. McGuiggan, *Science* **1989**, *246*, 919–922.
11 C. A. Helm, W. Knoll, J. N. Israelachvili, *Proc. Natl Acad. Sci. USA* **1991**, *88*, 8169–8173.
12 L. Chernomordik, M. M. Kozlov, J. Zimmerberg, *J. Membr. Biol.* **1995**, *146*, 1–14.
13 P. I. Kuzmin, J. Zimmerberg, Y. A. Chizmadzhev, F. S. Cohen, *Proc. Natl Acad. Sci. USA* **2001**, *98*, 7235–7240.
14 G. W. Kemble, T. Danieli, J. M. White, *Cell* **1994**, *76*, 383–391.
15 G. B. Melikyan, S. A. Brener, D. C. Ok, F. S. Cohen, *J. Cell Biol.* **1997**, *136*, 995–1005.
16 L. V. Chernomordik, V. A. Frolov, E. Leikina, P. Bronk, J. Zimmerberg, *J. Cell Biol.* **1998**, *140*, 1369–1382.
17 E. Leikina, L. V. Chernomordik, *Mol. Biol. Cell* **2000**, *11*, 2359–2371.
18 R. M. Markosyan, G. B. Melikyan, F. S. Cohen, *Biophys. J.* **2001**, *80*, 812–821.
19 J. Lee, B. R. Lentz, *Biochemistry* **1997**, *36*, 6251–6259.
20 M. E. Haque, T. J. McIntosh, B. R. Lentz, *Biochemistry* **2001**, *40*, 4340–4348.
21 K. O. Evans, B. R. Lentz, *Biochemistry* **2002**, *41*, 1241–1249.
22 D. P. Siegel, *Biophys. J.* **1993**, *65*, 2124–2140.
23 D. P. Siegel, *Biophys. J.* **1999**, *76*, 291–313.
24 Y. Kozlovsky, M. M. Kozlov, *Biophys. J.* **2002**, *82*, 882–895.
25 V. S. Markin, J. P. Albanesi, *Biophys. J.* **2002**, *82*, 693–712.
26 M. E. Haque, B. R. Lentz, *Biochemistry* **2004**, *43*, 3507–3517.
27 K. Katsov, M. Muller, M. Schick, *Biophys. J.* **2004**, *87*, 3277–3290.
28 H. Noguchi, M. Takasu, *J. Chem. Phys.* **2001**, *115*, 9547–9551.
29 M. Muller, K. Katsov, M. Schick, *J. Chem. Phys.* **2002**, *116*, 2342–2345.
30 M. Muller, K. Katsov, M. Schick, *Biophys. J.* **2003**, *85*, 1611–1623.
31 S. J. Marrink, A. E. Mark, *J. Am. Chem. Soc.* **2003**, *125*, 11144–11145.
32 M. J. Stevens, J. H. Hoh, T. B. Woolf, *Phys. Rev. Lett.* **2003**, *91*, 1881021–1881024.
33 V. A. Frolov, A. Y. Dunina-Barkovskaya, A. V. Samsonov, J. Zimmerberg, *Biophys. J.* **2003**, *85*, 1725–1733.
34 J. J. Skehel, K. Cross, D. Steinhauer, D. C. Wiley, *Biochem. Soc. Trans.* **2001**, *29*, 623–626.
35 L. J. Earp, S. E. Delos, H. E. Park, J. M. White, *Curr. Topics Microbiol. Immunol.* **2004**, *285*, 25–66.

36 M. J. Gething, R. W. Doms, D. York, J. White, *J. Cell Biol.* **1986**, *102*, 11–23.

37 D. A. Steinhauer, S. A. Wharton, J. J. Skehel, D. C. Wiley, *J. Virol.* **1995**, *69*, 6643–6651.

38 C. Schoch, R. Blumenthal, *J. Biol. Chem.* **1993**, *268*, 9267–9274.

39 H. Qiao, R. T. Armstrong, G. B. Melikyan, F. S. Cohen, J. M. White, *Mol. Biol. Cell* **1999**, *10*, 2759–2769.

40 K. J. Cross, S. A. Wharton, J. J. Skehel, D. C. Wiley, D. A. Steinhauer, *EMBO. J.* **2001**, *20*, 4432–4442.

41 W. Garten, F. X. Bosch, D. Linder, R. Rott, H. D. Klenk, *Virology* **1981**, *115*, 361–374.

42 R. T. Armstrong, A. S. Kushnir, J. M. White, *J. Cell Biol.* **2000**, *151*, 425–437.

43 R. F. Epand, J. C. Macosko, C. J. Russell, Y. K. Shin, R. M. Epand, *J. Mol. Biol.* **1999**, *286*, 489–503.

44 C. H. Kim, J. C. Macosko, Y. K. Shin, *Biochemistry* **1998**, *37*, 137–144.

45 R. F. Epand, C. M. Yip, L. V. Chernomordik, D. L. LeDuc, Y. K. Shin, R. M. Epand, *Biochim. Biophys. Acta* **2001**, *1513*, 167–175.

46 S. G. Peisajovich, O. Samuel, Y. Shai, *J. Mol. Biol.* **2000**, *296*, 1353–1365.

47 K. A. Baker, R. E. Dutch, R. A. Lamb, T. S. Jardetzky, *Mol. Cell* **1999**, *3*, 309–319.

48 L. Chen, J. J. Gorman, J. McKimm-Breschkin, L. J. Lawrence, P. A. Tulloch, B. J. Smith, P. M. Colman, M. C. Lawrence, *Structure (Camb.)* **2001**, *9*, 255–266.

49 K. Salzwedel, J. T. West, E. Hunter, *J. Virol.* **1999**, *73*, 2469–2480.

50 I. Munoz-Barroso, K. Salzwedel, E. Hunter, R. Blumenthal, *J. Virol.* **1999**, *73*, 6089–6092.

51 A. Saez-Cirion, M. J. Gomara, A. Agirre, J. L. Nieva, *FEBS Lett.* **2003**, *533*, 47–53.

52 D. H. Kweon, C. S. Kim, Y. K. Shin, *Nat. Struct. Biol.* **2003**, *10*, 440–447.

53 S. S. Chen, S. F. Lee, C. T. Wang, *J. Virol.* **2001**, *75*, 9925–9938.

54 P. Scheiffele, M. G. Roth, K. Simons, *EMBO J.* **1997**, *16*, 5501–5508.

55 S. Lin, H. Y. Naim, A. C. Rodriguez, M. G. Roth, *J. Cell Biol.* **1998**, *142*, 51–57.

56 G. B. Melikyan, H. Jin, R. A. Lamb, F. S. Cohen, *Virology* **1997**, *235*, 118–128.

57 L. K. Tamm, H. Hong, in *Protein Folding Handbook*, Buchner, J., Kiefhaber, T. (eds), Wiley-VCH, Weinheim, **2005**, Vol. 2, Part I, pp. 998–1031.

58 I. Martin, F. Defrise-Quertain, E. Decroly, M. Vandenbranden, R. Brasseur, J. M. Ruysschaert, *Biochim. Biophys. Acta* **1993**, *1145*, 124–133.

59 I. Martin, H. Schaal, A. Scheid, J. M. Ruysschaert, *J. Virol.* **1996**, *70*, 298–304.

60 R. Brasseur, M. Vandenbranden, B. Cornet, A. Burny, J. M. Ruysschaert, *Biochim. Biophys. Acta* **1990**, *1029*, 267–273.

61 J. P. Bradshaw, M. J. Darkes, T. A. Harroun, J. Katsaras, R. M. Epand, *Biochemistry* **2000**, *39*, 6581–6585.

62 M. Rafalski, J. D. Lear, W. F. DeGrado, *Biochemistry* **1990**, *29*, 7917–7922.

63 A. Saez-Cirion, J. L. Nieva, *Biochim. Biophys. Acta* **2002**, *1564*, 57–65.

64 S. G. Peisajovich, R. F. Epand, M. Pritsker, Y. Shai, R. M. Epand, *Biochemistry* **2000**, *39*, 1826–1833.

65 D. K. Chang, S. F. Cheng, W. J. Chien, *J. Virol.* **1997**, *71*, 6593–602.

66 K. F. Morris, X. Gao, T. C. Wong, *Biochim. Biophys. Acta* **2004**, *1667*, 67–81.

67 J. Yang, C. M. Gabrys, D. P. Weliky, *Biochemistry* **2001**, *40*, 8126–8137.

68 J. Yang, D. P. Weliky, *Biochemistry* **2003**, *42*, 11879–11890.

69 J. Yang, M. Prorok, F. J. Castellino, D. P. Weliky, *Biophys. J.* **2004**, *87*, 1951–1963.

70 L. M. Gordon, P. W. Mobley, R. Pilpa, M. A. Sherman, A. J. Waring, *Biochim. Biophys. Acta* **2002**, *1559*, 96–120.

71 L. M. Gordon, P. W. Mobley, W. Lee, S. Eskandari, Y. N. Kaznessis, M. A. Sherman, A. J. Waring, *Protein Sci.* **2004**, *13*, 1012–1030.

72 M. Murata, Y. Sugahara, S. Takahashi, S. Ohnishi, *J. Biochem. (Tokyo)* **1987**, *102*, 957–962.

73 J. D. Lear, W. F. DeGrado, *J. Biol. Chem.* **1987**, *262*, 6500–6505.

74 S. A. Wharton, S. R. Martin, R. W. Ruigrok, J. J. Skehel, D. C. Wiley, *J. Gen. Virol.* **1988**, *69*, 1847–1857.

75 C. Gray, S. A. Tatulian, S. A. Wharton, L. K. Tamm, *Biophys. J.* **1996**, *70*, 2275–2286.

76 X. Han, D. A. Steinhauer, S. A. Wharton, L. K. Tamm, *Biochemistry* **1999**, *38*, 15052–15059.

77 M. E. Haque, A. J. McCoy, J. Glenn, J. Lee, B. R. Lentz, *Biochemistry* **2001**, *40*, 14243–14251.

78 M. E. Haque, B. R. Lentz, *Biochemistry* **2002**, *41*, 10866–10876.

79 X. Han, L. K. Tamm, *Proc. Natl Acad. Sci. USA* **2000**, *97*, 13097–13102.

80 X. Han, L. K. Tamm, *J. Mol. Biol.* **2000**, *304*, 953–965.

81 X. Han, J. H. Bushweller, D. S. Cafiso, L. K. Tamm, *Nat. Struct. Biol.* **2001**, *8*, 715–720.

82 J. C. Macosko, C. H. Kim, Y. K. Shin, *J. Mol. Biol.* **1997**, *267*, 1139–1148.

83 J. Luneberg, I. Martin, F. Nussler, J. M. Ruysschaert, A. Herrmann, *J. Biol. Chem.* **1995**, *270*, 27606–27614.

84 P. V. Dubovskii, H. Li, S. Takahashi, A. S. Arseniev, K. Akasaka, *Protein Sci.* **2000**, *9*, 786–798.

85 C. H. Hsu, S. H. Wu, D. K. Chang, C. Chen, *J. Biol. Chem.* **2002**, *277*, 22725–22733.

86 Y. Li, A. L. Lai, X. Han, J. H. Bushweller, D. S. Cafiso, L. K. Tamm, *J. Virol.*, in press.

87 Y. Li, X. Han, L. K. Tamm, *Biochemistry* **2003**, *42*, 7245–7251.

88 S. G. Peisajovich, R. F. Epand, R. M. Epand, Y. Shai, *Eur. J. Biochem.* **2002**, *269*, 4342–4350.

89 O. Samuel, Y. Shai, *Biochemistry* **2001**, *40*, 1340–1349.

90 M. J. Gomara, P. Mora, I. Mingarro, J. L. Nieva, *FEBS Lett.* **2004**, *569*, 261–266.

91 Y. Modis, S. Ogata, D. Clements, S. C. Harrison, *Nature* **2004**, *427*, 313–319.

92 D. L. Gibbons, M. C. Vaney, A. Roussel, A. Vigouroux, B. Reilly, J. Lepault, M. Kielian, F. A. Rey, *Nature* **2004**, *427*, 320–325.

93 R. M. Epand, R. F. Epand, I. Martin, J. M. Ruysschaert, *Biochemistry* **2001**, *40*, 8800–8807.

94 A. Colotto, I. Martin, J. M. Ruysschaert, A. Sen, S. W. Hui, R. M. Epand, *Biochemistry* **1996**, *35*, 980–989.

95 M. L. Longo, A. J. Waring, D. A. Hammer, *Biophys. J.* **1997**, *73*, 1430–1439.

96 W. L. Lau, D. S. Ege, J. D. Lear, D. A. Hammer, W. F. DeGrado, *Biophys. J.* **2004**, *86*, 272–284.

97 R. Yang, M. Prorok, F. J. Castellino, D. P. Weliky, *J. Am. Chem. Soc.* **2004**, *126*, 14722–14723.

98 S. Kamath, T. C. Wong, *Biophys. J.* **2002**, *83*, 135–143.

99 Q. Huang, C. L. Chen, A. Herrmann, *Biophys. J.* **2004**, *87*, 14–22.

100 L. Vaccaro, K. Cross, J. Kleinjung, S. Strauss, D. Thomas, S. Wharton, J. Skehel, F. Fraternali, *Biophys. J.* **2005**, *88*, 25–36.

101 S. Tong, R. W. Compans, *Virology* **2000**, *270*, 368–376.

102 H. Jin, G. P. Leser, J. Zhang, R. A. Lamb, *EMBO J.* **1997**, *16*, 1236–1247.

103 D. A. Einfeld, E. Hunter, *J. Virol.* **1994**, *68*, 2513–2520.

104 R. J. Owens, C. Burke, J. K. Rose, *J. Virol.* **1994**, *68*, 570–574.

105 T. Pietschmann, H. Zentgraf, A. Rethwilm, D. Lindemann, *J. Virol.* **2000**, *74*, 4474–4482.

106 J. T. West, P. B. Johnston, S. R. Dubay, E. Hunter, *J. Virol.* **2001**, *75*, 9601–9612.

107 G. M. Taylor, D. A. Sanders, *Mol. Biol. Cell* **1999**, *10*, 2803–2815.

108 D. Z. Cleverley, J. Lenard, *Proc. Natl Acad. Sci. USA* **1998**, *95*, 3425–3430.

109 S. A. Tatulian, L. K. Tamm, *Biochemistry* **2000**, *39*, 496–507.

110 D. J. Schibli, R. C. Montelaro, H. J. Vogel, *Biochemistry* **2001**, *40*, 9570–9578.

111 A. Saez-Cirion, J. L. Arrondo, M. J. Gomara, M. Lorizate, I. Iloro, G. Melikyan, J. L. Nieva, *Biophys. J.* **2003**, *85*, 3769–3780.

112 M. D. Delahunty, I. Rhee, E. O. Freed, J. S. Bonifacino, *Virology* **1996**, *218*, 94–102.

113 E. O. Freed, D. J. Myers, R. Risser, *Proc. Natl Acad. Sci. USA* **1990**, *87*, 4650–4654.

114 L. Bergeron, N. Sullivan, J. Sodroski, *J. Virol.* **1992**, *66*, 2389–2397.

115 P. W. Mobley, A. J. Waring, M. A. Sherman, L. M. Gordon, *Biochim. Biophys. Acta* **1999**, *1418*, 1–18.

116 G. B. Melikyan, S. Lin, M. G. Roth, F. S. Cohen, *Mol. Biol. Cell* **1999**, *10*, 1821–1836.

117 G. B. Melikyan, R. M. Markosyan, M. G. Roth, F. S. Cohen, *Mol. Biol. Cell* **2000**, *11*, 3765–3775.
118 L. K. Tamm, X. Han, Y. Li, A. L. Lai, *Biopolymers* **2002**, *66*, 249–260.
119 C. M. Carr, P. S. Kim, *Cell* **1993**, *73*, 823–832.
120 L. K. Tamm, *Biochim. Biophys. Acta* **2003**, *1614*, 14–23.
121 J. Chen, J. J. Skehel, D. C. Wiley, *Proc. Natl Acad. Sci. USA* **1999**, *96*, 8967–8972.
122 H. E. Park, J. A. Gruenke, J. M. White, *Nat. Struct. Biol.* **2003**, *10*, 1048–1053.
123 T. Kanaseki, K. Kawasaki, M. Murata, Y. Ikeuchi, S. Ohnishi, *J. Cell Biol.* **1997**, *137*, 1041–1056.
124 S. A. Tatulian, P. Hinterdorfer, G. Baber, L. K. Tamm, *EMBO J.* **1995**, *14*, 5514–5523.
125 C. Gray, L. K. Tamm, *Protein Sci.* **1997**, *6*, 1993–2006.
126 C. Gray, L. K. Tamm, *Protein Sci.* **1998**, *7*, 2359–2373.
127 L. K. Tamm, J. Crane, V. Kiessling, *Curr. Opin. Struct. Biol.* **2003**, *13*, 453–466.
128 F. W. Tse, A. Iwata, W. Almers, *J. Cell Biol.* **1993**, *121*, 543–552.
129 X. Han, C. T. Wang, J. Bai, E. R. Chapman, M. B. Jackson, *Science* **2004**, *304*, 289–292.

Part 5
Cholesterol, Lipid Rafts, and Protein Sorting

13
Protein–Lipid Interactions in the Formation of Raft Microdomains in Biological Membranes

Akihiro Kusumi, Kenichi Suzuki, Junko Kondo, Nobuhiro Morone, and Yasuhiro Umemura

13.1
Many Plasma Membrane Functions are Mediated by Molecular Complexes, Microdomains and Membrane Skeleton-based Compartments

The biological membrane has been considered as a two-dimensional liquid, with the membrane-constituent molecules, i.e. the lipids and proteins, diffusing within the membrane more or less freely without affecting the overall morphology of the membrane. However, in the actual cellular plasma membrane, the situation may be quite different, as seen in Fig. 13.1 a, which shows schematic diagrams of the plasma membrane of the neuron and the intestine epithelial cell. If all the proteins and lipids in the membrane moved freely in the plasma membrane, then the plasma membrane would become featureless. However, the plasma membrane actually contains a variety of specialized regions, such as synapses, coated pits, caveolae, and cell–cell and cell–substrate adhesion structures, in which specific proteins and lipids are assembled to carry out specialized functions. Therefore, the cell must have some means to regulate the movement and assembly of specific membrane proteins and lipids in/on the plasma membrane, and to induce the recruitment of a variety of proteins from the cytoplasm, thus facilitating the interactions of assembled molecules to have them work. Understanding such mechanisms is one of the key issues in cell biophysics.

The examples given above are large structures with an average size greater than 50 nm. However, the plasma membrane contains a variety of smaller structures, perhaps with briefer lifetimes or with shorter residency times for the constituent molecules. These may include the clusters of signaling molecules and scaffolding proteins, and possibly raft domains in the plasma membrane, as well as the plasma membrane compartments formed by the membrane skeleton-based partitioning.

Note that in this chapter the term “membrane domains” is used in a very broad sense, covering a large variety of non-random assemblies of membrane molecules that may exhibit a wide range of sizes and lifetimes of assembly. These assemblies

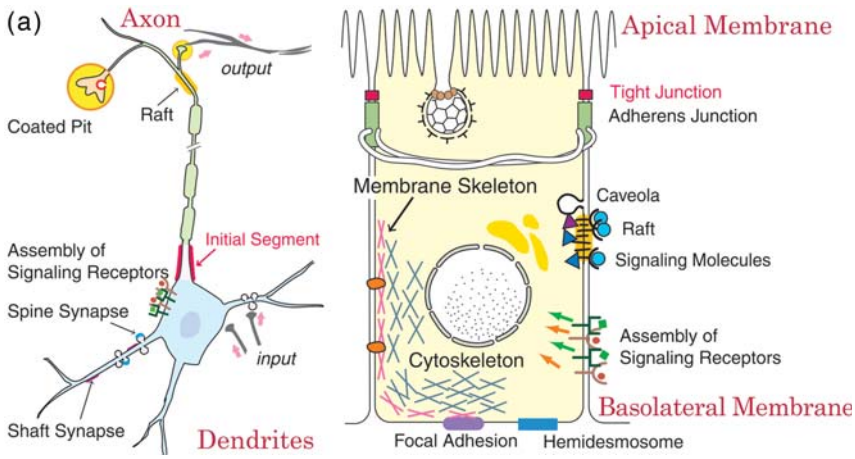

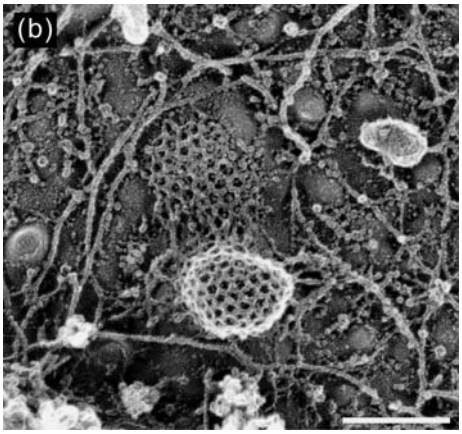

Fig. 13.1 (a) Schematic figures of the plasma membranes of a neuron (left) and an epithelial cell (right). The plasma membranes of these cell types are totally polarized into the axonal (left)–apical (right) membrane and the somatodendritic (left)–basolateral (right) membrane. These are some of the largest plasma membrane compartments. The plasma membrane contains a variety of specialized regions and molecular complexes with various time–space scales, collectively called membrane domains in this chapter (a broad definition is used here).
(b) Electron micrograph showing a forming clathrin-coated pit linked to the actin-based membrane skeleton. Such an electron micrograph gives the impression that clathrin-coated pits are stable structures, but in reality they form and dissociate from the membrane with a half-life of 40 s, on average.

include very small, transient domains or molecular complexes made of several proteins or lipids, on the one hand, as well as large, stable assemblies such as cell–cell adhesion domains and the apical membranes of epithelial cells, on the other hand. Between these two extreme cases are the raft domains: their sizes and lifetimes are likely to be between these two extreme cases, and they may be

greatly enhanced upon signaling or by the clustering of raft-associating proteins (Paladino et al. 2004), i.e. their sizes and lifetimes may vary greatly.

In this chapter, we feature the raft domains; however, before we concentrate on this specific type of membrane domain, we will first place the raft domain structure and dynamics in a larger perspective, to better understand the mechanisms by which they are formed in the non-ideal two-dimensional fluid mixture of many components, and are stabilized to become visible by optical and electron microscopic techniques. By placing the raft concept in the greater perspective of all kinds of membrane domains, the important structural, dynamic and functional characteristics of the raft domains that distinguish them from other membrane domains and protein assemblies may be clarified.

Then, we will discuss raft domains in steady-state cells (without stimulation) and in cells after extracellular or intracellular stimulation. Throughout this chapter, we emphasize the importance of bringing the concept of timescales into the research of membrane domains. The lifetime of the domain and the residency time of a molecule in a domain might be much shorter than generally assumed (of the order of seconds or less rather than on the order of minutes), and thus these timescales must always be considered to understand the membrane domains and their functions.

13.2 Timescales, Please!

Take a look at the ultrafine structure of the clathrin-coated pit as observed by electron microscopy (Fig. 13.1 b). Due to its large size and highly structured morphology, the clathrin-coated pit may appear to reside in the membrane for a long time. However, in reality, their half-lives are only 40 s long on average (Gaidarov et al. 1999). Another point to be noted is that even if the overall structure remains in the membrane, each individual molecule in the structure may be exchanging with the bulk pool or newly synthesized molecules much more rapidly. Consider the desmosome – a cellular organelle shared by two adhering cells. The desmosome is responsible for a strong type of cell–cell adhesion, described in the previous section as an example of a large, stable membrane domain. It can be as large as 10 μm in diameter in differentiated keratinocytes and requires 4 M guanidinium chloride, a very potent protein denaturant, for its disassembly *in vitro*. The lifetime of the desmosome may be as long as (or even longer than) the doubling time of the cell (over 60 h in some keratinocytes in culture), but the half-lives of the proteins that form the desmosome may be of the order of several hours (Pasdar and Nelson 1988 a, b, 1989).

These two points, the *lifetime* and the *residency time* (or the exchange rate), are the key issues addressed in this chapter, because they are the keys to understanding the structures and functions of all kinds of biomolecular systems in living cells, including membrane domains. The bottom line is that we always have to consider these membrane domains and structures as very dynamic entities, even when they are

large and clearly visible by light and electron microscopy, and this timescale viewpoint is even more important with smaller structures, like raft domains. Researchers have to apply these timescale concepts for understanding the mechanisms of the formation and function of microdomains, and for critically evaluating the limitations of various methods (time resolutions) used to study membrane domains. However, membrane researchers have been slow to adopt the timescale and time-resolution concepts, and this has caused major confusion in the membrane research field. In this chapter, we would like to address the timescales of molecular processes in the formation and the function of various membrane microdomains.

13.3
Four Types of Membrane Domains

First, we will briefly review the various membrane domains (as noted above, this term is used in a very broad sense here). The plasma membrane domains may be generally categorized into four classes.

Category 1: Large, stable structures that can be visualized by both electron microscopy and immunofluorescence microscopy, like synapses, desmosomes, clathrin-coated pits, etc., as described in Section 13.1.

Category 2: Partitioning of the plasma membrane into small compartments (Fig. 13.2 a), due to the presence of the actin-based membrane skeleton (fence, Fig. 13.2 b) and a variety of transmembrane proteins anchored to and lined up along the membrane skeleton (pickets, Fig. 13.2 c). This is likely to occur throughout the plasma membrane, except for the large, stable domains of Category 1, although the membrane skeleton is likely to associate intimately with these structures. Virtually all of the molecules incorporated in the plasma membrane (e.g. even the phospholipids residing in the outer leaflet of the plasma membrane) are affected by these pickets and fences (Fig. 13.2 a). They tend to undergo short-term confined diffusion within a compartment and long-term hop diffusion between these compartments. The compartment sizes are generally between 30 and 230 nm (cell-type dependent). The residency time of individual transmembrane proteins and phospholipids in a compartment may be of the order of 1–1000 ms (depending on the molecule and the cell type). The movement of the compartment itself or the membrane skeleton mesh has not been studied extensively. This model requires a paradigm shift of the plasma membrane concept. The traditional fluid-mosaic model of Singer and Nicolson (1972) may be true in the space scale of 10 nm (the size of the original cartoon published in their paper), but for longer-scale diffusion over 10 nm, the partitioning of the plasma membrane has to be considered (Fig. 13.2 a).

Category 3: Microdomains, called raft domains, where the lipid–lipid interaction plays a major role in their formation. Here, the "lipid" includes the alkyl chains that anchor the protein to the plasma membrane, like those for glycosylphosphatidylinositol (GPI)-anchored proteins, and the signaling molecules on the

cytoplasmic surface of the plasma membrane, such as some of the Src family kinases (SFKs) [note that in this chapter we do not differentiate between whether the alkyl chain is linked to other parts of the molecule via ester (acyl chains) or other bonds, like an ether bond, and we call all these chains alkyl chains]. In addition, we would like to emphasize the tendency of cholesterol to be excluded, if given a choice, from the bulk membrane domain enriched in unsaturated alkyl chains, and to partition into the domains rich in saturated alkyl chains and cholesterol (Crane and Tamm 2004). Thus, this situation is analogous to a hydrophobic interaction. In fact, cholesterol seems to form transient clusters of several cholesterol molecules with a lifetime of 1–100 ns in liposomes containing L-*α*-dioleoylphosphatidylcholine (DOPC) and cholesterol (Subczynski et al. 1990). The reason for the exclusion of cholesterol from the bulk domain enriched in unsaturated alkyl chains may be due to the lateral non-conformability between the rigid tetracyclic ring structure of cholesterol and the bent structure of the *cis* double bond in unsaturated lipids. In spite of the extensive and intensive efforts to understand raft domains in the plasma membrane of steady-state cells (in the absence of extracellular stimuli), their sizes and lifetimes are essentially unknown. One of the major reasons for the difficulty of determining these key figures may be their small size and instability in the steady state (without extracellular or intracellular stimulation). They are hard to detect *in situ* using optical and electron microscopy techniques (Glebov and Nichols 2004; Prior et al. 2003; Sharma et al. 2004; Varma and Mayor 1998). It seems only after extracellular stimulation, crosslinking of raft molecules or lowering the temperature that the raft domains become stabilized, which makes them visible by the concentration of raft-associated molecules (however, see Brugger et al. 2004).

Category 4: Oligomers of proteins in the membrane. These include dimers of G-protein-coupled receptors (Jordan and Devi 1999) and the ligand-induced signaling complexes of receptor-type tyrosine kinases, such as the ligand-induced epidermal growth factor dimers complexed with Shc, Grb2 and SOS. Such protein clusters are the smallest class of membrane domains. This type of cluster is becoming more important as the involvement of scaffolding proteins that stabilize the interaction of two functional molecules becomes clear.

"Scaffolding" may be a key term for all four of the domains described above. The large, stable domains of Category 1 are certainly important platforms for the functions that require large structures, e.g. internalizing various membrane molecules (clathrin-coated pits) or coping with large macroscopic mechanical stress (cell adhesion structures). The partitioning of the plasma membrane described in Category 2 would induce the strong confinement of molecules within a partitioned compartment upon their oligomerization or molecular complex formation (oligomerization-induced trapping within the compartment, see Fig. 13.3 and its legend; this is a good case of the cooperative action of membrane domains in different categories, Categories 2 and 4 in this particular case), which may be important for the short-term memory of where the external signal was received for the cellular chemotactic responses or localized/polarized

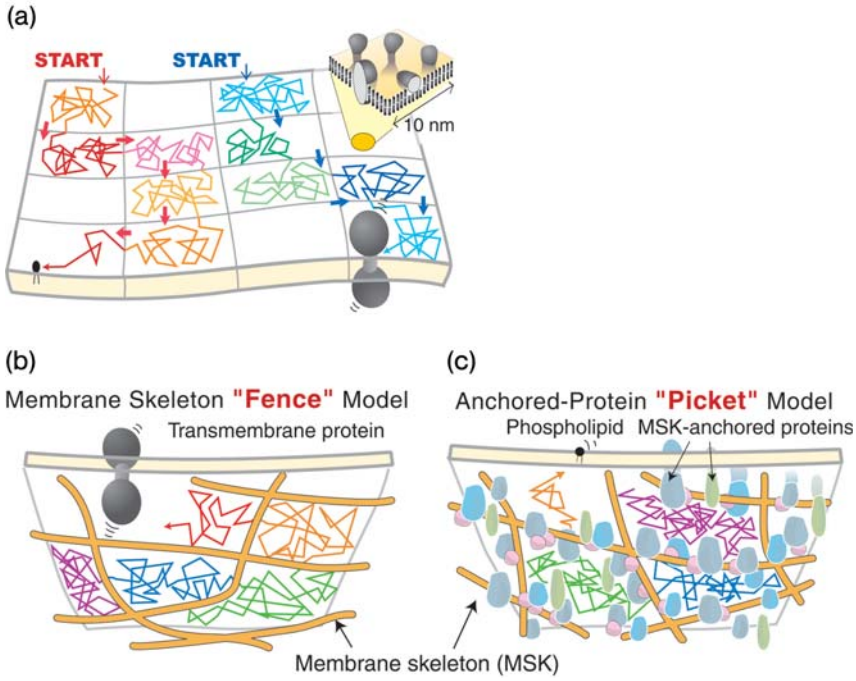

Fig. 13.2 Paradigm shift for the concept of the plasma membrane structure, from the two-dimensional continuum fluid to the partitioned fluid, due to the membrane skeleton 'fence' and the transmembrane protein 'pickets' anchored and aligned on the membrane skeleton fence.
(a) A paradigm shift for the concept of the plasma membrane structure in spatial scales larger than 10 nm may be required, from the two-dimensional continuum fluid to the partitioned fluid, in which its constituent molecules undergo short-term confined diffusion and long-term hop diffusion between the partitioned compartments. The fluid-mosaic model of the plasma membrane of Singer and Nicolson (1972) (see inset) is perfectly suitable on spatial scales less than 10 nm (incidentally, this is about the size of the original cartoon model in Singer and Nicolson's classical paper), but on spatial scales greater than 10 nm, one must consider the influence of the partitioning of the plasma membrane.
(b) Membrane skeleton 'fence' model. The membrane skeleton is chiefly made of actin filaments, which are also bound by many actin-associated proteins. The membrane skeleton is a part of the plasma membrane, since it plays important roles in many membrane functions, as well as a part of the cytoskeleton, since it is continuous with the cytoskeleton. The part of the cytoskeleton associated with the membrane has a different structure from that of the bulk cytoskeleton and contains specific proteins for interactions with the plasma membrane, and thus is called the membrane skeleton to distinguish it from the bulk cytoskeleton. Transmembrane proteins protrude into the cytoplasm, and in the fence model, the cytoplasmic domains of transmembrane proteins collide with the membrane skeleton, which induces temporary confinement of the transmembrane proteins within the membrane skeleton mesh.
(c) Anchored protein 'picket' model. About 15% of the transmembrane proteins are thought to be bound to the membrane skeleton and although their off-rates may be very high, they continually bind and re-associate rapidly. These bound transmembrane proteins form rows of pickets lined up along the membrane skeleton fence, which

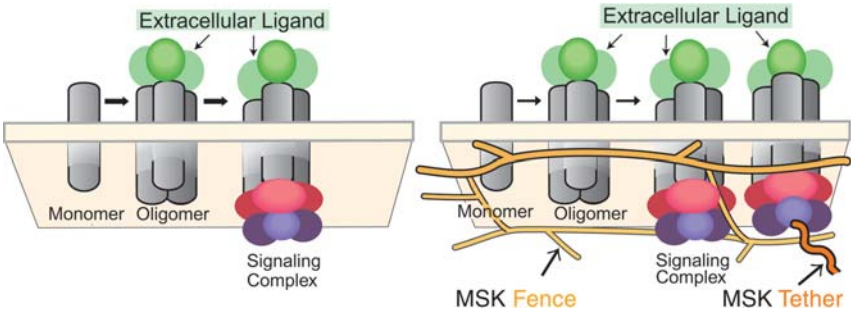

Fig. 13.3 Oligomerization-induced trapping model for membrane molecules upon oligomerization or molecular complex formation. Upon oligomerization or molecular complex formation, the hop rate across the intercompartmental barrier would be reduced greatly (right), because, in contrast to monomers, in the case of molecular complexes, all of the molecules within the complex have to hop across the picket-fence line simultaneously. In addition, due to the avidity effect, molecular complexes are more likely to be tethered to the membrane skeleton, perhaps temporarily, which also reduces their overall diffusion rate. The enhanced confinement and binding effects induced by oligomerization or molecular complex formation are collectively termed "oligomerization-induced trapping" (Iino et al. 2001). This would not occur in the absence of membrane skeleton fences and pickets (left): the diffusion theory by Saffman and Delbrück (1975), based on the fluid-mosaic model of Singer and Nicolson (1972), predicts that the diffusion rates of the oligomeric complexes would be almost the same as those of the single receptor molecules.

reorganization of the cytoskeleton. Categories 3 and 4 indicate the two major ways of scaffold formation for molecular interactions in and on the membrane: Category 3 emphasizes the lipid–lipid and protein–lipid interactions, whereas Category 4 mainly addresses the protein–protein interactions. The cells may take advantage of these two categories of domains, depending on the required number of molecules and molecular species, the levels of specificity in the molecular interaction and the lifetime of the complex. However, the boundary between these two types of domains is somewhat vague, because they tend to be mutually dependent on each other and one interaction tends to enhance the other.

effectively confine lipids, proteins, and virtually all of the molecules incorporated in the membrane. A Monte-Carlo simulation showed that when 20–30% of the compartment boundaries are occupied by anchored transmembrane protein pickets, temporary confinement of a lipid molecule on the order of 1–25 ms, as found in experiments, could be reproduced. This amount of bound transmembrane protein is consistent with the overall binding of 15% of the transmembrane proteins to the membrane skeleton. Since the membrane viscosity is high, about 100-fold greater than that in water, the presence of an immobile picket reduces the diffusion rate around it by several nanometers and thus the compartment boundaries do not have to be completely closed by the pickets. The average gap between immobilized anchored pickets is thought to be 3–10 nm or for the passage of the raft domain through the gap the effective size of the gap may be 2–9 nm, due to the exclusion of cholesterol from the boundary domain around the transmembrane proteins.

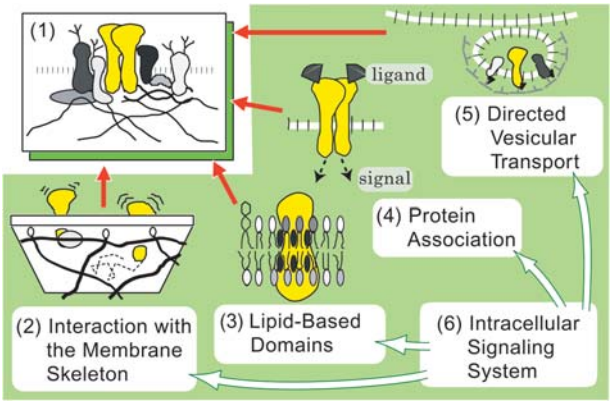

Fig. 13.4 Molecular processes that form the basis for the dynamics, structure and function of membrane molecules in the plasma membrane. (1) Multimolecular interactions forming large, stable membrane domains of Category 1. (2) Interaction with the membrane skeleton and associated transmembrane protein pickets, inducing membrane partitioning and the compartments of Category 2. (3) Lipid-based molecular interactions that may lead to the formation of raft domains (Category 3). (4) Protein oligomerization and complex formation, for example, induced by ligand binding (Category 4). This is likely to be a critical trigger for the initiation of a variety of membrane processes. This is also a key elementary process that greatly enhances the other molecular interactions described in this figure. (5) Directed vesicular transport, which may play crucial roles in the creation of concentration variations and specific membrane domains in the plasma membrane. (6) Intracellular signaling systems, which may be necessary for coordinating these molecular processes. This figure also shows that large, stable membrane domains may be generated by the actions of various elementary processes depicted here.

We further stress that these four classes of domains are interactive. Take the case of the creation of large, stable domains (Category 1) as an example (see Fig. 13.4). Molecular complex formation (Category 4) may lead to the stabilization of lipid raft domains (Category 3), and to confinement within the existing membrane skeleton compartment and/or transport to specific places by the membrane skeleton (Category 2). Such assemblies of molecules in the plasma membrane might act as platforms to recruit cytoplasmic molecules, perhaps including molecules loaded on the transport vesicles (shown as "(5)" in Fig. 13.4). In addition, signaling mechanisms may coordinate the various recruitment processes (shown as "(6)" in Fig. 13.4).

13.4 The Cell Membrane is a Two-dimensional Non-ideal Liquid Containing Dynamic Structures on Various Time-Space Scales

In the previous sections, we emphasized the presence of various membrane domains in the plasma membrane. However, at the same time, particularly in the context of raft domains and protein oligomers (molecular complexes), it is im-

portant to realize that the plasma membrane is not a simple liquid, but rather a non-ideal liquid mixture of molecules with various levels of miscibilities (in addition, it contains immobile molecules and domains that may be bound to the underlying membrane skeleton). Thus the plasma membrane naturally contains dynamic structures (like molecular complexes and domains), existing in various time and space scales, that are forming and dispersing continually within the cell membrane. As described in Section 13.1, these molecular complexes and domains range from protein clusters of small sizes with short lifetimes, like transient dimers of rhodopsin (Kusumi and Hyde 1982), to large micron-sized stable domains, like desmosomes (Pasdar and Nelson 1988a, b, 1989). Perhaps, the entire membrane should be viewed as a mosaic of microdomains (Maxfield 2002; Pierini and Maxfield 2001).

Based on the concept of a non-ideal liquid, we argue that the plasma membrane is always prepared for the formation of various domains and molecular clusters with enhanced sizes and lifetimes. We think that this concept is really a key toward understanding how the raft may be involved in the signaling and trafficking of raftophilic molecules.

13.5
A Definition of Raft Domains

Among the various membrane (micro)domains, the most controversial one is the so-called raft domain (Mukherjee and Maxfield 2004). From here, we now concentrate on raft domains. The first problem of writing about raft domains is that it is a word that has not been defined well. Lai called it an "unidentified floating object" (Lai 2003). Many researchers in related fields are uncomfortable with the status and the way the raft research field is being developed, and hastily demand a definition of the raft before one studies or talks about it. However, this seems to be a time to be patient about the *status quo* of raft research. The term "raft domain" is like the term "biophysics", which vaguely defines a research area: "biophysicists" basically know what it is (but with many grey areas), although they cannot specifically define it, and researchers in adjacent areas are often skeptical about its usefulness and scientific value. What is better about the term "raft" than "biophysics" is that we hope to be able to define the "raft" as we learn more about it in the near future. We will obtain a correct definition of raft when we really understand the membrane domain that is now vaguely called the "raft domain". To this end, we need a working definition for the "raft" and we have to make it useful for investigations of rafts. Therefore, in the context of seeing the membrane as non-ideal liquid mixture of molecules with various levels of miscibilities and also considering that the raft domains are involved in assembling molecules, we propose calling a molecular complex a "raft" when it involves more than two molecules (i.e. three or more molecules), and its formation requires the interactions of cholesterol and a saturated alkyl chain(s). This working definition may be surprising for many researchers,

because it includes very small molecular complexes as rafts. However, it is logical as well as useful, in the sense that it does not preclude anything without specific reasons (two-molecule complexes were excluded from the raft in this definition because one molecule is cholesterol and so the binding of another molecule would not contribute to enhancing molecular interactions or concentrating molecules).

13.6 The Original Raft Hypothesis

The proposal of a raft hypothesis was initially thought to be simple as well as (or because of its simplicity) fascinating (Brown and London 1998; Simons and Ikonen 1997; Simons and Toomre 2000; Simons and van Meer 1988). In the plasma membrane or the Golgi membrane, there may be many micron-sized domains of a liquid-ordered phase, consisting of glycosphingolipids, sphingomyelin and cholesterol, in which specific receptors (GPI-anchored receptors and some selected transmembrane receptors) and cytoplasmic signaling molecules, anchored to the cytoplasmic leaflet of the plasma membrane via saturated alkyl chains (such as Lyn or H-Ras), are concentrated, since these molecules have high affinities for the liquid-ordered phase. The ligand-induced enhanced partitioning of receptor molecules, perhaps due to clustering, into these pre-existing raft domains may trigger and facilitate the downstream signaling. This concentration of specific signaling proteins and the exclusion of other molecules (such as CD45) might play key roles in (de)selecting specific downstream signaling pathways.

13.7 Are there Raft Domains in Steady-state Cells in the Absence of Extracellular Stimulation?

Subsequent research revealed that some modifications may be necessary for the original raft hypothesis.

13.7.1 Standard Immunofluorescence or Immunoelectron Microscopy Failed to Detect Raft-like Domains in the Plasma Membrane of Steady-state Cells

In steady-state cells (in the absence of extracellular stimulation), membrane domains of several hundred nanometers or greater in diameter could not be found using conventional immunolabeling techniques, by either optical or electron microscopy. This suggests that the raft domains are small and the concentration of single species of raft-candidate molecules into a raft domain may not happen. There have been reports suggesting the presence of micron-sized raft domains, but these experiments almost always include the process of crosslinking (often

called chemical fixation) and/or lowering of temperature. Taken together, these results indicate that the micron-sized raft domains were not present in steady-state cells, but were *induced* by the crosslinking of raft-associating molecules or by the cold-enhanced assembly of molecules (including assembly due to exclusion from solidified domains). In chemotactic cells, large raft-like domains have been observed, but these can also be classified into induced rafts, as the cells were already actively engaged in crawling (Manes et al. 2003; Pierini et al. 2003).

The use of low concentrations of paraformaldehyde, which is generally assumed to "fix" the amino-containing molecules at their intrinsic locations, actually enhances the clustering of raftophilic molecules rather than fixing these molecules *in situ*, probably because sphingolipids and cholesterol, which are critically involved in raft formation, cannot be crosslinked by paraformaldehyde (Mayor et al. 1994). For observations at the light microscopy level, the use of at least 3% paraformaldehyde has been recommended (Mayor et al. 1994), whereas for observations at the electron microscopic level, the inclusion of (at least) 0.1% glutaraldehyde in the fixation medium appears to be essential (Hancock 2003; Mayor et al. 1994; Parton and Hancock 2001; Prior et al. 2003). For further details, see Subsection 13.9.1. Any milder chemical fixation may in fact induce enhanced assembly of molecules, leading to signaling events in the plasma membrane. Very often the oligomerization of molecules itself is already the beginning of the signaling events in the plasma membrane.

13.7.2
The Recovery of a Molecule in Detergent-resistant Membrane (DRM) Fractions Might Infer its Raft Association in the Cell Membrane, but the Relationship between DRM Fractions and Raft Domains is Complicated

The partitioning of a molecule in the liquid-ordered domain in artificial model membranes correlates well with its recovery in cold DRM fractions (London and Brown 2000; Schroeder et al. 1998). This inspired the thought that the lipid raft domain in the membrane is the domain in the liquid-ordered phase, and that a high correlation exists between the molecules recovered in the DRM fraction and those partitioned into raft domains in the membrane (reviewed in Simons and Vaz 2004). This has even reached the point in which the DRM association of a molecule has been accepted widely as the biochemical definition of its being a raft-associating molecule. However, there is no direct evidence that a molecule associated with the DRM fraction mostly resides in raft domains in the membrane *in situ*. Rather, cold-detergent treatment might induce macroscopic (of the order of a micron) precipitation of raftophilic molecules (Heerklotz 2002, 2003).

The following is our opinion on how to deal with the relationships between the DRM association and the raft partitioning of a molecule. It will still be correct that the DRM association of a molecule indicates a good possibility that it is associated with the raft domains in the plasma membrane and that the deter-

mination of DRM association is a good starting point for investigating a molecule's raft association in the plasma membrane. However, one has to clearly understand that DRM fractions and rafts are likely to be quite different. It will be perfectly reasonable to treat molecules that show a tendency for DRM association as raft-candidate molecules, but one has to realize that the DRM association of a molecule does not directly imply its raft association in the membrane. Therefore, in the biochemical literature, it is particularly important to make this distinction clear (Mayor and Rao 2004). DRM-associating molecules should not be called "raft" molecules. This loose terminology in the lipid raft literature is causing much confusion in raft-domain research. The DRM-associating molecules could simply be called "DRM molecules", or perhaps "raft-candidate molecules" or "raftophilic molecules" may be acceptable (Kusumi et al. 2004; Subczynski and Kusumi 2003).

In addition, the DRM association has to be described quantitatively, which is rarely done in the literature. For the majority of "DRM" molecules described in the literature, less than half of the total amounts of these molecules were associated with the DRM fractions. Therefore, another important reminder is that the "DRM molecules" described in the literature may actually be associated more frequently with non-DRM than with DRM fractions. To determine the level of DRM association of a molecule in the literature (even semiquantitatively), the information contained in the abstract of the paper is usually insufficient, and one has to look at the actual data with the hope that the gel-patterns presented in figures are representative and reveal the actual amounts of DRM association. There is an urgent need that this situation in raft research be improved.

Furthermore, many biochemical reports conclude that the level of DRM association changed, based on incorrect normalization methods. Often, the total amount of protein in each sodium dodecylsulfate–polyacrylamide gel electrophoresis (SDS-PAGE) lane is normalized to be the same. In many cases, this is a correct normalization method. However, in other cases where the changes in the raft association of a molecule are investigated, if such a normalization method is employed, then the changes in the partitioning (between DRM and non-DRM) of the target molecule cannot be evaluated (it shows how the relative amount with regard to all of the other molecules in the lane is changed and so if, for example, much more actin is recovered in DRM fraction after stimulation, then the amount of the molecule of interest in the DRM fraction may appear to be decreased after stimulation, even when the actual amount either did not change or even increased). A correct comparison can be made by loading equal "volumes" (or the total protein) from each fraction after sucrose-gradient centrifugation and keeping all conditions the same before and after stimulation. Regarding "keeping all the conditions the same", it is particularly important to keep both the total number and the density of cells used for the experiments constant because, when cold detergent extraction is carried out, both the concentration of the detergent and the ratio of the cell number/detergent concentration have to remain the same. In the absence of these precautions, reports of changes of DRM association are not useful.

13.7.3
The Size of Rafts in Plasma Membranes of Steady-state Cells may be 10 nm or Less

Sharma et al. (2004), using fluorescence lifetime imaging microscopy based on homo-fluorescence resonance energy transfer (FRET, between two of the same fluorescent molecules) between GPI-anchored proteins, folate receptor or Green Fluorescent Protein (GFP)-GPI, showed that 20–40% of these proteins may be in cholesterol-dependent clusters smaller than pentamers (below 5 nm), with the remaining 60–80% existing as monomers (Sharma et al. 2004; Varma and Mayor 1998). Such low levels of clustering of raftophilic molecules are consistent with the difficulty or variability in detecting hetero-FRET (between two different dye molecules) between raftophilic molecules. Due to the low clustering levels of GPI-anchored proteins or raftophilic molecules, the detection of hetero-FRET appears to strongly depend on the molecules, the cells, the relative concentration of the fluorescent probe molecule among other raftophilic molecules, the size of the region where measurements were made and other subtle variations in the experimental protocols among different laboratories (Feder et al. 1996; Glebov and Nichols 2004; Kenworthy and Edidin 1998; Kenworthy et al. 2000; Nagle 1992; Nichols 2003).

Direct evaluations of the raft size have been carried out in a series of elegant quantitative immunoelectron microscopy studies by Prior, Parton and Hancock (Parton and Hancock 2004; Prior et al. 2003; Plowman et al., personal communication). First, they greatly enhanced the labeling efficiency of their target molecules with their colloidal gold probes (probably over 50%) by employing 4-nm diameter gold particles with careful tuning of the antibody-conjugation method. Second, the images showing the distribution of gold probes bound to various raftophilic molecules (mostly localized on the inner surface of the membrane like H- and K-Ras) were digitized and subjected to a statistical analysis of Ripley's K function to detect the non-random distribution of the gold probes. They initially found 40-nm diameter raft domains that concentrate raftophilic molecules, like H-Ras (before its activation). However, this was further refined recently by considering the geometry of the bound IgG with respect to the gold particles, which gave around 15 nm as the diameter of the steady-state rafts (Parton and Hancock 2004).

Partitioning of the plasma membrane into compartments of 30–200 nm (the size depends on the cell type; Category 2 domain described in Section 13.3 and Fig. 13.2) due to the membrane skeleton fence and the anchored transmembrane protein pickets provides an interesting way to look into the raft size. In contrast to the situation of artificial membranes without partitioning, where the cluster size of the diffusant hardly affects the diffusion rate (Peters and Cherry 1982; Saffman and Delbrück 1975; Vaz et al. 1982), the diffusion rate in the cell membrane is a very sensitive monitor of molecular clustering. Upon clustering, membrane molecules, which rapidly hop across the picket-fences between the compartments as monomers, exhibit dramatically reduced hop rates (oligomeri-

zation-induced trapping, as described in Section 13.3 and Fig. 13.3). If the raft is larger than several nanometers and is stable (its lifetime and the residency time of its constituent molecules are long), one would expect that the diffusion coefficients of the raft-associating molecules would be much smaller than those for the membrane molecules that do not associate with raft domains. The results obtained by Vrljic et al. (2002) and Kenworthy et al. (2004) were at odds with this expectation. The diffusion rates were not different between these types of molecules in the majority of the cases and even when they were different, raft partitioning was not the cause for the difference.

Direct observations of the hop diffusion were carried out by Suzuki et al. using single-molecule techniques (at both 25-μs and 33-ms resolutions, using single-particle tracking and single fluorescent molecule video imaging) (Anderson and Jacobson 2002; Suzuki et al. 2001, 2002, 2003). Both the typical raft-preferring GPI-anchored receptor (GPI-AR) CD59 and the typical non-raftophilic, unsaturated phospholipid DOPE undergo short-term confined diffusion within a compartment of about the same size and long-term hop movement between the compartments, as expected. What was striking was the hop rate. Both molecules exhibited average hop rates that were basically the same, once every 25 ms (in the case of T24 epithelial cells). Taken together with the data by Vrljic et al. (2002) and Kenworthy et al. (2004), these results suggest that the raft size is much smaller than the average gap size between two transmembrane picket proteins, which was proposed to be 2–9 nm (see Section 13.7.4, also see Fig. 2 of Kusumi et al. 2004). Therefore the size of the raft in the steady state may be perhaps of the order of around 2 nm.

However, one has to be careful about this proposed raft size, estimated based on the diffusion measurements. It relates to the size that could fit into the gap between two transmembrane protein pickets anchored to and lined up along the membrane skeleton fence, and thus it is related to the size in the hydrophobic domain. These results suggest that the steady-state raft domains may have a mushroom (for those existing in a single layer of the membrane)- or dumbbell (for those spanning the whole membrane)-type shape with a size of about 10 nm in their hydrophilic part and around 2 nm in their hydrophobic part. This is probably made possible by the flexibility of glycochains that link the protein moiety and the phosphatidylinositol moiety, allowing assembly of saturated chains of GPI and cholesterol somewhere beneath the cluster of the protein moieties (Fig. 13.5, also see below). Furthermore, since the protein moiety is flexibly connected to the hydrophobic core region of the raft, the cluster of the protein moieties is likely to undergo rapid confined thermal oscillative motion on the membrane surface with respect to the hydrophobic raft core (which should undergo much slower diffusion due to 100-fold higher viscosity in the membrane), which would allow for the rapid passage of the cluster of the GPI-AR's protein moiety through the gap between two protruding extracellular hydrophilic domains of transmembrane protein pickets.

In line with these observations, McConnell and his colleagues have advanced the concept of the condensation complex (Anderson and McConnell 2001, 2002;

McConnell and Radhakrishnan 2003; McConnell and Vrljic 2003; Okonogi et al. 2002; Radhakrishnan et al. 2000, 2001), which might consist of 15–30 molecules (Radhakrishnan et al. 2000). The relationship between the condensation complex of cholesterol and saturated lipids with rafts has not been clarified.

Anderson and Jacobson (2002) proposed the model of a "lipid-shell" surrounding raft-associating protein molecules, based on the protein : lipid molar ratio in the DRM fraction (1 : 80). Eighty molecules of lipids would occupy a membrane area with an overall diameter of 7 nm in a single (outer) leaflet of the bilayer (assuming about a 1 : 1 molar ratio of polar lipids and cholesterol) wrapped around a raftophilic protein. This model is weak and not well supported by experimental data in several respects. First, there is no direct evidence that the protein : lipid ratio in the raft *in situ* is the same as that in DRM fractions. Second, it is difficult to think about any molecular interaction that could hold 80 molecules of lipids around a GPI-anchored or transmembrane protein. Anderson and Jacobson might have thought of the idea of "boundary lipids" around a transmembrane protein, but the residency time of a lipid in the boundary region is generally limited to about 0.1 μs (East et al. 1985; Horvath et al. 1988; Kusumi et al. 2004), i.e. much too short to have any effect on lateral diffusion

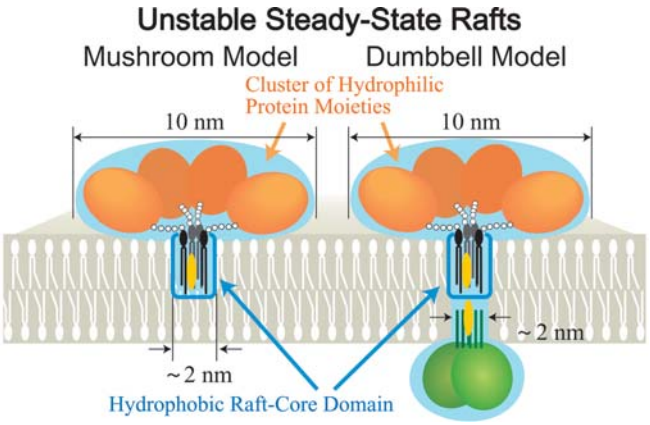

Fig. 13.5 Mushroom and dumbbell models for a small, unstable steady-state raft containing several GPI-anchored receptor molecules. Note that only a fraction of the GPI-ARs may be in such a complex and that the lifetime of such a steady-state raft may be short. The key feature of these models is the flexibility of the GPI-AR glyco-linker, which allows relocation of the PI moieties beneath the complex of hydrophilic protein moieties, leading to complex formation between cholesterol and the saturated alkyl chains of GPI from different molecules in the cluster. The large hydrophilic cluster of the protein moieties may be able to undergo rapid oscillative thermal motions on the membrane surface, due to the low viscosity of the aqueous domain and the flexibility of the glyco-linkers, facilitating rapid passage through the gap between two anchored protein pickets at the compartment boundaries. The protein moiety of this cluster may have a size of about 10 nm in diameter, whereas the hydrophobic core region of such a raft may have a diameter of only about 2 nm, which is much smaller than the average gap size between the pickets (2–9 nm).

of proteins in membranes. Third, although short-lived boundary lipids are detectable by spin-label electron paramagnetic resonance (EPR) spectroscopy, shells of lipids have never been detected by EPR or ^{1}H-nuclear magnetic resonance (NMR) of lipid probes in biological membranes. Fourth, a lipid shell extending to 7 nm diameter in both hydrophobic and hydrophilic domains is much greater than the gap between two picket transmembrane proteins lined up along the membrane skeleton (see Section 13.3), and thus the hop rate for such a large domain across the compartment boundaries in the plasma membrane should be substantially slower than that for single molecules of non-raft phospholipids and proteins, in contrast to actual diffusion measurements of raftophilic molecules and non-raft single molecules. As described above, the average gap between two pickets in a picket line may be about 2–9 nm (see Fig. 2 of Kusumi et al. 2004). This (apparent) contradiction has been explained by Anderson and Jacobson by assuming (1) that the lipid shell would have a longer lifetime than its residency time within a compartment, which is of the order of 1–25 ms, and (2) that the lipid shell is very soft and plastic, and thus may be able to readily cross the picket line. Lipids are unlikely to reside around proteins for as long as several milliseconds and at the same time have a plasticity that has essentially no effect on the hop rate across picket lines.

Single-particle tracking in the early era and photonic force microscopy suggested that the size of the raft ranges between 50 and 200 nm in diameter (Dietrich et al. 2002; Pralle et al. 2000; Sheets et al. 1997). The problem with both of these results is that gold or latex particles have been employed as probes that have tendencies to induce crosslinking. In this regard, much improved gold particles, but not latex beads, have been developed since these early experiments have been performed. In fact, when these improved single-particle probes are used, one no longer or only rarely observes raftophilic molecules confined to transient confinement zones, which are sites where the molecules temporarily stop diffusion (Kusumi and Jacobson, unpublished results). These transient confinements zones have often been interpreted to represent stabilized rafts.

13.7.4
Mushroom Model for the Steady-state Raft

In this section, we will first discuss the size and the shape of GPI-anchored proteins, and then, based on the structure of GPI-anchored proteins, we will reconsider how the proposed raft sizes and the number of molecules involved in a raft may be related. Keep in mind that we are still thinking about *rafts in steady-state cells*. The molecular sizes of GPI-anchored proteins can be roughly evaluated based on X-ray crystallographic data, assuming that the shapes of the protein moieties of these molecules are approximated by rectangular shapes: 16–34 (the expected height direction from the membrane) $\times$ 5 $\times$ 3 nm for decay-accelerating factor (CD55, the large uncertainty in the height direction is due to the undetermined structure of a part of the protein moiety) (Lukacik et al. 2004), 5 (the expected height direction from the membrane) $\times$ 8 $\times$ 3 nm for CD59 (Rudd

et al. 1997) and 7 (the expected height direction from the membrane) × 10 × 5 nm for the native dimer of placental alkaline phosphatase (PLAP) or the related shrimp alkaline phosphatase (de Backer et al. 2002; Le Du et al. 2001; Lehto and Sharom 2002). These results suggest that a 10-nm diameter protein portion of a single raft might be able to include only one to four molecules of GPI-anchored proteins, consistent with the evaluation by Sharma et al. (2004).

Consider as an example that is consistent with the data of Sharma et al. (2004), a cholesterol-dependent dimer or a tetramer of GPI-anchored proteins forming a raft domain. (This may be an oversimplification because many more GPI-anchored proteins may exist in the same membrane as monomers that are in equilibrium with these oligomers). Since alkaline phosphatases naturally occur as dimers, they could give a zeroth-order estimate for the distance between the two phosphatidylinositol (PI) molecules beneath the dimer of GPI-anchored proteins. Based on Fig. 8 in Lehto and Sharom (2002), the distance between the two carbonyl termini of the alkaline phosphatase dimer is about 4 nm. This is much greater than the size of the hydrophobic core of the raft, 1–2 nm, expected from the diffusive behavior of CD59 and other raftophilic molecules. Therefore, these results suggest that the flexible glyco-linker of a GPI-anchored protein allows for closer positioning of the two GPI-anchoring chains beneath the GPI-anchored cluster (Fig. 13.5). Within these approximately 2-nm diameter hydrophobic raft-core domains, two to four phospholipid molecules or three to six cholesterol molecules can be accommodated (assuming 0.65 and 0.44 nm^2 for their cross-sections, respectively) (Subczynski and Kusumi 2003). Such an estimate suggests that a steady-state raft with GPI-anchored proteins may contain one to four GPI-anchored proteins, a few molecules of glycolipid/phospholipid and a few cholesterol molecules. This is indeed a very small number of molecules located in a single raft. These molecules probably correspond to the molecules that stay in the hydrophobic core of the raft for prolonged periods of time, i.e. at least the residency time (1–25 ms) of GPI-anchored proteins within a membrane compartment made by plasma membrane partitioning. Since the hydrophilic part of this complex is expected to be on the order of 10 nm in diameter and the hydrophobic core part is thought to be of the order of around 2 nm in diameter, we call this model the "mushroom model" for steady-state rafts present in the outer leaflet of the plasma membrane (Fig. 13.5).

The hydrophobic part of the raft may extend slightly over this core region, but the raftophilic molecules that may be recruited to this extended region, particularly the raftophilic *lipid* molecules (because protein molecules cannot have easy access to the center of the raft, due to steric hindrance in the protein moieties), are likely to have a very short residency time in this domain. Its duration may be much shorter than the residency time of the raft within the membrane compartment. If not, the steady-state rafts could not hop as fast as single molecules of a non-raft phospholipid, DOPE. EPR spin-labeling experiments suggested that the rafts including hemagglutinin (HA) and cholesterol in the influenza virus envelope (plasma) membrane may be short-lived, and/or that the raftophilic probe molecules rapidly diffuse in and out of the raft, on a timescale

of 100 μs or less (Kawasaki et al. 2001), consistent with the short residency time of raftophilic molecules in the extended raft region around the core raft domain.

13.8
Stabilized Rafts Induced by Protein Clustering in Plasma and Golgi Membranes

13.8.1
Clustering of Raft Molecules by Ligand Binding or Crosslinking Induces Stabilized Rafts ("Receptor-cluster Rafts")

In contrast to a cell in the steady state (in the absence of extracellular stimulation), abundant evidence exists for the formation of greater, stabilized rafts upon stimulation by liganding or crosslinking raftophilic molecules, by the recruitment of raftophilic molecules in a cholesterol-dependent manner, to clusters of the activated receptor (Baird et al. 1999; Cherukuri et al. 2004a, b; Dietrich et al. 2001; Dykstra et al. 2003; Field et al. 1995; Harder et al. 1998; Janes et al. 1999; Pierce 2002; Pierini et al. 2003; Pierini and Maxfield 2001; Sheets et al. 1999; Shvartsman et al. 2003; Stoddart et al. 2002; Thomas et al. 1994; Young et al. 2003). These recruited raftophilic signaling molecules might include lipid-anchored signaling (raftophilic) molecules in both the outer and inner leaflet of the plasma membrane, which might facilitate interactions between different signaling molecules in/on a single receptor-cluster raft, leading to the activation of a signaling pathway.

Upon *de novo* synthesis of certain raftophilic molecules, they may be clustered in the Golgi (Paladino et al. 2004), perhaps by certain molecules that recognize them there. Such molecules have not been identified, but those that recognize GPI-anchored proteins may be strong candidates for such crosslinking/recognition molecules. The formation of clusters of GPI-anchored molecules would induce stabilized rafts in the Golgi membrane, possibly leading to enhanced trafficking to specific membrane compartments in the cell (Paladino et al. 2004).

13.8.2
How can Raft Molecule Clustering Induce Stabilized Rafts?

How can the clustering of GPI-anchored proteins (induced by ligands, lectins, pathogens or other reagents) induce greater, stabilized rafts? What makes the clustered raft molecules different from the monomeric raft molecules, i.e. what is the mechanism for recruiting the downstream signaling molecules only to the receptor-cluster rafts and not to steady-state rafts (see, e.g. Field et al. 1997; Pribluda et al. 1994; Sheets et al. 1999; Wu et al. 2004, for the case of the Fcε receptor)?

As an example, consider the hypothetical oligomerization of eight GPI-AR molecules, which induces the close assembly of eight to 16 saturated alkyl

chains. Note that since the protein moiety of a GPI-AR molecule is much larger (say 5 nm in diameter) than the two alkyl-chain anchors (say 0.6×1.2 nm), there is always enough space for other lipids to stay around the (8 to 16) anchoring chains in a GPI-AR cluster (say 15 nm in diameter). In such a GPI-AR cluster, eight to 16 saturated alkyl chains are concentrated and confined beneath the cluster of hydrophilic protein moieties of these GPI-AR molecules, and they may be brought close to each other because the glycochain that links the PI with the protein moiety in a GPI-AR is probably flexible (Lehto and Sharom 2002). We suggest that this concentration of saturated chains of GPI-ARs and their freedom of relocation within the GPI-AR cluster would be responsible for the formation, in the hydrophobic domain in the membrane, of (transient) complexes of these GPI-ARs' saturated alkyl chains together with cholesterol, glycosphingolipids, sphingomyelin and the saturated-lipid-anchoring chains of other lipid-anchored proteins, which would lead to the formation of enlarged, stabilized receptor-cluster rafts.

How might the concentration (plus confinement) and the relocation capability of the GPI-ARs' saturated anchoring chains beneath the GPI-AR cluster induce the recruitment of cholesterol and other raft components for the formation of receptor-cluster rafts?

First, cholesterol mixes well with saturated chains, while it tends to be excluded from the bulk, disordered liquid domains because of its poorer miscibility with unsaturated alkyl chains (Pasenkiewicz-Gierula et al. 1991; Subczynski et al. 1990). Therefore, if given a choice, cholesterol would move to the region where the saturated chains are concentrated.

Second, the long alkyl chains of sphingolipids might also be excluded from the bulk, disordered-liquid domain, due to mismatches in their hydrophobic lengths, particularly when the long saturated chains are in contact with cholesterol (Bretscher and Munro 1993; Gil et al. 1998; Kusumi and Hyde 1982). Thus, they tend to assemble in the clusters of GPI-AR–cholesterol, where the hydrophobic chains are longer and the membrane is thicker than in the bulk domain of the membrane.

Third, importantly, since the saturated alkyl chains of GPI-AR are concentrated and confined in the GPI-AR cluster, and can relocate within the cluster, the complex formation with cholesterol and other molecules with saturated alkyl chains beneath the cluster of the protein moieties of GPI-ARs may be greatly facilitated.

Fourth, since the cholesterol-saturated alkyl chain interaction enhances the *trans* conformation (Pasenkiewicz-Gierula et al. 1991; Subczynski et al. 1990), and thus orders saturated alkyl chains in the GPI-AR region, the thermal mobility in this region is reduced and the lifetime of the receptor-cluster rafts as well as the residency time of cholesterol, glycosphingolipids and sphingomyelin in this region is increased.

However, it is important to realize that the constituent lipid molecules of such "receptor-cluster rafts" may still be able to exchange with those in the bulk disordered-liquid domain, just like the lipids moving back and forth between the

ordered- and disordered-liquid-phase domains in artificial membranes (Simons and Ikonen 1997).

The receptor-cluster rafts are rafts that are directly involved in biological functions. The considerations given in this section suggest that the receptor-cluster rafts are poised to form in resting-state cells and that only small modulations of the delicate balance of molecular interactions, such as the clustering of GPI-ARs, are required to form receptor-cluster rafts. Therefore, the small, unstable steady-state rafts that are present before stimulation can be easily transformed into larger receptor-stabilized rafts.

13.9
Can Receptor-cluster Rafts Work as Platforms to Facilitate the Assembly of Raftophilic Molecules?

One of the keys for understanding the mechanism of raft-mediated or raft-facilitated signaling events may be how the raft may help to recruit and concentrate signaling molecules (Janes et al. 1999; Tavano et al. 2004). As a prelude to solving this issue, many studies have been performed to examine whether the crosslinking of a raftophilic molecule may induce the colocalization of another raftophilic molecule (with or without crosslinking). In the first subsection, we summarize the technical problems related to such immuno-colocalization experiments. In the following subsection, the results of colocalization experiments, mostly using immunofluorescence methods, will be presented (with supportive data using pull-down and immunoprecipitation assays). In the last subsection, we summarize the lack of robustness in such colocalization experiments, with variations and low levels of quantitative reproducibilities among different raftophilic molecules and cells, and subtle variations in the protocols from different laboratories.

13.9.1
Benchmarks for Experiments Examining the Colocalization of Raftophilic Molecules

Mayor et al. (1994) observed the colocalization of GPI-anchored proteins, folate receptor, CD55 and Thy-1, under various conditions using immunofluorescence microscopy. The experimental procedures and analysis described in this report in many respects represent the benchmark for such studies, and one should follow these protocols when this type of colocalization study is intended.

1. The normal fixation protocol using paraformaldehyde, employed in many studies, tends to induce the clustering of GPI-anchored proteins, rather than blocking it. To block the redistribution of GPI-anchored proteins by chemical fixation, the fixation with 3% paraformaldehyde has to be performed for over 1 h or with the inclusion of 0.3–0.5% glutaraldehyde (20–30 min). These fixation conditions have to be tested out for individual experimental systems.

2. Fixation should be carried out at room temperature without further lowering of the temperature, to avoid cold-enhanced formation of particular membrane domains. From today's viewpoint, it would be wise to compare the results with those obtained with fixation at 37 °C.

3. The colocalization levels of these GPI-anchored proteins have not usually been very high (even when colocalization appears to occur significantly by eye). They have been in the range of 35–55% in the case reported by Mayor et al. (1994). Since the colocalization levels are relatively low in this type of experiment, it is important to realize that the evaluation of colocalization must be done quantitatively and the random colocalization value must be given, as Mayor et al. did (also see Parmryd et al. 2003). Such random colocalization values can be conveniently obtained by shifting two superimposed images by, say, 1 μm relative to one another (Koyama-Honda et al. 2005).

4. Mayor et al. (1994) clearly described the colocalization percentages of one molecule's spots with the other molecule's spots. In many published studies, the relationships between molecules were not quantitatively described and, therefore, these results are less meaningful for obtaining quantitative measures of colocalization.

5. When membrane molecules are clustered, they tend to become colocalized in clathrin-coated pits and caveolae. If such events take place, then the colocalization of two molecules may not necessarily mean mutual binding to each other and may simply suggest recruitment to the same site. Therefore, when clustering is induced, colocalization with clathrin-coated pits, caveolae and the other internalization apparatus on the cell surface has to be examined, as done by Mayor et al. (1994).

6. In addition, other normal controls, like the partial depletion of cholesterol and the observation of non-raft molecules, such as transferrin receptor and unsaturated phospholipid, should be performed. The second control is important to do in addition to the cholesterol depletion control, as the antibody-induced clustering of raftophilic molecules may induce undulation and accumulation of the membrane in/near the clustered domain (Glebov and Nichols 2004).

13.9.2
Simultaneous Crosslinking of Two GPI-anchored Receptors

Mayor et al. (1994) found that when folate receptor, CD55 and Thy-1 were simultaneously (a combination of two molecules for each experiment) crosslinked with antibodies, they became colocalized at levels 3–5 times greater than the random colocalization controls. It was likely that the colocalization of these molecules took place in caveolae. Harder et al. (1998) also crosslinked PLAP, Thy-1 or influenza virus HA and the raft ganglioside GM_1 using antibodies and/or cholera toxin. The patches of these raft markers overlapped extensively at 12 °C

and less extensively at 37 °C, but not on the patches of non-raft markers, such as the transferrin and low-density lipoprotein receptors. In this study, it was not clear if the co-patched spots occurred in clathrin-coated pits. However, caveolae were not involved because colocalization also took place in caveolin-free T lymphocytes.

13.9.3
Sequential Crosslinking of One Species of GPI-anchored Receptors Followed by Crosslinking of a Second Species without Fixation

One key issue with the crosslinking of a second molecule appears to be the timing of the second crosslinking, i.e. whether the crosslinking of the second molecule occurs simultaneously with the first one or sequentially after the crosslinking of the first molecule is complete. (No chemical fixation is performed between the two crosslinking steps.)

Few sequential crosslinking experiments have been performed. Mayor et al. (1994), using folate receptor and Thy-1 (the order was permuted) found co-clustering of these molecules after crosslinking of the second species. Perhaps most of this co-clustering occurred in caveolae (see their Fig. 3).

13.9.4
Examination of the Recruitment of Non-crosslinked Second Raftophilic Molecules to Crosslinked GPI-anchored Receptor Clusters

Colocalization experiments were also conducted under conditions where the second crosslinking was omitted. Thus far, all of the observations in this class of experiments were carried out using fixed cells and in most experiments the fixation occurred after the crosslinking of the first GPI-AR. Different groups have obtained different results in different systems as described in the following. Mayor et al. (1994) did not detect any colocalization of the second species (folate receptor or Thy-1) to the crosslinked first molecular species (Thy-1 or folate receptor, respectively). Fra et al. (1994) also found that non-crosslinked Thy-1 or GM_1 was not recruited to pre-crosslinked GM_1 or Thy-1, respectively, in caveolin-free T cell hybridoma 2B2318 cells. Meanwhile, Harder et al. (1998) followed the distribution of non-crosslinked PLAP with patched HA or non-crosslinked HA with patched PLAP. They occasionally observed co-clustering of the two, but the co-patching behavior was quite variable.

Marwali et al. (2003) observed the colocalization of GM_1 with pre-crosslinked Thy-1 (see their Fig. 7). Caution is advised when interpreting these data because the cells were fixed only after the second species was stained. In their protocol, staining of the second species, GM_1, is expected to strongly affect the final results. The distribution of GM_1 was observed with the pentavalent B-subunit fragment of cholera toxin, which thus may collect five GM_1 molecules, and the staining was performed at 4 °C, which might enhance the formation of raft-like domains. Therefore, it is possible that the apparent colocalization of "non-cross-

linked GM_1" may be due to the recruitment of clustered GM_1. A reverse experiment was performed by Mitchell et al. (2002), who found that crosslinked GM_1 recruited the non-crosslinked GPI-AR CD59 (see their Fig. 5).

Interestingly, Harder et al. (1998) found that after crosslinking of PLAP, which is located in the *outer leaflet* of the plasma membrane, the SFK Fyn, which is anchored in the *cytoplasmic leaflet* of the plasma membrane via two saturated alkyl (one myristoyl and one palmitoyl) chains. These two alkyl chains may promote the partitioning of Fyn into raft domains with concentrated saturated alkyl chains beneath the PLAP clusters. This result is very interesting because the cytoplasmic leaflet does not contain appreciable amounts of sphingomyelin and it is not clear how the presence of an ordered lipid domain in the outer leaflet can induce an ordered lipid domain in the cytoplasmic leaflet.

13.9.5
Difficulty in Colocalization Experiments using Raftophilic Molecules: Low Levels of Colocalization and Quantitative Reproducibility Due to Sensitivity to Subtle Differences in Experimental Conditions and Protocols

As suggested in the previous subsections, colocalization experiments using raftophilic molecules turned out to be much more difficult than expected. In many colocalization experiments, the results were so clear that a statistical analysis of colocalization was practically unnecessary. However, in colocalization studies of raft molecules, as described in Section 13.9.1, the level of colocalization is typically only 3- to 5-fold greater than in random controls (Mayor et al. 1994; Parmryd et al. 2003).

Unfortunately, many investigators in this field experienced difficulties in reproducing data obtained by other laboratories. However, the differences tend to be quantitative rather than contradictory in most cases (e.g. 50% colocalization in one lab and 30% in another lab). Often, the robustness of the results appears to be lacking. The results appear to be sensitive to subtle differences in experimental conditions and protocols, and the types of molecules and cells that were used. We believe that this difficulty may be deeply rooted in (1) the essential nature of the colocalization of two raftophilic molecules, one of which may have been pre-clustered, and (2) the chemical fixation used for the observation of colocalization.

13.10
Timescales Again! Transient Colocalization of Raftophilic Molecules

An idea to explain the difficulty in colocalization experiments can be found in the experiments carried out by Shvartsman et al. (2003). These authors tried to observe the interaction between two antigenically distinct influenza HA proteins: a wild-type transmembrane HA and a GPI-anchored HA. They already knew that biochemical and immunofluorescence methods did not reveal any as-

sociation between these two molecular species. They developed a very smart approach for detecting the interaction of crosslinked with non-crosslinked molecular species. In live cells that coexpressed these two proteins, they measured by fluorescence recovery after photobleaching (FRAP) the lateral diffusion rate of wild-type HA before and after the aggregation of GPI-HA into immobile patches. They found that the presence of GPI-HA patches reduced the diffusion rate of wild-type HA, suggesting a *transient* binding of individual wild-type HA molecules to crosslinked GPI-HA.

This result also suggests the possibility that a variety of short-term interactions between raftophilic molecules exist that may be missed in immunofluorescence colocalization experiments and biochemical pull-down assays. Such dynamic on–off interactions or rapid association–dissociation may lie at the edge of the detectability limit of static immuno-colocalization observations, which involve the chemical fixation of transiently colocalized molecules. Such dynamic effects make the detectability of colocalization even more sensitive to subtle variations of molecules, cells and experimental protocols or reagents, leading to low levels (and thus large fluctuations) of static colocalization and poor quantitative reproducibility of the data from different laboratories or sometimes even among different researchers in the same group.

The results described in Sections 13.9.2 and 13.9.4 can be summarized as follows.

1. When two species of raftophilic molecules are individually crosslinked, they tend to show colocalization (although the quantitative level of colocalization may vary under different conditions).

2. When one species of raftophilic molecule is crosslinked and then the recruitment of another molecular species of raftophilic molecules is observed, the results are variable (even when the experiments are done by the same researchers; see, e.g. Harder et al. 1998) and colocalization is more difficult to detect.

We propose an explanation for these results by considering the dynamics of the interacting molecular species, i.e. *the timescales of interaction* (Fig. 13.6). We think that the interaction is transient, especially when the second molecular species is not crosslinked (Fig. 13.6, left), but also when two clusters are separately crosslinked (Fig. 13.6, right). If one chemically fixes such dynamical membrane systems, the level of colocalization will depend on both the frequency and duration of the molecular interactions, making colocalization experiments very sensitive to experimental details. This is true for the case where both of the two molecular species are crosslinked (Fig. 13.6, right) and even more so when the second molecular species is not crosslinked (Fig. 13.6, left). Single-molecule approaches may be the key to resolving the dynamics of such transient colocalization interactions. Efforts to directly observe homo- and heterotypic colocalization events at the single molecule level are underway in our laboratory.

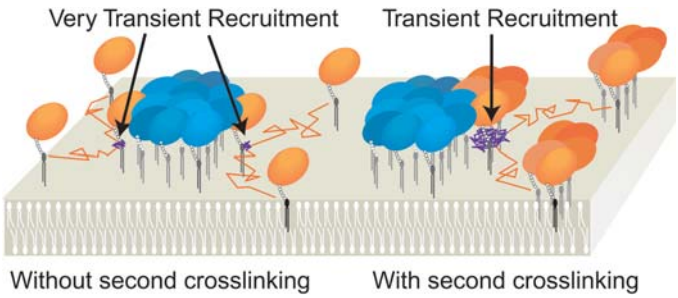

Fig. 13.6 Model of dynamic recruitment of raftophilic molecules, with or without crosslinking, to receptor-cluster rafts, explaining the lack of robustness in immunofluorescence colocalization experiments using chemically fixed cells. Colocalization events may occur very dynamically – to a stabilized raft of crosslinked GPI-anchored proteins a different species of raftophilic molecules may be recruited transiently. If these dynamic colocalization events are visualized by immunofluorescence after chemical fixation, the observed colocalization level may be low and near the detectability limit, making the colocalization detection sensitive to small experimental variations. Detectability of colocalization depends on the efficiency of chemical crosslinking, temperature, and how exactly crosslinking and chemical fixation are performed. When both of the observed molecular species are clustered, colocalization is observed at much higher rates than when only one of the two species is clustered. This suggests the following dynamic recruitment model: the efficiency of chemical fixation of the second molecule at the stabilized raft of the first clustered molecule becomes much higher after crosslinking of the second molecule because the duration of colocalization will be prolonged after clustering of the second molecule.

13.11 Modified Raft Hypothesis

We think that the original raft hypothesis, described in Section 13.6, is essentially correct, but we propose three modifications to the original model.

1. In the absence of extracellular stimulation or crosslinking of raftophilic molecules, the rafts in these steady-state cells are small and some of them may contain as few as one to four GPI-anchored proteins, together with a few molecules of glycolipids and/or phospholipids with saturated alkyl chains and a few molecules of cholesterol. The cluster size of the hydrophilic protein moieties of GPI-anchored receptors may be of the order of 10 nm in diameter, whereas the hydrophobic core of the steady-state raft may be only around 2 nm in diameter. This is described by the mushroom model (Fig. 13.5). One of the most important characteristics of such a steady-state raft is that the glyco-linker of GPI-AR is flexible, allowing fast oscillative thermal motion of the protein moiety and positional freedom for the GPI moiety beneath the protein moiety. For example, when a four-molecule GPI-AR cluster is formed, the GPI-anchoring chains can be close to each other beneath the cluster of protein moieties.

2. Enlarged stabilized rafts are induced by liganding or crosslinking of GPI-ARs, which leads to GPI-AR cluster formation. The cluster of the GPI-linked protein moieties will concentrate the saturated alkyl chains of the GPI anchors beneath the cluster, which in turn will attract cholesterol molecules, leading to further assembly of glycosphingolipids and sphingomyelin with saturated alkyl chains, and the formation of a receptor-cluster raft.

3. This enlarged stabilized raft forms a platform to facilitate the recruitment and assembly of various raftophilic molecules; however, this recruitment and the associated interactions are likely to occur only transiently.

These ideas and models need further testing. Importantly, all of these events have to be described in a quantitative fashion. Some of the most important quantitations that await experimental verification concern the sizes and lifetimes of steady-state and receptor-cluster rafts, and the duration of colocalization of individual raft components.

Acknowledgments
We thank the members of our laboratory for fruitful discussions and advice.

References

Anderson, R. G., K. Jacobson. **2002**. A role for lipid shells in targeting proteins to caveolae, rafts, and other lipid domains. *Science 296*, 1821–1825.

Anderson, T. G., H. M. McConnell. **2001**. Condensed complexes and the calorimetry of cholesterol–phospholipid bilayers. *Biophys. J. 81*, 2774–2785.

Anderson, T. G., H. M. McConnell. **2002**. A thermodynamic model for extended complexes of cholesterol and phospholipid. *Biophys. J. 83*, 2039–2052.

Baird, B., E. D. Sheets, D. Holowka. **1999**. How does the plasma membrane participate in cellular signaling by receptors for immunoglobulin E? *Biophys. Chem. 82*, 109–119.

Bretscher, M. S., S. Munro. **1993**. Cholesterol and the Golgi apparatus. *Science 261*, 1280–1281.

Brown, D. A., E. London. **1998**. Functions of lipid rafts in biological membranes. *Annu. Rev. Cell Dev. Biol. 14*, 111–136.

Brugger, B., C. Graham, I. Leibrecht, E. Mombelli, A. Jen, F. Wieland, R. Morris. **2004**. The membrane domains occupied by glycosylphosphatidylinositol-anchored prion protein and Thy-1 differ in lipid composition. *J. Biol. Chem. 279*, 7530–7536.

Cherukuri, A., R. H. Carter, S. Brooks, W. Bornmann, R. Finn, C. S. Dowd, S. K. Pierce. **2004a**. B cell signaling is regulated by induced palmitoylation of CD81. *J. Biol. Chem. 279*, 31973–31982.

Cherukuri, A., T. Shoham, H. W. Sohn, S. Levy, S. Brooks, R. Carter, S. K. Pierce. **2004b**. The tetraspanin CD81 is necessary for partitioning of coligated CD19/CD21–B cell antigen receptor complexes into signaling-active lipid rafts. *J. Immunol. 172*, 370–380.

Crane, J. M., L. K. Tamm. **2004**. Role of cholesterol in the formation and nature of lipid rafts in planar and spherical model membranes. *Biophys. J. 86*, 2965–2979.

de Backer, M., S. McSweeney, H. B. Rasmussen, B. W. Rise, P. Lindley, E. Hough. **2002**. The 1.9 Å crystal structure of heat-labile shrimp alkaline phosphatase. *J. Mol. Biol. 318*, 1265–1274.

Dietrich, C., Z. N. Volovyk, M. Levi, N. L. Thompson, K. Jacobson. **2001**. Partitioning of Thy-1, GM_1, and cross-linked phospho-

lipid analogs into lipid rafts reconstituted in supported model membrane monolayers. *Proc. Natl Acad. Sci. USA 98*, 10642–10647.

Dietrich, C., B. Yang, T. Fujiwara, A. Kusumi, K. Jacobson. **2002**. Relationship of lipid rafts to transient confinement zones detected by single particle tracking. *Biophys. J. 82*, 274–284.

Dykstra, M., A. Cherukuri, H.W. Sohn, S.J. Tzeng, S.K. Pierce. **2003**. Location is everything: lipid rafts and immune cell signaling. *Annu. Rev. Immunol. 21*, 457–481.

East, J.M., D. Melville, A.G. Lee. **1985**. Exchange rates and numbers of annular lipids for the calcium and magnesium ion dependent adenosine triphosphatase. *Biochemistry 24*, 2615–2623.

Feder, T.J., I. Brust-Mascher, J.P. Slattery, B. Baird, W.W. Webb. **1996**. Constrained diffusion or immobile fraction on cell surfaces: a new interpretation. *Biophys. J. 70*, 2767–2773.

Field, K.A., D. Holowka, B. Baird. **1995**. Fc epsilon RI-mediated recruitment of p53/56^{lyn} to detergent-resistant membrane domains accompanies cellular signaling. *Proc. Natl Acad. Sci. USA 92*, 9201–9205.

Field, K.A., D. Holowka, B. Baird. **1997**. Compartmentalized activation of the high affinity immunoglobulin E receptor within membrane domains. *J. Biol. Chem. 272*, 4276–4280.

Fra, A.M., E. Williamson, K. Simons, R.G. Parton. **1994**. Detergent-insoluble glycolipid microdomains in lymphocytes in the absence of caveolae. *J. Biol. Chem. 269*, 30745–30748.

Gaidarov, I., F. Santini, R.A. Warren, J.H. Keen. **1999**. Spatial control of coated-pit dynamics in living cells. *Nat. Cell Biol. 1*, 1–7.

Gil, T., J.H. Ipsen, O.G. Mouritsen, M.C. Sabra, M.M. Sperotto, M.J. Zuckermann. **1998**. Theoretical analysis of protein organization in lipid membranes. *Biochim. Biophys. Acta 1376*, 245–266.

Glebov, O.O., B.J. Nichols. **2004**. Lipid raft proteins have a random distribution during localized activation of the T-cell receptor. *Nat. Cell Biol. 6*, 238–243.

Hancock, J.F. **2003**. Ras proteins: different signals from different locations. *Nat. Rev. Mol. Cell Biol. 4*, 373–384.

Harder, T., P. Scheiffele, P. Verkade, K. Simons. **1998**. Lipid domain structure of the plasma membrane revealed by patching of membrane components. *J. Cell Biol. 141*, 929–942.

Heerklotz, H. **2002**. Triton promotes domain formation in lipid raft mixtures. *Biophys. J. 83*, 2693–2701.

Heerklotz, H., H. Szadkowska, T. Anderson, J. Seelig. **2003**. The sensitivity of lipid domains to small perturbations demonstrated by the effect of Triton. *J. Mol. Biol. 329*, 793–799.

Horvath, L.I., P.J. Brophy, D. Marsh. **1988**. Exchange rates at the lipid–protein interface of myelin proteolipid protein studied by spin-label electron spin resonance. *Biochemistry 27*, 46–52.

Iino, R., I. Koyama, A. Kusumi. **2001**. Single molecule imaging of green fluorescent proteins in living cells: E-cadherin forms oligomers on the free cell surface. *Biophys. J. 80*, 2667–2677.

Janes, P.W., S.C. Ley, A.I. Magee. **1999**. Aggregation of lipid rafts accompanies signaling via the T cell antigen receptor. *J. Cell Biol. 147*, 447–461.

Jordan, B.A., L.A. Devi. **1999**. G-protein-coupled receptor heterodimerization modulates receptor function. *Nature 399*, 697–700.

Kawasaki, K., J.J. Yin, W. K. Subczynski, J. S. Hyde, A. Kusumi. **2001**. Pulse EPR detection of lipid exchange between protein-rich raft and bulk domains in the membrane: methodology development and its application to studies of influenza viral membrane. *Biophys. J. 80*, 738–748.

Kenworthy, A.K., M. Edidin. **1998**. Distribution of a glycosylphosphatidylinositol-anchored protein at the apical surface of MDCK cells examined at a resolution of <100 Å using imaging fluorescence resonance energy transfer. *J. Cell Biol. 142*, 69–84.

Kenworthy, A. K., N. Petranova, M. Edidin. **2000**. High-resolution FRET microscopy of cholera toxin B-subunit and GPI-anchored proteins in cell plasma membranes. *Mol. Biol. Cell 11*, 1645–1655.

Kenworthy, A. K., B. J. Nichols, C. L. Remmert G. M. Hendrix, M. Kumar, J. Zimmerberg, J. Lippincott-Schwartz. **2004**. Dynamics of putative raft-associated proteins at the cell surface. *J. Cell Biol. 165*, 735–746.

Koyama-Honda, I., K. Ritchie, T. Fujiwara, R. Iino, H. Murakoshi, R. S. Kasai, A. Kusumi. **2005**. Fluorescence imaging for monitoring the colocalization of two single molecules in living cells. *Biophys. J. 88*, 2126–2136.

Kusumi, A., J. S. Hyde. **1982**. Spin-label saturation-transfer electron spin resonance detection of transient association of rhodopsin in reconstituted membranes. *Biochemistry 21*, 5978–5983.

Kusumi, A., I. Koyama-Honda, K. Suzuki. **2004**. Molecular dynamics and interactions for creation of stimulation-induced stabilized rafts from small unstable steady-state rafts. *Traffic 5*, 213–230.

Lai, E. C. **2003**. Lipid rafts make for slippery platforms. *J. Cell Biol. 162*, 365–370.

Le Du, M. H., T. Stigbrand, M. J. Taussig, A. Menez, E. A. Stura. **2001**. Crystal structure of alkaline phosphatase from human placenta at 18 Å resolution. Implication for a substrate specificity. *J. Biol. Chem. 276*, 9158–9165.

Lehto, M. T., F. J. Sharom. **2002**. Proximity of the protein moiety of a GPI-anchored protein to the membrane surface: a FRET study. *Biochemistry 41*, 8368–8376.

London, E., D. A. Brown. **2000**. Insolubility of lipids in Triton X-100: physical origin and relationship to sphingolipid/cholesterol membrane domains (rafts). *Biochim. Biophys. Acta 1508*, 182–195.

Lukacik, P., P. Roversi, J. White, D. Esser, G. P. Smith, J. Billington, P. A. Williams, P. M. Rudd, M. R. Wormald, D. J. Harvey, M. D. Crispin, C. M. Radcliffe, R. A. Dwek, D. J. Evans, B. P. Morgan, R. A. Smith, S. M. Lea. **2004**. Complement regulation at the molecular level: the structure of decay-accelerating factor. *Proc. Natl Acad. Sci. USA 101*, 1279–1284.

Manes, S., R. Ana Lacalle, C. Gomez-Mouton, A. C. Martinez. **2003**. From rafts to crafts: membrane asymmetry in moving cells. *Trends. Immunol. 24*, 320–326.

Marwali, M. R., J. Rey-Ladino, L. Dreolini, D. Shaw, F. Takei. **2003**. Membrane cholesterol regulates LFA-1 function and lipid raft heterogeneity. *Blood 102*, 215–222.

Maxfield, F. R. **2002**. Plasma membrane microdomains. *Curr. Opin. Cell Biol. 14*, 483–487.

Mayor, S., M. Rao. **2004**. Rafts: scale-dependent, active lipid organization at the cell surface. *Traffic 5*, 231–240.

Mayor, S., K. G. Rothberg, F. R. Maxfield. **1994**. Sequestration of GPI-anchored proteins in caveolae triggered by cross-linking. *Science 264*, 1948–1951.

McConnell, H. M., A. Radhakrishnan. **2003**. Condensed complexes of cholesterol and phospholipids. *Biochim. Biophys. Acta 1610*, 159–173.

McConnell, H. M., M. Vrljic. **2003**. Liquid–liquid immiscibility in membranes. *Annu. Rev. Biophys. Biomol. Struct. 32*, 469–492.

Mitchell, J. S., O. Kanca, B. W. McIntyre. **2002**. Lipid microdomain clustering induces a redistribution of antigen recognition and adhesion molecules on human T lymphocytes. *J. Immunol. 168*, 2737–2744.

Mukherjee, S., F. R. Maxfield. **2004**. Membrane domains. *Annu. Rev. Cell Dev. Biol. 20*, 839–866.

Nagle, J. F. **1992**. Long tail kinetics in biophysics? *Biophys. J. 63*, 366–370.

Nichols, B. J. **2003**. GM_1-containing lipid rafts are depleted within clathrin-coated pits. *Curr. Biol. 13*, 686–690.

Okonogi, T. M., A. Radhakrishnan, H. M. McConnell. **2002**. Two fatty acids can replace one phospholipid in condensed complexes with cholesterol. *Biochim. Biophys. Acta 1564*, 1–4.

Paladino, S., D. Sarnataro, R. Pillich, S. Tivodar, L. Nitsch, C. Zurzolo. **2004**. Protein oligomerization modulates raft partitioning and apical sorting of GPI-anchored proteins. *J. Cell Biol. 167*, 699–709.

Parmryd, I., J. Adler, R. Patel, A. I. Magee. **2003**. Imaging metabolism of phosphatidylinositol 4,5-bisphosphate in T-cell GM_1-enriched domains containing Ras proteins. *Exp. Cell Res. 285*, 27–38.

Parton, R. G., J. F. Hancock. **2001**. Caveolin and Ras function. *Methods Enzymol. 333*, 172–183.

Parton, R.G., J.F. Hancock. **2004**. Lipid rafts and plasma membrane microorganization: insights from Ras. *Trends Cell Biol. 14*, 141–147.

Pasdar, M., W.J. Nelson. **1988a**. Kinetics of desmosome assembly in Madin-Darby canine kidney epithelial cells: temporal and spatial regulation of desmoplakin organization and stabilization upon cell–cell contact.I. Biochemical analysis. *J. Cell Biol. 106*, 677–685.

Pasdar, M., W.J. Nelson. **1988b**. Kinetics of desmosome assembly in Madin-Darby canine kidney epithelial cells: temporal and spatial regulation of desmoplakin organization and stabilization upon cell–cell contact. II. Morphological analysis. *J. Cell Biol. 106*, 687–695.

Pasdar, M., W.J. Nelson. **1989**. Regulation of desmosome assembly in epithelial cells: kinetics of synthesis, transport, and stabilization of desmoglein I, a major protein of the membrane core domain. *J. Cell Biol. 109*, 163–177.

Pasenkiewicz-Gierula, M., W. K. Subczynski, A. Kusumi. **1991**. Influence of phospholipid unsaturation on the cholesterol distribution in membranes. *Biochimie 73*, 1311–1316.

Peters, R., R.J. Cherry. **1982**. Lateral and rotational diffusion of bacteriorhodopsin in lipid bilayers: experimental test of the Saffman-Delbruck equations. *Proc. Natl Acad. Sci. USA 79*, 4317–4321.

Pierce, S.K. **2002**. Lipid rafts and B-cell activation. *Nat. Rev. Immunol. 2*, 96–105.

Pierini, L.M., F.R. Maxfield. **2001**. Flotillas of lipid rafts fore and aft. *Proc. Natl Acad. Sci. USA 98*, 9471–9473.

Pierini, L.M., R.J. Eddy, M. Fuortes, S. Seveau, C. Casulo, F.R. Maxfield. **2003**. Membrane lipid organization is critical for human neutrophil polarization. *J. Biol. Chem. 278*, 10831–10841.

Pralle, A., P. Keller, E. L. Florin, K. Simons, J.K. Horber. **2000**. Sphingolipid–cholesterol rafts diffuse as small entities in the plasma membrane of mammalian cells. *J. Cell Biol. 148*, 997–1008.

Pribluda, V.S., C. Pribluda, H. Metzger. **1994**. Transphosphorylation as the mechanism by which the high-affinity receptor for IgE is phosphorylated upon aggregation. *Proc. Natl Acad. Sci. USA 91*, 11246–11250.

Prior, I.A., C. Muncke, R.G. Parton, J.F. Hancock. **2003**. Direct visualization of Ras proteins in spatially distinct cell surface microdomains. *J. Cell Biol. 160*, 165–170.

Radhakrishnan, A., T.G. Anderson, H.M. McConnell. **2000**. Condensed complexes, rafts, and the chemical activity of cholesterol in membranes. *Proc. Natl Acad. Sci. USA 97*, 12422–12427.

Radhakrishnan, A., X.M. Li, R.E. Brown, H. M. McConnell. **2001**. Stoichiometry of cholesterol–sphingomyelin condensed complexes in monolayers. *Biochim. Biophys. Acta 1511*, 1–6.

Rudd, P.M., B.P. Morgan, M.R. Wormald, D.J. Harvey, C.W. van den Berg, S.J. Davis, M.A. Ferguson, R.A. Dwek. **1997**. The glycosylation of the complement regulatory protein, human erythrocyte CD59. *J. Biol. Chem. 272*, 7229–7244.

Saffman, P.G., M. Delbrück. **1975**. Brownian motion in biological membranes. *Proc. Natl Acad. Sci. USA 72*, 3111–3113.

Schroeder, R.J., S.N. Ahmed, Y. Zhu, E. London, D.A. Brown. **1998**. Cholesterol and sphingolipid enhance the Triton X-100 insolubility of glycosylphosphatidylinositol-anchored proteins by promoting the formation of detergent-insoluble ordered membrane domains. *J. Biol. Chem. 273*, 1150–1157.

Sharma, P., R. Varma, R.C. Sarasij, Ira, K. Gousset, G. Krishnamoorthy, M. Rao, S. Mayor. **2004**. Nanoscale organization of multiple GPI-anchored proteins in living cell membranes. *Cell 116*, 577–589.

Sheets, E.D., G.M. Lee, R. Simson, K. Jacobson. **1997**. Transient confinement of a glycosylphosphatidylinositol-anchored protein in the plasma membrane. *Biochemistry 36*, 12449–12458.

Sheets, E.D., D. Holowka, B. Baird. **1999**. Critical role for cholesterol in Lyn-mediated tyrosine phosphorylation of FcepsilonRI and their association with detergent-resistant membranes. *J. Cell Biol. 145*, 877–887.

Shvartsman, D.E., M. Kotler, R.D. Tall, M.G. Roth, Y.I. Henis. **2003**. Differently

anchored influenza hemagglutinin mutants display distinct interaction dynamics with mutual rafts. *J. Cell Biol. 163*, 879–888.

Simons, K., E. Ikonen. **1997**. Functional rafts in cell membranes. *Nature 387*, 569–572.

Simons, K., D. Toomre. **2000**. Lipid rafts and signal transduction. *Nat. Rev. Mol. Cell Biol. 1*, 31–39.

Simons, K., G. van Meer. **1988**. Lipid sorting in epithelial cells. *Biochemistry 27*, 6197–6202.

Simons, K., W. L. Vaz. **2004**. Model systems, lipid rafts, and cell membranes. *Annu. Rev. Biophys. Biomol. Struct 33*, 269–295.

Singer, S. J., G. L. Nicolson. **1972**. The fluid mosaic model of the structure of cell membranes. *Science 175*, 720–731.

Stoddart, A., M. L. Dykstra, B. K. Brown, W. Song, S. K. Pierce, F. M. Brodsky. **2002**. Lipid rafts unite signaling cascades with clathrin to regulate BCR internalization. *Immunity 17*, 451–462.

Subczynski, W. K., A. Kusumi. **2003**. Dynamics of raft molecules in the cell and artificial membranes: approaches by pulse EPR spin labeling and single molecule optical microscopy. *Biochim. Biophys. Acta 1610*, 231–243.

Subczynski, W. K., W. E. Antholine, J. S. Hyde, A. Kusumi. **1990**. Microimmiscibility and three-dimensional dynamic structures of phosphatidylcholine–cholesterol membranes: translational diffusion of a copper complex in the membrane. *Biochemistry 29*, 7936–7945.

Suzuki, K., F. Sanematsu, T. Fujiwara, M. Edidin, A. Kusumi. **2001**. Rapid, continual formation/dispersion of raft-like domains in the resting cell membrane. *Mol. Biol. Cell 12*, 470a.

Suzuki, K., F. Sanematsu, T. Fujiwara, M. Edidin, A. Kusumi. **2002**. Stimulation-induced formation of temporal but stabilized rafts. *Biophys. J. 82*, 348a.

Suzuki, K., F. Sanematsu, T. Fujiwara, K. Ritchie, M. Edidin, A. Kusumi. **2003**. Crosslinking of a GPI-anchored protein creates signaling rafts from smaller, transient, lipid rafts. *Biophys. J. 84*, 487a.

Tavano, R., G. Gri, B. Molon, B. Marinari, C. E. Rudd, L. Tuosto, A. Viola. **2004**. CD28 and lipid rafts coordinate recruitment of Lck to the immunological synapse of human T lymphocytes. *J. Immunol. 173*, 5392–5397.

Thomas, J. L., D. Holowka, B. Baird, W. W. Webb. **1994**. Large-scale co-aggregation of fluorescent lipid probes with cell surface proteins. *J. Cell Biol. 125*, 795–802.

Varma, R., S. Mayor. **1998**. GPI-anchored proteins are organized in submicron domains at the cell surface. *Nature 394*, 798–801.

Vaz, W. L., M. Criado, V. M. Madeira, G. Schoellmann, T. M. Jovin. **1982**. Size dependence of the translational diffusion of large integral membrane proteins in liquid-crystalline phase lipid bilayers. A study using fluorescence recovery after photobleaching. *Biochemistry 21*, 5608–5612.

Vrljic, M., S. Y. Nishimura, S. Brasselet, W. E. Moerner, H. M. McConnell. **2002**. Translational diffusion of individual class II MHC membrane proteins in cells. *Biophys. J. 83*, 2681–2692.

Wu, M., D. Holowka, H. G. Craighead, B. Baird. **2004**. Visualization of plasma membrane compartmentalization with patterned lipid bilayers. *Proc. Natl Acad. Sci. USA 101*, 13798–13803.

Young, R. M., D. Holowka, B. Baird. **2003**. A lipid raft environment enhances Lyn kinase activity by protecting the active site tyrosine from dephosphorylation. *J. Biol. Chem. 278*, 20746–20752.

14
Protein and Lipid Partitioning in Locally Heterogeneous Model Membranes

Petra Schwille, Nicoletta Kahya, and Kirsten Bacia

14.1
Introduction: Why Should We Use Simple Model Membranes to Gain Insight Into Complex Membrane Organization?

The Singer and Nicholson model of the biological membrane implies a homogeneous lateral distribution of the bulk of lipids [1], which are thought to act mainly as a solvent for the proteins. As a modification of the Singer and Nicholson model, it was proposed that the bulk lipids, rather than forming homogeneous layers, might also be laterally organized [2]. Different mechanisms and aspects of lateral organization into domains were suggested, such as:

- Proteins ordering the lipid packing around them.
- *Lipid* phase separation as seen in model systems (liquid/gel phase).
- Lipid phase separation involving cholesterol.
- Physical alterations of membrane structure (e.g. curvature radius).
- Heterogeneity caused by transmembrane lipid asymmetry.

Much later, starting around 1998, the hypothesis of domain formation in cellular membranes, so far mainly discussed in the context of lipid chemistry, has provoked an enormous wave of interest among biologists. Most likely, the following three factors substantially contributed to this great attention.

14.1.1
Relation of Domain Structure to a Biological Function

In 1988, Simons et al. [3, 4] hypothesized that the quantitatively different lipid compositions of apical and basolateral membranes [apical membranes being richer in glycosphingolipids and poorer in phosphatidylcholine (PC)] could stem from lateral lipid sorting in the *trans*-Golgi membranes into domains similar to the ones known in lipid model systems. If protein and lipid sorting were linked,

the *lipid* sorting hypothesis would also provide a mechanism for selective *protein* targeting to the respective membranes, which is still a very attractive hypothesis [5]. In the plasma membrane, the same mechanism could have the function of providing a compartmentalized environment to endocytic (for review, see [6]) and signaling processes (for review, see [7]).

14.1.2 An Accessible Detection Method

In 1992, Brown and Rose [8] reported their studies on detergent-solubility of glycosylphosphatidylinositol (GPI)-anchored proteins. Taking the approach Skibbens et al. [9] had used on hemagglutinin, they examined the kinetics with which the GPI-anchored protein human placental alkaline phosphatase (PLAP) becomes insoluble to Triton X-100 (at 4 °C) during its biosynthetic course from the endoplasmic reticulum (ER) via the Golgi to the cell surface. The detergent insolubility assay was refined by adding a sucrose-gradient ultracentrifugation, which separates low-density, lipid-associated insoluble material from high-density, e.g. cytoskeleton-associated, insoluble material.

They concluded that PLAP becomes detergent insoluble in the Golgi before reaching the *trans*-Golgi (and remains so at the plasma membrane). Furthermore, tests of a variety of conditions made it appear unlikely that this insolubility was due to cytoskeleton interactions. Lipid analysis showed that the insoluble membrane fractions are richer in sphingolipids and poorer in glycerophospholipids than the total membrane and also suggested that the ratio of cholesterol : sphingolipid : glycerophospholipid in the insoluble fraction was around 1 : 1 : 1, i.e. similar to the composition of apical membranes in polarized cells. In conclusion, these experiments supported the model of lipid microdomains in the Golgi as a sorting mechanism for apical targeting and suggested the use of detergent insolubility as a criteria for cholesterol–sphingolipid microdomain association. Experiments on artificial liposomes (e.g. [10]) further supported the use of this methodological approach by demonstrating that sphingolipid–cholesterol-rich membranes (with the incorporated GPI-linked PLAP protein) tended to resist detergent extraction, whereas unsaturated PC bilayers were more readily extracted. In the last years, the preparation of detergent-resistant membranes, which requires equipment that is readily available in most biochemical laboratories, became the most widespread method used in studying biological membrane heterogeneity.

14.1.3 The Term "Raft"

The term "raft" was coined to denote functional platforms floating in membranes in a review by Simons and Ikonen [11], and has conveniently unified research in this field under a common, searchable keyword. It now commonly stands for [12]:

- Putative domains in native membranes (expected to be sphingolipid- and cholesterol-rich, but still poorly defined; there may be different types of domains).
- Liquid-ordered phase domains (clearly defined only in model membranes).
- Detergent-resistant fractions of membrane preparations (DRMs).
- Putative location of membrane constituents whose function is impaired by cholesterol extraction or inhibition of cholesterol synthesis.
- Areas in membranes with restricted diffusion behavior as observed by single-particle tracking (SPT).
- Domains in membranes that are observable by fluorescence microscopy.

Unfortunately, the relationship between these phenomena that are all referred to as "rafts" has not been irrevocably defined and they are clearly not synonyms. In particular, the detergent resistance does not appear to coincide precisely with liquid-ordered domain association. Detergent treatment and cooling change the thermodynamic state of membrane systems, and may actually induce the formation and organization of liquid-ordered phases [13, 14]. As described later in this chapter, recent model membrane work indicates that even "traditional raft markers" as judged by detergent resistance may predominantly associate with the liquid-disordered phase in the unperturbed state and prefer the liquid-ordered phase only upon crosslinking. These observations argue strongly against equating "rafts", liquid-ordered phase domains and DRMs. However, since it appears that "non-DRM" markers stay in the liquid-disordered phase even upon crosslinking [15], the detergent resistance assay may – despite its failure to mirror the *in vivo* situation – still serve as an indicator for raft *propensity*.

Research in the raft field in the past 5 years has yielded a huge amount of information about DRM association and functional dependency of specific proteins on cholesterol. However, the nature of live cell rafts has remained a fairly open question. This dilemma has been critically reflected in a series of current reviews [16–20]. Evidently, the aim to characterize submicron membrane heterogeneity based on weak molecular interactions in the fully complex live cell is set very high. One possible approach is to study live cell membranes with improved methods. Strategies towards this aim comprise minimizing the invasiveness and increasing the resolution of existing techniques used on cells as well as extending the use of more techniques from model membranes to cells. The other approach towards understanding native rafts is to continue the tradition of model membrane systems and to greatly increase their complexity in a stepwise manner. Possible steps in this direction are to use free-standing lipid bilayers as in giant unilamellar vesicles (GUVs) [21–23], to use native lipid compositions [24, 25], to include proteins in artificial lipid bilayers [26, 27] and to mimic the cell cytoskeleton [28]. The following sections describe the types of model membranes employed to study membrane heterogeneity, the methods used to study them, and the results obtained on different lipid and protein systems that are pertinent to the raft hypothesis.

14.2
Biomimetic Membranes

Biomolecular membrane research has a long tradition of development and application of artificial membranes as a model for complex biological membranes. To date, several model membranes have been made available for different purposes [29, 30]. Ideal model membranes should consist of a closed, spherical, single bilayer structure, in which integral or surface-associated peripheral membrane proteins can be inserted, such that the protein folding, activity, oligomeric state and lateral diffusion properties are maintained. The most popular membrane system used for biochemical assays is the liposome or vesicle (see Fig. 14.1 a) which provides a closed, stable and regular bilayer structure [31]. The diameter typically ranges from 15–50 nm [small unilamellar vesicles (SUVs)] up to 100–1000 nm [large unilamellar vesicles (LUVs)]. However, liposomes of this size are of no use for (single-molecule) optical microscopy, as the

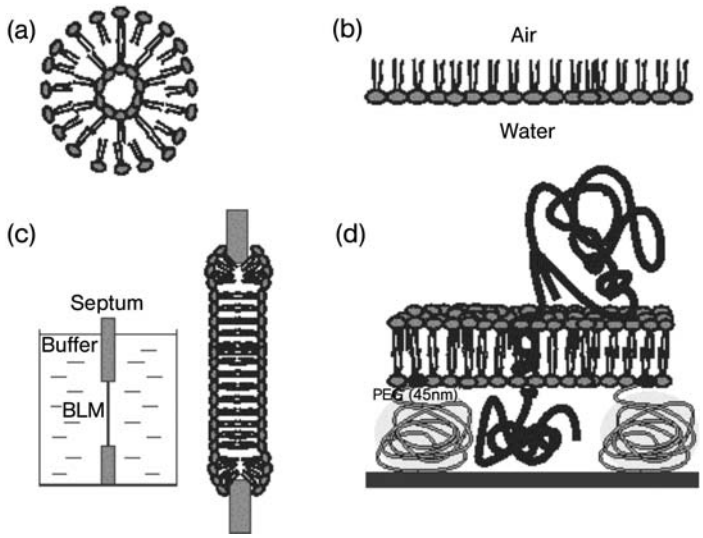

Fig. 14.1 Model membranes. (a) Schematic representation of a vesicle, a spherical closed bilayer, its size being 15–50 nm (SUVs) or 0.1–1 μm (LUVs) and (b) of a monolayer formed at water/air interfaces. (c) Layout of the experimental setup to prepare BLMs (left). On the septum (mostly made of Teflon foil, 15 μm thick) that supports the BLM a smooth, circular hole (100–200 μm diameter) is burned. An organic lipid solution is painted on the hole, after which spontaneous membrane thinning (right) occurs. (d) Tethered polymer-supported planar membranes are designed to separate the lipid bilayer from the solid substrate in order to accommodate the soluble residues of membrane proteins and prevent them from interacting with the support. If a functionalized form of the soft polymer PEG is employed, the space between the bilayer and the substrate is 4.5 nm thick. As a result of insertion of polymer, the lateral mobility of lipids and proteins increases, but artifacts may still arise. Inserted proteins may interact with the tethering polymers [35].

size of the membrane must be larger than the optical spatial resolution (around 300 nm). Hence, systems like monolayers, black lipid membranes (BLMs), (tethered) planar supported membranes and GUVs are the most popular models for optical microscopy.

Monolayers [32] are easy to prepare, provide a regular and stable structure (see Fig. 14.1 b), and the composition can be accurately controlled. Their ability to mimic biomembranes can be questioned, as they lack the second leaflet to form a bilayer. The first successful attempt to make membranes with a bilayer lipid arrangement was reported by Müller et al. [33] with the BLMs. Two compartments are separated by a thin partition (septum) and communicate through an aperture (100–200 μm in diameter) in this partition (see Fig. 14.1 c). An organic solution of lipids is brushed over the hole and then the compartments are filled with an aqueous medium. Dispersion of the solvent in the aqueous medium eventually leaves a bilayer on the hole (Fig. 14.1 c). In practice, however, there are many technical limitations that prevent the formation of an ideal BLM and lead to an irregular bilayer structure [34]. Furthermore, technical problems often frustrate reproducible protein reconstitution in BLMs. An alternative to BLMs consists of membranes assembled at the interface between a solid substrate and an aqueous phase. The early concept was based on the fusion of vesicles (SUVs) onto the hydrophilic surface of a clean polar substrate, such as glass or mica. This results in a supported membrane [30] floating on an ultrathin (around 1–2 nm) water layer. However, the lipid–substrate interactions are sources of severe artifacts. In particular, many membrane proteins protrude from the bilayer surface into the water phase, much further than 1–2 nm, hence their soluble residues interact with the solid substrate, leading to partial or complete loss of functionality. Furthermore, many biological reactions in membranes depend on the lateral mobility and spatial distribution of proteins. Therefore, to bear biological relevance, model membranes should provide an environment in which protein dynamics and mobility are similar to those in the native membrane. The strategy to solve these drawbacks led to the development of a tethered bilayer [30], which is composed of a solid substrate, a tethering layer (e.g. a soft polymer cushion) and a lipid bilayer (Fig. 14.1 d). The polymer should keep the lipid bilayer and rigid support far apart to preserve membrane fluidity. Tamm et al. [35] introduced a novel tethering system based on a polyethylene glycol (PEG)–phospholipid conjugate that can be covalently attached to silicate substrates. However, membrane proteins embedded in such a lipid matrix interact with the polymer and appear to be only partially mobile. In the post-genomic era, supported membranes provide an enormous potential for the production of biosensors, membrane chips [36] and membrane protein microarrays [37], constructed by lateral patterning of the bilayer substrate architectures either with microlithography techniques [38] or by blotting and stamping the desired patterns [39]. Nevertheless, the properties of integral membrane proteins in a supported planar membrane seem as yet far from those observed in the native cell membrane.

Potentially, the artifacts present in supported membranes are absent in GUVs, which is a rapidly emerging model in membrane research [40]. GUVs are spherical, closed, single bilayers, freely floating in aqueous solution. They are suitable

for single-molecule optical microscopy and exhibit a cell-like curvature, as their size ranges from 10 to 100 μm in diameter. GUV micromanipulation gives membrane researchers a unique opportunity to monitor a single colloidal particle exposed to controlled mechanical, thermal and/or (bio)chemical perturbations.

14.2.1 GUVs: Properties and Preparation

In our hands, the most appropriate and convenient procedure for preparing GUVs, i.e. truly unilamellar vesicles with a high yield, is the one based on electroformation, as developed by Dimitrov and Angelova [22, 41]. In the 1980s it was observed that electric fields can induce, facilitate or hinder lipid swelling and liposome formation. Electric fields were seen to significantly affect the rate of lipid swelling and induce liposome formation even when mere hydration failed to do so. Briefly, the method consists of depositing droplets of the lipid solution on either two parallel platinum wires or on two plane-parallel, nickel-covered electrodes. After the lipid layer has been dried under nitrogen, the chamber in which the wires are located is filled with water and an electric field is subsequently applied. In general, liposome formation depends on the dried lipid layer thickness, the lipid composition and the applied voltage. Neutral lipids, e.g. 1,2-dimyristoyl-*sn*-glycero-3-phosphocholine (DMPC; C_{14}, saturated, symmetric), formed just a few thin-walled liposomes in the absence of a field, but the yield increased remarkably (10- to 100-fold) when an AC field was applied. By monitoring lipid swelling by phase-contrast microscopy, it was observed that the membranes vibrated with the same frequency as the applied AC field. By increasing the amplitude of the field, the amplitude of the vibrations increased as well. At a fixed voltage, the amplitude of the vibration decreased with increasing AC frequency [22]. From this point of view, the action of an AC field is similar to the dispersion of energy into the system by a sonicator, albeit more gentle and thereby resulting in the formation of much larger vesicles. In both cases, mechanical stress exerted on the lipid layer induces separation and destabilization of the membranes in order to form unilamellar liposomes.

GUVs can be prepared by electroformation with a wide variety of phospholipids, zwitterionic and charged, and mixtures thereof. Importantly, however, the vesicles should be prepared at conditions where the lipids are fluid, i.e., above their gel-to-liquid-crystalline phase transition, because in the solid state, membrane viscosity prevents lipid swelling. In general, increasing the ionic strength decreased the efficiency of vesicle formation. In practice, only low ionic strengths were found tolerable, but the actual limitations depend on the type of buffer, lipid mixture, temperature and electric field applied.

14.3
Methods of Investigation of Domain Formation in Biomimetic Membranes

Over the years, we learned much about membrane physicochemical properties through thermodynamic measurements [by differential scanning calorimetry (DSC) and surface pressure-area isotherms), spectroscopic methods [nuclear magnetic resonance (NMR), electron spin resonance (ESR), IR spectroscopy, fluorescence quenching and resonance energy transfer] and analytical approaches (mass spectrometry and density gradient ultracentrifugation), which are reviewed in [18, 42, 43]. In recent years, the need for more direct methods to study the topological organization of membranes at the micro-/nanometer spatial scale has become pertinent. To this end, diverse microscopy techniques have been employed, yielding a very complex picture of the membrane architecture, where components are ordered at different spatial and temporal scales. Below, the most important microscopy techniques are listed (because of the limited space, only the studies on model membranes are quoted).

14.3.1
Electron Microscopy

Electron microscopy allows for visualization of the organization of components in the membrane with great spatial resolution (down to 2–4 nm for freeze-fracture electron microscopy). It is mainly used for (intra)cellular applications, although it also provided good insights into phase co-existence in artificial membranes; in particular, related to the equilibrium between the gel phase and liquid-disordered (l_d) phase [44]. Seeing the sample preparation procedures, the technique is rather invasive and developing reliable, artifact-free labeling protocols still represents a challenge.

14.3.2
Atomic Force Microscopy (AFM)

Mostly used as a surface imaging technique, AFM offers excellent spatial resolution for direct visualization of the membrane topology. Although the poor chemical specificity is currently being improved by the implementation of new tools (e.g. functionalized cantilevers), the present limitations of the technique – poor temporal resolution (tens of milliseconds) and rather high invasiveness – keep most applications limited to model membranes. The level of spatial detail allows for resolving lipid complexes that would not be seen by optical microscopy, as in the case of the ganglioside GM1, which affects domain morphology in sphingomyelin (SM)/1,2-dioleoyl-*sn*-glycero-3-phosphocholine (DOPC; C_{18}, *un*saturated, symmetric)/cholesterol mixtures when present in amounts larger than 2 mol%. By further increasing the amount of GM1, it has been shown that subdomains are formed, which are highly enriched in the ganglioside [45].

14.3.3
Near-field Scanning Optical Microscopy (NSOM)

Relying on an optical waveguide as a light source, which is located at very short distances (roughly nanometers) from the sample, NSOM provides high spatial resolution (around 30–50 nm), compared to wide-field fluorescence imaging techniques. The poor temporal resolution (comparable to AFM) and the technical challenges to work under physiological conditions limit the applications at the moment to model membranes [46].

14.3.4
Fluorescence Imaging (Confocal, Multi-photon)

Applied to model membranes, fluorescence imaging has allowed for a direct visualization of domains and a characterization of their topology, in the case of phase co-existence [23–25, 47]. Great care needs to be taken in assigning lipid phases on the basis of the partitioning behavior of the lipid probes as this may vary depending on the membrane lipid composition. Moreover, lipid analogs may not behave the same way as their natural counterparts. Finally, the visualization of domain assembly is bound to the diffraction limit (around 300 nm).

14.3.5
Fluorescence Photobleaching Recovery (FPR) or Fluorescence Recovery after Photobleaching (FRAP)

Although limited by the optical resolution, optical microscopy offers a suitable temporal resolution (within the characteristic time window of lateral diffusion) with low invasiveness. Because of this, FRAP has for a long time been employed to study lateral dynamics and rafts in live cells. Studies have also been carried out on artificial membranes [15, 24, 48]. The need for high degrees of labeling and strong illumination power may cause chemical- and/or heating-induced artifacts. The high laser powers needed and the chemical alteration of great fractions of the labeled species may yield artifactual results.

14.3.6
Single Particle Tracking (SPT)

Numerous SPT studies have been conducted to examine the diffusion characteristics of membrane components [49]. The technique relies on imaging and tracing single fluorescent molecules diffusing at the membrane surface. The high spatial resolution (around 30 nm) achieved by particle localization procedures combined with high temporal resolution (50 ms down to 25 μs) allows for a detailed characterization of lateral diffusion modes and particle aggregation/dissociation events. Great care has to be taken to obtain data with good statistical accuracy.

14.3.7
Fluorescence Correlation Spectroscopy (FCS)

This technique is based on the time correlation of temporal fluctuations of fluorescence detected in the focal volume, which is governed by dynamic parameters of a system at equilibrium [50, 51]. FCS explores dynamic events with high temporal resolution and good statistical accuracy [52], thereby providing reliable data analysis in much shorter times than SPT. Unlike FRAP, FCS assures low invasiveness, as it relies on single-molecule sensitivity, and a great versatility, as it gives information about a wide range of dynamic properties (e.g. translational mobility, association constants, chemical kinetic constants and lifetimes of some chromophore electronic states). In the past, FCS has been proven to be a powerful tool to follow lipid and protein dynamics *in vivo* [53] and in domain-forming GUVs [54].

14.4
Lipid Domain Assembly in GUVs

14.4.1
Phase Separation

14.4.1.1 Can Cellular Membrane Domains be Regarded as Phase Domains?

In thermodynamic terms, a phase is a part of a system that is homogeneous in its thermodynamic parameters. At the interface of the phase with another phase, thermodynamic parameters abruptly change. In three-dimensional systems, the interfaces are two-dimensional (surfaces); in lipid bilayers systems, they are one-dimensional (lines). Strictly speaking, true phases exist only in the limit of infinite extension. However, for practical purposes it suffices that the extension of the phase is large compared to the microscopic entities constituting the phase and that the number of particles involved in forming the interface is small relative to the bulk of the phase.

When describing the formation of lateral heterogeneities in membranes as the co-existence of domains of different phases it is therefore important to compare the domain to the particle dimension. Concepts of membrane domains range from "small, unstable steady-state rafts" consisting of a theoretical minimum of three molecules [55], over subresolution "rafts" of a few thousands lipids (around 50 nm diameter [56]) to domains or patches of more than 100 000 lipids (or more than 250 nm in diameter). The latter are visible under light microscopy, and usually obtained only after invasive treatments like crosslinking and cooling [7, 57]. Since the circumference scales with the square root of the area, the number of interfacial molecules scales with the square root of the number of molecules pertaining to the domain. Depending on the width of the boundary layer (line) between the phases, a domain consisting of 100 000 lipids would have a minimum of 1% of its molecules at the interface, but a smaller

domain with 1000 lipids would already have a minimum of 10% of its molecules at the interface (calculated for a boundary line width of one molecular diameter).

In addition to the "surface" (i.e. interfacial line) effects, the complexity of the lipid composition needs to be considered. Phase domains will no longer be homogeneous on their length scale if the lipid composition is too complex, i.e. if there are too many different lipid species with exceedingly different properties among the total number of molecules. In that case, the lipids do not mix into a single homogeneous macroscopic phase. In many model membrane studies, relatively simple lipid compositions are studied, i.e. binary or ternary lipid mixtures. The domains observed are often large (on the order of GUV size or about 10 μm); in this case, portrayal as a "phase" is quite appropriate [58]. Homogeneity within the GUV phases is supported, for instance, by the fact that diffusion coefficients obtained by FCS are independent of the positioning of the laser focus within the phase domain. The lipid composition in real membranes is, in contrast, much more complex.

Lateral membrane heterogeneity may not need to be macroscopic and describable as a phase co-existence to be physiologically relevant. It may also occur in the form of more or less extended and transient lateral fluctuations in lipid composition [59]. These fluctuations can become larger in the vicinity of phase transitions or for strongly non-ideal mixtures, i.e. when the interaction enthalpies between the different species (ΔH_{A-B}) are very different from the average interaction enthalpies between molecules of the same species (ΔH_{A-A} and ΔH_{B-B}). It appears difficult to "catch" these fluctuations experimentally without perturbing them; in particular, in a liquid bilayer where diffusion is rapid. Some techniques like AFM [60] or electron microscopy [61] have the spatial resolution to characterize nanoscale domains arising from these fluctuations. However, these techniques cannot follow the domains' dynamics. They involve some kind of fixation (like transfer to a solid substrate or even chemical crosslinking), meaning they produce "snapshots", which may suffer from perturbation during the fixating process. It seems very difficult to detect the lipid lateral distribution non-invasively, and at the same time to gain sufficient temporal and spatial resolution to detect submicron heterogeneity.

For this reason, various studies try to push towards understanding "rafts" in terms of collective properties, e.g. lipid phase behavior. Although used most extensively to describe pure lipid mixtures, the phase concept is able to accommodate proteins by regarding them as solutes that partition between different phases of lipid solvents (or accumulate at the interface) with a certain partition coefficient. Other studies, again, take a microscopic, particulate view by focusing on selected molecular complexes, which assemble due to molecular binding interactions. Such molecular complexes can consist of proteins, proteins and lipids (caveolin and cholesterol [62]) or lipids alone (the concept of condensed cholesterol–phospholipid complexes [63]).

14.4.1.2 **Properties of Lipid Bilayer Phases**

Among the phases formed by lipids in the presence of water, the bilayer (lamellar) phases are most important to understand domain formation (see Fig. 14.2):

1. The lamellar *gel* phases feature a highly ordered, all-*trans* configuration of the hydrocarbon chains. X-ray crystallography has identified different gel phases with distinct packing structures (e.g. tilted hydrocarbon chains relative to the bilayer plane or interdigitated hydrocarbon chains), but they are all characterized by the long-range translational order that impedes lateral movement. The gel phase is also called *solid*(-ordered) phase (s_o).

2. Upon increase of the temperature above the melting point (T_m), the entropy term becomes dominating, resulting in a *fluid*, so-called *liquid-crystalline* phase, L_α. It is characterized both by low conformational order in the hydrocarbon chains (lower internal order) and by low translational order (low packing order, high translational diffusion). Area-per-lipid, which is on the order of 0.5 nm^2 in the gel phase [64], increases by approximately 15 to 30% upon melting [65]. The L_α phase has more recently also been the termed *liquid-disordered* (l_d) phase to distinguish it from (3).

3. The *liquid-ordered* (l_o) phase. The addition of cholesterol results in a loss of cooperativity of the gel-to-liquid-crystalline phase transition. Magnet resonance studies indicate that this is due to the introduction of another equilibrium phase, l_o, in which there is high conformational order like in the gel phase, but the translational order is lost (fast translational diffusion) similar as in the L_α phase [66–69]. Theoretical studies [70] predict that the order–disorder transition of the hydrocarbon chains and the order–disorder transition of the packing do not need to be coupled, thus supporting the establishment of a new phase.

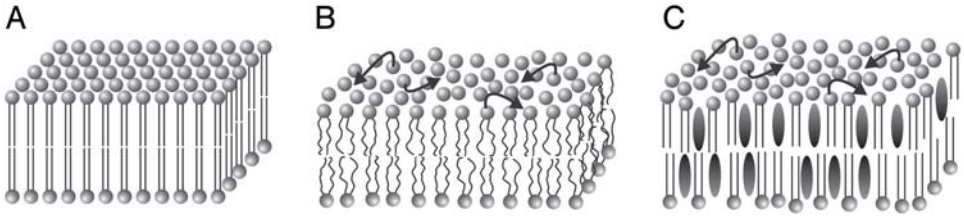

Fig. 14.2 Schematic views of different lamellar lipid phases. (A) The L_β gel phase (a solid-ordered s_o phase) is characterized by both high conformational and high translational order of the lipid chains. (B) In the L_α, liquid-crystalline (l_d) phase, the phospholipids show both lipid chain conformational and translational disorder (high lateral diffusibility). (C) In the l_o phase, the lipid chains are ordered due to interactions with the cholesterol (depicted as ellipses). However, there is translational disorder, allowing for lateral diffusion.

14.4.1.3 Co-existence of Lipid Bilayer Phases

A lipid bilayer system may exhibit one or more co-existing phases, depending on temperature, pressure and composition. Visualization of the gel and l_d phase in GUVs shows irregularly shaped domains due to the rigid (solid) structure of the gel phase [23]. Co-existence of l_o and l_d phases implies liquid–liquid immiscibility (translational disorder in both phases), leading to circular domain shapes [24, 71], since the system seeks to minimize the amount of energetically unfavorable packing at the phase interface (line tension).

The maximum number of co-existing phases can be deduced by the Gibbs Rule. It states the number of degrees of freedom, F, for a system consisting of C components and exhibiting P different phases. With the pressure being a constant, the remaining degrees of freedom are given by

$$F = C - P + 1$$

Note that for the composition of lipid bilayers in excess water, the water is usually not counted as a component (and the water concentration accordingly not as a degree of freedom).

For a single-lipid system ($C=1$), two phases ($P=2$) exist only right at the phase transition temperature T_m (no degree of freedom for the temperature). In contrast, a binary lipid system ($C=2$) can have a *region* of phase co-existence ($P=2$), where phase co-existence is maintained as the temperature is varied ($F=1$).

14.4.1.4 Lipid Phase Diagrams

The occurrence of lipid phases as a function of the state of a lipid system is depicted in a phase diagram. Phase diagrams are constructed based on experimental data on abrupt changes in thermodynamic parameters at phase transitions. They can only be constructed for simple systems and are often already quite complex for binary and, in particular, ternary lipid mixtures. Fig. 14.3 shows a schematic example of a phase diagram for a binary lipid mixture.

14.4.2 Binary Lipid Systems

Over the past 30 years, a large amount of work has been devoted to investigating the physicochemical properties of bilayers composed of binary lipid mixtures. Concerning lipid/sterol mixtures, a number of properties and the aspect of the phase diagram triggered McConnell et al. to introduce the hypothesis of condensed complexes [72]. Above 30–35 mol% of cholesterol, no extensive phase separation was observed within the optical resolution. Theoretical as well as experimental phase diagrams for similar binary mixtures show that at high cholesterol contents one homogeneous l_o phase is formed. Low T_m PC lipids, saturated and unsaturated, never exhibited domain formation, at least within the optical resolution. The presence of micrometer-scale domains has been ruled out

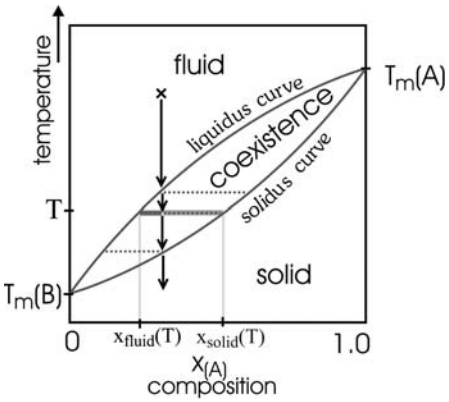

Fig. 14.3 Typical phase diagram for a binary mixture of saturated PCs that differ only in their chain lengths, e.g. A = DPPC and B = DMPC [115, 116]. The lipids show complete miscibility in the solid (gel) and the fluid (liquid-crystalline) phase. However, due to their different melting temperatures (here T_m(A) = 41 °C and T_m(B) = 24 °C), there is a solid–fluid co-existence region. Upon cooling a mixture (depicted by the cross and the arrows), a DPPC-enriched mixture starts to solidify at the liquidus curve, increasing the DMPC content of the remaining liquid. Hence in the co-existence region DPPC-enriched solid is in equilibrium with DMPC-enriched liquid. At a chosen temperature *T*, the compositions of the phases x_{fluid} and x_{solid} are fixed. They can be read from where the horizontal dotted line, a so-called tie-line, intersects the liquidus and the solidus curves. The relative amounts of liquid and solid can be calculated from material conservation ("lever rule").

also by other techniques, such as FRET in submicrometer vesicles and calorimetry [42, 63]. When using lipids of different chain length, the question arises whether cholesterol would be equally soluble in all of the considered lipids. Whereas little information on that issue comes from optical imaging, FCS data obtained from mixtures of up to 65 mol% of cholesterol showed that different nominal sterol densities gave rise to different dynamics, implying that the solubility limit was not reached in these mixtures (see Section 14.4.5).

For bilayers composed of equimolar mixtures of saturated and unsaturated PCs, a network of intricate and interwoven domains in the gel phase is at equilibrium with a l_d phase. Contrast between distinct phases was provided here by the differential partitioning behavior of DiI-C_{18} (*cf.* the homogeneous fluorescence at the surface of DOPC GUVs in Fig. 14.4 A). (DiI-C_n = 1,1′-dialkyl-3,3,3′,3′-tetramethylindocarbocyanine perchlorate, fluorescent lipid analogs where *n* indicates alkyl chain length, e.g. C_{18} = octadecyl chains.) For 1,2-dipalmitoyl-*sn*-glycero-3-phosphocholine (DPPC; C_{16}, saturated, symmetric)/DOPC 1:1 GUVs (Fig. 14.4 B), the lipid probe preferentially partitioned in the gel phase (ratio around 4:1), whereas in 1,2-distearoyl-*sn*-glycero-3-phosphocholine (DSPC; C_{18}, saturated, symmetric)/DOPC 1:1 GUVs (Fig. 14.4 C), it is mostly found (ratio 1:4) in the l_d-, DOPC-enriched phase [73]. No phase separation was visible in DOPC/SM 1:1 GUVs by using DiI-C_{18} [47], but liquid domains have

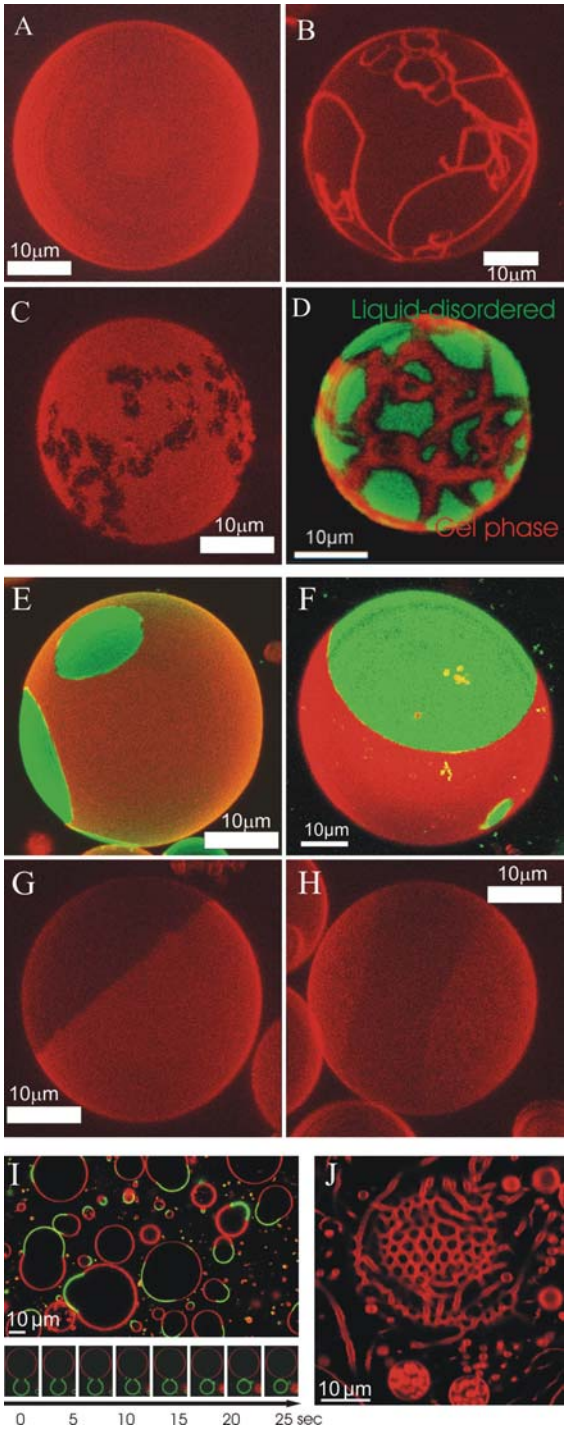
A
10μm
B
10μm
C
10μm
D
Liquid-disordered
Gel phase
10μm
E
10μm
F
10μm
G
10μm
H
10μm
I
10μm
0
5
10
15
20
25 sec
J
10μm

been observed by using PC analogs labeled with the fluorophore Bodipy (4,4-difluoro-4-bora-3a,4a-diaza-*s*-indacene. By mixing saturated PCs, domain formation is a result of a hydrophobic mismatch of at least four C atoms difference in chain length between the two lipids, e.g. for 1,2-dilauroyl-*sn*-glycero-3-phosphocholine (DLPC, PC with C_{12}, saturated, symmetric fatty acids)/DPPC at different ratios (Fig. 14.4 D) [23].

14.4.3 Ternary Lipid Systems

Bulk studies on the phase behavior of ternary mixtures containing cholesterol and phospholipids were mainly based on calorimetry, IR, fluorescence and magnetic (NMR and ESR) spectroscopy. They established the basis for two prominent effects of cholesterol: (1) cholesterol interacts non-randomly with different phospholipid components within the same bilayer and (2) high cholesterol levels promote intermixing of lipids that exhibit phase separation in the absence of cholesterol. In recent years, the molecular basis of liquid-liquid immiscibility could be investigated with high spatial resolution by optical microscopy and AFM. Lipid domains were visualized by one- and two-photon fluorescence microscopy in GUVs by several groups. The pioneering work by Korlach et al. [23] has paved the way to the establishment of a tool that conclusively demonstrated the co-existence of lipid phases in DLPC/DPPC/cholesterol mixtures, thereby unraveling details of the topology of these domains on the vesicle surface. In DLPC/DPPC mixtures at various ratios, co-existing gel and l_d phases could be visualized by exploiting the differential partitioning behavior of two lipid probes, DiI-C_{20} and Bodipy-PC, in distinct phases. Ordered domains enriched in DPPC in the gel phase formed elongated bands interwoven in an intricate network on

Fig. 14.4 Lipid organization in GUVs from binary and ternary lipid mixtures. Three-dimensional projections obtained from confocal images (0.4 µm thickness) of GUVs composed of (A) 100% DOPC and 0.1% DiI-C_{18}, (B) DOPC/DPPC 1:1 and 0.1% DiI-C_{18}, (C) DOPC/DSPC 1:1 and 0.1% DiI-C_{18}, and (D) DLPC/DPPC 0.4:0.6 and 0.1% DiI-C_{20} (red) and 0.1% Bodipy-PC (green). Note that this vesicle is multilamellar and was obtained from a different preparation procedure (adapted from [23]). (E–F) Three-dimensional projections of GUVs composed of DOPC/SM 1:1, 0.1% GM_1, 0.1% DiI-C_{18} (red) and AF-CTB (green), and 20% (E) or 33% (F) cholesterol. (G and H) Three-dimensional projections of GUVs produced from (G) DOPC/DPPC 1:1, 20% cholesterol and 0.1% DiI-C_{18}, and (H) DOPC/DSPC 1:1, 33% cholesterol and 0.1% DiI-C_{18}. (I) Confocal slice images of GUVs prepared from a 1:1:1 lipid mixture of sphingomyelin, cholesterol and DOPC with 0.1% GM_1. The l_d phase is labeled with DiI-C_{18} in red and the l_o phase with AF-CTB in green. The l_o phase exhibits an increased positive curvature, which eventually leads to budding to the outside, as seen in the time series. (J) GUVs containing cholesterol sulfate instead of cholesterol and labeled only with DiI-C_{18}. No phase domains within the membranes were observed. However, the membranes formed vesicles, multivesicular structures, membrane tubules and reticulate structures, such as the network seen here.

the vesicle surface. These regions, enriched in DiI-C_{20}, were exactly complementary to the fluid, DLPC-enriched regions, in which Bodipy-PC was mainly found. Interestingly, the paper also showed the changes in domain morphology upon addition of small (up to 5 mol%) amounts of cholesterol, as the band-like regions became more elongated. One important piece of information was the establishment of the superposition of phase domains in inner and outer leaflets, for all of the lipid mixtures analyzed.

Co-existing fluid phases were visualized by optical imaging in further works by Dietrich et al. [24]. Here, various lipid mixtures and, in particular, the more physiologically relevant SM/POPC/cholesterol 1:1:1 mixture exhibited spatial segregation in round domains on the vesicle surface of both planar supported bilayers and GUVs. A more detailed investigation of the morphology of co-existing domains in lipid mixtures that are relevant to the raft issue was performed on SM/DOPC/cholesterol mixture at various ratios [47]. Cholesterol was shown to promote segregation of DOPC and SM in distinct phases for a defined region of the lipid phase diagram. Phase assignment was carried out by using the fluorescent lipid probe DiI-C_{18}, which strongly favored one of the two phases by a factor of around 50 and the Alexa Fluor 488-labeled cholera toxin B subunit (AF-CTB) that binds the ganglioside GM1 and marks the SM-enriched phases. In Fig. 14.4 E–H, three-dimensional image projections of GUVs composed of SM/DOPC/cholesterol at various ratios are reported. AF-CTB (green) marked only the regions of the GUV surface from which DiI-C_{18} (red, Fig. 14.4 E and F) was almost completely excluded, thereby identifying the raft-like, sphingolipid-enriched areas. DiI-C_{18} exhibited the opposite partitioning behavior from that in DPPC/DOPC mixtures (without cholesterol), in which it favored the DPPC gel phase. The explanation at the molecular level we have so far is that the molecular packing in the gel phase for DPPC greatly differs from that of SM/cholesterol in the l_o phase, in which cholesterol tightly intercalates between SM molecules, thereby "squeezing out" DiI-C_{18} molecules. Note that the amount of GM1 added to these lipid mixtures was at most 0.1 mol%, an amount that was shown by AFM not to affect the domain morphology of the SM/DOPC/cholesterol mixtures. By optical imaging, we did see changes in domain morphology upon addition of 1–2 mol% of GM1 (N. Kahya, unpublished results). By increasing the cholesterol levels from 10 up to 33 mol% (added to SM/DOPC 1:1 mixtures), the large round-shaped domains did not change, but the total surface covered by the SM/cholesterol-enriched areas clearly increased, although no detailed quantitative analysis was carried out. At and above 50 mol% of cholesterol, lipid mixing occurred, thereby yielding homogeneous fluorescence (within the optical resolution) from the GUV surface. Furthermore, by varying the ratio of SM/DOPC within the ternary mixtures, one realizes that the region of phase co-existence in the phase diagram is not symmetric around the central axis. At SM/DOPC above 1:1, lipid spatial segregation took place, whereas no domain formation was observed for low SM/DOPC ratios [47].

Within the 30 years of research of membrane biophysics, the issue whether cholesterol engages in a special interaction with SM rather than with saturated

glycerophospholipids was raised pretty recently [74, 75]. In this respect, SM has been shown to have a peculiar affinity for cholesterol, which was estimated to be much higher than for other lipids. Phase co-existence for the SM/DOPC/cholesterol mixture was characterized by optical imaging, and compared to that in the DPPC/DOPC/cholesterol and DSPC/DOPC/cholesterol mixtures, in which SM (18:0) has been replaced by a saturated glycerophospholipid of comparable chain length. Liquid–liquid immiscibility was readily observed approximately within the same region of the phase diagram. However, the two-phase region, which yielded GUVs with large round (hence liquid) domains, was found to increase with DPPC < DSPC < SM. This is entirely consistent with previous work [74] and confirmed the enhanced ability of cholesterol of creating a differential molecular packing in the presence of SM rather than with saturated glycerophospholipids. Surprisingly, the lipid probe DiI-C_{18} favored the l_d phase in the DPPC/DOPC/cholesterol mixture, as for the SM, but favored the l_o phase in the DSPC/DOPC/cholesterol mixture.

Finally, optical imaging was carried out in ternary lipid mixtures in which cholesterol was added to saturated glycerophospholipids of different length (i.e. DLPC and DMPC) [75a] and SM. Cholesterol was shown in the early literature to interact more strongly with saturated than with unsaturated phospholipids. Consistent with this, a two-phase region appeared only at high cholesterol content, close to the solubility limits of cholesterol. Below this level, lipid mixing yielded a homogeneous spatial distribution of the fluorescence signal (from the probe DiI-C_{18}) on the GUV surface.

14.4.4
Effect of Sterols on Lipid Segregation

Cholesterol, with its rigid sterol structure, very efficiently imposes order onto neighboring aliphatic lipid chains, causing formation of the l_o phase and thus producing liquid–liquid immiscibility. Its unique role is emphasized by the fact that it is highly conserved as the major sterol in animal cell membranes, making up about 30% of the plasma membrane in many cells [76]. Other sterols, i.e. stigmasterol and sitosterol, may play a similar role as cholesterol in higher plant cells [77]; ergosterol is thought to have a similar role in yeast [78].

Cholesterol has a dominant role in animal cells, but cells also produce other sterols and steroids with the same basic ring structure. While the signaling functions of membrane-permeating steroid hormones have been the subject of numerous investigations, the structural roles of non-cholesterol sterols/steroids as membrane constituents have not yet been studied very extensively. Can these also form a l_o phase? Do they have the potential to fulfill their own specialized structural roles in membranes, maybe even at low relative concentrations?

Lanosterol is of interest as a biosynthetic and potentially also evolutionary precursor to cholesterol [79]. Spectroscopic data and Monte-Carlo simulations [80, 81] indicate that lanosterol should be a weaker inducer of the l_o phase than cholesterol. This observation is explained by the protrusion of the 14′ methyl group

from the steroid surface that renders the molecule less "smooth". Cholesterol sulfate (CS), which has the same "smooth" structure as cholesterol, but carries a sulfate instead of the 3′-hydroxy group, is present in a wide range of human tissues. CS concentrations are particularly high in the stratum corneum of the skin, where the cholesterol/CS ratio can reach 5:1 (and even 1:1 in the case of recessive X-linked ichthyosis), and in sperm, where CS may constitute 20% or more of the area of the head of the sperm [82]. Calorimetry [83] and molecular dynamics calculations [84] indicate that CS, like cholesterol, has a condensing effect on saturated PC, albeit possibly a weaker one than cholesterol.

GUVs are excellent tools to directly visualize phase separation for modified sterols. Incorporation of different sterols together with DOPC and SM (1:1:1) shows that slight modifications of the sterol structure can make the difference between no observable phase separation, on the one hand, and clear liquid–liquid immiscibility, on the other hand. Cholesteryl *sulfonate* (a synthetic sterol), for example, has been observed to produce phase separation, but the above-mentioned *sulfate* (CS) appeared homogeneous under comparable conditions [84a]. Moreover, for the sterols that produce phase separation, diffusional mobility of a fluorescent marker (cholesteryl-Bodipy) measured by FCS in the l_o phase depends strongly on the modification of the sterol, whereas marker mobilities are similar in the l_d phases of these GUVs. Finally, combination or replacement of cholesterol with the natural sterols lanosterol and CS were observed to modulate membrane curvature, budding processes (Fig. 14.4I), and the formation of tubular and even reticulate structures (Fig. 14.4J). Thus, the sterol structure significantly affects processes that may have important implications for intracellular trafficking.

14.4.5
Lipid Dynamics in Domain-exhibiting GUVs

The lipid diffusion coefficient is a crucial parameter to characterize membrane properties, and to understand the global picture of spatial and temporal organization of membrane components, for several reasons:

- Putative microdomains in cells are most likely not static structures, but rather they are dynamic in size and composition.
- Translational diffusion has, in general, a large impact on protein oligomerization and enzyme-mediated chemical reactions occurring at and around cellular membranes.
- Lipid diffusion coefficients give insight into the membrane structure, e.g. they give indications for phase composition.

A variety of data on lipid binary systems combining cholesterol with saturated or unsaturated PCs [68, 85–87] show the co-existence of l_o phases, cholesterol-depleted l_d phases and/or gel phases, depending on the temperature, pressure and sterol content. Furthermore, cholesterol exhibits different lipid/sterol interaction energies, depending on the saturation/unsaturation length of the phos-

pholipid aliphatic chain. The effects of cholesterol on the lipid mobility were systematically investigated by FCS in GUVs of various compositions. Two main effects were observed.

14.4.5.1 "Fluidizing" Effect of Cholesterol for High-T_m Lipids

Our observations of a sterol-induced increase in the lipid lateral diffusion rates are based on SM/DPPC and DSPC/cholesterol bilayers (see Fig. 14.5, top left). The data is consistent with previous DSC findings [87], which showed that cholesterol progressively decreased the T_m of PC bilayers with saturated acyl chains of 18 or more carbon atoms and the hydrophobic length of cholesterol was esti-

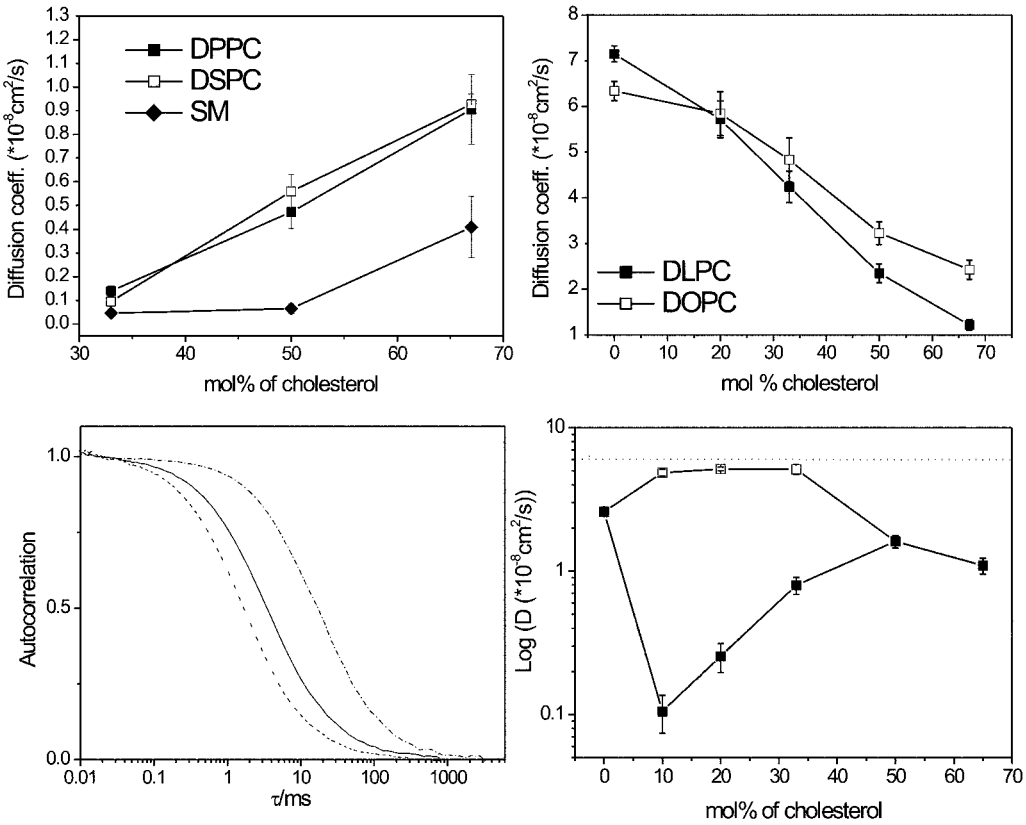

Fig. 14.5 Lipid dynamics explored by FCS. Average values of lipid diffusion coefficient, as determined from fitting the FCS data, plotted against molar percentage of cholesterol for lipid binary mixtures of (top left) DPPC/cholesterol, DSPC/cholesterol and SM/cholesterol, and (top right) DLPC/cholesterol and DOPC/cholesterol. Bottom left: FCS curves recorded from GUVs composed of DOPC/SM 1:1 (solid line) and DOPC/SM/cholesterol 1:1:1 (dashed, l_d phase; dash-dotted, l_o phase). Bottom right: Average values of lipid diffusion coefficient as determined from the FCS data, plotted against molar percentage of cholesterol for ternary mixtures with DOPC/SM 1:1 (adapted from [47]). The lipid probe was DiI-C_{18} (0.001 mol%).

mated to be equivalent to that of a saturated acyl chain with 17 carbon atoms. No difference in the sterol effect on lipid dynamics can be appreciated between DPPC and DSPC, but a significant difference exists between sphingolipids and glycerophospholipids of similar chain length. An explanation for the slower changes of diffusion coefficient upon increase of sterol levels in SM bilayers can be found in the stronger network of hydrogen bonds between SM molecules, which keeps the molecules more tightly bound to each other and overall less mobile. This result is in agreement with a considerable amount of data that indicates that cholesterol favors SM over other PCs in bilayers and monolayers [42, 88, 89]. It has been shown that water permeability is lower in SM/cholesterol membranes than in PC/cholesterol bilayers, indicative of a more dense lateral packing density and a stronger interaction in the former system [90]. Furthermore, the rate of cholesterol desorption from SM bilayers is known to be much slower than desorption from membranes containing phospholipids with acyl chains of comparable length [88, 89].

14.4.5.2 "Condensing" Effect of Cholesterol for Low-T_m Lipids

Lipid lateral mobility was found to continuously decrease upon an increase of cholesterol concentrations for unsaturated and saturated short-chain glycerophospholipids (Fig. 14.5, top right), consistent with the idea that there might be no phase transition in these binary mixtures. DOPC bilayers yielded a trend of diffusion coefficient with a smaller slope compared to that for DLPC, thereby suggesting a higher affinity of cholesterol for saturated than for unsaturated lipids [54].

It is established in the literature that lipids in the gel phase virtually do not undergo translational diffusion, whereas the l_d and l_o phases are characterized by a high lipid mobility. The difference hypothesized for the l_d and l_o phases mostly concerns the degree of freedom lipids have in surfing the conformational landscape. When cholesterol and phospholipids form the l_o phase, the flat sterol makes the phospholipid chains more rigid, thereby imposing a conformational order upon the aliphatic chains. The idea is that, despite the imposed molecular ordering, the degree of translational freedom of lipids would be conserved and the molecular mobility in the l_o and l_d phases would be similar (by a factor of around 2 [24]). However, by employing FCS to probe the lipid translational diffusion in distinct co-existing phases of the SM/DOPC/cholesterol mixtures (Fig. 14.5, bottom), we demonstrated that the lipid mobility in the l_o and l_d phases can differ by a factor up to 40. In addition, cholesterol controls the lipid diffusion coefficient in the l_o phase and can tune it within one order of magnitude.

Within the two-phase region, the lipid diffusion coefficient measured in one phase is very close to that of pure DOPC and rather independent of the cholesterol level. On the other hand, lipid mobility in the other phase is very low and strongly cholesterol dependent. From this data, it is possible to assign distinct phases, independent of the optical imaging.

Lipid dynamics in the two-phase region did not change significantly by replacing SM with DSPC and DPPC. However, significant changes were appreciated when replacing DOPC by DLPC or DMPC, due to the ability of cholesterol to engage in significant interactions with both SM and DLPC/DMPC. This implies a more homogeneous distribution of cholesterol between distinct phases in the case of lipid segregation and a rather high level of mixing of the phospholipids [75 a].

14.5 Spatial Organization and Dynamics of Membrane Proteins in GUVs

Proteins represent an essential part of biological membranes and are indispensable for cellular functioning. The protein/lipid ratio varies with the type of membrane, ranging from 1:4 to 4:1 by dry mass [91], where 1:1 by mass corresponds to roughly 1:50 by molar ratio. If domains are formed solely based on lipid phase separation, then some characteristic partitioning of proteins between the given phases should be observable. In addition, proteins as solutes in a lipid solvent are also expected to influence the thermodynamics and the kinetics of the lipid phase separation. GUVs represent a new tool for studying the partitioning of proteins between phases. In this controlled system, lipids and proteins of choice can be combined, and potential changes in partitioning observed. Furthermore, in addition to the imaging of macroscopic phase effects, GUVs are amenable to investigating nanoscopic effects like protein oligomerization or lipid clustering around proteins by using FCS and other spectroscopic techniques.

However, reconstitution of proteins into GUVs is not trivial. Detergent removal methods allow for reconstitution of transmembrane and membrane-anchored proteins only into relatively small liposomes. These have sizes of tens to hundreds of nanometers and are therefore too small for visualization of phase separation. Unfortunately, the conventional methods to produce GUVs entail dissolving the lipids in organic solvent. These procedures are thereby generally unsuitable for protein incorporation. Yet, a method to insert transmembrane proteins into GUVs should fulfill a number of requirements: (1) stability/reproducibility of the incorporation, (2) restoring a regular and unilamellar vesicle structure, (3) correct insertion of the protein, which should maintain the proper folding and activity, and (4) possibility of controlling the insertion process and the amount of reconstituted protein. To this end, two work-arounds can be performed:

The first method relies on a biochemical protocol based on peptide-induced membrane fusion [26]. Proteoliposomes of submicrometer size carry a *de novo* synthesized peptide with excellent fusogenic properties [92]. Small amounts (between 1 and 5 mol%) of peptide covalently bound to the lipids suffice to bring about full fusion of closely apposing bilayers, which was assayed by lipid and aqueous contents mixing. Such engineered liposomes are able to dock onto

GUVs, which carry a positively charged transfection agent, also present in low amounts (1–5 mol%), which promotes the docking step by electrostatic attraction (the fusogenic peptide on the surface of the proteo-LUVs is negatively charged). GUV–LUV fusion has been characterized in detail, showing that full fusion occurs at an efficiency of 4–10 LUVs/μm^2 of GUV surface [26]. First, bacteriorhodopsin (BRh) from *Halobacterium halobium* was proven to be functionally reconstituted into GUVs of homogeneous spatial lipid distribution and its lateral diffusion characterized under different experimental conditions [93]. Furthermore, a modification of this method, which extended the applicability to vesicles composed of large amounts of negatively charged lipids, was applied to the lactose transporter (LacS) from *Streptococcus thermophilus* [94].

The second one involves a gentle dehydration–rehydration procedure applied to the small proteoliposomes, which replaces the deposition of the lipids by evaporation of organic solvent. Although not all membrane proteins might withstand this method, it is successful with a number of proteins, including the SNARE (soluble *N*-ethylmaleimide-sensitive factor attachment protein receptor) proteins syntaxin and synaptobrevin [27], BRh [94a], the GPI-anchored protein PLAP [94b], the mechanosensitive channel from *Escherichia coli* and the LacS from *Streptococcus thermophilus* (N. Kahya and B. Poolman, unpublished results and [94c]). In the drying process, cryoprotectants (ethylene glycol, sugars) can be added to avert damage from the protein. In the case of the SNARE proteins, conservation of functionality after the reconstitution procedure was demonstrated by binding to the complementary SNARE motifs. For BRh, functionality was confirmed by measuring under the light microscope a transmembrane pH gradient generated by its light-induced proton-pumping activity. Interestingly, this also confirmed that BRh retained a preferential (inside-out) orientation during the dehydration–rehydration cycles. The putative raft-associated human placental alkaline phosphatase, PLAP, likewise retained its activity after reconstitution into GUVs. These four proteins have been reconstituted into the phase-separating lipid mixture of DOPC:SM:cholesterol=1:1:1. The experiments have yielded the striking result that all of these proteins exhibit a preference for the l_d rather than the l_o phase (see Fig. 14.6). Since the GPI-anchored protein PLAP is a prime example of a DRM-associated ("raft") protein, and since syntaxin clustering and SNARE-mediated exocytosis have been considered cholesterol-dependent processes [95], this result was not expected. Concerning PLAP, only 20–30% of the protein is targeted to the l_o phase, whereas it is mostly retained in the membrane fragments (SM and cholesterol-enriched) when detergent extraction is carried out at 4 °C [94b]. It is reasonable to believe that functional rafts are formed on the basis of a delicate balance of lipid–lipid and lipid–protein interactions, which might be very sensitive to subtle changes in parameters such as temperature, pressure and (detergent-induced) changes in the molecular packing. A similar redistribution behavior has been found for the bovine intestine alkaline phosphatase, a GPI-anchored protein homologous to PLAP, as reconstituted in GUVs prepared from analogous lipid mixtures (N. Kahya and S. Morandat, unpublished results).

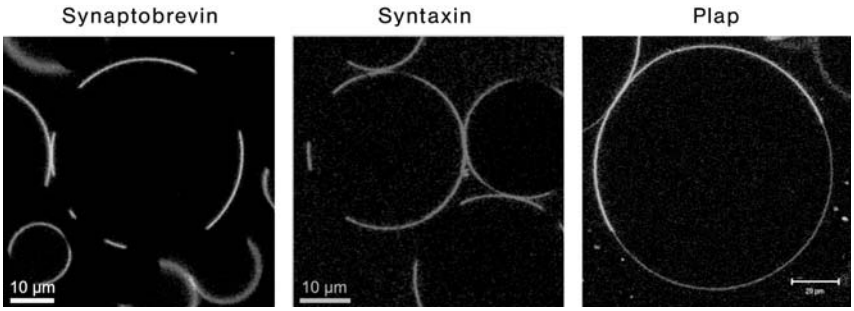

Fig. 14.6 Reconstitution of membrane proteins into domain-exhibiting GUVs.
Left: Reconstitution of synaptobrevin 2 into GUVs with the same lipid composition as in Fig. 14.4 F, but no fluorescent labels other than Alexa Fluor 488 covalently attached to the synaptobrevin. The protein is strongly enriched in one type of domain, which can be assigned to the l_d phase by using either FCS or counterstaining with red fluorescent cholera toxin (not shown).
Middle: Reconstitution of Alexa Fluor 488-labeled syntaxin 1A into the same type of GUVs. Using FCS or counterstaining, it can be determined that the preferred phase is the l_d phase [27].
Right: Reconstitution of rhodamine-labeled placental alkaline phosphatase into GUVs composed of DOPC/SM/cholesterol 1 : 1 : 1 (protein concentration of 0.05 mol%). Using FCS and/or counterstaining with green fluorescent cholera toxin (not shown), it was determined that PLAP favors the l_d phase [94 b].

Recently, PLAP has also been inserted into supported planar bilayers and its spatial organization observed by AFM [96]. Here, the protein was exclusively localized into the l_o phase from synthetic lipid mixtures of SM and DOPC, both in the presence and in the absence of cholesterol. The difference in targeting efficiency to rafts between the AFM and the GUV study might be related to the use of a bilayer support (with a mica surface interfaced to the lipid bilayer) and/or to its protocol of preparation. How can we reconcile these results with earlier findings obtained from DRMs? It is now accepted that co-purification with DRM fragments alone does not provide the constitute proof of an association with pre-existing domains in cells and/or model membranes. Possible artifacts intrinsic to this technique arise from the potential coalescence of detergent-insoluble components and/or removal of components caused by the action of the detergent at low temperatures. Recent studies by Heerklotz et al. [13, 14] have described the potential changes occurring in the thermodynamics of the membrane system as a function of addition of detergents and change of temperature. Consistent with those findings, our data show that there is a significant difference in terms of composition and raft-association of proteins and lipids between a free-standing bilayer and the DRMs, in particular those obtained at low temperatures.

Although the issue of identifying the nature of rafts is still strongly debated, it is widely accepted that, in specific cellular contexts of sorting and signaling, larger and more stable platforms are formed. Lateral crosslinking has been shown to induce patching of membrane proteins and lipids, leading to forma-

tion of stabilized domains. Clustering of membrane components that exhibit affinity for a certain phase region might induce cooperative effects, which strengthen the association with that phase. It has been shown in supported monolayers that chemical crosslinking of lipids shifts their partition coefficient in favor of the l_o phase with respect to the l_d phase [15]. In GUVs, we have recently observed that the binding of naturally pentavalent cholera toxin to GM1 initially commences in the l_d phase, with the fluorescence signal subsequently migrating to the l_o phase and giving rise to the typical pattern of a cholera toxin-labeled l_o phase [84a]. Use of a synthetic GM1 ganglioside with a modified tail prevented its redistribution to the l_o phase upon cholera toxin addition.

14.6
From Model to Cellular Membranes

How do the findings on the model membranes relate to native cellular membranes? Model membranes are certainly a far way from the complexity of native cellular membranes, but their use has three important aspects.

14.6.1
Model Membranes Constitute Test Systems for Developing New and Improving Existing Detection Techniques

New methods have to be tested on simple systems. The FPR/FRAP concept was, for example, tested on a thin layer of aqueous dye solution [97]. FRAP was then found to be readily applicable to cell membranes [98, 99], but interpreting the fluorescence recoveries obtained on cells in terms of structural membrane features is still a difficult issue [100, 101]. Similarly, early implementations of FCS used both three-dimensional diffusion in solution and planar lipid bilayers as model systems [102]. However, extending the use from model membranes to native cells proved more difficult with FCS than with FRAP, since the autofluorescent background in cells is a major problem for FCS, which uses low probe concentrations and requires single-molecule sensitivity. Fortunately, large technological advances [103] have meanwhile made FCS applicable to cell membranes [104]. While all of the techniques mentioned in this chapter can be used with model membranes, not all of them have yet proven applicable to cell membranes or, in some instances, the results obtained in native membrane applications have remained elusive. Model membranes hence provide a good "playground" for improving the sensitivity and, in particular, the target specificity of techniques to make them applicable to native membranes.

14.6.2
Direct Comparison Between Results Obtained on Model and Native Membranes

When results obtained on complex, native membranes are hard to interpret, direct comparison with model membranes can help to improve understanding. For example, the hint that a phase phenomenon could be the underlying cause for the sphingolipid- and cholesterol-rich compositions of detergent-resistant membrane fractions from cells came from application of the technique to artificial liposomes [8]. Other examples are FCS measurements that were performed on native cell membranes using long-chain DiI as a marker [104]. Due to its preference for ordered phases, long-chain DiI had been considered a putative raft component [105–107]. The reduction in diffusional mobility that we observed upon cholesterol depletion with methyl-β-cyclodextrin (MβCD) appeared therefore counter-intuitive, until we performed comparative measurements of DiI in l_d/l_o phase-separated GUVs, where DiI was seen to prefer the l_d phase. GUVs were then treated with MβCD and the same qualitative results were obtained as on the cells [108].

14.6.3
Model Membranes Demonstrate What Structures Can be Potentially Formed by Lipids and Proteins, and Suggest Mechanisms for Fulfilling *in vivo* Functions

Model membranes have exemplified that cooperative lipid interactions involving the biologically relevant saturated (sphingo-) lipids and cholesterol are sufficient to produce a kind of lateral inhomogeneity akin to phase separation. While exact domain composition and *in vivo* domain sizes remain at the moment unclear, some factors that can potentially determine domain size, such as temperature, lipid composition and involvement of proteins are starting to be addressed *in vitro*. The controllability of the model membrane system also makes it valuable for singling out environmental parameters in the study of membrane proteins. While studies of potential "raft association" of proteins in cells by different methods have yielded ambiguous results, model membranes can answer the question of intrinsic l_o phase affinity in a simple system where environmental parameters are better controlled and cellular response activities eliminated [27, 94b]. Another example is the cell biological hypothesis that crosslinking leads to directed, dynamic changes in domain composition (sorting). This hypothesis is supported by a few, but intriguing observations on model membranes and merits more comprehensive investigations. Yet another example is the membrane shape transformation that could be relevant for endocytosis and intracellular trafficking processes. This kind of shape transformation has been theoretically predicted [109–111], and experimentally observed both in uniform [112] and phase-separated GUVs [58, 113]. As mentioned above, even in pure lipidic systems, GUVs can display a specific, composition-dependent behavior of domain curvatures and budding from l_o domains (Fig. 14.4I). In contrast, investigations of membrane shape transformations in cells have focused on mem-

brane sculpting by proteins, such as vesicular coat proteins (COP I- and II-type vesicles) and clathrin coats. The reason for this is that in cells, proteins are more accessible to genetic manipulation than lipids, while in GUVs lipid composition is more easily controlled. In the future, model membrane systems will hopefully allow for looking into the interplay of proteins and lipids in membrane shape transformations. Towards this aim, a few transmembrane proteins have so far been reconstituted into GUVs as discussed above, components of the actin cytoskeleton have been introduced to GUVs [28] and membranous tubules have been pulled from GUVs using the motor protein kinesin and microtubules [114]. We are expecting more insight into membrane functions, as these techniques will be further developed and integrated, aiming for a continuously more complex model of the plasma membrane and finally an "artificial model cell".

References

1 S. J. Singer, G. L. Nicolson, *Science* **1972**, *175*, 720–731.
2 M. J. Karnovsky, A. M. Kleinfeld, R. L. Hoover, R. D. Klausner, *J. Cell Biol.* **1982** 94, 1–6.
3 K. Simons, G. van Meer, *Biochemistry* **1988**, *27*, 6197–6202.
4 K. Simons, A. Wandinger-Ness, *Cell* **1990**, *62*, 207–210.
5 G. van Meer, H. Sprong, *Curr. Opin. Cell Biol.* **2004**, *16*, 373–378.
6 R. G. Parton, A. A. Richards, *Traffic* **2003**, *4*, 724–738.
7 K. Simons, D. Toomre, *Nat. Rev. Mol. Cell Biol.* **2000**, *1*, 31–39.
8 D. A. Brown, J. K. Rose, *Cell* **1992**, *68*, 533–544.
9 J. E. Skibbens, M. G. Roth, K. S. Matlin, *J. Cell Biol.* **1989**, *108*, 821–832.
10 R. Schroeder, E. London, D. Brown, *Proc. Natl Acad. Sci. USA* **1994**, *91*, 12130–12134.
11 K. Simons, E. Ikonen, *Nature* **1997**, *387*, 569–572.
12 C. N. Shrimpton, K. Gousset, F. Tablin, J. A. Lopez, *Methods Mol. Biol.* **2004**, *273*, 213–228.
13 H. Heerklotz, *Biophys. J.* **2002**, *83*, 2693–2701.
14 H. Heerklotz, H. Szadkowska, T. Anderson, J. Seelig, *J. Mol. Biol.* **2003**, *329*, 793–799.
15 C. Dietrich, Z. N. Volovyk, M. Levi, N. L. Thompson, K. Jacobson, *Proc. Natl Acad. Sci. USA* **2001**, *98*, 10642–10647.
16 S. Munro, *Cell* **2003**, *115*, 377–388.
17 M. Edidin, *Annu. Rev. Biophys. Biomol. Struct.* **2003**, *32*, 257–283.
18 K. Simons, W. L. Vaz, *Annu. Rev. Biophys. Biomol. Struct.* **2004**, *33*, 269–295.
19 L. J. Pike, *Biochem. J.* **2004**, *378*, 281–292.
20 T. P. W. McMullen, R. N. A. H. Lewis, R. N. McElhaney, *Curr. Opin. Colloid Interface Sci.* **2004**, *8*, 459–468.
21 J. P. Reeves, R. M. Dowben, *J. Cell. Physiol.* **1968**, *73*, 49–60.
22 M. I. Angelova, D. S. Dimitrov, *Faraday Discuss. Chem. Soc.* **1986**, *81*, 303–311.
23 J. Korlach, P. Schwille, W. W. Webb, G. W. Feigenson, *Proc. Natl Acad. Sci. USA* **1999**, *96*, 8461–8466.
24 C. Dietrich, L. A. Bagatolli, Z. N. Volovyk, N. L. Thompson, M. Levi, K. Jacobson, E. Gratton, *Biophys. J.* **2001**, *80*, 1417–1428.
25 J. B. de la Serna, J. Perez-Gil, A. C. Simonsen, L. A. Bagatolli, *J. Biol. Chem.* **2004**, *279*, 40715–40722.
26 N. Kahya, E. I. Pécheur, W. P. de Boeij, D. A. Wiersma, D. Hoekstra, *Biophys. J.* **2001**, *81*, 1464–1474.
27 K. Bacia, C. G. Schuette, N. Kahya, R. Jahn, P. Schwille, *J. Biol. Chem.* **2004**, *279*, 37951–37955.

28 L. Limozin, M. Barmann, E. Sackmann, *Eur. Phys. J. E* **2003**, *10*, 319–330.

29 D. D. Lasic, *Trends Biotechnol.* **1998**, *16*, 307–321.

30 E. Sackmann, *Science* **1996**, *271*, 43–48.

31 J. L. Rigaud, D. Levy, G. Mosser, O. Lambert, *Eur. Biophys. J.* **1998**, *27*, 305–319.

32 M. M. Lipp, K. Y. C. Lee, J. A. Zasadzinski, A. J. Waring, *Science* **1996**, *273*, 1196–1199.

33 P. Mueller, D. O. Rudin, H. T. Tien, W. C. Wescott, *Nature* **1962**, *194*, 979–981.

34 U. Meseth, *PhD Thesis*, Ecole Politechnique Federale de Lausanne, **1998**.

35 M. L. Wagner, L. K. Tamm, *Biophys. J.* **2000**, *79*, 1400–1414.

36 E. K. Sinner, W. Knoll, *Curr. Opin. Chem. Biol.* **2001**, *5*, 705–711.

37 Y. Fang, A. G. Frutos, J. Lahiri, *J. Am. Chem. Soc.* **2002**, *124*, 2394–2395.

38 J. T. Groves, N. Ulman, S. G. Boxer, *Science* **1997**, *275*, 651–653.

39 J. S. Hovis, S. G. Boxer, *Langmuir* **2000**, *16*, 894–897.

40 F. M. Menger, J. S. Keiper, *Adv. Mater.* **1998**, *10*, 888–890.

41 D. S. Dimitrov, M. I. Angelova, *Bioelectrochem. Bioenerg.* **1988**, *19*, 323–333.

42 J. R. Silvius, *Biochim. Biophys. Acta* **2003**, *1610*, 174–183.

43 S. Mayor, M. Rao, *Traffic* **2004**, *5*, 231–240.

44 C. W. M. Grant, S. H.-W. Wu, H. M. McConnell, *Biochim. Biophys. Acta* **1974**, *363*, 151–158.

45 C. Yuan, J. Furlong, P. Burgos, L. J. Johnston, *Biophys. J.* **2002**, *82*, 2526–2535.

46 J. Hwang, L. K. Tamm, C. Böhm, T. S. Ramalingam, E. Betzig, M. Edidin, *Science* **1995**, *270*, 610–614.

47 N. Kahya, D. Scherfeld, K. Bacia, B. Poolman, P. Schwille, *J. Biol. Chem.* **2003**, *278*, 28109–28115.

48 P. F. Almeida, W. L. Vaz, T. E. Thompson, *Biochemistry* **1992**, *31*, 7198–7210.

49 G. J. Schuetz, H. Schindler, T. Schmidt, *Biophys. J.* **1997**, *73*, 1073–1080.

50 M. Eigen, R. Rigler, *Proc. Natl Acad. Sci. USA* **1994**, *91*, 5740–5747.

51 P. Schwille, J. Korlach, W. W. Webb, *Cytometry* **1999**, *36*, 176–182.

52 D. E. Koppel, *Phys. Rev. A* **1974**, *10*, 1938–1945.

53 P. Schwille, *Cell. Biochem. Biophys.* **2001**, *34*, 383–408.

54 N. Kahya, D. Scherfeld, K. Bacia, P. Schwille, *J. Struct. Biol.* **2004**, *147*, 77–89.

55 A. Kusumi, I. Koyama-Honda, K. Suzuki, *Traffic* **2004**, *5*, 213–230.

56 A. Pralle, P. Keller, E. L. Florin, K. Simons, J. K. Horber, *J. Cell Biol.* **2000**, *148*, 997–1008.

57 T. Harder, P. Scheiffele, P. Verkade, K. Simons, *J. Cell Biol.* **1998**, *141*, 929–942.

58 S. L. Veatch, S. L. Keller, *Biophys. J.* **2003**, *85*, 3074–3083.

59 L. K. Nielsen, A. Vishnyakov, K. Jorgensen, T. Bjornholm, O. G. Mouritsen, *J. Phys. Cond. Matt.* **2000**, *12*, A309–A314.

60 L. K. Nielsen, T. Bjornholm, O. G. Mouritsen, *Nature* **2000**, *404*, 352.

61 I. A. Prior, C. Muncke, R. G. Parton, J. F. Hancock, *J. Cell Biol.* **2003**, *160*, 165–170.

62 M. Murata, J. Peranen, R. Schreiner, F. Wieland, T. V. Kurzchalia, K. Simons, *Proc. Natl Acad. Sci. USA* **1995**, *92*, 10339–10343.

63 H. M. McConnell, M. Vrljic, *Annu. Rev. Biophys. Biomol. Struct.* **2003**, *32*, 469–492.

64 J. F. Nagle, S. Tristram-Nagle, *Biochim. Biophys. Acta* **2000**, *1469*, 159–195.

65 J. M. Seddon, R. H. Templer. *Handbook of Biological Physics*. Elsevier, Amsterdam, **1995**.

66 D. J. Recktenwald, H. M. McConnell, *Biochemistry* **1981**, *20*, 4505–4510.

67 J. H. Ipsen, G. Karlstrom, O. G. Mouritsen, H. Wennerstrom, M. J. Zuckermann, *Biochim. Biophys. Acta* **1987**, *905*, 162–172.

68 M. R. Vist, J. H. Davis, *Biochemistry* **1990**, *29*, 451–464.

69 H. W. Meyer, K. Semmler, P. J. Quinn, *Mol. Membr. Biol.* **1997**, *14*, 187–193.

70 M. Nielsen, L. Miao, J. H. Ipsen, M. J. Zuckermann, O. G. Mouritsen, *Phys. Rev. E Stat. Phys. Plasmas Fluids Relat. Interdiscip. Topics* **1999**, *59*, 5790–5803.

71 S. L. Veatch, S. L. Keller, *Phys. Rev. Lett.* **2002**, *89*, 268101.

72 H.M. McConnell, A. Radhakrishnan, *Biochim. Biophys. Acta* **2003**, *1610*, 159–173.

73 D. Scherfeld, N. Kahya, P. Schwille, *Biophys. J.* **2003**, *85*, 3758–3768.

74 B. Ramstedt, J.P. Slotte, *Biophys. J.* **1999**, 76:908–915.

75 B. Ramstedt, J.P. Slotte, *FEBS Lett.* **2002**, *531*, 33–37.

75a N. Kahya, D. Scherfeld, P. Schwille, *Chem. Phys. Lip.* **2005**, in press.

76 Yeagle, P.L. *The Structure of Biological Membranes*. CRC Press, Boca Raton, FL, **1991**.

77 S. Mongrand, J. Morel, J. Laroche, S. Claverol, J.P. Carde, M.A. Hartmann, M. Bonneu, F. Simon-Plas, R. Lessire, J.J. Bessoule, *J. Biol. Chem.* **2004**, *279*, 36277–36286.

78 M. Bagnat, S. Keranen, A. Shevchenko, A. Shevchenko, K. Simons, *Proc. Natl Acad. Sci. USA* **2000**, *97*, 3254–3259.

79 L. Miao, M. Nielsen, J. Thewalt, J.H. Ipsen, M. Bloom, M.J. Zuckermann, O.G. Mouritsen, *Biophys. J.* **2002**, *82*, 1429–1444.

80 X. Xu, E. London, *Biochemistry* **2000**, *39*, 843–849.

81 X. Xu, R. Bittman, G. Duportail, D. Heissler, C. Vilcheze, E. London, *J. Biol. Chem.* **2001**, *276*, 33540–33546.

82 C.A. Strott, Y. Higashi, *J. Lipid. Res.* **2003**, *44*, 1268–1278.

83 N. Kitson, M. Monck, K. Wong, J. Thewalt, P. Cullis, *Biochim. Biophys. Acta* **1992**, *1111*, 127–133.

84 A.M. Smondyrev, M.L. Berkowitz, *Biophys. J.* **2000**, *78*, 1672–1680.

84a K. Bacia, P. Schwille, T. Kurzchalia, *Proc. Natl. Acad. Sci. USA* **2005**, *102*, 3272–3277.

85 J.P. Hagen, H.M. McConnell, *Biochim. Biophys. Acta* **1997**, *1329*, 7–11.

86 P.F.F. Almeida, W.L.C. Vaz, T.E. Thompson, *Biophys. J.* **1993**, *64*, 399–412.

87 T.P.W. McMullen, R.N. McElhaney, *Biochim. Biophys. Acta* **1995**, *1234*, 90–98.

88 P. Mattjus, J.P. Slotte, *Chem. Phys. Lipids* **1996**, *81*, 69–80.

89 J.P. Slotte, *Chem. Phys. Lipids* **1999**, *102*, 13–27.

90 D. Needham, R.S. Nunn, *Biophys. J. 1990, 58*, 997–1009.

91 R.B. Gennis. *Biomembranes, Molecular Structure and Function*. Springer, Berlin, **1989**.

92 E.-I. Pécheur, D. Hoekstra, J. Sainte-Marie, L. Maurin, A. Bienvenue, J.R. Philippot, *Biochemistry* **1997**, *36*, 3773–3781.

93 N. Kahya, D.A. Wiersma, B. Poolman, D. Hoekstra. *J. Biol. Chem.* **2002**, *277*, 39304.

94 N. Kahya, *PhD Thesis*, University of Groningen, **2003**.

94a P. Girard, J. Pecreaux, G. Lenoir, P. Falson, J.L. Rigaud, P. Bassereau, *Biophys. J.* **2004**, *87*, 419–429.

94b N. Kahya, D.A. Brown, P. Schwille, *Biochemistry* **2005**, in press.

94c M.K. Doeven, J.H. Folgering, V. Krasnikov, E.R. Geertsma, G. van den Bogaart, B. Poolman, *Biophys. J.* **2005**, *88*, 1134–1142.

95 T. Lang, D. Bruns, D. Wenzel, D. Riedel, P. Holroyd, C. Thiele, R. Jahn, *EMBO J.* **2001**, *20*, 2202–2213.

96 D.E. Saslowsky, J. Lawrence, X. Ren, D.A. Brown, R.M. Henderson, J.M. Edwardson, *J. Biol. Chem.* **2002**, *277*, 26966–26970.

97 D.E. Koppel, D. Axelrod, J. Schlessinger, E.L. Elson, W.W. Webb, *Biophys. J.* **1976**, *16*, 1315–1329.

98 J. Schlessinger, D. Axelrod, D.E. Koppel, W.W. Webb, E.L. Elson, *Science* **1977**, *195*, 307–309.

99 J. Schlessinger, E.L. Elson, W.W. Webb, I. Yahara, U. Rutishauser, G.M. Edelman, *Proc. Natl Acad. Sci. USA* **1977**, *74*, 1110–1114.

100 J.C. Owicki, H.M. McConnell, *Biophys. J.* **1980**, *30*, 383–397.

101 A.K. Kenworthy, B.J. Nichols, C.L. Remmert, G.M. Hendrix, M. Kumar, J. Zimmerberg, J. Lippincott-Schwartz, *J. Cell Biol.* **2004**, *165*, 735–746.

102 P.F. Fahey, D.E. Koppel, L.S. Barak, D.E. Wolf, E.L. Elson, W.W. Webb, *Science* **1977**, *195*, 305–306.

103 E.L. Elson, *J. Biomed. Opt.* **2004**, *9*, 857–864.

104 P. Schwille, J. Korlach, W.W. Webb, *Cytometry* **1999**, *36*, 176–182.

105 R. D. Klausner, D. E. Wolf, *Biochemistry* **1980**, *19*, 6199–6203.

106 J. L. Thomas, D. Holowka, B. Baird, W. W. Webb, *J. Cell Biol.* **1994**, *125*, 795–802.

107 M. Hao, S. Mukherjee, F. R. Maxfield, *Proc. Natl Acad. Sci. USA* **2001**, *98*, 13072–13077.

108 K. Bacia, D. Scherfeld, N. Kahya, P. Schwille, *Biophys. J.* **2004**, *87*, 1034–1043.

109 R. Lipowsky, *Nature* **1991**, *349*, 475–481.

110 F. Julicher, R. Lipowsky, *Phys. Rev. Lett.* **1993**, *70*, 2964–2967.

111 F. Julicher, R. Lipowsky, *Phys. Rev. E* **1996**, *53*, 2670–2683.

112 J. Kas, E. Sackmann, *Biophys. J.* **1991**, *60*, 825–844.

113 T. Baumgart, S. T. Hess, W. W. Webb, *Nature* **2003**, *425*, 821–824.

114 A. Roux, G. Cappello, J. Cartaud, J. Prost, B. Goud, P. Bassereau, *Proc. Natl Acad. Sci. USA* **2002**, *99*, 5394–5399.

115 E. J. Shimshick, H. M. McConnell, *Biochemistry* **1973**, *12*, 2351–2360.

116 D. Marsh. *CRC Handbook of Lipid Bilayers*. CRC Press, Boca Raton, FL, **1990**.

Part 6
Targeting of Extrinsic Membrane Protein Modules to Membranes and Signal Transduction

15
In vitro and Cellular Membrane-binding Mechanisms of Membrane-targeting Domains

Wonhwa Cho and Robert V. Stahelin

15.1
Introduction

It has been shown that a large number of cytoplasmic proteins involved in cell signaling and membrane trafficking reversibly translocate to different cellular membranes in response to specific stimuli (Teruel and Meyer 2000). Many of these peripheral proteins (as opposed to integral membrane proteins) contain one or more modular domains specialized in lipid binding. These lipid-binding structural modules, also known as membrane-targeting domains, include protein kinase C (PKC) *C*onserved *1* (C1) (Brose and Rosenmund 2002; Cho 2001; Yang and Kazanietz 2003), PKC *C*onserved *2* (C2) (Cho 2001; Nalefski and Falke 1996; Rizo and Sudhof 1998), *P*leckstrin *H*omology (PH) (Ferguson et al. 2000; Lemmon and Ferguson 2000, 2001), *F*ab1, *Y*OTB, *V*ac1, and *E*arly endosomal antigen 1 (FYVE) (Stenmark et al. 2002), *P*ho*x* (PX) (Wishart et al. 2001; Xu et al. 2001 b), *E*psin *N*-*T*erminal *H*omology (ENTH) (De Camilli et al. 2002; Itoh and Takenawa 2002), AP180 *N*-*T*erminal *H*omology (ANTH) (De Camilli et al. 2002; Itoh and Takenawa 2002), *B*in *A*mphiphysin *R*vs (BAR) (Habermann 2004), Band *4*.1, *E*zrin, *R*adixin, *M*oesin (FERM) (Bretscher et al. 2002) and tubby domains (Carroll et al. 2004). This chapter summarizes the recent progress in our understanding of the mechanisms by which reversible binding of membrane-targeting domains and their host proteins to different cell membranes is mediated and regulated, with an emphasis on how kinetics and energetics of their membrane–protein interactions are modulated by different factors.

15.2
Membrane Interactions of Membrane-targeting Domains

15.2.1
Interfacial Location of Membrane-targeting Domains

Liquid-crystallographic determination of the structure of a 1,2-dioleoyl-*sn*-glycero-3-phosphocholine bilayer showed that the lipid bilayer has a highly polarized structure that consists of a central hydrocarbon core region and two flanking interfacial regions (see Fig. 15.1) (Wiener and White 1992). The hydrocarbon region and the combined interfacial regions have comparable width (around 30 Å each) so that the interfaces account for roughly 50% of the total thickness of the bilayer. The interfacial regions consist of a complex mixture of water, lipid backbone phosphate groups, headgroups, and the polar portion of the acyl chains and the polarity profile changes dramatically over the 15-Å span of an interface, from the hydrocarbon region to the aqueous solution. Due to this complex nature of the lipid bilayer, the location of the protein in the bilayer is a critical factor that governs the kinetics and energetics of its membrane interactions. Based on their membrane location, membrane targeting proteins can be arbitrarily subdivided into three groups: (1) S-type proteins that are localized at the membrane surface and in the shallow interfacial region (i.e. outside of the level of the backbone phosphate group; see Fig. 15.1) and interact predominantly with the polar headgroups, (2) I-type proteins that penetrate significantly into

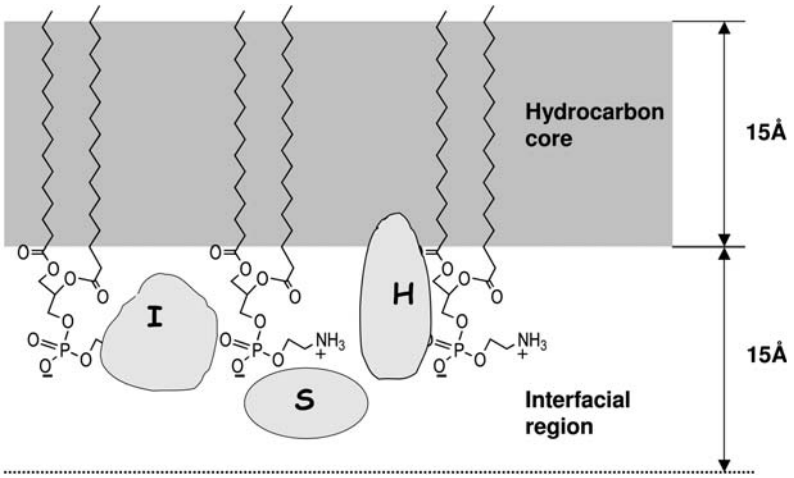

Fig. 15.1 The structure of a phospholipid bilayer and the membrane location of three classes of peripheral proteins. The bilayer is composed of the hydrocarbon core region and the interfacial region with approximately equal thickness. I- and H-type proteins penetrate below the lipid phosphate group, whereas S-type proteins show little interfacial penetration. See the text for further description. Only a monolayer of a PC bilayer is shown here.

the interfacial region (i.e. inside the level of the phosphate), and (3) H-type proteins that penetrate into the hydrocarbon core region of the lipid bilayer. Both I- and H-type peripheral proteins interact with both the polar headgroups and the hydrocarbon of the bilayer.

15.2.2
Energetics and Kinetics of Membrane–Protein Interactions

In protein–protein interactions the initial formation of non-specific collisional complexes, driven by diffusion and electrostatic forces, is followed by the formation of tightly bound complexes, which are stabilized by specific interactions (Cunningham and Wells 1993; Northrup and Erickson 1992). For the ligand binding of human growth hormone receptor, attractive electrostatic forces were shown to enhance the second-order rate constant for association (k_a), whereas specific interactions that stabilize tightly bound complexes primarily lowered the dissociation rate constant (k_d) (Cunningham and Wells 1993).

All intracellular membranes contain a varying degree of anionic lipids and a majority of peripheral proteins (and membrane-targeting domains) contain cationic surfaces, at least locally. Recent biophysical studies of membrane–protein interactions using a large number of membrane-targeting domains, their host proteins and respective mutants have revealed that binding of these proteins to anionic membranes also follows a two-step mechanism, in which the initial formation of non-specific collisional complexes, driven by diffusion and electrostatic forces, is followed by the formation of tightly bound complexes, which are stabilized by specific interactions and/or membrane penetration (see Fig. 15.2) (Cho 2001; Cho and Stahelin 2005; Stahelin and Cho 2001; Stahelin et al. 2002, 2003a, b). Both theoretical and experimental work has shown that although non-specific electrostatic interactions may not be sufficient to anchor peripheral proteins at membrane surfaces, they are necessary for the membrane recruitment of these proteins (Murray et al. 2002). The initial membrane adsorption of peripheral proteins facilitates specific interactions with lipids (and/or membrane proteins) by effectively reducing the dimensionality of the space through which the protein interacts with its lipid ligand (Kholodenko et al. 2000; McCloskey and Poo 1986). That is, the enhanced effective concentration of the protein at the membrane increases the probability that the protein is able to interact with both effectors and substrates.

The initial membrane attachment can also facilitate the penetration of hydrophobic and aromatic residues on the surfaces of peripheral proteins (mainly H/I types) into the interfacial and hydrocarbon core regions of the lipid bilayer. Since hydrophobic side-chains of proteins are not normally exposed to the molecular surface, membrane penetration of membrane-targeting domains and peripheral proteins often involves the conformational change of proteins at the membrane interface that exposes the buried hydrophobic side-chains. Biological activities of some peripheral proteins depend heavily on their partial membrane insertion (Ford et al. 2002; Stahelin et al. 2002, 2003a, b). Specific lipid binding

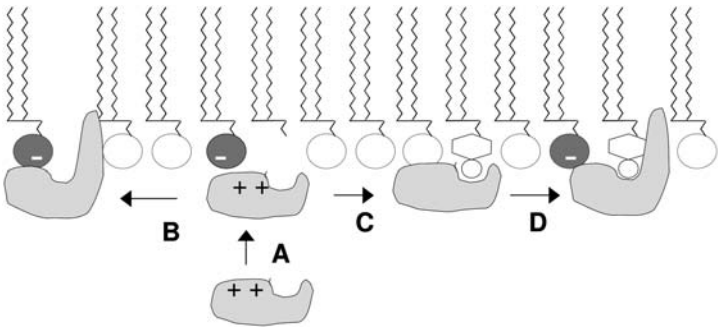

Fig. 15.2 Membrane-binding mechanisms of peripheral proteins. Initial membrane adsorption of peripheral proteins (Step A) is driven by non-specific electrostatic interactions and diffusion. Step A can be either autonomously performed or triggered by a Ca^{2+}-induced electrostatic switch. The membrane-attached protein can either undergo membrane penetration (Step B) or bind a specific lipid (Step C) to achieve a more stable membrane–protein complex. For many phosphoinositide-binding proteins, specific lipid binding also leads to the membrane penetration of the protein (Step D).

and membrane penetration are not mutually exclusive, as it has been shown that specific lipid binding of some phosphoinositide-binding domains, such as FYVE (Stahelin et al. 2002), PX (Stahelin et al. 2003 a) and ENTH domains (Stahelin et al. 2003 b), also induces their membrane penetration. Resulting specific interactions and/or hydrophobic interactions provide the proteins with extra binding energy that is necessary for their membrane recruitment and activity.

In general, protein residues (e.g. cationic membrane-binding residues) and other factors (e.g. Ca^{2+} or phosphorylation) that enhance the non-specific, long-range electrostatic interactions primarily accelerate the association of proteins to anionic membranes (i.e. k_a effect), whereas protein residues and other factors that increase short-range specific interactions and/or membrane penetration mainly slow the membrane dissociation (i.e. k_d effect) (Cho 2001; Stahelin and Cho 2001). Aromatic residues, particularly Trp, play a unique and crucial role in binding to zwitterionic phosphatidylcholine (PC)-rich membranes (Gelb et al. 1999; Han et al. 1999) by affecting both membrane association and dissociation steps (Stahelin and Cho 2001). Recent cell studies using Green Fluorescence Protein (GFP) derivatives and GFP-fusion proteins showed that these proteins can freely diffuse in the cytosol despite molecular crowding (Teruel and Meyer 2000). Therefore, the cellular membrane–protein binding is also expected to follow a similar two-step mechanism, although protein–protein interactions might also contribute to the binding process in the cell.

15.3
C1 Domains

15.3.1
Occurrence and Structure

The C1 domain (about 50 amino acids) was first identified as the interaction site for diacylglycerol (DAG) and phorbol ester in PKCs (Ono et al. 1989; Osada et al. 1990). More than 50 different mammalian proteins in the current protein database have the C1 domain (Brose and Rosenmund 2002; Shirai and Saito 2002; Yang and Kazanietz 2003). A large number of these proteins, including PKCs, contain multiple copies of C1 domains. In general, C1 domains show a high degree of amino acid sequence homology. However, minor sequence variations in the ligand-binding region dramatically affect affinity for DAG and phorbol ester. Structural analyses have shown that these small cysteine-rich domains are composed of five short β-strands, a short α-helix and two zinc ions (see Fig. 15.3) (Canagarajah et al. 2004; Xu et al. 1997; Zhang et al. 1995). Among all known C1 domains, those from conventional and novel PKCs, protein kinase D, chimaerins, Ras-GRPs, Unc13/Munc-13 isoforms and DAG kinases (β and γ isoforms) have been shown to bind DAG and/or phorbol ester (Brose and Rosenmund 2002; Yang and Kazanietz 2003).

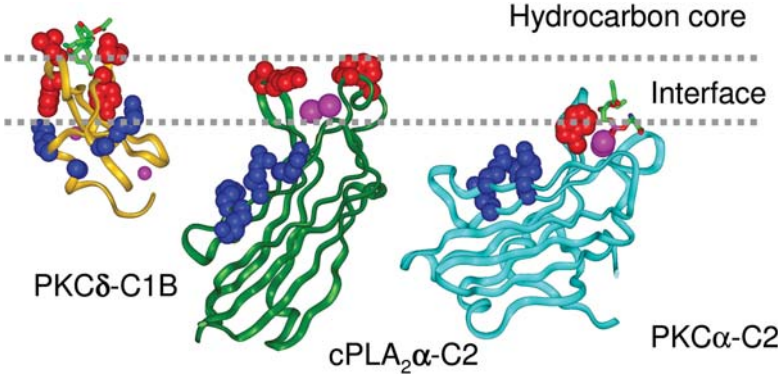

Fig. 15.3 Proposed membrane binding modes for PKCδ C1B, cPLA$_2\alpha$ C2 and PKCα C2 domains. The backbones of the three domains and the specific lipid ligands (phorbol ester for PKCδ-C1B and PS for PKCα-C2) are shown in ribbon diagram and stick model, respectively. Membrane-penetrating aromatic and hydrophobic residues are shown in space-filling representation and colored red. Cationic residues involved in non-specific membrane interactions (for the C1 domain) or specific lipid binding (for the C2 domains) are shown in blue. Zinc (C1) and calcium (C2) ions are shown in magenta. For cPLA$_2\alpha$-C2 (Frazier et al. 2002) and PKCα-C2 (Kohout et al. 2003), the depth of membrane penetration and the membrane-bound orientation have been determined by EPR analysis.

15.3.2
Lipid Specificity

The X-ray crystal structure of the PKCδ C1B domain–phorbol 13-acetate complex revealed how the C1 domain achieves the ligand selectivity. The domain has a polar binding pocket for DAG/phorbol ester located at the tip of the molecule and the main chain peptide groups in the pocket form hydrogen bonds with polar moieties of the phorbol ester (Zhang et al. 1995). It has been generally thought that the C1 domain interacts with DAG and phorbol ester by the same mode. However, recent studies have shown that many C1 domains have disparate affinities for DAG and phorbol esters. For instance, C1A and C1B domains of PKCα and PKCδ have opposite affinities for DAG and phorbol ester, i.e. the C1A domain has high affinity for DAG and the C1B domain has high affinity for phorbol ester (Ananthanarayanan et al. 2003; Stahelin et al. 2004b). Although the structural basis of differential DAG and phorbol ester affinities of these C1 domains is not fully understood at present, these findings call for careful re-examination of DAG and phorbol ester affinities of C1 domains. The C1B domains of PKCδ and PKCε have been also reported to interact with ceramide and arachidonic acid (Kashiwagi et al. 2002; Schultz et al. 2004), but their binding sites have not been located. The PKC C1 domains have been shown to bind alcohols with high stereospecificity (Slater et al. 2003), presumably via a non-DAG-binding site (Das et al. 2004).

15.3.3
Membrane-binding Mechanisms

The C1 domain represents a prototype H-type protein that follows a two-step membrane-binding mechanism in which the initial membrane adsorption by non-specific electrostatic interactions is followed by the membrane penetration. The X-ray crystal structure of the PKCδ C1B domain shows that it has unique structural features that are consistent with this membrane-binding mechanism (Zhang et al. 1995). The lipid-binding pocket is surrounded by hydrophobic and aromatic residues, which are adjoined by a ring of cationic residues in the middle part of the molecule (see Fig. 15.3). Mutational studies of PKCα showed that clustered cationic residues in the C1A domain are involved in non-specific electrostatic interactions with anionic phospholipids, which accelerate the initial membrane adsorption of the C1 domain (k_a effect) and also properly position the C1 domain at the membrane surface (Bittova et al. 2001). A nuclear magnetic resonance (NMR) study of the PKCγ C1B domain (Xu et al. 1997), a monolayer penetration study of PKCα (Medkova and Cho 1999), as well as vesicle-binding studies of the PKCδ C1B domain (Wang et al. 2001), showed that the hydrophobic and aromatic residues surrounding the DAG-binding pocket penetrate the membrane. The surface plasmon resonance (SPR) measurements indicate that DAG binding increases the vesicle affinity (K_a) of the PKC C1 domains by more than two orders of magnitude mainly by reducing the k_d (Anan-

thanarayanan et al. 2003; Stahelin et al. 2004b), as is the characteristic of a protein that interacts with membranes through specific or hydrophobic interactions. A monolayer penetration study of the PKCα C1A domain indicated that membrane penetration of the C1 domain is necessary for DAG binding (Medkova and Cho 1998; Medkova and Cho 1999), since the glycerol moiety of DAG is expected to be located deep within the interfacial region. The depth of membrane penetration by the C1 domain has not been quantitatively measured yet; however, from the NMR spectra of the PKCγ C1B domain interacting with lipid micelles (Xu et al. 1997) it is estimated to be at least 10 Å below the level of the lipid phosphate, hence the classification as H-type (see Fig. 15.3). Since hydrophobic and aromatic residues surrounding the DAG-binding pocket are exposed, isolated C1 domains typically have a high tendency to aggregate in solution. Thus, the C1 domain in the full-length protein is expected to be buried in the inactive form of the enzyme and becomes accessible to DAG or phorbol esters only after an inter-domain conformational change (Bittova et al. 2001; Canagarajah et al. 2004; Medkova and Cho 1999; Stahelin et al. 2004b); in the case of PKCα, C1 domains are exposed upon Ca^{2+}-dependent, C2 domain-mediated membrane binding of the proteins (Bittova et al. 2001; Medkova and Cho 1999; Oancea and Meyer 1998; Stahelin et al. 2004b).

15.3.4
Subcellular Localization

The cellular membrane recruitment of isolated C1 domains and their host proteins, mostly PKCs, in response to DAG and phorbol esters has been measured in various mammalian cells transfected with GFP-tagged proteins. Normally, C1 domains and host proteins will migrate to the membrane that contains DAG or phorbol ester. For instance, C1 domain (Oancea et al. 1998) and PKC isoforms (Kazanietz et al. 1995; Oancea and Meyer 1998; Raghunath et al. 2003; Stahelin et al. 2004b; Szallasi et al. 1994) are recruited to the plasma membrane in response to exogenous phorbol 12-myristate 13-acetate (PMA) or stimuli that induce the endogenous DAG formation because PMA and DAG are localized primarily at the plasma membrane. When less hydrophobic PMA or DAG is fed into the cell or DAG is formed at other intracellular membranes, the spatiotemporal dynamics of C1 domains and host proteins has been shown to follow that of their C1 ligands (Baron and Malhotra 2002; Bivona et al. 2003; Wang et al. 2000). In general, residues essential for the *in vitro* membrane binding of C1 domains, particularly membrane-penetrating hydrophobic and aromatic residues, have also been found to play an important role in the subcellular targeting of PKC isoforms (Ananthanarayanan et al. 2003; Stahelin et al. 2004b), indicating good correlation between *in vitro* and cellular membrane binding properties of C1 domains. Further discussion on the subcellular localization of C1 domain-containing proteins can be found in recent reviews (Brose and Rosenmund 2002; Shirai and Saito 2002; Yang and Kazanietz 2003).

15.4 C2 Domains

15.4.1 Occurrence and Structure

The C2 domain (around 130 residues) was first discovered as the Ca^{2+}-binding site in conventional PKCs (Kikkawa et al. 1989). More than 200 mammalian proteins containing a C2 domain have been identified since, and most of them are involved in signal transduction [e.g. PKC, group IVA cytosolic phospholipase A_2 (cPLA$_2\alpha$), phospholipase C (PLC), plant phospholipase D (PLD) and phosphatidylinositol 3-kinase] or membrane trafficking (e.g. synaptotagmins, rabphilin-3A and Munc-13) (Cho 2001; Nalefski and Falke 1996; Rizo and Sudhof 1998). Structural analyses of multiple C2 domains have indicated that all C2 domains share a common fold with eight-stranded antiparallel β-sandwich connected by variable loops (see Fig. 15.3) (Essen et al. 1997; Perisic et al. 1998; Sutton et al. 1995; Sutton and Sprang 1998). The Ca^{2+}-binding sites are composed of three variable loops that contain ligands for multiple Ca^{2+} ions and most Ca^{2+}-dependent C2 domain bind two to three Ca^{2+} ions. When compared with C1 domains, C2 domains show much lower sequence homology, particularly in the loop regions, which is consistent with their greater functional diversity. Some of the Ca^{2+}-independent C2 domains, such as that of PTEN (Das et al. 2003; Lee et al. 1999), still bind the membrane, whereas others, such as the C2 domains of PLC β1 and β2, are involved in protein–protein interactions (Wang et al. 1999).

15.4.2 Lipid Specificity

C2 domains are unique among membrane-targeting domains in that they do not have a well-defined lipid-binding pocket and thus show relatively weak lipid specificity. Most Ca^{2+}-dependent membrane-binding C2 domains, including the C2 domains of conventional PKCs (Kohout et al. 2002; Stahelin et al. 2003c; Verdaguer et al. 1999), PLCδ1 (Essen et al. 1997) and synaptotagmins (Chae et al. 1998), prefer anionic membranes to zwitterionic ones. In particular, the PKCα (Stahelin et al. 2003c) and PLCδ1 C2 domains (Essen et al. 1997) exhibit phosphatidylserine (PS) selectivity, which is consistent with their localization to the PS-rich plasma membrane. In contrast, the C2 domains of cPLA$_2\alpha$ (Nalefski and Falke 1998; Stahelin et al. 2003c) and 5-lipoxygenase strongly favor PC membranes (Kulkarni et al. 2002).

Several C2 domains, including synaptotagmin-C2B (Mehrotra et al. 2000), JFC1-C2A (Catz et al. 2002), Rsp5-C2 (Dunn et al. 2004) and PKCα-C2 (Corbalan-Garcia et al. 2003), have been reported to bind phosphoinositides, presumably via the cationic cluster in the β-sandwich region in a Ca^{2+}-independent manner (see Fig. 15.3). For synaptotagmin-C2B, it has been proposed that its Ca^{2+}-independent binding to PtdIns(4,5)P_2 prelocalizes the protein to PtdIns(4,5)P_2-rich membranes

(Schiavo et al. 1996). Since the cationic patch is conserved in virtually all C2 domains, this Ca^{2+}-independent phosphoinositide (or other anionic lipids) binding may represent a common membrane-binding mechanism of C2 domains at low Ca^{2+} concentrations, which may in turn prime C2 domains for stronger Ca^{2+}-dependent membrane binding. However, the cationic cluster of the C2 domain is buried in some C2 domain-containing peripheral proteins and may not be accessible for anionic lipid binding (Johnson et al. 1997). Most recently, the C2 domain of cPLA$_2\alpha$ was shown to specifically bind ceramide-1-phosphate via the cationic cluster (Stahelin and Cho, unpublished observation).

15.4.3
Membrane Binding Mechanisms

Ca^{2+} plays critical roles in the membrane targeting of a majority of C2 domains by inducing an electrostatic switch (Murray and Honig 2002; Rizo and Sudhof 1998), inducing conformational changes in the calcium-binding regions (Bittova et al. 1999; Kulkarni et al. 2002; Shao et al. 1998), or directly coordinating a lipid through calcium bridging or chelation (Verdaguer et al. 1999). In general, anionic lipid-selective C2 domains are I-type and PC-preferring C2 domains are H-type. For the I-type C2 domains, Ca^{2+} ions primarily function as an electrostatic switch and/or a bridge. Ca^{2+} binding dramatically enhances the positive electrostatic potential surrounding the Ca^{2+}-binding loops, which accelerates the association to the anionic membrane (Murray and Honig 2002; Rizo and Sudhof 1998). Ca^{2+} can also mediate partial (i.e. around 5 Å below the phosphate) membrane penetration (Kohout et al. 2003) and/or PS coordination (Verdaguer et al. 1999), both of which slow the membrane dissociation of the domain (k_d effect). For PS-selective PKCα and PLCδ1 C2 domains, a single Asn residue [Asn189 for PKCα (Stahelin et al. 2003c) and Asn647 for PLCδ1 (Ananthanarayanan et al. 2002)] in the Ca^{2+}-binding loops also plays a pivotal role in PS headgroup recognition and membrane residence of the domains.

In the case of the H-type cPLA$_2\alpha$-C2 and the 5-lipoxygenase-C2, Ca^{2+}-induced electrostatic neutralization in the Ca^{2+}-binding loops has been proposed to promote the insertion of hydrophobic and aromatic residues into interfacial and hydrophobic regions (i.e. around 10 Å below the phosphate) (Bittova et al. 1999; Frazier et al. 2002; Kulkarni et al. 2002; Murray and Honig 2002). Thus, the main role of Ca^{2+} in this case is to reduce k_d through hydrophobic interactions. Mutational studies of the C2 domains of cPLA$_2\alpha$ and 5-lipoxygenase showed that aromatic and hydrophobic residues located in their Ca^{2+}-binding loops are important for their PC selectivity and membrane penetration (i.e. k_d effect) (Kulkarni et al. 2002; Stahelin et al. 2003c). Electron paramagnetic resonance (EPR) analysis has shown that PKCα-C2 binds to the membrane in an orientation that optimizes its electrostatic interactions with the anionic membranes (Kohout et al. 2003), whereas cPLA$_2\alpha$-C2 binds to the membrane in an orientation that optimizes the membrane penetration of its hydrophobic and aromatic residues (Frazier et al. 2002) (see Fig. 15.3).

15.4.4
Subcellular Localization

The subcellular targeting of GFP-tagged C2 domains and their host proteins has been studied in different mammalian cells. In general, the subcellular localization behaviors of C2 domains are consistent with their *in vitro* membrane binding properties. For instance, PS-selective C2 domains translocate to the PS-rich plasma membrane (Ananthanarayanan et al. 2002; Corbalan-Garcia et al. 1999; Stahelin et al. 2003 c) whereas PC-preferring C2 domains move to the PC-abundant perinuclear region in response to Ca^{2+} (Evans et al. 2004; Kulkarni et al. 2002; Stahelin et al. 2003 c). PtdIns(4,5)P_2-binding C2 domains are found in the PtdIns(4,5)P_2-rich region of the plasma membrane (Evans et al. 2004). The C2A domain of JFC1 is localized to the plasma membrane via 3-phosphoinositides (Catz et al. 2002). The C2 domain of yeast ubiquitin ligase Rsp5, which binds PtdIns(3)P and PtdIns(3,5)P_2 but not PS, is localized in late endosomes and multivesicular bodies (Dunn et al. 2004). Also, this subcellular localization pattern of isolated C2 domains correlates with that of their host proteins, if the C2 domain is the only membrane targeting domain in the molecule (e.g. cPLA$_2\alpha$) (Gijon et al. 1999). Even those with multiple membrane-targeting domains, such as conventional PKCs with both C1 and C2 domains, the C2 domain still plays an important role in both their subcellular location and the kinetics and energetics of their membrane binding (Medkova and Cho 1999).

15.5
PH Domains

15.5.1
Occurrence, Structure and Lipid Specificity

PH domains are composed of 100–120 amino acids and found in over 250 mammalian proteins, making them one of the most common domains. PH domains generally show low (i.e. less than 30%) sequence homology (Ferguson et al. 2000; Lemmon et al. 2002), but all PH domains of known structure have a very similar fold containing a β-sandwich fold and a C-terminal α-helix (Lemmon 2003; Lemmon et al. 2002). The same structural fold has been observed in several other domains, such as phosphotyrosine binding (PTB) domain (Zhou et al. 1995), the Enabled/VASP homology domain-1 (EVH1) (Prehoda et al. 1999) and the Ran binding domain (Vetter et al. 1999).

About 15% of known PH domains bind phosphoinositides with relative high affinity; however, their specificity varies widely (see Table 15.1). The PH domain of PLCδ1 binds PtdIns(4,5)P_2 (Ferguson et al. 1995; Garcia et al. 1995; Rebecchi et al. 1992), whereas the Btk and Grp1 PH domains have specificity for PtdIns(3,4,5)P_3. Also, the PH domain of Akt/PKB binds both PtdIns(3,4)P_2 and PtdIns(3,4,5)P_3 (Kavran et al. 1998; Marte and Downward 1997). Moreover, PH

Table 15.1 Membrane-targeting domains specific for the lipids involved in cell signaling and membrane trafficking

Lipids	Main cellular location	Domains
DAG	Plasma membrane, Golgi, endoplasmic reticulum	C1 (PKC, DAG kinase, Ras-GRP, chimaerin, Unc-13)
PtdIns(3)P	Early endosome	FYVE PX ($p40^{phox}$, Vam7p, sorting nexin3) PH (PEPP1)
PtdIns(4)P	Golgi	PX (Bem1p) PH (FAPP1, oxysterol-binding protein) ENTH (epsinR)
PtdIns(5)P	(plasma membrane)	PHD (ACF, MLZF)
PtdIns(3,4)P_2	(plasma membrane)	PX ($p47^{phox}$) PH (Tapp) ENTH (HIP1)
PtdIns(3,5)P_2	Late endosome	PH (centaurin β2) ENTH (Ent3p, Ent5p, HIP1-related protein)
PtdIns(4,5)P_2	Plasma membrane	PH (PLCδ1) PX (CPK) ENTH (epsin), ANTH (AP180/CALM) FERM Tubby PTB (Disabled-1) PDZ (syntenin, Tiam-1, CASK, PTP-BL) C2 (PKC*a*, synaptotagmin)
PtdIns(3,4,5)P_3	Plasma membrane (endosomes)	PH (Btk, Grp1, ARNO, *Akt, Dapp1*) PX (PLD1)
Ceramide	Golgi	C1 (PKCδ)
Ceramide-1-phosphate	Golgi	C2 ($cPLA_2\alpha$)

Cellular locations shown in parenthesis indicate putative locations.

domains that bind PtdIns(3)P, PtdIns(4)P and PtdIns(3,5)P_2 have been identified (Dowler et al. 2000). Many of PH domains have low phosphoinositide affinities and do not yet have known functions. All phosphoinositide-binding PH domains show pronounced electrostatic polarization with the strong positive located in the phosphoinositide-binding surface (Blomberg et al. 1999; Blomberg and Nilges 1997; Lemmon and Ferguson 2000; Rameh et al. 1997; Yoon et al. 1994). Additional information on PH domains and their host proteins can be found in several recent reviews (DiNitto et al. 2003; Lemmon and Ferguson 2000; Lemmon and Ferguson 2001).

15.5.2
Membrane-binding Mechanisms

Most PH domains are S-type proteins whose membrane binding does not involve significant interfacial penetration. Unlike other H- and I-type phosphoinositide-binding domains, such as FYVE, PX and ENTH domains, PH domains do not have a deep ligand-binding pocket or hydrophobic and aromatic residues in the vicinity of the pocket. Thus, the membrane binding of PH domain is initially driven by non-specific electrostatic interactions, which is followed by specific phosphoinositide binding (Singh and Murray 2003). However, a recent solid-state NMR study suggests that hydrophobic residues of the PLCδ1 PH domain might penetrate the interfacial region to achieve hydrophobic interactions (Tuzi et al. 2003).

15.5.3
Subcellular Localization

In general, the PH domains with high phosphoinositide affinity recruit their host proteins in a phosphoinositide-dependent manner. For instance, the PH domain of PLCδ1 is required for the plasma membrane localization of the enzyme. Similarly, the PH domain of Akt/PKB recruits the protein to the PtdIns(3,4,5)P_3 site in the plasma membrane in response to phosphoinositide 3-kinase activation (Kavran et al. 1998; Marte and Downward 1997). The cellular function of a large majority of PH domains with weak phosphoinositide affinity has not been well defined. Lemmon and Ferguson have proposed that some of these PH domains, such as dynamins, increase their phosphoinositide affinity through oligomerization in host proteins (Klein et al. 1998; Lemmon and Ferguson 2000). Some PH domains may interact with both phosphoinositide and membrane proteins. For instance, the PH domain of the β-adrenergic receptor kinase, which has low PtdIns(4,5)P_2 affinity, drives the membrane targeting of the host protein by simultaneously interacting with the $G_{\beta\gamma}$ subunit of heterotrimeric G proteins (Mahadevan et al. 1995; Pitcher et al. 1995; Touhara et al. 1995).

15.6
FYVE Domains

15.6.1
Occurrence, Structure and Lipid Specificity

FYVE domains are small (70–80 amino acids) Cys-rich domains that contain two zinc ions (Stenmark et al. 2002). They are named for the first letters of the first four proteins in which they were identified: Fablp, YOTB, Vac1p and early endosomal antigen 1 (EEA1). FYVE domains are highly homologous and a large majority of FYVE domains specifically bind PtdIns(3)P that plays a key role in membrane trafficking (Patki et al. 1998). The recent X-ray structure of EEA1-

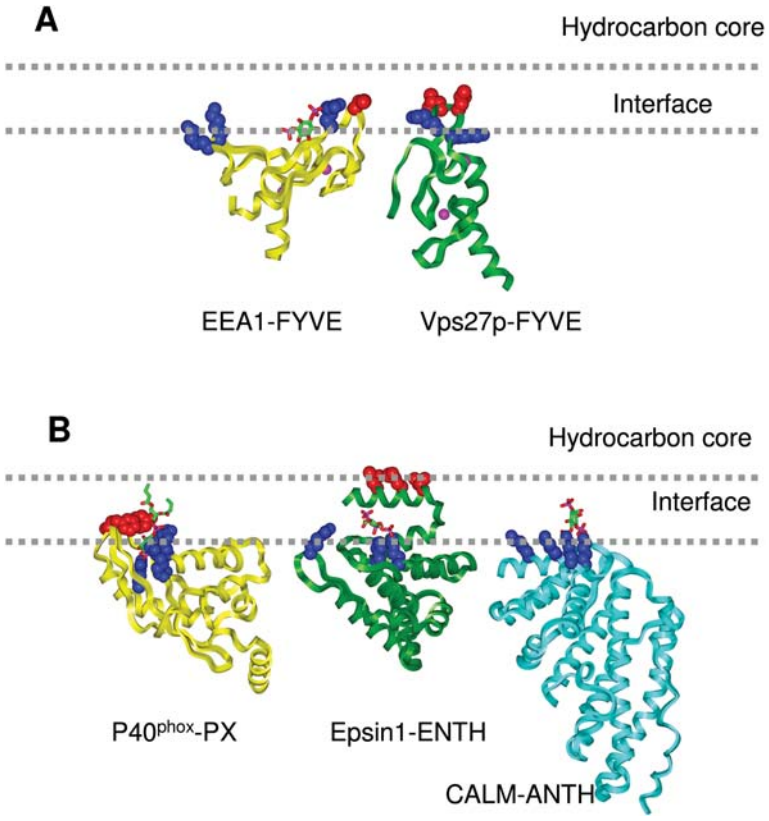

Fig. 15.4 Proposed membrane-binding modes for (A) two FYVE domains, and (B) $p40^{phox}$ PX, epsin1 ENTH and CALM ANTH domains. The backbones of the three domains and the specific lipid ligands ($Ins(1,3)P_2$ for EEA1-FYVE, PtdIns(3)P for $p40^{phox}$ PX, and $Ins(1,4,5)P_3$ for ENTH/ANTH domains) are shown in ribbon diagram and stick model, respectively. Membrane-penetrating aromatic and hydrophobic residues are shown in space-filling representation and colored red. Cationic residues involved in ligand and membrane interactions are shown in blue. Some of these residues are involved in non-specific electrostatic interactions, whereas others are involved in both specific phosphoinositide coordination and non-specific membrane binding. Zinc ions (FYVE domains) are shown in magenta. The depth of membrane penetration and the membrane-bound orientation have not been directly determined for these domains.

FYVE domain–inositol 1,3-bisphosphate complex demonstrates how the FYVE domain stereospecifically recognizes the PtdIns(3)P head group (see Fig. 15.4) (Dumas et al. 2001). In addition to their role in membrane trafficking, FYVE domain-containing proteins have been implicated in receptor signaling (Seet and Hong 2001; Tsukazaki et al. 1998) and actin cytoskeleton regulation (Estrada et al. 2001). Recently, the plant homeodomain (PHD), a domain common to

many chromatin-regulatory proteins, was shown to have FYVE domain-like structure (Pascual et al. 2000), and bind PtdIns(5)P both *in vitro* and *in vivo* (Gozani et al. 2003).

15.6.2 Membrane-binding Mechanism

The membrane-binding mechanism of FYVE domains has been extensively studied. FYVE domains are H- or I-type domains (i.e. the depth of interfacial penetration is unknown as of yet) whose membrane binding involves initial membrane adsorption by non-specific electrostatic interactions (Diraviyam et al. 2003; Kutateladze et al. 2004; Stahelin et al. 2002), specific lipid binding (Patki et al. 1998), interfacial penetration (Stahelin et al. 2002) and perhaps protein dimerization (Dumas et al. 2001; Hayakawa et al. 2004; Mao et al. 2000). Several different membrane-binding orientations have been proposed for FYVE domains. Based on similarity between the structures of the Vps27p-FYVE and the C1B domain of PKCδ, Misra and Hurley proposed that the FYVE domain binds to the membrane in a "side-on" orientation such that the long axis of the domain is perpendicular to the membrane surface (see Fig. 15.4). This would enable the binding of PtdIns(3)P to the pocket and simultaneous interfacial penetration of two Leu residues (Leu185 and Leu186) in an exposed loop (termed the turret loop). Based on the structure of the tandem VHS-FYVE domains from *Drosophila* Hrs, however, Mao et al. (2000) proposed a different membrane-binding mechanism in which a dimeric Hrs–FYVE complex interacts with the PtdIns(3)P-containing membrane in a distinct orientation. Subsequent NMR studies of the FYVE domain of EEA1 in the presence and absence of a soluble PtdIns(3)P and/or *n*-dodecyl phosphocholine micelles support the membrane binding orientation proposed by Misra and Hurley (Kutateladze and Overduin 2001; Kutateladze et al. 2004). More recently, Dumas et al. determined the X-ray structure of EEA1-FYVE–inositol 1,3-bisphosphate complex (Dumas et al. 2001), in which the protein forms a homodimer stabilized by a coiled-coil conformation of the N-terminal extension. The authors proposed that the long axis of the PtdIns(3)P-bound FYVE domain makes approximately a 45° angle with respect to the membrane surface ("angled") as opposed to the perpendicular "side-on" orientation (see Fig. 15.4).

Recent biophysical and computational studies of the FYVE domains have shed new light on the membrane-binding mechanism and orientation of FYVE domains. The electrostatic potential calculation of Vps27p and Hrs FYVE domains showed that due to the presence of cationic residues, the turret loop and neighboring region is surrounded by highly positive electrostatic potential, which drives the initial membrane association (k_a effect) (Stahelin et al. 2002). This membrane adsorption is followed by specific PtdIns(3)P binding, which then induces the interfacial penetration of hydrophobic and aromatic residues in the turret loop (Stahelin et al. 2002). SPR vesicle binding and monolayer penetration measurements indicated that PtdIns(3)P binding serves as an electro-

static switch that greatly reduces the positive potential surrounding the turret loop and thereby promotes the interfacial penetration of hydrophobic/aromatic turret loop residues (see Fig. 15.4) (Diraviyam et al. 2003; Stahelin et al. 2002). Local conformational changes in the turret loop region caused by PtdIns(3)P binding has also been observed. Both specific PtdIns(3)P binding and interfacial penetration slow the membrane dissociation (k_d effect) and thus stabilizes the membrane–protein complex. This mechanism is further supported by a recent computational study of FYVE domain-phospholipids interactions using the Finite Difference Poisson Boltzmann method (Diraviyam et al. 2003). Furthermore, this calculation predicted that Vps27p-FYVE and EEA1-FYVE would have the "side-on" and "angled" membrane orientation, respectively, due to their distinct electrostatic potential distributions and different minimal free energy orientations at the membrane surface.

15.6.3
Subcellular Localization

PtdIns(3)P plays a key role in membrane trafficking and is found in specific subcellular locales, including the cytoplasmic face of early endosomes and internal vesicles of multivesicular bodies (Gillooly et al. 2000; Stenmark 2001; Stenmark and Gillooly 2001). Consistent with its *in vitro* PtdIns(3)P specificity, many FYVE domain-containing proteins have also been shown to be localized to these membranes (Itoh et al. 2002; Ridley et al. 2001; Seet and Hong 2001). However, among all FYVE domains characterized so far only a few FYVE domains (e.g. those of endofin, FENS-1 and SARA) have been shown to be readily targeted to endosomal membranes when ectopically expressed in the cell (Itoh et al. 2002; Ridley et al. 2001; Seet and Hong 2001). Other FYVE domains do not seem to have high enough affinity for PtdIns(3)P-containing membranes to function as autonomous membrane-targeting domains. This raises questions as to whether lipid–protein interactions alone provide enough driving force for the subcellular targeting of the FYVE domains and whether other factors, such as domain oligomerization or other protein–protein interactions, are required for their membrane targeting. Dimerization-mediated endosomal targeting of FYVE domains has been proposed for several FYVE domains (Dumas et al. 2001; Hayakawa et al. 2004; Mao et al. 2000). FYVE domains differ in their hydrophobicity in the putative dimer interface, which is proposed from the dimeric crystal structures of EEA1 and Hrs, and this difference could contribute to the differential dimerization and subcellular localization of FYVE domains. In support of this notion, a tandem fusion construct of the FYVE domains of Hrs was shown to readily translocate to endosomes while a monomeric construct could not (Gillooly et al. 2001). It was also reported (Hayakawa et al. 2004) that the homodimerization of the SARA FYVE domain plays an important role in its endosomal localization. Our recent study showed that minor structural variations in the turret loops of FYVE domains dramatically changed their *in vitro* membrane binding properties and subcellular localization behaviors without causing domain dimerization

(Blatner et al. 2004). Furthermore, when a panel of mutants with structural variations in the turret loop were characterized, good quantitative correlation was observed between their K_d values for *in vitro* vesicle binding and subcellular localization to early endosomes, with a presence of a sharp range of threshold K_d necessary for the endosomal localization (Blatner et al. 2004). This suggests that the membrane recruitment of membrane-targeting domains and their host proteins can be readily turned on and off by slight changes in membrane affinity, which can be induced by many different factors, including a conformational change of protein and a change in the local concentration of a specific lipid.

15.7 PX Domains

15.7.1 Occurrence, Structure and Lipid Specificity

The PX domain is a structural module composed of 100–140 amino acids that was first identified in the $p40^{phox}$ and the $p47^{phox}$ subunits of NADPH oxidase (Ponting 1996) and has since been found in a variety of other proteins involved in membrane trafficking (e.g. Mvp1p, Vps5p, Bem1p and Grd19p, and the sorting nexin family of proteins) and cell signaling (e.g. PLD, phosphoinositide 3-kinases, cytokine-independent survival kinase and FISH) (Wishart et al. 2001). Recently, PX domains have been shown to interact with different phosphoinositides via conserved basic residues and target the host proteins to specific subcellular locations (Kanai et al. 2001; Xu et al. 2001a). PX domains are similar to the PH domain in that they exhibit broad phosphoinositide specificity (see Tab. 15.1). Many PX domains, including those of Vam7p (Cheever et al. 2001), sorting nexin 3 (Xu et al. 2001a) and $p40^{phox}$ (Kanai et al. 2001), and most yeast PX domains (Yu and Lemmon 2001), specifically interact with PtdIns(3)P. However, the PX domain of class II phosphoinositide 3-kinase-C2*α* (CPK) interacts with PtdIns(4,5)P_2 (Song et al. 2001), while the $p47^{phox}$ PX domain preferentially interacts with PtdIns(3,4)P_2 (Kanai et al. 2001). Also, the PX domains of the yeast protein Bem1p (Ago et al. 2001) and PLD1 (Stahelin et al. 2004a) have specificity for PtdIns(4)P and PtdIns(3,4,5)P_3, respectively. The PX domain of Nox organizing protein 1 was reported to bind PtdIns(4)P, PtdIns(5)P and PtdIns(3,5)P_2 (Cheng and Lambeth 2004).

The crystal structure of the $p40^{phox}$–PtdIns(3)P complex illustrated how the domain achieves the stereospecific recognition of PtdIns(3)P (Fig. 15.4) (Bravo et al. 2001), i.e. Arg58, that is conserved among many PX domains, specifically forms the hydrogen bond with the 3′-phosphate of PtdIns(3)P. The PX domains lacking the conserved Arg at position 58 bind other phosphoinositides. The X-ray structure of the PX domain of $p47^{phox}$ revealed that this PX domain has two phospholipid binding sites – the first basic pocket that putatively interact with PtdIns(3,4)P_2 and a second basic pocket which binds phosphatidic acid

(PA) and PS, but not phosphoinositides (Karathanassis et al. 2002b). The recent crystal structures of free and PtdIns(3)P-bound PX domain of yeast Grd19p protein showed the lipid-induced local conformational changes involving putative membrane-penetrating hydrophobic residues (Zhou et al. 2003).

15.7.2 Membrane-binding Mechanism

In vitro membrane-binding studies of the PX domains of $p40^{phox}$ and $p47^{phox}$ indicated that these PX domains are H- or I-type proteins (i.e. the depth of their interfacial penetration is unknown) whose membrane-binding mechanism is similar to that of FYVE domains (see Fig. 15.4). That is, initial membrane adsorption driven by non-specific electrostatic interactions between the cationic surface of the PX domain and the anionic membrane is followed by the specific phosphoinositide binding, and subsequent interfacial penetration of hydrophobic and aromatic residues (Karathanassis et al. 2002b; Stahelin et al. 2003a). The $p47^{phox}$ PX domain with two separate phospholipid-binding pockets follows a similar, but more complex, mechanism. In this case, PtdIns(3,4)P_2 and PA (or PS) induces the interfacial penetration of hydrophobic residues located near their respective binding sites by modulating local electrostatic potential changes (Karathanassis et al. 2002b) and potentially causing conformational changes (Zhou et al. 2003). Simultaneous occupation of the binding pockets by ligands dramatically reduces the positive electrostatic potential, which in turn promotes more effective interfacial penetration of the domain; hence the synergistic effect of PtdIns(3,4)P_2 and PA (or PS) on the membrane affinity of the $p47^{phox}$ PX domain (Karathanassis et al. 2002a). The molecular modeling of the PLD1 PX domain suggested the presence of a second lipid-binding pocket that is similar to that of $p47^{phox}$-PX. However, this putative binding pocket non-specifically interacts with anionic lipids (Stahelin et al. 2004a), and neither specific PtdIns(3,4,5)P_3 binding nor non-specific anionic lipid binding significantly induces the interfacial penetration of the domain, suggesting that the PLD1 PX domain is a S-type protein whose initial membrane attachment by non-specific electrostatic interactions is followed by specific phosphoinositide binding. More recently, it was suggested that the membrane binding of the cytokine-independent survival kinase PX domain might involve the domain homodimerization in addition to the phosphoinositide-induced interfacial penetration, based on the finding that this PX domain tends to dimerize in the presence of the linker between the PX domain and the catalytic domain (Xing et al. 2004).

15.7.3 Subcellular Localization

Many PtdIns(3)P-binding PX domains, including the $p40^{phox}$ PX domain, have been shown to be localized at early endosomes when ectopically expressed in the cell (Bravo et al. 2001; Kanai et al. 2001; Xu et al. 2001a). This suggests that

these PX domains have higher affinity for PtdIns(3)P-containing membranes than most FYVE domains that are not targeted to endosomes. In fact, the affinity of $p40^{phox}$-PX for PtdIns(3)P-containing vesicles is more than 10 times higher than that of the FYVE domains of Vps27p and Hrs, and is above the threshold value for endosomal localization determined for FYVE domains (see above) (Stahelin et al. 2003a). Cell studies with GFP-tagged $p40^{phox}$-PX mutants in HEK293 cells showed good correlation between *in vitro* affinity for PtdIns(3)P-containing vesicles and the endosomal localization (Stahelin et al. 2003a). In particular, hydrophobic and aromatic residues involved in interfacial penetration were crucial for the endosomal targeting of $p40^{phox}$-PX. Among 15 PtdIns(3)P-binding PX domains found in *Saccharomyces cerevisiae* only four PX domains strongly bind PtdIns(3)P-containing vesicles and are likely to be capable of driving endosomal localization (Yu and Lemmon 2001). Notably, many of the yeast proteins containing low affinity PX domains have been found in multi-protein complexes. One example is the sorting nexin family, in which some family members have coiled-coil regions that can drive the homo and/or hetero-oligomerization and endosomal targeting (Xu et al. 2001b). The GFP-tagged $p47^{phox}$-PX was found in the cytosol in HEK293 cells presumably because of low cellular concentration of PtdIns(3,4)P_2 (Stahelin et al. 2003a). When PtdIns(3,4)P_2 was fed into cells and distributed among intracellular membranes, however, the $p47^{phox}$-PX was selectively targeted to the PS-rich plasma membrane, indicating that the secondary lipid-binding site might play a key role in the membrane targeting of $p47^{phox}$-PX (Stahelin et al. 2003a).

Sequence comparisons of PX domains have shown that the domain contains several conserved regions, including a Pro-rich motif [R(K)XXPXXP] that is characteristic of SH3 domain-binding motifs. Thus, it was speculated that some PX domains might be interacting partners of SH3 domain proteins (Ponting 1996). Recently, it was demonstrated that the PX domain of $p47^{phox}$ interacts intramolecularly with its C-terminal SH3 domain and inhibits binding of the PX domain to PtdIns(3,4)P_2-containing membranes. When five C-terminal Ser residues are phosphorylated, this interdomain interaction is disrupted and the PX domain is allowed to interact with the membrane (Karathanassis et al. 2002b). Similarly, the PX domain of Scd2 has been shown to interact with its SH3 domain, preventing its binding to Cdc42 until Scd1 unleashes this interaction (Endo et al. 2003). PX domains may also be involved in interactions with other cellular proteins, e.g. the PX domains of $p40^{phox}$ and $p47^{phox}$ have been shown to bind moesin (Wientjes et al. 2001). However, the structural basis and the physiological role of this interaction have not been clarified.

15.8
ENTH and ANTH Domains

15.8.1
Occurrence, Structure and Lipid Specificity

The ENTH domain is about 140 amino acids in length and has a compact globular structure of eight α-helices connected by loops of varying length (De Camilli et al. 2002). This domain was first identified in the 90-kDa epsin protein that binds the clathrin adaptor AP-2 (Kay et al. 1999). Subsequently, the ENTH domain was identified through homology searches in a number of proteins, such as CALM and AP180 (a brain-specific analog of CALM), involved in the early stages of the endocytic pathway. X-ray crystallographic and NMR studies have shown that these domains have similar structures despite the low sequence homology (see Fig. 15.4) (Ford et al. 2001, 2002; Itoh et al. 2001).

Recent reports have indicated that ENTH domains can bind PtdIns(4,5)P_2 (Ford et al. 2001; Itoh et al. 2001). The X-ray structure of the ENTH domain of AP180/CALM revealed that a cluster of basic residues bind phosphate groups of PtdIns(4,5)P_2 (Ford et al. 2001). Surprisingly, the ENTH domain of epsin1, which lacks this basic region, also binds PtdIns(4,5)P_2 (Itoh et al. 2001). The subsequent X-ray structure of the epsin1 ENTH domain complexed with Ins(1,4,5)P_3 revealed that Ins(1,4,5)P_3 induces the formation of an N-terminal amphiphilic α-helix that constitutes the binding pocket for Ins(1,4,5)P_3 (Ford et al. 2002). Also, the structure suggested that hydrophobic residues on the same face of the amphiphilic α-helix penetrate the membrane, which is essential for membrane deformation and vesicle budding during clathrin-mediated endocytosis.

In contrast to the epsin1 ENTH domain, the CALM/AP180 ENTH domain does not induce membrane deformation. Based on these different membrane properties, ENTH domains are therefore subdivided into two classes: ENTH for epsin1 and its homologs, and ANTH for AP180/CALM. Recently, the ENTH domains with different phosphoinositide specificity have been reported. The ENTH domain of epsin-related protein (epsinR) binds PtdIns(4)P (Mills et al. 2003) whereas the ENTH domains of yeast proteins Ent3p and Ent5p have specificity for PtdIns(3,5)P_2 (Eugster et al. 2004; Friant et al. 2003). Also, the ENTH domains of Huntingtin-interacting protein1 (HIP1) and HIP1-related protein bind PtdIns(3,4)P_2 and PtdIns(3,5)P_2 (Hyun et al. 2004).

15.8.2
Membrane-binding Mechanism

Our recent biophysical analysis of the epsin ENTH and AP180 ANTH domains showed that these two domains have distinctly different membrane-binding mechanisms (Stahelin et al. 2003b). The epsin ENTH domain is a H-type protein which initially binds anionic membranes by non-specific electrostatic interactions, which is followed by the facilitated PtdIns(4,5)P_2 binding on the mem-

brane surface. The initial membrane binding and/or PtdIns(4,5)P_2 binding induce dramatic conformation changes of the domain, leading to the formation of the amphipathic N-terminal α-helix (Ford et al. 2002). As in the case with FYVE (Stahelin et al. 2002) and PX domains (Stahelin et al. 2003 a), PtdIns(4,5)P_2 binding also serves as an electrostatic switch to neutralize the strong positive electrostatic potential on the membrane-binding surface and thereby promotes the interfacial penetration of hydrophobic and aromatic residues of the N-terminal α-helix. The depth of membrane penetration by the ENTH domain has not been determined; however, it is expected to penetrate into the hydrocarbon core region from the putative membrane binding orientation of the domain and the length the N-terminal α-helix (see Fig. 15.4). This PtdIns(4,5)P_2-induced penetration provides a biophysical explanation for the vesicle tubulation activity of the epsin ENTH domain (Ford et al. 2002).

In contrast, the AP180 ANTH domain is a S-type protein that binds the membrane by non-specific electrostatic forces and subsequent specific interaction with PtdIns(4,5)P_2 acting as an electrostatic bridge between the protein and the membrane (see Fig. 15.5). This ANTH domain has smaller k_a and larger k_d than the epsin-ENTH because of weaker positive electrostatic potential and lack of interfacial penetration (Stahelin et al. 2003 b), respectively. The latter property is also consistent with its inability to tubulate liposomes (Ford et al. 2002). Intriguingly, there are many peripheral proteins, such as FYVE (Stahelin et al. 2002), PX (Stahelin et al. 2003 a) and C1 domains (Medkova and Cho 1999), which penetrate lipid monolayers as well as or more effectively than the epsin ENTH domain without inducing liposome tubulation. Although further studies are required to understand the molecular basis of this special activity of the epsin ENTH domain, it would seem that the insertion of a rigid α-helix distorts the membrane and causes curvature changes much more efficiently than a flexible loop, as was seen with many surface active amphiphilic peptides (Ludtke et al. 1994; Moll et al. 2000).

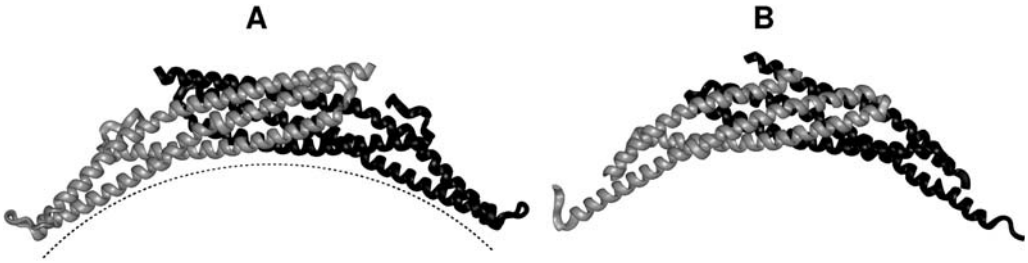

Fig. 15.5 Crystal structures of BAR domains of *Drosophila* amphiphysin (A) and arfaptin2 (B). Both proteins form a crescent-shaped homodimer. Two monomeric units are shown in black and grey ribbon diagrams, respectively. The concave face and both ends of the amphiphysin BAR domain have a number of cationic residues. The concave surface of the amphiphysin BAR domain would fit a curved membrane with a diameter of 22 nm (shown in a dotted line). The flexible N-terminal extension of the amphiphysin BAR domain is not shown.

15.9
BAR Domains

BAR domains (around 250 amino acids) were originally identified as a highly conserved N-terminal domain of the BAR family proteins that include mammalian bridging-integrators (Bin-1 and Bin-2), amphiphysins, and the yeast Rvs161p and Rvs167p (Zhang and Zelhof 2002). This domain has been since found in a large number of proteins, including endophilins, arfaptins, nadrin, centaurin β2, oligophrenins and sorting nexins (Habermann 2004). Amphiphysins, endophilins and their BAR domains have been shown to bind, bend and tubulate vesicles *in vitro* (Farsad et al. 2001; Takei et al. 1999) and *in vivo* (Peter et al. 2004). The recently determined structure of the *Drosophila* amphiphysin BAR domain provides the basis of its unique membrane interaction properties (Peter et al. 2004). This domain forms a crescent-shaped dimer of two coiled-coils (see Fig. 15.5), each made of three long kinked α-helices, and this structure is strikingly similar to that of another BAR domain from apfaptin2 (Tarricone et al. 2001). The concave surface of the dimer harbors several cationic clusters, which interact with anionic membranes primarily through non-specific electrostatic interactions (Peter et al. 2004; Zimmerberg and McLaughlin 2004). Consequently, amphiphysin and other BAR domains show low lipid selectivity except for the arfaptin BAR domain (Peter et al. 2004) that shows selectivity for PtdIns(4)P (Stahelin and Cho, unpublished observation). It is interesting to note that the membrane-interacting surface of yeast Sec23/24–Sar1 complex, that is involved in COPII-coated vesicle formation on the endoplasmic reticulum, is also concave and positively charged (Bi et al. 2002).

Owing to the rigid concave shape of their membrane-binding surfaces, it has been proposed that BAR domains can "sense" the membrane curvature, i.e. the domain should bind with higher affinity for those membranes whose geometric curvature approaches that of the BAR domain (a curved membrane with a diameter of around 22 nm for the amphiphysin BAR domain) (Peter et al. 2004). A similar membrane-curvature sensing function was also proposed for ArfGAP protein in COPI-mediated vesicle coat assembly (Bigay et al. 2003). In fact, some BAR domains, such as those of sorting nexin 1 (Carlton et al. 2004), centaurin β2 and oligophrenin1 (the latter two were studied as BAR + PH domain hybrids) (Peter et al. 2004), showed differential affinities for vesicles of different size. Interestingly, those BAR domains with high vesicle tubulation activity, which include those of amphiphysins, endophilins and nadrin, show little sensitivity to the vesicle size (Peter et al. 2004). These BAR domains commonly have an N-terminal extension, which is induced to form an amphiphilic α-helix by lipid binding in the case of the *Drosophila* amphiphysin BAR domain (Peter et al. 2004). This induced helical structure appears to play an important role in vesicle tubulation, as in the case of the epsin ENTH domain (Ford et al. 2002). Our recent studies (Stahelin and Cho, unpublished observation) show that amphiphysin and endophilin BAR domains follow a two-step membrane-binding mechanism in which the initial non-specific electrostatic binding is followed by

the membrane penetration by the N-terminal extension. The latter step is abrogated by the deletion of the extension. Thus, it appears that the BAR domains without the N-terminal extension act as S-type proteins that mainly interact with curved anionic membrane surfaces through non-specific electrostatic interactions and consequently are sensitive to the membrane curvature. By contrast, the BAR domains with the extension (also known as N-BAR domains) function as H-type proteins and cause the membrane deformation through membrane penetration. Due to the extra hydrophobic membrane binding energies conferred on these BAR domains, their vesicle affinity is much less sensitive to the vesicle curvature (Peter et al. 2004). Some BAR domains, including the arfaptin2 BAR domain (Tarricone et al. 2001), have been also shown to bind the small GTPase using the concave surface (Habermann 2004). It is unclear whether this activity is common to all BAR domains and how the membrane binding and the protein interaction are coordinated for those BAR domains that bind both membranes and the small GTPase.

15.10 FERM Domains

The FERM domain is composed of about 300 amino acids, and found in the N-terminal region of ezrin/radixin/moesin (ERM) family of proteins that function as cross-linkers between plasma membranes and actin filaments (Bretscher et al. 2002; Hamada et al. 2000; Pearson et al. 2000; Smith et al. 2003). The FERM or FERM-like domain has been also identified in various other proteins, including a subset of protein tyrosine phosphatases. It has been reported that the FERM domain binds PtdIns(4,5)P_2 *in vitro* (Hamada et al. 2000) and that PtdIns(4,5)P_2 binding by ezrin is important for its cellular function. The interdomain interaction between the FERM domain and the C-terminal domain keeps ERM proteins in a dormant conformation in the cytoplasm. Phosphorylation of the C-terminal tail weakens this intramolecular interaction, allowing the FERM domain to interact with PtdIns(4,5)P_2 and membrane proteins in the plasma membrane (Edwards and Keep 2001). The crystal structure of the radixin FERM domain shows that the domain is composed of three subdomains and that the PtdIns(4,5)P_2 binding site is formed in a basic cleft between two subdomains (Hamada et al. 2000, 2001; Pearson et al. 2000; Smith and Cerione 2002; Smith et al. 2003). Although the membrane binding of the FERM domain has not been fully characterized, the FERM domain is not expected to significantly penetrate the PtdIns(4,5)P_2-containing membranes since its binding pocket is exposed similarly to the PH domain and lacks the presence of hydrophobic/aromatic residues. It has also been reported that FERM domains may have multiple non-specific PtdIns(4,5)P_2 binding motifs (Bompard et al. 2003).

15.11
Tubby Domains

Tubby domains are highly conserved domains of about 260 amino acids located in the C-terminus of all TULP (tubby-like protein) family proteins (Carroll et al. 2004; Santagata et al. 2001). The Tub protein, a founding member of TULPs, shows dual subcellular localization at the plasma membrane and in the nucleus, which is achieved through the presence of competing localization signals in the N-terminal and C-terminal (i.e. tubby domain) domains. The N-terminal domain has a nuclear localization sequence and adopts completely nuclear localization, whereas the tubby domain on its own is localized to the plasma membrane. The Tub tubby domain has been shown to bind PtdIns(4,5)P_2 as well as PtdIns(3,4)P_2 and PtdIns(3,4,5)P_3, but not PtdIns(3,5)P_2 and singly-phosphorylated phosphoinositides (Santagata et al. 2001). The X-ray structure of the tubby domain of Tub shows that the domain adopts a 12-stranded antiparallel β-barrel conformation that is filled with a central α-helix (Santagata et al. 2001). The PtdIns(4,5)P_2 binding site is formed between three β-strands and an external helix, its PtdIns(4,5)P_2 binding mode is similar to that of CALM ANTH domain (Ford et al. 2001). Mutation of cationic residue involved in PtdIns(4,5)P_2 binding abrogates the plasma membrane localization of the tubby domain (Santagata et al. 2001). Although further studies are needed to elucidate the membrane-binding mechanism of the tubby domain, it would seem that the domain is a S-type domain whose membrane-binding mechanism is similar to that of the ANTH domain. Interestingly, it has been proposed that PtdIns(4,5)P_2-mediated plasma membrane binding of the tubby domain sequesters the TULP away from its effectors that are located in the nucleus (Santagata et al. 2001). Thus, membrane binding of tubby domains serves to keep their host proteins dormant in contrast to other membrane-targeting domains whose membrane binding lead to the activation of their host proteins.

15.12
Other Phosphoinositide-binding Domains

In addition to the membrane-targeting domains listed above, other modular signaling domains have been reported to bind phosphoinositides, PtdIns(4,5)P_2 in particular. PTB domains bind phosphorylated (Kavanaugh and Williams 1994) and non-phosphorylated (Yan et al. 2002) tyrosines in receptor tyrosine kinases and other signaling proteins (Kavanaugh and Williams 1994). It has been reported that PTB domains can also bind phosphoinositides (Ravichandran et al. 1997; Takeuchi et al. 1998), which is not surprising given their structural similarity to PH domains (Zhou et al. 1995). A recent crystal structure of the Disabled-1 PTB domain showed that this PTB domain (Stolt et al. 2003) has a PtdIns(4,5)P_2-binding site, composed of multiple basic residues, that is distinct from its peptide-binding site and structurally similar to the PtdIns(4,5)P_2-bind-

ing sites found in other PH domains. The *P*ostsynaptic density protein, *d*isks large, *z*onula occludens (PDZ) domain is another signaling domain that has been reported to bind PtdIns(4,5)P_2. PDZ domains play essential roles in signal transduction by acting as molecular scaffolds for the assembly of multiprotein complexes (Fanning and Anderson 1999; Saras and Heldin 1996). They bind to short peptide sequences, typically C-terminal four to five amino acids of their targets. Recently, PDZ domains from syntenin, Tiam-1, CASK and PTP-BL, have been shown to bind phosphoinositides (Zimmermann et al. 2002). In particular, high-affinity PtdIns(4,5)P_2 binding was seen for syntenin through the synergistic effect of two PDZ domains.

15.13 Perspectives

It is becoming increasingly clear that membrane–protein interactions play important roles in the execution and regulation of many cellular processes, including cell signaling and membrane trafficking. Progress in our understanding of the membrane-binding mechanisms of membrane targeting proteins and their host proteins has been substantial over the past decade thanks to rapid progress in structural biology, computational biology, *in vitro* biophysical studies and microscopic cell imaging. With the availability of whole-genome sequence information for many different organisms, it is expected that an increasing number of membrane-targeting domains and peripheral proteins will be identified in the near future. Thus, future research on membrane–protein interactions will entail more comprehensive studies. Structural biology of membrane-targeting domains and peripheral proteins will continue to play an important role in deciphering the structural basis of specific lipid binding and membrane interactions. Computational biology and bioinformatics will allow identification of putative membrane binding domains and motifs from the protein database, and prediction of their tertiary structures. Biophysical studies using model membranes will be essential for obtaining critical mechanistic information, including the depth of interfacial penetration of peripheral proteins. Also, *in vitro* and cellular single-molecule studies of peripheral proteins will provide detailed information about the molecular events involved in membrane–protein interactions. Recent development in various fluorescence spectroscopic techniques, such as fluorescence correlation spectroscopy, offers exciting new opportunities to determine the kinetic and thermodynamic parameters of membrane–protein interactions in living cells. These parameters will undoubtedly provide the most direct and critical information about the cellular membrane targeting of peripheral proteins. Collectively, these multidisciplinary studies will elucidate the mechanisms by which cellular membrane binding and activation of a wide range of membrane-targeting domains and their host proteins is regulated.

References

Ago, T., Takeya, R., Hiroaki, H., Kuribayashi, F., Ito, T., Kohda, D., Sumimoto, H. **2001**. The PX domain as a novel phosphoinositide-binding module. *Biochem. Biophys. Res. Commun. 287*, 733–738.

Ananthanarayanan, B., Das, S., Rhee, S.G., Murray, D., Cho, W. **2002**. Membrane targeting of C2 domains of phospholipase C-delta isoforms. *J. Biol. Chem. 277*, 3568–3575.

Ananthanarayanan, B., Stahelin, R.V., Digman, M.A., Cho, W. **2003**. Activation mechanisms of conventional protein kinase C isoforms are determined by the ligand affinity and conformational flexibility of their C1 domains. *J. Biol. Chem. 278*, 46886–46894.

Baron, C.L., Malhotra, V. **2002**. Role of diacylglycerol in PKD recruitment to the TGN and protein transport to the plasma membrane. *Science 295*, 325–328.

Bi, X., Corpina, R.A., Goldberg, J. **2002**. Structure of the Sec23/24-Sar1 pre-budding complex of the COPII vesicle coat. *Nature 419*, 271–277.

Bigay, J., Gounon, P., Robineau, S., Antonny, B. **2003**. Lipid packing sensed by ArfGAP1 couples COPI coat disassembly to membrane bilayer curvature. *Nature 426*, 563–566.

Bittova, L., Sumandea, M., Cho, W. **1999**. A structure–function study of the C2 domain of cytosolic phospholipase A2. Identification of essential calcium ligands and hydrophobic membrane binding residues. *J. Biol. Chem. 274*, 9665–9672.

Bittova, L., Stahelin, R.V., Cho., W. **2001**. Roles of ionic residues of the C1 domain in protein kinase C-alpha activation and the origin of phosphatidylserine specificity. *J. Biol. Chem. 276*, 4218–4226.

Bivona, T.G., Perez De Castro, I., Ahearn, I.M., Grana, T.M., Chiu, V.K., Lockyer, P.J., Cullen, P.J., Pellicer, A., Cox, A.D., Philips, M.R. **2003**. Phospholipase Cgamma activates Ras on the Golgi apparatus by means of RasGRP1. *Nature 424*, 694–698.

Blatner, N.R., Stahelin, R.V., Diraviyam, K., Hawkins, P.T., Hong, W., Murray, D., Cho, W. **2004**. The molecular basis of the differential subcellular localization of FYVE domains. *J. Biol. Chem. 279*, 53818–53827.

Blomberg, N., Baraldi, E., Nilges, M., Saraste, M. **1999**. The PH superfold: a structural scaffold for multiple functions. *Trends Biochem. Sci. 24*, 441–445.

Blomberg, N., Nilges, M. **1997**. Functional diversity of PH domains: an exhaustive modelling study. *Fold. Des. 2*, 343–355.

Bompard, G., Martin, M., Roy, C., Vignon, F., Freiss, G. **2003**. Membrane targeting of protein tyrosine phosphatase PTPL1 through its FERM domain via binding to phosphatidylinositol 4,5-bisphosphate. *J. Cell Sci. 116*, 2519–2530.

Bravo, J., Karathanassis, D., Pacold, C.M., Pacold, M.E., Ellson, C.D., Anderson, K.E., Butler, P.J., Lavenir, I., Perisic, O., Hawkins, P.T., et al. **2001**. The crystal structure of the PX domain from $p40^{phox}$ bound to phosphatidylinositol 3-phosphate. *Mol. Cell 8*, 829–839.

Bretscher, A., Edwards, K., Fehon, R.G. **2002**. ERM proteins and merlin: integrators at the cell cortex. *Nat. Rev. Mol. Cell Biol. 3*, 586–599.

Brose, N., Rosenmund, C. **2002**. Move over protein kinase C, you've got company: alternative cellular effectors of diacylglycerol and phorbol esters. *J. Cell Sci. 115*, 4399–4411.

Canagarajah, B., Leskow, F.C., Ho, J.Y., Mischak, H., Saidi, L.F., Kazanietz, M.G., Hurley, J.H. **2004**. Structural mechanism for lipid activation of the Rac-specific GAP, beta2-chimaerin. *Cell 119*, 407–418.

Carlton, J., Bujny, M., Peter, B.J., Oorschot, V.M., Rutherford, A., Mellor, H., Klumperman, J., McMahon, H.T., Cullen, P.J. **2004**. Sorting nexin-1 mediates tubular endosome-to-TGN transport through coincidence sensing of high-curvature membranes and 3-phosphoinositides. *Curr. Biol. 14*, 1791–1800.

Carroll, K., Gomez, C., Shapiro, L. **2004**. Tubby proteins: the plot thickens. *Nat. Rev. Mol. Cell Biol. 5*, 55–63.

Catz, S.D., Johnson, J.L., Babior, B.M. **2002**. The C2A domain of JFC1 binds to 3′-phosphorylated phosphoinositides and

directs plasma membrane association in living cells. *Proc. Natl Acad. Sci. USA 99*, 11652–11657.

Chae, Y.K., Abildgaard, F., Chapman, E.R., Markley, J.L. **1998**. Lipid binding ridge on loops 2 and 3 of the C2A domain of synaptotagmin I as revealed by NMR spectroscopy. *J. Biol. Chem. 273*, 25659–25663.

Cheever, M.L., Sato, T.K., de Beer, T., Kutateladze, T.G., Emr, S.D., Overduin, M. **2001**. Phox domain interaction with $PtdIns_3P$ targets the Vam7 t-SNARE to vacuole membranes. *Nat. Cell Biol. 3*, 613–618.

Cheng, G., Lambeth, J.D. **2004**. NOXO1, regulation of lipid binding, localization, and activation of Nox1 by the Phox homology (PX) domain. *J. Biol. Chem. 279*, 4737–4742.

Cho, W. **2001**. Membrane targeting by C1 and C2 domains. *J. Biol. Chem. 276*, 32407–32410.

Cho, W., Stahelin, R.V. **2005**. Membrane–protein interactions in cell signaling and membrane trafficking. *Annu. Rev. Biophys. Biomol. Struct. 34*, 119–151.

Corbalan-Garcia, S., Garcia-Garcia, J., Rodriguez-Alfaro, J.A., Gomez-Fernandez, J.C. **2003**. A new phosphatidylinositol 4,5-bisphosphate-binding site located in the C2 domain of protein kinase Calpha. *J. Biol. Chem. 278*, 4972–4980.

Corbalan-Garcia, S., Rodriguez-Alfaro, J.A., Gomez-Fernandez, J.C. **1999**. Determination of the calcium-binding sites of the C2 domain of protein kinase Calpha that are critical for its translocation to the plasma membrane. *Biochem. J. 337*, 513–521.

Cunningham, B.C., Wells, J.A. **1993**. Comparison of a structural and a functional epitope. *J. Mol. Biol. 234*, 554–563.

Das, S., Dixon, J.E., Cho, W. **2003**. Membrane-binding and activation mechanism of PTEN. *Proc. Natl Acad. Sci. USA 100*, 7491–7496.

Das, J., Addona, G.H., Sandberg, W.S., Husain, S.S., Stehle, T., Miller, K.W. **2004**. Identification of a general anesthetic binding site in the diacylglycerol-binding domain of protein kinase Cd. *J. Biol. Chem. 279*, 37964–37972.

De Camilli, P., Chen, H., Hyman, J., Panepucci, E., Bateman, A., Brunger, A.T. **2002**. The ENTH domain. *FEBS Lett. 513*, 11–18.

DiNitto, J.P., Cronin, T.C., Lambright, D.G. **2003**. Membrane recognition and targeting by lipid-binding domains. *Sci. STKE 2003*, re16.

Diraviyam, K., Stahelin, R.V., Cho, W., Murray, D. **2003**. Computer modeling of the membrane interaction of FYVE domains. *J. Mol. Biol. 328*, 721–736.

Dowler, S., Currie, R.A., Campbell, D.G., Deak, M., Kular, G., Downes, C.P., Alessi, D.R. **2000**. Identification of pleckstrin-homology-domain-containing proteins with novel phosphoinositide-binding specificities. *Biochem. J. 351*, 19–31.

Dumas, J.J., Merithew, E., Sudharshan, E., Rajamani, D., Hayes, S., Lawe, D., Corvera, S., Lambright, D.G. **2001**. Multivalent endosome targeting by homodimeric EEA1. *Mol. Cell 8*, 947–958.

Dunn, R., Klos, D.A., Adler, A.S., Hicke, L. **2004**. The C2 domain of the Rsp5 ubiquitin ligase binds membrane phosphoinositides and directs ubiquitination of endosomal cargo. *J. Cell Biol. 165*, 135–144.

Edwards, S.D., Keep, N.H. **2001**. The 2.7 Å crystal structure of the activated FERM domain of moesin: an analysis of structural changes on activation. *Biochemistry 40*, 7061–7068.

Endo, M., Shirouzu, M., Yokoyama, S. **2003**. The Cdc42 binding and scaffolding activities of the fission yeast adaptor protein Scd2. *J. Biol. Chem. 278*, 843–852.

Essen, L.O., Perisic, O., Lynch, D.E., Katan, M., Williams, R.L. **1997**. A ternary metal binding site in the C2 domain of phosphoinositide-specific phospholipase C-delta1. *Biochemistry 36*, 2753–2762.

Estrada, L., Caron, E., Gorski, J.L. **2001**. Fgd1, the Cdc42 guanine nucleotide exchange factor responsible for faciogenital dysplasia, is localized to the subcortical actin cytoskeleton and Golgi membrane. *Hum. Mol. Genet. 10*, 485–495.

Eugster, A., Pecheur, E.I., Michel, F., Winsor, B., Letourneur, F., Friant, S. **2004**. Ent5p is required with Ent3p and Vps27p for ubiquitin-dependent protein sorting into the multivesicular body. *Mol. Biol. Cell 15*, 3031–3041.

Evans, J.H., Gerber, S.H., Murray, D., Leslie, C.C. **2004**. The calcium binding loops of the cytosolic phospholipase A2 C2 domain specify targeting to Golgi and ER in live cells. *Mol. Biol. Cell 15*, 371–383.

Fanning, A.S., Anderson, J.M. **1999**. Protein modules as organizers of membrane structure. *Curr. Opin. Cell Biol. 11*, 432–439.

Farsad, K., Ringstad, N., Takei, K., Floyd, S.R., Rose, K., De Camilli, P. **2001**. Generation of high curvature membranes mediated by direct endophilin bilayer interactions. *J. Cell Biol. 155*, 193–200.

Ferguson, K.M., Lemmon, M.A., Schlessinger, J., Sigler, P.B. **1995**. Structure of the high affinity complex of inositol trisphosphate with a phospholipase C pleckstrin homology domain. *Cell 83*, 1037–1046.

Ferguson, K.M., Kavran, J.M., Sankaran, V.G., Fournier, E., Isakoff, S.J., Skolnik, E.Y., Lemmon, M.A. **2000**. Structural basis for discrimination of 3-phosphoinositides by pleckstrin homology domains. *Mol. Cell 6*, 373–384.

Ford, M.G., Pearse, B.M., Higgins, M.K., Vallis, Y., Owen, D.J., Gibson, A., Hopkins, C.R., Evans, P.R., McMahon, H.T. **2001**. Simultaneous binding of PtdIns(4,5)P_2 and clathrin by AP180 in the nucleation of clathrin lattices on membranes. *Science 291*, 1051–1055.

Ford, M.G., Mills, I.G., Peter, B.J., Vallis, Y., Praefcke, G.J., Evans, P.R., McMahon, H.T. **2002**. Curvature of clathrin-coated pits driven by epsin. *Nature 419*, 361–366.

Frazier, A.A., Wisner, M.A., Malmberg, N.J., Victor, K.G., Fanucci, G.E., Nalefski, E.A., Falke, J.J., Cafiso, D.S. **2002**. Membrane orientation and position of the C2 domain from cPLA2 by site-directed spin labeling. *Biochemistry 41*, 6282–6292.

Friant, S., Pecheur, E.I., Eugster, A., Michel, F., Lefkir, Y., Nourrisson, D., Letourneur, F. **2003**. Ent3p is a PtdIns(3,5)P_2 effector required for protein sorting to the multivesicular body. *Dev. Cell 5*, 499–511.

Garcia, P., Gupta, R., Shah, S., Morris, A.J., Rudge, S.A., Scarlata, S., Petrova, V., McLaughlin, S., Rebecchi, M.J. **1995**. The pleckstrin homology domain of phospholipase C-delta 1 binds with high affinity to phosphatidylinositol 4,5-bisphosphate in bilayer membranes. *Biochemistry 34*, 16228–16234.

Gelb, M.H., Cho, W., Wilton, D.C. **1999**. Interfacial binding of secreted phospholipase A2: more than electrostatics and a major role for tryptophan. *Curr. Opin. Struct. Biol. 9*, 428–432.

Gijon, M.A., Spencer, D.M., Kaiser, A.L., Leslie, C.C. **1999**. Role of phosphorylation sites and the C2 domain in regulation of cytosolic phospholipase A2. *J. Cell Biol. 145*, 1219–1232.

Gillooly, D.J., Morrow, I.C., Lindsay, M., Gould, R., Bryant, N.J., Gaullier, J.M., Parton, R.G., Stenmark, H. **2000**. Localization of phosphatidylinositol 3-phosphate in yeast and mammalian cells. *EMBO J. 19*, 4577–4588.

Gillooly, D.J., Simonsen, A., Stenmark, H. **2001**. Cellular functions of phosphatidylinositol 3-phosphate and FYVE domain proteins. *Biochem. J. 355*, 249–258.

Gozani, O., Karuman, P., Jones, D.R., Ivanov, D., Cha, J., Lugovskoy, A.A., Baird, C.L., Zhu, H., Field, S.J., Lessnick, S.L., et al. **2003**. The PHD finger of the chromatin-associated protein ING2 functions as a nuclear phosphoinositide receptor. *Cell 114*, 99–111.

Habermann, B. **2004**. The BAR-domain family of proteins: a case of bending and binding? *EMBO Rep. 5*, 250–255.

Hamada, K., Shimizu, T., Matsui, T., Tsukita, S., Hakoshima, T. **2000**. Structural basis of the membrane-targeting and unmasking mechanisms of the radixin FERM domain. *EMBO J. 19*, 4449–4462.

Hamada, K., Shimizu, T., Matsui, T., Tsukita, S., Hakoshima, T. **2001**. Crystallographic characterization of the radixin FERM domain bound to the cytoplasmic tail of the adhesion protein ICAM-2. *Acta Crystallogr. D Biol. Crystallogr. 57*, 891–892.

Han, S.K., Kim, K.P., Koduri, R., Bittova, L., Munoz, N.M., Leff, A.R., Wilton, D.C., Gelb, M.H., Cho, W. **1999**. Roles of Trp31 in high membrane binding and proinflammatory activity of human group V phospholipase A2. *J. Biol. Chem. 274*, 11881–11888.

Hayakawa, A., Hayes, S.J., Lawe, D.C., Sudharshan, E., Tuft, R., Fogarty, K.,

Lambright, D., Corvera, S. **2004**. Structural basis for endosomal targeting by FYVE domains. *J. Biol. Chem. 279*, 5958–5966.

Hyun, T.S., Rao, D.S., Saint-Dic, D., Michael, L.E., Kumar, P.D., Bradley, S.V., Mizukami, I.F., Oravecz-Wilson, K.I., Ross, T.S. **2004**. HIP1 and HIP1r stabilize receptor tyrosine kinases and bind 3-phosphoinositides via epsin N-terminal homology domains. *J. Biol. Chem. 279*, 14294–14306.

Itoh, T., Takenawa, T. **2002**. Phosphoinositide-binding domains: Functional units for temporal and spatial regulation of intracellular signalling. *Cell Signal. 14*, 733–743.

Itoh, T., Koshiba, S., Kigawa, T., Kikuchi, A., Yokoyama, S., Takenawa, T. **2001**. Role of the ENTH domain in phosphatidylinositol-4,5-bisphosphate binding and endocytosis. *Science 291*, 1047–1051.

Itoh, F., Divecha, N., Brocks, L., Oomen, L., Janssen, H., Calafat, J., Itoh, S., Dijke Pt, P. **2002**. The FYVE domain in Smad anchor for receptor activation (SARA) is sufficient for localization of SARA in early endosomes and regulates TGF-beta/Smad signalling. *Genes Cells 7*, 321–331.

Johnson, J.E., Edwards, A.S., Newton, A.C. **1997**. A putative phosphatidylserine binding motif is not involved in the lipid regulation of protein kinase C. *J. Biol. Chem. 272*, 30787–30792.

Kanai, F., Liu, H., Field, S.J., Akbary, H., Matsuo, T., Brown, G.E., Cantley, L.C., Yaffe, M.B. **2001**. The PX domains of $p47^{phox}$ and $p40^{phox}$ bind to lipid products of PI(3)K. *Nat. Cell Biol. 3*, 675–678.

Karathanassis, D., Stahelin, R.V., Bravo, J., Perisic, O., Pacold, C.M., Cho, W., Williams, R.L. **2002a**. Binding of the PX domain of $p47^{phox}$ to phosphatidylinositol 3,4-bisphosphate and phosphatidic acid is masked by an intramolecular interaction. *EMBO J. 21*, 5057–5068.

Karathanassis, D., Stahelin, R.V., Bravo, J., Perisic, O., Pacold, C.M., Cho, W., Williams, R.L. **2002b**. Binding of the PX domain of $p47^{phox}$ to phosphatidylinositol 3,4-bisphosphate and phosphatidic acid is masked by an intramolecular interaction. *EMBO J. 21*, 5057–5068.

Kashiwagi, K., Shirai, Y., Kuriyama, M., Sakai, N., Saito, N. **2002**. Importance of C1B domain for lipid messenger-induced targeting of protein kinase C. *J. Biol. Chem. 277*, 18037–18045.

Kavanaugh, W.M., Williams, L.T. **1994**. An alternative to SH2 domains for binding tyrosine-phosphorylated proteins. *Science 266*, 1862–1865.

Kavran, J.M., Klein, D.E., Lee, A., Falasca, M., Isakoff, S.J., Skolnik, E.Y., Lemmon, M.A. **1998**. Specificity and promiscuity in phosphoinositide binding by pleckstrin homology domains. *J. Biol. Chem. 273*, 30497–30508.

Kay, B.K., Yamabhai, M., Wendland, B., Emr, S.D. **1999**. Identification of a novel domain shared by putative components of the endocytic and cytoskeletal machinery. *Protein Sci. 8*, 435–438.

Kazanietz, M.G., Wang, S., Milne, G.W.A., Lewin, N.E., Liu, H.L., Blumberg, P.M. **1995**. Residues in the second cysteine-rich region of protein kinase Cδ relevant to phorbol ester binding as revealed by site-directed mutagenesis. *J. Biol. Chem. 270*, 21852–21859.

Kholodenko, B.N., Hoek, J.B., Westerhoff, H.V. **2000**. Why cytoplasmic signalling proteins should be recruited to cell membranes. *Trends Cell Biol. 10*, 173–178.

Kikkawa, U., Kishimoto, A., Nishizuka, Y. **1989**. The protein kinase C family: heterogeneity and its implications. *Annu. Rev. Biochem. 58*, 31–44.

Klein, D.E., Lee, A., Frank, D.W., Marks, M.S., Lemmon, M.A. **1998**. The pleckstrin homology domains of dynamin isoforms require oligomerization for high affinity phosphoinositide binding. *J. Biol. Chem. 273*, 27725–27733.

Kohout, S.C., Corbalan-Garcia, S., Torrecillas, A., Gomez-Fernandez, J.C., Falke, J.J. **2002**. C2 domains of protein kinase C isoforms alpha, beta, and gamma: activation parameters and calcium stoichiometries of the membrane-bound state. *Biochemistry 41*, 11411–11424.

Kohout, S.C., Corbalan-Garcia, S., Gomez-Fernandez, J.C., Falke, J.J. **2003**. C2 domain of protein kinase C alpha: elucidation of the membrane docking surface by site-directed fluorescence and spin labeling. *Biochemistry 42*, 1254–1265.

Kulkarni, S., Das, S., Funk, C. D., Murray, D., Cho, W. **2002**. Molecular basis of the specific subcellular localization of the C2-like domain of 5-lipoxygenase. *J. Biol. Chem. 277*, 13167–13174.

Kutateladze, T., Overduin, M. **2001**. Structural mechanism of endosome docking by the FYVE domain. *Science 291*, 1793–1796.

Kutateladze, T. G., Capelluto, D. G., Ferguson, C. G., Cheever, M. L., Kutateladze, A. G., Prestwich, G. D., Overduin, M. **2004**. Multivalent mechanism of membrane insertion by the FYVE domain. *J. Biol. Chem. 279*, 3050–3057.

Lee, J. O., Yang, H., Georgescu, M. M., Di Cristofano, A., Maehama, T., Shi, Y., Dixon, J. E., Pandolfi, P., Pavletich, N. P. **1999**. Crystal structure of the PTEN tumor suppressor: implications for its phosphoinositide phosphatase activity and membrane association. *Cell 99*, 323–334.

Lemmon, M. A. **2003**. Phosphoinositide recognition domains. *Traffic 4*, 201–213.

Lemmon, M. A., Ferguson, K. M. **2000**. Signal-dependent membrane targeting by pleckstrin homology (PH) domains. *Biochem. J. 350*, 1–18.

Lemmon, M. A., Ferguson, K. M. **2001**. Molecular determinants in pleckstrin homology domains that allow specific recognition of phosphoinositides. *Biochem. Soc. Trans. 29*, 377–384.

Lemmon, M. A., Ferguson, K. M., Abrams, C. S. **2002**. Pleckstrin homology domains and the cytoskeleton. *FEBS Lett. 513*, 71–76.

Ludtke, S. J., He, K., Wu, Y., Huang, H. W. **1994**. Cooperative membrane insertion of magainin correlated with its cytolytic activity. *Biochim. Biophys. Acta 1190*, 181–184.

Mahadevan, D., Thanki, N., Singh, J., McPhie, P., Zangrilli, D., Wang, L. M., Guerrero, C., LeVine, H., 3rd, Humblet, C., Saldanha, J., et al. **1995**. Structural studies on the PH domains of Db1, Sos1, IRS-1, and beta ARK1 and their differential binding to G beta gamma subunits. *Biochemistry 34*, 9111–9117.

Mao, Y., Nickitenko, A., Duan, X., Lloyd, T. E., Wu, M. N., Bellen, H., Quiocho, F. A. **2000**. Crystal structure of the VHS and FYVE tandem domains of Hrs, a protein involved in membrane trafficking and signal transduction. *Cell 100*, 447–456.

Marte, B. M., Downward, J. **1997**. PKB/Akt: connecting phosphoinositide 3-kinase to cell survival and beyond. *Trends Biochem. Sci. 22*, 355–358.

McCloskey, M. A., Poo, M. M. **1986**. Rates of membrane-associated reactions: reduction of dimensionality revisited. *J. Cell Biol. 102*, 88–96.

Medkova, M., Cho, W. **1998**. Differential membrane-binding and activation mechanisms of protein kinase C-alpha and -epsilon. *Biochemistry 37*, 4892–4900.

Medkova, M., Cho, W. **1999**. Interplay of C1 and C2 domains of protein kinase C-alpha in its membrane binding and activation. *J. Biol. Chem. 274*, 19852–19861.

Mehrotra, B., Myszka, D. G., Prestwich, G. D. **2000**. Binding kinetics and ligand specificity for the interactions of the C2B domain of synaptagmin II with inositol polyphosphates and phosphoinositides. *Biochemistry 39*, 9679–9686.

Mills, I. G., Praefcke, G. J., Vallis, Y., Peter, B. J., Olesen, L. E., Gallop, J. L., Butler, P. J., Evans, P. R., McMahon, H. T. **2003**. EpsinR: an AP1/clathrin interacting protein involved in vesicle trafficking. *J. Cell Biol. 160*, 213–222.

Moll, G. N., Brul, S., Konings, W. N., Driessen, A. J. **2000**. Comparison of the membrane interaction and permeabilization by the designed peptide Ac-MB21-NH_2 and truncated dermaseptin S3. *Biochemistry 39*, 11907–11912.

Murray, D., Abbruzova, A., Honig, B., McLaughlin, S. **2002**. The role of electrostatic and nonpolar interactions in the association of peripheral proteins with membranes. *Curr. Topics Membr. 52*, 277–307.

Murray, D., Honig, B. **2002**. Electrostatic control of the membrane targeting of C2 domains. *Mol. Cell 9*, 145–154.

Nalefski, E. A., Falke, J. J. **1996**. The C2 domain calcium-binding motif: structural and functional diversity. *Protein Sci. 5*, 2375–2390.

Nalefski, E. A., Falke, J. J. **1998**. Location of the membrane-docking face on the Ca^{2+}-activated C2 domain of cytosolic phospholipase A2. *Biochemistry 37*, 17642–17650.

Northrup, S.H., Erickson, H.P. **1992**. Kinetics of protein–protein association explained by Brownian dynamics computer simulation. *Proc. Natl Acad. Sci. USA 89*, 3338–3342.

Oancea, E., Meyer, T. **1998**. Protein kinase C as a molecular machine for decoding calcium and diacylglycerol signals. *Cell 95*, 307–318.

Oancea, E., Teruel, M.N., Quest, A.F., Meyer, T. **1998**. Green fluorescent protein (GFP)-tagged cysteine-rich domains from protein kinase C as fluorescent indicators for diacylglycerol signaling in living cells. *J. Cell Biol. 140*, 485–498.

Ono, Y., Fujii, T., Igarashi, K., Kuno, T., Tanaka, C., Kikkawa, U., Nishizuka, Y. **1989**. Phorbol ester binding to protein kinase C requires a cysteine-rich zinc-finger-like sequence. *Proc. Natl Acad. Sci. USA 86*, 4868–4871.

Osada, S., Mizuno, K., Saido, T.C., Akita, Y., Suzuki, K., Kuroki, T., Ohno, S. **1990**. A phorbol ester receptor/protein kinase, nPKC eta, a new member of the protein kinase C family predominantly expressed in lung and skin. *J. Biol. Chem. 265*, 22434–22440.

Pascual, J., Martinez-Yamout, M., Dyson, H.J., Wright, P.E. **2000**. Structure of the PHD zinc finger from human Williams-Beuren syndrome transcription factor. *J. Mol. Biol. 304*, 723–729.

Patki, V., Lawe, D.C., Corvera, S., Virbasius, J.V., Chawla, A. **1998**. A functional PtdIns(3)P-binding motif. *Nature 394*, 433–434.

Pearson, M.A., Reczek, D., Bretscher, A., Karplus, P.A. **2000**. Structure of the ERM protein moesin reveals the FERM domain fold masked by an extended actin binding tail domain. *Cell 101*, 259–270.

Perisic, O., Fong, S., Lynch, D.E., Bycroft, M., Williams, R.L. **1998**. Crystal structure of a calcium-phospholipid binding domain from cytosolic phospholipase A2. *J. Biol. Chem. 273*, 1596–1604.

Peter, B.J., Kent, H.M., Mills, I.G., Vallis, Y., Butler, P.J., Evans, P.R., McMahon, H.T. **2004**. BAR domains as sensors of membrane curvature: the amphiphysin BAR structure. *Science 303*, 495–499.

Pitcher, J.A., Touhara, K., Payne, E.S., Lefkowitz, R.J. **1995**. Pleckstrin homology domain-mediated membrane association and activation of the beta-adrenergic receptor kinase requires coordinate interaction with G beta gamma subunits and lipid. *J. Biol. Chem. 270*, 11707–11710.

Ponting, C.P. **1996**. Novel domains in NADPH oxidase subunits, sorting nexins, and PtdIns 3-kinases: binding partners of SH3 domains? *Protein Sci. 5*, 2353–2357.

Prehoda, K.E., Lee, D.J., Lim, W.A. **1999**. Structure of the enabled/VASP homology 1 domain-peptide complex: a key component in the spatial control of actin assembly. *Cell 97*, 471–480.

Raghunath, A., Ling, M., Larsson, C. **2003**. The catalytic domain limits the translocation of protein kinase C alpha in response to increases in Ca^{2+} and diacylglycerol. *Biochem. J. 370*, 901–912.

Rameh, L.E., Arvidsson, A., Carraway, K.L., 3rd, Couvillon, A.D., Rathbun, G., Crompton, A., VanRenterghem, B., Czech, M.P., Ravichandran, K.S., Burakoff, S.J., et al. **1997**. A comparative analysis of the phosphoinositide binding specificity of pleckstrin homology domains. *J. Biol. Chem. 272*, 22059–22066.

Ravichandran, K.S., Zhou, M.M., Pratt, J.C., Harlan, J.E., Walk, S.F., Fesik, S.W., Burakoff, S.J. **1997**. Evidence for a requirement for both phospholipid and phosphotyrosine binding via the Shc phosphotyrosine-binding domain *in vivo*. *Mol. Cell Biol. 17*, 5540–5549.

Rebecchi, M., Peterson, A., McLaughlin, S. **1992**. Phosphoinositide-specific phospholipase C-delta 1 binds with high affinity to phospholipid vesicles containing phosphatidylinositol 4,5-bisphosphate. *Biochemistry 31*, 12742–12747.

Ridley, S.H., Ktistakis, N., Davidson, K., Anderson, K.E., Manifava, M., Ellson, C.D., Lipp, P., Bootman, M., Coadwell, J., Nazarian, A., et al. **2001**. FENS-1 and DFCP1 are FYVE domain-containing proteins with distinct functions in the endosomal and Golgi compartments. *J. Cell Sci. 114*, 3991–4000.

Rizo, J., Sudhof, T.C. **1998**. C2-domains, structure and function of a universal Ca^{2+}-

binding domain. *J. Biol. Chem. 273*, 15879–15882.

Santagata, S., Boggon, T.J., Baird, C.L., Gomez, C.A., Zhao, J., Shan, W.S., Myszka, D.G., Shapiro, L. **2001**. G-protein signaling through tubby proteins. *Science 292*, 2041–2050.

Saras, J., Heldin, C.H. **1996**. PDZ domains bind carboxy-terminal sequences of target proteins. *Trends Biochem. Sci. 21*, 455–458.

Schiavo, G., Gu, Q.M., Prestwich, G.D., Sollner, T.H., Rothman, J.E. **1996**. Calcium-dependent switching of the specificity of phosphoinositide binding to synaptotagmin. *Proc. Natl Acad. Sci. USA 93*, 13327–13332.

Schultz, A., Ling, M., Larsson, C. **2004**. Identification of an amino acid residue in the protein kinase C C1b domain crucial for its localization to the Golgi network. *J. Biol. Chem. 279*, 31750–31760.

Seet, L.F., Hong, W. **2001**. Endofin, an endosomal FYVE domain protein. *J. Biol. Chem. 276*, 42445–42454.

Shao, X., Fernandez, I., Sudhof, T.C., Rizo, J. **1998**. Solution structures of the Ca^{2+}-free and Ca^{2+}-bound C2A domain of synaptotagmin I: does Ca^{2+} induce a conformational change? *Biochemistry 37*, 16106–16115.

Shirai, Y., Saito, N. **2002**. Activation mechanisms of protein kinase C: maturation, catalytic activation, and targeting. *J. Biochem. (Tokyo) 132*, 663–668.

Singh, S.M., Murray, D. **2003**. Molecular modeling of the membrane targeting of phospholipase C pleckstrin homology domains. *Protein Sci. 12*, 1934–1953.

Slater, S.J., Cook, A.C., Seiz, J.L., Malinowski, S.A., Stagliano, B.A., Stubbs, C.D. **2003**. Effects of ethanol on protein kinase C alpha activity induced by association with Rho GTPases. *Biochemistry 42*, 12105–12114.

Smith, W.J., Cerione, R.A. **2002**. Crystallization and preliminary crystallographic analysis of the ezrin FERM domain. *Acta Crystallogr. D Biol. Crystallogr. 58*, 1359–1361.

Smith, W.J., Nassar, N., Bretscher, A., Cerione, R.A., Karplus, P.A. **2003**. Structure of the active N-terminal domain of Ezrin. Conformational and mobility changes identify keystone interactions. *J. Biol. Chem. 278*, 4949–4956.

Song, X., Xu, W., Zhang, A., Huang, G., Liang, X., Virbasius, J.V., Czech, M.P., Zhou, G.W. **2001**. Phox homology domains specifically bind phosphatidylinositol phosphates. *Biochemistry 40*, 8940–8944.

Stahelin, R.V., Cho, W. **2001**. Differential roles of ionic, aliphatic, and aromatic residues in membrane–protein interactions: a surface plasmon resonance study on phospholipases A2. *Biochemistry 40*, 4672–4678.

Stahelin, R.V., Long, F., Diraviyam, K., Bruzik, K.S., Murray, D., Cho, W. **2002**. Phosphatidylinositol 3-phosphate induces the membrane penetration of the FYVE domains of Vps27p and Hrs. *J. Biol. Chem. 277*, 26379–26388.

Stahelin, R.V., Burian, A., Bruzik, K.S., Murray, D., Cho, W. **2003a**. Membrane binding mechanisms of the PX domains of NADPH oxidase $p40^{phox}$ and $p47^{phox}$. *J. Biol. Chem. 278*, 14469–14479.

Stahelin, R.V., Long, F., Peter, B.J., Murray, D., De Camilli, P., McMahon, H.T., Cho, W. **2003b**. Contrasting membrane interaction mechanisms of AP180 N-terminal homology (ANTH) and epsin N-terminal homology (ENTH) domains. *J. Biol. Chem. 278*, 28993–28999.

Stahelin, R.V., Rafter, J.D., Das, S., Cho, W. **2003c**. The molecular basis of differential subcellular localization of C2 domains of protein kinase C-alpha and group IVa cytosolic phospholipase A2. *J. Biol. Chem. 278*, 12452–12460.

Stahelin, R.V., Ananthanarayanan, B., Blatner, N.R., Bruzik, K.S., Murray, D., Cho, W. **2004a**. Mechanism of membrane binding of the phospholipase D1 PX domain. *J. Biol. Chem. 279*, 54918–54926.

Stahelin, R.V., Digman, M.A., Medkova, M., Ananthanarayanan, B., Rafter, J.D., Melowic, H.R., Cho, W. **2004b**. Mechanism of diacylglycerol-induced membrane targeting and activation of protein kinase Cdelta. *J. Biol. Chem. 279*, 29501–29512.

Stenmark, H. **2001**. Introduction. Trafficking of lipids. *Semin. Cell Dev. Biol. 12*, 135–137.

Stenmark, H., Gillooly, D. J. **2001**. Intracellular trafficking and turnover of phosphatidylinositol 3-phosphate. *Semin. Cell Dev. Biol. 12*, 193–199.

Stenmark, H., Aasland, R., Driscoll, P. C. **2002**. The phosphatidylinositol 3-phosphate-binding FYVE finger. *FEBS Lett. 513*, 77–84.

Stolt, P. C., Jeon, H., Song, H. K., Herz, J., Eck, M. J., Blacklow, S. C. **2003**. Origins of peptide selectivity and phosphoinositide binding revealed by structures of disabled-1 PTB domain complexes. *Structure (Camb.) 11*, 569–579.

Sutton, R. B., Sprang, S. R. **1998**. Structure of the protein kinase Cbeta phospholipid-binding C2 domain complexed with Ca^{2+}. *Structure 6*, 1395–1405.

Sutton, R. B., Davletov, B. A., Berghuis, A. M., Sudhof, T. C., Sprang, S. R. **1995**. Structure of the first C2 domain of synaptotagmin I: a novel Ca^{2+}/phospholipid-binding fold. *Cell 80*, 929–938.

Szallasi, Z., Smith, C. B., Pettit, G. R., Blumberg, P. M. **1994**. Differential regulation of protein kinase C isozymes by bryostatin 1 and phorbol 12-myristate 13-acetate in NIH 3T3 fibroblasts. *J. Biol. Chem. 269*, 2118–2124.

Takei, K., Slepnev, V. I., Haucke, V., De Camilli, P. **1999**. Functional partnership between amphiphysin and dynamin in clathrin-mediated endocytosis. *Nat. Cell Biol. 1*, 33–39.

Takeuchi, H., Matsuda, M., Yamamoto, T., Kanematsu, T., Kikkawa, U., Yagisawa, H., Watanabe, Y., Hirata, M. **1998**. PTB domain of insulin receptor substrate-1 binds inositol compounds. *Biochem. J. 334*, 211–218.

Tarricone, C., Xiao, B., Justin, N., Walker, P. A., Rittinger, K., Gamblin, S. J., Smerdon, S. J. **2001**. The structural basis of Arfaptin-mediated cross-talk between Rac and Arf signalling pathways. *Nature 411*, 215–219.

Teruel, M. N., Meyer, T. **2000**. Translocation and reversible localization of signaling proteins: a dynamic future for signal transduction. *Cell 103*, 181–184.

Touhara, K., Koch, W. J., Hawes, B. E., Lefkowitz, R. J. **1995**. Mutational analysis of the pleckstrin homology domain of the beta-adrenergic receptor kinase. Differential effects on G beta gamma and phosphatidylinositol 4,5-bisphosphate binding. *J. Biol. Chem. 270*, 17000–17005.

Tsukazaki, T., Chiang, T. A., Davison, A. F., Attisano, L., Wrana, J. L. **1998**. SARA, a FYVE domain protein that recruits Smad2 to the TGFbeta receptor. *Cell 95*, 779–791.

Tuzi, S., Uekama, N., Okada, M., Yamaguchi, S., Saito, H., Yagisawa, H. **2003**. Structure and dynamics of the phospholipase C-delta1 pleckstrin homology domain located at the lipid bilayer surface. *J. Biol. Chem. 278*, 28019–28025.

Verdaguer, N., Corbalan-Garcia, S., Ochoa, W. F., Fita, I., Gomez-Fernandez, J. C. **1999**. Ca^{2+} bridges the C2 membrane-binding domain of protein kinase Calpha directly to phosphatidylserine. *EMBO J. 18*, 6329–6338.

Vetter, I. R., Nowak, C., Nishimoto, T., Kuhlmann, J., Wittinghofer, A. **1999**. Structure of a Ran-binding domain complexed with Ran bound to a GTP analogue: implications for nuclear transport. *Nature 398*, 39–46.

Wang, Q. J., Fang, T. W., Fenick, D., Garfield, S., Bienfait, B., Marquez, V. E., Blumberg, P. M. **2000**. The lipophilicity of phorbol esters as a critical factor in determining the pattern of translocation of protein kinase C delta fused to green fluorescent protein. *J. Biol. Chem. 275*, 12136–12146.

Wang, Q. J., Fang, T. W., Nacro, K., Marquez, V. E., Wang, S., Blumberg, P. M. **2001**. Role of hydrophobic residues in the C1b domain of protein kinase C delta on ligand and phospholipid interactions. *J. Biol. Chem. 276*, 19580–19587.

Wang, T., Pentyala, S., Rebecchi, M. J., Scarlata, S. **1999**. Differential association of the pleckstrin homology domains of phospholipases C-beta 1, C-beta 2, and C-delta 1 with lipid bilayers and the beta gamma subunits of heterotrimeric G proteins. *Biochemistry 38*, 1517–1524.

Wiener, M. C., White, S. H. **1992**. Structure of a fluid dioleoylphosphatidylcholine bilayer determined by joint refinement of X-ray and neutron diffraction data. III. Complete structure. *Biophys. J. 61*, 437–447.

Wientjes, F. B., Reeves, E. P., Soskic, V., Furthmayr, H., Segal, A. W. **2001**. The

NADPH oxidase components p47^{phox} and p40^{phox} bind to moesin through their PX domain. *Biochem. Biophys. Res. Commun. 289*, 382–388.

Wishart, M. J., Taylor, G. S., Dixon, J. E. **2001**. Phoxy lipids: revealing PX domains as phosphoinositide binding modules. *Cell 105*, 817–820.

Xing, Y., Liu, D., Zhang, R., Joachimiak, A., Songyang, Z., Xu, W. **2004**. Structural basis of membrane targeting by the phox homology domain of cytokine-independent survival kinase (CISK-PX). *J. Biol. Chem. 279*, 30662–30669.

Xu, R. X., Pawelczyk, T., Xia, T. H., Brown, S. C. **1997**. NMR structure of a protein kinase C-gamma phorbol-binding domain and study of protein–lipid micelle interactions. *Biochemistry 36*, 10709–10717.

Xu, Y., Hortsman, H., Seet, L., Wong, S. H., Hong, W. **2001 a**. SNX3 regulates endosomal function through its PX-domain-mediated interaction with PtdIns(3)P. *Nat. Cell Biol. 3*, 658–666.

Xu, Y., Seet, L. F., Hanson, B., Hong, W. **2001 b**. The Phox homology (PX) domain, a new player in phosphoinositide signalling. *Biochem. J. 360*, 513–530.

Yan, K. S., Kuti, M., Zhou, M. M. **2002**. PTB or not PTB – that is the question. *FEBS Lett. 513*, 67–70.

Yang, C., Kazanietz, M. G. **2003**. Divergence and complexities in DAG signaling: looking beyond PKC. *Trends Pharmacol. Sci. 24*, 602–608.

Yoon, H. S., Hajduk, P. J., Petros, A. M., Olejniczak, E. T., Meadows, R. P., Fesik, S. W. **1994**. Solution structure of a pleckstrin-homology domain. *Nature 369*, 672–675.

Yu, J. W., Lemmon, M. A. **2001**. All phox homology (PX) domains from Saccharomyces cerevisiae specifically recognize phosphatidylinositol 3-phosphate. *J. Biol. Chem. 276*, 44179–44184.

Zhang, B., Zelhof, A. C. **2002**. Amphiphysins: raising the BAR for synaptic vesicle recycling and membrane dynamics. Bin-Amphiphysin-Rvsp. *Traffic 3*, 452–460.

Zhang, G., Kazanietz, M. G., Blumberg, P. M., Hurley, J. H. **1995**. Crystal structure of the cys2 activator-binding domain of protein kinase C delta in complex with phorbol ester. *Cell 81*, 917–924.

Zhou, C. Z., de La Sierra-Gallay, I. L., Quevillon-Cheruel, S., Collinet, B., Minard, P., Blondeau, K., Henckes, G., Aufrere, R., Leulliot, N., Graille, M., et al. **2003**. Crystal structure of the yeast Phox homology (PX) domain protein Grd19p complexed to phosphatidylinositol-3-phosphate. *J. Biol. Chem. 278*, 50371–50376.

Zhou, M. M., Ravichandran, K. S., Olejniczak, E. F., Petros, A. M., Meadows, R. P., Sattler, M., Harlan, J. E., Wade, W. S., Burakoff, S. J., Fesik, S. W. **1995**. Structure and ligand recognition of the phosphotyrosine binding domain of Shc. *Nature 378*, 584–592.

Zimmerberg, J., McLaughlin, S. **2004**. Membrane curvature: how BAR domains bend bilayers. *Curr. Biol. 14*, R250–R252.

Zimmermann, P., Meerschaert, K., Reekmans, G., Leenaerts, I., Small, J. V., Vandekerckhove, J., David, G., Gettemans, J. **2002**. PIP_2-PDZ domain binding controls the association of syntenin with the plasma membrane. *Mol. Cell 9*, 1215–1225.

16
Structure and Interactions of C2 Domains at Membrane Surfaces

David S. Cafiso

16.1
Introduction

The attachment of proteins to membrane interfaces is an important event for many cellular processes, including membrane trafficking and cell signaling. Membrane attachment regulates the biochemistry of the cell through a number of different mechanisms.

1. The substrates for many enzymes involved in signaling are lipids and membrane association brings these enzymes in proximity to their substrates.
2. Membrane binding limits protein diffusion to a two-dimensional surface, and this reduction in dimensionality enhances the probability of appropriate protein–protein interactions and allows for the assembly of proteins into localized domains that function in signaling.
3. Membrane binding may promote structural changes in proteins and rearrangements of structural domains resulting in enzymatic activation. As a result, the reversible mechanisms by which proteins become attached to membrane surfaces become critical regulators of cellular events.

There are several mechanisms by which proteins become attached to membrane surfaces. Protein acylation is one general mechanism that can attach proteins to interfaces and this typically involves either myristoylation or palmitoylation [1]. Protein acylation sometimes takes place in tandem with an electrostatic interaction between a basic (positively charged) protein motif and a membrane interface containing phosphatidylserine (PS) or other negatively charged lipids. These general mechanisms can be regulated by events such as phosphorylation. In the case of the myristoylated alanine-rich C-kinase substrate (MARCKS), both myristoylation and electrostatic interactions are present; however, neither interaction alone is sufficient for membrane attachment [2, 3]. As a result, phosphorylation within the highly charged effector domain of MARCKS (MARCKS-ED) reduces the electrostatic interaction and dissociates the MARCKS from the membrane.

In addition to acylation and basic sequences, protein domains have been identified that bind membrane surfaces by recognizing specific lipids or lipid surfaces. C2 and PH domains are some of the best characterized of these lipid-binding domains; although other domains that recognize specific phosphorylated inositols, such as FYVE, ENTH and PX domains, have been identified. Membrane-binding domains function in a highly coordinated fashion to regulate cell-signaling events and membrane trafficking, and their importance to the cell is underscored by the observation that they are the most abundant domains found in proteins [4]. In this chapter the function of C2 domains and the physical chemistry that guides their association with membrane interfaces will be discussed.

16.2
C2 Domains: Ca^{2+}-dependent and Ca^{2+}-independent Membrane Binding

C2 domains were first identified as the second conserved domain in calcium-dependent isoforms of protein kinase C (PKC) and they have been identified in numerous Ca^{2+}-regulatory proteins found in eukaryotic systems [5, 6]. These domains are found in a wide range of signaling proteins that are central to the production of lipid-derived second messengers, protein phosphorylation, membrane trafficking, protein ubiquitination, membrane pore formation and GTPase regulation [5, 6]. For example, cytosolic phospholipase A_2-α ($cPLA_2$) is a water-soluble lipase with a C2 domain that mediates binding to specific intracellular membranes in a Ca^{2+}-dependent manner [7]. Upon membrane association, the enzymatic domain hydrolyzes target lipids to release arachidonic acid, triggering

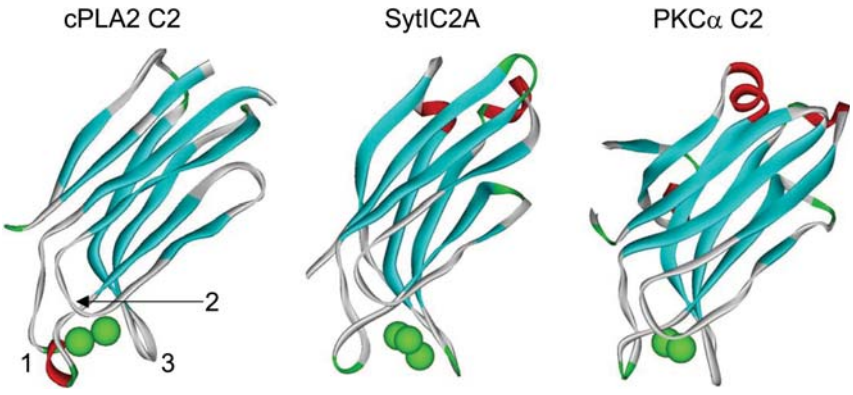

Fig. 16.1 Structures of C2 domains. $cPLA_2$ C2 (1BCI) [14], sytIC2A (1BYN) [15] and PKCα (1DSY) [27]. Three loops on one end of the β-sandwich surround the Ca^{2+} sites. Bound Ca^{2+} ions are highlighted in green. The $cPLA_2$ C2 domain is topology type II; both the PKCα and sytI domains are type I.

the synthesis of eicosanoids that activate various pathways including inflammation (8–10). High-resolution structures have been obtained for a number of C2 domains including those found in $cPLA_2$, synaptotagmin, PKC and phospholipase C (PLC) [11–19].

Fig. 16.1 shows high-resolution structures of several C2 domains. C2 domains are relatively compact and have a common fold consisting of an eight-stranded antiparallel β-sandwich. There are two types of morphologies of C2 domains, depending upon the position of the C- and N-termini within the domain fold [20], and three loops at one end of the sandwich that generally bind two or more Ca^{2+} ions.

In general, C2 domains appear to function as membrane-binding modules and C2 domains are often found to bind to membranes in a Ca^{2+}-dependent fashion. However, C2 domains have been identified that bind to membranes in a Ca^{2+}-independent fashion, such as the domain from a human coagulation factor [21]. In addition, there are reports that C2 domains function as protein-binding modules [22–24].

16.3 What Drives Membrane Targeting of C2 Domains?

As indicated above, many C2 domains acquire the capacity to bind to membrane surfaces in the presence of Ca^{2+} and several different forces have been proposed to drive the interaction between the C2 domain and the membrane interface. For example, the C2 domains from synaptotagmin I (sytI) require negatively charged lipid such as PS or phosphatidylinositol (PI) for membrane binding. In this case, the binding is more dependent upon surface charge density than the headgroup type and positively charged residues near the Ca^{2+} binding sites appear to be important in membrane binding [25]. As a result, it has been proposed that Ca^{2+} binding induces membrane attachment through a long-range Coulombic interaction by creating a positively charged protein surface. In this model, the binding of Ca^{2+} to the C2 domain acts as an electrostatic switch. This long-range electrostatic interaction does not appear to play a role in the Ca^{2+}-dependent binding of the C2 domain from $cPLA_2$, which does not require negatively charged lipid and will bind to membranes containing only zwitterionic lipids, such as phosphatidylcholine (PC).

In addition to electrostatics, several other interactions are thought to attach C2 domains to membranes. For example, Ca^{2+} binding to the C2 domain of PLCδ1 has been proposed to induce structural changes in the loops, thereby opening up a binding site for phospholipid and exposing hydrophobic residues that insert into the membrane interface [26]. However, many C2 domains do not appear to exhibit significant structural changes upon Ca^{2+} binding that would trigger such an interaction [15]. Direct coordination between the lipid headgroup and the C2 domain has also been proposed to drive binding. Indeed, high-resolution crystal structures of the C2 domain from PKCα indicate that

there is a direct coordination between the phosphoryl group of PS and one of the bound Ca^{2+} ions [27].

Evidence for the direct role of coordination comes from observations showing that C2 domains have higher affinity for Ca^{2+} in the presence of lipid [28]. The first C2 domain of sytI (sytIC2A) has three Ca^{2+}-binding sites (see Fig. 16.1) and, in solution, one of these sites is incompletely coordinated by the protein [23]. In solution, this third binding site also has a low affinity for Ca^{2+}, which increases by approximately two orders of magnitude upon membrane binding. This increase in Ca^{2+} binding could result from coordination of the third Ca^{2+}-binding site, and it has been proposed that phospholipids, such as PS, provide the coordination for this third site and contribute to the driving force for membrane attachment [25]. However, it should be noted that some fraction of this binding affinity increase may be attributed to an increased Ca^{2+} concentration at the membrane interface. Membranes containing negative charged lipids have a negative surface potential, and, in response to this electrostatic surface potential, Ca^{2+} will be more concentrated at the interface [29] and the apparent Ca^{2+} affinity will be raised. For example, with a negative surface potential of –40 mV, Ca^{2+} will be concentrated at the membrane surface by a factor of 20 over that in the bulk aqueous phase.

16.4
Electrostatic Binding of Simple Linear Protein Motifs

Positively charged regions of proteins are known to attach to negatively charged membrane surfaces as a result of a long-range electrostatic interaction [30], and some of the principles by which these simple motifs attach are also likely to play a role in the membrane attachment of C2 and other membrane-binding domains. Fig. 16.2 shows a model for the interaction of the effector domain of MARCKS-ED based upon both nuclear magnetic resonance (NMR) and electron paramagnetic resonance (EPR) data [31–33]. This motif (MARCKS 151–175–181) has the sequence KKKKKRFSFKKSFKLSGFSFKKNKK and contains 13 positive charged side-chains within its 25-residue stretch. It interacts electrostatically with membranes composed of PS, but penetrates the bilayer with its five phenylalanine residues buried within the lipid interface; thus, hydrophobic interactions clearly also contribute to the interaction. The importance and interplay of electrostatic and hydrophobic interactions of MARCKS-ED is revealed by the binding and location of this motif lacking the five phenylalanine residues (FA-MARCKS) [34]. Fig. 16.2 also shows the position of this derivative, which binds approximately 3–5 Å above the membrane interface and lies within the aqueous double layer. This interaction is electrostatic and although this segment binds, it does not contact the membrane interface. It is prevented from contacting as a result of a short-range dehydration force that becomes important close to the membrane surface. This dehydration force may have several components, including a Born repulsion resulting from the interaction of the electrostatic

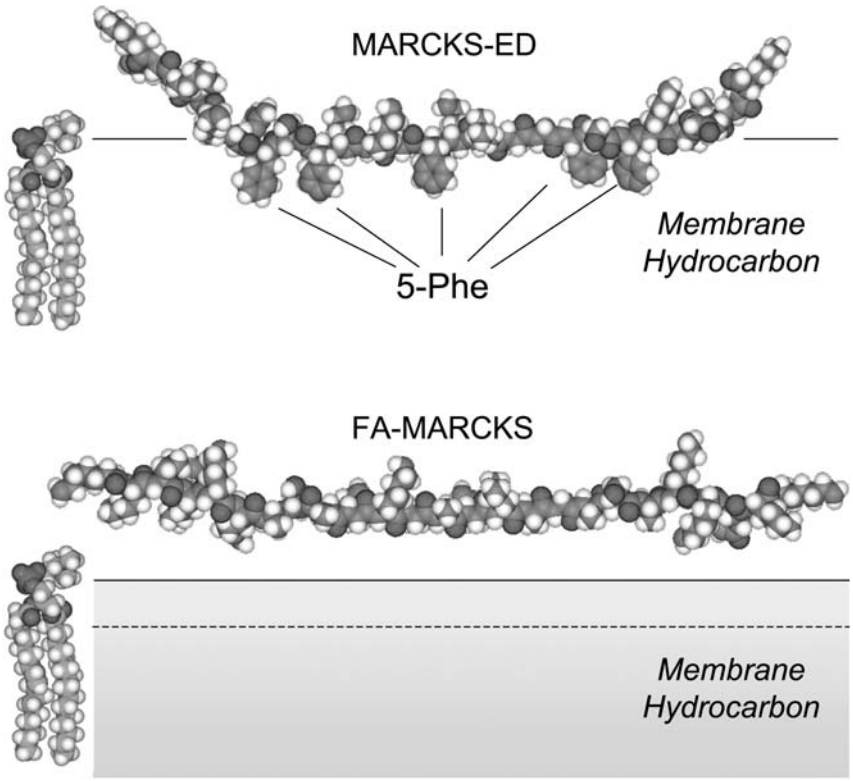

Fig. 16.2 Top: Model for the position of MARCKS-ED on the membrane interface from data obtained by NMR and site-directed spin labeling [32, 33, 36]. The five phenylalanine residues are positioned within the membrane hydrocarbon near the interface. This position is a result of the action of three forces: a long-range Coulombic attraction, a repulsive dehydration force and a hydrophobic interaction. Bottom: Model for the position of FA-MARCKS, which lacks the five phenylalanines, on the membrane interface based upon site-directed spin-labeling [34]. The hydrophobic contribution to the binding has been eliminated, and the position of the peptide in the double layer is determined by the balance between a short-range dehydration force and a long-range electrostatic attraction.

field from the charged side-chains with the low-dielectric membrane interior and a conformational entropy loss that is experienced by the peptide near the membrane interface [35–38].

Phosphatidylinositol 4,5-bisphosphate [PI(4,5)P_2] plays a central role as a signaling molecule and as a precursor to other second messengers [39], and MARCKS may function as a key regulator of PI(4,5)P_2 activity within the membrane. In addition to its interaction with membranes containing PS, MARCKS-ED interacts strongly with membranes containing PI(4,5)P_2. Remarkably, this segment binds more strongly to PC membranes containing 1 mol% PI(4,5)P_2 than to PC membranes containing 17 mol% PS [40, 41]. The interaction be-

tween MARCKS-ED and PI(4,5)P_2 membranes is also driven by electrostatics, but the strong interaction with PI(4,5)P_2 is due the valence on this lipid ($z=-3$ to -4 at pH 7.0) and the fact that three to four PI(4,5)P_2 associate with MARCKS in the plane of the membrane [42]. This interaction sequesters PI(4,5)P_2 within the plane of the membrane and this is a process that has been observed for a number of other positively charged protein motifs [43–46]. It has been proposed that a primary role of MARCKS is to sequester PI(4,5)P_2. Phosphorylation of the effector domain or binding of the effector domain to Ca^{2+}-CaM removes MARCKS from the membrane surface and increases the availability of PI(4,5)P_2 within the plane of the bilayer.

The position of the positively charged lysine and arginine residues of MARCKS-ED at the membrane surface appears to enhance the interaction of this motif with PI(4,5)P_2. When FA-MARCKS is examined (which is not attached to the membrane interface; see Fig. 16.2), its capacity to sequester PI(4,5)P_2 is reduced relative to that of MARCKS-ED [46]. Electrostatic calculations indicate that the proximity of the charged residues of MARCKS-ED to the membrane interface extends the electrostatic field from these changed sidechains in the plane of the membrane and is responsible for enhancing peptide–lipid electrostatic interactions [42].

16.5
The Results of Electrostatic Calculations on C2 Domains

The electrostatic potentials on the C2 domains of cPLA_2 and sytIC2A have been calculated and compared, and the results reveal two possible roles for an electrostatic regulation of membrane attachment [47]. Fig. 16.3 shows electrostatic potential surfaces for the C2 domain from cPLA_2 and sytIC2A. For sytIC2A, the binding of Ca^{2+} alters the potential near the membrane-binding surface of the domain so that it takes on a positive electrostatic potential. This suggests that Ca^{2+} may drive the membrane binding of the sytIC2A domain through a long-range Coulombic attraction. Thus, the same type of electrostatic interaction that drives membrane association of MARCKS-ED may also drive the association of sytIC2A. For the C2 domain from cPLA_2, the electrostatic potential at the membrane-binding surface of the domain is dramatically reduced in the presence of Ca^{2+}, so that this surface has neither a high negative nor positive potential. It has been proposed that Ca^{2+} binding lowers the dehydration energy for this end of the domain, allowing it to insert into neutral PC membranes.

These electrostatic potential profiles make functional sense when one considers that the sytIC2A domain requires negatively charged lipid to bind, whereas the cPLA_2 C2 domain does not.

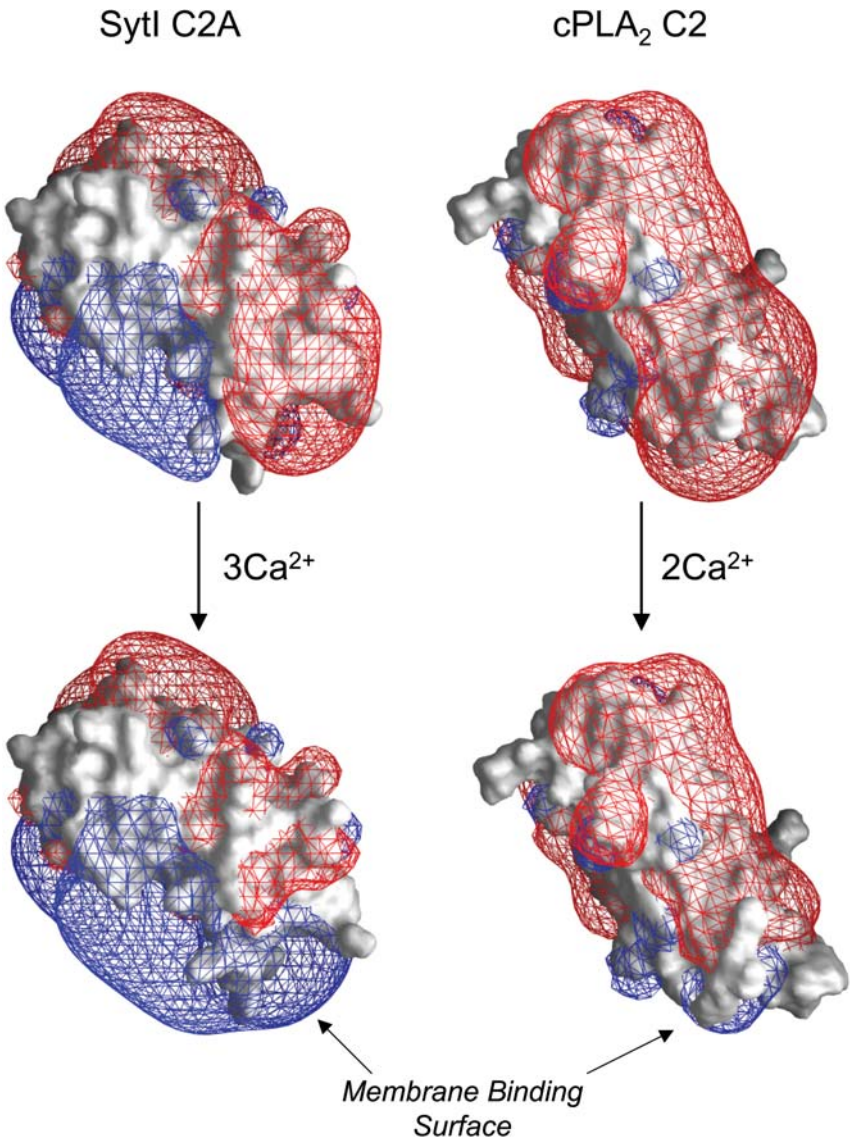

Fig. 16.3 Electrostatic potential surfaces on the $cPLA_2$ C2 and sytIC2A domains without and with bound Ca^{2+} ions calculated using the finite-difference Poisson Boltzmann method [47] determined for 0.1 M KCl. Blue: $+kT/e$ and red: $-kT/e$. Ca^{2+} binding polarizes the membrane binding surface of the sytI domain, whereas Ca^{2+} binding to the $cPLA_2$ domain lowers the electrostatic potential and reduces the dehydration energy for the membrane binding face. (The figures were kindly provided by Diana Murray).

16.6
Determining the Interactions and Positions of C2 Domains

Although high-resolution structures for C2 domains have been obtained through crystallography and solution NMR spectroscopy, these methods do not provide information regarding the membrane orientation and depth of penetration of C2 domains. As indicated above, several different forces may drive the association of C2 domains with membrane interfaces, and information on the orientation and position of these domains should help determine which forces are important. If the lipid headgroup provides coordination for protein bound Ca^{2+}, the Ca^{2+}-binding sites would be expected to lie close to the membrane interface. If the interactions of the domain are purely electrostatic (as they are for FA-MARCKS, see Fig. 16.2), penetration of the domain into the membrane interior should not take place. Information on the membrane orientation and penetration of C2 domains may also prove critical to understanding their function. For example, in the case of the C2 domains from sytI, the membrane interactions of these domains may also provide insight into the mechanisms by which these C2 domains trigger neuronal exocytosis.

16.6.1
Site-directed Mutagenesis

Information on the interactions made by C2 domains with membrane interfaces has been obtained using a number of different approaches. For example, site-directed mutagenesis has been used to identify residues responsible for the membrane binding of C2 domains. Mutation of the aspartic acid residues that bind Ca^{2+} in the C2 domain of $cPLA_2$ dramatically reduces $cPLA_2$ membrane binding and enzymatic activity, as does mutation of a number of hydrophobic residues positioned in the Ca^{2+}-binding loops [48, 49]. On the other hand, mutation of four cationic residues in a β-strand has a minimal effect on the binding of the $cPLA_2$ C2 domain to zwitterionic or anionic membranes [49]. Taken together, these data indicate that the membrane binding of the $cPLA_2$ domain is driven largely by hydrophobic interactions.

A similar mutagenesis study on the C2 domain of PKCα identified arginine and tryptophan residues that were important in electrostatic binding and membrane penetration of the C2 domain [50]. Like the study on the $cPLA_2$ domain, mutagenesis of the Asp residues participating in Ca^{2+} binding showed that they were important in binding but not equivalent in their importance for function.

16.6.2
Chemical Labeling

Chemical labeling approaches have been used to examine the binding of C2 domains. For example, evidence has been obtained for Ca^{2+}-dependent penetration of C2 domains into membranes through photolabeling with [^{125}I]TID [3-(tri-

fluoromethyl)-3-(*m*-[^{125}I]iodophenyl)diazirine] [51]. This reagent labels hydrophobic surfaces of proteins and was shown to extensively label the cPLA$_2$ C2 domain when it was membrane bound, but not label the sytIC2A domain when it was membrane bound. This finding is consistent with the idea that the cPLA$_2$ C2 domain interacts primarily through hydrophobic interactions whereas the sytIC2A interacts electrostatically.

16.6.3
Fluorescence

Fluorescence methods represent a powerful approach to determine the membrane orientation and penetration of C2 domains. This has typically involved the incorporation of site-specific fluorescence probes either by site-directed mutagenesis to tryptophan or to cysteine, followed by labeling (in the case of cysteine) with a sulfhydryl reactive fluorescent probe. The membrane-binding region of the C2 domain of cPLA$_2$ was determined through the fluorescein derivatization of single cysteine residues [52]. The fluorescence emission spectra of these labels change intensity and wavelength as a function of Ca^{2+} and membrane binding, and indicate the sites of interaction between the domain and the membrane interface. The use of aqueous quenchers, such as iodine, reveals the labeled residues that become protected from the aqueous environment upon membrane binding. The results of these experiments indicated that fluorescent labels from each of the three Ca^{2+}-binding loops penetrated the membrane interface. For this same C2 domain, a series of mutants containing single tryptophan residues were used along with membrane bound nitroxides as quenchers. Using this approach the data indicate that the first and third Ca^{2+}-binding loops of the cPLA$_2$ C2 domain penetrate the lipid bilayer [48].

Using a fluorescence approach single, native phenylalanine residues were replaced by tryptophans within the Ca^{2+}-binding region of the sytIC2A domain [53]. The quenching of fluorescence produced by lipids with spin-labels at different depths indicated that some of these tryptophans penetrated deeply into the lipid hydrocarbon. This result contrasts somewhat with the work described above using chemical labeling, which indicates little penetration of the domain.

16.6.4
Site-directed Spin Labeling (SDSL) to Determine C2 Domain Orientation

SDSL is an approach that involves a combination of site-directed mutagenesis and EPR spectroscopy, and it has been used successfully to determine protein structure, conformational changes and dynamics in both membrane and soluble proteins [54–57]. SDSL involves the incorporation of a single reactive site by site-directed mutagenesis, which is typically a cysteine, followed by the reaction of that residue by a chemically reactive spin-label. This approach replaces the normal protein side-chain with a spin-labeled side-chain. Although a range of probes can be chosen, the side-chain termed “R1” is typically incorporated (see

Fig. 16.4). The EPR line shapes that result from this protein associated spin-label reflect the local secondary structure and tertiary environment of the label. This connection between line shape and structure takes place because averaging of the anisotropic magnetic interactions of this label are determined by its rates and amplitudes of motion, which are in turn uniquely determined by the local environment and structure [58].

Information on the distance of nitroxides along the bilayer normal may be obtained by measuring the effect of a secondary paramagnetic species, such as oxygen or a paramagnetic metal, on the relaxation rates of the nitroxide. The enhancements in relaxation rate produced by oxygen or paramagnetic metal are proportional to their local concentration. These relaxation rates can be determined either by continuous wave or pulse methods [59–61].

The first measurements to determine the orientation of a C2 domain using SDSL were carried out on the C2 domain from cPLA$_2$. In this study, distances of spin-labels from the membrane interface were determined by measuring the effect of potassium tris (oxalato) chromate (CrOx) on the power saturation behavior of the nitroxide [62]. In the presence of a highly charged lipid interface, a concentration gradient in CrOx (a negatively charged chelate) is established within the aqueous double layer. Distance information is obtained by measuring the enhancement produced by CrOx in the spin-lattice relaxation rate (T_{1e}) of a nitroxide attached to the C2 domain. This enhancement is directly proportional to the collision frequency with CrOx and hence its local concentration. Because the distance dependence of the concentration of CrOx through the interface is known, this measurement yields a position for the label.

An alternate method for aligning this C2 domain with respect to the membrane interface involves measuring the enhancement in T_{1e} produced by both oxygen and Ni(II)EDDA, a neutral paramagnetic species. These data may then be used to obtain a membrane depth parameter [63]. As described elsewhere, these two paramagnetic species exhibit opposite gradients through the interface and their effect upon the relaxation behavior of a nitroxide allows the position of that nitroxide to be determined within the bilayer interior [60].

The advantage of the first approach (using CrOx) is that it is sensitive to distances within a Debye length of the membrane interface, whereas the O_2–Ni(II) measurement becomes insensitive to distances more than 5 Å on the aqueous

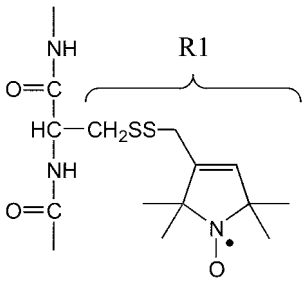

Fig. 16.4 Reaction of a free cysteine with a sulfhydryl specific methanethiosulfonate spin-label [(1-oxyl-2,2,5,5-tetramethyl-Δ^3-pyrroline-3-methyl)-methanethiosulfonate] produces the spin-labeled side-chain R1 [87].

side of the membrane interface. Thus, the CrOx approach has the potential to provide distance constraints for many labels that may lie well within the aqueous phase. A disadvantage of the approach using CrOx is that it requires the use of unusual membrane compositions with high negative surface potentials. In addition, the charge on CrOx is not well defined and this approach assumes that the ionization state of the protein does not change near the interface. Nonetheless, this method is likely to be appropriate for membrane-binding domains that are not strongly influenced by electrostatic interactions with the membrane interface.

Using distance constraints obtained through either method, the position of the domain at the membrane interface may be determined to medium resolution by finding the best fit of the orientation and depth of the C2 domain to the experimental distances. This fitting presumes that the high-resolution structure of the domain, obtained by NMR or crystallography, is maintained upon membrane binding. In the case of the C2 domain from $cPLA_2$, both approaches to generate distances produce similar results for the orientation and binding of the domain. As shown in Fig. 16.5, the domain penetrates the membrane interface and interacts primarily through its first and third Ca^{2+}-binding loops.

This model indicates that significant hydrophobic contact occurs between this domain and the membrane interior, and that several of the labeled sites penetrate deeply within the membrane interface. This finding is consistent with the results of electrostatic calculations, which indicate that the binding of Ca^{2+} to the membrane interacting loops of this domain functions to reduce the hydration energy of these loops thereby permitting membrane insertion (see Fig. 16.3). A more detailed study of the interaction of the $cPLA_2$ C2 domain has been carried out, by making measurements on spin-labels at nearly every position within the membrane binding loops [64]. This work indicates that there are minimal changes in loop structure upon Ca^{2+} binding or membrane binding for this domain.

A similar approach has been used to determine the membrane interactions made by the first C2 domain of sytI, and the best fit orientation of this domain is shown in Fig. 16.5. The orientation of this domain is similar to that of the $cPLA_2$ domain, with both the first and third Ca^{2+}-binding loops penetrating below the level of the lipid phosphates. The sytIC2A domain does not appear sit as deep within the membrane interface as does the domain from $cPLA_2$, a result that is consistent with the idea that a long-range Coulombic attraction between the domain and the membrane interface plays a role in the Ca^{2+}-dependent binding of sytIC2A. The interaction of the C2A domain with the membrane interface is, however, not purely electrostatic as a number of residues in the Ca^{2+}-binding loop regions are buried within the bilayer interface.

In the case of the sytIC2A domain, Ca^{2+} binding appears to alter the dynamics of the Ca^{2+}-binding loops. EPR spectra have been shown to be sensitive to local backbone motion [65, 66] and the effect of Ca^{2+} on the EPR spectra obtained for site T176R1 in the first Ca^{2+}-binding loop are shown in Fig. 16.6. The changes in these spectra do not result from tertiary contact of the label, but reflect a change

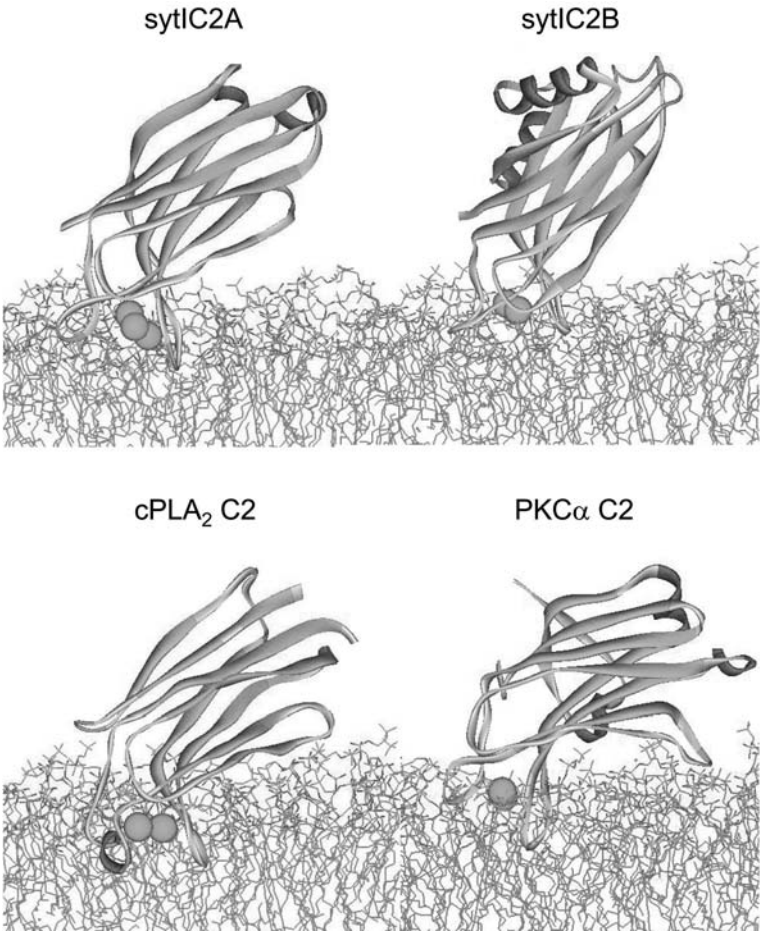

Fig. 16.5 Medium-resolution models for the membrane position of the C2 domains from sytI, $cPLA_2$ and PKCα determined by site-directed spin-labeling [63, 64, 67–69]. The domains make similar interactions with the interface; however, the $cPLA_2$ domain appears to make more hydrophobic contact with the membrane interface. The models are shown superimposed on a simulated bilayer [88].

in backbone motion. The simulations of these EPR spectra are also shown (grey lines) and indicate that Ca^{2+} produces to a 2-fold increase in the order parameter of the nitroxide, which if related totally to backbone dynamics would correspond to an increase in backbone rocking motion of about 8°. Although it is difficult to quantitatively assess, this result suggests that Ca^{2+} binding to the domain may also enhance membrane binding by reducing a conformational entropy loss which might otherwise take place upon membrane binding [67].

Site-directed spin-labeling has also been used to determine the orientations for the C2 domain from PKCα [68] and sytIC2B [69]. For these domains, both

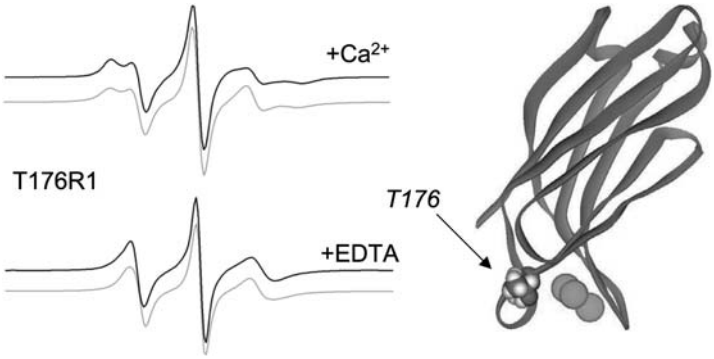

Fig. 16.6 X-band EPR spectra of the R1 spin-label at position 176 in sytIC2A, which is located in the first Ca^{2+}-binding loop of the domain. Binding and removing Ca^{2+} alters the EPR spectrum at this site and this likely reflects a change in backbone dynamics upon Ca^{2+} coordination [67]. Simulated spectra are shown below in grey and indicate that Ca^{2+} removal decreases the order parameter for the label by about 2-fold. If this change in label ordering were attributed entirely to backbone dynamics, it would represent a roughly 8° change in the amplitude of backbone motion on the nanosecond timescale.

the first and third Ca^{2+} binding loops are found to penetrate the bilayer interface with the bound Ca^{2+} ions lying near a plane defined by the lipid headgroup (see Fig. 16.5). Both these domains require negatively charged lipid for binding, and the binding of Ca^{2+} ions to the domain is likely to increase the membrane affinity in part by modifying the long-range electrostatic attraction to the membrane interface. There are some minor differences in the interactions made by these domains, e.g. sytIC2A seems to penetrate a bit deeper than sytIC2B; however, these differences are within the experimental error of the method and the data currently available.

In summary, the results of SDSL indicate that a number of C2 domains that bind in a Ca^{2+}-dependent fashion make similar interactions with the membrane interface. The primary role of Ca^{2+} is to modify the electrostatics at the membrane-binding surface of the protein. For C2 domains that require negatively charged lipids (e.g. sytIC2A, sytI C2B and PKCα C2), the binding of Ca^{2+} produces a long-range Coulombic attraction between the protein and the membrane interface. Hydrophobic interactions from residues within the Ca^{2+}-binding loops, and perhaps Ca^{2+} coordination with lipid headgroups, provide an additional interaction that attaches the protein to the interface. For the $cPLA_2$ C2 domain, Ca^{2+} binding also acts as an electrostatic switch. However, in this case the change in electrostatics facilitates attachment by reducing a repulsive force (a dehydration penalty) between the C2 domain and the membrane interface, thereby allowing the membrane insertion of hydrophobic residues on the Ca^{2+}-binding loops of the domain.

16.7
Proteins with Multiple C2 Domains

A number of proteins have multiple C2 domains. Synaptotagmins are proteins that are involved in membrane trafficking and repair (for reviews, see [70–73]). They are anchored to the membrane through a single transmembrane pass towards the N-terminus, with two C2 domains located towards their C-terminus. SytI is the best studied of the isoforms and genetic studies indicate that it functions as the Ca^{2+} sensor for neuronal exocytosis (for a review, see [74]). However, the precise molecular function that the two C2 domains in sytI have in regulating fusion is not understood.

Other proteins that contain multiple C2 domains include the copines, which are family of ubiquitous proteins containing two C2 domains involved in Ca^{2+}-dependent membrane binding. The copines also contain a region that resembles the protein-binding domain of integrins [75]. Tricalbins are a recently discovered family of proteins derived from yeast, which appear to have an N-terminal transmembrane segment and three C2 domains [76]. These proteins are thought to be homologues of synaptotagmin and have been implicated in membrane trafficking. Myoferlin and a homologous protein dysferlin have six C2 domains with a transmembrane domain located at their C-terminus [77–79]. The first C2 domain, C2A, of these proteins has been shown to bind to PC:PS membranes in a Ca^{2+}-dependent manner. Dysferlin has been implicated in membrane repair and defects in dysferlin may lead to forms of muscular degeneration. Indeed, a point mutation in the C2A of dysferlin, which has been shown to produce a form of muscular dystrophy, reduces the Ca^{2+}-dependent membrane binding of C2A.

What is the role of multiple C2 domains? As discussed elsewhere, two or more domains may be better than one [39]. The free energy of multiple membrane binding domains has often been found to be additive and multiple C2 domains may function to enhance the membrane binding of the protein. Indeed, it has been shown that there are synergistic interactions between the two domains of sytI. Neither C2A nor C2B alone will bind to isolated chromaffin granules; however, an isolated soluble fragment containing both the C2A and C2B domains readily binds granules [80].

Another function of multiple C2 domains might be to display different lipid specificities and allow binding of the protein to membranes of altered composition. Indeed, differences in the interactions made by the C2A and C2B of sytI suggest that they may be designed to recognize different lipid compositions (see below). Finally, multiple C2 domains might function by allowing a connection to be formed across two membranes, such as the synaptic vesicle and plasma membranes.

16.8
Interactions of Phosphoinositides with C2 Domains

C2 domains have been reported to bind to membranes containing polyphosphoinositides and to interact with soluble inositol phosphates. Interactions with polyphosphoinositides, such as $PI(4,5)P_2$ and $PI(3,4,5)P_3$, have been observed for the C2 domains of Rabphilin3a [81], the C2 domain of PKCα [82] as well as the C2 domains of synaptotagmin. For sytI, a number of studies have focused on its second C2 domain (C2B) as being a membrane-binding module with specificity for phosphoinositides (see, e.g. [83]). One recent study indicates that C2B binds to $PI(4,5)P_2$ membranes in either the absence or presence of Ca^{2+}, but that Ca^{2+}-dependent attachment of C2B takes place more rapidly [84]. C2B also appears to assume a different orientation when bound to $PI(4,5)P_2$ in the absence of Ca^{2+} [69, 84]. It has been suggested that $PI(4,5)P_2$ enables sytI to drive target and vesicle membranes closer together, thereby driving membrane fusion. In contrast, sytIC2A when expressed as an isolated domain does not bind $PI(4,5)P_2$-containing membranes in the presence of physiologically relevant levels of $PI(4,5)P_2$, but binds strongly to PC:PS bilayers. C2A is reported to penetrate bilayers composed of $PI(4,5)P_2$, but only when expressed in tandem with C2B. Similarly, C2B is reported to interact more strongly and penetrate more deeply into PC:PS when it is expressed and studied as a tandem soluble construct containing C2A. Thus, both the C2A and C2B domains of sytI appear to interact differently with membranes when they are present together in a single protein than when they are studied as isolated domains, and both domains of sytI appear to show a preference for different lipid surfaces.

SytIC2B has a β-strand (termed the polybasic strand) that contains a number of positively charged residues making one of its surfaces highly positively charged. This strand appears to be important in the Ca^{2+}-independent binding of C2B to $PI(4,5)P_2$ containing membranes [84]. As indicated above, highly or moderately basic segments of proteins such as the effector domain from MARCKS have the capacity to bind and interact with $PI(4,5)P_2$. A similar interaction may occur with the polybasic strand of C2B. Indeed mutation of the lysine resides within this strand of sytIC2B disrupts its Ca^{2+}-independent binding to membranes containing $PI(4,5)P_2$. Such electrostatic interactions are not expected to be specific and other highly phosphorylated inositol phosphates would also be expected to interact with these highly charged segments. Presently, detailed information on the position and interactions made by C2B with $PI(4,5)P_2$-containing membranes is not available.

In addition to interactions with membrane-bound polyphosphoinositols, soluble inositol phosphates appear to interact with C2 domains. For example, the binding of sytI to $PI(4,5)P_2$ and other phosphorylated lipids is an interaction that is blocked by inositol phosphates [83]. The inositol phosphates (IP_4, IP_5 and IP_6) have been found to bind to C2B and have been proposed to act as a negative regulator of membrane fusion [85]. The interaction of these soluble IPs also appears to be directed towards the polybasic region of sytIC2B [86].

Acknowledgments

We thank Stuart McLaughlin and Diana Murray for many useful discussions, and Diana Murray for providing the electrostatic potential plots used in Fig. 16.3. Portions of the author's work that were described in this chapter were supported by NIH grants GM62305 and GM072694.

References

1 Resh, M. D. **1999**. Fatty acylation of proteins: new insights into membrane targeting of myristoylated and palmitoylated proteins, *Biochim. Biophys. Acta 1451*, 1–16.

2 Kim, J. K., Blackshear, P. J., Johnson, D. J., McLaughlin, S. A. **1994**. Phosphorylation reverses the membrane association of peptides that correspond to the calmodulin-binding domains of MARCKS and neuromodulin, *Biophys. J. 67*, 227–237.

3 McLaughlin, S., Aderem, A. **1995**. The myristoyl-electrostatic switch: a modulator of reversible protein–membrane interactions, *Trends Biochem. Sci. 20*, 272–276.

4 DiNitto, J. P., Cronin, T. C., Lambright, D. G. **2003**. Membrane recognition and targeting by lipid-binding domains, *Sci. STKE 2003*, re16.

5 Nalefski, E. A., Slazas, M. M., Falke, J. J. **1997**. Ca^{2+}-signaling cycle of a membrane-docking C2 domain, *Biochemistry 36*, 12011–12018.

6 Nalefski, E. A., Wisner, M. A., Chen, J. Z., Sprang, S. R., Fukuda, M., Mikoshiba, K., Falke, J. J. **2001**. C2 domains from different Ca^{2+} signaling pathways display functional and mechanistic diversity, *Biochemistry 40*, 3089–3100.

7 Evans, J. H., Spencer, D. M., Zweifach, A., Leslie, C. C. **2001**. Intracellular calcium signals regulating cytosolic phospholipase A_2 translocation to internal membranes, *J. Biol. Chem. 276*, 30150–30160.

8 Kramer, R. M., Sharp, J. D. **1997**. Structure, function and regulation of Ca^{2+}-sensitive cytosolic phospholipase A_2 ($cPLA_2$), *FEBS Lett. 410*, 49–53.

9 Dessen, A. **2000**. Structure and mechanism of human cytosolic phospholipase A_2, *Biochim. Biophys. Acta 1488*, 40–47.

10 Hirabayashi, T., Shimizu, T. **2000**. Localization and regulation of cytosolic phospholipase A_2, *Biochim. Biophys. Acta 1488*, 124–138.

11 Sutton, R. B., Davletoc, B. A., Berghuis, A. M., Sudhof, T. C., Sprang, S. R. **1995**. Structure of the first C2 domain of synaptotagmin I: a novel Ca^{2+}/phospholipid-binding fold, *Cell 80*, 929–938.

12 Essen, L. O., Perisic, P., Katan, M., Williams, R. L. **1996**. Crystal structure of a mammalian phosphoinositide-specific phospholipase C, *Nature 380*, 595–602.

13 Pappa, H., Murray-Rust, J., Dekker, L. V., Parker, P. J., McDonald, N. Q. **1998**. Crystal structure of the C2 domain from protein kinase C-delta, *Structure 6*, 855–894.

14 Xu, G.-Y., McDonagh, T., Yu, H.-A., Nalefski, E. A., Clark, J. D., Cumming, D. A. **1998**. Solution structure and membrane interactions of the C2 domain of cytosolic phospholipase A_2, *J. Mol. Biol. 280*, 485–500.

15 Shao, X., Fernandez, I., Sudhof, T. C., Rizo, J. **1998**. Solution structures of the Ca^{2+}-free and Ca^{2+}-bound C2A domain of synaptotagmin I: does Ca^{2+} induce a conformational change?, *Biochemistry 37*, 16106–16115.

16 Perisic, O., Fong, S., Lynch, D. E., Bycroft, M., Williams, R. L. **1998**. Crystal structure of a calcium-phospholipid binding domain from cytosolic phospholipase A_2, *J. Biol. Chem. 273*, 2596–2604.

17 Sutton, R. B., Sprang, S. R. **1998**. Structure of the protein kinase C beta phospholipid-binding C2 domain complexed with Ca^{2+}, *Structure 6*, 1395–1405.

18 Sutton, R. B., Ernst, J. A., Brunger, A. T. **1999**. Crystal structure of the cytosolic C2A–C2B domains of synaptotagmin III: implications for Ca^{2+}-independent SNARE complex interaction, *J. Cell Biol. 147*, 589–598.

19 Fernandez, I., Arac, D., Ubach, J., Gerber, S. H., Shin, O., Gao, Y., Anderson, R. G., Sudhof, T. C., Rizo, J. **2001**. Three-dimensional structure of the synaptotagmin 1 C2B-domain: synaptotagmin 1 as a phospholipid binding machine, *Neuron 32*, 1057–1069.

20 Nalefski, E. A., Falke, J. J. **1996**. The C2 domain calcium-binding motif: structural and functional diversity, *Protein Sci. 5*, 2375–2390.

21 Macedo-Ribeiro, S., Bode, W., Huber, R., Quinn-Allen, M. A., Kim, S. W., Ortel, T. L., Bourenkov, G. P., Bartunik, H. D., Stubbs, M. T., Kane, W. H., Fuentes-Prior, P. **1999**. Crystal structures of the membrane-binding C2 domain of human coagulation factor V, *Nature 402*, 434–439.

22 Chapman, E. R., An, S., Edwardson, J. M., Jahn, R. **1996**. A novel function for the second C2 domain of synaptotagmin. Ca^{2+}-triggered dimerization, *J. Biol. Chem. 271*, 5844–5849.

23 Ubach, J., Zhang, X., Shao, X., Sudhof, T. C., Rizo, J. **1998**. Ca^{2+} binding to synaptotagmin: how many Ca^{2+} ions bind to the tip of a C2-domain?, *EMBO J. 17*, 3921–3930.

24 Desai, R. C., Vyas, B., Earles, C. A., Littleton, J. T., Kowalchyck, J. A., Martin, T. F., Chapman, E. R. **2000**. The C2B domain of synaptotagmin is a Ca^{2+}-sensing module essential for exocytosis, *J. Cell Biol. 150*, 1125–1136.

25 Zhang, X., Rizo, J., Sudhof, T. C. **1998**. Mechanism of phospholipid binding by the C2A-domain of synaptotagmin I, *Biochemistry 37*, 12395–12403.

26 Grobler, J. A., Essen, L.-O., Williams, R. L., Hurley, J. H. **1996**. C2 domain conformational changes in phospholipase C-d1, *Nat. Struct. Biol. 3*, 788–795.

27 Verdaguer, N., Corbalan-Garcia, S., Ochoa, W. F., Gomez-Fernandez, J. C. **1999**. Ca^{2+} bridges the C2 membrane-binding domain of protein kinase C*a* directly to phosphatidylserine, *EMBO J. 18*, 6329–6338.

28 Davletov, B. A., Sudhof, T. C. **1993**. A single C2 domain from synaptotagmin I is sufficient for high affinity Ca^{2+}/phospholipid binding, *J. Biol. Chem. 268*, 26386–26390.

29 McLaughlin, S. A. **1977**. Electrostatic potentials at membrane-solution interfaces, *Curr. Topics Membr. Transport 9*, 71–144.

30 Mosior, M., McLaughlin, S. A. **1992**. Electrostatics and dimensionality can produce apparent cooperativity when protein kinase C and its substrates bind to acidic lipids in membranes, In *Protein Kinase C: Current Concepts and Future Perspectives*, Epand, R., Lester, D. (eds), Ellis Horwood, New York.

31 Qin, Z., Wertz, S. L., Jacob, J., Savino, Y., Cafiso, D. S. **1996**. Defining protein–protein interactions using site-directed spin-labeling: the binding of protein kinase C substrates to calmodulin, *Biochemistry 35*, 13272–13276.

32 Zhang, W., Crocker, E., McLaughlin, S., Smith, S. O. **2003**. Binding of peptides with basic and aromatic residues to bilayer membranes: phenylalanine in the myristoylated alanine-rich C kinase substrate effector domain penetrates into the hydrophobic core of the bilayer, *J. Biol. Chem. 278*, 21459–21466.

33 Ellena, J. F., Burnitz, M. C., Cafiso, D. S. **2003**. Location of the myristoylated alanine-rich C-kinase substrate (MARCKS) effector domain in negatively charged phospholipid bicelles, *Biophys. J. 85*, 2442–2448.

34 Victor, K., Jacob, J., Cafiso, D. S. **1999**. Interactions controlling the membrane binding of basic protein domains, *Biochemistry 38*, 12527–12536.

35 Ben-Tal, N., Honig, B., Peitzsch, R. M., Denisov, G., McLaughlin, S. **1996**. Binding of small basic peptides to membranes containing acidic lipids: theoretical models and experimental results, *Biophys. J. 71*, 561–575.

36 Qin, Z., Cafiso, D. S. **1996**. Membrane structure of the PKC and calmodulin binding domain of MARCKS determined by site-directed spin-labeling, *Biochemistry 35*, 2917–2925.

37 Ben-Tal, N., Honig, B., Miller, C., McLaughlin, S. **1997**. Electrostatic binding of proteins to membranes. Theoreti-

cal predictions and experimental results with charybdotoxin and phospholipid vesicles, *Biophys. J. 73*, 1717–1727.

38 Murray, D., Arbuzova, A., Hangyas-Mihalyne, G., Gambhir, A., Ben-Tal, N., Honig, B., McLaughlin, S. **1999**. Electrostatic properties of membranes containing acidic lipids and adsorbed basic peptides: theory and experiment, *Biophys. J. 77*, 3176–3188.

39 McLaughlin, S., Wang, J., Gambhir, A., Murray, D. **2002**. PIP_2 and proteins: interactions, organization, and information flow, *Annu. Rev. Biophys. Biomol. Struct. 31*, 151–175.

40 Arbuzova, A., Wang, L., Wang, J., Hangyas-Mihalyne, G., Murray, D., Honig, B., McLaughlin, S. **2000**. Membrane binding of peptides containing both basic and aromatic residues. Experimental studies with peptides corresponding to the scaffolding region of caveolin and the effector region of MARCKS, *Biochemistry 39*, 10330–10339.

41 Wang, J., Arbuzova, A., Hangyas-Mihalyne, G., McLaughlin, S. **2001**. The effector domain of myristoylated alanine-rich C kinase substrate binds strongly to phosphatidylinositol 4,5-bisphosphate, *J. Biol. Chem. 276*, 5012–5019.

42 Wang, J., Gambhir, A., McLaughlin, S., Murray, D. **2004**. A computational model for the electrostatic sequestration of $PI(4,5)P_2$ by membrane-adsorbed basic peptides, *Biophys. J. 86*, 1969–1986.

43 Rauch, M.E., Ferguson, C.G., Prestwich, G.D., Cafiso, D.S. **2002**. Myristoylated alanine-rich C kinase substrate (MARCKS) sequesters spin-labeled phosphatidylinositol 4,5-bisphosphate in lipid bilayers, *J. Biol. Chem. 277*, 14068–14076.

44 Wang, J., Gambhir, A., Hangyas-Mihalyne, G., Murray, D., Golebiewska, U., McLaughlin, S. **2002**. Lateral sequestration of phosphatidylinositol 4,5-bisphosphate by the basic effector domain of myristoylated alanine-rich C kinase substrate is due to nonspecific electrostatic interactions, *J. Biol. Chem. 277*, 34401–34412.

45 Ellena, J.F., Moulthrop, J., Wu, J., Rauch, M., Jaysinghne, S., Castle, J.D., Cafiso, D.S. **2004**. Membrane position of a basic aromatic peptide that sequesters phosphatidylinositol 4,5 bisphosphate determined by site-directed spin labeling and high-resolution NMR, *Biophys. J. 87*, 3221–3233.

46 Gambhir, A., Hangyas-Mihalyne, G., Zaitseva, I., Cafiso, D.S., Wang, J., Murray, D., Pentyala, S.N., Smith, S.O., McLaughlin, S. **2004**. Electrostatic sequestration of PIP_2 on phospholipid membranes by basic/aromatic regions of proteins, *Biophys. J. 86*, 2188–2207.

47 Murray, D., Honig, B. **2002**. Electrostatic control of the membrane targeting of C2 domains, *Mol. Cell 9*, 145–154.

48 Perisic, O., Paterson, H.F., Mosedale, G., Lara-Gonzalez, S., Williams, R.L. **1999**. Mapping the phospholipid-binding surface and translocation determinants of the C2 domain from cytosolic phospholipase A_2, *J. Biol. Chem. 274*, 14979–14987.

49 Bittova, L., Sumandea, M., Cho, W. **1999**. A structure–function study of the C2 domain of cytosolic phospholipase A_2, *J. Biol. Chem. 274*, 9665–9672.

50 Medkova, M., Cho, W. **1998**. Mutagenesis of the C2 domain of protein kinase C-alpha. Differential roles of Ca^{2+} ligands and membrane binding residues, *J. Biol. Chem. 273*, 17544–17552.

51 Davletov, B., Perisic, O., Williams, R.L. **1998**. Calcium-dependent membrane penetration is a hallmark of the C2 domain of cytosolic phospholipase A2 whereas the C2A domain of synaptotagmin binds membranes electrostatically, *J. Biol. Chem. 273*, 19093–19096.

52 Nalefski, E.A., Falke, J.J. **1998**. Location of the membrane-docking face on the Ca^{2+}-activated c2 domain of cytosolic phospholipase A_2, *Biochemistry 37*, 17642–17650.

53 Chapman, E.R., Davis, A.F. **1998**. Direct interaction of a Ca^{2+}-binding loop of synaptotagmin with lipid bilayers, *J. Biol. Chem. 273*, 13995–14001.

54 Hubbell, W., Altenbach, C. **1994**. Investigation of structure and dynamics in membrane proteins using site-directed spin labeling, *Curr. Opin. Struct. Biol. 4*, 566–578.

55 Hubbell, W.L., Cafiso, D.S., Altenbach, C. **2000**. Conformational changes with site directed spin labeling, *Nat. Struct. Biol. 7*, 735–739.

56 Hubbell, W.L., Gross, A., Langen, R., Lietzow, M.A. **1998**. Recent advances in site-directed spin labeling of proteins, *Curr. Opin. Struct. Biol. 8*, 649–656.

57 Hubbell, W.L., Mchaourab, H.S., Altenbach, C., Lietzow, M.A. **1996**. Watching proteins move using site-directed spin labeling, *Structure 4*, 779–783.

58 Mchaourab, H., Lietzow, M., Hideg, K., Hubbell, W. **1996**. Motion of spin-labeled side-chains in T4 lysozyme. (I) Correlation with protein structure and dynamics, *Biochemistry 35*, 7692–7704.

59 Altenbach, C., Froncisz, W., Hyde, J.S., Hubbell, W.L. **1989**. Conformation of spin-labeled melittin at membrane surfaces investigated by pulse saturation recovery and continuous wave power saturation electron paramagnetic resonance, *Biophys. J. 56*, 1183–1191.

60 Altenbach, C., Greenhalgh, D.A., Khorana, H.G., Hubbell, W.L. **1994**. A collision gradient-method to determine the immersion depth of nitroxides in lipid bilayers. Application to spin-labeled mutants of bacteriorhodopsin, *Proc. Natl Acad. Sci. USA 91*, 1667–1671.

61 Canaan, S., Nielsen, R., Ghomashchi, F., Robinson, B.H., Gelb, M.H. **2002**. Unusual mode of binding of human group IIA secreted phospholipase A2 to anionic interfaces as studied by continuous wave and time domain electron paramagnetic resonance spectroscopy, *J. Biol. Chem. 277*, 30984–30990.

62 Ball, A., Nielsen, R., Gelb, M.H., Robinson, B.H. **1999**. Interfacial membrane docking of cytosolic phospholipase A_2 C2 domain using electrostatic potential-modulated spin relaxation magnetic resonance, *Proc. Natl Acad. Sci. USA 96*, 6637–6642.

63 Frazier, A.A., Wisner, M.A., Malmberg, N.J., Victor, K.G., Fanucci, G.E., Nalefski, E.A., Falke, J.J., Cafiso, D.S. **2002**. Membrane orientation and position of the C2 domain from $cPLA_2$ by site-directed spin labeling, *Biochemistry 41*, 6282–6292.

64 Malmberg, N.J., Van Buskirk, D.R., Falke, J.J. **2003**. Membrane-docking loops of the $cPLA_2$ C2 domain: detailed structural analysis of the protein-membrane interface via site-directed spin-labeling, *Biochemistry 42*, 13227–13240.

65 Columbus, L., Hubbell, W.L. **2004**. Mapping backbone dynamics in solution with site-directed spin labeling: GCN4-58 bZip free and bound to DNA, *Biochemistry 43*, 7273–7287.

66 Columbus, L., Hubbell, W.L. **2002**. A new spin on protein dynamics, *Trends Biochem. Sci. 27*, 288–295.

67 Frazier, A.A., Roller, C.R., Havelka, J.J., Hinderliter, A., Cafiso, D.S. **2003**. Membrane-bound orientation and position of the synaptotagmin I C2A domain by site-directed spin labeling, *Biochemistry 42*, 96–105.

68 Kohout, S.C., Corbalan-Garcia, S., Gomez-Fernandez, J.C., Falke, J.J. **2003**. C2 domain of protein kinase C alpha: elucidation of the membrane docking surface by site-directed fluorescence and spin labeling, *Biochemistry 42*, 1254–1265.

69 Rufener, E., Frazier, A., Wieser, C.M., Hinderliter, A., Cafiso, D.S. **2005**. Membrane bound orientation and position of the synaptotagmin C2B domain determined by site-directed spin labeling, *Biochemistry 44*, 18–28.

70 Sudhof, T.C., Rizo, J. **1996**. Synaptotagmins: C2-domain proteins that regulate membrane traffic, *Neuron 17*, 379–388.

71 Chapman, E.R. **2002**. Synaptotagmin: a Ca^{2+} sensor that triggers exocytosis?, *Nat. Rev. Mol. Cell. Biol. 3*, 498–508.

72 Sudhof, T.C. **2002**. Synaptotagmins: why so many?, *J. Biol. Chem. 277*, 7629–7632.

73 Bai, J., Chapman, E.R. **2004**. The C2 domains of synaptotagmin – partners in exocytosis, *Trends Biochem. Sci. 29*, 143–151.

74 Koh, T.W., Bellen, H.J. **2003**. Synaptotagmin I, a Ca^{2+} sensor for neurotransmitter release, *Trends Neurosci. 26*, 413–422.

75 Tomsig, J.L., Creutz, C.E. **2000**. Biochemical characterization of copine: a ubiquitous Ca^{2+}-dependent phospholipid-binding protein, *Biochemistry 39*, 16163–16175.

76 Schulz, T. A., Creutz, C. E. **2004**. The tricalbin C2 domains: lipid-binding properties of a novel, synaptotagmin-like yeast protein family, *Biochemistry 43*, 3987–3995.

77 Davis, D. B., Doherty, K. R., Delmonte, A. J., McNally, E. M. **2002**. Calcium-sensitive phospholipid binding properties of normal and mutant ferlin C2 domains, *J. Biol. Chem. 277*, 22883–22888.

78 Doherty, K. R., McNally, E. M. **2003**. Repairing the tears: dysferlin in muscle membrane repair, *Trends Mol. Med. 9*, 327–330.

79 Bansal, D., Campbell, K. P. **2004**. Dysferlin and the plasma membrane repair in muscular dystrophy, *Trends Cell Biol. 14*, 206–213.

80 Damer, C. K., Creutz, C. E. **1994**. Synergistic membrane interactions of the two C2 domains of synaptotagmin, *J. Biol. Chem. 49*, 31115–31123.

81 Chung, S. H., Song, W. J., Kim, K., Bednarski, J. J., Chen, J., Prestwich, G. D., Holz, R. W. **1998**. The C2 domains of Rabphilin3A specifically bind phosphatidylinositol 4,5-bisphosphate containing vesicles in a Ca^{2+}-dependent manner. In vitro characteristics and possible significance, *J. Biol. Chem. 273*, 10240–10248.

82 Corbalan-Garcia, S., Garcia-Garcia, J., Rodriguez-Alfaro, J. A., Gomez-Fernandez, J. C. **2003**. A new phosphatidylinositol 4,5-bisphosphate-binding site located in the C2 domain of protein kinase C alpha, *J. Biol. Chem. 278*, 4972–4980.

83 Schiavo, G., Gu, Q. M., Prestwich, G. D., Sollner, T. H., Rothman, J. E. **1996**. Calcium-dependent switching of the specificity of phosphoinositide binding to synaptotagmin, *Proc. Natl Acad. Sci. USA 93*, 13327–13332.

84 Bai, J., Tucker, W. C., Chapman, E. R. **2004**. PIP_2 increases the speed of response of synaptotagmin and steers its membrane-penetration activity toward the plasma membrane, *Nat. Struct. Mol. Biol. 11*, 36–44.

85 Mikoshiba, K., Fukuda, M., Ibata, K., Kabayama, H., Mizutani, A. **1999**. Role of synaptotagmin, a Ca^{2+} and inositol polyphosphate binding protein, in neurotransmitter release and neurite outgrowth, *Chem. Phys. Lipids 98*, 59–67.

86 Fukuda, M., Kojima, T., Aruga, J., Niinobe, M., Mikoshiba, K. **1995**. Functional diversity of C2 domains of synaptotagmin family. Mutational analysis of inositol high polyphosphate binding domain, *J. Biol. Chem. 270*, 26523–26527.

87 Berliner, L. J., Grunwald, J., Hankovszky, H. O., Hideg, K. **1982**. A novel reversible thiol-specific spin label: papain active site labeling and inhibition, *Anal. Biochem. 119*, 450–455.

88 Tieleman, D. P., Berendsen, H. J., Sansom, M. S. **1999**. Surface binding of alamethicin stabilizes its helical structure: molecular dynamics simulations, *Biophys. J. 76*, 3186–3191.

17
Structural Mechanisms of Allosteric Regulation by Membrane-binding Domains

Bertram Canagarajah, William J. Smith, and James H. Hurley

17.1
Introduction

Membrane targeting of proteins is a fundamental regulatory mechanism in cell signaling. The specific interaction of conserved protein modules with membrane lipids is one prominent mechanism for membrane targeting. The best known of these are the C1, C2, ENTH, FYVE, PH and PX domains [1–10] (see also Chapter 15), but the number continues to grow. Reversible binding of signaling proteins to membranes has a variety of consequences. The most obvious effect is relocalization, which typically brings a signaling protein to its site of action at a cell membrane. In a few cases, membrane localization instead sequesters a protein at the membrane and thereby removes it from its site of action. Relocalization has become straightforward to measure *in vivo* by using fluorescent protein fusions as probes and countless proteins have now been shown to undergo regulation by reversible changes in subcellular localization. Many excellent reviews on this topic are available [1–10].

Targeting is not the only function of membrane-binding domains. Many enzymes that act at the membrane interface contain membrane-binding domains that are rigidly attached to, but distinct from, their catalytic domain. In these systems, the membrane-binding domain serves as a rigid "handle" to position the catalytic domain on the membrane [11, 12]. The function of a rigidly attached handle, which targets and positions, stands in contrast to a flexibly tethered anchor, which targets but does not position.

Yet another consequence of membrane binding can be to allosterically alter the activity of a protein by inducing conformational changes. The protein kinase Cs (PKCs) are the archetypal examples of allosteric regulation by membrane binding domains, and most of the concepts in the field were first established by studies of PKC activation by diacylglycerol (DAG) and phosphatyidylserine [5, 13–19]. Biochemical and, ultimately, structural analysis is required to charac-

terize these allosteric activation mechanisms. It is correspondingly harder to study these mechanisms as compared to simple targeting mechanisms.

There are few structures of full-length, or nearly full-length, membrane-binding domain-containing proteins. Some of these structures are best interpreted in terms of targeting and positioning roles for the membrane-binding domain, with no large structural changes produced by membrane binding domain engagement. The structures of the C2 domain-containing proteins phospholipase Cδ [20, 21], cytosolic phospholipase A_2 [22], PTEN [23] and phosphoinositide 3-kinase [24] fall into this category. The same might hold for the PH domain-containing lipid phosphatase myotubularin [25], although the lipid-binding properties of its outlier PH domain (formerly known as a "GRAM" domain) have not been reported to date. This chapter will focus on the handful of PH and PKC C1 domain-containing proteins for which structures are available, and for which there is at least some reason to believe that membrane binding leads to regulatory conformational changes. While only a few such structures are available, the small number of structures probably has more to do with the technical challenges of coaxing large, conformationally heterogeneous signaling proteins to form crystals. The total number of proteins in this regulatory class is probably far greater than is represented by existing structures.

17.2
How Membranes and PH Domains Regulate Rho Family-specific Guanine Nucleotide Exchange Factors (GEFs)

The GTP-binding proteins Cdc42, Rho and Rac are part of the Rho subfamily of small-molecular-weight Ras-like GTPases, and are at the center of many fundamental cellular events including the establishment of cell polarity, transcriptional regulation, actin cytoskeleton rearrangement, intracellular trafficking and endocytosis. These small G-proteins are intimately associated with phospholipid membranes [26–31]. The GTPases serve as molecular switches whereby the GTP bound form is active in signaling, while the GDP form is largely inert. Small GTPases have very poor intrinsic enzyme activity, and are helped through their catalytic cycle by GTPase-activating proteins (GAPs) and GEFs. GAPs turn off signaling by activating GTP hydrolysis, while GEFs turn the signal on by loading GTP onto the GTPases.

A GTP-binding protein has two highly conserved regions that serve as the site for interactions with a variety of targets and regulatory proteins. These two regions are centered around the GTP-binding pocket, and have been dubbed switch I and switch II (Fig. 17.1), due to their propensity to undergo a conformational change upon binding to either a magnesium-coordinated GTP or GDP molecule [32]. The Rho family members are post-translationally modified at their C-terminus with a prenyl moiety that allows for their direct insertion into membrane compartments and organelles [33, 34].

17.2.1
DH and PH Domain Rho GEFs

The Rho family-specific GEFs consist of a Dbl homology followed by a PH domain, and together they are referred to as a DHPH module. The minimal catalytic unit, the DH domain, is largely α-helical and possesses three conserved regions, referred to as CR1–3, that are critical for function. The mechanism of GEF-mediated guanine nucleotide exchange on the Rho family protein members by the DH domain is modeled as a three-step process. The DH domain first interacts with the conformational-rigid $\beta 2$–$\beta 3$ strands (Fig. 17.1) between switch I and II of their cognate GTPase. This "lock and key" association is followed by an "induced fit" mechanism that results in a conformational movement of switch I and switch II and consequently destabilization of the guanine nucleotide. The combined intrusion of Ala59 into the Mg^{2+}-binding site and a steric clash of Ile33 with the nucleotide sugar promotes GDP dissociation (Fig. 17.1). The complex allows unobstructed access to the guanine nucleotide-binding pocket where subsequent GTP binding leads to remodeling of the switch regions and destabilization of the GEF/GTPase complex, resulting in the dissociation of the GEF and an active GTPase [35–37].

17.2.2
Regulation of GEF Activity by PH Domains

While some isolated DH domains catalyze the exchange of GDP for GTP, the presence of the PH domain is required in others [38–41]. In the GEF–GTPase complex of Tiam1–Rac1, residues important for efficient GEF-stimulated guanine nucleotide exchange are present within the DH domain. A critical interaction between Arg66 within switch II of the GTP-binding protein, Rac1, forms an ion pair with Glu1239 within the DH domain of Tiam1, an interaction that is essential for the GEF activity on Rac1 [37]. However, in Dbs (*D*bl's *b*ig *s*ister) the conserved Glu residue is absent. To restore GEF activity, the PH domain of these GEFs must contribute a hydrogen bond from Tyr889 and the carbonyl oxygen of Pro887 to a hydrogen bond network with Arg66 within switch II of Cdc42 (Fig. 17.1). However, mutation of Arg66 does not compromise the GEF activity of Dbs and it is thought that Tyr889 promotes GEF catalysis by stabilizing the electronic polarization of the imidazole group of His814 within the DH domain [37]. Thus, with the requirement of Tyr889 from the PH domain of Dbs in facilitating efficient guanine nucleotide exchange on its cognate GTP-binding protein, Cdc42 (or Rho), any alteration of the positioning of the PH domain relative to its DH domain would have a direct effect on the catalytic activity of the GEF.

There are two leading models for the allosteric regulation of the GEF, which are not mutually exclusive. In the first, stabilizing interactions or structural rigidity imparted by the membrane on the GEFs (or other accessory proteins) to optimize GEF-stimulated guanine nucleotide exchange activity. In the second model, membrane binding to the PH domain induces conformational changes

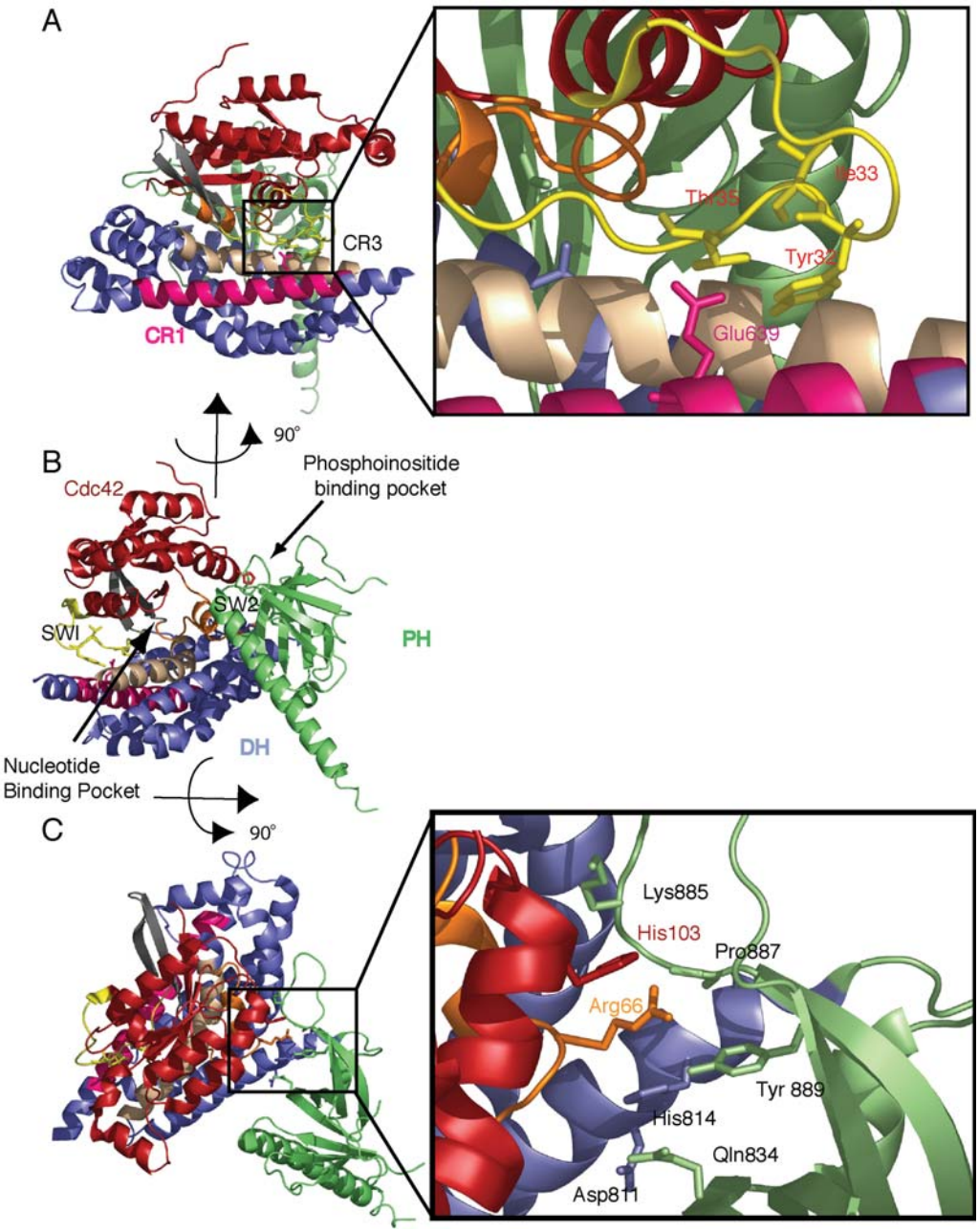
A
CR3
CR1
Ile33
Thr35
Tyr32
Glu639
90°
B
Cdc42
Phosphoinositide
binding pocket
SW2
SWI
PH
DH
Nucleotide
Binding Pocket
90°
C
Lys885
His103
Pro887
Arg66
Tyr 889
His814
Qln834
Asp811

in the DHPH module that enhance GEF-stimulated guanine nucleotide exchange.

Dbs appears to fall into the first category. The PH domain of Dbs can rotate around the C-terminal helix (α6) with the DH domain. This rotation allows the PH domain in Dbs to directly interact with Cdc42 [37]. The crystal structure of the isolated unbound DHPH module of Dbs revealed a similar orientation of the DHPH module as observed when complexed with Cdc42 [42, 43]. Although the structures are similar, Worthylake et al. argue that the subtle differences between the GTPase-bound and unbound DHPH module of Dbs show how phosphoinositide and membrane binding to the PH domain restricts the conformational heterogeneity between the DH and PH domain [43]. This restriction in conformational flexibility would then favor direct interaction between the PH domain and GTPase to allow for elevated GEF-stimulated guanine nucleotide exchange [43]. Mutations that block the binding of the PH domain to phosphoinositides preserve GEF-stimulated nucleotide exchange *in vitro* and maintain proper localization in the cell, but do not activate their cognate GTPases *in vivo* [39, 44]. A similar scenario applies to Trio [45]. The PH domain of Trio does not bind to phosphoinositides by itself, but RhoG greatly enhances the association of Trio with phosphoinositides [45]. In summary, first the GTPase is bound to the membrane, in close proximity to a phosphoinositide patch (Fig. 17.2). Second, the GEF is recruited to the GTPase by unobstructed access of the DH domain to the GTP-binding protein, however GEF activity is minimal. Finally, the PH domain engages the phosphoinositide directly through residues within the β1–β2 and β3–β4 loop, and stabilizes the catalytic loop contributed by the PH domain to assist in GEF activity. The case of Trio is a variation of the last step in which the basic tail of RhoG acts as a bridge by interacting with the PH domain of Trio and with membranes.

Allosteric regulation of the PH domain within the DHPH module may occur by gross reorientations of the DH and PH domains. In the crystal structure of

Fig. 17.1 Structural basis of Rho-GEF-stimulated guanine-nucleotide exchange on Rho family GTP-binding proteins: structure of Cdc42 (red) bound to the DHPH module of Dbs (PDB: 1KZ7). Switch I (yellow), switch II (orange) and the β2–β3 (interswitch and colored charcoal) region that are responsible for the association with target/effector and regulator molecules.
(A) Guanine nucleotide exchange occurs with the association of the DH domain (blue) (slate) with the β2–β3 "interswitch" concurrently with the conformational disruption of switch I and II in the GTPase. The conserved region's 1 and 2 (CR1 and CR2) that interact with the GTPase and facilitate GEF-stimulated guanine nucleotide exchange are highlighted in beige and hot-pink, respectively.
(B) Orthogonal view to (A), highlighting the relative accessibility of the nucleotide-binding pocket and the association of loop regions within the β1–β2 and β3–β4 strands that serve to coordinate membrane-bound phosphoinositides.
(C) Dbs coordinates Arg66 within switch II (orange) of Cdc42 with residues contributed from the DH domain (His814) and PH domain (Tyr889 and Pro887, green) that are critical for GEF activity. All figures were rendered with MacPyMOL (www.pymol.org)].

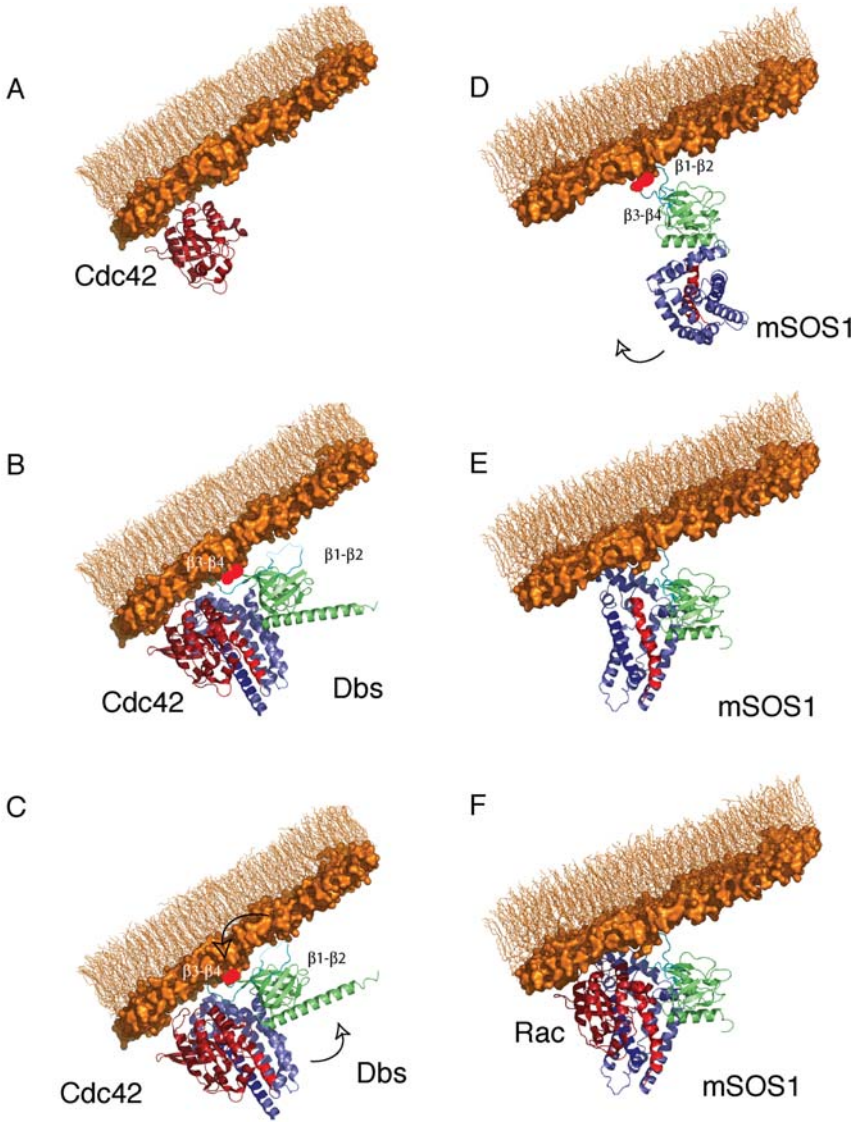

Fig. 17.2 Allosteric regulation of GEF-stimulated guanine nucleotide exchange by phospholipid membranes.
(A) Cdc42 (red) associates with a membrane surface through its geranylgeranyl moiety.
(B) Dbs is recruited to the membrane through the interaction with the DH domain and Cdc42, however GEF activity is minimal.
(C) Dbs' PH domain undergoes a stabilized conformational change via interactions of $\beta 1$–$\beta 2$ and $\beta 3$–$\beta 4$ loops with the exposed phosphoinositide (pink) and contributes key residues within the PH to facilitate GEF-facilitated exchange.
(D) The conformational and catalytically unavailable DHPH domain of mSOS is recruited to the membrane via phosphoinositide and PH (green) interactions.
(E) Membrane curvature, close proximity of the membrane and/or accessory factors induce a conformational change of the DH domain (slate) through a gross movement toward the membrane via an unstructured linker region between the PH and DH domain.
(F) The DH domain is able to engage the GTPase and catalyze GEF-stimulated guanine nucleotide exchange.

the isolated DHPH domain from mSos1 in the absence of a GTPase, the PH domain sterically blocks the main catalytic surface of the DH domain [41]. The crystal structure of the LARG DHPH module alone or bound to RhoA highlights a conformational change that occurs upon association with the small GTPase. A roughly 30° rotation of the PH domain relative to the DH domain occurs through a bend in the flexible helix between the DH and PH domains. This conformational change allows for the PH domain to move into a position to directly contribute to efficient guanine nucleotide exchange [40]. Thus, in model 2, the GEF is first targeted to the membrane via direct electrostatic interactions contributed from the positively charged polarized surface of the PH domain (Fig. 17.2). Second, the membrane, assisted by additional protein effectors, induces a conformational change in the PH domain which in turn leads to a conformational change in the unstructured loop between the DH and PH domains, which then engages the membrane. Finally, the GEF is positioned to engage the GTPase and GEF-stimulated guanine nucleotide exchange occurs.

In summary, the DHPH GEFs have a conserved modular structure, yet are regulated by diverse mechanisms. In some cases membrane engagement by the PH domain functions indirectly by positioning the DH; in other cases, structural changes are induced that rigidify the overall DHPH assembly and promote direct interactions between the PH domain and the small GTPase; and in at least one case it appears that conformational changes are required to relieve a steric block of the active site by the PH domain.

17.3
Regulation of G-protein Receptor Kinase (GRK) 2 Activity by Lipids and the G$\beta\gamma$ Subunit at the Membrane

GRKs are serine/threonine kinases that phosphorylate the C-terminal tail of activated G-protein-coupled receptors (GPCRs). The phosphorylation of activated GPCRs is followed by binding of specific arrestins to the phosphorylated receptors, which uncouples the receptors from their G-proteins and ultimately leads to the desensitization of these receptors [46]. At the level of G-proteins, GRKs prevent complex formation between Gα and G$\beta\gamma$ subunits. GRK2 (previously referred to as β-adrenergic receptor kinase) is an 80-kDa protein containing three modular domains: an N-terminal regulator of G-protein signaling (RGS) homology (RH) domain, a central protein kinase domain, and a C-terminal PH domain that is unique to GRK2 and GRK3 [47]. GRK2 is recruited from the cytosol to the plasma membrane by interacting with G$\beta\gamma$ and anionic phospholipids through its PH domain [48, 49].

The crystal structure of the GRK2–G$\beta\gamma$ complex (Fig. 17.3) has been determined in the presence of detergent micelles [50]. This structure suggests how GRK2 function is intricately regulated by the interaction between its domains and its interactions with Gqα, G$\beta\gamma$ and anionic lipid [50]. This structure illustrates how GRK2 is able to interact with Gα, G$\beta\gamma$, GPCR and phospholipids si-

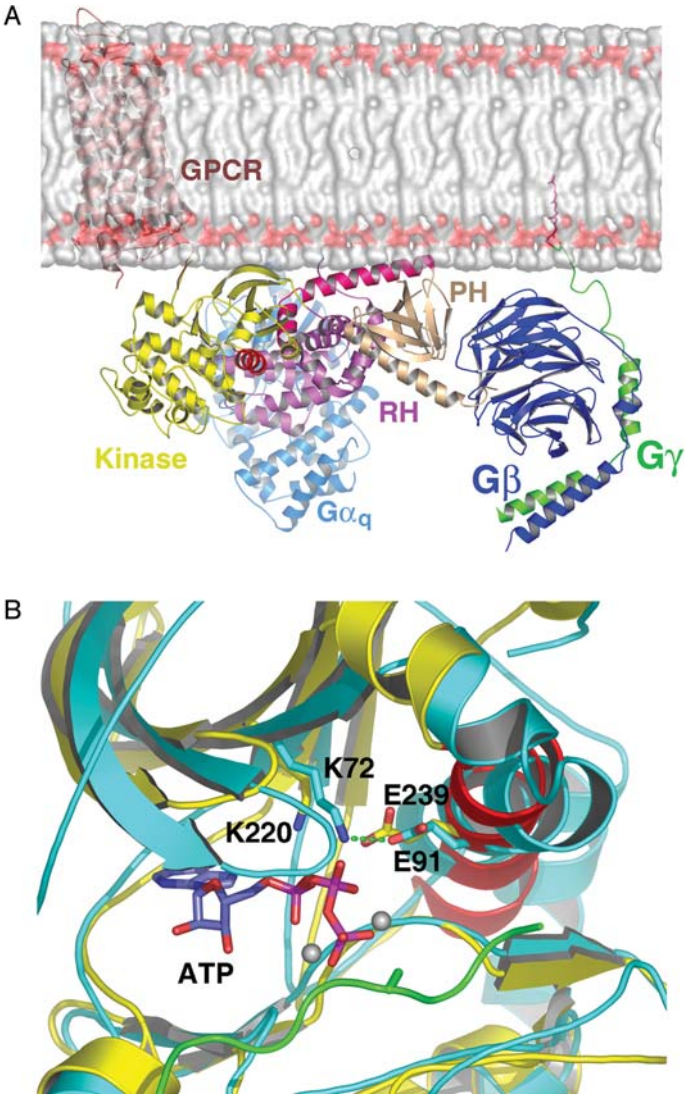

Fig. 17.3 Structural mechanism for allosteric regulation of GRK2.
(A) Side view of the GRK2–G$\beta\gamma$ complex bound to Gqα and GPCR at the membrane. The PH domain of GRK2 is tan, the RH domain is violet and the kinase domain is yellow. The two helices (α10 and α11) that are separate from the rest of the RH domain in the primary sequence are colored magenta. The Gβ_1 subunit is blue and Gγ_2 is green. The model was built using the GRK2–G$\beta_1\gamma_2$ complex (PDB: 1OMW), the inactive crystal structure of rhodopsin (PDB: 1L9H) as activated GPCR (maroon) and a homology model of Gqα (cyan) built based on the structure of Giα in complex with RGS4 (PDB: 1AGR). The membrane is depicted as a translucent surface.
(B) A close-up view of the kinase domain. The inactive kinase domain of GRK2 in yellow is superimposed on the active kinase structure of PKA (PDB: 1ATP) in cyan using the C-terminal lobes. The difference between the relative orientation of the lobes and the orientation of the C helix is apparent. The catalytically important Lys72 and Glu91 of PKA, the corresponding residues in GRK2, and the ATP are drawn as sticks. The hydrogen bond between Lys72 and Glu91 is drawn as a green dashed line. Two manganese ions of PKA are shown as white spheres.

multaneously, and to down-regulate G-protein mediated signaling at the level of GPCRs and G-proteins.

The kinase domain of GRK2 is very similar to the other known structures of AGC family of kinases, including protein kinase A (PKA) and protein kinase B (PKB). The kinase domain in the complex is in an open, inactive conformation. The nucleotide-binding gate is disordered and the αC-helix is oriented as seen in other inactive kinase structures. The kinase activity of GRK2 is regulated by its interactions with the substrate, the membrane and protein ligands. Unlike the other AGC kinases, it is not regulated by phosphorylation on residues on the activation loop or other sites [51]. The kinase domain makes extensive contacts with RH domain. The α10 helix lies at the RH–kinase domain interface, and consists of several hydrophobic contacts and an ion pair. Any change in the conformation of RH domain could be relayed to the kinase domain.

The phospholipid-binding site of the PH domain is adjacent to the RH domain–PH domain interface. The structure also displays significant differences in the conformation of the C-terminal region of the domain compared to the nuclear magnetic resonance structure of the PH domain [52]. This conformational change could be a result of G$\beta\gamma$ binding to the GRK2 PH domain. It is possible that the binding of phospholipids and G$\beta\gamma$ to PH domain could be communicated to the rest of the protein through the RH–PH domain interface. This interface, consisting of hydrophobic interactions, a salt bridge and two ion pairs, plays a significant role in the allosteric regulation of GRK2. Site-directed mutagenesis of one of these ion pairs has been shown to impair the phospholipid-mediated activation of GRK2 [53].

The similarities between the inactive structure of c-Src [54, 55] and the RH–kinase domain core of GRK2 led to the concept that binding of other proteins and/or domains to the RH domain could be coupled to the activity of the kinase domain. In particular, the similarity of the α10 helix to the Src homology-2 (SH2) kinase linker of c-Src places the α10 helix at an important position to regulate the enzymatic activity of GRK2. Changes in the rest of the protein produced by the interactions of Gα, G$\beta\gamma$ and phospholipids could change the conformation of the RH domain. The RH domain is in direct contact with both the PH and kinase domains, and thus able to coordinate various interactions with the activation of the kinase. A change in the conformation of RH domain resulting from the binding of phospholipids, G$\beta\gamma$ and Gα could then shift the kinase domain to the active conformation.

In summary, the structure of GRK2 offers a clear-cut example of a positioning role, whereby the PH domain interacts with membranes and G$\beta\gamma$ to bring the kinase into proximity to its GPCR substrate. The observation of an inactive conformation even in the presence of detergent and G$\beta\gamma$ shows that these ligands are insufficient to fully activate the kinase. It seems clear that further activation by phospholipids or other ligands not present in the crystal structure must induce a conformational change in the kinase core in order to reposition the αC-helix for catalysis.

17.4
Lipid Activation of Rac-GAP Activity: β2-Chimaerin

DAG is a paradigmatic lipid second messenger in metazoan cell signaling, the first to be discovered [13–16]. DAG is a central mediator of downstream signaling by a host of hormones coupled through G_q and phospholipase Cβ, growth factors coupled to tyrosine kinase-linked receptors and phospholipase Cγ, and many other extra- and intracellular stimuli [16]. The PKC isozyme family has historically been the most intensively studied class of targets for DAG signaling [5, 13–16, 56, 57]. Conventional and novel PKC isozymes, and the protein kinase D isozymes, translocate to membranes and are activated by DAG and phorbol esters by virtue of their direct binding to motifs known as protein kinase C homology-1 (C1) domains [5, 15, 16, 56, 58, 59].

There are several major classes of C1 domain-containing DAG receptors in addition to PKC. One example is β2-chimaerin, a phorbol ester- and DAG-responsive GTPase-activating protein [60–64]. β2-chimaerin contains three conserved domains. The N-terminal SH2 domain is presumed competent to bind phosphotyrosine-containing proteins, but its physiological partner is unknown. The central C1 domain is followed by a C-terminal GAP domain with homology to many other Rho, Rac and Cdc42 GAPs. The GAP activity of β2-chimaerin is specific for Rac as opposed to other small G-proteins [65].

17.4.1
The C1 Domain of β2-Chimaerin is Buried

The overall structure of β2-chimaerin [66] shows that the C1 domain is the linchpin that holds together the larger assembly of domains (Fig. 17.4). The C1 domain is in contact with both the SH2 and Rac-GAP domains, with the N-terminal region and with the SH2-C1 linker. Much of the surface of the C1 domain is deeply buried in contacts with the rest of the protein. The C1 domain surfaces buried in these contacts overlap extensively with the surfaces involved in phospholipid and phorbol ester binding. Of the six hydrophobic side-chains believed to insert into the membrane, four are completely buried, and two are partially buried in contacts with the rest of the protein. The main-chain NH and CO groups on Gly235 are presumed to interact with the 3- and 4-hydroxyls of phorbol ester, as seen for Gly253 of PKCδ. In β2-chimaerin, the amide group of the side-chain of Gln32 replaces this interaction and sterically blocks the phorbol ester-binding site. This implies that the observed conformation of β2-chimaerin is incompatible with phorbol ester and phospholipid membrane binding.

The cost in free energy to break the extensive interactions between the C1 domain and these four protein regions must be considerable. This is consistent with the observation that intact β2-chimaerin translocates to membranes at higher doses of phorbol ester than required for the C1 domain alone or for proteins with less buried C1 domains. β2-chimaerin translocation to cell membranes requires a dose around 100-fold higher than translocation of PKCα [67].

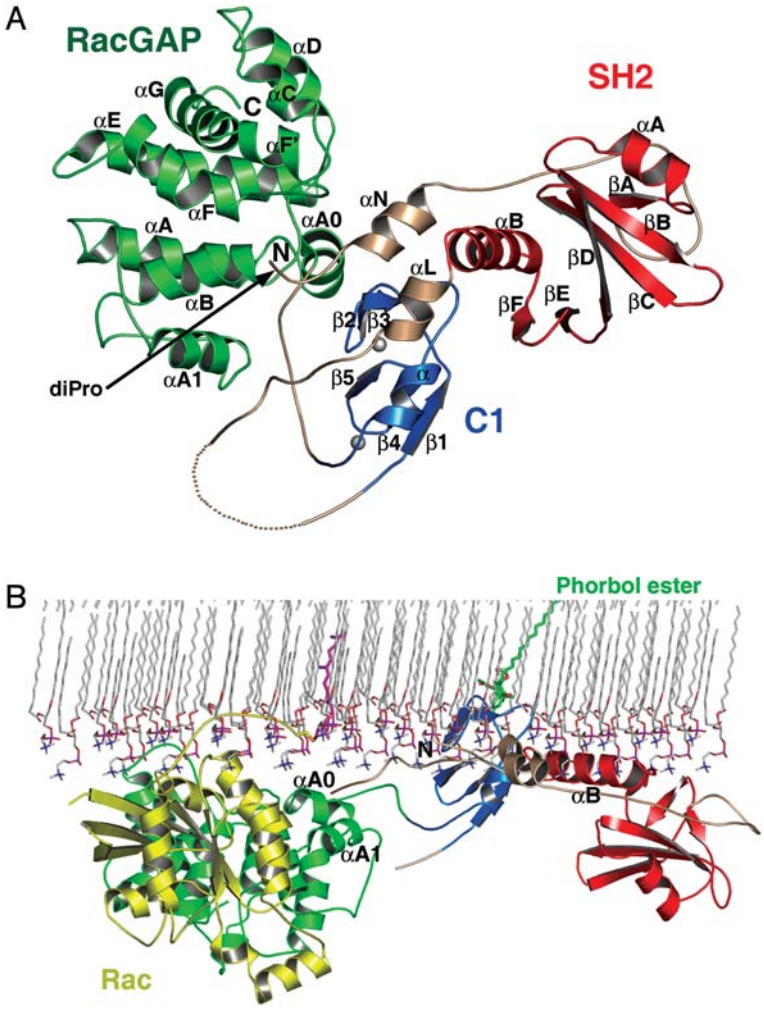

Fig. 17.4 Allosteric regulation of the β2-chimaerin at the membrane.
(A) The overall structure of the β2-chimaerin: SH2 domain (red), C1 (blue), Rac-GAP (green) and linkers (tan).
(B) Model for membrane-docked, active β2-chimaerin. The geranylgeranyl group is taken from the structure of Rac (yellow) bound to its guanine nucleotide dissociation inhibitor.

β1-chimaerin, the product of alternative splicing of the same gene as β2-chimaerin, lacks the SH2 domain of β2-chimaerin and therefore has fewer intramolecular interactions with the C1 domain. β1-Chimaerin translocates to membranes at a much lower dose of phorbol ester than β2-chimaerin, consistent with a greater degree of solvent exposure of its C1 domain.

Point mutants in any of the four regions that contact the C1 domain destabilize the inactive conformation and thereby decrease the EC_{50} for phorbol ester-

induced translocation, with the sensitization ranging from 15- to 90-fold. The smallest enhancement, 15-fold, is seen in the Q32A mutant, which obliterates polar interactions, rather than the hydrophobic interactions lost in other mutants. The largest enhancements of phorbol ester sensitivity, 90-fold, are seen in the mutants L28A and I130A. Leu28 buries itself against the junction between αL and the C1 domain, while Ile130 is buried in the αN/C1 interface. Mutating residues that stabilize more than one interdomain contact thus produces the largest sensitivity enhancements. Thus, the cooperative collapse of all of these interactions is a prerequisite for membrane binding. In other words, membrane binding by β2-chimaerin is coupled to a massive conformational change involving the entire protein.

17.4.2
Mechanism of Allosteric Rac-GTPase Activation by the C1 Domain

The β2-chimaerin structure, taken together with modeling of the β2-chimaerin/Rac transition state complex, shows how β2-chimaerin promotes the GTPase activity of Rac. Based on the model, Arg311 of β2-chimaerin acts as the "arginine finger", reaches into the active site of Rac, and directly stabilizes the transition state for GTP hydrolysis. The observed β2-chimaerin structure appears to be inactive for catalysis in two respects. First, Pro21 and Pro22 directly occlude the Rac-binding site (Fig. 17.4). Second, the αF′ helix is locked in the unliganded conformation by contacts with Pro22 (Fig. 17.4). The liganded conformation of p50-Rho-GAP shows the likely conformation of the β2-chimaerin Rac-GAP domain in complex with substrate. The liganded complex predicts that a movement of the helix by around 6 Å in order to make contact with Rac. The diPro unit is structurally rigid, the local environment in the Rac-binding cleft is conformationally restrictive and it is not apparent how such a structural change could occur without moving the residues that connect the diPro unit to the rest of β2-chimaerin. The next two residues in sequence, Ile23 and Trp24, are wedged between the C1 and Rac-GAP domain and the N-terminus is thereby anchored to both domains via extensive hydrophobic interactions. These interactions need to be broken in order to free the diPro motif to move out of the GAP active site.

In summary, β2-chimaerin provides the most clear-cut example available for a large-scale activating conformational change triggered by membrane engagement of a membrane binding domain. The membrane-penetrating and phorbol ester-binding sites on β2-chimaerin are occluded by intramolecular interactions with four separate regions of the protein. The Rac-binding site on β2-chimaerin is occluded. Rac binding requires the removal of the N-terminal region from the Rac-GAP domain active site. The N-terminal segment is tightly anchored by the C1 and Rac-GAP domain, and it participates directly in the occlusion of the phospholipid-binding site. Acidic phospholipid membranes compete with intramolecular interactions for binding to the C1 domain. When the former bind,

the latter interactions are disrupted. The disruption of these intramolecular interactions allows the N-terminus sufficient flexibility to leave the Rac-GAP active site, removes steric inhibition of Rac binding, and permits the αF′ helix to adopt the active conformation.

Acknowledgment
W. J. S. thanks Juan Bonifacino for his support.

References

1 E. A. Nalefski, J. J. Falke, *Protein. Sci.* **1996**, *5*, 2375–2390.
2 M. J. Rebecchi, S. Scarlata, *Annu. Rev. Biophys. Biomol. Struct.* **1998**, *27*, 503–528.
3 M. A. Lemmon, K. M. Ferguson, *Biochem. J.* **2000**, *350*, 1–18.
4 M. A. Lemmon, *Traffic* **2003**, *4*, 201–213.
5 A. C. Newton, J. J. Johnson, *Biochim. Biophys. Acta Rev. Biomembr.* **1998**, *1376*, 155–172.
6 J. H. Hurley, T. Meyer, *Curr. Opin. Cell. Biol.* **2001**, *13*, 146–152.
7 W. Cho, *J. Biol. Chem.* **2001**, *276*, 32407–32410.
8 J. H. Hurley, S. Misra, *Annu. Rev. Biophys. Biomol. Struct.* **2000**, *29*, 49–79.
9 J. H. Hurley, B. Wendland, *Cell* **2002**, *111*, 143–146.
10 A. Simonsen, A. E. Wurmser, S. D. Emr, H. Stenmark, *Curr. Opin. Cell Biol.* **2001**, *13*, 485–492.
11 J. H. Hurley, J. A. Grobler, *Curr. Opin. Struct. Biol.* **1997**, *7*, 557–565.
12 J. H. Hurley, Y. Tsujishita, M. A. Pearson, *Curr. Opin. Struct. Biol.* **2000**, *10*, 737–743.
13 U. Kikkawa, A. Kishimoto, Y. Nishizuka, *Annu. Rev. Biochem.* **1989**, *58*, 31–44.
14 Y. Nishizuka, *Nature* **1988**, *334*, 661–665.
15 Y. Nishizuka, *Science* **1992**, *258*, 607–614.
16 Y. Nishizuka, *FASEB J.* **1995**, *9*, 484–496.
17 J. W. Orr, L. M. Keranen, A. C. Newton, *J. Biol. Chem.* **1992**, *267*, 15263–15266.
18 J. W. Orr, A. C. Newton, *J. Biol. Chem.* **1994**, *269*, 8383–8387.
19 A. C. Newton, *Trends Pharmacol. Sci.* **2004**, *25*, 175–177.
20 L. O. Essen, O. Perisic, R. Cheung, M. Katan, R. L. Williams, *Nature* **1996**, *380*, 595–602.
21 J. A. Grobler, L. O. Essen, R. L. Williams, J. H. Hurley, *Nat. Struct. Biol.* **1996**, *3*, 788–795.
22 A. Dessen, J. Tang, H. Schmidt, M. Stahl, J. D. Clark, J. Seehra, W. S. Somers, *Cell* **1999**, *97*, 349–360.
23 J. O. Lee, H. J. Yang, M. M. Georgescu, A. Di Cristofano, T. Maehama, Y. G. Shi, J. E. Dixon, P. Pandolfi, N. P. Pavletich, *Cell* **1999**, *99*, 323–334.
24 E. H. Walker, O. Perisic, C. Ried, L. Stephens, R. L. Williams, *Nature* **1999**, *402*, 313–320.
25 M. J. Begley, G. S. Taylor, S. A. Kim, D. M. Veine, J. E. Dixon, J. A. Stuckey, *Mol. Cell* **2003**, *12*, 1391–1402.
26 S. Bagrodia, B. Dérijard, R. J. Davis, R. A. Cerione, *J. Biol. Chem.* **1995**, *270*, 27995–27998.
27 O. A. Coso, M. Chiariello, J. C. Yu, H. Teramoto, P. Crespo, N. Xu, T. Miki, J. S. Gutkind, *Cell* **1995**, *81*, 1137–1146.
28 A. Hall, *Science* **1998**, *279*, 509–514.
29 C. S. Hill, J. Wynne, R. Treisman, *Cell* **1995**, *81*, 1159–1170.
30 R. Kozma, S. Ahmed, A. Best, L. Lim, *Mol. Cell Biol.* **1995**, *15*, 1942–1952.
31 A. J. Ridley, A. Hall, *Cell* **1992**, *70*, 389–399.
32 A. M. De Vos, L. Tong, M. V. Milburn, P. M. Matias, J. Jancarik, S. Noguchi, S. Nishimura, K. Miura, E. Ohtsuka, S. H. Kim, *Science* **1988**, *239*, 888–893.
33 Y. Fukumoto, K. Kaibuchi, Y. Hori, H. Fujioka, S. Araki, T. Ueda, A. Kikuchi, Y. Takai, *Oncogene* **1990**, *5*, 1321–1328.

34 T. Nomanbhoy, R. A. Cerione, *Biochemistry* **1999**, *38*, 15878–15884.

35 D. K. Worthylake, K. L. Rossman, J. Sondek, *Nature* **2000**, *408*, 682–688.

36 J. T. Snyder, D. K. Worthylake, K. L. Rossman, L. Betts, W. M. Pruitt, D. P. Siderovski, C. J. Der, J. Sondek, *Nat. Struct. Biol.* **2002**, *9*, 468–475.

37 K. L. Rossman, D. K. Worthylake, J. T. Snyder, D. P. Siderovski, S. L. Campbell, J. Sondek, *EMBO J.* **2002**, *21*, 1315–13126.

38 Y. Zheng, M. J. Hart, R. A. Cerione, *Methods Enzymol.* **1995**, *256*, 77–84.

39 K. L. Rossman, L. Cheng, G. M. Mahon, R. J. Rojas, J. T. Snyder, I. P. Whitehead, J. Sondek, *J. Biol. Chem.* **2003**, *278*, 18393–18400.

40 R. Kristelly, G. Gao, J. J. Tesmer, *J. Biol. Chem.* **2004**, *279*, 47352–47362.

41 S. M. Soisson, A. S. Nimnual, M. Uy, D. Bar-Sagi, J. Kuriyan, *Cell* **1998**, *95*, 259–268.

42 K. L. Rossman, D. K. Worthylake, J. T. Snyder, L. Cheng, I. P. Whitehead, J. Sondek, *J. Biol. Chem.* **2002**, *277*, 50893–50898.

43 D. K. Worthylake, K. L. Rossman, J. Sondek, *Structure (Camb.)* **2004**, *12*, 1078–1086.

44 M. A. Baumeister, L. Martinu, K. L. Rossman, J. Sondek, M. A. Lemmon, M. M. Chou, *J. Biol. Chem.* **2003**, *278*, 11457–11464.

45 K. R. Skowronek, F. Guo, Y. Zheng, N. Nassar, *J. Biol. Chem.* **2004**.

46 K. L. Pierce, R. T. Premont, R. J. Lefkowitz, *Nat. Rev. Mol. Cell Biol.* **2002**, *3*, 639–650.

47 J. A. Pitcher, N. J. Freedman, R. J. Lefkowitz, *Annu. Rev. Biochem.* **1998**, *67*, 653–692.

48 S. K. Debburman, J. Ptasienski, J. L. Benovic, M. M. Hosey, *J. Biol. Chem.* **1996**, *271*, 22552–22562.

49 J. A. Pitcher, K. Touhara, E. S. Payne, R. J. Lefkowitz, *J. Biol. Chem.* **1995**, *270*, 11707–11710.

50 D. T. Lodowski, J. A. Pitcher, W. D. Capel, R. J. Lefkowitz, J. J. G. Tesmer, *Science* **2003**, *300*, 1256–1262.

51 L. N. Johnson, M. E. M. Noble, D. J. Owen, *Cell* **1996**, *85*, 149–158.

52 D. Fushman, T. Najmabadi-Haske, S. Cahill, J. Zheng, H. I. Levine, D. Cowburn, *J. Biol. Chem.* **1998**, *273*, 2835–2843.

53 C. V. Carman, L. S. Barak, C. Chen, L. Liu-Chen, J. J. Onorato, S. P. Kennedy, M. G. Caron, J. L. Benovic, *J. Biol. Chem.* **2000**, *275*, 10443–10452.

54 W. Q. Xu, S. C. Harrison, M. J. Eck, *Nature* **1997**, *385*, 595–602.

55 F. Sicheri, I. Moarefi, J. Kuriyan, *Nature* **1997**, *385*, 602–609.

56 D. Ron, M. G. Kazanietz, *FASEB J.* **1999**, *13*, 1658–1676.

57 H. Mellor, P. J. Parker, *Biochem. J.* **1998**, *332*, 281–292.

58 Y. Ono, T. Fujii, K. Igarashi, T. Kuno, C. Tanaka, U. Kikkawa, Y. Nishizuka, *Proc. Natl Acad. Sci. USA* **1989**, *86*, 4868–4871.

59 J. H. Hurley, A. C. Newton, P. J. Parker, P. M. Blumberg, Y. Nishizuka, *Protein Sci.* **1997**, *6*, 477–480.

60 T. Leung, B. E. How, E. Manser, L. Lim, *J. Biol. Chem.* **1994**, *269*, 12888–12892.

61 S. Ahmed, J. Lee, R. Kozma, A. Best, C. Monfries, L. Lim, *J. Biol. Chem.* **1993**, *268*, 10709–10712.

62 L. B. Areces, M. G. Kazanietz, P. M. Blumberg, *J. Biol. Chem.* **1994**, *269*, 19553–19558.

63 M. J. Caloca, N. Fernandez, N. E. Lewin, D. X. Ching, R. Modali, P. M. Blumberg, M. G. Kazanietz, *J. Biol. Chem.* **1997**, *272*, 26488–26496.

64 M. J. Caloca, M. L. Garcia-Bermejo, P. M. Blumberg, N. E. Lewin, E. Kremmer, H. Mischak, S. M. Wang, K. Nacro, B. Bienfait, V. E. Marquez, M. G. Kazanietz, *Proc. Natl Acad. Sci. USA* **1999**, *96*, 11854–11859.

65 M. J. Caloca, H. B. Wang, M. G. Kazanietz, *Biochem. J.* **2003**, *375*, 313–321.

66 B. Canagarajah, F. Collucio Leskow, Y. S. J. Ho, H. Mischak, L. Saidi, M. G. Kazanietz, J. H. Hurley, *Cell* **2004**, *119*, 407–418.

67 M. J. Caloca, H. B. Wang, A. Delemos, S. M. Wang, M. G. Kazanietz, *J. Biol. Chem.* **2001**, *276*, 18303–18312.

Subject Index